DIRECT STRENGTH METHOD FOR THE DESIGN OF COLD-FORMED STEEL SECTIONS UNDER LOCALISED LOADING

by

VAN VINH NGUYEN

A thesis submitted in partial fulfilment of requirements for

the degree of Doctor of Philosophy

School of Civil Engineering

Faculty of Engineering and IT

The University of Sydney

Australia

Sydney, August 2017

This is to certify that to the best of my knowledge, the content of this thesis is my own work. This thesis has not been submitted for any degree or other purposes.

I certify that the intellectual content of this thesis is the product of my own work and that all the assistance received in preparing this thesis and sources have been acknowledged.

Sydney, 2nd August 2017

Van Vinh Nguyen

ABSTRACT

The main objective of the thesis is the development of the Direct Strength Method (DSM) for the design of cold-formed steel sections under general localised loading. In order to calibrate the DSM equations, it is necessary to have three main input variables which are the buckling load, the yield load and the experimental data.

The first objective of this research is the development of the Finite Strip Method (FSM) theory for analysis of thin-walled sections under localised loading with general end boundary conditions to determine the buckling load as described in Chapters 3 and 4 of the thesis. The theory is included in Version 2.0 of the THIN-WALL-2 program which can be used for analysing structural members under generalised loading conditions as described in Chapter 5.

The second objective is the formulation of plastic mechanism models to estimate the yield load of thin-walled sections subjected to localised loading. In order to establish these models, observations are performed from experiments to ascertain the failure modes of structural members under localised loading with different cross-sections, load cases and flange fastening conditions. From the data, new simple plastic mechanism models are built-up based on the concept of the balance between the internal energy of the structural member and the external energy of the applied loads to estimate the yield load as described in Chapter 6.

The third objective is collating the experimental data of thin-walled sections under localised loading. The data is collected from previous literature for different types of cross-sections: un-lipped plain-C, lipped plain-C, SupaCee and Dimond Hi-Span channel (DHS) sections subjected to all load cases. In addition, both flange fastened and unfastened conditions are assembled in the experimental database as described in Chapter 6.

From these three input variables, the DSM design equations are proposed for structural members under general localised loading. The method is a consistent and simplified model generalised for all localised load cases. It includes both an inelastic reserve component as observed in testing and a yield load component. Also, a reliability analysis calibration is performed to validate the accuracy of the DSM predictions with the collected experimental data as described in Chapter 7.

PREFACE

This thesis is submitted to the University of Sydney, Australia for the degree of Doctor of Philosophy. The work described in this thesis was carried out by the candidate during the years 2014 to 2017 in the School of Civil Engineering, the University of Sydney under the supervision of Dr. Cao Hung Pham and Professor Gregory J. Hancock.

In accordance with the Bylaws of the University of Sydney governing the requirements for the degree of Doctor of Philosophy, the candidate submits that the work presented in this thesis is original unless otherwise referenced within the text. The Finite Strip Method (FSM) theory for the analyses of thin-walled sections under localised loading for Simply Supported boundary condition was devised by Professor Gregory J. Hancock. The candidate further developed this theory for general end boundary conditions by the inclusion of appropriate longitudinal displacement functions. In addition, the theory has been included in Version 2.0 of the THIN-WALL-2 program which is a combination of two programs:

1. Graphical User Interface (GUI) program written by the candidate and Dr. Cao Hung Pham using Matlab.

2. Finite Strip Method module written by the candidate in Matlab for analyses of thin-walled sections under localised loading for general end boundary conditions.

A separate Version 1.0 of the THIN-WALL-2 program for pre-buckling and buckling analyses of thin-walled sections under localised loading with simply supported boundary condition alone contains C++ modules written by Professor Gregory J. Hancock and is not claimed as part of this thesis.

New plastic mechanism models are proposed by the candidate to estimate the yield load (P_y) of structural members under localised loading. Also, the author proposes new Direct Strength Method (DSM) design equations to predict the capacities of structural members subjected to localised loading.

Four journal papers and five conference papers, which are based on the work presented in this thesis, have been published, submitted or are prepared for publication. In addition, four research reports have been published which are also based on the work presented in this thesis.

PUBLICATIONS

Journal papers

1. Nguyen, V.V., G.J. Hancock, and C.H. Pham, *Analyses of thin-walled sections under localised loading for general end boundary conditions - Part 1: Pre-buckling.* Thin-Walled Structures, 2017. **(accepted for publication)**

2. Nguyen, V.V., G.J. Hancock, and C.H. Pham, *Analyses of thin-walled sections under localised loading for general end boundary conditions - Part 2: Buckling.* Thin-Walled Structures, 2017. **(accepted for publication)**

3. Nguyen, V.V., G.J. Hancock, and C.H. Pham, *A consistent and simplified Direct Strength Method (DSM) for design of cold-formed steel sections under localised loading.* Journal of Structural Engineering (ASCE), 2017. **(in preparation)**

4. Nguyen, V.V., G.J. Hancock, and C.H. Pham, *Application of the THIN-WALL-2 V2.0 program for analysis of thin-walled sections under localised loading.* Computers & Structures, 2017. **(in preparation)**

Conference papers

1. Nguyen, V.V., G.J. Hancock, and C.H. Pham, *Development of the THIN-WALL-2 program for buckling analysis of thin-walled sections under generalised loading*, in *Eighth International Conference on Advances in Steel Structures*. 2015: Lisbon, Portugal.

2. Nguyen, V.V., G.J. Hancock, and C.H. Pham, *Analyses of thin-walled sections under localised loading for general end boundary conditions - Part 1: Pre-buckling*, in *CCFSS2016*. 2016: Baltimore, Maryland, USA.

3. Nguyen, V.V., G.J. Hancock, and C.H. Pham, *Analyses of thin-walled section under localised loading for general end boundary conditions - Part 2: Buckling*, in *CCFSS2016*. 2016: Baltimore, Maryland, USA.

4. Nguyen, V.V., G.J. Hancock, and C.H. Pham, *New developments in the Direct Strength Method (DSM) for design of cold-formed steel sections under localised loading*, in *Eurosteel Copenhagen 2017*. 2017: Copenhagen, Denmark.

5. Nguyen, V.V., G.J. Hancock, and C.H. Pham, *Applications of the THIN-WALL-2 V2.0 program for analysis of thin-walled sections under localised loading*, in *International conference CIGOS2017 - New challenges in Civil Engineering*. 2017: Ho Chi Minh city, Viet Nam.

Research reports

1. Nguyen, V.V., G.J. Hancock, and C.H. Pham, *Pre-buckling analysis of thin-walled sections under localised loading for general end boundary conditions*, in *Research report R958*. 2016, The University of Sydney: Sydney, Australia.

2. Nguyen, V.V., G.J. Hancock, and C.H. Pham, *Buckling analysis of thin-walled sections under localised loading for general end boundary conditions*, in *Research report R959*. 2016, The University of Sydney: Sydney, Australia.

3. Nguyen, V.V., G.J. Hancock, and C.H. Pham, *Experimental data, buckling loads and plastic mechanism models used in the Direct Strength Method (DSM) applied to localised loading*, in *Research Report R965*. 2017, The University of Sydney: Sydney, Australia.

4. Nguyen, V.V., G.J. Hancock, and C.H. Pham, *A consistent and simplified Direct Strength Method (DSM) for design of cold-formed steel sections under localised loading*, in *Research Report R966*. 2017, The University of Sydney: Sydney, Australia.

ACKNOWLEDGEMENT

I also wish to thank Ms Daniela Entenmann who supported me during my research, especially in getting the top up scholarship for my tuition fees and living costs from the School of Civil Engineering, the University of Sydney.

I'm grateful for my mother, Mrs Thi Ha Nguyen, who bore me, raised me very hard after my father passed away in 1993. She always encourages me to study and go overseas to do PhD research. Also, I appreciate my parents-in-law, Mr Ngoc Thang Hoang and Mrs Thi Ty Nguyen, who gave me advice and financial support during my period of time in Australia.

Lastly, I would like to thank my wife, Mrs Thi Bich Tra Hoang, who is always beside me. She gave up her job in Viet Nam to come to Australia with me and worked as a casual worker in Sydney. She looked after our sons, Hoang Linh Nguyen and Hoang Long Nguyen, very well when I was busy with my study. I'm more confident when living overseas with all members of my family, obviously I can focus 100% on my research and finish my thesis on time.

TABLE OF CONTENTS

LIST OF APPENDICES

LIST OF TABLES

LIST OF FIGURES

NOTATION

LATIN LETTERS

Notation	Meaning	Unit
$[B_{Fm}]$	Strain matrix of flexural displacement	
$[B_{Mm}]$	Strain matrix of membrane displacement	
$[C]$	Transformation matrix	
$[C_F]$	Evaluation matrix of the flexural displacement functions at the nodal lines	
$[C_M]$	Evaluation matrix of the membrane displacement functions at the nodal lines	
$[D_F]$	Property matrix of flexural displacement of a strip	
$[D_M]$	Property matrix of membrane displacement of a strip	
$[G]$	Stability matrix of section	
$[g_{\alpha Fmn}]$	Flexural stability matrix of a strip	
$[g_{\alpha Mmn}]$	Membrane stability matrix of a strip	
$[G_G]$	Global stability matrix of a strip	
$[G_L]$	Local stability matrix of a strip	
$[K]$	Stiffness matrix of section	
$[k_{\alpha Fmn}]$	Flexural stiffness matrix of a strip	
$[k_{\alpha Mmn}]$	Membrane stiffness matrix of a strip	
$[K_G]$	Global stiffness matrix of a strip	
$[K_L]$	Local stiffness matrix of a strip	
$[R]$	Rotation matrix	
$\{F\}$	Load vector	
$\{F_{Xm}\}$	Load vector component in X direction	
$\{F_{Ym}\}$	Load vector component in Y direction	
$\{F_{Zm}\}$	Load vector component in Z direction	
A	Strip area	mm^2
A_w	Web area	mm^2

b	Strip width	mm
B_f	Flange width	mm
CC	Both ends clamped	
CF	One end clamped and one end free	
C_l	Coefficient of bearing length	
C_r	Coefficient of inside bent radius	
C_w	Coefficient of web slenderness	
D	Section depth	mm
d_1	Web depth	mm
D_X	Displacement by transverse direction	mm
D_Y	Displacement by vertical direction	mm
D_Z	Displacement by longitudinal direction	mm
EN	End node	
EOF	End one-flange loading	
ETF	End two-flange loading	
E_x	Young's modulus by longitudinal direction	MPa
E_y	Modulus of elasticity by transverse direction	MPa
$f_{1m}(y)$	Polynomial function for flexural transverse variation	
FF	Both ends free	
f_{od}	Elastic distortional buckling stress of the section in bending	MPa
f_{ol}	Elastic local buckling stress of the section in bending	
f_u	Ultimate strength of steel	MPa
$f_{um}(y)$	Polynomial function for membrane transverse variation	
$f_{vm}(y)$	Polynomial function for membrane transverse variation	
$F_X(Z)$	Distributed lines load in X direction	
f_y	Yield strength of steel	MPa
$F_Y(Z)$	Distributed lines load in Y direction	
$F_Z(Z)$	Distributed lines load in Z direction	
G	Shear modulus of a strip	MPa
h	Plastic hinge depth	mm

i	Strip number	
IOF	Interior one-flange loading	
ITF	Interior two-flanges loading	
j	Node (nodal line) number	
k	DSM coefficient	
k_v	Shear buckling coefficient	
L	Strip length	mm
L_1, L_2	Lip lengths	mm
l_b	Actual bearing length	mm
L_o	Beam length	mm
m	Series term m^{th}	
M_{od}	Elastic distortional buckling moment of the section	kNm
M_{ol}	Elastic local buckling moment of the section	kNm
M_p	Plastic moment per unit length of plate	kNm
M_y	Yield moment of the section	kNm
N	Bearing length	mm
n	Node number of a section	nodes
N_{cd}	Nominal capacity of a member in compression for distortional buckling	kN
N_{ce}	Nominal member capacity of a member in compression	kN
N_{cl}	Nominal capacity of a member in compression for local buckling	kN
N_m	Yield-line length	mm
N_{oc}	The least of the elastic compression member buckling load in flexural, torsional and flexural-torsional buckling	kN
N_{od}	Distortional buckling load	kN
N_{ol}	Elastic local buckling load	kN
N_y	Nominal yield capacity of the member in compression	kN
p	Start node of a strip	
P^*	Applied load	kN
P_{cr}	Buckling load	kN
P_{exp}	Experiment load	kN

P_n	Nominal capacity	kN
P_y	Yield load	kN
q	End node of a strip	
r	Centre radius	mm
r_1, r_2	Corner radii	mm
R_b	Nominal capacity for concentrated load or reaction for one solid web	kN
R_c	Nominal capacity for concentrated load or reaction for one solid web with holes	kN
r_e	Outer radius	mm
r_i	Inner radius	mm
s	Strip number of a section	
SC	One end simply supported and one end clamped	
SF	One end simply supported and one end free	
SN	Start node	
SS	Both ends simply supported	
t	Thickness	mm
t_E	Thickness for bending	mm
t_f	Thickness of flange	mm
t_G	Thickness for shear	mm
t_w	Thickness of web	mm
U	Total strain energy of a strip	
u	Longitudinal membrane displacement of a strip	mm
U_F	Flexural strain energy stored in a strip	
U_M	Membrane strain energy stored in a strip	
V	Total potential energy of external forces or membrane stresses	
V	Strip volume	mm^3
v	Transverse membrane displacement of a strip	mm
V_{cr}	Elastic shear buckling force of web	kN
V_F	Flexural potential energy of the membrane stresses	

V_{FL}	Flexural potential energy of the longitudinal stress	
V_{FS}	Flexural potential energy of the shear stress	
V_{FT}	Flexural potential energy of the transverse stress	
V_M	Membrane potential energy of the membrane stresses	
V_{Mu}	Membrane potential energy of the longitudinal stress by longitudinal direction	
V_{Mv}	Membrane potential energy of the longitudinal stress by transverse direction	
V_y	Yield load of web	kN
w	Flexural displacement of a strip	mm
X	Transverse axis	
$X_{1m}(x)$	Displacement function for flexural longitudinal variation and membrane transverse variation	
$X_{2m}(x)$	Displacement function for membrane longitudinal variation	
Y	Vertical axis	
Z	Longitudinal axis	
Z_e	Section modulus	mm^3
Z_f	Section modulus about a horizontal axis of the full section	mm^3
$\bar{y}$	Variable	

GREEK LETTERS

Notations	Meaning	Unit
$\{\alpha_{Fm}\}$	Vector of polynomial coefficients of flexural deformations	
$\{\alpha_{Mm}\}$	Vector of polynomial coefficients of membrane deformations	
$\{\delta_{Fm}\}$	Flexural displacement vector of a strip	
$\{\delta_{Mm}\}$	Membrane displacement vector of a strip	
$\{\varepsilon_{Fm}\}$	Flexural strain vector	
$\{\varepsilon_{Mm}\}$	Membrane strain vector	
$\{\sigma_{Fm}\}$	Flexural stress vector	
$\{\sigma_{Mm}\}$	Membrane stress vector	
α	Plastic hinge depth factor	
β	Yield-line slope factor	
β_1	Slope factor	
β_o	Slope factor depends on the bearing length ratio (N/D)	
δ_b	Buckling displacement (deformation)	mm
δ_p	Pre-buckling displacement (deformation)	mm
ϕ	Total potential energy	
γ	Factor depends on the radius ratio (r_i/t)	
λ	Section slenderness	
λ	Load factor against buckling	
λ_d	Non-dimensional slenderness used to determine M_{bd}	
λ_l	Non-dimensional slenderness used to determine M_{bl}	
λ_v	Non-dimensional slenderness used to determine V_v	
μ	Number of series terms	
v_x, v_y	Poisson's ratios	
θ	Rotation angle of web	
ρ_x	Curvature in x direction	
ρ_{xy}	Twist in x direction	

ρ_y	Curvature in y direction	
ρ_{yx}	Twist in y direction	
σ_x	Longitudinal stress	MPa
σ_y	Transverse stress	MPa
σ_{cr}	Elastic critical stress	MPa
τ_{xy}	Shear stress	MPa
ξ	Variable, $\xi = \pi x / L$	

ρ_y Curvature in y direction

CHAPTER 1

INTRODUCTION

1.1. INTRODUCTION ABOUT COLD-FORMED STEEL STRUCTURES

Cold-formed steel can be seen as an alternative to hot-rolled steel. Members made from cold-formed steel have been used widely and effectively around the world with many applications such as roof trusses (Fig.1.1a), decking (Fig.1.1b), beams, storage racks, houses (Fig.1.1c), purlins, portal frames (Fig.1.1d), roof sheeting and floor decks. In addition, these members can be used as non-building members in transportation vehicles such as cars, railway cars or coaches. High strength steel is often used to create cold-formed steel members, thus the members are thinner and lighter than hot-rolled steel members. The thickness can be as thin as 0.42mm with a high yield stress of 550MPa [1]. Obviously, the self-weight of structures is reduced which makes the structures more efficient to transport and erect.

(a) Roof trusses	(b) Decking
(c) Houses	(d) Portal frames

Figure 1.1: Applications of cold-formed steel

The cold-formed steel members are manufactured by bending flat sheets at ambient temperatures which allows the creation of many shapes of cross-sections such as roof sheeting, channels, zeds, hats and proprietary sections such as SupaCees, SupaZeds, Dimond Hi-Span (DHS) channels, built-up-I sections with and without stiffeners in the web and flanges as shown in Fig.1.2. It means that there are more options for member cross-sections when using cold-formed steel than hot-rolled steel.
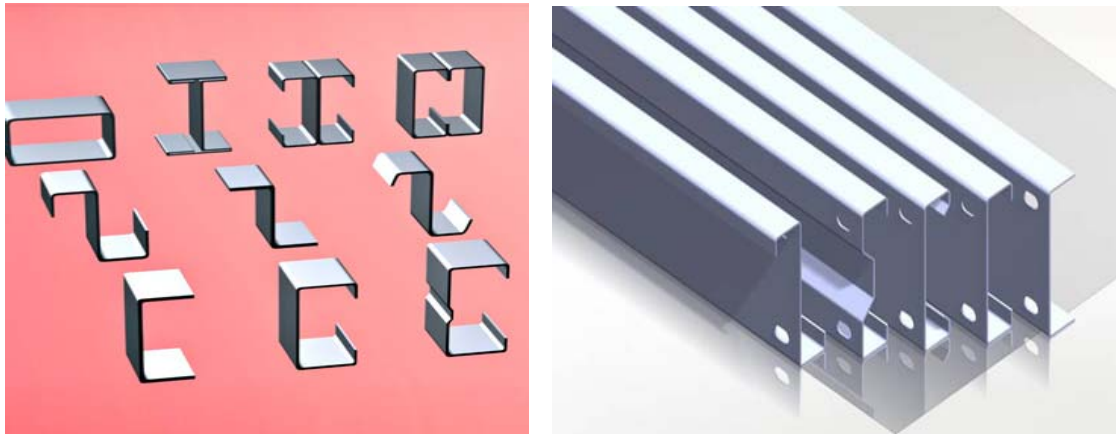
Figure 1.2: Cold-formed steel (thin-walled) sections

However, because of the thinner sections, cold-formed steel members have modes of failure and deformation which are not commonly encountered in normal structural steel design as shown in Fig.1.3, and so design specifications and standards are required which provide guidance for the design of thin-walled members. In addition, the cold-forming process often produces structural imperfections and residual stresses which are quite different from those of traditional hot-rolled and welded members. Consequently, design specifications and standards have been produced specifically for cold-formed structural members [2], [3], [4], [5], [6].

Figure 1.3: Failures of cold-formed steel structures

Recently, with the development of high strength steels, improvements of rolling and forming technology and evolution of complex shapes, cold-formed steel members are being fabricated with higher yield strength materials and used as an effective alternative to the hot-rolled steel members.

1.2. SIGNIFICANCE OF STUDY

Cold-formed members may fail because of compression, flexure (bending), shear or combinations of these forces. Many investigations have been focused on these areas. The design rules have been developed and included in both the North American Specification for the Design of Cold-Formed Steel Structural Members AISI S100-2012 [2] and the Australian/New Zealand Standard AS/NZS 4600:2005 [3]. However, in some structures, cold-formed members are connected together and there is a direct transfer of localised loading from one to each other as shown in Fig.1.4. Web crippling at points of concentrated load and supports can be a critical problem in cold-formed steel structural members and sheeting for several reasons. Firstly, in cold-formed design, it is often not practical to provide load bearing and end bearing stiffeners. This is always the case in continuous sheeting and decking spanning several support points. Secondly, the depth to thickness ratios of the webs of cold-formed members usually is larger than for hot-rolled structural members. Thirdly, in many cases, the webs are inclined rather than vertical. Finally, the intermediate element between the flange to which the load is applied, and the web of a cold-formed member usually consists of a bend of finite radius, thus the load is applied eccentrically from the web.

Figure 1.4: Localised loading

Localised loading, patch loading and web crippling have the same phenomena; however, in this thesis the term localised loading has been used throughout.

From the locations of the localised load, there are four loading cases which are referred in design in the North American Specification for the Design of Cold-Formed Steel Structural Members AISI S100-2012 [2] and the Australian/New Zealand Standard AS/NZS 4600:2005 [3] of thin-walled

sections. These are Interior one-flange loading (IOF), End one-flange loading (EOF), Interior two-flange loading (ITF) and End two-flange loading (ETF). The failure modes of structural members under the four different localised load cases are shown in Fig.1.5(a), (b), (c) and (d) respectively.

(a) IOF load case [7]   (b) EOF load case [8]
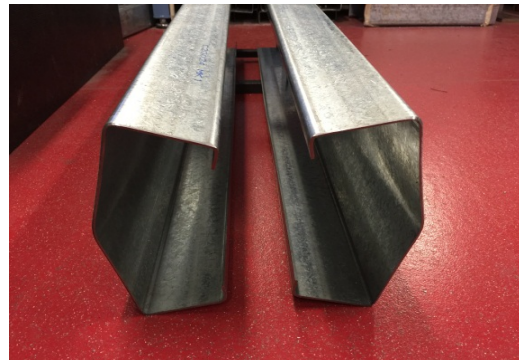
(c) ITF load case [9]   (d) ETF load case [10]

Figure 1.5: Web crippling failure modes

Currently, many experimental investigations have been performed to study cold-formed steel members under localised loading; however, there is limited theoretical research focusing on this area due to the difficulty in the buckling analysis and yielding analysis when the load is concentrated. Thus, it is necessary to have a theoretical combined with experimental investigation for cold-formed structural members subjected to localised loading.

The common design methods used to estimate the capacities of structural members are the Effective Width Method (EWM) and the Direct Strength Method (DSM). The DSM is a recent alternative to the traditional EWM for design of cold-formed sections. The DSM has been developed by Schafer and Pekoz [11] and well established for design rules of cold-formed steel structural members under compression, bending and shear. In addition, the DSM of design was included in the North American Specification for the Design of Cold-Formed Steel Structural Members AISI S100-2012 [2] (NAS) for the three load cases above and the Australian/New Zealand Standard AS/NZS

4600:2005 [3] for compression and bending. However, the NAS S100:2012 and 2016 Editions have not included the DSM for design of thin-walled sections under localised loading. Thus, it is important that the DSM is extended to localised loading so that the method is completely general. In order to establish the DSM for design of cold-formed sections under localised loading, it is necessary to have three main input variables as the buckling load, the yield load and the experimental data.

The elastic buckling load is an important input to the DSM design equations for web crippling. Some investigations have been performed to determine the buckling load of cold-formed sections under localised loading; however, they still have limitations. Recently, Hancock and Pham [12] have developed the Semi-Analytical Finite Strip Method (SAFSM) for buckling analysis of thin-walled sections under localised loading; however, the theory is only available for the simply-supported boundary conditions at both ends of structural members. In normal structures, cold-formed members are connected by bolts or welds, thus the boundary conditions are different from simply-supported. Thus, it is necessary to develop the theory for analyses of cold-formed sections under localised loading with general end boundary conditions.

In addition to the buckling load, the yield load is another key input to the DSM design equations for web crippling. Some mechanism and yield models have been proposed as described in Chapter 2 to estimate the yield load of thin-walled sections under localised loading; however, these predictions still have some disadvantages. Thus, it is necessary to develop simplified and consistent models to determine the yield load for web crippling for general cold-formed steel sections, load cases and flange fastened conditions.

1.3. OBJECTIVES OF STUDY

The main objectives which have been presented in the thesis are listed as follows:

1. To develop the FSM theory for pre-buckling and buckling analyses of thin-walled sections under localised loading with general end of boundary conditions.

2. To investigate elastic buckling stresses of thin-walled sections under localised loading and to determine various buckling modes as well as to get the critical load (P_{cr}) of the thin-walled sections.

3. To collect the experimental data of structural members subjected to localised loading from previous literature.

4. To create simple plastic mechanism models to estimate the yield load (P_y) of structural members under localised loading using the data in 4.

5. To develop a consistent and simplified Direct Strength Method (DSM) for the design of cold-formed steel sections under localised loading.

1.4. RESEARCH METHODOLOGY

1.4.1. Finite Strip Method

The Finite Strip Method (FSM) [13] is an effective method for the static, stability, post-buckling and vibration analyses of thin-walled structures. In comparison with the Finite Element Method (FEM), this method has various advantages. Firstly, structural members are divided into strips instead of elements in analyses, thus the number of degrees of freedom is reduced. Secondly, there are no compatibility problems between flexural and membrane displacements at plate junctions in using the FSM. In addition, it is easy to define the geometry of the structural problem.

In the FSM, simple polynomial functions are used to describe the transverse variations, while continuous harmonic series functions are usually employed to describe the longitudinal variation of strip displacements. This approach is different from the FEM which uses the polynomial functions for both the longitudinal and transverse directions to describe the element displacements. In general, in order to give compatibility between the strips, the longitudinal harmonic series chosen for flexural and membrane deformations are the same. When harmonic functions are chosen based on analytical solutions, the FSM is commonly known as the Semi-Analytical Finite Strip Method (SAFSM). In another case, local spline functions may be used instead of the harmonic series functions in the longitudinal direction to account for the different end boundary conditions. This is known as the Spline Finite Strip Method (SFSM).

Cheung [13] originally developed the SAFSM for stress analysis of isotropic and orthotropic variable thickness plates in bending with simply supported boundary conditions. In this research, a polynomial function is used in the transverse direction, while a harmonic series function which is assumed to take the form of a half sine wave is employed in the longitudinal direction. This choice of displacement functions is consistent with the boundary condition of simply supported ends. This method was also extended to plates with clamped and free-end boundary conditions. In addition, Cheung [13] further extended the method incorporating the membrane displacements in addition to the plate flexural displacements for the stress analysis of folded plate structures. The displacements

along each nodal line is described by only four degrees of freedom, thus the numerical work was reduced considerably in comparison with the FEM. The SAFSM was first used by Przmieniecki [14] for buckling analysis of plates involving only flexural deformations. Plank and Wittrick [15] extended this study to develop a complex finite strip method for the buckling analysis of plates under loading combinations such as longitudinal compression and bending, transverse compression and shear. Recently, Hancock and Pham [12] have used the SAFSM for the analysis of thin-walled sections under localised loading with simply-supported at both ends of the structural members.

For other boundary conditions, the displacement functions may be different from harmonic functions. In this thesis, the FSM has been developed for both pre-buckling and buckling analyses of thin-walled sections under localised loading for general end boundary conditions as described in the Chapters 3 and 4. The theory has been included in the THIN-WALL-2 V2.0 program as shown in Fig.1.6 and described in detail in Chapter 5. The general end boundary conditions theory has used a combination of longitudinal displacement functions from Cheung [13] and Bradford and Azhari [16]. Li and Schafer [17] have subsequently used the Bradford and Azhari's functions for buckling analysis.
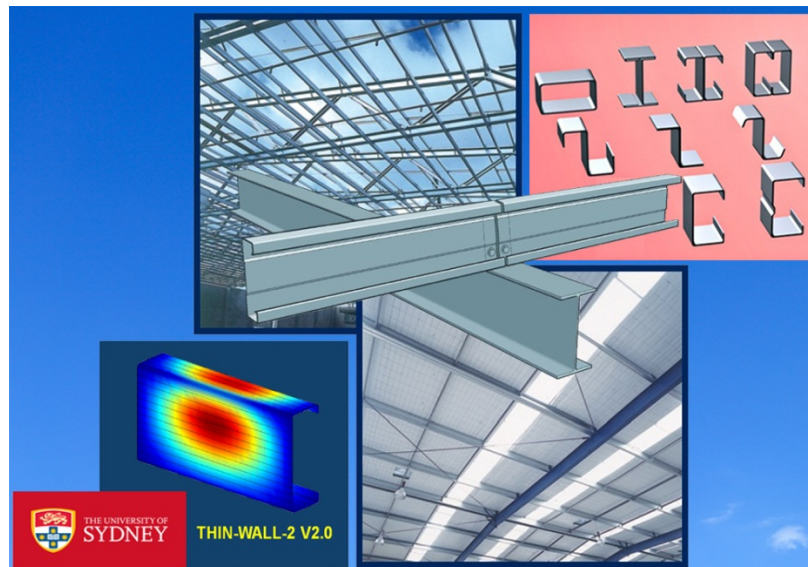
Figure 1.6: THIN-WALL-2 V2.0 program appearance
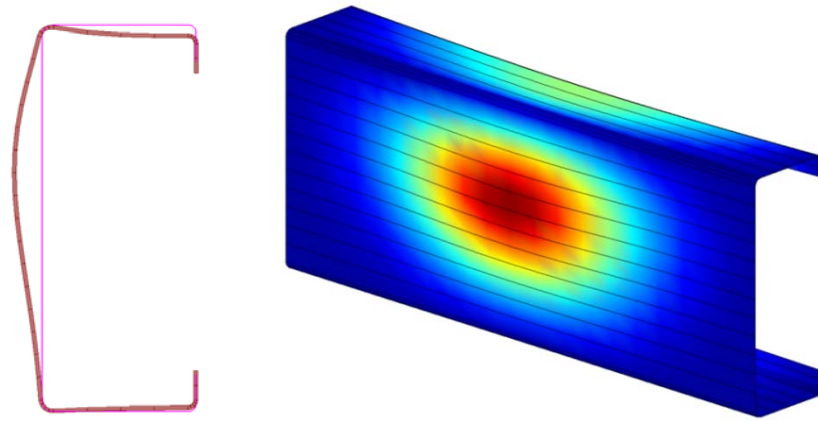
Figure 1.7: Localised loading buckling modes in 2D and 3D views from THIN-WALL-2 V2.0

THIN-WALL-2 V2.0 is written to define input data using a Graphical User Interface (GUI) to perform pre-buckling and buckling analyses of thin-walled sections under generalised loading. The loading may contain uniform stresses or localised loading. The GUI is then used to display the results of the analysis. It is also possible to use this program to perform a cross-section analysis to generate the section properties. The cross-sections can be formed from different shapes includes open and closed sections or mixed sections. In this research, the THIN-WALL-2 V2.0 program is used to estimate the buckling load and buckling modes of structural members under localised loading as shown in Fig.1.7. The buckling load is a key input to develop the DSM for web crippling.

1.4.2. Plastic mechanism models

The yield load is another important input variable to the DSM for web crippling. Some models have been proposed to estimate the yield load of thin-walled sections under localised loading. For example, Keerthan et al. [18], Sundararajah et al. [19] and Dara and Yu [20] determined the yield load from an equivalent web yield capacity. Natário, Silvestre and Camotim [21] employed the yield-line method to calculate the yield load for different cross-sections, different flange fastened conditions, under both two-flange load cases. Young and Hancock [22] developed plastic mechanism models to estimate the yield load of un-lipped channel sections under localised load cases. In this thesis, observations are performed from experiments to ascertain the failure modes of structural members under localised loading with different cross-sections, load cases and flange fastened conditions as shown in Fig.1.8. From the data, simple and consistent plastic mechanism models are built up based on the concept of the balance between the internal energy of the structural member and the external energy of the applied loads to estimate the yield load. Currently, the models are available for different types of cross-

section such as unlipped plain-C, lipped plain-C, SupaCee and Dimond Hi-Span (DHS) for all localised loading cases.

An example of a plastic mechanism model for a lipped channel section under the interior one-flange loading (IOF) is shown in Fig.1.9. The models for other cross-sections subjected to other localised load cases are described in Chapter 6 of the thesis.

(a) Experiment   (b) Failure modes
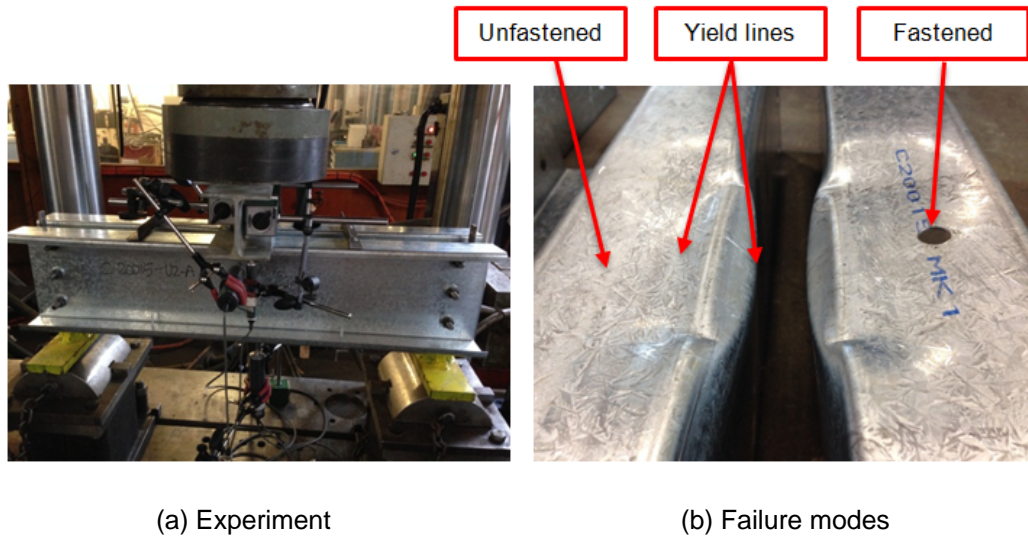
Figure 1.8: The IOF load case [7]
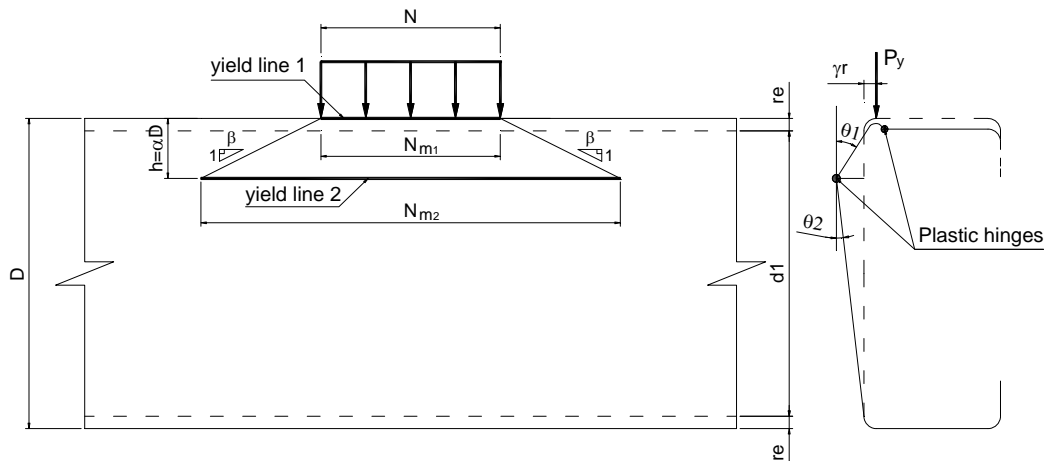
Figure 1.9: Plastic mechanism model for the IOF load case

where N is the bearing length and N_{m1}, N_{m2} are the yield-line lengths

The models are simplified with horizontal hinges of length N_{m1} and N_{m2} to facilitate easy design.

The internal energy of the structural member must be equal to the external energy of the applied loads as given:

$$P_y \gamma r \theta_1 = M_p \theta_1 N_{m1} + M_p \left(\theta_1 + \theta_2 \right) N_{m2}$$

(1.1)

Hence, the yield load (P_y) is given by:

$$P_y = \frac{M_p}{\gamma r}\left[N_{m1} + \left(\frac{D}{D-h} \right) N_{m2} \right]$$

(1.2)

where

N is the bearing length

N_{m1}, N_{m2} are the yield-line lengths

γr is the load eccentricity from the web centre

M_p is the plastic moment per unit length of plate

This example has been included here so as to provide a demonstration of the nature and simplicity of the equations.

1.4.3. Experimental investigations

Experimental investigations have been performed by many researchers to study the behaviour of cold-formed steel members subjected to localised loading. Four localised loading cases (IOF, EOF, ITF and ETF) have been tested as shown in Fig.1.10. In addition, different cross-sections have been conducted in the experiments such as un-lipped plain-C, lipped plain-C, Supacee, DHS, lipped plain-Z, SupaZed and built-up-I sections. Also, both unfastened and fastened flanges have been considered in the tests. The experimental data has been collected from different sources to estimate the yield loads by the plastic mechanism models and the buckling loads using the THIN-WALL-2 V2.0 program based on the FSM as described in the Chapter 6. Full details are given in Chapters 2 and 6 of the thesis.
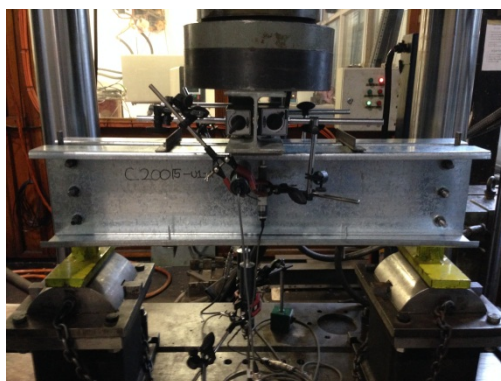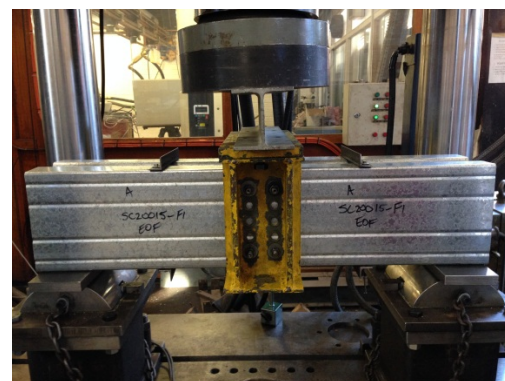
(a) IOF test [7]   (b) EOF test [8]
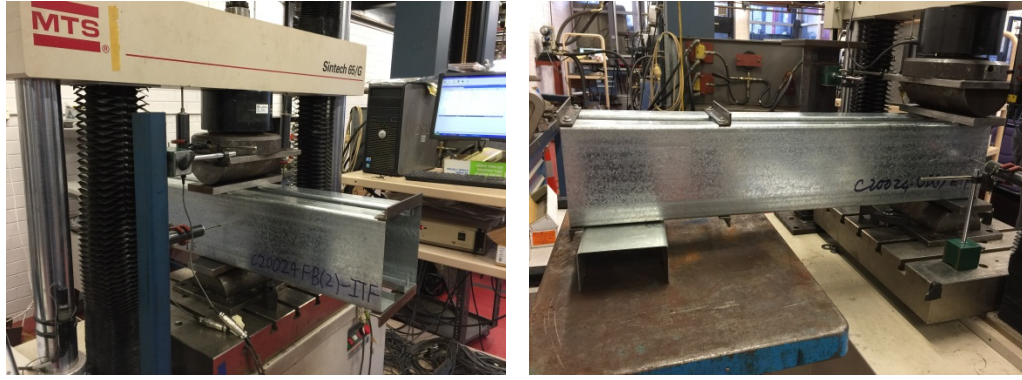
(c) ITF test [9] (d) ETF test [10]

Figure 1.10: Experiments of cold-formed steel members under localised loading

1.4.4. Direct Strength Method

The purpose of this research is the development of the DSM for the design of cold-formed steel sections under localised loading. Three main input variables to establish the DSM for web crippling are the elastic buckling load (P_{cr}), yield load (P_y) and experimental data (P_{exp}). The elastic buckling load is obtained from the THIN-WALL-2 V2.0 program based on the Finite Strip Method (FSM), while the yield load is determined from the plastic mechanism models and the experimental data is collected from different sources for all load cases as described in Chapter 6. From these three components, a general set of DSM equations is proposed to predict the nominal strength of the structural members under localised loading. To introduce these equations in a general form, Eqs.(1.3) and (1.4) which are Eqs. (7.1) and (7.2) in Chapter 7, are summarised here. Eq.(1.4) is used to predict the yield nominal capacity, while the Eq.(1.3) is used to predict the inelastic reserve nominal capacity of structural members subjected to the different localised load cases.

$$\frac{P_n}{P_y} = \left[1 + \left(1 - \frac{\lambda}{\lambda_o} \right) (k_4 - 1) \right] \qquad \text{for} \qquad \lambda \leq \lambda_o \qquad (1.3)$$

$$\frac{P_n}{P_y} = k_1 \left[1 - k_2 \left(\frac{P_{cr}}{P_y} \right)^{k3} \right] \left(\frac{P_{cr}}{P_y} \right)^{k3} \qquad \text{for} \qquad \lambda > \lambda_o \qquad (1.4)$$

where:

λ is the sectional slenderness, $\lambda = \sqrt{P_y / P_{cr}}$

λ_o is the sectional slenderness when $P_n / P_y = 1$

k_1, k_2, k_3 are simplified coefficients and exponents calibrated through fitting the set of ratios $P_{\exp} / P_y$ to the right hand side of Eq.(1.4) which was proposed previously by Natário et al. [21] where a non-linear regression procedure was used. For different load cases, different coefficients and exponents are employed to build up suitable DSM design equations.

k_4 is a mechanism strengthening effect coefficient. It has been chosen as k_4=1.8 in this study. The mechanism strengthening effect, which is observed experimentally, is probably caused by the moving hinge position in the flange under significant plastic deformation for stockier sections.

Eq.(1.4) is plotted in Fig.1.11 by a continuous curve. The cut-off $\left(P_n / P_y = 1 \right)$ is defined as the slenderness range for which the estimated web crippling load equals the yield load (P_y). From Eq.(1.3), the inelastic reserve capacity is plotted by a dash line in the same figure. The DSM design curve is the combination of the continuous curve when $\lambda > \lambda_o$ and the dash line when $\lambda \leq \lambda_o$ as shown in Fig.1.11. The DSM equations for different localised load cases are described in Chapter 7. The inelastic reserve capacity curve is similar to those for bending in the AISI S100:2012 Specification (Appendix 1, Sections 1.2.2.1.2.1.2 and 1.2.2.1.3.1.2).
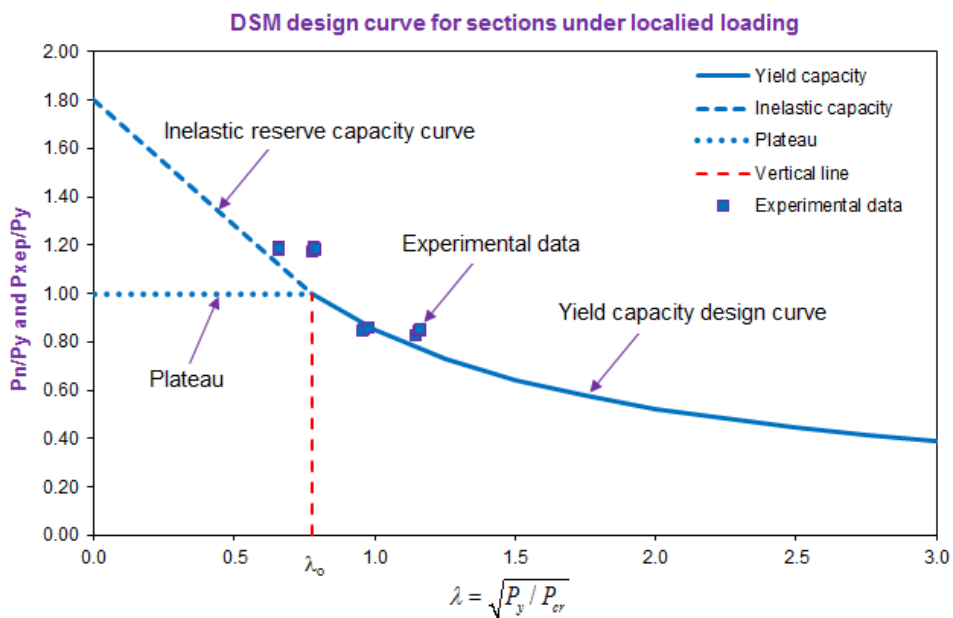
Figure 1.11: Proposal DSM design curve for web crippling

1.4.5. Finite Element Method

The Finite Element Method (FEM) which is the most powerful and versatile tool for solutions in structural analysis, is now well known and established. Many investigations have been performed to

develop the Finite Element Method for thin-walled structural members. In 1974, Cook [23] developed a solution procedure involving a combination of increment load or displacement control coupled with full or modified Newton-Raphson iterations and provided the basis for most nonlinear finite element computer programs.

Rajasekaran and Murray [24] studied the effects of local and member buckling and developed a formulation for elastic and inelastic buckling of thin-walled beams with local and member buckling interaction. A finite element model was developed from this formulation for elastic wide flange beams and the finite element stiffness matrices were derived from these equations for the wide flange I – sections. An investigation of the coupling for the section was carried out. The detail of a procedure for analysing inelastic beams and beam-column problems of arbitrary thin-walled open cross-section, under the assumption of no strain reversal were also presented by Rajasekaran and Murray [24]. The finite element formulation associated with such a procedure, and the expressions for programming the necessary computation of section properties and element matrices were given.

Hancock and Trahair [25] extended the finite element buckling analysis method to allow for any combinations of continuous restraints which are uniform along the element, and the analysis of mono-symmetric beam-columns with moment gradients. In other research, Hancock and Roos [26] used the finite element analysis based on an one dimensional mono-symmetric element to study the flexural-torsional buckling mode of columns forming the upright frames of industrial steel storage racks. The FEM was further extended by Clarke and Hancock [27] in a nonlinear analysis applied to study the strength and behaviour of stressed arch frames. The analysis simulated geometric nonlinear behaviour and plasticity in the stressed arch, particularly at the top chord.

The finite element program ABAQUS was used to establish the numerical modelling of ultimate strength of cold-formed steel members by Schafer [28]. The author reviewed the existing literature on the geometric imperfections, residual stress and stress-strain curve. The conservative bounds for imperfection magnitudes were established. The average flexural residual stresses were suggested to be used in modelling of residual stresses. Schafer and Peköz [29] provided detail of geometric imperfection and residual stresses in cold-formed members.

Recently, Natário et al. [30] performed an investigation on the use of quasi-static analyses with explicit integration to evaluate the web crippling behaviour of cold-formed steel beams. In this work, the Abaqus code was employed to implement Shell Finite Element (SFE) models aimed at replicating

an experimental test and quasi-static analyses with an explicit integration scheme were adopted. In addition, the SFE models were developed in Abaqus code to study the flange crushing failure of a plain channel beam subjected to Internal Two Flange (ITF) loading conditions as described in [31].

In this research the FEM is used to model structural members under localised loading using Abaqus [32]. The elastic buckling results are compared with the results from the THIN-WALL-2 V2.0 program to validate the accuracy of the FSM theory as given in Chapters 3 and 4. In addition, the FEM is used to simulate structural members from experiments to validate the test results and extend the data range based on the reliable data.

The use of the FEM in the research methodology is shown in Fig.1.12.
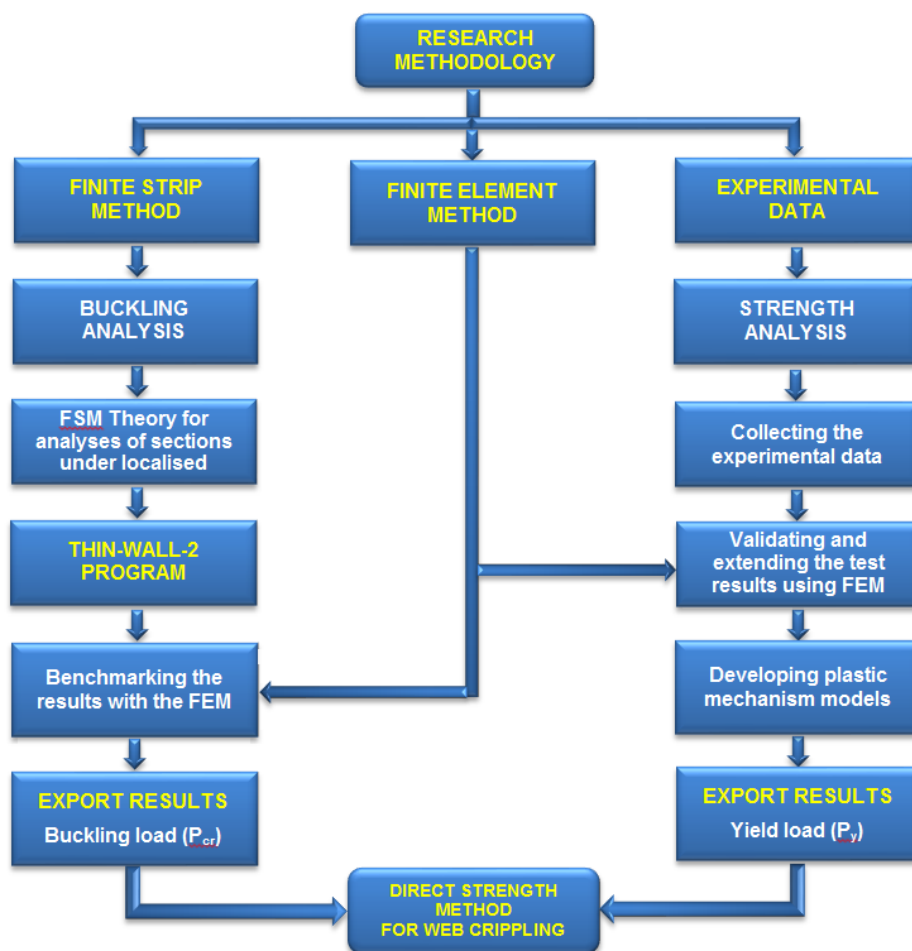
Figure 1.12: Use of FEM in research methodology

CHAPTER 2

LITERATURE REVIEW

2.1. INTRODUCTION

This Chapter introduces the literature for rules in the current Specifications (Standards) for the design of cold-formed steel members subjected to web crippling in Section 2.2. In addition, the existing experimental data of cold-formed steel members under localised loading is summarized in Section 2.3. Section 2.4 gives the elastic buckling solutions for plates and complete sections. The yielding analysis of cold-formed steel sections under localised loading is reviewed in Section 2.5 including plastic mechanism models. The Chapter also gives the background of the Direct Strength Method (DSM) development for the design of cold-formed steel sections subjected to localised loading in Section 2.6.

2.2. DESIGN CODE PREDICTIONS FOR WEB CRIPPLING

2.2.1. Eurocode 3: Part 1.3 (ENV 1993-1-3:1996)

The Eurocode-3 [5] provides a set of equations to avoid crushing, crippling or buckling of webs subjected to support reactions or other local transverse loads applied through the flanges. For a cross-section with a single unstiffened web, the local transverse resistance of the web is determined as given in EN 1993-1-3:2006 6.1.7.2 [5]. These equations are empirically based on a range of experiments over many years.

2.2.1.1. For a single local load or support reaction

1. When $c \leq 1.5h_w$ clear from a free end as shown in Fig.2.1 (this corresponds to the EOF load case)
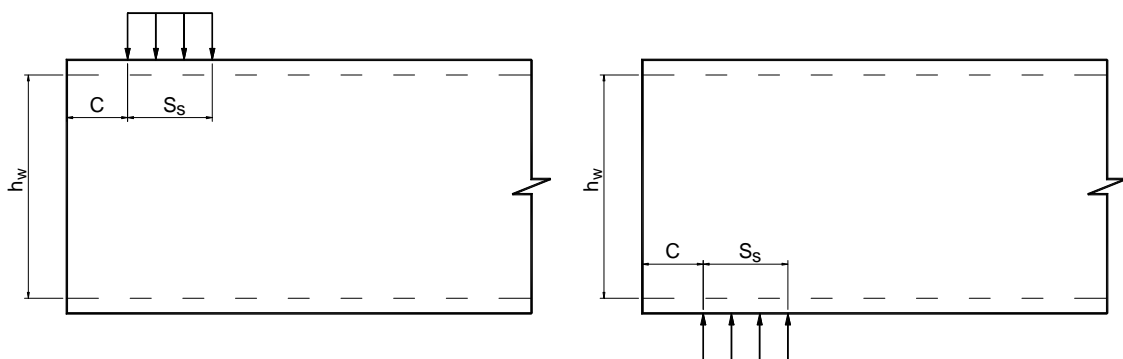
Figure 2.1: Single local load or support reaction with $c \leq 1.5h_w$ [5]

For a cross-section with stiffened flanges:

$$R_{w,Rd} = \frac{k_1 k_2 k_3 \left[9.04 - \frac{h_w/t}{60} \right]\left[1 + 0.01\frac{S_s}{t} \right] t^2 f_{yb}}{\gamma_{M1}}$$ (2.1)

For a cross-section with unstiffened flanges:

If $S_s/t \le 60$

$$R_{w,Rd} = \frac{k_1 k_2 k_3 \left[5.92 - \frac{h_w/t}{132} \right]\left[1 + 0.01\frac{S_s}{t} \right] t^2 f_{yb}}{\gamma_{M1}}$$ (2.2)

If $S_s/t > 60$

$$R_{w,Rd} = \frac{k_1 k_2 k_3 \left[5.92 - \frac{h_w/t}{132} \right]\left[0.71 + 0.015\frac{S_s}{t} \right] t^2 f_{yb}}{\gamma_{M1}}$$ (2.3)

2. When $c > 1.5 h_w$ clear from a free end as shown in Fig.2.2 (this corresponds to the IOF load case)
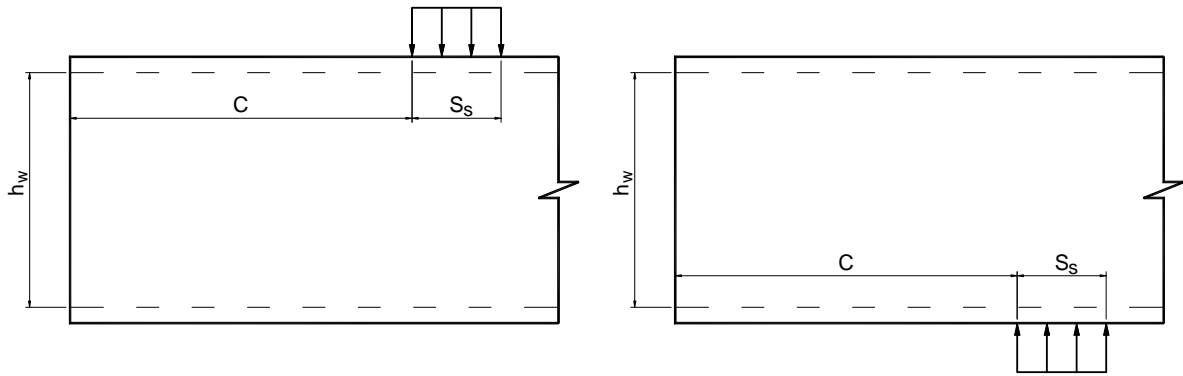
Figure 2.2: Single local load or support reaction with $c > 1.5 h_w$ [5]

If $S_s/t \le 60$

$$R_{w,Rd} = \frac{k_3 k_4 k_5 \left[14.7 - \frac{h_w/t}{49.5} \right]\left[1 + 0.007\frac{S_s}{t} \right] t^2 f_{yb}}{\gamma_{M1}}$$ (2.4)

If $S_s/t > 60$

$$R_{w,Rd} = \frac{k_3 k_4 k_5 \left[14.7 - \frac{h_w/t}{49.5} \right]\left[0.75 + 0.011\frac{S_s}{t} \right] t^2 f_{yb}}{\gamma_{M1}}$$ (2.5)

2.2.1.2. For two opposing local transverse forces closer together than 1,5hw

1. When $c \le 1.5 h_w$ clear from a free end as shown in Fig.2.3 (this corresponds to the ETF load case)
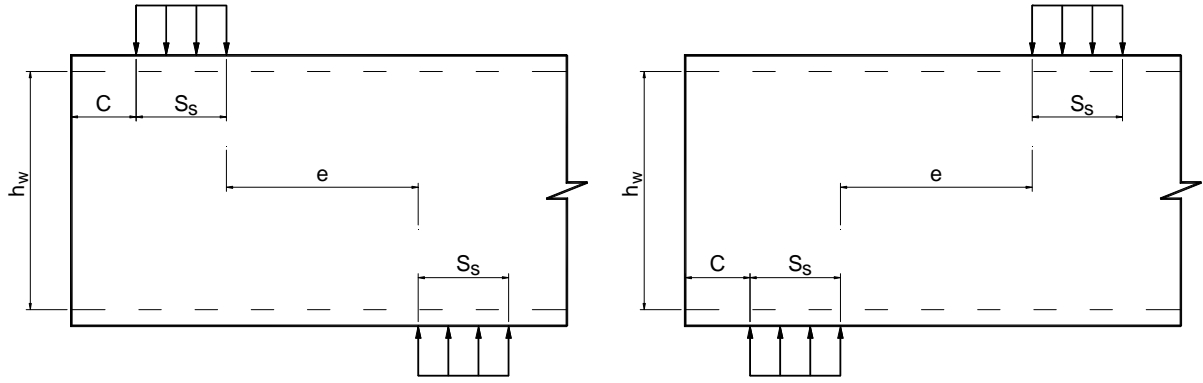
Figure 2.3: Two opposing local transverse forces with $c \leq 1.5 h_w$ [5]

$$R_{w,Rd} = \frac{k_1 k_2 k_3 \left[6.66 - \frac{h_w / t}{64} \right] \left[1 + 0.01 \frac{S_s}{t} \right] t^2 f_{yb}}{\gamma_{M1}} \quad (2.6)$$

2. When $c > 1.5 h_w$ clear from a free end as shown in Fig.2.4 (this corresponds to the ITF load case)
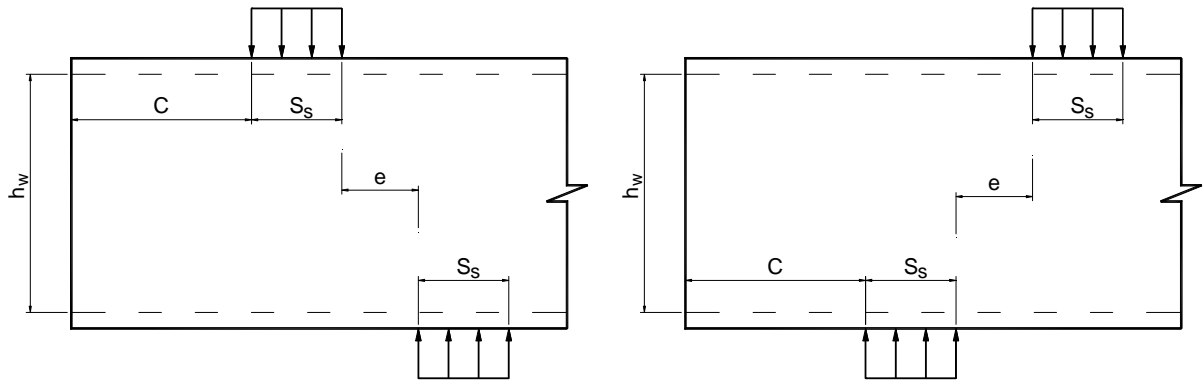
Figure 2.4: Two opposing local transverse forces with $c > 1.5 h_w$ [5]

$$R_{w,Rd} = \frac{k_3 k_4 k_5 \left[21.0 - \frac{h_w / t}{16.3} \right] \left[1 + 0.0013 \frac{S_s}{t} \right] t^2 f_{yb}}{\gamma_{M1}} \quad (2.7)$$

where:

c is the distance from loading to the closest end of the beam

S_s is the nominal length of stiff bearing

f_{yb} is the design strength (MPa)

r is internal radius of the corner

h_w is the web height between the midline of the flanges

t is the web thickness

ϕ is the angle of the web relative to the flange

$$k_1 = \left(1.33 - 0.33k\right) \qquad\qquad k_2 = \left(1.15 - 0.15\frac{r}{t}\right) \text{ and } 0.5 \le k_2 \le 1.0$$

$$k_3 = 0.7 + 0.3\left(\frac{\phi}{90}\right)^2 \qquad\qquad k_4 = \left(1.22 - 0.22k\right)$$

$$k_5 = \left(1.06 - 0.06\frac{r}{t}\right) \le 1.0 \qquad\qquad k = \frac{f_{yb}}{228}$$

The above equations are applied within the following limits:

$$\frac{h_w}{t} \le 200 \ ; \ \frac{r}{t} < 6 \ ; \ 45^o \le \phi \le 90^o$$

2.2.1.3. For section with the web rotation prevented (fastened flanges)

If the web rotation is prevented either by suitable restraint or because of the section geometry

(e.g. I-beams) then the local transverse resistance of a web $R_{w,Rd}$ may be determined as follows:

a. For a single load or support reaction

1). $c < 1.5h_w$ (near of at free end): for a cross-section of stiffened or unstiffened flanges:

$$R_{w,Rd} = \frac{k_7\left[8.8 + 1.1\sqrt{\dfrac{S_s}{t}}\right]t^2 f_{yb}}{\gamma_{M1}} \tag{2.8}$$

2). $c > 1.5h_w$ (far from free end): for a cross-section of stiffened or unstiffened flanges:

$$R_{w,Rd} = \frac{k_5^* k_6\left[13.2 + 2.87\sqrt{\dfrac{S_s}{t}}\right]t^2 f_{yb}}{\gamma_{M1}} \tag{2.9}$$

b. For opposite loads or reactions

1). $c < 1.5h_w$ (near of at free end): for a cross-section of stiffened or unstiffened flanges:

$$R_{w,Rd} = \frac{k_{10} k_{11}\left[8.8 + 1.1\sqrt{\dfrac{S_s}{t}}\right]t^2 f_{yb}}{\gamma_{M1}} \tag{2.10}$$

2). $c > 1.5h_w$ (loads or reactions far from free end): for a cross-section of stiffened or unstiffened

flanges:

$$R_{w,Rd} = \frac{k_8 k_9\left[13.2 + 2.87\sqrt{\dfrac{S_s}{t}}\right]t^2 f_{yb}}{\gamma_{M1}} \tag{2.11}$$

where the values of coefficients k^*_5 to k_{11} should be determined as follows:

$$k^*_5 = 1.49 - 0.53k \geq 0.6 \qquad\qquad k_6 = 0.88 - \frac{0.12t}{1.9}$$

$$k_7 = 1 + \frac{S_s/t}{750} \quad \text{if} \quad S_s/t < 150; \qquad k_7 = 1.20 \quad \text{if} \quad S_s/t > 150$$

$$k_8 = \frac{1}{k} \quad \text{if} \quad S_s/t < 66.5; \qquad k_8 = \frac{\left(1.10 - \dfrac{S_s/t}{665}\right)}{k} \quad \text{if} \quad S_s/t > 66.5$$

$$k_9 = 0.82 + \frac{0.15t}{1.9} \qquad\qquad k_{10} = \frac{\left(0.98 - \dfrac{S_s/t}{865}\right)}{k}$$

$$k_{11} = 0.64 + \frac{0.31t}{1.9}$$

2.2.2. Australian and New Zealand Standard (AS/NZS 4600)

The AS/NZS 4600 [3] equations are based on the AISI S100:2012 [2] using a different notation. The commentary to the AISI Specifications [33] gives the full database used to calibrate the equations.

2.2.2.1. Bearing without holes (AS/NZS 4600 3.3.6.2)

The nominal capacity for concentrated load or reaction for one solid web connecting top and bottom flanges (R_b) shall be determined as follows:

$$R_b = Ct_w^2 f_y \sin\theta \left(1 - C_r\sqrt{\frac{r_i}{t_w}}\right)\left(1 + C_l\sqrt{\frac{l_b}{t_w}}\right)\left(1 - C_w\sqrt{\frac{d_1}{t_w}}\right) \qquad (2.12)$$

where

C is a coefficient

f_y is the yield strength of steel

t_w is the web thickness

θ is the angle between the plane of the web and the plane of the bearing surface. θ shall be within the following limits: $45^o \leq \theta \leq 90^o$

C_r is the coefficient of inside bent radius

r_i is the inside bent radius

C_l is the coefficient of bearing length

l_b is the actual bearing length. For the case of two equal and opposite concentrated loads distributed over unequal bearing length, the smaller value of l_b shall be taken

C_w is the coefficient of web slenderness

d_1 is the depth of the flat portion of the web measured along the plane of the web

The coefficients and capacity reduction factors are given in Tables 2.1 to 2.5.

Webs of members in bending for which $d_1/t_w > 200$ shall be provided with adequate means of transmitting concentrated actions or reactions directly into the web(s). R_b is the nominal capacity for load or reaction for one solid web connecting top and bottom flanges. For webs consisting of two or more such sheets, R_b shall be calculated for each individual sheet and the results added to obtain the nominal load or reaction for the full section.

One-flange loading or reaction occurs when the clear distance between the bearing edges of adjacent opposite concentrated actions or reactions is greater than $1.5d_1$. Two-flange loading or reaction occurs when the clear distance between the bearing edges of adjacent opposite concentrated actions or reactions is less than or equal to $1.5d_1$. End loading or reaction occurs when the distance from the edge of the bearing to the end of the member is less than or equal to $1.5d_1$. Interior loading or reaction occurs when the distance from the edge of the bearing to the end of the member is greater than or equal to $1.5d_1$.

Table 2.1: Back-to-back channel sections [3]

Support and flange conditions		Load cases	C	C_r	C_l	C_w	ϕ_w	Limits
Fastened to support	Stiffened or partially stiffened flanges	EOF	10	0.14	0.28	0.001	0.75	$r_i/t_w \le 5$
		IOF	20	0.15	0.05	0.003	0.90	$r_i/t_w \le 5$
Unfastened to support	Stiffened or partially stiffened flanges	EOF	10	0.14	0.28	0.001	0.75	$r_i/t_w \le 5$
		IOF	20.5	0.17	0.11	0.001	0.85	$r_i/t_w \le 3$
		ETF	15.5	0.09	0.08	0.04	0.75	$r_i/t_w \le 3$
		ITF	36	0.14	0.08	0.04	0.75	
	Unstiffened flanges	EOF	10	0.14	0.28	0.001	0.75	$r_i/t_w \le 5$
		IOF	20.5	0.17	0.11	0.001	0.85	$r_i/t_w \le 3$

Table 2.1 applies to I-beam made from two channels connected back-to-back

The coefficients in Table 2.1 apply if $l_b/t_w \le 210$; $l_b/d_1 \le 1$ and $\theta = 90^o$

Table 2.2: Single web channel-sections and C-sections [3]

Support and flange conditions		Load cases	C	C_r	C_l	C_w	ϕ_w	Limits
Fastened to support	Stiffened or partially stiffened flanges	EOF	4	0.14	0.35	0.02	0.85	$r_i/t_w \leq 9$
		IOF	13	0.23	0.14	0.01	0.90	$r_i/t_w \leq 5$
		ETF	7.5	0.08	0.12	0.048	0.85	$r_i/t_w \leq 12$
		ITF	20	0.10	0.08	0.031	0.85	$r_i/t_w \leq 12$
Unfastened to support	Stiffened or partially stiffened flanges	EOF	4	0.14	0.35	0.02	0.80	$r_i/t_w \leq 5$
		IOF	13	0.23	0.14	0.01	0.90	
		ETF	13	0.32	0.05	0.04	0.90	$r_i/t_w \leq 3$
		ITF	24	0.52	0.15	0.001	0.80	
	Unstiffened flanges	EOF	4	0.40	0.60	0.03	0.85	$r_i/t_w \leq 2$
		IOF	13	0.32	0.10	0.01	0.85	$r_i/t_w \leq 1$
		ETF	2	0.11	0.37	0.01	0.75	$r_i/t_w \leq 1$
		ITF	13	0.47	0.25	0.04	0.80	

The coefficients in Table 2.2 apply if $l_b/t_w \leq 210$; $l_b/d_1 \leq 2$ and $\theta = 90^o$

Table 2.3: Single web Z-sections [3]

Support and flange conditions		Load cases	C	C_r	C_l	C_w	ϕ_w	Limits
Fastened to support	Stiffened or partially stiffened flanges	EOF	4	0.14	0.35	0.02	0.85	$r_i/t_w \leq 9$
		IOF	13	0.23	0.14	0.01	0.90	$r_i/t_w \leq 5$
		ETF	9	0.05	0.16	0.052	0.85	$r_i/t_w \leq 12$
		ITF	24	0.07	0.07	0.04	0.80	$r_i/t_w \leq 12$
Unfastened to support	Stiffened or partially stiffened flanges	EOF	5	0.09	0.02	0.001	0.85	$r_i/t_w \leq 5$
		IOF	13	0.23	0.14	0.01	0.90	
		ETF	13	0.32	0.05	0.04	0.90	$r_i/t_w \leq 3$
		ITF	24	0.52	0.15	0.001	0.80	
	Unstiffened flanges	EOF	4	0.40	0.60	0.03	0.85	$r_i/t_w \leq 2$
		IOF	13	0.32	0.10	0.01	0.85	$r_i/t_w \leq 1$
		ETF	2	0.11	0.37	0.01	0.75	$r_i/t_w \leq 1$
		ITF	13	0.47	0.25	0.04	0.80	

The coefficients in Table 2.3 apply if $d_1/t_w \leq 200$; $l_b/t_w \leq 210$; $l_b/d_1 \leq 2$ and $\theta = 90^o$

Table 2.4: Single web H-sections [3]

Support and flange conditions	Load cases	C	C_r	C_l	C_w	ϕ_w	Limits
Fastened to support	EOF	4	0.25	0.68	0.04	0.75	$r_i/t_w \leq 5$
	IOF	17	0.13	0.13	0.04	0.80	$r_i/t_w \leq 10$
	ETF	9	0.10	0.07	0.03	0.85	$r_i/t_w \leq 10$
	ITF	10	0.14	0.22	0.02	0.85	
Unfastened to support	EOF	4	0.25	0.68	0.04	0.75	$r_i/t_w \leq 4$
	IOF	17	0.13	0.13	0.04	0.90	

The coefficients in Table 2.4 apply if $d_1/t_w \leq 200$; $l_b/t_w \leq 200$; $l_b/d_1 \leq 2$ and $\theta = 90^o$

Table 2.5: Multi-web deck sections [3]

Support and flange conditions	Load cases	C	C_r	C_l	C_w	ϕ_w	Limits
Fastened to support	EOF	4	0.04	0.25	0.025	0.90	$r_i/t_w \leq 20$
	IOF	8	0.10	0.17	0.004	0.85	$r_i/t_w \leq 10$
	ETF	9	0.12	0.14	0.040	0.85	$r_i/t_w \leq 10$
	ITF	10	0.11	0.21	0.020	0.85	
Unfastened to support	EOF	3	0.04	0.29	0.028	0.60	$r_i/t_w \leq 20$
	IOF	8	0.10	0.17	0.004	0.85	
	ETF	6	0.16	0.15	0.050	0.90	$r_i/t_w \leq 5$
	ITF	17	0.10	0.10	0.046	0.90	

The coefficients in Table 2.5 apply if $d_1/t_w \leq 200$; $l_b/t_w \leq 210$; $l_b/d_1 \leq 3$ and $45^o \leq \theta \leq 90^o$

2.2.2.2. Bearing with holes (AS/NZS 4600 3.3.6.3)

When a web hole is within the bearing length (l_b), a bearing stiffener shall be used. For beam webs with holes, the web crippling strength shall be calculated in accordance with Clause 3.3.6.2 multiplied by the reduction factor (R_c), given in this Clause.

Web crippling strength of channel-section webs with holes, as determined by Clause 3.3.6.2, shall be applicable within the following limits:

(a) $d_{wh}/d_1 < 0.7$

(b) $d_1/t \leq 200$

(c) Holes centred at mid-depth of the web

(d) Clear distance between holes is greater than or equal to 450mm

(e) Distance between the end of the member and the edge of the hole is greater than or equal to d

(f) Non-circular holes corner radii greater than or equal to 2t

(g) Non-circular holes with $d_{wh}/t \leq 65$ mm and $b \leq 115$ mm

(h) Circular holes diameters less than or equal to 150 mm.

(i) $d_{wh}/t > 15$ mm

When a web hole is not within the bearing length ($l_b \geq 25$ mm)

$$R_c = 1.01 - \frac{0.325d_{wh}}{d_1} + \frac{0.083x}{d_1} \leq 1.0 \tag{2.13}$$

When any portion of a web hole is not within the bearing length ($l_b \geq 75$mm)

$$R_c = 0.90 - \frac{0.047d_{wh}}{d_1} + \frac{0.053x}{d_1} \leq 1.0 \tag{2.14}$$

where:

l_b is the bearing length

d is the depth of cross-section

x is the nearest distance between the web hole and the edge bearing

Although this thesis does not include web crippling with holes, this brief summary for the Australian/New Zealand Standard AS/NZS 4600:2005 [3] shows approach used currently.

2.3. EXPERIMENTAL INVESTIGATIONS FOR WEB CRIPPLING

Experimental investigations have been performed by many researchers to study the behaviour of cold-formed steel sections subjected to web crippling. Different cross-sections have been tested such as unlipped plain-C, lipped plain-C, SupaCee, Dimond Hi-Span (DHS), lipped plain-Z and built-up-I sections. In addition, four localised load cases (IOF, EOF, ITF, ETF) and both flange unfastened and fastened conditions have been considered in the experiments. Table.2.6 summarises the experimental investigations for web crippling. This selected data for comparison in this thesis is the regarding to the test data since 1995. Generally, these tests have been performed following the Standard Test Method for determining the web crippling strength of cold-formed steel beams S909-08 [34] and include high strength steels. The data on Z-sections and back to back channels has been excluded. The detailed experimental data used for the development of the DSM for design of cold-formed steel sections based on Table 2.6 is given in Chapter 6.

Table 2.6: Web crippling experiments

Authors	Years	Sections	Load case	Number of tests	Flange fastened conditions	Places
Cain and LaBoube [35]	1995	Lipped plain-Z	EOF	28	Unfastened	The Missouri University of Science and Technology, USA
		Built-up-I-section	IOF	14		
Beshara and Schuster [36]	2000	Lipped plain-C	ITF	18	Fastened	The University of Waterloo, Canada
			ETF	18		
		Lipped plain-Z	ITF	18		
			ETF	18		
Young and Hancock [22]	2001	Unlipped plain-C	IOF	24	Unfastened	The University of Sydney, Australia
			EOF	24		
			ITF	14		
			ETF	12		
Macdonald et al. [37]	2008	Lipped plain-C	EOF	18	Fastened	Glasgow Caledonian University, Glasgow, UK
			ETF	18		
Uzzaman et al. [38]	2012	Lipped plain-C	ITF	10	Unfastened & Fastened	Queen's University, Belfast, UK
			ETF	14		
Uzzaman et al. [39]	2012		ETF	23		
Morelli et al. [40]	2014	Lipped plain-C	IOF	16	Unfastened & Fastened	The University of Sydney, Australia
		DHS		16		
Khatale et al. [41]	2014	Lipped plain-C	ITF	8	Unfastened & Fastened	The University of Sydney, Australia
			ETF	8		
		DHS	ITF	8		
			ETF	8		
Sundararajah et al. [19]	2015	Lipped plain-C	ITF	18	Unfastened	Queensland University of Technology, Australia
			ETF	18		
	2016	SupaCee	ITF	15	Unfastened	

			ETF	21		
Efendy et al. [7]	2015	Lipped plain-C	IOF	16	Unfastened & Fastened	The University of Sydney, Australia
		SupaCee		16		
Hadchiti et al. [8]	2015	Lipped plain-C	EOF	16	Unfastened & Fastened	The University of Sydney, Australia
		SupaCee		16		
Bartlett et al. [9]	2016	Lipped plain-C	ITF	16	Unfastened & Fastened	The University of Sydney, Australia
		SupaCee		16		
Htet and Pham [10]	2016	Lipped plain-C	ETF	16	Unfastened & Fastened	The University of Sydney, Australia
		SupaCee		16		
Lian et al. [42]	2016	Lipped plain-C	EOF	22	Unfastened & Fastened	Queen's University, Belfast, UK

2.4. ELASTIC BUCKLING FOR WEB CRIPPLING

2.4.1. Elastic buckling analysis for rectangular plates

A plate element subjected to compression, bending and shear or a combination of these stresses in its plane may buckle or distort locally at a low stress level (namely local buckling stress). Local buckling involves flexural displacements of the plate elements, with the line junctions between plate elements remaining straight. The elastic critical stress for local buckling has been extensively investigated and summarized by numerous researchers. Saint-Venant [43] derived the differential equation describing buckling of an elastic plate which is loaded in plane:

$$\frac{\partial^4 w}{\partial x^4} + 2\frac{\partial^4 w}{\partial x^2 \partial y^2} + \frac{\partial^4 w}{\partial y^4} + \frac{\sigma t}{D}\frac{\partial^2 w}{\partial x^2} = 0 \tag{2.15}$$

$$D = \frac{Et^3}{12(1-v^2)} \tag{2.16}$$

where:

E is the modulus of elasticity of cold-formed steel

w is the plate deflection perpendicular to surface

σ is the applied compressive stress in transverse direction

t is the plate thickness

v is Poisson's ratio

D is the plate flexural rigidity

The critical buckling stress of a plate as shown in Fig.2.5 was solved by Bryan [44] using differential equation based on the small defection theory as given in Eq.(2.15). Consequently, the critical local buckling stress for a rectangular plate subjected to compression stress in one direction can be calculated by Eq.(2.17).
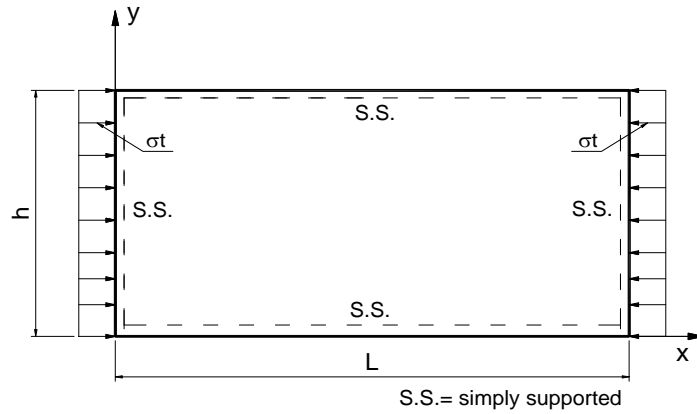
Figure 2.5: Rectangular plate subjected to compression stress [45]

$$\sigma_{cr} = \frac{k\pi^2 E}{12\left(1-v^2\right)}\left(\frac{t}{h}\right)^2 \tag{2.17}$$

where:

σ_{cr} is the elastic critical stress

t and h are the plate thickness and width respectively

k is the plate buckling coefficient which depends on support conditions. The values of k is shown in Fig.2.6 for different L/h ratios.

$$k = \left[m\left(\frac{h}{L}\right) + \frac{1}{m}\left(\frac{L}{h}\right)\right]^2 \tag{2.18}$$

m is the number of the half sine-waves in the x direction
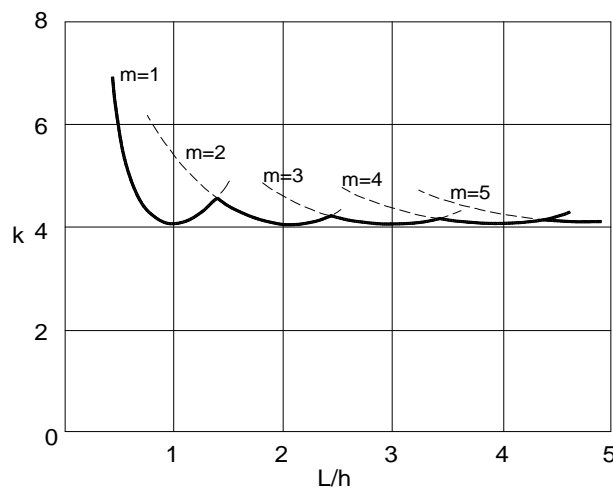
Figure 2.6: Buckling coefficient for flat rectangular plates [45]

For a plate subjected to a concentrated force as shown in Fig.2.9(c), the stress distribution throughout the plate varies considerably and this causes mathematical difficulties which have to be resolved. Despite this, the first solution for the problem was published by Timoshenko and Gere [46]. Since then, several solutions have been published to solve the above problem. Girkmann [47] investigated the buckling analysis of a rectangular plate with simply supported edges subjected to a single edge force. However, the results were only applied to plates with L/h<1.1 and the solution was only given in the form of a determinant which had to be evaluated for any particular case.

Khan and Walker [48] studied the buckling of two plates subjected to distributed edge loads. The first case is a rectangular plate loaded along parts of two opposite sides as shown in Fig.2.7(a), the length of the loading can vary between being a point load and being uniformly distributed along the edges (*n=L*). The second one is a plate subjected to locally distributed edge load which is balanced by the shear stresses along the vertical edges as shown in Fig. 2.7(b). For both these loading cases, the buckling loads are calculated for plates having zero torsional restraint along the edges, this theory corresponds to theoretical simply supported boundary conditions. The buckling load of the plate subjected to these load cases is calculated by Eq.(2.19). The values of the buckling coefficients (*k*) for the opposite locally distributed edge loads (case 1) are shown in Fig.2.8(a) and for the locally distributed edge load (case 2) are shown in Fig.2.8(b) with two different ratios of *n/h*.

(a) Opposite locally distributed edge loads   (b) Locally distributed edge load
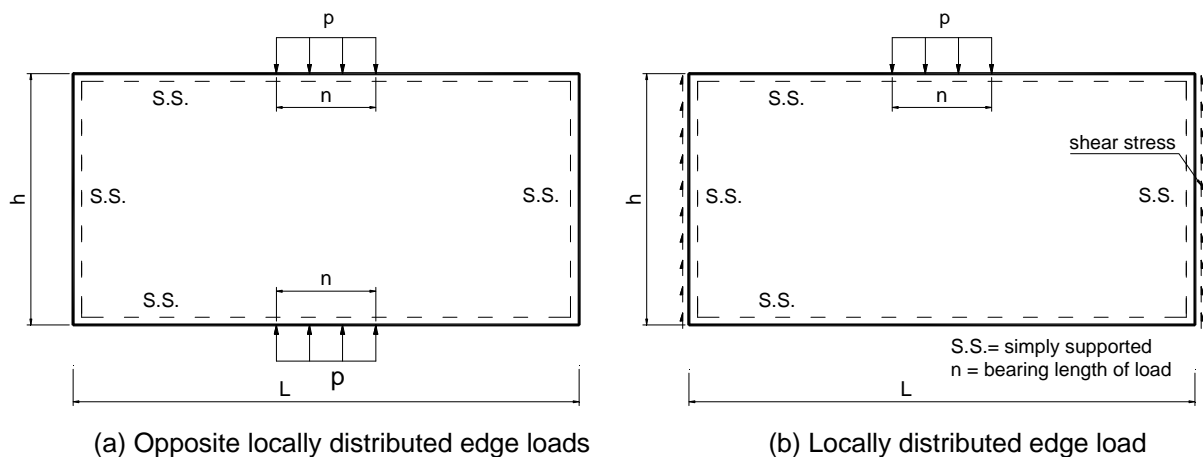
Figure 2.7: Plate geometry and typical load conditions [48]

$$P_{cr} = \frac{k\pi^2 D}{h}$$

(2.19)

where

    n is the bearing length

    P_{cr} is the buckling load, $P_{cr} = \sigma_{cr} tn$

From Eq.(2.19), the buckling stress of plate can be calculated as given:

$$\sigma_{cr} = \frac{k\pi^2 E}{12\left(1-v^2\right)\left(\dfrac{h}{t}\right)^2\left(\dfrac{n}{h}\right)}$$

(2.20)

(a) Opposite locally distributed edge loads   (b) Locally distributed edge load
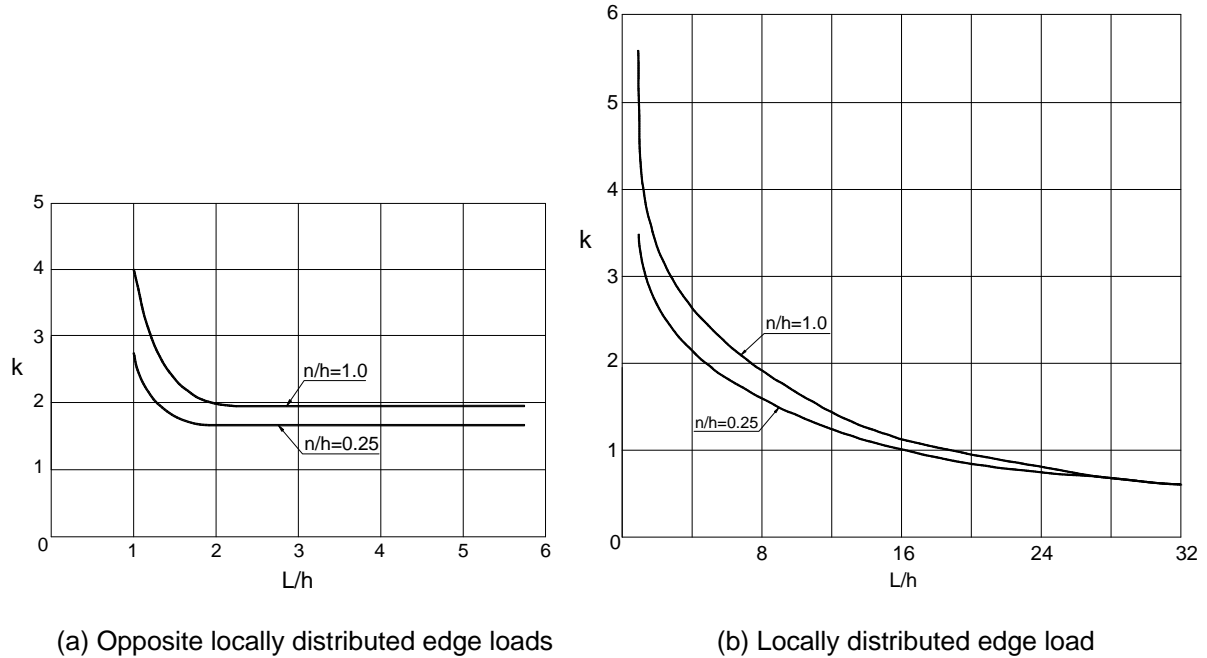
Figure 2.8: Variation of buckling coefficient with length/depth ratios [48]

Zetlin [49] studied an elastic stability analysis of a plate supported at both ends and subjected to locally distributed edge load. Zetlin assumed that the plate was simply supported with lateral movement prevented along all four edges and without restraint in the plane of the plate. The applied load was supported at the ends of the plate by distributed shear stresses along the transverse edges as shown in Fig.2.7(b). The buckling coefficients (*k*) are given in Table.2.7.

Rockey and Bagchi [50] investigated the buckling of plate girder webs subjected to locally distributed edge load with simply supported edges. The system studied was similar to Fig. 2.7(b). The flexural and torsional properties of the flanges were included in the analysis using the FEM to solve the buckling coefficients (*k*) of the plates. The values of *k* are given in Table.2.7.

In other research, Khan et al. [51] studied the buckling analysis of a plate subjected to locally edge load as shown in Fig.2.7(b). The solution was developed in a more computer friendly direction. The buckling coefficients (*k*) are given in Table.2.7. It is found that there is agreement between these results with those presented by Rockey and Bagchi [50] for *L/h*<3.0.

Chin et al. [52] studied the behaviour of a plate which was the same as described in Rockey and Bagchi [50] and Khan et al. [51] to check the quality of a newly developed finite element. The initial

aim of this research was not mainly focusing on the buckling of a simply supported plate subjected to partial edge load; however, the results were matched with those obtained by Rockey and Bagchi [50] and Khan et al. [51] as shown in Table.2.7.

Table 2.7: Buckling coefficients (*k*) for simply supported plates (Fig.2.7(b)) [53]

L/h ratios	*n/h* ratios	Zetlin [49]	Rockey and Bagchi [50]	Khan et al. [51]	Chin et al. [52]
1.0	0		3.25		3.20
	1/65	3.32			
	0.05	3.36	3.27		
	0.1		3.34		
	0.2		3.45		3.35
	0.25			3.42	
	0.3		3.60		
	0.4		3.70		3.70
	0.5		3.95	3.9	
	0.6		4.15		4.20
	0.75		4.50	4.65	
	0.8		4.80		4.80
	0.9		5.10		
	1.0	6.20	5.55	5.57	5.60
2.0	0		2.40		
	0.1		2.45		
	0.2		2.50		
	0.25			2.41	
	0.4		2.6		
	0.5			2.59	
	0.6		2.80		
	0.75			2.84	
	0.8		2.90		
	1.0		3.20	3.15	
	0.25			2.32	

	0.50			2.43	
3.0	0.75			2.66	
	1.0			2.95	
	4/65	2.15			
	0.20	2.12			
4.0	0.25			2.21	
	0.50			2.34	
	0.75			2.54	
	1.0			2.80	

Johansson and Lagerqvist [53] used a set of 46 *k* values, as given in Table.2.7, which were obtained from Zetlin [49], Rockey and Bagchi [50], Khan et al. [51] and Chin et al. [52] to find a reasonable simple equation for *k* values as follow:

$$k = 2.1 + 1.2\left(\frac{h}{L}\right)^2 + \left(\frac{n}{h}\right)^2\left[0.4 + 2.0\left(\frac{h}{L}\right)^2\right] \qquad (2.21)$$

with $n/h \leq 1.0$

Natário et al. [54] reviewed the analytical studies as well as fundamental background of localised buckling analysis of thin web plates. Webs of steel members can be idealised as rectangular thin plates simply supported along the edges, subjected to locally distributed in-plane edge compressive forces. The critical elastic buckling load can be computed by relatively simple rational analytical formulae. Four cases of localised edge loads were considered in this review as shown in Fig.2.9. The buckling load (P_{cr}) of the thin plate can be written in a simple form as given in Eq.(2.22). The buckling coefficient *k* depends on the type of distribution of the edge loads. The values of *k* can be calculated by Eq.(2.21) and these values are shown in Fig.2.10 for all four load cases with different *n/h* ratios.

$$P_{cr} = k\frac{\pi^2 E t^3}{12\left(1-v^2\right)h} \qquad (2.22)$$
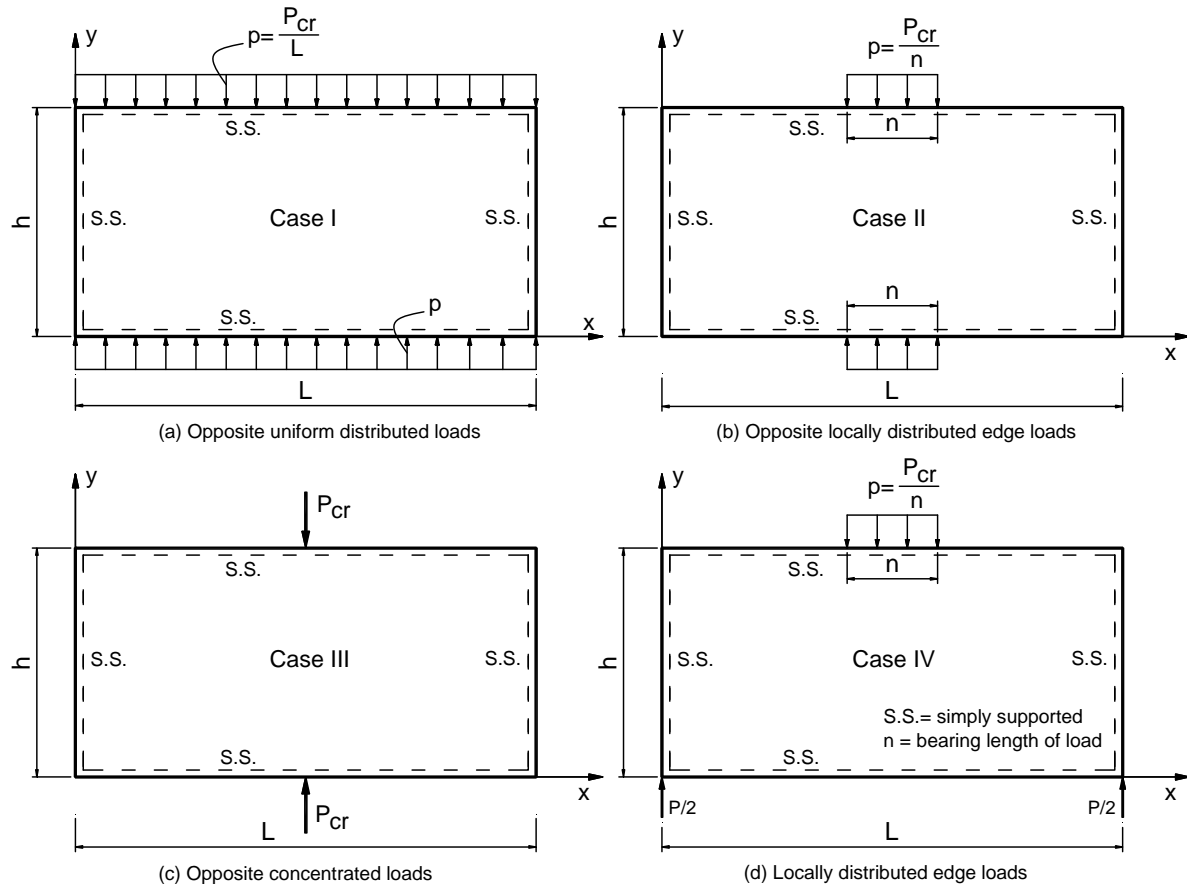
Figure 2.9: Localised load cases for plate buckling analysis [54]

(a) Cases I, II, III (Fig.2.9) (b) Case IV (Fig.2.9)
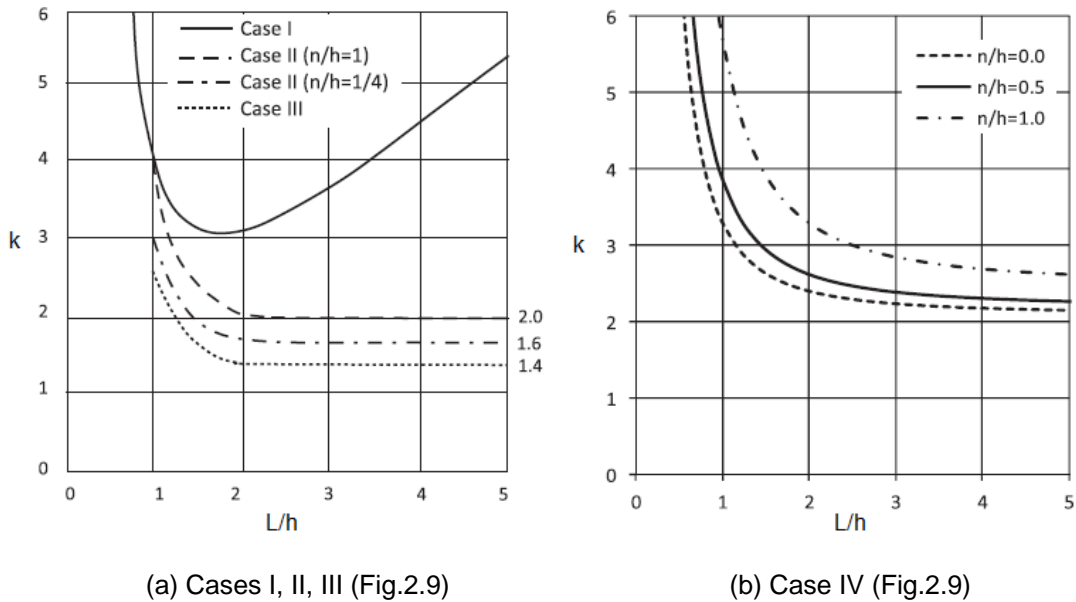
Figure 2.10: Variation of buckling coefficient *k* with length/depth ratio (*L/h*) [54]

Figs.2.9 and 2.10 indicate that Case I and Case III represent limiting situations of edge loading.

For a given load bearing length (*n*), while Case II and Case IV represent the most common situations.

The difference between the Case II and Case IV can be seen in two main reasons:

▪ Due to two opposite locally loads on both sides of the plate, Case II always has lower buckling coefficients (*k*) in comparison with Case IV, regardless of the plate length-to-high ratio *L/h*. It means that Case II is much more prone to buckling than Case IV (see Fig. 2.10 for *n/h*=1)

▪ For a given value of *L/h*, the influence of the lateral simply supported ends on the coefficient *k* is much more effective for Case IV than for Case II: the *k* values are almost unchanged for *L/h*>2.0 in case II and *L/h*>5.0 in Case IV.

The approaches for elastic buckling analysis of rectangular plates have been investigated for different localised load cases. However, the limitation is that only rectangular plates with simply supported end boundary condition has been covered. Thus, it will be less accurate when applying these equations to calculate the buckling load of completed sections with corners, flanges, fastened flanges condition and different end boundary conditions.

2.4.2. Elastic buckling analysis for structural members with complete sections

The theoretical analysis of web crippling for cold-formed steel flexural members is extremely complicated for beams having webs connected to flanges because it involves the following factors: non-uniform stress distribution under the applied load, elastic and inelastic stability of the web element, bending produced by eccentric load when it is applied on the bearing flange at a distance beyond the curved transition of the web, various edge restraints provided by beam flanges and the interaction between flange and web elements. Some advanced investigations have been approached to determine the buckling load of structural members under localised loading using the Generalised Beam Theory (GBT), the Finite Strip Method (FSM) and the Finite Element Method (FEM).

2.4.2.1. Elastic buckling analysis using General Beam Theory (GBT)

Natário et al. [54] developed computer software namely GBTWEB to analyse the elastic web buckling of thin-walled steel beams under concentrated loads. The program is based on the GBT formulation as described in [54] to calculate all first-order plane stress components (either uniform or non-uniform), which may then be included in the geometric stiffness matrix for the ensuing buckling analysis. Due to the nature of the web crippling phenomenon, which is potentially influenced by combinations of all stress components, GBTWEB is viewed as a good alternative method to handle this problem, combining a reasonably low pre-processing effort with an accurate structural analysis [21]. The GBTWEB software [55] is based on three main windows that follow the corresponding main steps of the buckling analysis in the GBT framework: (i) cross-section analysis, (ii) first-order and buckling

analysis and (iii) buckling solution. Fig.2.11 shows the graphical user interface for the cross-section and structural member data input and analysis.
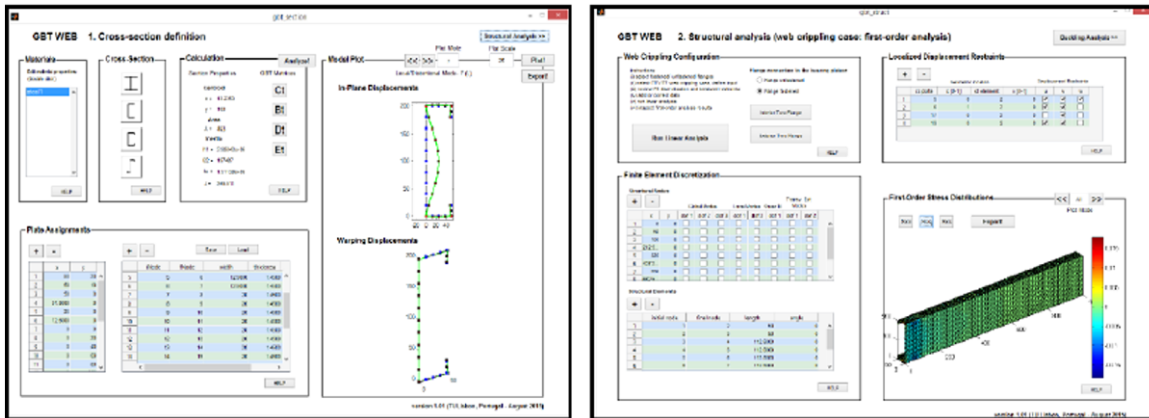
Figure 2.11: GBTWEB main window [55]

The software was used by the authors to determine the elastic buckling load of cold-formed steel sections to develop the DSM for web crippling of beams under the ETF load cases as described in [21]. In this research GBTWEB was seen as an effective option to calculate the buckling load of unlipped plain-C sections from Young and Hancock [22], lipped plain-C and build-up-I sections from Hetrakul and Yu [56], lipped plain-C and lipped plain-Z sections from Beshara and Schuster [36] and lipped plain-C sections from Macdonald et al. [37]. In order to validate the GBT results, Shell Finite Element (SFE) models were performed to carry out the non-linear analyses and corresponding elastic buckling analyses. In general, the GBT and SFE analyses have similar results, not only in terms of the web buckling modes configuration but also concerning the buckling load (P_{cr}).
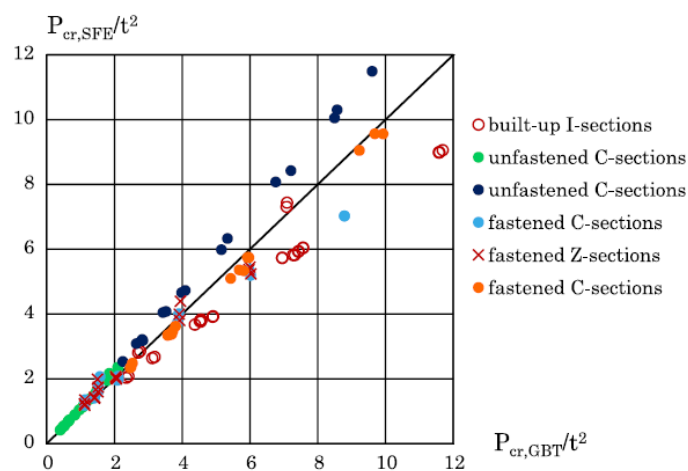
Figure 2.12: Comparison between the buckling loads obtained from SFE ($P_{cr,SFE}$) and GBT ($P_{cr,GBT}$) analyses – values divided by t^2 [21]

It can be seen that for some cross-sections the GBT solutions are too high such as unfastened C sections and too low in others such as built-up I sections as shown in Fig.2.12. This may be because of the lower accuracy of the GBT solutions in the buckling analysis for some cross-sections and fastened flange conditions.

2.4.2.2. Elastic buckling analysis using Finite Strip Method (FSM)

The FSM developed by Cheung [13] is an efficient method of analysis in comparison with the FEM. This method is used extensively in the DSM of design of cold-formed sections in the North American Specification for the Design of Cold-Formed Steel Structural Members AISI S100-2012 [2] and the Australian/New Zealand Standard AS/NZS 4600:2005 [3]. It is therefore essential to extend the FSM of buckling analysis to localised loading. The SAFSM was applied in Chu et al. [57] and Bui [58] to the buckling analysis of thin-walled sections under more general loading conditions, where multiple series terms were used to capture the modulation of the buckles. The limitation of these investigations is that the transverse compression and shear are not included. Thus, Hancock and Pham [59] applied the FSM to the buckling analysis of thin-walled sections subjected to shear forces.

More recently, Hancock and Pham [12] have extended the SAFSM to the analysis of thin-walled sections under localised loading with simply supported boundary condition using multiple series terms in the longitudinal direction. A pre-buckling analysis was performed to compute stresses prior to the buckling analysis using these stresses. Solution convergence with increasing numbers of series terms was provided. The theory was included in a computer program namely bfinst10.cpp [12] written in Visual C++ to assemble the stiffness equations and stability equations to solve for the pre-buckling displacements and pre-buckling stresses, the buckling load factors and buckling modes. In the numerical examples, the authors performed buckling analyses for a plate under localised load along one longitudinal edge at the centre of the plate, unlipped and lipped sections under the IOF and ITF load cases. Fig.2.13 shows the buckling modes from bfinst10.cpp of a rectangular plate and an unlipped channel section under localised loading. The comparison between the results from SAFSM using bfinst10.cpp and FEM using ABAQUS is shown in Tables.2.8 to.2.10
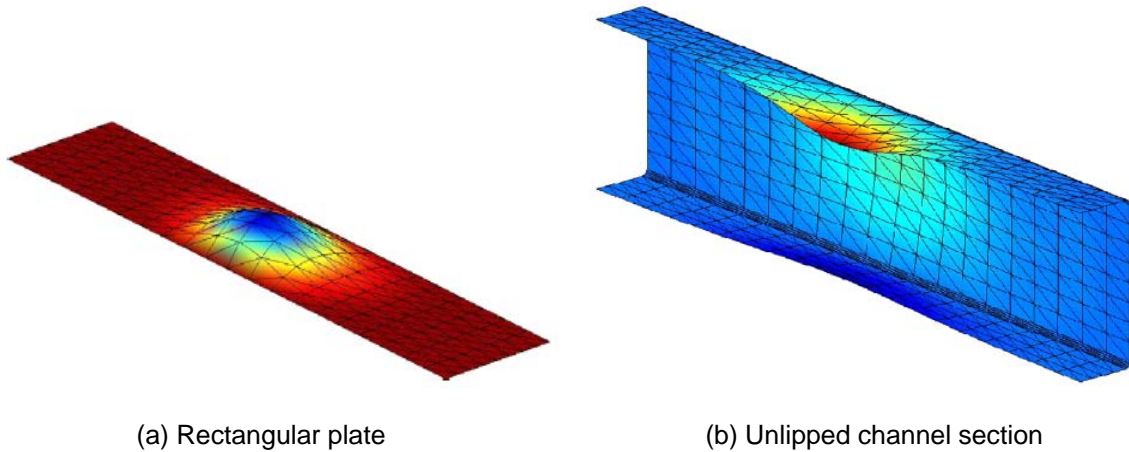
(a) Rectangular plate   (b) Unlipped channel section

Figure 2.13: Buckling modes from bfinst10.cpp [12]

Table 2.8: Buckling coefficients k for simply supported rectangular plates [12]

Load case	Load length ratio (n/L)	Aspect length ratio (L/h)	SAFSM (bfinst10.cpp)		FEM (ABAQUS)
			Series terms (μ)	Buckling coefficient (k)	
IOF load case	0.25	1	5	3.48	3.399
			11	3.478	
	0.05	2	5	2.421	2.368
			11	2.404	
			15	2.404	
	0.2	2	5	2.549	2.515
			11	2.545	
	0.05	5	11	2.066	1.991
			19	2.018	
	0.2	5	7	2.697	2.59
			11	2.597	
	0.025	10	25	1.433	1.392

It is concluded that the SAFSM for buckling analysis of thin-walled sections subjected to localised loading with simply supported ends has been developed and benchmarked against the FEM. However, in practice, cold-formed members are connected together by welds or bolts so that the end boundary conditions are expected to be different from simply supported. Thus, it is necessary to extend this method to the analysis of thin-walled sections under localised loading for general end boundary conditions.

Table 2.9: Unlipped channel section buckling load in kN [12]

Load case	Length (mm)	Load length (mm)	SAFSM (bfinst10.cpp)		FEM (ABAQUS)	
			Series terms (μ)	Buckling coefficient (k)	Web only SS	Whole section SS
IOF load case	933	90	11	464.3	455.36	455.4
			15	463.5		
ITF load case	838	90	11	304.2	299.78	302.28
			15	304.1		

SS: simply supported

Table 2.10: Buckling coefficients k for lipped channel section [12]

Load case	Length (mm)	Load length (mm)	SAFSM (bfinst10.cpp)		FEM (ABAQUS)	
			Series terms (μ)	Buckling coefficient (k)	Web only SS	Whole section SS
IOF load case	1000	200	7	6.024	5.410	5.009
			11	6.017		
			15	6.016		
		50	7	5.303	4.766	5.175
			11	5.234		
			15	5.221		
ITF load case	1000	200	7	3.051	2.731	3.056
			11	3.049		
			15	3.039		
		50	7	2.746	2.472	2.727
			11	2.737		
			15	2.735		

SS: simply supported

2.4.2.3. Elastic buckling analysis using Finite Element Method

The Finite Element Method (FEM) is a powerful and versatile solution for structural analysis. The method is applicable for any geometry, boundary conditions and material variation. The FEM was included in the ABAQUS software [32] which has been used effectively and widely. Dara and Yu [20] used ABAQUS to perform buckling analysis of lipped plain-C and lipped plain-Z sections under the IOF load case as shown in Fig.2.14 and the EOF load cases. In this research, the ABAQUS models simulated the actual loading and boundary conditions of the tests adopted from the literature.
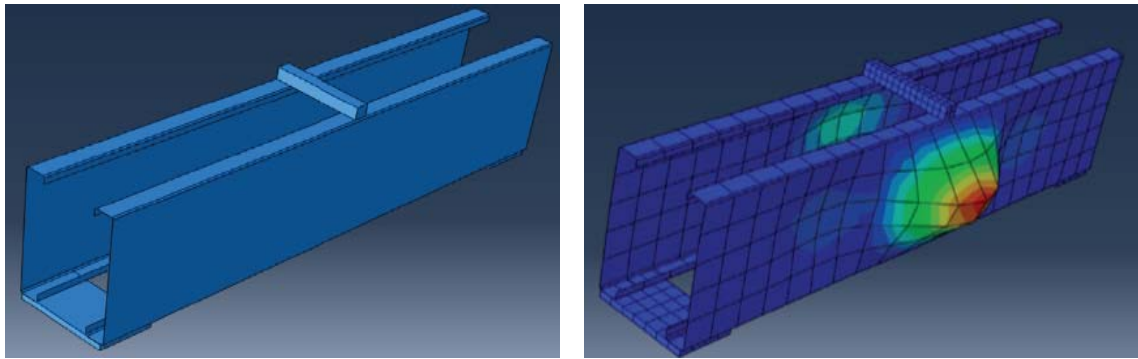
(a) Assembly of C-sections and bearing plates   (b) Buckling modes

Figure 2.14: FEM model on ABAQUS [20]

In other investigations, Hancock and Pham [12] used ABAQUS to model a rectangular plate under the IOF load case, unlipped channel and lipped channel sections under both the IOF and ITF load cases. The buckling loads and buckling coefficients (*k*) from ABAQUS were used to validate those from SAFSM developed by the authors as shown in Tables.2.8 to.2.10. Fig.2.15 shows the SFE model for an unlipped channel section under the IOF load case.
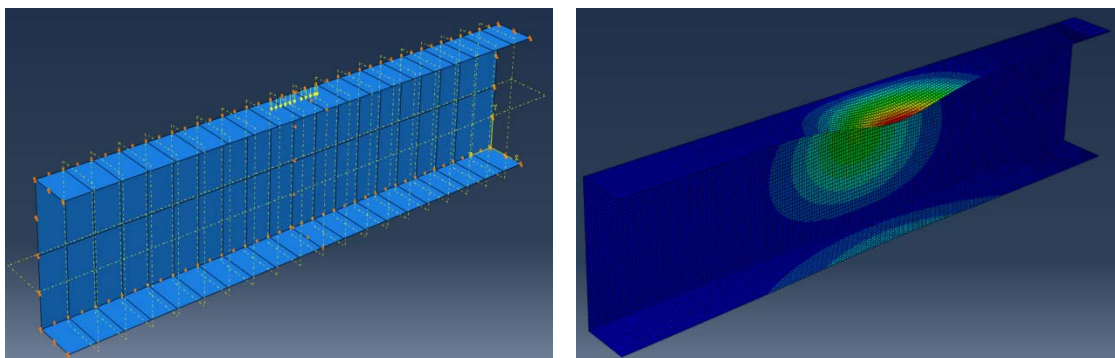
(a) Loading and boundary condition   (b) Buckling modes

Figure 2.15: Unlipped channel section under the IOF load case

Natário et al. [21] used ABAQUS to perform SFE models of unlipped plain-C, lipped plain-C, lipped plain-Z and build-up-I sections under the ETF load case. The buckling loads obtained from these models were used to validate those from the GTB theory developed by the authors as shown in Fig.2.12.

2.5. ESTIMATION OF THE YIELD LOAD FOR WEB CRIPPLING

2.5.1. Equivalent web yield capacity method

Yield load is an important component which contributes to the determination of the strength of structural members subjected to web crippling. Keerthan et al. [18] and Sundararajah et al. [19] determined the yield load from the equivalent web yield capacity method which is used for hot-rolled

steel sections as given in the Australian/New Zealand Standard AS/NZS 4100:1998 [60]. The yield load estimation for the interior two-flange (ITF) and end two-flange (ETF) load cases is given in Eqs.(2.23) and (2.24). However, the behaviour and failure modes of cold-formed steel members is different from the hot-rolled steel members. This method seems to be not accurate to estimate the yield load of cold-formed steel members subjected to web crippling as it does not account for corner radius effects.

$$P_y = f_y t_w \left(N + \frac{d_1}{2} \right) \qquad \text{for the ETF load case} \qquad (2.23)$$

$$P_y = f_y t_w \left(N + d_1 \right) \qquad \text{for the ITF load case} \qquad (2.24)$$

where:

P_y is the yield load

N is the bearing length

d_1 is the flat portion of the web

t_w is the web thickness

f_y is the yield strength of steel

2.5.2. Plastic mechanism models

In 2001, Young and Hancock [22] proposed analysis models to estimate the bearing capacity of un-lipped stocky channel sections under localised loading. In this research, the selected plastic mechanism models for the derivation of a P_y formula depends on the observation of experimental and/or numerical (non-linear SFE) results. The models to calculate the yield load of un-lipped channel sections under the different localised load cases are shown in Figs.2.16 to 2.19 and the P_y calculation is given in Eq.(2.25).
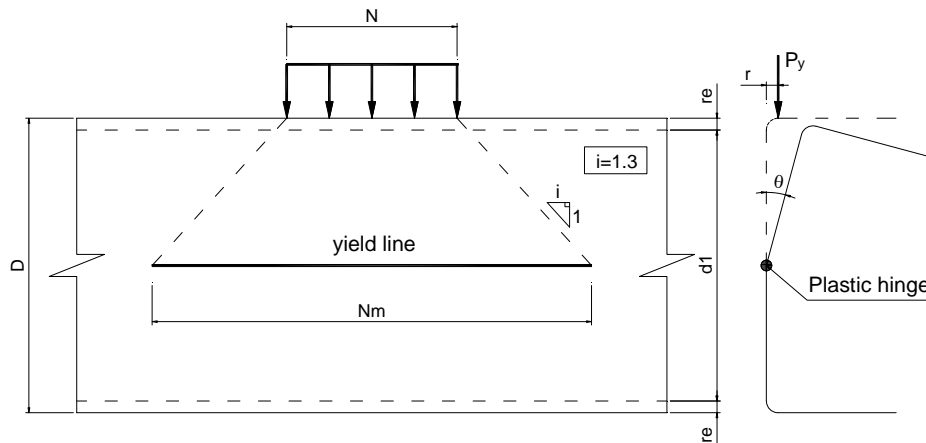
Figure 2.16: Plastic mechanism models for the IOF load case [22]
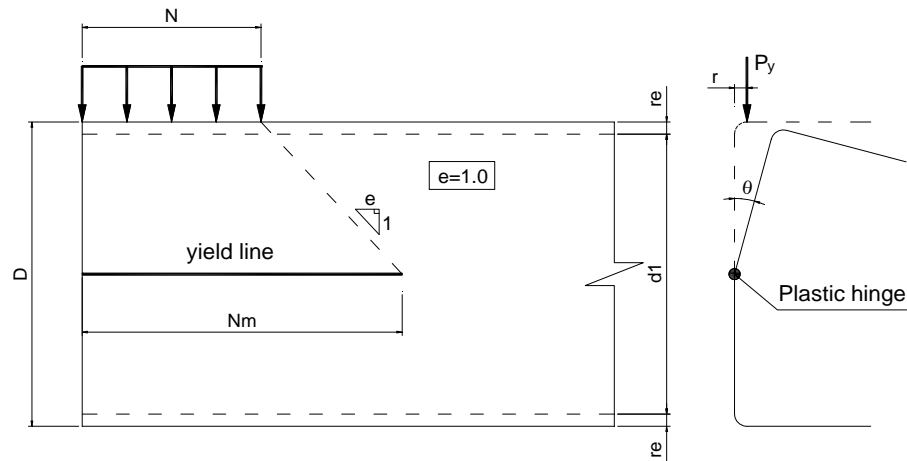
Figure 2.17: Plastic mechanism models for the EOF load case [22]
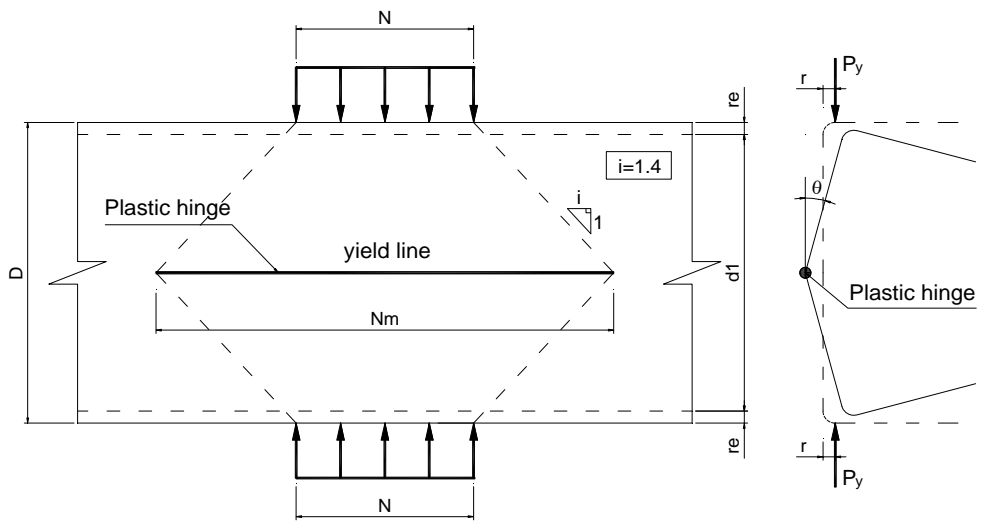
Figure 2.18: Plastic mechanism models for the ITF load case [22]
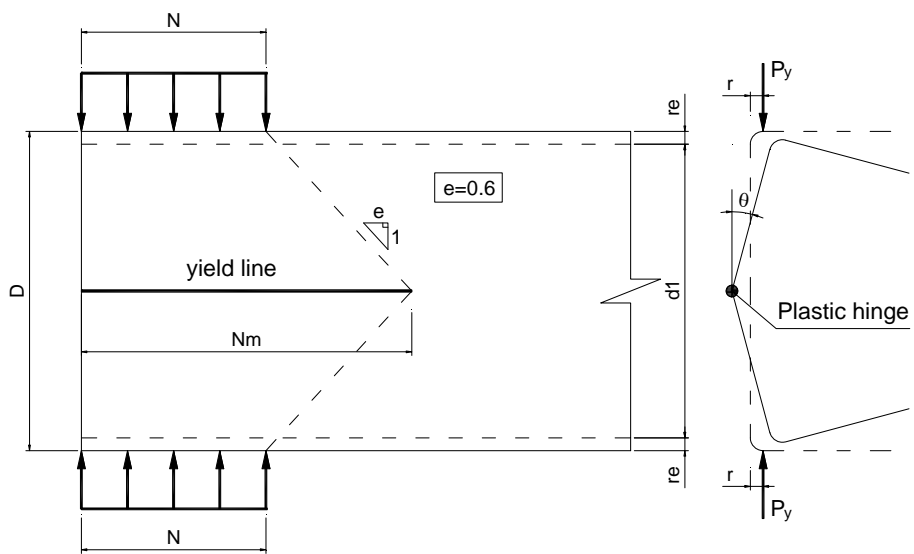
Figure 2.19: Plastic mechanism models for the ETF load case [22]

Yield capacity of sections given by:

$$P_y = \frac{M_p N_m}{r} \tag{2.25}$$

where:

M_p is the plastic moment per unit length

$$M_p = \frac{f_y t_w^2}{4} \tag{2.26}$$

r, r_i and r_e are centre-line, inside and outside corner radii, respectively

$$r = r_i + \frac{t_w}{2} \text{ and } r_e = r_i + t_w$$

D is the overall depth of the section

N_m is the yield-line length

$$N_m = N + iD \qquad \text{for interior loading} \tag{2.27}$$

$$N_m = N + \frac{eD}{2} \qquad \text{for end loading} \tag{2.28}$$

i=1.3   for the IOF load case

i=1.4   for the ITF load case

i=1.0   for the EOF load case

i=0.6   for the ETF load case

These are simple models for the calculation of the yield load of un-lipped stocky sections. It means that the sections are thick and compact and without flange stiffeners. However, the failure modes of slender sections with different shapes, flange stiffeners and flange fastened conditions might be different from the stocky un-lipped channel sections. Thus, it is necessary to develop plastic mechanism models to determine the yield load of general cold-formed sections subjected to web crippling.

2.5.3. Elastic-plastic analysis using Shell Finite Element method (SFE)

Natário et al. [61] used the SFE model to evaluate the 1st order elastic-plastic (EF) behaviour of cold-formed steel beams under four different localised load cases (IOF, EOF, ITF and ETF). The distributions of plastic strains of the 1st order elastic-plastic collapse mechanisms are shown in Fig.2.20. The yield loads from these models were used as well as the buckling loads obtained from the GBT to predict the strength of web crippling of structural members.

a. IOF load case

b. EOF load case

c. ITF load case
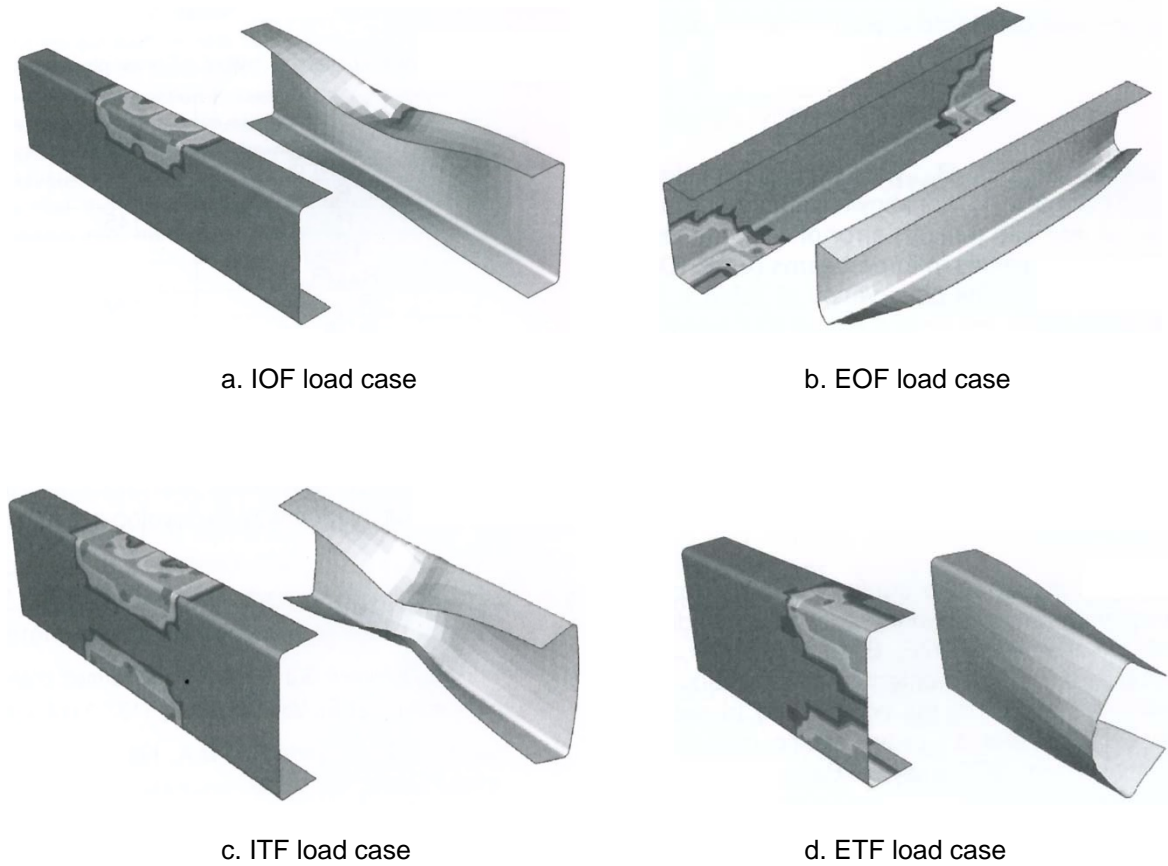
d. ETF load case

Figure 2.20: Elastic-plastic models using the SFE [61]

2.5.4. Yield-line mechanism

Natário et al. [21] gathered the experimental data from previous literature to study the behaviour of thin-walled sections under the ITF and ETF load cases. The authors employed the yield-line method based on the rigid plastic analysis to determine the yield load. In this method, the formulae to calculate P_y are derived, using the principle of virtual work, on the basic of the observed yield-line mechanisms. For lipped plain-C sections with unfastened flange conditions under the ETF load case, the yield-line mechanism was proposed in Fig.2.21 and the yield capacity of the member is given in Eq.(2.29).

$$P_y = f_y N_m \left(\sqrt{4r^2 + t^2} - 2r \right) \tag{2.29}$$

$$N_m = N + 2.5r_e + \frac{d_1}{2} \tag{2.30}$$
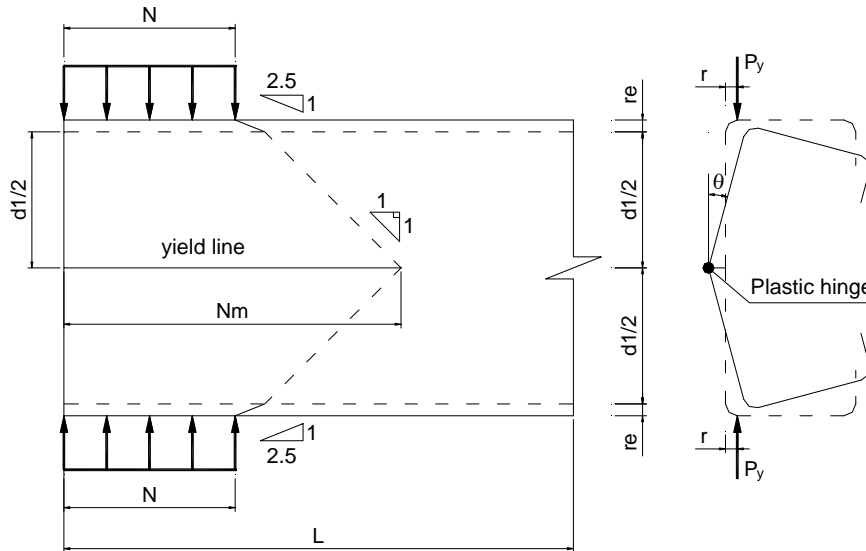
Figure 2.21: Yield-line mechanism for C-sections beams with unfastened flanges [21]

The yield-line mechanism for lipped plain-C sections under the ETF load case shown in Fig (2.22) and the yield load can be calculated by Eq.(2.31).
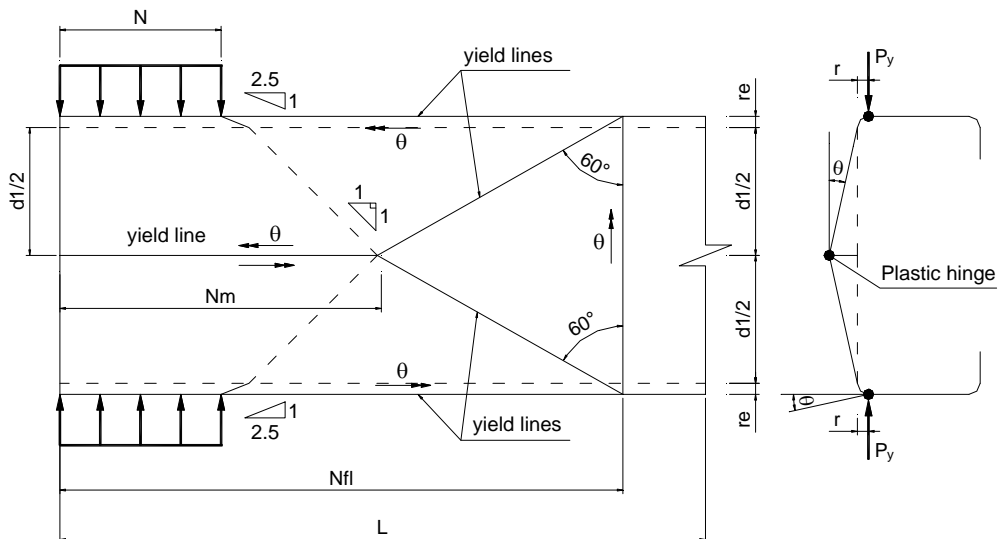
Figure 2.22: Yield-line mechanism for C-sections beams with fastened flanges [21]

$$P_y = f_y N_m \left(-2r + \sqrt{4r^2 + t^2 \frac{N^*}{N_m}} \right) \qquad (2.31)$$

$$N^* = 2N_m + \frac{4\sqrt{3}}{3}(d_1 + 2r) \qquad (2.32)$$

$$N_m = N + 2.5r_e + \frac{d_1}{2} \qquad (2.33)$$

The yield-line mechanism was proposed for plain-Z sections under the ETF load case shown in Fig.2.23 and the yield load of the member under this load case is determine by Eq.(2.34).

$$P_y = \frac{f_y N_m}{2(1+c_1)} \left(-4r_m(1-c_1) + \sqrt{\left[4r_m(1-c_1)\right]^2 + 4(1+c_1)t^2 \frac{N^*}{N_m}} \right) \tag{2.34}$$

$$N_{vert} = h_w + 2r_m ; \; N_m = L_s + 2.5r_{ext} + \frac{h_w}{3} \tag{2.35}$$

$$c_1 = \frac{\frac{h_w}{3} + r_m}{\frac{2h_w}{3} + r_m} ; \; c_2 = \frac{\frac{h_w}{3} + r_m}{\frac{\sqrt{3}}{2} N_{vert}} \tag{2.36}$$

$$N^* = \left(2N_m + \frac{\sqrt{3}}{2} N_{vert}\right)(1+c_1) + \frac{\sqrt{3}}{2} N_{vert} \left[c_1 + \frac{2\sqrt{3}}{3} c_2 + c_2^2\left(1+\frac{1}{c_1}\right) + 1\right] \tag{2.37}$$
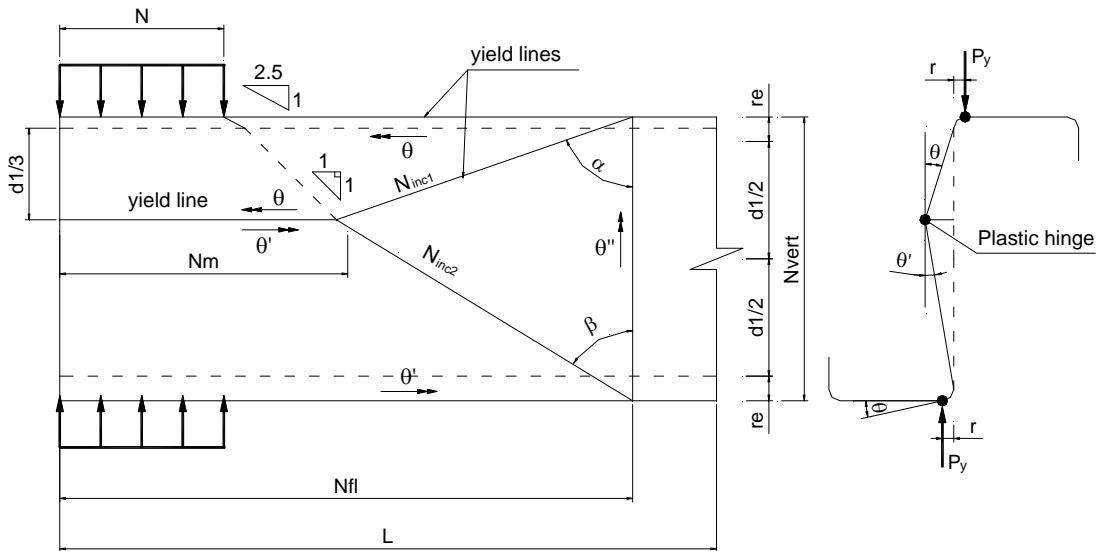
Figure 2.23: Yield-line mechanism for plain-Z sections with fastened flanges [21]

Fig.2.24 shows the yield-line mechanism for the built-up-I-sections, while Eq.(2.38) gives the calculation of the yield load of this type of cross-section under the ETF load case.

$$P_y = \frac{4}{3} f_y N_m \left[\sqrt{r_m^2 + \left(\frac{3}{2}t\right)^2} - r_m \right] \tag{2.38}$$

$$N_m = \min\left\{ L; L_s + 2.5r_{ext} + \frac{d_1}{2} \right\} \tag{2.39}$$
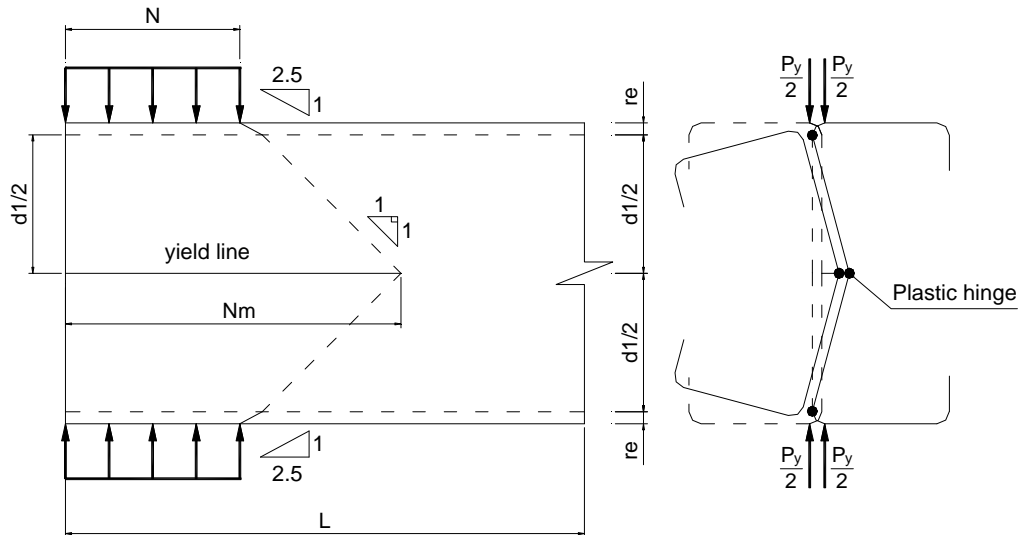
Figure 2.24: Yield-line mechanism for built-up-I-sections [21]

The yield-line models proposed by Natário et al. [21] have been seen as effective models to determine the yield load of thin-walled sections under localised loading. However, these models seem to be too complex for different cross-sections and fastened flange conditions for easy application in design standards. In addition, these models are available for the ETF load case but they are still not available for the IOF, EOF and ITF load cases. Thus, it is necessary to investigate simple and consistent models to calculate the yield load for different cross-sections, fastened flange conditions and loading conditions.

2.6. DIRECT STRENGTH METHOD OF DESIGN FOR WEB CRIPPLING APPROACHES

Investigations have been performed to establish the DSM equations for web crippling based on experimental data. In 2014, Keerthan et al. [18] performed an investigation of cold-formed steel hollow flange channel beams known as LiteSteel beams (LSBs) subjected to the ITF and ETF load cases. In this research, the buckling load (P_{cr}) is calculated by the elastic buckling equation of rectangular plates as given in Eq.(2.22), while the yield load (P_y) is determined from equivalent web yield capacity as given in Eqs.(2.23) and (2.24). The DSM design equations for the LiteSteel beams subjected to the ITF and ETF load cases are given in Eqs.(2.40) and (2.41).

$$\frac{P_n}{P_y} = 0.5\left[1 - 0.05\left(\frac{P_{cr}}{P_y}\right)^{0.78}\right]\left(\frac{P_{cr}}{P_y}\right)^{0.78} \quad \text{for the ETF load case} \tag{2.40}$$

$$\frac{P_n}{P_y} = 0.56\left[1 - 0.05\left(\frac{P_{cr}}{P_y}\right)^{0.75}\right]\left(\frac{P_{cr}}{P_y}\right)^{0.75} \quad \text{for the ITF load case} \tag{2.41}$$

where:

P_y is the yield load

P_{cr} is the buckling load

P_n is the nominal capacity of structural members under localised loading

In other research, thirty-six tests were conducted by Sundararajah et al. [19] to assess the web crippling behaviour and strengths of Lipped channel beams (LCBs) under the two-flanges load cases (ITF and ETF). The buckling load and the yield load are calculated the same as the calculations in [18]. From these two main input variables and the experimental data the authors proposed the DSM design equations for lipped channels beams subjected to the ITF and ETF load cases as given in Eqs.(2.42) and (2.43).

$$\frac{P_n}{P_y} = 0.23 \left[1 - 0.05 \left(\frac{P_{cr}}{P_y} \right)^{0.67} \right] \left(\frac{P_{cr}}{P_y} \right)^{0.67} \qquad \text{for the ETF load case} \qquad (2.42)$$

$$\frac{P_n}{P_y} = 0.46 \left[1 - 0.05 \left(\frac{P_{cr}}{P_y} \right)^{0.67} \right] \left(\frac{P_{cr}}{P_y} \right)^{0.67} \qquad \text{for the ITF load case} \qquad (2.43)$$

In 2015, Dara and Yu [20] performed an investigation for C and Z sections subjected to the IOF and EOF load cases. In this research, the buckling load was obtained from models simulated by FEM on Abaqus, while the yield load was determined from equivalent web yield capacity. The DSM equations were proposed to estimate the nominal web crippling strength as follows:

$$P_n = AP_y \qquad \text{for} \qquad \lambda \le \alpha \tag{2.44}$$

$$P_n = BP_y \lambda^{-c} \qquad \text{for} \qquad \lambda > \alpha \tag{2.45}$$

where

α, A, B and C values changes, as given in Table 2.11, with the respect to the loading condition and member cross-section shape.

λ is the non-dimensional slenderness used to determine P_n, $\lambda = \sqrt{P_y / P_{cr}}$

P_y is the yield load, calculated by

$$P_y = f_y N t \tag{2.46}$$

t is the section thickness

Table 2.11: Generalization of developed design equations

Sections	Load cases	Stiffening flange conditions	Fastening flange conditions	α	A	B	C
Lipped plain-C	IOF	Stiffened	Unfastened	<=0.48	0.680	-	-
				>=0.48	-	0.31	-1.05
	EOF	Unstiffened	Unfastened	<=0.40	-0.360	-	-
				>=0.40	-	0.21	-0.53
		Stiffened	Fastened	<=0.76	0.290	-	-
				>=0.76	-	0.21	-1.08
		Stiffened	Unfastened	<=0.44	0.280	-	-
				>=0.44	-	0.19	-0.52
Lipped plain-Z	IOF	Stiffened	Fastened	<=0.82	0.250	-	-
				>=0.82	-	0.19	-0.93
	EOF	Stiffened	Unfastened	<=0.75	0.200	-	-
				>=0.75	-	0.17	-0.33

Recently, Natário et al. [21], [62], [63] collected the experimental data from Hetrakul and Yu [56], Young and Hancock [22], Beshara and Schuster [36] and Macdonald et al. [64] to investigate the web crippling behaviour of structural members under the ITF and ETF load cases. From the test data, the authors used the yield-line method to calculate the yield load, while the buckling load was obtained from GBTWEB software which is based on a GBT formulation previously developed by the authors. Then, the DSM equations were proposed to estimate the capacity of structural members under localised loading as given in Eqs.(2.47) and (2.48).

For the ETF load case:

$$\frac{P_n}{P_y} = \begin{cases} 1 & for \quad \lambda \le 0.415 \\ 0.474\left[1-0.115\left(\frac{P_{cr}}{P_y}\right)^{0.728}\right]\left(\frac{P_{cr}}{P_y}\right)^{0.728} & for \quad \lambda > 0.415 \end{cases} \quad (2.47)$$

For the ITF load case:

$$\frac{P_n}{P_y} = \begin{cases} 1 & for \quad \lambda \le 0.517 \\ 0.732\left[1-0.156\left(\frac{P_{cr}}{P_y}\right)^{0.516}\right]\left(\frac{P_{cr}}{P_y}\right)^{0.516} & for \quad \lambda > 0.517 \end{cases} \quad (2.48)$$

More recently, Sundararajah et al. [65] conducted 36 experiments of SupaCee sections and used the previous data for lipped channel sections subjected to the ITF and ETF load cases. The authors calculated the buckling load by the elastic buckling equation of rectangular plates the same as their previous research [19], while the yield-line models were employed to determine the yield load. The DSM design equations were proposed to estimate the capacity of both lipped channel and SupaCee sections as given in Eqs.(2.49) and (2.50).

$$\frac{P_n}{P_y} = \left[1 - 0.2\left(\frac{P_{cr}}{P_y}\right)^{1.0}\right]\left(\frac{P_{cr}}{P_y}\right)^{1.0} \quad \text{for the ETF load case} \tag{2.49}$$

$$\frac{P_n}{P_y} = \left[1 - 0.2\left(\frac{P_{cr}}{P_y}\right)^{0.9}\right]\left(\frac{P_{cr}}{P_y}\right)^{0.9} \quad \text{for the ITF load case} \tag{2.50}$$

Currently, there is one set of DSM equations from Dara and Yu [20] to estimate the nominal capacity of structural members with C and Z sections subjected to the IOF and EOF load cases. However, these DSM equations seem to be too complex with many coefficients which depend on the cross-section types, flange stiffening conditions and flange fastened conditions as shown in Table.2.11. Also, in this investigation, the yield load is obtained from equivalent web yield capacity which is used for hot-rolled steel members, thus it may not predict accurately for cold-formed steel members with rounded corners.

There are four sets of DSM design equations to determine the nominal capacity of structural members subjected to the ITF and ETF load cases. The equations from Keerthan et al. [18] are used for hollow channel sections, the proposals from Sundararajah et al. [19] are used for lipped plain-C sections and from Sundararajah et al. [65] for both lipped plain-C and SupaCee sections, while the DSM equations from Natário et al. [21] can be used for un-lipped plain-C, lipped plain-C, lipped plain-Z and I sections. It is clear that three sets of DSM equations from [19], [65] and [21] can be used to estimate the nominal capacity of lipped plain-C sections under the ITF and ETF load cases; however, the DSM coefficients for each set of equations are totally different.

CHAPTER 3

PRE-BUCKLING ANALYSIS OF THIN-WALLED SECTIONS UNDER LOCALISED LOADING FOR GENERAL END BOUNDARY CONDITIONS

3.1. INTRODUCTION

In order to carry out an elastic buckling analysis of a thin-walled member under localised loading, it is necessary to compute the pre-buckling membrane stresses in the member. The pre-buckling analysis described in this Chapter is a linear elastic analysis step to provide stresses for conducting the elastic buckling analysis described in Chapter 4. This process of pre-buckling analysis then buckling analysis is also given in Natário et al. [66] in a research about localised failure of thin-walled steel members subjected to concentrated loads.

This Chapter summaries the displacement functions for different end boundary conditions of structural members. The theory of the FSM for pre-buckling analysis of thin walled sections under localised loading for general end boundary conditions is given and also built into Version 2.0 of the THIN-WALL-2 as described in detail in Chapter 5. Numerical examples have been performed using the THIN-WALL-2 program and compared with the results from the FEM analyses using ABAQUS [32] to validate the accuracy. The results from the pre-buckling analysis step are membrane stresses and deformations of the structural member which are used for the elastic buckling analysis described in Chapter 4. A convergence study of stresses with the number of series terms is also provided in this Chapter.

The most significant development of this Chapter is the choice and validation of the displacement functions for different boundary conditions. Consequently, this Chapter introduces the displacement functions first before giving the full derivation of the stiffness matrices and load vector based on energy principles.

3.2. BOUNDARY CONDITION

Boundary condition refers to the support conditions at the ends of structural members (plates or beams) in the analyses of thin-walled sections under loading. The structural member is divided into strips and for different supports and loading conditions, different displacement functions are required for the displacements of the structural member.

The simply supported boundary condition (S) as shown in Fig.3.1(a) is a common type of support for structural members. The main feature of this boundary condition is that the strips can rotate about the transverse direction at the end edges and move freely in the longitudinal direction. At the simply supported ends, there are only shear forces while the moments and the axial forces vanish.

The clamped boundary condition (C) as shown in Fig.3.1(b) is the second type of support for structural members. The main feature of this boundary condition is that the strips can deform freely in the longitudinal direction but they cannot rotate about the transverse axis or expand transversely at the end edges. At the clamped ends, there are moments and shear forces, while the axial force vanishes.

a. Both ends Simply supported   b. One end Clamped and one end Free
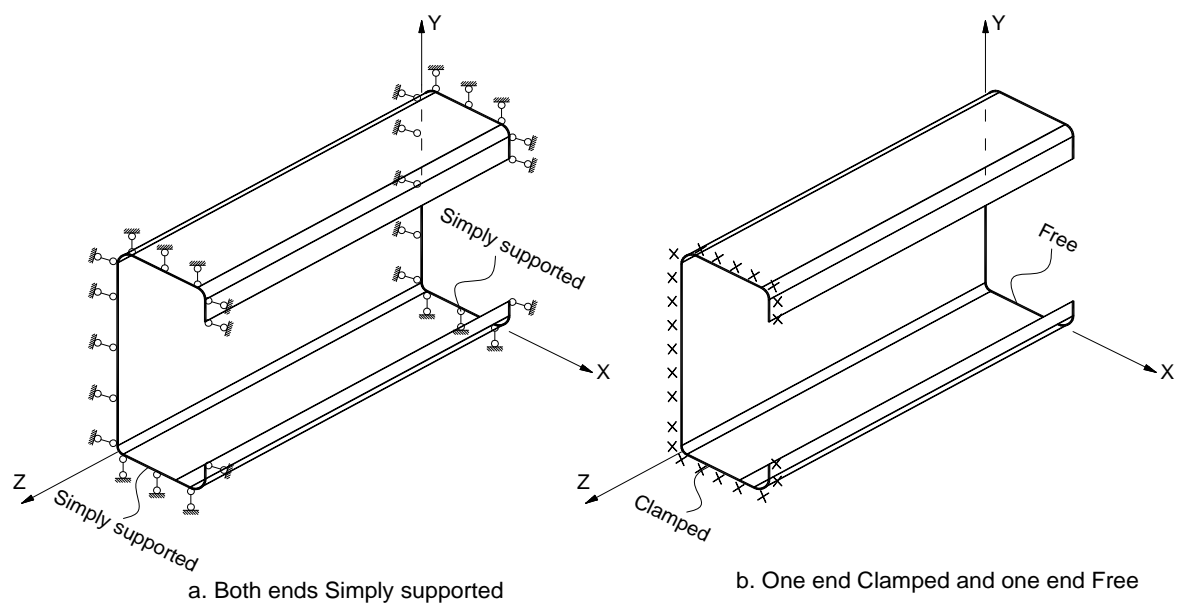
Figure 3.1: Boundary conditions

The free boundary condition (F) as shown in Fig.3.1(b) is the third type of support for structural members. It appears when the ends of the structural members are free and not connected with other members. The main feature of this boundary condition is that strips can rotate about the transverse axis at the end edges and deform freely in all directions. Thus, there are no forces, moments or stresses at the free ends.

By combining two from these three boundary conditions, there are possible different combinations of boundary conditions which can be applied to strips of structural members:

1. Both ends simply supported (SS),

2. One end simply supported and the other end clamped (SC),

3. One end simply supported and the other end free (SF),

4. Both ends clamped (CC),

5. One end clamped and the other end free (CF),

6. Both ends free (FF).

3.3. LOCALISED LOADING CASES

In general, it is possible to analyse thin-walled sections under arbitrary localised loading. The loading is located at any position along the beam. In addition, the loading can be applied from one side or both sides of the structural member. The applied loads and the reaction loads at the supports lead to the buckling of the structural member. From the locations of the localised load, there are four loading cases which are referred in design in the North American Specification for the Design of Cold-Formed Steel Structural Members AISI S100-2012 [2] and the Australian/New Zealand Standard AS/NZS 4600:2005 [3] of thin-walled section under localised loading, as follows:

1. Interior one-flange loading (IOF),

2. Interior two-flange loading (ITF),

3. End one-flange loading (EOF),

4. End two-flange loading (ETF).

In the interior one-flange loading (IOF) case as shown in Fig.3.2(a), the localised load is applied in the interior of the beam with the required distance from the support to the bearing plate greater than 1.5 times the web depth to avoid the effect of two external support conditions. In this case, the buckle appears at the area of the web under localised loading since the end reaction points are stiffened.

In the interior two-flange loading (ITF) case as shown in Fig.3.2(b), the localised load is applied on both sides of the cross-section of the beam. The required distance from the beam end to the bearing plate is greater than 1.5 times the web depth. With these loading conditions, the buckle appears in the area of the web between the applied load and the reaction.

In the end one-flange loading (EOF) case as shown in Fig.3.2(c), the load is applied in the interior of the beam at a stiffened loading point in order to prevent failure around this area. With this loading condition, reactions appear at the ends of the beam and the buckle is enforced appear in the area of the web above the external supports.

In the end two-flange loading (ETF) case as shown in Fig.3.2(d), the load is applied at the end of the beam which leads to the appearance of a reaction at the opposite supports. The buckle appears in the area of the web between these loads.

a. IOF: Interior One-Flange Loading

b. ITF: Interior Two-Flange Loading

c. EOF: End One-Flange Loading

d. ETF: End Two-Flange Loading
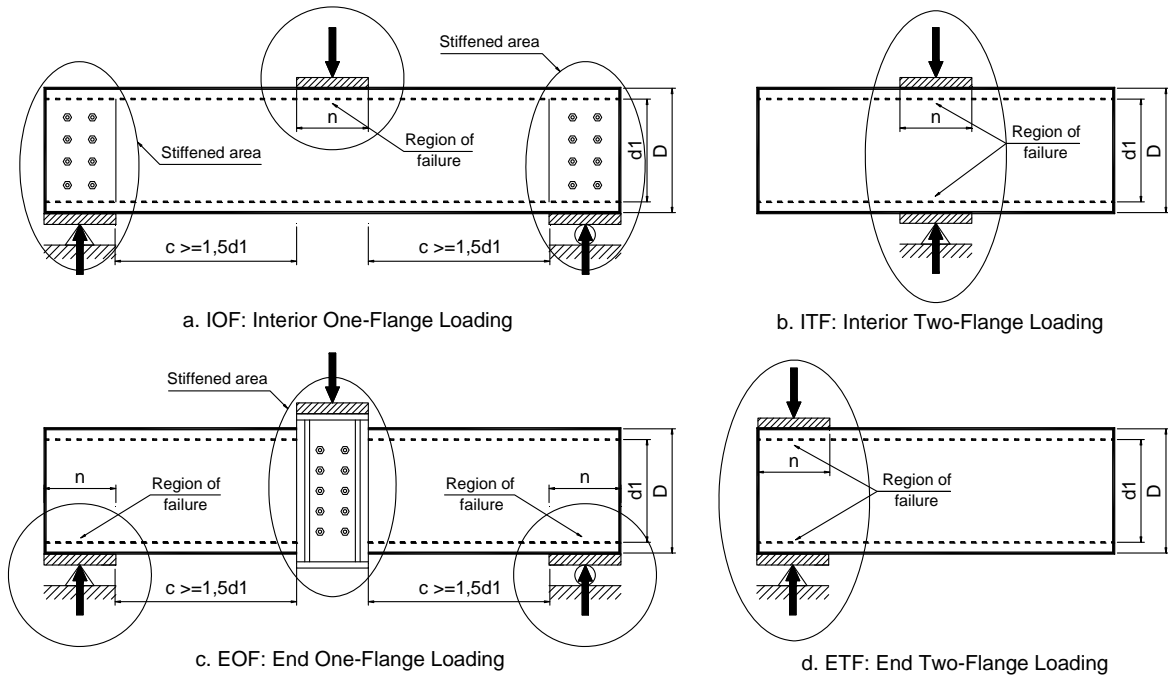
Figure 3.2: Localised loading cases

3.4. DISPLACEMENT FUNCTIONS

3.4.1. Choice of displacement functions

In the Finite Strip Method (FSM), it is vital that the choice of suitable displacement functions for a strip is the most important stage of the analysis, and great care must be exercised at this stage. An incorrectly chosen displacement function may lead to results which converge to incorrect solutions for successively refined meshes. The FSM can be considered as a special form of the FEM procedure using the displacement approach. Unlike the standard FEM which uses the polynomial displacement functions in all directions, the FSM employs simple polynomials in the transverse direction and continuously differentiable smooth series in the longitudinal direction, so that such series should satisfy the boundary conditions at the ends of the strips. The displacements of a strip are a combination of the flexural displacements perpendicular to the strip and membrane displacements in the plane of the strip. Generally, the form of the displacement function is given as a product of polynomials and smooth series. The notation used in this Chapter 3 and Chapter 4 for the FSM is the same as used by Hancock and Pham [12]. The local x, y, z axes are the same orientation as Timoshenko and Gere [46].

3.4.2. The flexural displacement functions of a strip in local x, y, z axes

An isometric view of flexural displacements of a strip is shown in Fig.3.3

The plate flexural deformations *w* of a strip can be described by the summation over *μ* series terms as:

$$w = \sum_{m=1}^{\mu} f_{1m}(y) X_{1m}(x) \tag{3.1}$$

where:

μ is the number of series terms of the harmonic longitudinal function

X_{1m}(x) is the function for longitudinal variation

f_{1m}(y) is a polynomial function for transverse variation. This function for the *m^{th}* series term is given by:

$$f_{1m}(y) = \alpha_{1Fm} + \alpha_{2Fm}\left(\frac{y}{b}\right) + \alpha_{3Fm}\left(\frac{y}{b}\right)^2 + \alpha_{4Fm}\left(\frac{y}{b}\right)^3 \tag{3.2}$$

$\{\alpha_{Fm}\}$ is the vector of polynomial coefficients for the *m^{th}* series term which depend on the nodal line flexural deformations of the strip

$$\{\alpha_{Fm}\} = \begin{bmatrix} \alpha_{1Fm} & \alpha_{2Fm} & \alpha_{3Fm} & \alpha_{4Fm} \end{bmatrix}^T \tag{3.3}$$

t, b and *L* are the strip thickness, width and length respectively.
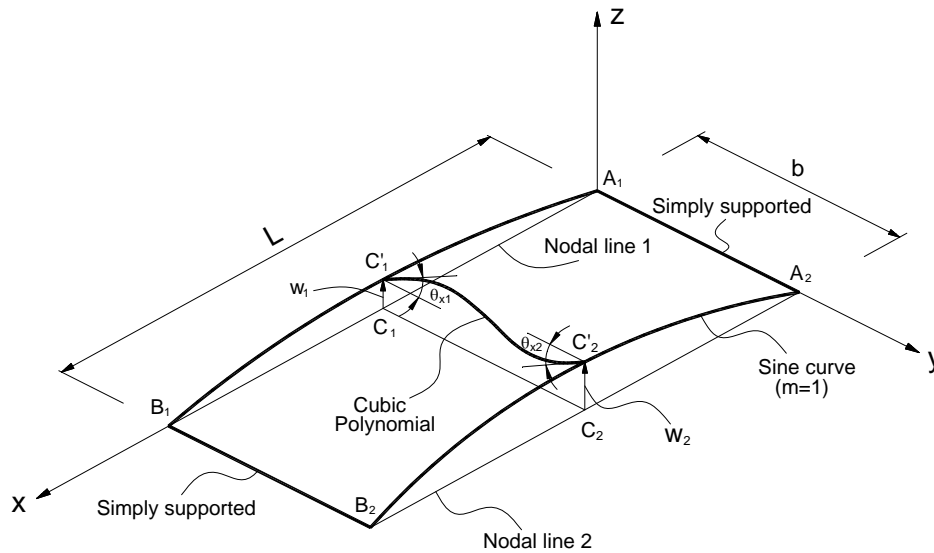
Figure 3.3: Flexural displacements of a strip

3.4.3. The membrane displacement functions of a strip in local x, y, z axes

An isometric view of membrane displacements of a strip is shown in Fig.3.4
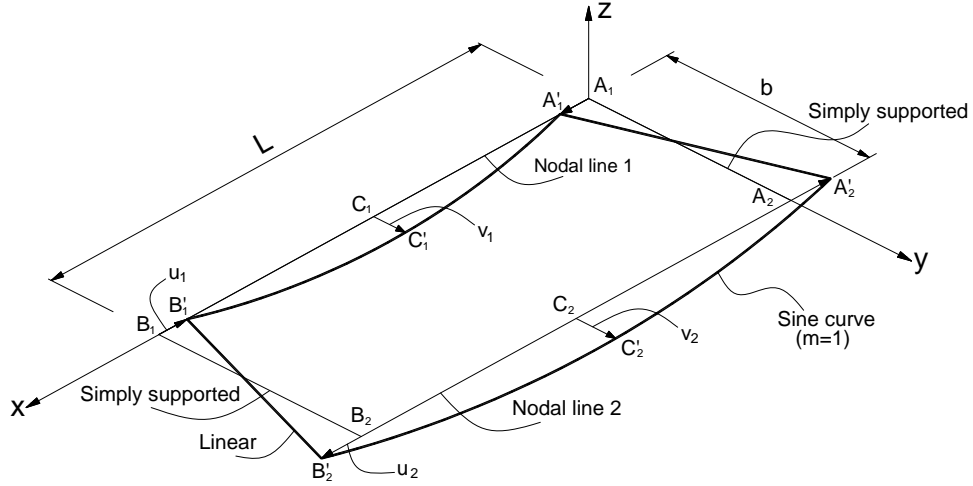
Figure 3.4: Membrane displacements of a strip

The membrane deformations in the longitudinal and transverse directions of a strip can be described by the summation over *µ* series terms as:

$$v = \sum_{m=1}^{\mu} f_{vm}(y) X_{1m}(x) \tag{3.4}$$

$$u = \sum_{m=1}^{\mu} f_{um}(y) X_{2m}(x) \tag{3.5}$$

where:

$X_{1m}(x)$ and $X_{2m}(x)$ are the longitudinal variation functions for the membrane transverse *v* and longitudinal *u* deformations respectively

$f_{vm}(y)$ and $f_{um}(y)$ are the transverse variations. These functions for the mth series term are given:

$$f_{vm}(y) = \alpha_{1Mm} + \alpha_{2Mm}\left(\frac{y}{b}\right) \tag{3.6}$$

$$f_{um}(y) = \alpha_{3Mm} + \alpha_{4Mm}\left(\frac{y}{b}\right) \tag{3.7}$$

$\{\alpha_{Mm}\}$ is the vector of polynomial coefficients for the mth series term which depends on the nodal line membrane deformations of the strips

$$\{\alpha_{Mm}\} = \begin{bmatrix} \alpha_{1Mm} & \alpha_{2Mm} & \alpha_{3Mm} & \alpha_{4Mm} \end{bmatrix}^{T} \tag{3.8}$$

3.4.4. Available displacement functions for different boundary conditions

a. Both ends simply supported (SS)

The displacement functions by Cheung [13] are:

$$X_{1m}(x) = \sin\left(\frac{m\pi x}{L}\right)$$ (3.9)

$$X_{2m}(x) = \cos\left(\frac{m\pi x}{L}\right)$$ (3.10)

These displacement functions for the SS case with m=3 are shown in Fig.3.5.
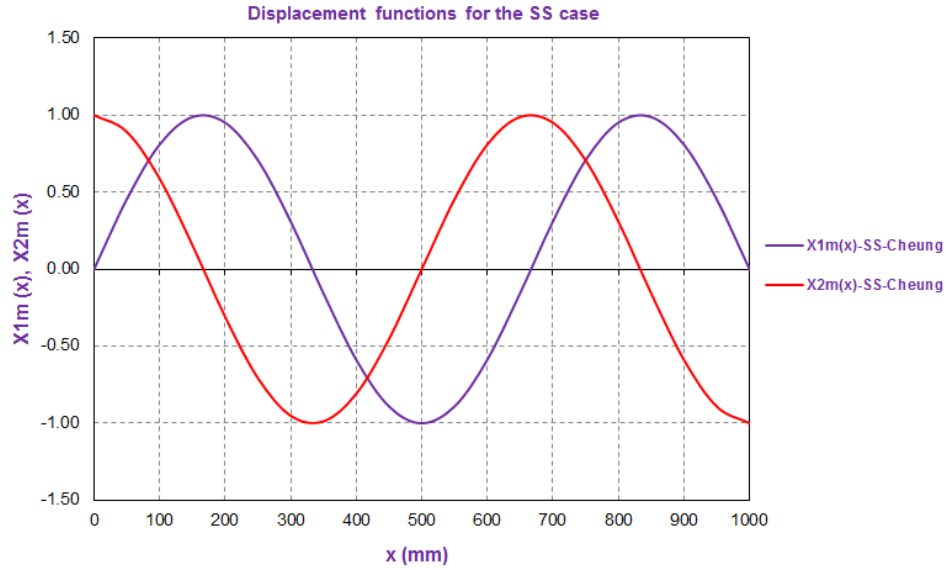
Figure 3.5: Displacement functions for the SS case with m=3

b. One end simply supported and the other end clamped (SC)

The displacement functions by Cheung [13] are:

$$X_{1m}(x) = \sin\left(\frac{\mu_m x}{L}\right) - \alpha_m \sinh\left(\frac{\mu_m x}{L}\right)$$ (3.11)

$$X_{2m}(x) = \cos\left(\frac{\mu_m x}{L}\right) - \alpha_m \cosh\left(\frac{\mu_m x}{L}\right)$$ (3.12)

with $\quad \mu_m = 3.9266, 7.0685, 10.2102, ..., \dfrac{4m+1}{4}\pi$

$m = 1, 2, 3, ..., \infty$ and $\alpha_m = \dfrac{\sin \mu_m}{\sinh \mu_m}$

The functions have been chosen in preference to the Bradford and Azhari functions [16] because they better satisfy equilibrium at the ends as required for the pre-buckling analysis. The Bradford and Azhari functions were chosen to satisfy the kinematic boundary conditions for buckling analyses.

These displacement functions for the SS case with m=3 are shown in Fig.3.6.
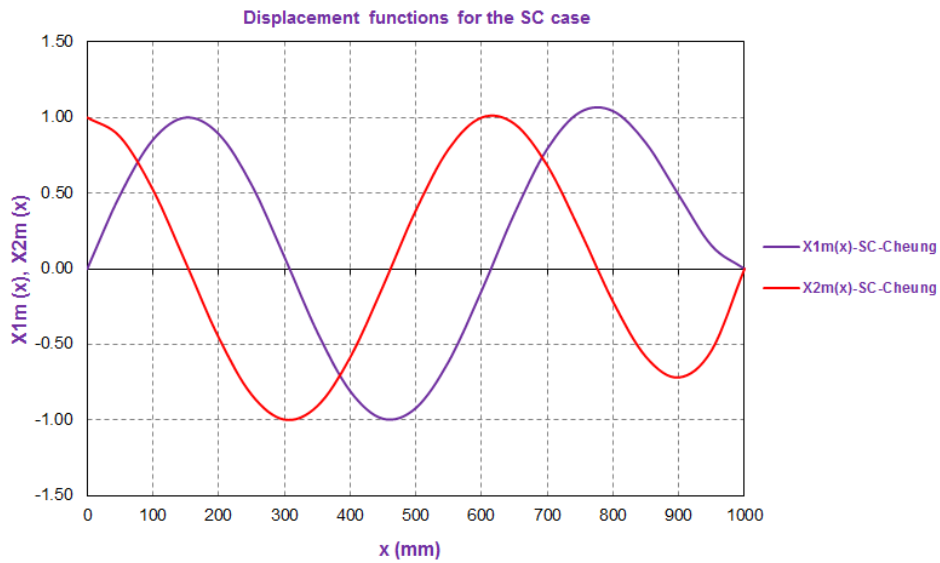
Figure 3.6: Displacement functions for the SC case with m=3

c. One end simply supported and the other end free (SF)

The displacement functions by Cheung [13] are:

Case 1: $m = 1$ and $\mu_1 = 1$

$$X_{11}(x) = \frac{x}{L} \text{ and } X_{21}(x) = 1 \tag{3.13}$$

Case 2:

$$m = 2, 3, 4, 5, ..., \infty \text{ and } \alpha_m = \frac{\sin \mu_m}{\sinh \mu_m}$$

$$\mu_m = 3.9266, 7.0685, 10.2102, 13.3520, ..., \frac{4m-3}{4}\pi$$

$$X_{1m}(x) = \sin\left(\frac{\mu_m x}{L}\right) + \alpha_m \sinh\left(\frac{\mu_m x}{L}\right) \tag{3.14}$$

$$X_{2m}(x) = \cos\left(\frac{\mu_m x}{L}\right) + \alpha_m \cosh\left(\frac{\mu_m x}{L}\right) \tag{3.15}$$

The displacement functions for the SF case with m=3 are shown in Fig.3.7.
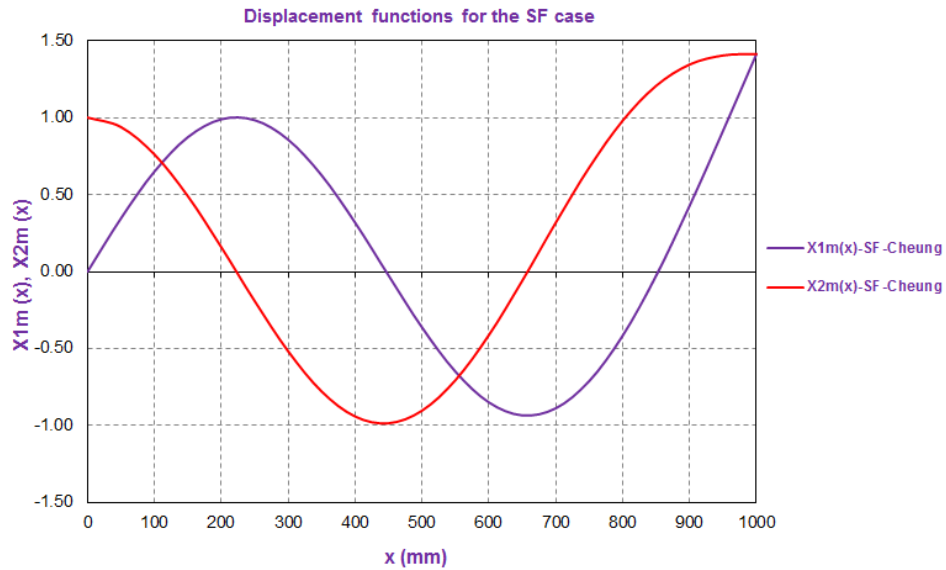
Figure 3.7: Displacement functions for the SF case with m=3

d. Both ends clamped (CC)

The displacement functions by Cheung [13] are:

$$X_{1m}(x) = \sin\left(\frac{m\pi x}{L}\right) \tag{3.16}$$

$$X_{2m}(x) = \sin\left[\frac{(m+1)\pi x}{L}\right] \tag{3.17}$$

These functions were selected in Chapter 3 of Cheung [13]. Cheung developed these functions to satisfy the natural boundary conditions and have been proven successful in static analyses. The displacement functions for the CC case with m=3 are shown in Fig.3.8.
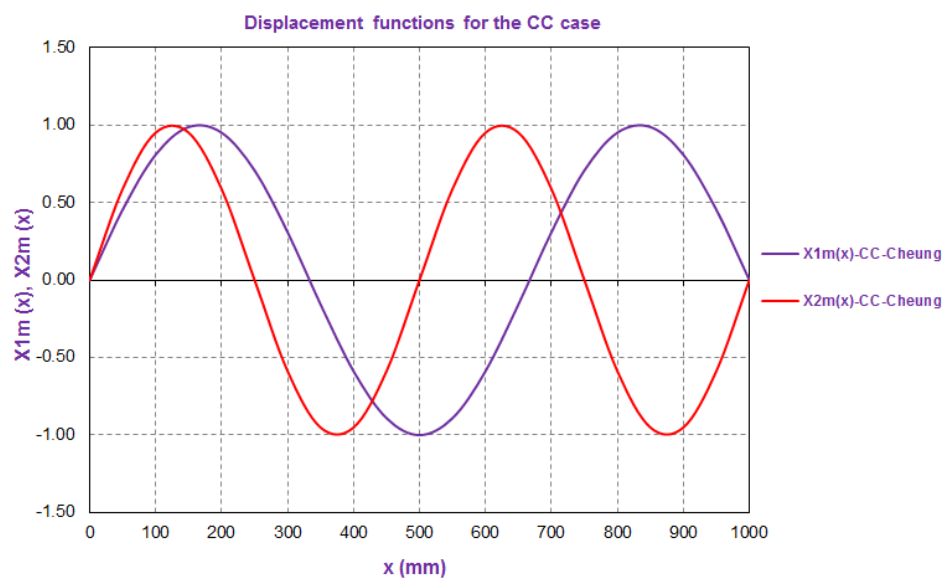
Figure 3.8: Displacement functions for the CC case with m=3

e. One end clamped and the other end free (CF)

The displacement functions by Bradford and Azhari [16] are:

$$X_{1m}(x) = 1 - \cos\left[\left(m - \frac{1}{2}\right)\frac{\pi x}{L}\right] \tag{3.18}$$

$$X_{2m}(x) = \left(\frac{2m-1}{2m}\right)\sin\left[\left(m - \frac{1}{2}\right)\frac{\pi x}{L}\right] \tag{3.19}$$

These functions have been chosen as they are simpler to implement in Chapter 4 - Buckling described later. They are different from those developed by Cheung [13].

The displacement functions for the CF case with m=3 are shown in Fig.3.9.
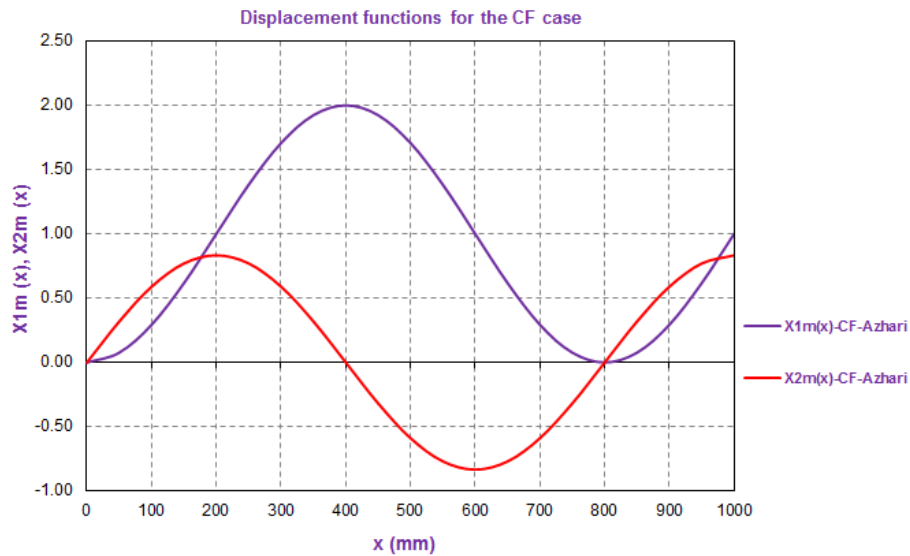
Figure 3.9: Displacement functions for the CF case with m=3

f. Both ends free (FF)

The new displacement functions used in this research are:

Case 1: $m = 1$

$$X_{11}(x) = 1 \text{ and } X_{21}(x) = 0 \tag{3.20}$$

Case 2: $m = 2$

$$X_{12}(x) = 1 - \frac{2x}{L} \text{ and } X_{22}(x) = -\frac{1}{\pi} \tag{3.21}$$

Case 3: $m \geq 3$

$$X_{1m}(x) = 1 - 2\sin\left[\frac{(2m-5)\pi x}{L}\right] \tag{3.22}$$

$$X_{2m}(x) = -2\left(\frac{2m-5}{m}\right)\cos\left[\frac{(2m-5)\pi x}{L}\right]$$

(3.23)

These functions have been chosen as they are simpler to implement in Chapter 4 - Buckling as described later. In a similar manner to those chosen for the CC case, they satisfy equilibrium when a series is taken and have no kinematic restrictions as would occur for the FF case.

The displacement functions for the FF case with m=3 and m=4 are shown in Fig.3.10 and Fig.3.11. respectively.
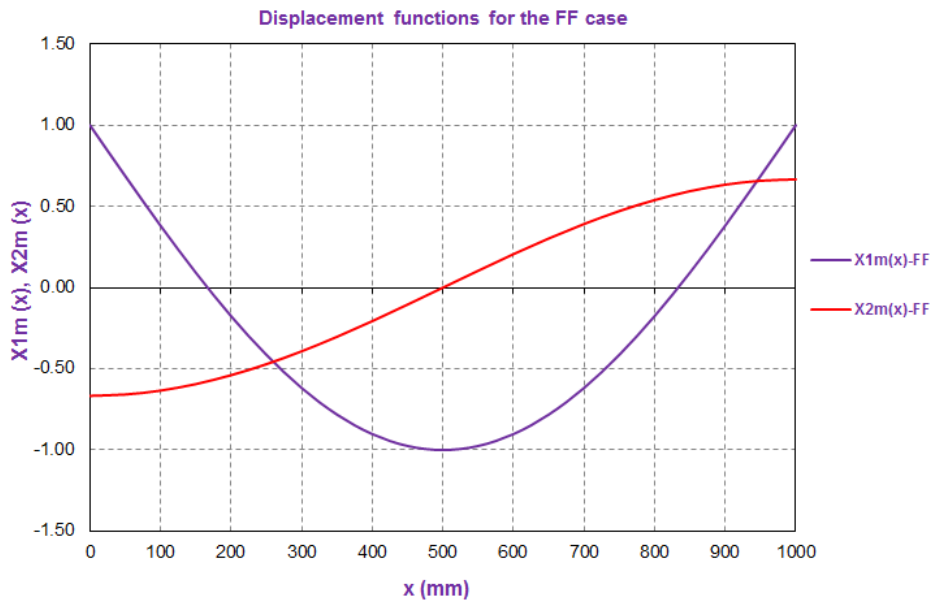
Figure 3.10: Displacement functions for the FF case with m=3
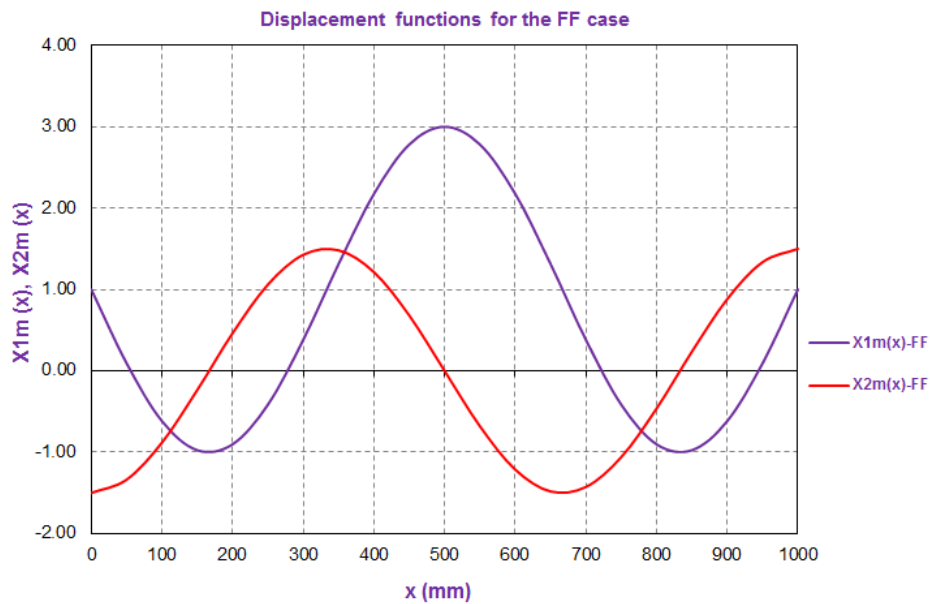
Figure 3.11: Displacement functions for the FF case with m=4

3.5. THE FLEXURAL STIFFNESS MATRIX OF A STRIP

3.5.1. The flexural displacement functions

The displacement function from Eq.(3.1) can be rewritten as matrix format.

$$w = \left[M_{Fm} \right] \left\{ \alpha_{Fm} \right\}$$

(3.24)

where:

$$\left[M_{Fm} \right] = \left[\; X_{1m} \quad \bar{y} X_{1m} \quad \bar{y}^2 X_{1m} \quad \bar{y}^3 X_{1m} \; \right]$$

$$\bar{y} = \frac{y}{b}$$

3.5.2. Bending stresses and curvatures of a strip

Stress distribution
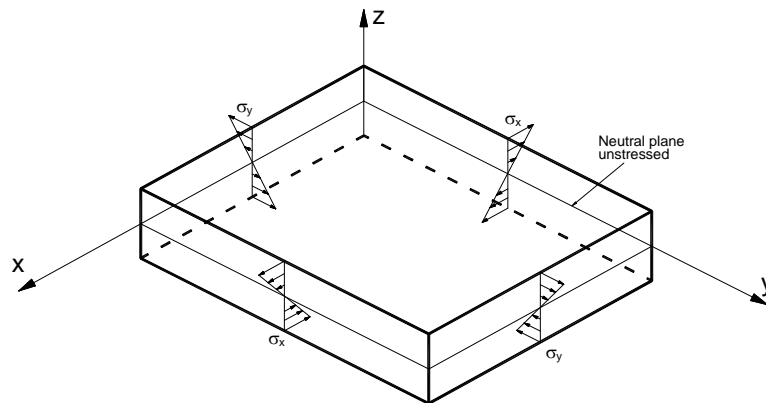
Figure 3.12: Stress distribution
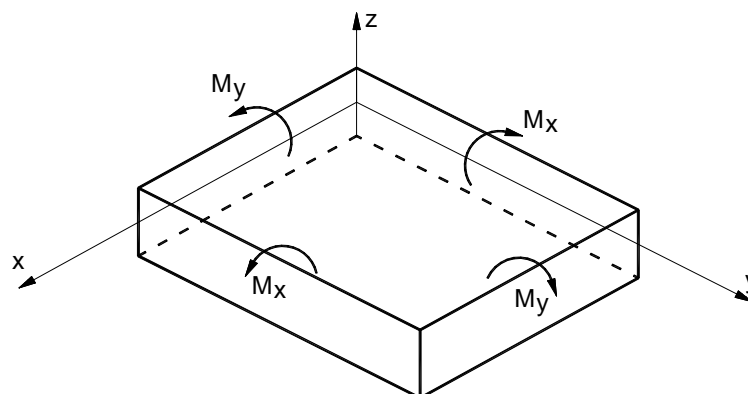
Stress resultants

Figure 3.13: Stress resultants
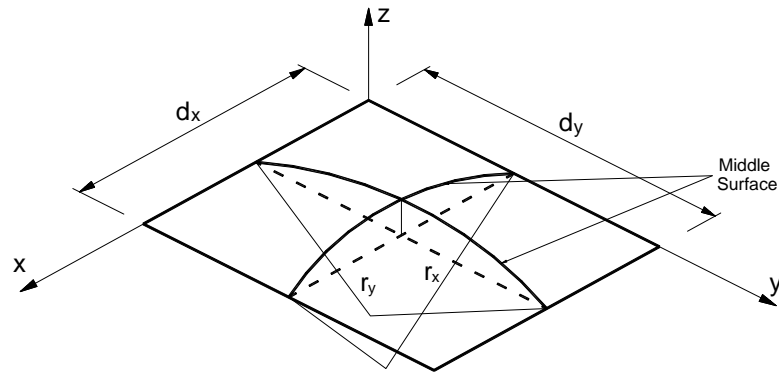
Curvatures

Figure 3.14: Curvatures

$$\text{Curvature in x direction} = \frac{1}{r_x} = \frac{-\partial^2 w}{\partial x^2} = \rho_x \tag{3.25}$$

$$\text{Curvature in y direction} = \frac{1}{r_y} = \frac{-\partial^2 w}{\partial y^2} = \rho_y \tag{3.26}$$

3.5.3. Twisting stresses and deformations of a strip

Stress distribution
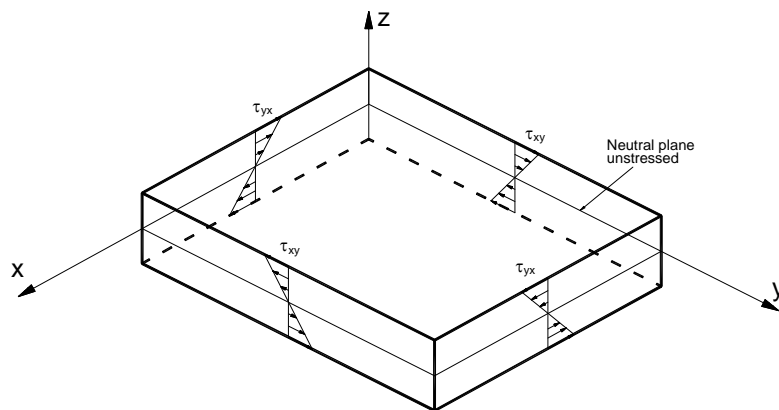
Figure 3.15: Stress distribution
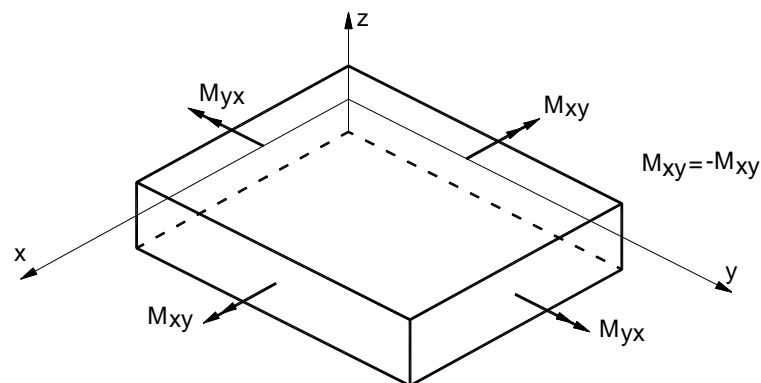
Stress resultants

Figure 3.16: Stress resultants
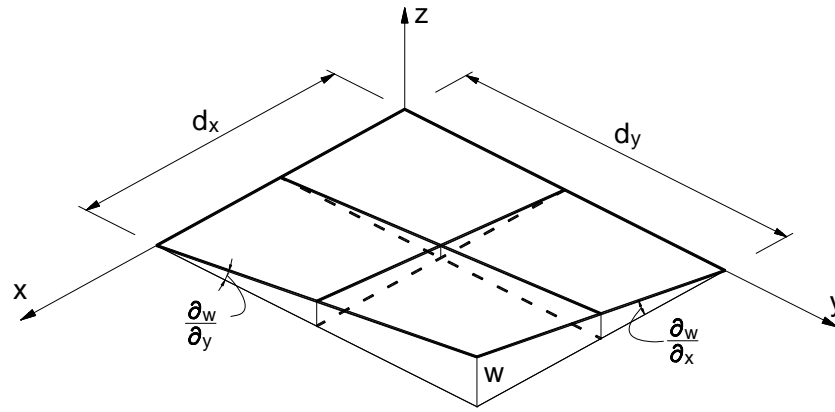
Curvatures

Figure 3.17: Curvatures

$$\text{Twist in y direction} = \frac{\partial}{\partial y}\left(\frac{\partial w}{\partial x}\right) = \frac{\partial^2 w}{\partial y \partial x} = \frac{1}{2r_{xy}} = \frac{\rho_{xy}}{2} \tag{3.27}$$

$$\text{Twist in x direction} = \frac{\partial}{\partial x}\left(\frac{\partial w}{\partial y}\right) = \frac{\partial^2 w}{\partial x \partial y} = \frac{1}{2r_{xy}} = \frac{\rho_{xy}}{2} \tag{3.28}$$

3.5.4. Flexural property matrix

The relationships between plate flexural and torsional rigidity are given as:

$$M_x = \frac{E_x t^3}{12(1-\nu_y \nu_x)}\left(-\frac{\partial^2 w}{\partial x^2} - \nu_y \frac{\partial^2 w}{\partial y^2}\right) = D_x \rho_x + D_1 \rho_y \tag{3.29}$$

$$M_y = \frac{E_y t^3}{12(1-\nu_y \nu_x)}\left(-\frac{\partial^2 w}{\partial y^2} - \nu_x \frac{\partial^2 w}{\partial x^2}\right) = D_y \rho_y + D_1 \rho_x \tag{3.30}$$

$$M_{xy} = \frac{G t^3}{12}\left(\frac{2\partial^2 w}{\partial x \partial y}\right) = D_{xy} \rho_{xy} \tag{3.31}$$

In which:

$$D_x = \frac{E_x t^3}{12(1-\nu_y \nu_x)} \qquad\qquad D_y = \frac{E_y t^3}{12(1-\nu_y \nu_x)} \tag{3.32}$$

$$D_1 = \nu_x D_y = \nu_y D_x \qquad\qquad D_{xy} = \frac{G t^3}{12}$$

Writing these relationships in Matrix format

$$\{\sigma_{Fm}\} = [D_F]\{\in_{Fm}\} \tag{3.33}$$

where:

$\{\sigma_{Fm}\}$ is the flexural stress vector:
$$\{\sigma_{Fm}\} = \begin{bmatrix} M_x & M_y & M_{xy} \end{bmatrix}^T$$

$\{\in_{Fm}\}$ is the flexural strain vector:
$$\{\in_{Fm}\} = \begin{bmatrix} \rho_x & \rho_y & \rho_{xy} \end{bmatrix}^T$$

$[D_F]$ is the property matrix of flexural displacement of a strip, given in Appendix A of the thesis

3.5.5. Strain of a strip

The second derivative of *w* by *x*

$$\frac{-\partial^2 w}{\partial x^2} = \begin{bmatrix} -X_{1m}^{"} & -\overline{y}X_{1m}^{"} & -\overline{y}^2 X_{1m}^{"} & -\overline{y}^3 X_{1m}^{"} \end{bmatrix} \begin{Bmatrix} \alpha_{1Fm} \\ \alpha_{2Fm} \\ \alpha_{3Fm} \\ \alpha_{4Fm} \end{Bmatrix} \qquad (3.34)$$

The second derivative of *w* by *y*

$$\frac{-\partial^2 w}{\partial y^2} = \begin{bmatrix} 0 & 0 & -\dfrac{2}{b^2} X_{1m} & -\dfrac{6\overline{y}}{b^2} X_{1m} \end{bmatrix} \begin{Bmatrix} \alpha_{1Fm} \\ \alpha_{2Fm} \\ \alpha_{3Fm} \\ \alpha_{4Fm} \end{Bmatrix} \qquad (3.35)$$

The second derivative of *w* by both *x* and *y*

$$2\frac{\partial^2 w}{\partial x \partial y} = \begin{bmatrix} 0 & \dfrac{2}{b} X_{1m}^{'} & \dfrac{4\overline{y}}{b} X_{1m}^{'} & \dfrac{6\overline{y}^2}{b} X_{1m}^{'} \end{bmatrix} \begin{Bmatrix} \alpha_{1Fm} \\ \alpha_{2Fm} \\ \alpha_{3Fm} \\ \alpha_{4Fm} \end{Bmatrix} \qquad (3.36)$$

The strain of a strip

$$\{\in_{Fm}\} = \begin{Bmatrix} \rho_x \\ \rho_y \\ \rho_{xy} \end{Bmatrix} = \begin{bmatrix} B_{Fm} \end{bmatrix} \{\alpha_{Fm}\} \qquad (3.37)$$

where $[B_{Fm}]$ is the strain matrix of flexural displacement, given in Appendix A of the thesis

3.5.6. The flexural strain energy in a strip

The energy of a strip because of loads (bending and twisting) as described in [15] and [12] is given by:

$$U_F = \frac{1}{2} \int_0^L \int_0^b \left(-M_x \frac{\partial^2 w}{\partial x^2} - M_y \frac{\partial^2 w}{\partial y^2} + 2M_{xy} \frac{\partial^2 w}{\partial x \partial y} \right) dy dx \qquad (3.38)$$

$$\Rightarrow U_F = \frac{1}{2} \int_0^L \int_0^b \{\sigma_{Fm}\}^T \{\in_{Fm}\} dy dx \qquad (3.39)$$

For orthogonal plate with *m* and *n* series terms and the summation of strain energy is given:

$$U_F = \frac{1}{2} \int\limits_0^L \int\limits_0^b \sum_{m=1}^{\mu} \sum_{n=1}^{\mu} \{\sigma_{Fm}\}^T \{\in_{Fn}\} \, dy dx \tag{3.40}$$

Replacement Eqs.(3.33) and (3.37) to Eq.(3.40):

$$U_F = \frac{1}{2} \int\limits_o^L \int\limits_o^b \sum_{m=1}^{\mu} \sum_{n=1}^{\mu} \{\alpha_{Fm}\}^T [B_{Fm}]^T [D_F][B_{Fn}]\{\alpha_{Fn}\} \, dy dx \tag{3.41}$$

This equation can be rewritten in other variables as:

$$U_F = \frac{1}{2} \left(\frac{bL}{\pi} \right) \int\limits_o^{\xi} \int\limits_o^{\bar{y}} \sum_{m=1}^{\mu} \sum_{n=1}^{\mu} \{\alpha_{Fm}\}^T [B_{Fm}]^T [D_F][B_{Fn}]\{\alpha_{Fn}\} \, d\bar{y} d\xi \tag{3.42}$$

where:

$$\{\alpha_{Fm}\} = [C_F]^{-1} \{\delta_{Fm}\}$$

$$\xi = \frac{\pi x}{L}, \ \xi = 0 \rightarrow \pi \text{ when } x = 0 \rightarrow L$$

$$\bar{y} = \frac{y}{b}, \ \bar{y} = 0 \rightarrow 1 \text{ when } y = 0 \rightarrow b$$

{σ_{Fn}} is the flexural displacement vector of a strip

$$\{\delta_{Fn}\} = \begin{bmatrix} w_{1n} & \theta_{x1n} & w_{2n} & \theta_{x2n} \end{bmatrix}^T$$

[C_F] is the evaluation matrix of the flexural displacement functions at the nodal lines, given in Appendix A of the thesis.

Eq.(3.42) can be rewritten as:

$$U_F = \frac{1}{2} \left(\frac{bL}{\pi} \right) \int\limits_o^{\xi} \int\limits_o^{\bar{y}} \sum_{m=1}^{\mu} \sum_{n=1}^{\mu} \{\delta_{Fm}\}^T [C_F]^{-T} [B_{Fm}]^T [D_F][B_{Fn}][C_F]^{-1} \{\delta_{Fn}\} \, d\bar{y} d\xi \tag{3.43}$$

$$\Rightarrow \ U_F = \frac{1}{2} \{\delta_{Fm}\}^T [C_F]^{-T} \left[\left(\frac{bL}{\pi} \right) \int\limits_o^{\xi} \int\limits_o^{\bar{y}} \sum_{m=1}^{\mu} \sum_{n=1}^{\mu} [B_{Fm}]^T [D_F][B_{Fn}] \, d\bar{y} d\xi \right] [C_F]^{-1} \{\delta_{Fn}\} \tag{3.44}$$

3.5.7. The flexural stiffness matrix of a strip

The flexural strain energy from Eq.(3.44) can be written as given:

$$U_F = \{\delta_{Fm}\}^T [k_{Fmn}]\{\delta_{Fn}\} \tag{3.45}$$

where [k_{Fmn}] is the flexural stiffness matrix of a strip

$$[k_{Fmn}] = [C_F]^{-T}[k_{\alpha Fmn}][C_F]^{-1}$$ (3.46)

$$[k_{\alpha Fmn}] = \left[\left(\frac{bL}{\pi}\right)\int_o^\xi\int_o^{\bar{y}}\sum_{m=1}^\mu\sum_{n=1}^\mu[B_{Fm}]^T[D_F][B_{Fn}]d\bar{y}d\xi\right]$$ (3.47)

Matrix A

$$A = [D_F][B_{Fn}]$$ (3.48)

Matrix B

$$B = [B_{Fm}]^T[D_F][B_{Fn}]$$ (3.49)

Matrix C

$$C = \int_0^{\bar{y}=1}[B_{Fm}]^T[D_F][B_{Fn}]d\bar{y}$$ (3.50)

Matrix D

$$D = \int_0^{\xi=\pi}\int_0^{\bar{y}=1}[B_{Fm}]^T[D_F][B_{Fn}]d\bar{y}d\xi$$ (3.51)

$$\Rightarrow [k_{\alpha Fmn}] = \frac{A}{\pi}[D]$$ (3.52)

In which:

A is the area of a strip: *A=bL*

[$k_{\alpha Fmn}$] is the flexural stiffness matrix of a strip

The values of matrices *A,B,C* and *D* are shown in Appendix A of the thesis

3.6. THE MEMBRANE STIFFNESS MATRIX OF A STRIP

3.6.1. The membrane displacement functions

The membrane displacement function from Eqs.(3.4) and (3.5) can be rewritten in matrix format.

$$\{f_{Mm}\} = [M_{Mm}]\{\alpha_{Mm}\}$$ (3.53)

where:

$$\{f_{Mm}\} = [v \quad u]^T$$

$$[M_{Mm}] = \begin{bmatrix} X_{1m} & \bar{y}X_{1m} & 0 & 0 \\ 0 & 0 & X_{2m} & \bar{y}X_{2m} \end{bmatrix}$$

3.6.2. Membrane stresses and strains

Stress distribution
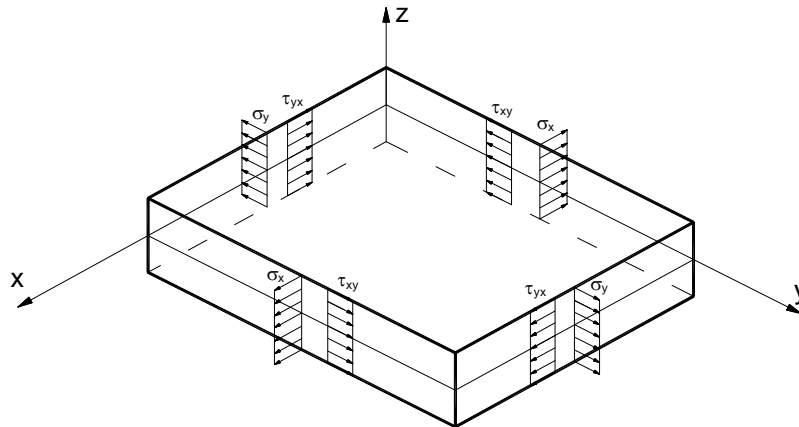
Figure 3.18: Stress distribution

Longitudinal strain
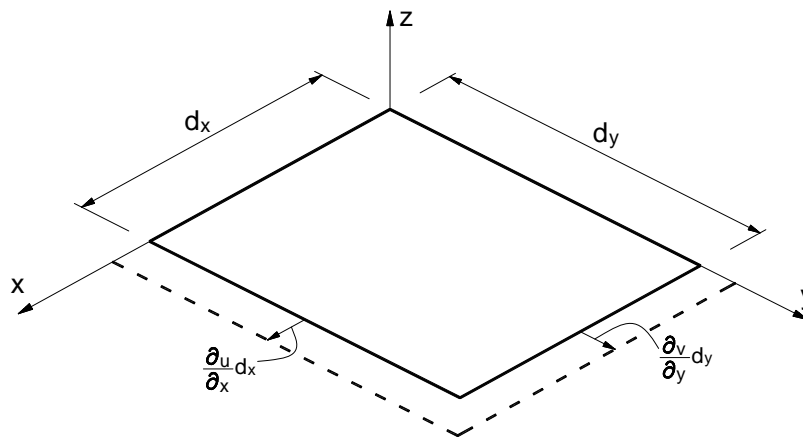
Figure 3.19: Longitudinal strain

Shear strain
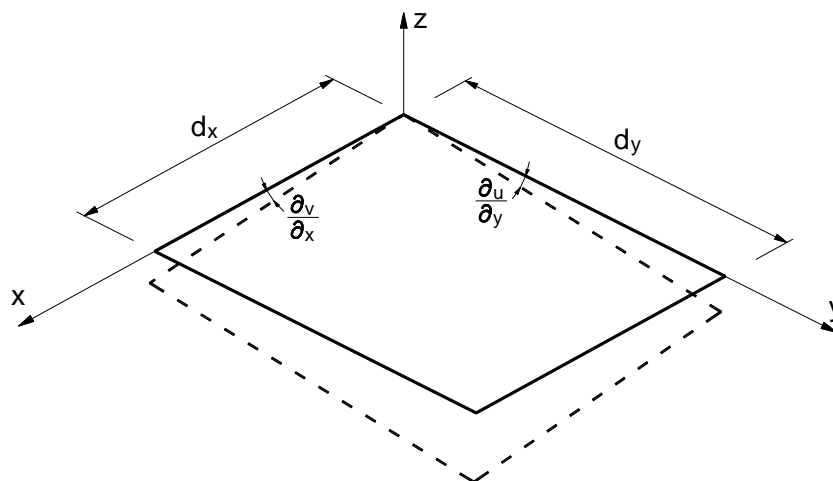
Figure 3.20: Shear strain

3.6.3. Membrane property matrix

The relationships between the flexural and torsional rigidity of a strip:

$$\sigma_x = \frac{E_x}{(1-\nu_y\nu_x)}\left(\frac{\partial u}{\partial x}+\nu_y\frac{\partial v}{\partial y}\right) = E_2\in_x +E_{12}\in_y \tag{3.54}$$

$$\sigma_y = \frac{E_y}{(1-\nu_y\nu_x)}\left(\frac{\partial v}{\partial y}+\nu_x\frac{\partial v}{\partial x}\right) = E_{12}\in_x +E_1\in_y \tag{3.55}$$

$$\tau_{xy} = G\left(\frac{\partial v}{\partial x}+\frac{\partial u}{\partial y}\right) = G\gamma_{xy} \tag{3.56}$$

where:

$$E_2 = \frac{E_x}{(1-\nu_y\nu_x)}\,; \qquad E_1 = \frac{E_y}{(1-\nu_y\nu_x)}\,;$$

$$E_{12} = \frac{\nu_x E_y}{(1-\nu_y\nu_x)} = \frac{\nu_y E_x}{(1-\nu_y\nu_x)} \tag{3.57}$$

Writing these relationships in Matrix format

$$\{\sigma_{Mm}\} = [D_M]\{\in_{Mm}\} \tag{3.58}$$

In which:

$\{\sigma_{Mm}\}$ is the stress vector

$$\{\sigma_{Mm}\} = \left\{\sigma_x \quad \sigma_y \quad \tau_{xy}\right\}^T$$

$\{\in_{Mm}\}$ is the strain vector

$$\{\in_{Mm}\} = \left\{\in_x \quad \in_y \quad \gamma_{xy}\right\}^T = \left\{\frac{\partial u}{\partial x} \quad \frac{\partial v}{\partial y} \quad \left(\frac{\partial v}{\partial x}+\frac{\partial u}{\partial y}\right)\right\}^T$$

$[D_M]$ is the property matrix of membrane displacement, given in Appendix A of the thesis

3.6.4. Strain of a strip

The first derivative u by x:

$$\frac{\partial u}{\partial x} = \begin{bmatrix} 0 & 0 & X'_{2m} & \overline{y}X'_{2m} \end{bmatrix} \begin{Bmatrix} \alpha_{1Mm} \\ \alpha_{2Mm} \\ \alpha_{3Mm} \\ \alpha_{4Mm} \end{Bmatrix} \tag{3.59}$$

The first derivative of v by y:

$$\frac{\partial v}{\partial y} = \begin{bmatrix} 0 & \frac{1}{b}X_{1m} & 0 & 0 \end{bmatrix} \begin{Bmatrix} \alpha_{1Mm} \\ \alpha_{2Mm} \\ \alpha_{3Mm} \\ \alpha_{4Mm} \end{Bmatrix} \tag{3.60}$$

The summation of the first derivatives:

The first derivative u by y:

$$\frac{\partial u}{\partial y} = 0 + \alpha_{4Mm}\frac{1}{b}X_{2m} \tag{3.61}$$

The first derivative v by x:

$$\frac{\partial v}{\partial x} = \alpha_{1Mm}X'_{1m} + \alpha_{2Mm}\overline{y}X'_{1m} \tag{3.62}$$

The summation:

$$\frac{\partial u}{\partial y} + \frac{\partial v}{\partial x} = \alpha_{1Mm}X'_{1m} + \alpha_{2Mm}\overline{y}X'_{1m} + \alpha_{3Mm}0 + \alpha_{4Mm}\frac{1}{b}X_{2m}$$

$$\Rightarrow \quad \frac{\partial u}{\partial y} + \frac{\partial v}{\partial x} = \begin{bmatrix} X'_{1m} & \overline{y}X'_{1m} & 0 & \frac{1}{b}X_{2m} \end{bmatrix} \begin{Bmatrix} \alpha_{1Mm} \\ \alpha_{2Mm} \\ \alpha_{3Mm} \\ \alpha_{4Mm} \end{Bmatrix} \tag{3.63}$$

The strain of a strip:

$$\{\in_{Mm}\} = [B_{Mm}]\{\alpha_{Mm}\} \tag{3.64}$$

where $[B_{Mm}]$ is the strain matrix of membrane displacement, given in Appendix A of the thesis

3.6.5. Membrane strain energy in a strip

The membrane strain energy of a strip because of load as described in [15] and [12] is given by:

$$U_M = \frac{1}{2}\int_0^L\int_0^b\left(\sigma_x\in_x + \sigma_y\in_y + \tau_{xy}\gamma_{xy}\right)tdydx$$

$$= \frac{1}{2}\int_0^L\int_0^b\begin{Bmatrix}\sigma_x & \sigma_y & \tau_{xy}\end{Bmatrix}\begin{Bmatrix}\in_x \\ \in_y \\ \gamma_{xy}\end{Bmatrix}tdydx = \frac{1}{2}\int_0^L\int_0^b\{\sigma_M\}^T\{\in_M\}tdydx \tag{3.65}$$

The m and n terms must be introduced and the summation taken over the m and n, hence

$$U_M = \frac{1}{2}\int_0^L\int_0^b\sum_{m=1}^\mu\sum_{n=1}^\mu\{\sigma_{Mm}\}^T\{\in_{Mn}\}tdydx \tag{3.66}$$

Substituting Eqs.(3.58) and (3.64) into Eq.(3.66):

$$U_M = \frac{1}{2} \int_0^L \int_0^b \sum_{m=1}^{\mu} \sum_{n=1}^{\mu} \{\alpha_{Mm}\}^T [B_{Mm}]^T [D_M][B_{Mn}]\{\alpha_{Mn}\} t \, dy \, dx \tag{3.67}$$

This equation can be rewritten in other variables as:

$$U_M = \frac{1}{2}\left(\frac{bLt}{\pi}\right) \int_0^{\xi=\pi} \int_0^{\bar{y}=1} \sum_{m=1}^{\mu} \sum_{n=1}^{\mu} \{\alpha_{Mm}\}^T [B_{Mm}]^T [D_M][B_{Mn}]\{\alpha_{Mn}\} \, d\bar{y} \, d\xi \tag{3.68}$$

Eq.(3.68) can be rewritten as:

$$U_M = \frac{1}{2}\left(\frac{bLt}{\pi}\right) \int_0^{\xi=\pi} \int_0^{\bar{y}=1} \sum_{m=1}^{\mu} \sum_{n=1}^{\mu} \{\delta_{Mm}\}^T [C_M]^{-T} [B_{Mm}]^T [D_M][B_{Mn}][C_M]^{-1}\{\delta_{Mn}\} \, d\bar{y} \, d\xi \tag{3.69}$$

$$U_M = \frac{1}{2}\{\delta_{Mm}\}^T [C_M]^{-T} \left[\left(\frac{bLt}{\pi}\right) \int_0^{\xi=\pi} \int_0^{\bar{y}=1} \sum_{m=1}^{\mu} \sum_{n=1}^{\mu} [B_{Mm}]^T [D_M][B_{Mn}] \, d\bar{y}\xi\right] [C_M]^{-1}\{\delta_{Mn}\} \tag{3.70}$$

where:

$$\{\alpha_{Mm}\} = [C_M]^{-1}\{\delta_{Mm}\}$$

$\{\delta_{Mn}\}$ is the vector of membrane displacement, $\{\delta_{Mn}\} = \begin{bmatrix} u_{1n} & v_{1n} & u_{2n} & v_{2n} \end{bmatrix}^T$

$[C_M]$ is the evaluation matrix of the membrane displacement functions at nodal line, given in Appendix A of the thesis

3.6.6. The membrane stiffness matrix of a strip

The membrane strain energy from Eq.(3.70) can be written as given:

$$U_M = \{\delta_{Mn}\}^T [k_{Mmn}]\{\delta_{Mn}\} \tag{3.71}$$

where $[k_{Mmn}]$ is the membrane stiffness matrix of a strip

$$[k_{Mmn}] = [C_M]^{-T}[k_{\alpha Mmn}][C_M]^{-1} \tag{3.72}$$

$$[k_{\alpha Mm}] = \left[\left(\frac{bLt}{\pi}\right) \int_0^{\xi=\pi} \int_0^{\bar{y}=1} \sum_{m=1}^{\mu} \sum_{n=1}^{\mu} [B_{Mm}]^T [D_M][B_{Mn}] \, d\bar{y} \, d\xi\right] \tag{3.73}$$

Matrix M:

$$M = [D_M][B_{Mn}] \tag{3.74}$$

Matrix N:

$$N = [B_{Mm}]^T [D_M][B_{Mn}] \tag{3.75}$$

Matrix P:

$$P = \int\limits_{0}^{\overline{y}=1} \left[B_{Mm}\right]^{T} \left[D_{M}\right] \left[B_{Mn}\right] d\overline{y} \tag{3.76}$$

Matrix Q:

$$Q = \int\limits_{0}^{\xi=\pi} \int\limits_{0}^{\overline{y}=1} \left[B_{Mm}\right]^{T} \left[D_{M}\right] \left[B_{Mn}\right] d\overline{y}d\xi \tag{3.77}$$

$$\Rightarrow \quad \left[k_{\alpha Mmn}\right] = \frac{V}{\pi}\left[Q\right] \tag{3.78}$$

In which:

V is the volume of strip, *V=bLt*

[$k_{\alpha Mmn}$] is the membrane stiffness matrix of a strip

The values of matrices *M,N,P* and *Q* are shown in Appendix A of the thesis

3.7. TRANSFORMATION FROM LOCAL TO GLOBAL COORDINATES

Each member has its own local axis system with the y and z axes lie in the plane of the cross-sections, while the x axis is along the member. The axes were chosen to align with Timoshenko and Gere [46] for plate buckling. However, the global axis system used in the finite strip analysis has been chosen to conform with that normally chosen in structural analysis of thin-walled members. The X and Y axes lie in the plane of the cross-section, while the Z axis is located along the member (along the strips) as shown in Fig.3.21.
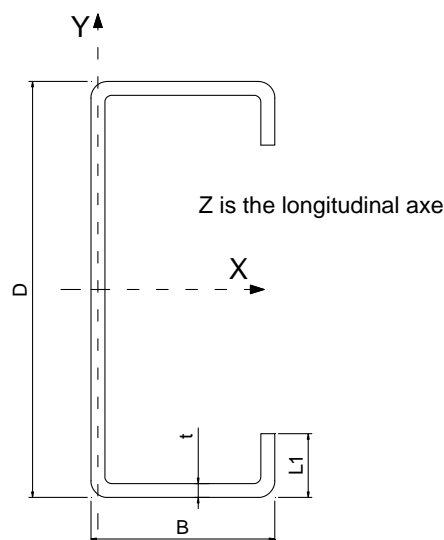
Figure 3.21: Global coordinate for the Finite strip method

The global and local displacements are shown in Fig.3.22
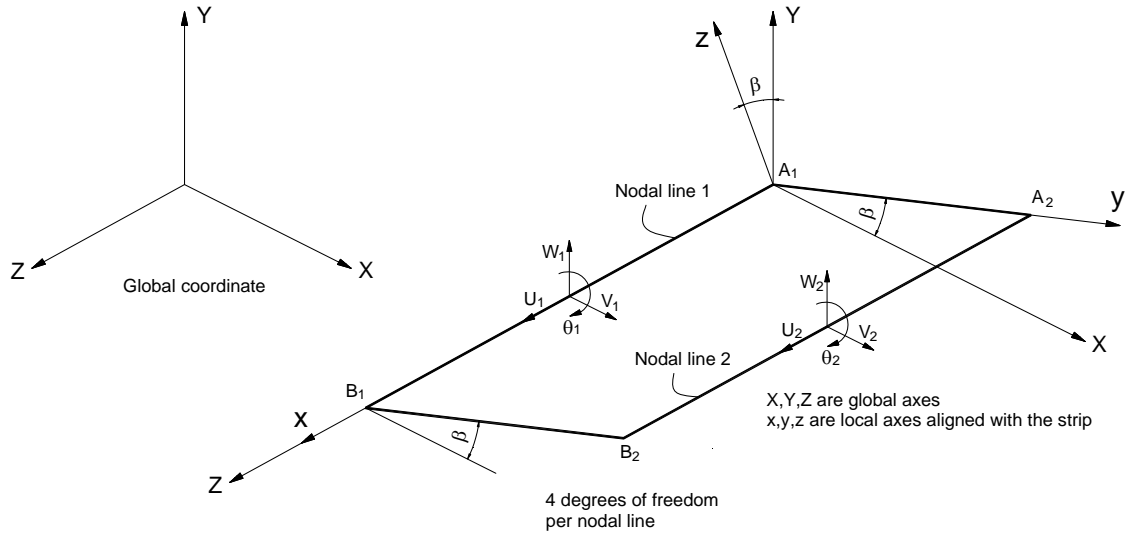
Figure 3.22: Global and local displacements

Load vector of plate with two nodal lines in the local coordinate:

$$\{f_m\} = [C]^{-T}\{\alpha_m\} \tag{3.79}$$

where:

$\{f_m\}$ is the vector of a strip displacement in local axes

$$\{f_m\} = \left\{ F_{x1m} \quad F_{y1m} \quad F_{z1m} \quad M_{z1m} \quad F_{x2m} \quad F_{y2m} \quad F_{z2m} \quad M_{z2m} \right\}^T$$

$\{\alpha_m\}$ is the vector of polynomial coefficients.

$$\{\alpha_{Fm}\} = \left[\alpha_{1Fm} \quad \alpha_{2Fm} \quad \alpha_{3Fm} \quad \alpha_{4Fm} \quad \alpha_{1Mm} \quad \alpha_{2Mm} \quad \alpha_{3Mm} \quad \alpha_{4Mm} \right]^T$$

$[C]^{-T}$ is the transformation matrix, given in Appendix A of the thesis

Changing load vector from the local coordinate to the global coordinate:

$$\{F_m\} = [R]\{f_m\} \tag{3.80}$$

where:

$\{F_m\}$ is the load vector of a strip in global axes

$$\{F_m\} = \left\{ F_{X1m} \quad F_{Y1m} \quad F_{Z1m} \quad M_{Z1m} \quad F_{X2m} \quad F_{Y2m} \quad F_{Z2m} \quad M_{Z2m} \right\}^T$$

$[R]$ is the rotation matrix, given in Appendix A of the thesis

3.8. THE STIFFNESS MATRIX OF THE SECTION

The stiffness matrix of a strip in the local coordinate system is assembled from both the flexural stiffness matrix and the membrane stiffness matrix, thus the stiffness matrix [K_L] is an 8x8 size matrix.

$$\left[K_L \right] = \begin{bmatrix} \left[k_{\alpha Fmn} \right] & 0 \\ 0 & \left[k_{\alpha Mmn} \right] \end{bmatrix} \tag{3.81}$$

where [K_L] is the local stiffness matrix of a strip

The stiffness matrix of a strip in the global coordinate is determined by a multiplication of the stiffness matrix in the local coordinate with transformation matrices as given:

$$\left[K_G \right] = \left[A \right] \left[K_L \right] \left[A \right]^T \tag{3.82}$$

where:

[K_G] is the stiffness matrix in the global coordinate,

[A] and [A]^T are transformation matrices from local to global coordinates, given in Appendix A of the thesis.

The relationship between the load vector and the displacement vector is given by:

$$\left\{ W_m \right\} = \left[K_G \right] \left\{ \delta_n \right\} \tag{3.83}$$

$$\begin{bmatrix} \left\{ W_{1m} \right\} \\ \left\{ W_{2m} \right\} \end{bmatrix} = \begin{bmatrix} \left[K_{ppmn} \right] & \left[K_{pqmn} \right] \\ \left[K_{qpmn} \right] & \left[K_{qqmn} \right] \end{bmatrix} \begin{bmatrix} \left\{ \delta_{1n} \right\} \\ \left\{ \delta_{2n} \right\} \end{bmatrix} \tag{3.84}$$

It means that:

$$\left[K_G \right] = \begin{bmatrix} \left[K_{ppmn} \right] & \left[K_{pqmn} \right] \\ \left[K_{qpmn} \right] & \left[K_{qqmn} \right] \end{bmatrix}$$

where:

p, q are the start node and end node of a strip

{W_{1m}} and {W_{2m}} are the load vectors of the start node and the end node of a strip

$$\left\{ W_{1m} \right\} = \left\{ W_{X1m} \quad W_{Y1m} \quad W_{Z1m} \quad W_{M1m} \right\}^T$$

$$\left\{ W_{2m} \right\} = \left\{ W_{X2m} \quad W_{Y2m} \quad W_{Z2m} \quad W_{M2m} \right\}^T$$

{δ_{1n}} and {δ_{2n}} are the displacement vectors of the start node and the end node of a strip

$$\left\{ \delta_{1n} \right\} = \left\{ \delta_{X1n} \quad \delta_{Y1n} \quad \delta_{Z1n} \quad \theta_{Z1n} \right\}^T$$

$$\left\{ \delta_{2n} \right\} = \left\{ \delta_{X2n} \quad \delta_{Y2n} \quad \delta_{Z2n} \quad \theta_{Z2n} \right\}^T$$

$[K_{ppmn}]$, $[K_{pqmn}]$, $[K_{qpmn}]$ and $[K_{qqmn}]$ are four components of the stiffness matrix of a strip in the global coordinate

The stiffness matrix of the section for each mode is assembled from the stiffness matrices of nodes in strips, thus the size of this matrix is 4 times the number of nodes. The stiffness matrix at each point of this matrix is determined by doing the summation of stiffness matrix components of strips which have the same node. The stiffness matrix of the whole section is assembled from the stiffness matrices of series terms as shown in Fig.3.23, thus the size of this matrix is 4 times the number of series terms and the number of nodes.

$$r = 4 \times \mu \times n$$

where:

r is the size of the stiffness matrix $[K]$

μ is the number of series terms

n is the number of nodes of the section
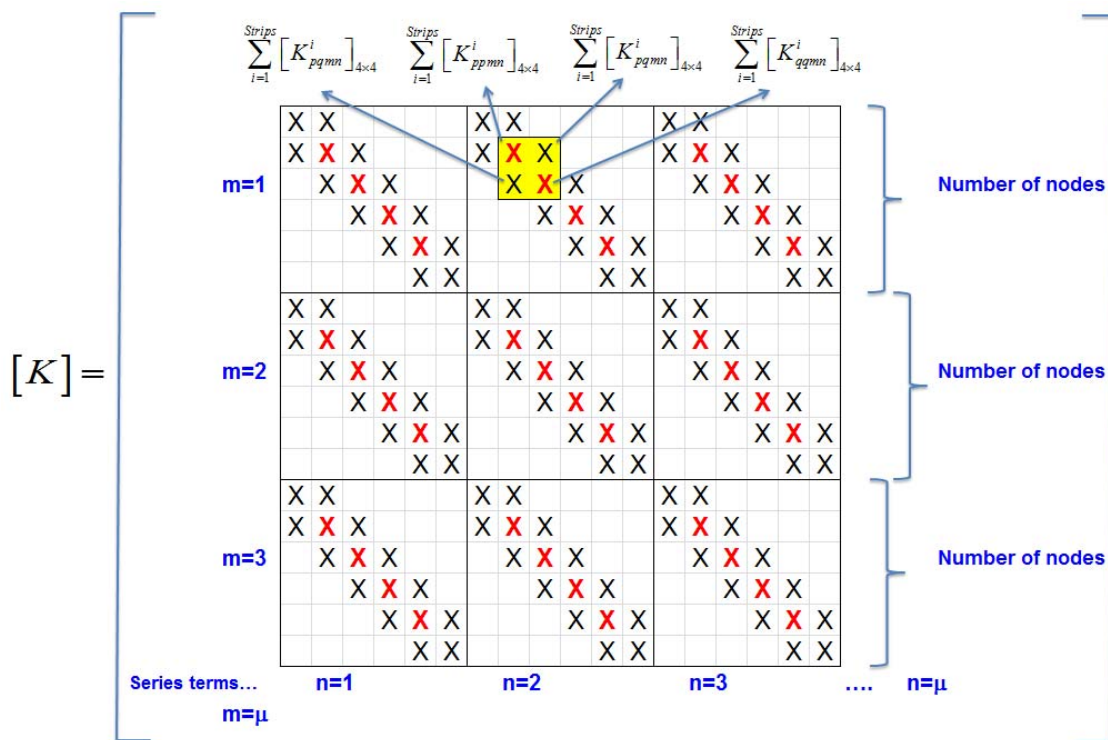
Figure 3.23: Stiffness matrix for whole section

3.9. LOAD VECTOR

The localised load applied on the structural member is assumed to be a line load along a nodal line as shown in the Fig.3.24. The loads may be applied in different directions and at any position along the structural member.
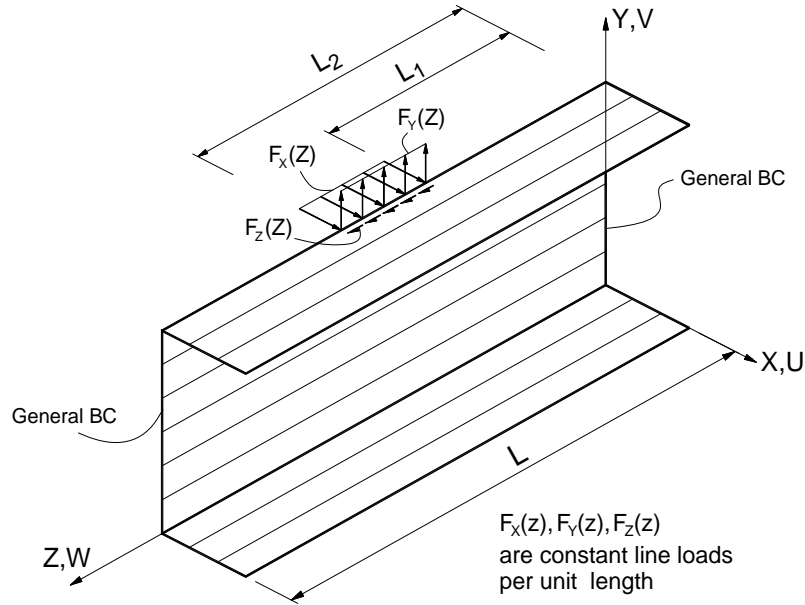
Figure 3.24: Localised loading applied on a strip

The deformation of the nodal line U,V,W in X,Y,Z directions is given by:

$$U = U_{1m}X_{1m}(Z)$$
$$V = V_{1m}X_{1m}(Z)$$
$$W = W_{1m}X_{2m}(Z)$$

(3.85)

where:

$X_{1m}(Z)$ is the longitudinal variation curve for the transverse deformation (U,V)

$X_{2m}(Z)$ is the longitudinal variation curve for the longitudinal deformation (W)

U_{1m}, V_{1m}, W_{1m}, are amplitude deformations of the loaded nodal line for the mth series term

The load vector for nodal line j can be derived for the potential energy of the external forces as given in Eq.(3.90):

$$\left\{ F_m^j \right\} = \left\{ F_{Xm} \quad F_{Ym} \quad F_{Zm} \quad F_{Mm} \right\}^T$$

(3.86)

In which

$$F_{Xm} = \int_{L_1}^{L_2} F_X(Z)X_{1m}(Z)dZ \; ; \; F_{Ym} = \int_{L_1}^{L_2} F_Y(Z)X_{1m}(Z)dZ$$

(3.87)

$$F_{Zm} = \int_{L_1}^{L_2} F_Z(Z)X_{2m}(Z)dZ$$

The load vector for each series term is assembled from the load vectors of nodal lines, thus the size of this vector is 4 times the number of nodes. The load vector of whole section is assembled from the load vectors of series terms as shown in Fig.3.25, thus the size of this vector is 4 times the number of series terms and the number of nodes.
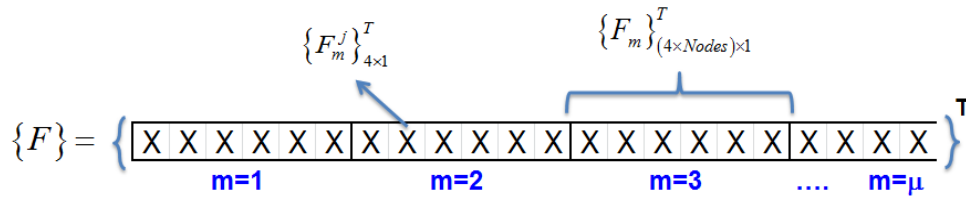
Figure 3.25: Load vector of whole section

where:

L_1 and L_2 are the starting and ending points of the line loads respectively as shown in Fig.3.24

$F_X(Z)$, $F_Y(Z)$, $F_Z(Z)$ are the distributed lines load in the X,Y,Z directions. These loads may be constant or vary with Z

F_{Xm}, F_{Ym}, F_{Zm} are the X,Y,Z components of the load vector for each nodal line for the mth series terms.

$\{F^j_m\}$ is the load vectors for of nodal line j at the series term m^{th}

$\{F_m\}$ is the load vectors for of the section at the series term m^{th}

$\{F\}$ is the load vectors for of the whole section

3.10. PRE-BUCKLING ANALYSIS

3.10.1. Minimization of the potential energy

The strain energy of a strip is given by:

$$U = U_F + U_M$$

(3.88)

In matrix format:

$$U = \{\delta_p\}^T [K]\{\delta_p\}$$

(3.89)

where $\{\delta_p\}$ is the pre-buckling displacement of the section, called pre-buckling modes

The potential energy due to the external forces can be written as:

$$V = -\left\{\delta_p\right\}^T \left\{F\right\}$$

(3.90)

where $\{F\}$ is the load vector of the whole section as given in Section 3.9

The total potential energy is the sum of the elastic strain energy stored in a strip and the potential energy of the external loads, thus:

$$\phi = U + V$$

(3.91)

$$\phi = \left\{\delta_p\right\}^T \left[K\right]\left\{\delta_p\right\} - \left\{\delta_p\right\}^T \left\{F\right\}$$

(3.92)

The principle of minimum total potential energy requires that:

$$\left\{\frac{\partial \phi}{\partial \left\{\delta_p\right\}}\right\} = \left\{0\right\}$$

(3.93)

Hence:

$$\left[K\right]\left\{\delta_p\right\} - \left\{F\right\} = \left\{0\right\}$$

(3.94)

$$\left[K\right]\left\{\delta_p\right\} = \left\{F\right\}$$

(3.95)

3.10.2. The pre-buckling displacements

The relationship among the load vector, the displacement vector and the stiffness matrix from Eq.(3.95) is rewritten by:

$$\left\{\delta_{pA}\right\} = \left[K\right]^{-1}\left\{F\right\}$$

(3.96)

where $\{\delta_{pA}\}$ is the amplitude of the displacement vector for the whole section

The vector $\{\delta_{pA}\}$ has the same size with the load vector $\{F\}$ as shown in Fig.3.26. It means that the size of this vector is 4 times the number of series terms and the number of nodes.
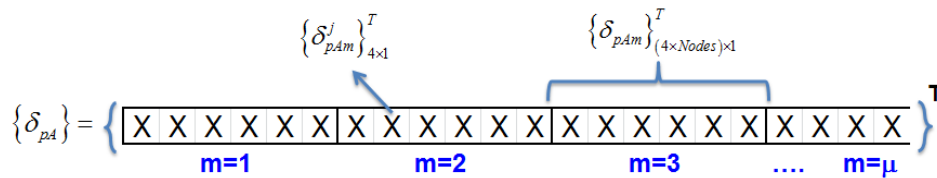
Figure 3.26: Amplitude of displacement vector

The displacement vector $\{\delta_{pA}\}$ is splitted up to the displacement vectors for each mode $\{\delta_{pAm}\}$ and the displacement vectors for each nodal line $\{\delta^j_{pAm}\}$

$$\left\{\delta^j_{pAm}\right\} = \left\{\delta^j_{pAXm} \quad \delta^j_{pAYm} \quad \delta^j_{pAZm} \quad \theta^j_{pAZm}\right\}^T$$

where:

j is the nodal line

$\{\delta_{pAm}\}$ is the amplitude of the displacement vector for mode m

$\{\delta^j_{pAm}\}$ is the amplitude of the displacement vector of nodal line j, mode m

The amplitudes of the pre-buckling displacements are multiplied with the displacement functions to get the pre-buckling deformations for all sections along the structural member.

$$\delta^j_{pXm} = \delta^j_{pAXm} X_{1m}(x_{sec}); \quad \delta^j_{pYm} = \delta^j_{pAYm} X_{1m}(x_{sec})$$

$$\delta^j_{pZm} = \delta^j_{pAZm} X_{2m}(x_{sec}); \quad \theta^j_{pZm} = \theta^j_{pAZm} X_{1m}(x_{sec})$$

(3.97)

where:

δ^j_{pAXm}, δ^j_{pAYm}, δ^j_{pAZm}, θ^j_{pAZm} are the amplitudes of displacement of nodal line j, mode m

δ^j_{pXm}, δ^j_{pYm}, δ^j_{pZm}, θ^j_{pZm} are the displacements of node j, mode m

x_{sec} is the location of sections along the beam

The displacement of nodes along the beam is determined by doing the summation of the displacement in all series terms.

$$\delta^j_{pX} = \sum_{m=1}^{\mu} \delta^j_{pXm} \,; \; \delta^j_{pY} = \sum_{m=1}^{\mu} \delta^j_{pYm}$$

(3.98)

$$\delta^j_{pX} = \sum_{m=1}^{\mu} \delta^j_{pZm} \,; \; \theta^j_Z = \sum_{m=1}^{\mu} \theta^j_{Zm}$$

(3.99)

where δ^j_{pX}, δ^j_{pY}, δ^j_{pZ}, θ^j_{pZ} are the displacements of node j

3.10.3. The polynomial coefficients

The relationship between the polynomial coefficients vector and the amplitude displacement vector of each strip in each mode is given by:

$$\left\{ \alpha^i_m \right\} = \left[A \right]^T \left\{ \delta^i_{pAm} \right\}$$

(3.100)

where:

$\{\delta^i_{pAm}\}$ is the amplitude displacement vector of the strip i

$$\left\{ \delta^i_{pAm} \right\} = \left\{ \delta^{SN}_{pAXm} \quad \delta^{SN}_{pAYm} \quad \delta^{SN}_{pAZm} \quad \theta^{SN}_{pAZm} \quad \delta^{EN}_{pAXm} \quad \delta^{EN}_{pAYm} \quad \delta^{EN}_{pAZm} \quad \theta^{EN}_{pAZm} \right\}^T$$

i is the strip number

SN and EN are the start node and the end node of the strip i respectively

$\{\alpha^i_m\}$ is the polynomial coefficients vector of the strip *i* in the mode *m*

$$\left\{\alpha^i_m\right\} = \left\{\left\{\alpha^i_{Fm}\right\} \quad \left\{\alpha^i_{Mm}\right\}\right\} \tag{3.101}$$

In which

$$\left\{\alpha^i_{Fm}\right\}^T = \begin{bmatrix} \alpha^i_{1Fm} & \alpha^i_{2Fm} & \alpha^i_{3Fm} & \alpha^i_{4Fm} \end{bmatrix}^T \tag{3.102}$$

$$\left\{\alpha^i_{Mm}\right\}^T = \begin{bmatrix} \alpha^i_{1Mm} & \alpha^i_{2Mm} & \alpha^i_{3Mm} & \alpha^i_{4Mm} \end{bmatrix}^T \tag{3.103}$$

3.10.4. The membrane stresses

The membrane stresses of a strip are given by:

$$\{\sigma_{Mm}\} = [D_M]\{\in_{Mm}\} \tag{3.104}$$

where $\{\in_{Mm}\}$ is the membrane strain vector:

$$\{\in_{Mm}\} = [B_{Mm}]\{\alpha_{Mm}\} \tag{3.105}$$

Hence:

$$\{\sigma_{Mm}\} = [D_M][B_{Mm}]\{\alpha_{Mm}\} \tag{3.106}$$

$$\Rightarrow \quad \{\sigma_{Mm}\} = \begin{Bmatrix} \sigma_x \\ \sigma_y \\ \tau_{xy} \end{Bmatrix} = \begin{bmatrix} 0 & \dfrac{E_{12}}{b}X_{1m} & E_2 X'_{2m} & E_2 \bar{y} X'_{2m} \\ 0 & \dfrac{E_1}{b}X_{1m} & E_{12}X'_{2m} & E_{12}\bar{y}X'_{2m} \\ GX'_{1m} & G\bar{y}X'_{1m} & 0 & \dfrac{G}{b}X_{2m} \end{bmatrix} \begin{Bmatrix} \alpha_{1Mm} \\ \alpha_{2Mm} \\ \alpha_{3Mm} \\ \alpha_{4Mm} \end{Bmatrix} \tag{3.107}$$

Evaluation of the membrane stresses at nodal line of each strip:

At nodal line 1: $\bar{y} = \dfrac{y}{b} = 0$

$$\{\sigma_{Mm}\} = \begin{Bmatrix} \sigma_x \\ \sigma_y \\ \tau_{xy} \end{Bmatrix} = \begin{bmatrix} 0 & \dfrac{E_{12}}{b}X_{1m} & E_2 X'_{2m} & 0 \\ 0 & \dfrac{E_1}{b}X_{1m} & E_{12}X'_{2m} & 0 \\ GX'_{1m} & 0 & 0 & \dfrac{G}{b}X_{2m} \end{bmatrix} \begin{Bmatrix} \alpha_{1Mm} \\ \alpha_{2Mm} \\ \alpha_{3Mm} \\ \alpha_{4Mm} \end{Bmatrix} \tag{3.108}$$

At nodal line 2: $\bar{y} = \dfrac{y}{b} = 1$

$$\{\sigma_{Mm}\} = \begin{Bmatrix} \sigma_x \\ \sigma_y \\ \tau_{xy} \end{Bmatrix} = \begin{bmatrix} 0 & \dfrac{E_{12}}{b}X_{1m} & E_2 X_{2m}^{'} & E_2 X_{2m}^{'} \\ 0 & \dfrac{E_1}{b}X_{1m} & E_{12}X_{2m}^{'} & E_{12}X_{2m}^{'} \\ GX_{1m}^{'} & GX_{1m}^{'} & 0 & \dfrac{G}{b}X_{2m} \end{bmatrix} \begin{Bmatrix} \alpha_{1Mm} \\ \alpha_{2Mm} \\ \alpha_{3Mm} \\ \alpha_{4Mm} \end{Bmatrix} \qquad (3.109)$$

The summation can be taken over the m series terms at any longitudinal position to get the membrane stresses for all sections:

$$\{\sigma_M\} = \sum_{m=1}^{\mu} \{\sigma_{Mm}\} \qquad (3.110)$$

3.11. NUMERICAL EXAMPLE

A pre-buckling analysis has been performed for a lipped channel section with rounded corners under localised loading using the THIN-WALL-2 V2.0 program. The geometry of the beam and the loading are shown in Fig.3.27. The beam is analysed with different boundary conditions for the web and the flanges of the end sections. In addition, lateral restraints are applied along the beam at Nodal Lines 11 and 35 to avoid twisting caused by eccentric loading. In the Simply-Free (SF) and Free-Free (FF) cases, the beam can deform freely in the longitudinal direction, thus longitudinal restraints are applied at Nodal Lines 11 and 35 along the beam to prevent this movement. Furthermore, in the Free-Free (FF) case, the beam has no supports at both ends, thus vertical restraints are applied at Nodal Line 35 along the beam to prevent the movement of the beam in the vertical direction. The results from the pre-buckling analysis of the beam under localised loading include deformations and stresses. The stress and deformation values are obtained from Nodal Line 23 in the middle of the section for all sections along the beam.

The beam has been also analysed using a pre-buckling analysis by ABAQUS with equivalent loading and boundary conditions. It was meshed into 5mm x 5mm, except at the section's corners. The corners were modeled with 1mm x 5mm mesh to accurately represent the influence of corner radius. The stress and deformation values are obtained from a group of nodes at the same positions as the nodal lines from THIN-WALL-2.
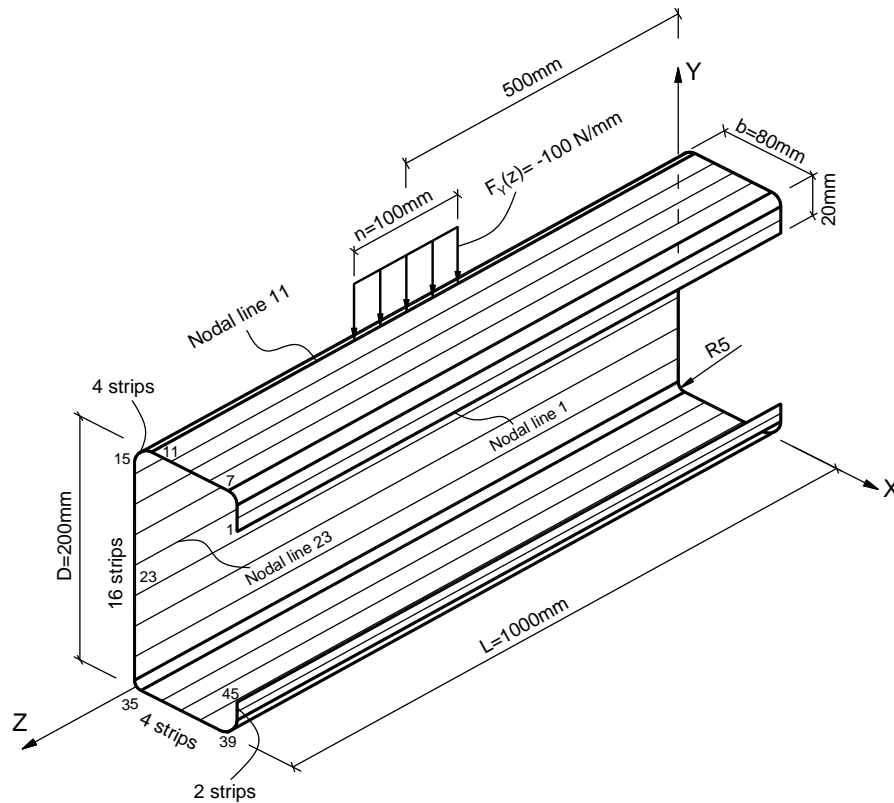
Figure 3.27: Lipped channel section under localised loading

The beam is subdivided into 21 equally spaced sections to calculate and plot the deformations and stresses along the beam. The comparison between the stresses and deformations from the FSM and the FEM are shown in Figs.3.28 to 3.34 for the Clamped - Free (CF) case which uses the Bradford and Azhari [16] displacement functions. The results for other boundary conditions are shown in Figs.B-1 to B-35 in Appendix B of the thesis. The comparisons demonstrate the accuracy of the FSM when 25 series terms are used particularly for the transverse and shear stresses. There is a small difference in the local peak of the longitudinal stress at the center in some cases but this is unlikely to have an effect on the elastic buckling analysis in Chapter 4. The only significant discrepancy appears to be the shear stresses in Fig.B-10. The shear forces resulting from these stresses are in equilibrium with the applied load but the different stress gradients in Fig.B-8 have resulted in the different shear stresses. To confirm these functions, the stiffness matrix has been evaluated both analytically and numerically. The alternative Bradford and Azhari functions [16] for this case show a greater discrepancy and therefore cannot be used as an alternative. Despite the discrepancy, the effect on the buckling loads in Chapter 4 is negligible.

Stress comparison:
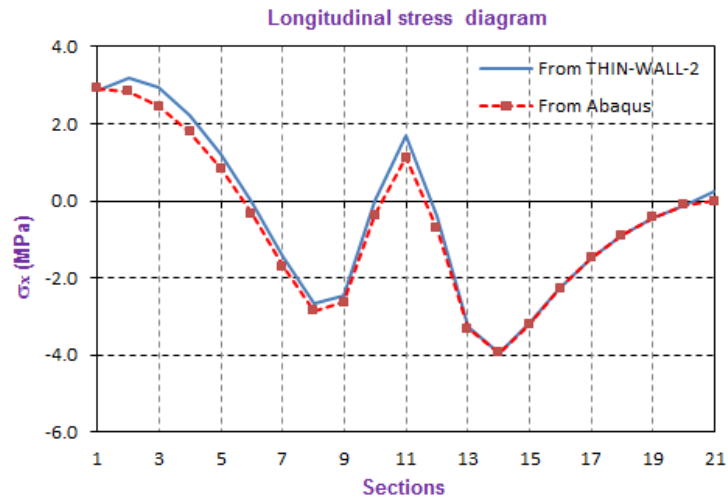
Figure 3.28: Longitudinal stress at Nodal Line 23 along the beam for the CF case
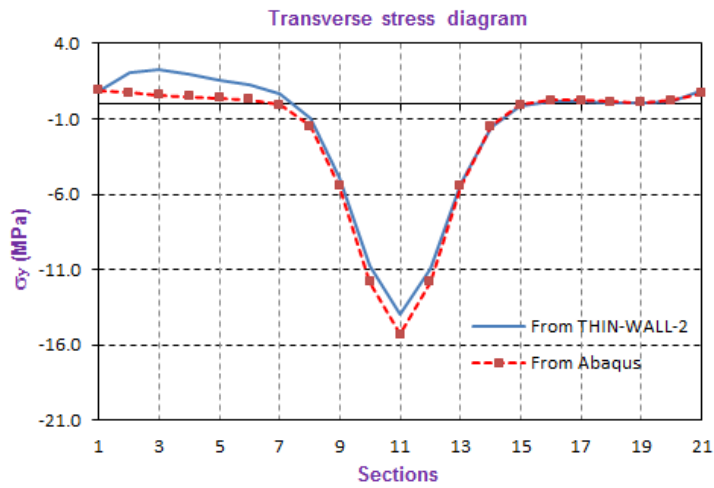
Figure 3.29: Transverse stress at Nodal Line 23 along the beam for the CF case
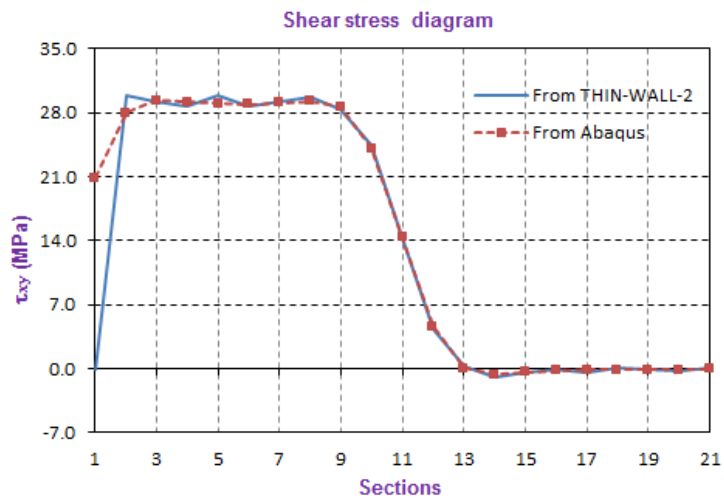
Figure 3.30: Shear stress at Nodal Line 23 along the beam for the CF case

Pre-buckling deformation comparison:

(a) From THIN-WALL-2   (b) From Abaqus
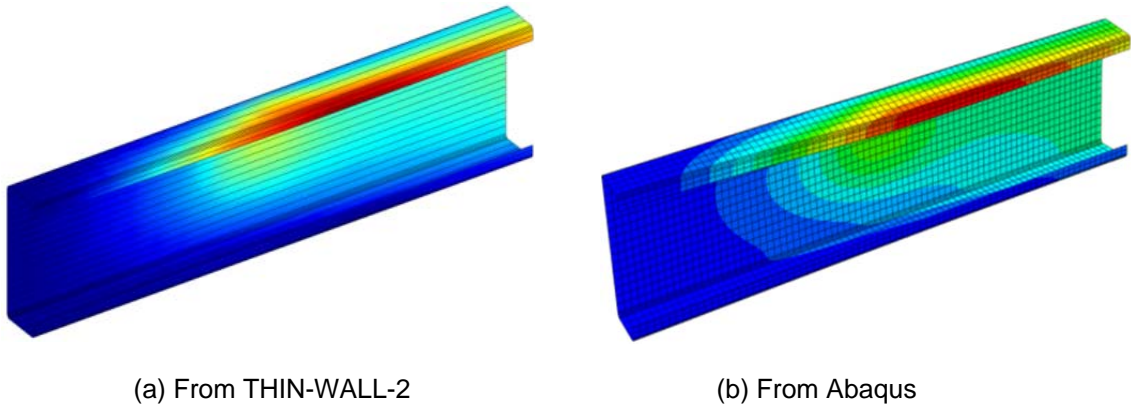
Figure 3.31: Pre-buckling deformation comparison for the CF case
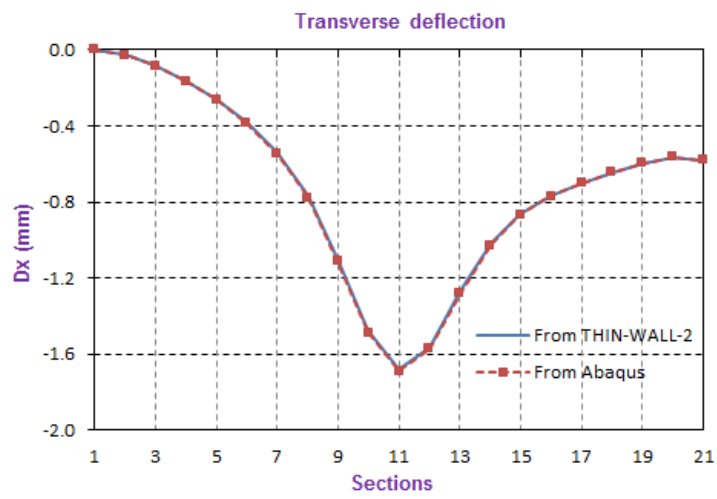
Figure 3.32: Transverse pre-buckling deformation at Nodal Line 23 along the beam for the CF case
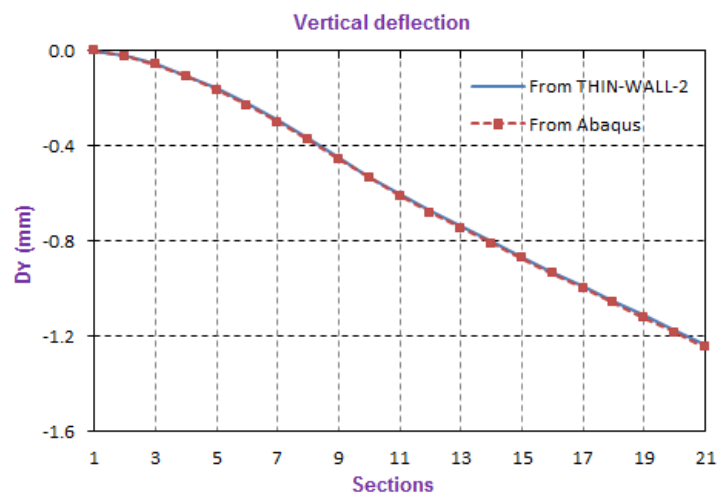
Figure 3.33: Vertical pre-buckling deformation at Nodal Line 23 along the beam for the CF case
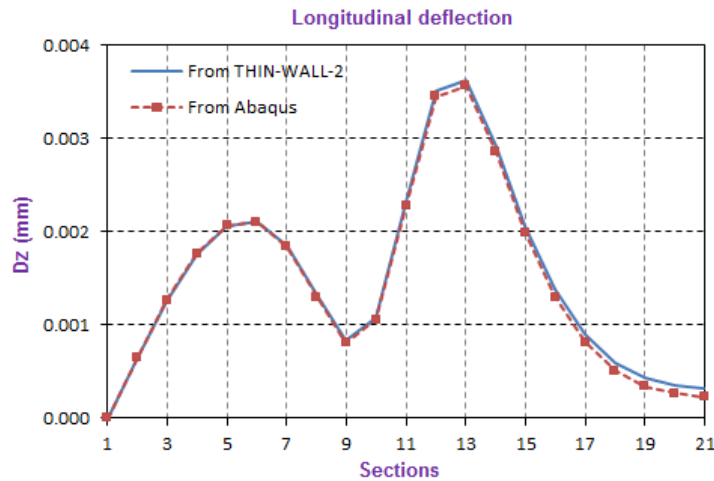
Figure 3.34: Longitudinal pre-buckling deformation at Nodal Line 23 along the beam for the CF case

3.12. CONVERGENCE STUDY

A study has been performed for the lipped channel section in Section 3.11 with different boundary conditions and different numbers of series terms to find the acceptable number of series terms for the pre-buckling analysis. The longitudinal and transverse stresses are obtained from Nodal Line 23, Section 11 at the middle of the beam, while the shear stresses are obtained from Nodal Line 23, Section 1 for the SS, SC, SF and CC cases and Section 9 for the CF and FF cases. The relationships between the longitudinal stress and the number of series terms are shown in Fig.3.35 for different boundary conditions. The solutions are converged for the longitudinal stress when the number of series terms reaches 25 as shown in Table 3.1. Similarly, the transverse stress and shear stress are converged when the number of series terms reaches 25 as given in Tables 3.2 and 3.3 and shown in Fig.3.36 and Fig.3.37. It means that about 25 series terms are required to get the converged stresses as well as deformations in the pre-buckling analysis for a localised load one tenth the length of the member.

Table 3.1: Convergence of longitudinal stress at Section 11 and Nodal Line 23

(L=1000mm, n=100mm)

Series terms (μ)	Longitudinal stress, σ_x (MPa)					
	SS	SC	SF	CC	CF	FF
3	-2.960	-2.459	-0.149	-1.806	-2.028	-1.084
5	-1.678	-1.181	1.410	-0.627	-1.029	1.587
7	-0.721	-0.249	2.787	0.235	0.327	2.797
9	-0.181	0.278	3.558	0.707	1.005	2.978
11	0.074	0.524	3.906	0.938	1.458	2.977
13	0.178	0.625	4.035	1.012	1.589	2.973
15	0.214	0.659	4.069	1.046	1.677	2.973
17	0.223	0.669	4.081	1.041	1.678	2.973
19	0.224	0.670	4.075	1.046	1.693	2.973
21	0.224	0.670	4.081	1.038	1.684	2.972
23	0.224	0.669	4.075	1.041	1.689	2.971
25	0.224	0.669	4.075	1.041	1.689	2.971

Table 3.2: Convergence of transverse stress at Section 11 and Nodal Line 23

(L=1000mm, n=100mm)

Series terms (μ)	Transverse stress, σ_y (MPa)					
	SS	SC	SF	CC	CF	FF
3	-9.745	-9.604	-5.409	-9.283	-5.951	-7.697
5	-12.430	-12.162	-8.724	-11.884	-10.282	-12.344
7	-13.850	-13.576	-10.660	-13.398	-12.092	-13.414
9	-14.496	-14.176	-11.374	-14.057	-13.386	-13.490
11	-14.753	-14.437	-11.690	-14.326	-13.631	-13.476
13	-14.843	-14.514	-11.737	-14.421	-13.910	-13.474
15	-14.868	-14.544	-11.766	-14.443	-13.872	-13.477
17	-14.874	-14.546	-11.753	-14.453	-13.943	-13.479
19	-14.875	-14.549	-11.758	-14.449	-13.903	-13.480
21	-14.874	-14.547	-11.753	-14.453	-13.933	-13.481
23	-14.875	-14.549	-11.757	-14.450	-13.910	-13.482
25	-14.875	-14.548	-11.755	-14.452	-13.928	-13.483

Table 3.3: Convergence of shear stress at Nodal Line 23,

at Section 1 for the SS, SC, SF, CF and Section 9 for the CC and FF cases

(L=1000mm, n=100mm)

Series terms (μ)	Shear stress, τ_{xy} (MPa)					
	SS	SC	SF	CC	CF	FF
3	12.524	12.281	27.297	16.078	26.103	6.023
5	15.394	15.977	23.960	16.559	23.712	9.265
7	13.974	13.934	25.492	14.782	29.892	10.449
9	14.626	14.770	24.825	14.526	28.854	10.418
11	14.355	14.361	25.078	13.916	28.594	10.404
13	14.455	14.483	25.001	13.626	29.236	10.393
15	14.424	14.426	25.016	13.335	29.134	10.394
17	14.431	14.430	25.017	13.126	29.234	10.399
19	14.430	14.423	25.015	12.950	28.953	10.401
21	14.430	14.419	25.016	12.805	28.930	10.394
23	14.430	14.417	25.016	12.685	29.136	10.397
25	14.430	14.414	25.015	12.581	29.135	10.396
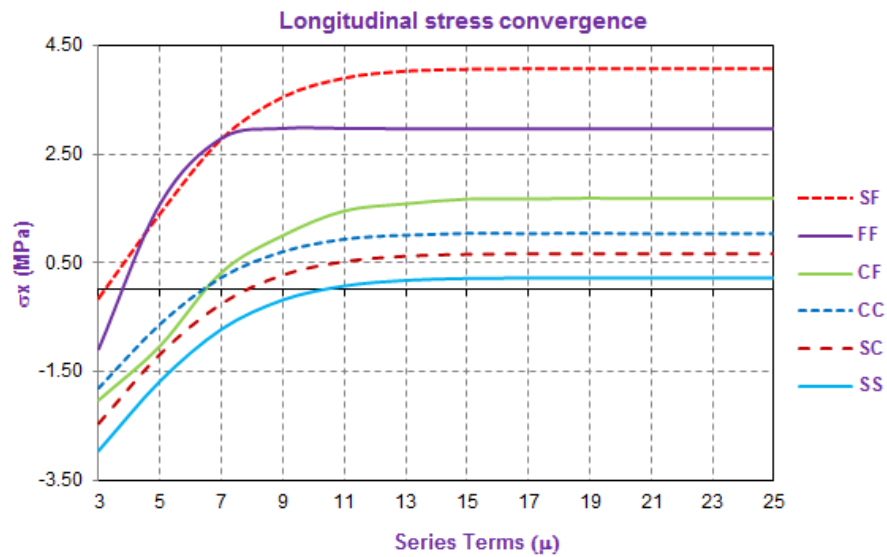
Figure 3.35: Convergences of longitudinal stress (σ_x) at Section 11 and Nodal Line 23

(L=1000mm, n=100mm)
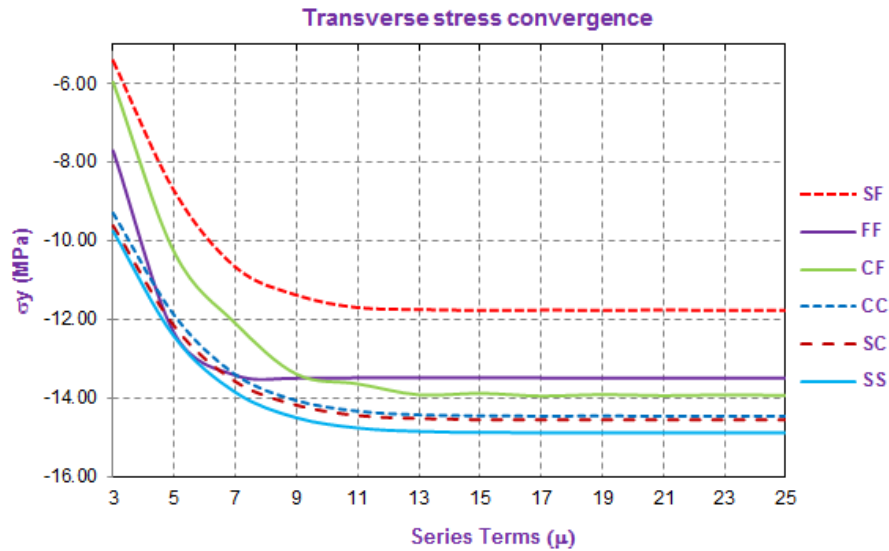
Figure 3.36: Convergences of transverse stress (σ_y) at Section 11 and Nodal Line 23
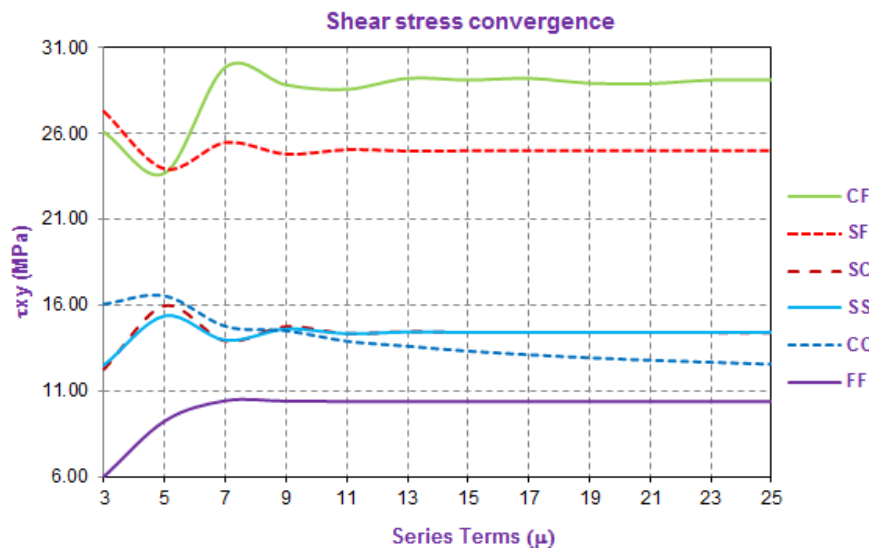
Figure 3.37: Convergences of shear stress (τ_{xy}) at Nodal Line 23, Section 1 for the SS, SC, SF, CC

cases and Section 9 for the CF and FF cases

Similar convergence study has been performed for the same lipped channel section in Section 3.11 with the beam length 1000mm and the load length 50mm. The convergence of the stresses are given in Tables.3.4 to 3.6 and shown in Figs.3.38 to 3.40. It can be seen that the solutions are converged for the longitudinal stress, transverse stress and shear stress when the number of series terms reaches 25 as for previous example.

Table 3.4: Convergence of longitudinal stress at Section 11 and Nodal Line 23

(L=1000mm, n=50mm)

Series terms (μ)	Longitudinal stress, σ_x (MPa)					
	SS	SC	SF	CC	CF	FF
3	-1.479	-1.232	-0.075	-0.909	-1.036	-0.546
5	-0.770	-0.525	0.751	-0.247	-0.499	0.900
7	-0.196	0.039	1.530	0.280	0.267	1.658
9	0.165	0.390	2.001	0.605	0.705	1.805
11	0.362	0.583	2.238	0.790	1.013	1.806
13	0.459	0.676	2.335	0.869	1.137	1.794
15	0.502	0.719	2.367	0.911	1.216	1.789
17	0.519	0.735	2.374	0.919	1.235	1.787
19	0.525	0.741	2.368	0.922	1.250	1.786
21	0.526	0.742	2.366	0.923	1.249	1.785
23	0.526	0.742	2.359	0.924	1.251	1.785
25	0.525	0.741	2.360	0.920	1.249	1.785

Table 3.5: Convergence of transverse stress at Section 11 and Nodal Line 23

(L=1000mm, n=50mm)

Series terms (μ)	Transverse stress, σ_y (MPa)					
	SS	SC	SF	CC	CF	FF
3	-4.942	-4.877	-2.719	-4.707	-3.003	-3.856
5	-6.382	-6.254	-4.428	-6.104	-5.251	-6.261
7	-7.191	-7.058	-5.455	-6.961	-6.263	-6.856
9	-7.590	-7.433	-5.851	-7.369	-7.002	-6.892
11	-7.767	-7.611	-6.021	-7.554	-7.188	-6.867
13	-7.839	-7.675	-6.050	-7.629	-7.365	-6.855
15	-7.864	-7.702	-6.057	-7.652	-7.364	-6.853
17	-7.871	-7.707	-6.041	-7.661	-7.406	-6.853
19	-7.872	-7.709	-6.035	-7.660	-7.388	-6.853
21	-7.871	-7.707	-6.026	-7.661	-7.461	-6.854
23	-7.870	-7.707	-6.025	-7.658	-7.389	-6.854
25	-7.869	-7.706	-6.020	-7.659	-7.397	-6.854

Table 3.6: Convergence of shear stress at Nodal Line 23,

at Section 1 for the SS, SC, SF, CC and Section 9 for the CF and FF cases

(L=1000mm, n=50mm)

Series terms (μ)	Shear stress, τ_{xy} (MPa)					
	SS	**SC**	**SF**	**CC**	**CF**	**FF**
3	6.204	6.065	13.663	8.007	13.074	1.020
5	7.758	8.071	11.956	8.325	11.990	4.800
7	6.931	6.891	12.777	7.359	15.216	5.487
9	7.351	7.436	12.388	7.290	14.769	5.457
11	7.151	7.144	12.554	6.943	14.628	5.457
13	7.239	7.258	12.494	6.824	14.743	5.452
15	7.204	7.201	12.510	6.662	14.869	5.448
17	7.216	7.216	12.510	6.567	14.856	5.449
19	7.213	7.208	12.506	6.473	14.765	5.450
21	7.213	7.208	12.510	6.405	14.755	5.449
23	7.214	7.206	12.507	6.341	14.808	5.448
25	7.213	7.205	12.509	6.291	14.801	5.447
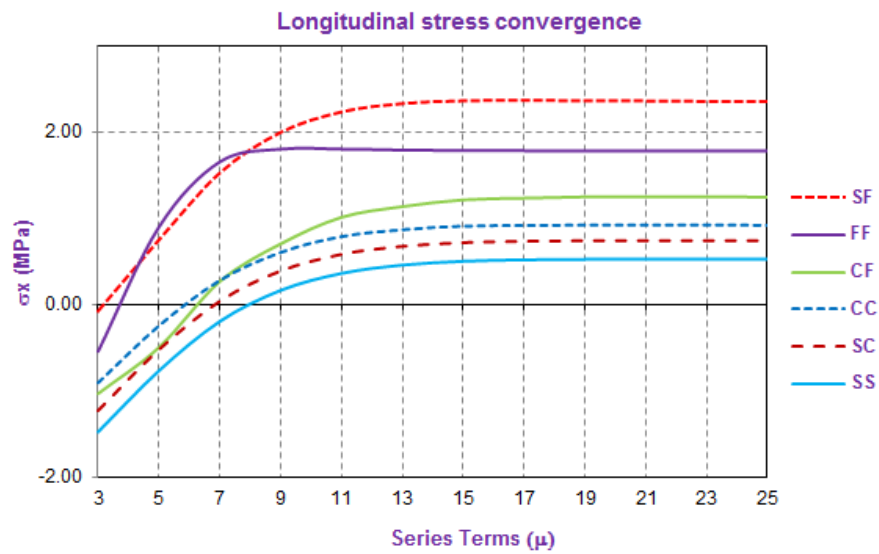
Figure 3.38: Convergences of longitudinal stress (σ_x) at Section 11 and Nodal Line 23
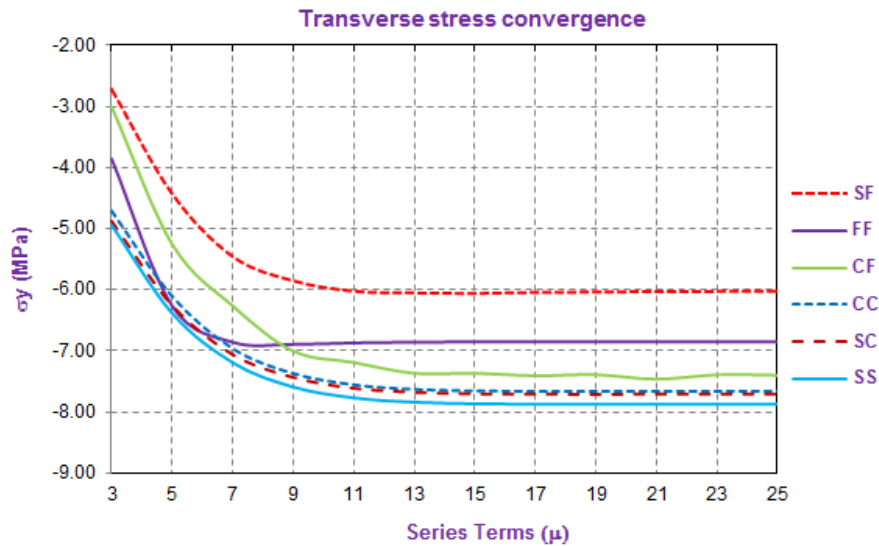
Figure 3.39: Convergences of transverse stress (σ_y) at Section 11 and Nodal Line 23
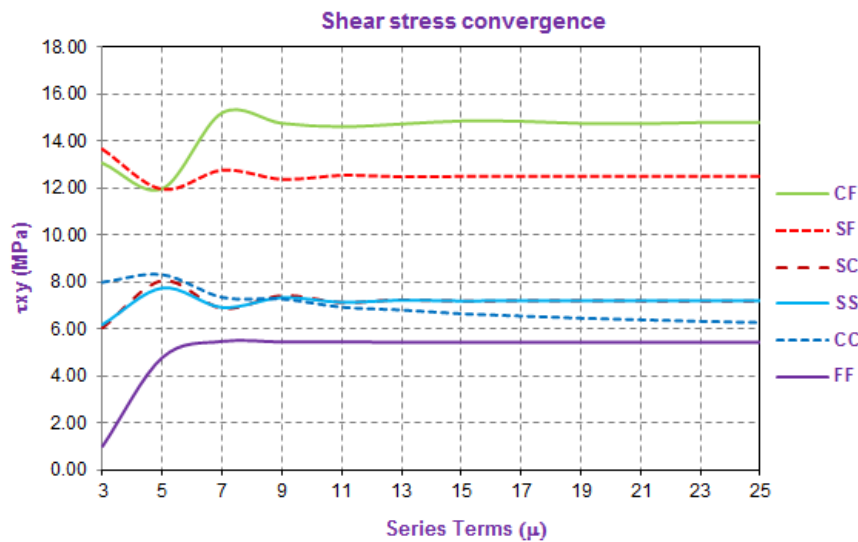
Figure 3.40: Convergences of shear stress (τ_{xy}) at Nodal Line 23, Section 1 for the SS, SC, SF, CC

cases and Section 9 for the CF and FF cases

3.13. CONCLUSIONS

A Finite Strip Method of pre-buckling analysis of thin-walled section under localised loading has been developed for general end boundary conditions. This method has been benchmarked against the Finite Element Method.

Suitable displacement functions are used for different support and loading conditions for both flexural and membrane displacements. For a load over one-twentieth to one-tenth of the span, approximately 25 series terms are required in the analysis process to get accurate pre-buckling results, particularly stress.

CHAPTER 4

BUCKLING ANALYSIS OF THIN-WALLED SECTIONS UNDER LOCALISED LOADING FOR GENERAL END BOUNDARY CONDITIONS

4.1. INTRODUCTION

In order to develop the Direct Strength Method (DSM) for design of cold-formed steel sections under localised loading, it is necessary to calculate the buckling load of structural members. The elastic buckling analysis described in this Chapter is an important step which provides the buckling load to establish the DSM design equations for web crippling as described in Chapter 7.

This Chapter introduces the functions used to compute the stress distributions in the strips of the structural member for different end boundary conditions as described in Chapter 3. In addition, the theory of the FSM for the elastic buckling analysis of thin walled sections under localised loading for general end boundary conditions is developed. Numerical examples have been performed by the FSM built into Version 2.0 of the THIN-WALL-2 program as described in detail in Chapter 5. The numerical solutions are compared with those from the analyses by the Finite Element Method (FEM) using ABAQUS [32] to validate the accuracy including a convergence study.

The most significant development of this Chapter is the choice and validation of the stress functions based on the displacement functions, as described in Chapter 3, for different boundary conditions. Consequently, this Chapter introduces the stress functions first before giving the full derivation of the stability matrices based on energy principles.

4.2. STRIP BUCKLING DISPLACEMENTS

4.2.1. Flexural buckling displacement

An isometric view of flexural displacements of a strip is shown in Fig.3.3 in Chapter 3.

The flexural deformations w of a strip can be described by the summation over μ series terms as:

$$w = \sum_{m=1}^{\mu} f_{1m}(y) X_{1m}(x) \tag{4.1}$$

where:

μ is the number of series terms of the harmonic longitudinal function

$X_{1m}(x)$ is the function for longitudinal variation

$f_{1m}(y)$ is a polynomial function for transverse variation. This function for the mth series term is given by:

$$f_{1m}(y) = \alpha_{1Fm} + \alpha_{2Fm}\left(\frac{y}{b}\right) + \alpha_{3Fm}\left(\frac{y}{b}\right)^2 + \alpha_{4Fm}\left(\frac{y}{b}\right)^3 \tag{4.2}$$

$\{\alpha_{Fm}\}$ are the vector polynomial coefficients for the mth series term which depend on the nodal line flexural deformations of the strip

$$\{\alpha_{Fm}\} = \begin{bmatrix} \alpha_{1Fm} & \alpha_{2Fm} & \alpha_{3Fm} & \alpha_{4Fm} \end{bmatrix}^T \tag{4.3}$$

t, b and L are the strip thickness, width and length respectively

The flexural deformations w can be written in matrix format:

$$w = \sum_{m=1}^{\mu} X_{1m}(x)[\Gamma_{FL}][C_F]^{-1}\{\delta_{Fm}\} \tag{4.4}$$

where:

$$\{\alpha_{Fm}\} = [C_F]^{-1}\{\delta_{Fm}\}$$

$$f_{1m}(y) = [\Gamma_{FL}]\{\alpha_{Fm}\}$$

$$[\Gamma_{FL}] = \begin{bmatrix} 1 & (y/b) & (y/b)^2 & (y/b)^3 \end{bmatrix}$$

$\{\delta_{Fm}\}$ is the flexural displacement vector for nodal line displacements for the mth series term

$$\{\delta_{Fm}\} = \begin{bmatrix} w_{1m} & \theta_{x1m} & w_{2m} & \theta_{x2m} \end{bmatrix}^T$$

$[C_F]$ is the evaluation matrix of the flexural displacement functions at the nodal lines, given in Appendix C of the thesis

In the computation of the flexural potential energy described later, the derivatives of the flexural deformation are required. The derivatives used are as follows:

The derivative of the flexural displacement functions by x variable:

$$\frac{\partial w}{\partial x} = \sum_{m=1}^{\mu} X'_{1m}(x)[\Gamma_{FL}]\{\alpha_{Fm}\} \tag{4.5}$$

$$\Rightarrow \left(\frac{\partial w}{\partial x}\right)^2 = \sum_{m=1}^{\mu}\sum_{n=1}^{\mu} \{\alpha_{Fm}\}^T[\Gamma_{FL}]^T X'_{1m}(x)X'_{1n}(x)[\Gamma_{FL}]\{\alpha_{Fn}\} \tag{4.6}$$

The derivative of the flexural displacement functions by y variable:

$$\frac{\partial w}{\partial y} = \sum_{m=1}^{\mu} X_{1m}(x) \frac{1}{b} \left[\Gamma_{FT}\right]\{\alpha_{Fm}\} \tag{4.7}$$

$$\Rightarrow \left(\frac{\partial w}{\partial y}\right)^2 = \sum_{m=1}^{\mu}\sum_{n=1}^{\mu} \frac{1}{b^2} \{\alpha_{Fm}\}^T \left[\Gamma_{FT}\right]^T X_{1m}(x) X_{1n}(x) \left[\Gamma_{FT}\right]\{\alpha_{Fn}\} \tag{4.8}$$

The derivative of the flexural displacement functions by *x* and *y* variables:

$$\frac{\partial w}{\partial x}\frac{\partial w}{\partial y} = \sum_{m=1}^{\mu}\sum_{n}^{\mu} \{\alpha_{Fm}\}^T \left[\Gamma_{FL}\right]^T X_{1m}^{'}(x)\frac{1}{b} X_{1n}(x)\left[\Gamma_{FT}\right]\{\alpha_{Fn}\} \tag{4.9}$$

$$\frac{\partial w}{\partial y}\frac{\partial w}{\partial x} = \sum_{m=1}^{\mu}\sum_{n}^{\mu} \{\alpha_{Fm}\}^T \left[\Gamma_{FT}\right]^T \frac{1}{b} X_{1m}(x) X_{1n}^{'}(x)\left[\Gamma_{FL}\right]\{\alpha_{Fn}\} \tag{4.10}$$

where $\left[\Gamma_{FL}\right] = \begin{bmatrix} 1 & (y/b) & (y/b)^2 & (y/b)^3 \end{bmatrix}$

4.2.2. Membrane buckling displacement

An isometric view of membrane displacements of a strip is shown in Fig.3.4 in Chapter 3.

The membrane deformations in the longitudinal and transverse directions of a strip can be described by the summation over μ series terms as:

$$v = \sum_{m=1}^{\mu} f_{vm}(y) X_{1m}(x) \tag{4.11}$$

$$u = \sum_{m=1}^{\mu} f_{um}(y) X_{2m}(x) \tag{4.12}$$

where:

$X_{1m}(x)$ and $X_{2m}(x)$ are the longitudinal variation functions for the membrane transverse *v* and longitudinal *u* deformations respectively

$f_{vm}(y)$ and $f_{um}(y)$ are the transverse variations. These functions for the mth series term are given:

$$f_{vm}(y) = \alpha_{1Mm} + \alpha_{2Mm}\left(\frac{y}{b}\right) \tag{4.13}$$

$$f_{um}(y) = \alpha_{3Mm} + \alpha_{4Mm}\left(\frac{y}{b}\right) \tag{4.14}$$

$\{\alpha_{Mm}\}$ is the vector of polynomial coefficients for the mth series term which depends on the nodal line membrane deformations of the strips

$$\{\alpha_{Mm}\} = \begin{bmatrix} \alpha_{1Mm} & \alpha_{2Mm} & \alpha_{3Mm} & \alpha_{4Mm} \end{bmatrix}^T \tag{4.15}$$

The membrane deformations of the strip can be written in matrix format:

$$v = \sum_{m=1}^{\mu} X_{1m}(x) [\Gamma_{Mv}] [C_M]^{-1} \{\delta_{Mm}\} \tag{4.16}$$

$$u = \sum_{m=1}^{\mu} X_{2m}(x) [\Gamma_{Mu}] [C_M]^{-1} \{\delta_{Mm}\} \tag{4.17}$$

where:

$$\{\alpha_{Mm}\} = [C_M]^{-1} \{\delta_{Mm}\}$$

$$f_{vm}(y) = [\Gamma_{Mv}] \{\alpha_{Mm}\} \qquad \text{and} \qquad f_{um}(y) = [\Gamma_{Mu}] \{\alpha_{Mm}\}$$

$$[\Gamma_{Mv}] = [1 \quad (y/b) \quad 0 \quad 0] \qquad \text{and} \qquad [\Gamma_{Mu}] = [0 \quad 0 \quad 1 \quad (y/b)]$$

$\{\delta_{Mm}\}$ is the vector of membrane displacement for the mth series term

$$\{\delta_{Mm}\} = [u_{1m} \quad v_{1m} \quad u_{2m} \quad v_{2m}]^T$$

$[C_M]$ is the evaluation matrix of the membrane displacement functions at nodal line, given in Appendix C of the thesis

In the computation of the membrane potential energy described later, the derivatives of the membrane deformations are required. The derivatives used are as follows:

The derivative of the membrane deformation *v* by *x* variable

$$\frac{\partial v}{\partial x} = \sum_{m=1}^{\mu} X_{1m}'(x) [\Gamma_{Mv}] \{\alpha_{Mm}\} \tag{4.18}$$

$$\Rightarrow \left(\frac{\partial v}{\partial x}\right)^2 = \sum_{m=1}^{\mu} \sum_{n=1}^{\mu} \{\alpha_{Mm}\}^T [\Gamma_{Mv}]^T X_{1m}'(x) X_{1n}'(x) [\Gamma_{Mv}] \{\alpha_{Mn}\} \tag{4.19}$$

The derivative of the membrane deformation *u* by *x* variable

$$\frac{\partial u}{\partial x} = \sum_{m=1}^{\mu} X_{2m}'(x) [\Gamma_{Mu}] \{\alpha_{Mm}\} \tag{4.20}$$

$$\Rightarrow \left(\frac{\partial u}{\partial x}\right)^2 = \sum_{m=1}^{\mu} \sum_{n=1}^{\mu} \{\alpha_{Mm}\}^T [\Gamma_{Mu}]^T X_{2m}'(x) X_{2n}'(x) [\Gamma_{Mu}] \{\alpha_{Mn}\} \tag{4.21}$$

4.3. MEMBRANE STRESSES

4.3.1. Membrane stress calculation

The membrane stresses of a strip for the kth series term of the pre-buckling as in Chapter 3 are given by:

$$\{\sigma_{Mk}\} = [D_M]\{\in_{Mk}\} \qquad (4.22)$$

where

$[D_M]$ is the property matrix of membrane displacement, given in Appendix C of the thesis

$\{\in_{Mk}\}$ is the membrane strain vector:

$$\{\in_{Mk}\} = [B_{Mk}]\{\alpha_{Mk}\} \qquad (4.23)$$

Hence:

$$\{\sigma_{Mk}\} = [D_M][B_{Mk}]\{\alpha_{Mk}\} \qquad (4.24)$$

where $[B_{Mk}]$ is the strain matrix of membrane displacement, given in Appendix C of the thesis

4.3.2. Stress distribution in a strip

A strip subjected to loading will have complex stresses as shown in the Fig.4.1 where the stresses due to the *k*=1 series term are drawn. The stresses are obtained from the pre-buckling analysis step described in Chapter 3.

x,y,z are local axes aligned with strip
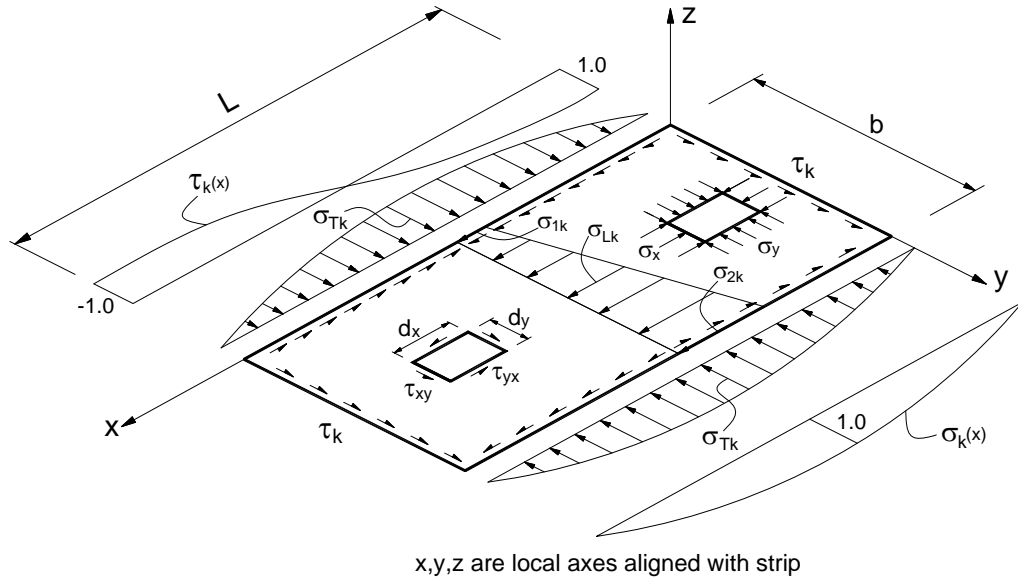
Figure 4.1: Stress distribution of a strip with both ends simply supported (*k*=1)

The longitudinal stress for elastic buckling analysis which is obtained from Eq.(4.24) varies in both the longitudinal and transverse directions and is given by:

$$\sigma_x(x) = \sum_{k=1}^{\mu} \sigma_{1k}(x)\sigma_{L1k} + \sum_{k=1}^{\mu} \sigma_{2k}(x)\left[\sigma_{L2k} + \sigma_{L3k}\frac{y}{b}\right] \qquad (4.25)$$

where:

k is the series term of the stress functions

$\sigma_x(x)$ is the longitudinal stress of the strip

σ_{L1k}, σ_{L2k}, σ_{L3k} are the amplitude components of the longitudinal stress at series term k^{th}

$$\sigma_{L1k} = \alpha_{2Mm}\frac{E_{12}}{b}; \sigma_{L2k} = \alpha_{3Mm}E_2 \text{ and } \sigma_{L3k} = \alpha_{4Mm}E_2$$

$\sigma_{1k}(x)$, $\sigma_{2k}(x)$ are the functions for the variation of the longitudinal stress along the strip

$$\sigma_{1k}\left(x\right) = X_{1k}\left(x\right) \text{ and } \sigma_{2k}\left(x\right) = X_{2k}^{'}\left(x\right)$$

E_1, E_2, E_{12} are given in Appendix C of the thesis

The transverse stress for elastic buckling analysis which is obtained from Eq.(4.24) is the average transverse stress in a strip and is given by:

$$\sigma_y\left(x\right) = \sum_{k=1}^{\mu}\sigma_{1k}\left(x\right)\sigma_{T1k} + \sum_{k=1}^{\mu}\sigma_{2k}\left(x\right)\sigma_{T2k} \tag{4.26}$$

where:

$\sigma_y(x)$ is the transverse stress of the strip

σ_{T1k}, σ_{T2k} re the amplitude components of the transverse stress of the strip at series term k^{th}

$$\sigma_{T1k} = \alpha_{2Mm}\frac{E_1}{b} \text{ and } \sigma_{T2k} = \left[\alpha_{3Mm}E_{12} + \frac{1}{2}\alpha_{4Mm}E_{12}\right]$$

$\sigma_{1k}(x)$, $\sigma_{2k}(x)$ are the functions for the variation of the transverse stress along the strip

$$\sigma_{1k}\left(x\right) = X_{1k}\left(x\right) \text{ and } \sigma_{2k}\left(x\right) = X_{2k}^{'}\left(x\right)$$

The shear stress for elastic buckling analysis which is obtained from Eq.(4.24) is the average stress in a strip and is given by:

$$\tau_{xy}\left(x\right) = \sum_{k=1}^{\mu}\tau_{1k}\left(x\right)\tau_{1k} + \sum_{k=1}^{\mu}\tau_{2k}\left(x\right)\tau_{2k} \tag{4.27}$$

where:

$\tau_{xy}(x)$ is the shear stress of the strip

τ_{1k}, τ_{2k} re the amplitude components of the shear stress of the strip at series term k^{th}

$$\tau_{1k} = \left[\alpha_{1Mm}G + \frac{1}{2}\alpha_{2Mm}G\right] \text{ and } \tau_{2k} = \alpha_{4Mm}\frac{G}{b}$$

$\tau_{1k}(x)$, $\tau_{2k}(x)$ are the functions for the variation of the shear stress along the strip

$$\tau_{1k}\left(x\right) = X_{1m}^{'}\left(x\right) \text{ and } \tau_{2k}\left(x\right) = X_{2m}\left(x\right)$$

G is the shear modulus

For different boundary conditions, different functions are required for flexural and membrane displacements, as described in Chapter 3.

4.4. THE FLEXURAL STABILITY MATRIX OF A STRIP

4.4.1. The flexural potential energy of the membrane forces

The flexural potential energy of the membrane forces as described in [15] and [12] is given by:

$$V_F = -\frac{1}{2}\int_0^L\int_0^b\left[\sigma_x(x)\left(\frac{\partial w}{\partial x}\right)^2 + \sigma_y(x)\left(\frac{\partial w}{\partial y}\right)^2 + \tau_{xy}(x)\left(\frac{\partial w}{\partial x}\right)\left(\frac{\partial w}{\partial y}\right) + \tau_{xy}(x)\left(\frac{\partial w}{\partial y}\right)\left(\frac{\partial w}{\partial x}\right)\right]t\,dy\,dx \quad (4.28)$$

$$\Rightarrow \quad V_F = V_{FL} + V_{FT} + V_{FS1} + V_{FS2} \quad (4.29)$$

where:

V_{FL} is the flexural potential energy of the longitudinal stress

$$V_{FL} = -\frac{1}{2}\int_0^L\int_0^b\left[\sigma_x(x)\left(\frac{\partial w}{\partial x}\right)^2\right]t\,dy\,dx \quad (4.30)$$

V_{FT} is the flexural potential energy of the transverse stress

$$V_{FT} = -\frac{1}{2}\int_0^L\int_0^b\left[\sigma_y(x)\left(\frac{\partial w}{\partial y}\right)^2\right]t\,dy\,dx \quad (4.31)$$

V_{FS} is the flexural potential energy of the shear stress

$$V_{FS} = V_{FS1} + V_{FS2} \quad (4.32)$$

$$V_{FS1} = -\frac{1}{2}\int_0^L\int_0^b\left[\tau_{xy}(x)\left(\frac{\partial w}{\partial x}\right)\left(\frac{\partial w}{\partial y}\right)\right]t\,dy\,dx \quad (4.33)$$

$$V_{FS2} = -\frac{1}{2}\int_0^L\int_0^b\left[\tau_{xy}(x)\left(\frac{\partial w}{\partial y}\right)\left(\frac{\partial w}{\partial x}\right)\right]t\,dy\,dx \quad (4.34)$$

4.4.2. The flexural potential energy of the longitudinal stress

Longitudinal stress distribution in a strip is shown in the Fig.4.2

x,y,z are local axes aligned with strip
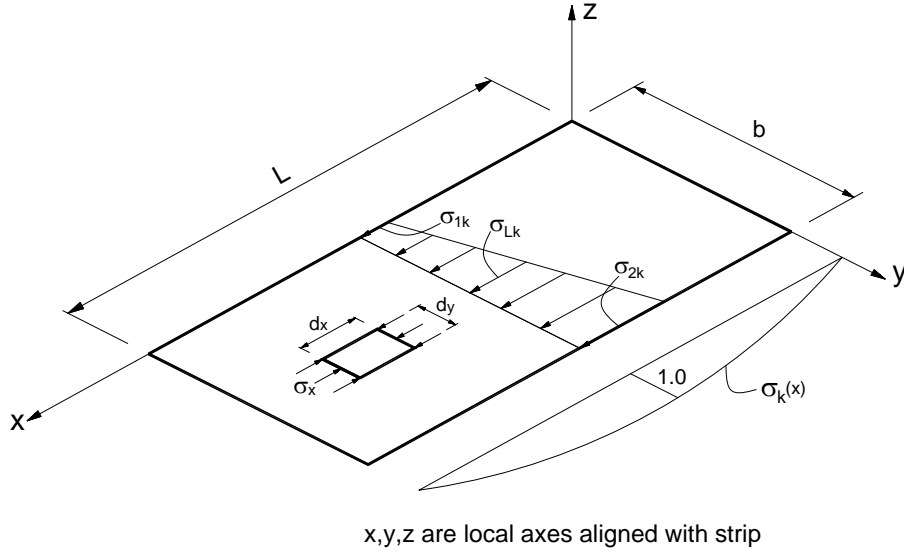
Figure 4.2: Longitudinal stress distribution in a strip with both ends simply supported

Elemental shortening and potential energy
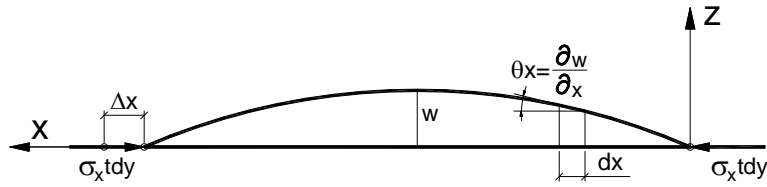
Figure 4.3: Elemental shortening and potential energy

Shortening of element

$$d_x = \frac{1}{2}\left(\frac{\partial w}{\partial x}\right)^2 dx \tag{4.35}$$

Integrating along length of strip

$$\Delta_x = \int_0^L \frac{1}{2}\left(\frac{\partial w}{\partial x}\right)^2 dx \tag{4.36}$$

Increase in potential energy of membrane forces resulting from flexural deformations:

$$V_{FL} = -\frac{1}{2}\int_0^L\int_0^b \left[\sigma_x\left(x\right)\left(\frac{\partial w}{\partial x}\right)^2\right]tdydx \tag{4.37}$$

Substitute (4.25) and (4.6) to (4.37) equation and do the summation taken over μ series terms of the potential energy of of the longitudinal stress:

$$V_{FL} = -\frac{1}{2}\int_0^L\int_0^b \sum_{m=1}^{\mu}\sum_{n=1}^{\mu}\left\{\alpha_{Fm}\right\}^T\left[\Gamma_{FL}\right]^T X_{1m}^{'}\left(x\right)\left(\sum_{k=1}^{\mu}\sigma_{1k}\left(x\right)\sigma_{L1k} + \sum_{k=1}^{\mu}\sigma_{2k}\left(x\right)\left[\sigma_{L2k} + \sigma_{L3k}\frac{y}{b}\right]\right). \tag{4.38}$$
$$X_{1n}^{'}\left(x\right)\left[\Gamma_{FL}\right]\left\{\alpha_{Fn}\right\}tdydx$$

Separate the V_{FL} into V_{FL1} and V_{FL2}

$$V_{FL1} = -\frac{1}{2}\int_0^L\int_0^b\sum_{m=1}^{\mu}\sum_{n=1}^{\mu}\{\alpha_{Fm}\}^T[\Gamma_{FL}]^T X_{1m}'(x)\left(\sum_{k=1}^{\mu}\sigma_{1k}(x)\sigma_{L1k}\right)X_{1n}'(x)[\Gamma_{FL}]\{\alpha_{Fn}\}tdydx \qquad (4.39)$$

$$V_{FL2} = -\frac{1}{2}\int_0^L\int_0^b\sum_{m=1}^{\mu}\sum_{n=1}^{\mu}\{\alpha_{Fm}\}^T[\Gamma_{FL}]^T X_{1m}'(x)\left(\sum_{k=1}^{\mu}\sigma_{L2k}(x)\left[\sigma_{2k}+\sigma_{L3k}\frac{y}{b}\right]\right)\cdot \qquad (4.40)$$
$$X_{1n}'(x)[\Gamma_{FL}]\{\alpha_{Fn}\}tdydx$$

These equations can be rewritten in other variables as:

$$V_{FL1} = -\frac{1}{2}\left(\frac{Lbt}{\pi}\right)\int_0^{\bar{y}=1}\int_0^{\xi=\pi}\sum_{m=1}^{\mu}\sum_{n=1}^{\mu}\{\alpha_{Fm}\}^T[\Gamma_{FL}]^T X_{1m}'(\xi)\left(\sum_{k=1}^{\mu}\sigma_{1k}(\xi)\sigma_{L1k}\right)\cdot \qquad (4.41)$$
$$X_{1n}'(\xi)[\Gamma_{FL}]\{\alpha_{Fn}\}d\xi d\bar{y}$$

$$V_{FL2} = -\frac{1}{2}\left(\frac{Lbt}{\pi}\right)\int_0^{\bar{y}=1}\int_0^{\xi=\pi}\sum_{m=1}^{\mu}\sum_{n=1}^{\mu}\{\alpha_{Fm}\}^T[\Gamma_{FL}]^T X_{1m}'(\xi)\left(\sum_{k=1}^{\mu}\sigma_{2k}(\xi)\left[\sigma_{L2k}+\sigma_{L3k}\bar{y}\right]\right)\cdot \qquad (4.42)$$
$$X_{1n}'(\xi)[\Gamma_{FL}]\{\alpha_{Fn}\}d\xi d\bar{y}$$

Rearrange these equations:

$$V_{FL1} = -\frac{1}{2}\left(\frac{Lbt}{\pi}\right)\sum_{k=1}^{\mu}\left(\begin{array}{c}\int_0^{\bar{y}=1}\sigma_{L1k}[\Gamma_{FL}]^T[\Gamma_{FL}]d\bar{y}\cdot \\ \int_0^{\xi=\pi}\sum_{m=1}^{\mu}\sum_{n=1}^{\mu}\{\alpha_{Fm}\}^T X_{1m}'(\xi)\sigma_{1k}(\xi)X_{1n}'(\xi)\{\alpha_{Fn}\}d\xi\end{array}\right) \qquad (4.43)$$

$$V_{FL2} = -\frac{1}{2}\left(\frac{Lbt}{\pi}\right)\sum_{k=1}^{\mu}\left(\begin{array}{c}\int_0^{\bar{y}=1}\left[\sigma_{L2k}+\sigma_{L3k}\bar{y}\right][\Gamma_{FL}]^T[\Gamma_{FL}]d\bar{y}\cdot \\ \int_0^{\xi=\pi}\sum_{m=1}^{\mu}\sum_{n=1}^{\mu}\{\alpha_{Fm}\}^T X_{1m}'(\xi)\sigma_{2k}(\xi)X_{1n}'(\xi)\{\alpha_{Fn}\}d\xi\end{array}\right) \qquad (4.44)$$

where:

$$\{\alpha_{Fm}\} = [C_F]^{-1}\{\delta_{Fm}\}$$

$$\xi = \frac{\pi x}{L}, \ \xi = 0 \rightarrow \pi \text{ when } x = 0 \rightarrow L$$

$$\bar{y} = y/b, \ \bar{y} = 0 \rightarrow 1 \text{ when } y = 0 \rightarrow b$$

$\{\delta_{Fn}\}$ is the flexural displacement vector of a strip

$$\{\delta_{Fn}\} = \begin{bmatrix} w_{1n} & \theta_{x1n} & w_{2n} & \theta_{x2n} \end{bmatrix}^T$$

[C_F] is the evaluation matrix of the flexural displacement functions at the nodal lines, given in Appendix C of the thesis

Eqs.(4.43) and (4.44) can be rewritten as:

$$V_{FL1} = -\frac{1}{2}\left(\frac{Lbt}{\pi}\right)\sum_{k=1}^{\mu}\begin{pmatrix} \int_0^{\bar{y}=1} \sigma_{L1k}[\Gamma_{FL}]^T[\Gamma_{FL}]d\bar{y}. \\ \int_0^{\xi=\pi}\sum_{m=1}^{\mu}\sum_{n=1}^{\mu}\{\delta_{Fm}\}^T[C_F]^{-T}X'_{1m}(\xi)\sigma_{1k}(\xi)X'_{1n}(\xi)[C_F]^{-1}\{\delta_{Fn}\}d\xi \end{pmatrix} \tag{4.45}$$

$$V_{FL2} = -\frac{1}{2}\left(\frac{Lbt}{\pi}\right)\sum_{k=1}^{\mu}\begin{pmatrix} \int_0^{\bar{y}=1} [\sigma_{L2k}+\sigma_{L3k}\bar{y}][\Gamma_{FL}]^T[\Gamma_{FL}]d\bar{y}. \\ \int_0^{\xi=\pi}\sum_{m=1}^{\mu}\sum_{n=1}^{\mu}\{\delta_{Fm}\}^T[C_F]^{-T}X'_{1m}(\xi)\sigma_{2k}(\xi)X'_{1n}(\xi)[C_F]^{-1}\{\delta_{Fn}\}d\xi \end{pmatrix} \tag{4.46}$$

In other format:

$$V_{FL1} = -\frac{1}{2}\left(\frac{V}{\pi}\right)\sum_{k=1}^{\mu}\left(B_{FL1}\sum_{m=1}^{\mu}\sum_{n=1}^{\mu}\{\delta_{Fm}\}^T[C_F]^{-T}C_{Lw1mnk}[C_F]^{-1}\{\delta_{Fn}\}\right) \tag{4.47}$$

$$V_{FL2} = -\frac{1}{2}\left(\frac{V}{\pi}\right)\sum_{k=1}^{\mu}\left(B_{FL2}\sum_{m=1}^{\mu}\sum_{n=1}^{\mu}\{\delta_{Fm}\}^T[C_F]^{-T}C_{Lw2mnk}[C_F]^{-1}\{\delta_{Fn}\}\right) \tag{4.48}$$

where:

V is the volume of the strip, $V=Lbt$

A_{FL}, B_{FL1}, B_{FL2}, C_{Lw1mnk}, C_{Lw2mnk} are given in Appendix C of the thesis

Hence:

$$V_{FL1} = -\frac{1}{2}\{\delta_{Fm}\}^T[C_F]^{-T}[g_{\alpha FL1mn}][C_F]^{-1}\{\delta_{Fn}\} \tag{4.49}$$

$$V_{FL2} = -\frac{1}{2}\{\delta_{Fm}\}^T[C_F]^{-T}[g_{\alpha FL2mn}][C_F]^{-1}\{\delta_{Fn}\} \tag{4.50}$$

where $[g_{\alpha FL1mn}]$ and $[g_{\alpha FL2mn}]$ are given in Appendix C of the thesis

4.4.3. The flexural potential energy of the transverse stress

Transverse stress distribution in a strip is shown in the Fig.4.4

x,y,z are local axes aligned with strip
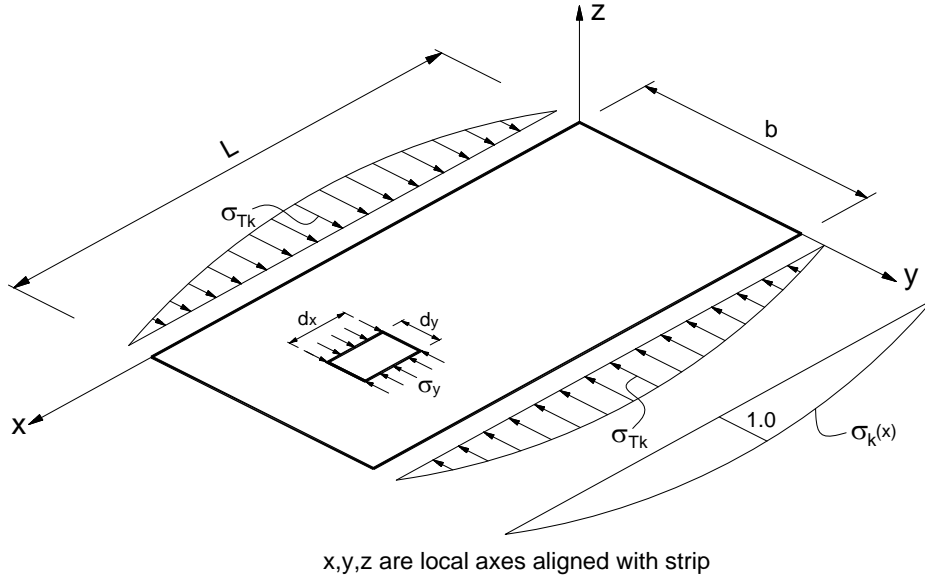
Figure 4.4: Transverse stress distribution in a strip with both ends simply supported

The flexural potential energy of the transverse stress

$$V_{FT} = -\frac{1}{2}\int_0^L\int_0^b\left[\sigma_y(x)\left(\frac{\partial w}{\partial y}\right)^2\right]tdydx \tag{4.51}$$

Substitute (4.26) and (4.8) to (4.51) and do the summation taken over μ series terms of the potential energy of of the transverse stress:

$$V_{FT} = -\frac{1}{2}\int_0^L\int_0^b\sum_{m=1}^{\mu}\sum_{n=1}^{\mu}\frac{1}{b^2}\{\alpha_{Fm}\}^T\left[\Gamma_{FT}\right]^T X_{1m}(x)\left[\sum_{k=1}^{\mu}\sigma_{1k}(x)\sigma_{T1k} + \sum_{k=1}^{\mu}\sigma_{2k}(x)\sigma_{T2k}\right]. \tag{4.52}$$
$$X_{1n}(x)[\Gamma_{FT}]\{\alpha_{Fn}\}tdydx$$

Separate the V_{FT} into V_{FT1} and V_{FT2}

$$V_{FT1} = -\frac{1}{2}\int_0^L\int_0^b\sum_{m=1}^{\mu}\sum_{n=1}^{\mu}\frac{1}{b^2}\{\alpha_{Fm}\}^T\left[\Gamma_{FT}\right]^T X_{1m}(x)\left[\sum_{k=1}^{\mu}\sigma_{1k}(x)\sigma_{T1k}\right]. \tag{4.53}$$
$$X_{1n}(x)[\Gamma_{FT}]\{\alpha_{Fn}\}tdydx$$

$$V_{FT2} = -\frac{1}{2}\int_0^L\int_0^b\sum_{m=1}^{\mu}\sum_{n=1}^{\mu}\frac{1}{b^2}\{\alpha_{Fm}\}^T\left[\Gamma_{FT}\right]^T X_{1m}(x)\left[\sum_{k=1}^{\mu}\sigma_{2k}(x)\sigma_{T2k}\right]. \tag{4.54}$$
$$X_{1n}(x)[\Gamma_{FT}]\{\alpha_{Fn}\}tdydx$$

These equations can be rewritten in other variables as:

$$V_{FT1} = -\frac{1}{2}\left(\frac{Lbt}{\pi b^2}\right)\int_0^{\bar{y}=1}\int_0^{\xi=\pi}\sum_{m=1}^{\mu}\sum_{n=1}^{\mu}\{\alpha_{Fm}\}^T\left[\Gamma_{FT}\right]^T X_{1m}(\xi)\left[\sum_{k=1}^{\mu}\sigma_{1k}(\xi)\sigma_{T1k}\right]. \tag{4.55}$$
$$X_{1n}(\xi)[\Gamma_{FT}]\{\alpha_{Fn}\}d\xi d\bar{y}$$

$$V_{FT2} = -\frac{1}{2}\left(\frac{Lbt}{\pi b^2}\right)\int_0^{\overline{y}=1}\int_0^{\xi=\pi}\sum_{m=1}^{\mu}\sum_{n=1}^{\mu}\{\alpha_{Fm}\}^T[\Gamma_{FT}]^T X_{1m}(\xi)\left[\sum_{k=1}^{\mu}\sigma_{2k}(\xi)\sigma_{T2k}\right]. \\ X_{1n}(\xi)[\Gamma_{FT}]\{\alpha_{Fn}\}d\xi d\overline{y}$$

(4.56)

Rearrange these equations:

$$V_{FT1} = -\frac{1}{2}\left(\frac{Lbt}{\pi b^2}\right)\sum_{k=1}^{\mu}\left(\begin{array}{c}\int_0^{\overline{y}=1}\sigma_{T1k}[\Gamma_{FT}]^T[\Gamma_{FT}]d\overline{y}.\\ \int_0^{\xi=\pi}\sum_{m=1}^{\mu}\sum_{n=1}^{\mu}\{\alpha_{Fm}\}^T X_{1m}(\xi)\sigma_{1k}(\xi)X_{1n}(\xi)\{\alpha_{Fn}\}d\xi\end{array}\right)$$

(4.57)

$$V_{FT2} = -\frac{1}{2}\left(\frac{Lbt}{\pi b^2}\right)\sum_{k=1}^{\mu}\left(\begin{array}{c}\int_0^{\overline{y}=1}\sigma_{T2k}[\Gamma_{FT}]^T[\Gamma_{FT}]d\overline{y}.\\ \int_0^{\xi=\pi}\sum_{m=1}^{\mu}\sum_{n=1}^{\mu}\{\alpha_{Fm}\}^T X_{1m}(\xi)\sigma_{2k}(\xi)X_{1n}(\xi)\{\alpha_{Fn}\}d\xi\end{array}\right)$$

(4.58)

These above equations can be rewritten as:

$$V_{FT1} = -\frac{1}{2}\left(\frac{Lbt}{\pi b^2}\right)\sum_{k=1}^{\mu}\left(\begin{array}{c}\int_0^{\overline{y}=1}\sigma_{T1k}[\Gamma_{FT}]^T[\Gamma_{FT}]d\overline{y}.\\ \int_0^{\xi=\pi}\sum_{m=1}^{\mu}\sum_{n=1}^{\mu}\{\delta_{Fm}\}^T[C_F]^{-T}X_{1m}(\xi)\sigma_{1k}(\xi)X_{1n}(\xi)[C_F]^{-1}\{\delta_{Fn}\}d\xi\end{array}\right)$$

(4.59)

$$V_{FT2} = -\frac{1}{2}\left(\frac{Lbt}{\pi b^2}\right)\sum_{k=1}^{\mu}\left(\begin{array}{c}\int_0^{\overline{y}=1}\sigma_{T2k}[\Gamma_{FT}]^T[\Gamma_{FT}]d\overline{y}.\\ \int_0^{\xi=\pi}\sum_{m=1}^{\mu}\sum_{n=1}^{\mu}\{\delta_{Fm}\}^T[C_F]^{-T}X_{1m}(\xi)\sigma_{2k}(\xi)X_{1n}(\xi)[C_F]^{-1}\{\delta_{Fn}\}d\xi\end{array}\right)$$

(4.60)

In other format:

$$V_{FT1} = -\frac{1}{2}\left(\frac{V}{\pi b^2}\right)\sum_{k=1}^{\mu}\left(B_{FT1}\sum_{m=1}^{\mu}\sum_{n=1}^{\mu}\{\delta_{Fm}\}^T[C_F]^{-T}C_{T1mnk}[C_F]^{-1}\{\delta_{Fn}\}\right)$$

(4.61)

$$V_{FT2} = -\frac{1}{2}\left(\frac{V}{\pi b^2}\right)\sum_{k=1}^{\mu}\left(B_{FT2}\sum_{m=1}^{\mu}\sum_{n=1}^{\mu}\{\delta_{Fm}\}^T[C_F]^{-T}C_{T2mnk}[C_F]^{-1}\{\delta_{Fn}\}\right)$$

(4.62)

where A_{FT}, B_{FT1}, B_{FT2}, C_{T1mnk}, C_{T2mnk} are given in Appendix C of the thesis

Hence:

$$V_{FT1} = -\frac{1}{2}\{\delta_{Fm}\}^T[C_F]^{-T}[g_{\alpha FT1mn}][C_F]^{-1}\{\delta_{Fn}\}$$

(4.63)

$$V_{FT2} = -\frac{1}{2}\{\delta_{Fm}\}^T [C_F]^{-T} [g_{\alpha FT2mn}][C_F]^{-1}\{\delta_{Fn}\}$$

(4.64)

where $[g_{\alpha FT1mn}]$ and $[g_{\alpha FT2mn}]$ are given in Appendix C of the thesis

4.4.4. The flexural potential energy of the shear stress

Shear stress distribution in a strip is shown in the Fig.4.5
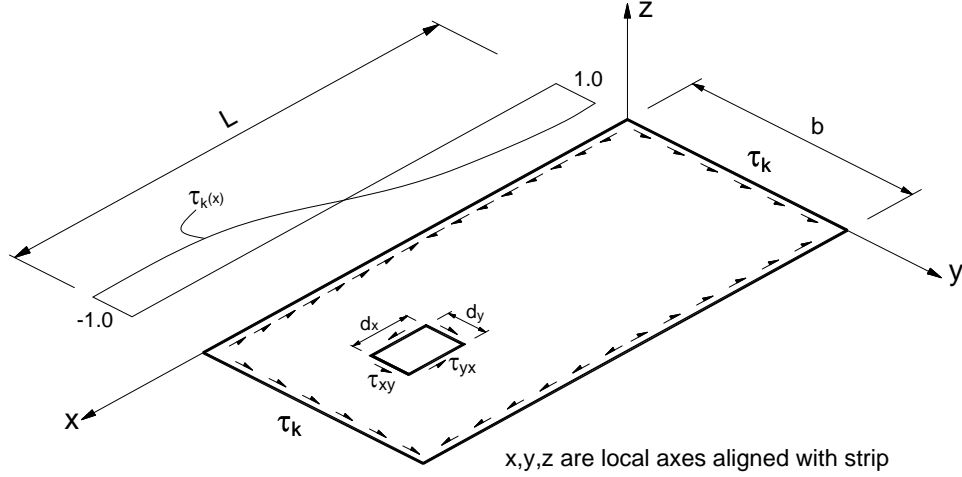
Figure 4.5: Shear stress distribution in a strip with both ends simply supported

The flexural potential energy of the shear stress

$$V_{FS} = V_{FS1} + V_{FS2}$$

(4.65)

$$V_{FS1} = -\frac{1}{2}\int_0^L\int_0^b \left[\tau_{xy}(x)\left(\frac{\partial w}{\partial x}\right)\left(\frac{\partial w}{\partial y}\right) \right] tdydx$$

(4.66)

$$V_{FS2} = -\frac{1}{2}\int_0^L\int_0^b \left[\tau_{xy}(x)\left(\frac{\partial w}{\partial y}\right)\left(\frac{\partial w}{\partial x}\right) \right] tdydx$$

(4.67)

Substitute (4.27), (4.9) and (4.10) to Eqs.(4.66) and (4.67) and do the summation taken over *μ* series terms of the potential energy of of the shear stress:

$$V_{FS1} = -\frac{1}{2}\int_0^L\int_0^b \sum_{m=1}^{\mu}\sum_{n}^{\mu}\{\alpha_{Fm}\}^T[\Gamma_{FL}]^T X_{1m}'(x)\left[\sum_{k=1}^{\mu}\tau_{1k}(x)\tau_{1k} + \sum_{k=1}^{\mu}\tau_{2k}(x)\tau_{2k} \right]. \\ \frac{1}{b}X_{1n}(x)[\Gamma_{FT}]\{\alpha_{Fn}\}tdydx$$

(4.68)

$$V_{FS2} = -\frac{1}{2}\int_0^L\int_0^b \sum_{m=1}^{\mu}\sum_{n}^{\mu}\{\alpha_{Fm}\}^T[\Gamma_{FT}]^T \frac{1}{b}X_{1m}(x)\left[\sum_{k=1}^{\mu}\tau_{1k}(x)\tau_{1k} + \sum_{k=1}^{\mu}\tau_{2k}(x)\tau_{2k} \right]. \\ X_{1n}'(x)[\Gamma_{FL}]\{\alpha_{Fn}\}tdydx$$

(4.69)

Separate the V_{FS1} into V_{FS11} and V_{FS12}

$$V_{FS11} = -\frac{1}{2} \int_0^L \int_0^b \sum_{m=1}^{\mu} \sum_n^{\mu} \{\alpha_{Fm}\}^T [\Gamma_{FL}]^T X_{1m}^{'}(x) \left[\sum_{k=1}^{\mu} \tau_{1k}(x)\tau_{1k} \right]. \qquad (4.70)$$
$$\frac{1}{b} X_{1n}(x)[\Gamma_{FT}]\{\alpha_{Fn}\} t\, dy\, dx$$

$$V_{FS12} = -\frac{1}{2} \int_0^L \int_0^b \sum_{m=1}^{\mu} \sum_n^{\mu} \{\alpha_{Fm}\}^T [\Gamma_{FL}]^T X_{1m}^{'}(x) \left[\sum_{k=1}^{\mu} \tau_{2k}(x)\tau_{2k} \right]. \qquad (4.71)$$
$$\frac{1}{b} X_{1n}(x)[\Gamma_{FT}]\{\alpha_{Fn}\} t\, dy\, dx$$

Separate the V_{FS2} into V_{FS21} and V_{FS22}

$$V_{FS21} = -\frac{1}{2} \int_0^L \int_0^b \sum_{m=1}^{\mu} \sum_n^{\mu} \{\alpha_{Fm}\}^T [\Gamma_{FT}]^T \frac{1}{b} X_{1m}(x) \left[\sum_{k=1}^{\mu} \tau_{1k}(x)\tau_{1k} \right]. \qquad (4.72)$$
$$X_{1n}^{'}(x)[\Gamma_{FL}]\{\alpha_{Fn}\} t\, dy\, dx$$

$$V_{FS22} = -\frac{1}{2} \int_0^L \int_0^b \sum_{m=1}^{\mu} \sum_n^{\mu} \{\alpha_{Fm}\}^T [\Gamma_{FT}]^T \frac{1}{b} X_{1m}(x) \left[\sum_{k=1}^{\mu} \tau_{2k}(x)\tau_{2k} \right]. \qquad (4.73)$$
$$X_{1n}^{'}(x)[\Gamma_{FL}]\{\alpha_{Fn}\} t\, dy\, dx$$

These equations can be rewritten in other variables as:

$$V_{FS11} = -\frac{1}{2} \left(\frac{Lbt}{\pi b} \right) \int_0^{\bar{y}=1} \int_0^{\xi=\pi} \sum_{m=1}^{\mu} \sum_{n=1}^{\mu} \{\alpha_{Fm}\}^T [\Gamma_{FL}]^T X_{1m}^{'}(\xi) \sum_{k=1}^{\mu} \tau_{1k}(\xi)\tau_{1k}. \qquad (4.74)$$
$$X_{1n}(\xi)[\Gamma_{FT}]\{\alpha_{Fn}\} d\xi\, d\bar{y}$$

$$V_{FS12} = -\frac{1}{2} \left(\frac{Lbt}{\pi b} \right) \int_0^{\bar{y}=1} \int_0^{\xi=\pi} \sum_{m=1}^{\mu} \sum_{n=1}^{\mu} \{\alpha_{Fm}\}^T [\Gamma_{FL}]^T X_{1m}^{'}(\xi) \sum_{k=1}^{\mu} \tau_{2k}(\xi)\tau_{2k}. \qquad (4.75)$$
$$X_{1n}(\xi)[\Gamma_{FT}]\{\alpha_{Fn}\} d\xi\, d\bar{y}$$

$$V_{FS21} = -\frac{1}{2} \left(\frac{Lbt}{\pi b} \right) \int_0^{\bar{y}=1} \int_0^{\xi=\pi} \sum_{m=1}^{\mu} \sum_{n=1}^{\mu} \{\alpha_{Fm}\}^T [\Gamma_{FT}]^T X_{1m}(\xi) \sum_{k=1}^{\mu} \tau_{1k}(\xi)\tau_{1k}. \qquad (4.76)$$
$$X_{1n}^{'}(\xi)[\Gamma_{FL}]\{\alpha_{Fn}\} d\xi\, d\bar{y}$$

$$V_{FS22} = -\frac{1}{2} \left(\frac{Lbt}{\pi b} \right) \int_0^{\bar{y}=1} \int_0^{\xi=\pi} \sum_{m=1}^{\mu} \sum_{n=1}^{\mu} \{\alpha_{Fm}\}^T [\Gamma_{FT}]^T X_{1m}(\xi) \sum_{k=1}^{\mu} \tau_{2k}(\xi)\tau_{2k}. \qquad (4.77)$$
$$X_{1n}^{'}(\xi)[\Gamma_{FL}]\{\alpha_{Fn}\} d\xi\, d\bar{y}$$

Rearrange these equations:

$$V_{FS11} = -\frac{1}{2}\left(\frac{Lbt}{\pi b}\right)\sum_{k=1}^{\mu}\left(\begin{array}{c}\displaystyle\int_0^{\bar{y}=1}\tau_{1k}\left[\Gamma_{FL}\right]^T\left[\Gamma_{FT}\right]d\bar{y}.\\[2ex]\displaystyle\int_0^{\xi=\pi}\sum_{m=1}^{\mu}\sum_{n=1}^{\mu}\{\alpha_{Fm}\}^T X_{1m}^{'}\left(\xi\right)\tau_{1k}\left(\xi\right)X_{1n}\left(\xi\right)\{\alpha_{Fn}\}d\xi\end{array}\right)$$ (4.78)

$$V_{FS12} = -\frac{1}{2}\left(\frac{Lbt}{\pi b}\right)\sum_{k=1}^{\mu}\left(\begin{array}{c}\displaystyle\int_0^{\bar{y}=1}\tau_{2k}\left[\Gamma_{FL}\right]^T\left[\Gamma_{FT}\right]d\bar{y}.\\[2ex]\displaystyle\int_0^{\xi=\pi}\sum_{m=1}^{\mu}\sum_{n=1}^{\mu}\{\alpha_{Fm}\}^T X_{1m}^{'}\left(\xi\right)\tau_{2k}\left(\xi\right)X_{1n}\left(\xi\right)\{\alpha_{Fn}\}d\xi\end{array}\right)$$ (4.79)

$$V_{FS21} = -\frac{1}{2}\left(\frac{Lbt}{\pi b}\right)\sum_{k=1}^{\mu}\left(\begin{array}{c}\displaystyle\int_0^{\bar{y}=1}\tau_{1k}\left[\Gamma_{FT}\right]^T\left[\Gamma_{FL}\right]d\bar{y}.\\[2ex]\displaystyle\int_0^{\xi=\pi}\sum_{m=1}^{\mu}\sum_{n=1}^{\mu}\{\alpha_{Fm}\}^T X_{1m}\left(\xi\right)\tau_{1k}\left(\xi\right)X_{1n}^{'}\left(\xi\right)\{\alpha_{Fn}\}d\xi\end{array}\right)$$ (4.80)

$$V_{FS22} = -\frac{1}{2}\left(\frac{Lbt}{\pi b}\right)\sum_{k=1}^{\mu}\left(\begin{array}{c}\displaystyle\int_0^{\bar{y}=1}\tau_{2k}\left[\Gamma_{FT}\right]^T\left[\Gamma_{FL}\right]d\bar{y}.\\[2ex]\displaystyle\int_0^{\xi=\pi}\sum_{m=1}^{\mu}\sum_{n=1}^{\mu}\{\alpha_{Fm}\}^T X_{1m}\left(\xi\right)\tau_{2k}\left(\xi\right)X_{1n}^{'}\left(\xi\right)\{\alpha_{Fn}\}d\xi\end{array}\right)$$ (4.81)

These above equations can be rewritten as:

$$V_{FS11} = -\frac{1}{2}\left(\frac{Lbt}{\pi b}\right)\sum_{k=1}^{\mu}\left(\begin{array}{c}\displaystyle\int_0^{\bar{y}=1}\tau_{1k}\left[\Gamma_{FL}\right]^T\left[\Gamma_{FT}\right]d\bar{y}.\\[2ex]\displaystyle\int_0^{\xi=\pi}\sum_{m=1}^{\mu}\sum_{n=1}^{\mu}\{\delta_{Fm}\}^T\left[C_F\right]^{-T} X_{1m}^{'}\left(\xi\right)\tau_{1k}\left(\xi\right)X_{1n}\left(\xi\right)\left[C_F\right]^{-1}\{\delta_{Fn}\}d\xi\end{array}\right)$$ (4.82)

$$V_{FS12} = -\frac{1}{2}\left(\frac{Lbt}{\pi b}\right)\sum_{k=1}^{\mu}\left(\begin{array}{c}\displaystyle\int_0^{\bar{y}=1}\tau_{2k}\left[\Gamma_{FL}\right]^T\left[\Gamma_{FT}\right]d\bar{y}.\\[2ex]\displaystyle\int_0^{\xi=\pi}\sum_{m=1}^{\mu}\sum_{n=1}^{\mu}\{\delta_{Fm}\}^T\left[C_F\right]^{-T} X_{1m}^{'}\left(\xi\right)\tau_{2k}\left(\xi\right)X_{1n}\left(\xi\right)\left[C_F\right]^{-1}\{\delta_{Fn}\}d\xi\end{array}\right)$$ (4.83)

$$V_{FS21} = -\frac{1}{2}\left(\frac{Lbt}{\pi b}\right)\sum_{k=1}^{\mu}\left(\begin{array}{c}\displaystyle\int_0^{\bar{y}=1}\tau_{1k}\left[\Gamma_{FT}\right]^T\left[\Gamma_{FL}\right]d\bar{y}.\\[2ex]\displaystyle\int_0^{\xi=\pi}\sum_{m=1}^{\mu}\sum_{n=1}^{\mu}\{\delta_{Fm}\}^T\left[C_F\right]^{-T} X_{1m}\left(\xi\right)\tau_{1k}\left(\xi\right)X_{1n}^{'}\left(\xi\right)\left[C_F\right]^{-1}\{\delta_{Fn}\}d\xi\end{array}\right)$$ (4.84)

$$V_{FS22} = -\frac{1}{2}\left(\frac{Lbt}{\pi b}\right)\sum_{k=1}^{\mu}\left(\begin{array}{l}\int_{0}^{\bar{y}=1}\tau_{2k}\left[\Gamma_{FT}\right]^{T}\left[\Gamma_{FL}\right]d\bar{y}.\\ \int_{0}^{\xi=\pi}\sum_{m=1}^{\mu}\sum_{n=1}^{\mu}\{\delta_{Fm}\}^{T}\left[C_{F}\right]^{-T}X_{1m}(\xi)\tau_{2k}(\xi)X_{1n}'(\xi)\left[C_{F}\right]^{-1}\{\delta_{Fn}\}d\xi\end{array}\right)$$ (4.85)

In other format:

$$V_{FS11} = -\frac{1}{2}\left(\frac{V}{\pi b}\right)\sum_{k=1}^{\mu}\left(B_{FS11}\sum_{m=1}^{\mu}\sum_{n=1}^{\mu}\{\delta_{Fm}\}^{T}\left[C_{F}\right]^{-T}C_{S11mnk}\left[C_{F}\right]^{-1}\{\delta_{Fn}\}\right)$$ (4.86)

$$V_{FS12} = -\frac{1}{2}\left(\frac{V}{\pi b}\right)\sum_{k=1}^{\mu}\left(B_{FS12}\sum_{m=1}^{\mu}\sum_{n=1}^{\mu}\{\delta_{Fm}\}^{T}\left[C_{F}\right]^{-T}C_{S12mnk}\left[C_{F}\right]^{-1}\{\delta_{Fn}\}\right)$$ (4.87)

$$V_{FS21} = -\frac{1}{2}\left(\frac{V}{\pi b}\right)\sum_{k=1}^{\mu}\left(B_{FS21}\sum_{m=1}^{\mu}\sum_{n=1}^{\mu}\{\delta_{Fm}\}^{T}\left[C_{F}\right]^{-T}C_{S21mnk}\left[C_{F}\right]^{-1}\{\delta_{Fn}\}\right)$$ (4.88)

$$V_{FS22} = -\frac{1}{2}\left(\frac{V}{\pi b}\right)\sum_{k=1}^{\mu}\left(B_{FS22}\sum_{m=1}^{\mu}\sum_{n=1}^{\mu}\{\delta_{Fm}\}^{T}\left[C_{F}\right]^{-T}C_{S22mnk}\left[C_{F}\right]^{-1}\{\delta_{Fn}\}\right)$$ (4.89)

where A_{FS1}, A_{FS2}, B_{FS11}, B_{FS12}, B_{FS21}, B_{FS22}, C_{S11mnk}, C_{S12mnk}, C_{S21mnk}, C_{S22mnk} are given in Appendix C of the thesis

Hence:

$$V_{FS11} = -\frac{1}{2}\{\delta_{Fm}\}^{T}\left[C_{F}\right]^{-T}\left[g_{\alpha FS11mn}\right]\left[C_{F}\right]^{-1}\{\delta_{Fn}\}$$ (4.90)

$$V_{FS12} = -\frac{1}{2}\{\delta_{Fm}\}^{T}\left[C_{F}\right]^{-T}\left[g_{\alpha FS12mn}\right]\left[C_{F}\right]^{-1}\{\delta_{Fn}\}$$ (4.91)

$$V_{FS21} = -\frac{1}{2}\{\delta_{Fm}\}^{T}\left[C_{F}\right]^{-T}\left[g_{\alpha FS21mn}\right]\left[C_{F}\right]^{-1}\{\delta_{Fn}\}$$ (4.92)

$$V_{FS22} = -\frac{1}{2}\{\delta_{Fm}\}^{T}\left[C_{F}\right]^{-T}\left[g_{\alpha FS22mn}\right]\left[C_{F}\right]^{-1}\{\delta_{Fn}\}$$ (4.93)

where $\left[g_{\alpha FS11mn}\right], \left[g_{\alpha FS12mn}\right], \left[g_{\alpha FS21mn}\right], \left[g_{\alpha FS22mn}\right]$ and $\left[g_{\alpha FT2mn}\right]$ are given in Appendix C of the thesis

4.4.5. The flexural stability matrix of a strip

The total flexural potential energy of the membrane stresses from Eq.(4.29) can be written as given:

$$V_F = -\frac{1}{2}\{\delta_{Fm}\}^{T}\left[g_{Fmn}\right]\{\delta_{Fn}\}$$ (4.94)

where

$[g_{Fmn}]$ is the flexural stability matrix of a strip

$$[g_{Fmn}] = [C_F]^{-T}[g_{\alpha Fmn}][C_F]^{-1} \tag{4.95}$$

$[g_{\alpha Fmn}]$ is given in Appendix C of the thesis

4.5. THE MEMBRANE STABILITY MATRIX OF A STRIP

4.5.1. The membrane potential energy of the membrane stresses

The membrane potential energy of the membrane stresses as stated in [15]: "to calculate the loss of potential energy of the stress $\sigma_x(x)$ we make use of the following non-linear expression for the longitudinal strain ε_x":

$$\varepsilon_x = \frac{\partial u}{\partial x} + \frac{1}{2}\left\{\left(\frac{\partial u}{\partial x}\right)^2 + \left(\frac{\partial v}{\partial x}\right)^2 + \left(\frac{\partial w}{\partial x}\right)^2\right\} \tag{4.96}$$

The first term has already been accounted for in deriving internal energy, whilst the last term, involving w, has been used in Eq.(4.28) in the calculation of the loss of potential energy of the basic stresses due to the flexural displacement. Thus, the appropriate expression for the loss of potential energy of the basic stresses due to the membrane displacement is:

$$V_M = -\frac{1}{2}\int_0^L\int_0^b \left(\sigma_x(x)\left(\frac{\partial v}{\partial x}\right)^2 + \sigma_x(x)\left(\frac{\partial u}{\partial x}\right)^2\right) t\, dy\, dx \tag{4.97}$$

As stated in [15], it is believed that there are no membrane instabilities associated with transverse stress and shear stress so that there are no term in above equation associated with these. This equation is written as below:

$$V_M = V_{Mv} + V_{Mu} \tag{4.98}$$

where:

V_{Mv} is the membrane potential energy of the longitudinal stress by transverse direction

$$V_{Mv} = -\frac{1}{2}\int_0^L\int_0^b \left[\sigma_x(x)\left(\frac{\partial v}{\partial x}\right)^2\right] t\, dy\, dx \tag{4.99}$$

V_{Mu} is the membrane potential energy of the longitudinal stress by longitudinal direction

$$V_{Mu} = -\frac{1}{2}\int_0^L\int_0^b \left[\sigma_x(x)\left(\frac{\partial u}{\partial x}\right)^2\right] t\, dy\, dx \tag{4.100}$$

4.5.2. The membrane potential energy of the stress by the transverse direction

Membrane deformations
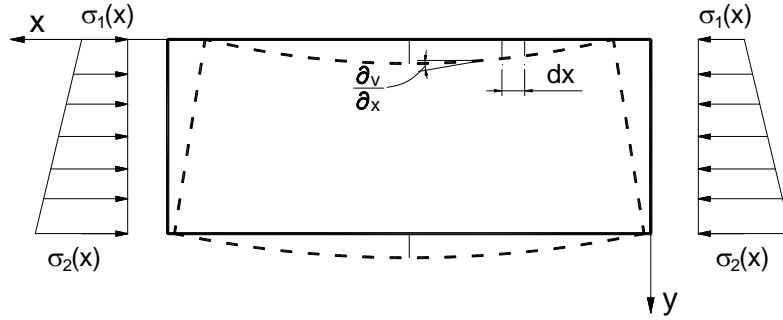
Figure 4.6: Membrane deformations of a strip

Increase in potential energy of membrane forces resulting from membrane deformations:

$$V_{Mv} = -\frac{1}{2}\int_0^L\int_0^b\left[\sigma_x(x)\left(\frac{\partial v}{\partial x}\right)^2\right]tdydx \tag{4.101}$$

Substitute Eqs.(4.25) and (4.19) to Eq.(4.101) and do the summation taken over μ series terms of the potential energy of the longitudinal stress:

$$V_{Mv} = -\frac{1}{2}\int_0^L\int_0^b\sum_{m=1}^{\mu}\sum_{n=1}^{\mu}\{\alpha_{Mm}\}^T[\Gamma_{Mv}]^T X_{1m}'(x)\left(\sum_{k=1}^{\mu}\sigma_{1k}(x)\sigma_{L1k}+\sum_{k=1}^{\mu}\sigma_{2k}(x)\left[\sigma_{L2k}+\sigma_{L3k}\frac{y}{b}\right]\right). \tag{4.102}$$
$$X_{1n}'(x)[\Gamma_{Mv}]\{\alpha_{Mn}\}tdydx$$

Separate the V_{Mv1} into V_{Mv1} and V_{Mv2}

$$V_{Mv1} = -\frac{1}{2}\int_0^L\int_0^b\sum_{m=1}^{\mu}\sum_{n=1}^{\mu}\{\alpha_{Mm}\}^T[\Gamma_{Mv}]^T X_{1m}'(x)\left(\sum_{k=1}^{\mu}\sigma_{1k}(x)\sigma_{L1k}\right)X_{1n}'(x)[\Gamma_{Mv}]\{\alpha_{Mn}\}tdydx \tag{4.103}$$

$$V_{Mv2} = -\frac{1}{2}\int_0^L\int_0^b\sum_{m=1}^{\mu}\sum_{n=1}^{\mu}\{\alpha_{Mm}\}^T[\Gamma_{Mv}]^T X_{1m}'(x)\left(\sum_{k=1}^{\mu}\sigma_{2k}(x)\left[\sigma_{L2k}+\sigma_{L3k}\frac{y}{b}\right]\right). \tag{4.104}$$
$$X_{1n}'(x)[\Gamma_{Mv}]\{\alpha_{Mn}\}tdydx$$

These equations can be rewritten in other variables as:

$$V_{Mv1} = -\frac{1}{2}\left(\frac{Lbt}{\pi}\right)\int_0^{\overline{y}=1}\int_0^{\xi=\pi}\sum_{m=1}^{\mu}\sum_{n=1}^{\mu}\{\alpha_{Mm}\}^T[\Gamma_{Mv}]^T X_{1m}'(\xi)\left(\sum_{k=1}^{\mu}\sigma_{1k}(\xi)\sigma_{L1k}\right). \tag{4.105}$$
$$X_{1n}'(\xi)[\Gamma_{Mv}]\{\alpha_{Mn}\}d\xi d\overline{y}$$

$$V_{Mv2} = -\frac{1}{2}\left(\frac{Lbt}{\pi}\right)\int_0^{\bar{y}=1}\int_0^{\xi=\pi}\sum_{m=1}^{\mu}\sum_{n=1}^{\mu}\{\alpha_{Mm}\}^T[\Gamma_{Mv}]^T X_{1m}'(\xi)\left(\sum_{k=1}^{\mu}\sigma_{2k}(\xi)\left[\sigma_{L2k}+\sigma_{L3k}\frac{y}{b}\right]\right).$$
$$X_{1n}'(\xi)[\Gamma_{Mv}]\{\alpha_{Mn}\}d\xi d\bar{y} \tag{4.106}$$

Rearrange these equations:

$$V_{Mv1} = -\frac{1}{2}\left(\frac{Lbt}{\pi}\right)\sum_{k=1}^{\mu}\left(\begin{array}{c}\int_0^{\bar{y}=1}\sigma_{L1k}[\Gamma_{Mv}]^T[\Gamma_{Mv}]d\bar{y}.\\[6pt]\int_0^{\xi=\pi}\sum_{m=1}^{\mu}\sum_{n=1}^{\mu}\{\alpha_{Mm}\}^T X_{1m}'(\xi)\sigma_{1k}(\xi)X_{1n}'(\xi)\{\alpha_{Mn}\}d\xi\end{array}\right) \tag{4.107}$$

$$V_{Mv2} = -\frac{1}{2}\left(\frac{Lbt}{\pi}\right)\sum_{k=1}^{\mu}\left(\begin{array}{c}\int_0^{\bar{y}=1}\left[\sigma_{L2k}+\sigma_{L3k}\bar{y}\right][\Gamma_{Mv}]^T[\Gamma_{Mv}]d\bar{y}.\\[6pt]\int_0^{\xi=\pi}\sum_{m=1}^{\mu}\sum_{n=1}^{\mu}\{\alpha_{Mm}\}^T X_{1m}'(\xi)\sigma_{2k}(\xi)X_{1n}'(\xi)\{\alpha_{Mn}\}d\xi\end{array}\right) \tag{4.108}$$

In other format:

$$V_{Mv1} = -\frac{1}{2}\left(\frac{V}{\pi}\right)\sum_{k=1}^{\mu}\left(B_{Mv1}\sum_{m=1}^{\mu}\sum_{n=1}^{\mu}\{\delta_{Mm}\}^T[C_M]^{-T}C_{Lv1mnk}[C_M]^{-1}\{\delta_{Mn}\}\right) \tag{4.109}$$

$$V_{Mv2} = -\frac{1}{2}\left(\frac{V}{\pi}\right)\sum_{k=1}^{\mu}\left(B_{Mv2}\sum_{m=1}^{\mu}\sum_{n=1}^{\mu}\{\delta_{Mm}\}^T[C_M]^{-T}C_{Lv2mnk}[C_M]^{-1}\{\delta_{Mn}\}\right) \tag{4.110}$$

where A_{Mv}, B_{Mv1}, B_{Mv2}, C_{Lv1mnk}, C_{Lv2mnk} are given in Appendix C of the thesis

The above equations can be rewritten as:

$$V_{Mv1} = -\frac{1}{2}\{\delta_{Mm}\}^T[C_M]^{-T}[g_{\alpha Mv1mn}][C_M]^{-1}\{\delta_{Mn}\} \tag{4.111}$$

$$V_{Mv2} = -\frac{1}{2}\{\delta_{Mm}\}^T[C_M]^{-T}[g_{\alpha Mv2mn}][C_M]^{-1}\{\delta_{Mn}\} \tag{4.112}$$

where $[g_{\alpha Mv1mn}]$ and $[g_{\alpha Mv2mn}]$ are given in Appendix C of the thesis

4.5.3. The membrane potential energy of the stress by the longitudinal direction

Increase in potential energy of membrane forces resulting from membrane deformations:

$$V_{Mu} = -\frac{1}{2}\int_0^L\int_0^b\left[\sigma_x(x)\left(\frac{\partial u}{\partial x}\right)^2\right]tdydx \tag{4.113}$$

Substitute Eqs.(4.25) and (4.21) to Eq.(4.113) and do the summation taken over μ series terms of the potential energy of the longitudinal stress:

$$V_{Mu} = -\frac{1}{2}\int_0^L\int_0^b\sum_{m=1}^{\mu}\sum_{n=1}^{\mu}\{\alpha_{Mm}\}^T[\Gamma_{Mu}]^T X_{2m}'(x)\left(\sum_{k=1}^{\mu}\sigma_{1k}(x)\sigma_{L1k} + \sum_{k=1}^{\mu}\sigma_{2k}(x)\left[\sigma_{L2k}+\sigma_{L3k}\frac{y}{b}\right]\right).$$

$$X_{2n}'(x)[\Gamma_{Mu}]\{\alpha_{Mn}\}tdydx \qquad (4.114)$$

Separate the V_{Mu} into V_{Mu1} and V_{Mu2}

$$V_{Mu1} = -\frac{1}{2}\int_0^L\int_0^b\sum_{m=1}^{\mu}\sum_{n=1}^{\mu}\{\alpha_{Mm}\}^T[\Gamma_{Mu}]^T X_{2m}'(x)\left(\sum_{k=1}^{\mu}\sigma_{1k}(x)\sigma_{L1k}\right).$$

$$X_{2n}'(x)[\Gamma_{Mu}]\{\alpha_{Mn}\}tdydx \qquad (4.115)$$

$$V_{Mu2} = -\frac{1}{2}\int_0^L\int_0^b\sum_{m=1}^{\mu}\sum_{n=1}^{\mu}\{\alpha_{Mm}\}^T[\Gamma_{Mu}]^T X_{2m}'(x)\left(\sum_{k=1}^{\mu}\sigma_{2k}(x)\left[\sigma_{L2k}+\sigma_{L3k}\frac{y}{b}\right]\right).$$

$$X_{2n}'(x)[\Gamma_{Mu}]\{\alpha_{Mn}\}tdydx \qquad (4.116)$$

These equations can be rewritten in other variables as:

$$V_{Mu1} = -\frac{1}{2}\left(\frac{Lbt}{\pi}\right)\int_0^{\bar{y}=1}\int_0^{\xi=\pi}\sum_{m=1}^{\mu}\sum_{n=1}^{\mu}\{\alpha_{Mm}\}^T[\Gamma_{Mu}]^T X_{1m}'(\xi)\left(\sum_{k=1}^{\mu}\sigma_{1k}(\xi)\sigma_{L1k}\right).$$

$$X_{2n}'(\xi)[\Gamma_{Mu}]\{\alpha_{Mn}\}d\xi d\bar{y} \qquad (4.117)$$

$$V_{Mu2} = -\frac{1}{2}\left(\frac{Lbt}{\pi}\right)\int_0^{\bar{y}=1}\int_0^{\xi=\pi}\sum_{m=1}^{\mu}\sum_{n=1}^{\mu}\{\alpha_{Mm}\}^T[\Gamma_{Mu}]^T X_{1m}'(\xi)\left(\sum_{k=1}^{\mu}\sigma_{2k}(\xi)\left[\sigma_{L2k}+\sigma_{L3k}\frac{y}{b}\right]\right).$$

$$X_{2n}'(\xi)[\Gamma_{Mu}]\{\alpha_{Mn}\}d\xi d\bar{y} \qquad (4.118)$$

Rearrange these equations:

$$V_{Mu1} = -\frac{1}{2}\left(\frac{Lbt}{\pi}\right)\sum_{k=1}^{\mu}\left(\begin{array}{c}\int_0^{\bar{y}=1}\sigma_{L1k}[\Gamma_{Mu}]^T[\Gamma_{Mu}]d\bar{y}.\\ \int_0^{\xi=\pi}\sum_{m=1}^{\mu}\sum_{n=1}^{\mu}\{\alpha_{Mm}\}^T X_{2m}'(\xi)\sigma_{1k}(\xi)X_{2n}'(\xi)\{\alpha_{Mn}\}d\xi\end{array}\right) \qquad (4.119)$$

$$V_{Mu2} = -\frac{1}{2}\left(\frac{Lbt}{\pi}\right)\sum_{k=1}^{\mu}\left(\begin{array}{c}\int_0^{\bar{y}=1}\left[\sigma_{L2k}+\sigma_{L3k}\bar{y}\right][\Gamma_{Mu}]^T[\Gamma_{Mu}]d\bar{y}.\\ \int_0^{\xi=\pi}\sum_{m=1}^{\mu}\sum_{n=1}^{\mu}\{\alpha_{Mm}\}^T X_{2m}'(\xi)\sigma_{1k}(\xi)X_{2n}'(\xi)\{\alpha_{Mn}\}d\xi\end{array}\right) \qquad (4.120)$$

In other format:

$$V_{Mu1} = -\frac{1}{2}\left(\frac{V}{\pi}\right)\sum_{k=1}^{\mu}\left(B_{Mu1} \sum_{m=1}^{\mu}\sum_{n=1}^{\mu}\{\delta_{Mm}\}^{T}\left[C_{M}\right]^{-T} C_{Lu1mnk}\left[C_{M}\right]^{-1}\{\delta_{Mn}\} \right) \tag{4.121}$$

$$V_{Mu2} = -\frac{1}{2}\left(\frac{V}{\pi}\right)\sum_{k=1}^{\mu}\left(B_{Mu2} \sum_{m=1}^{\mu}\sum_{n=1}^{\mu}\{\delta_{Mm}\}^{T}\left[C_{M}\right]^{-T} C_{Lu2mnk}\left[C_{M}\right]^{-1}\{\delta_{Mn}\} \right) \tag{4.122}$$

where A_{Mu}, B_{Mu1}, B_{Mu2}, C_{Lu1mnk}, C_{Lu2mnk} are given in Appendix C of the thesis

These above equations can be rewritten as:

$$V_{Mu1} = -\frac{1}{2}\{\delta_{Mm}\}^{T}\left[C_{M}\right]^{-T}\left[g_{\alpha Mu1mn}\right]\left[C_{M}\right]^{-1}\{\delta_{Mn}\} \tag{4.123}$$

$$V_{Mu2} = -\frac{1}{2}\{\delta_{Mm}\}^{T}\left[C_{M}\right]^{-T}\left[g_{\alpha Mu2mn}\right]\left[C_{M}\right]^{-1}\{\delta_{Mn}\} \tag{4.124}$$

where $\left[g_{\alpha Mu1mn}\right]$ and $\left[g_{\alpha Mu2mn}\right]$ are given in Appendix C of the thesis

4.5.4. The membrane stability of a strip

The total membrane potential energy of the membrane stresses from Eq.(4.98) can be written as given:

$$V_{M} = -\frac{1}{2}\{\delta_{Mm}\}^{T}\left[g_{Mmn}\right]\{\delta_{Mn}\} \tag{4.125}$$

where

$\left[g_{Mmn}\right]$ is the membrane stability matrix of a strip

$$\left[g_{Mmn}\right] = \left[C_{M}\right]^{-T}\left[g_{\alpha Mmn}\right]\left[C_{M}\right]^{-1} \tag{4.126}$$

$\left[g_{\alpha Mmn}\right]$ is given in Appendix C of the thesis

4.6. THE STABILITY MATRIX OF THE SECTION

The stability matrix of a strip in the local coordinate is assembled from both the flexural stability matrix and the membrane stability matrix, thus the stability matrix $\left[G_{L}\right]$ is an 8x8 size matrix.

$$\left[G_{L}\right] = \begin{bmatrix} \left[g_{\alpha Fmn}\right] & 0 \\ 0 & \left[g_{\alpha Mmn}\right] \end{bmatrix} \tag{4.127}$$

where $[G_{L}]$ is the stability matrix in the local coordinate.

The stability matrix of a strip in the global coordinate is determined by a multiplication of the stability matrix in the local coordinate with transformation matrices as given:

$$[G_G] = [A][G_L][A]^T \qquad (4.128)$$

where:

$[G_G]$ is the stability matrix in the global coordinate,

$[A]$ and $[A]^T$ are transformation matrices from local to global coordinates, given in Appendix C of the thesis

The global stability matrix of a strip is divided into four parts which are based on the number of nodes of each strip as given:

$$[G_G] = \begin{bmatrix} \begin{bmatrix} G_{ppmn} \end{bmatrix} & \begin{bmatrix} G_{pqmn} \end{bmatrix} \\ \begin{bmatrix} G_{qpmn} \end{bmatrix} & \begin{bmatrix} G_{qqmn} \end{bmatrix} \end{bmatrix} \qquad (4.129)$$

where p and q are the start node and the end node of each strip

The stability matrix of the section for each series term is assembled from the stability matrices of nodes in strips, thus the size of this matrix is 4 times the number of nodes. The stability matrix at each point of this matrix is determined by doing the summation of stability matrix components of strips which have the same node. The stability matrix of the whole section is assembled from the stability matrices of series terms as shown in Fig.4.7, thus the size of this matrix is 4 times the number of series terms and the number of nodes.
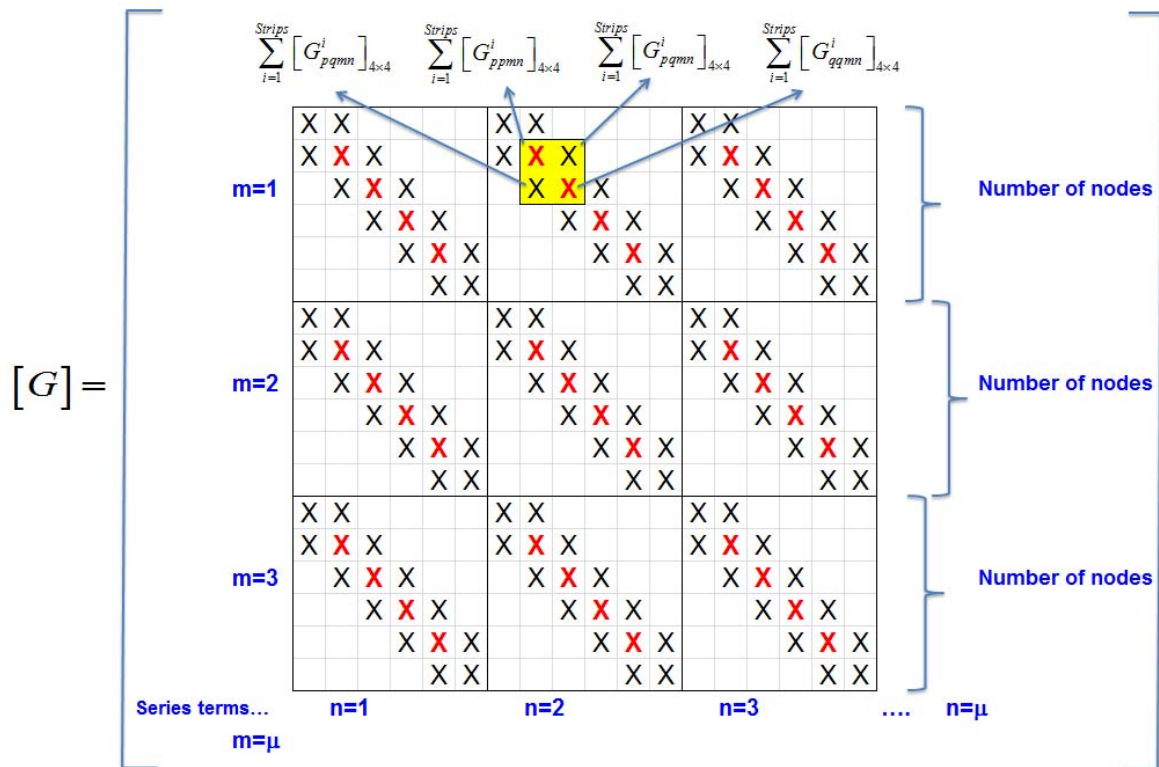
Figure 4.7: The stability matrix for whole section

4.7. ELASTIC BUCKLING ANALYSIS

4.7.1. Minimization of the potential energy

The strain energy of a strip is given by:

$$U = U_F + U_M \tag{4.130}$$

In matrix format:

$$U = \{\delta_b\}^T [K] \{\delta_b\} \tag{4.131}$$

where $\{\delta_b\}$ is the buckling displacement of the section, called buckling mode.

The potential energy due to the membrane stresses can be written as:

$$V = V_F + V_M \tag{4.132}$$

In matrix format:

$$V = \{\delta_b\}^T [G] \{\delta_b\} \tag{4.133}$$

The total potential energy is the sum of the elastic strain energy stored in a strip and the potential energy of the membrane stresses, thus:

$$\phi = U + V \tag{4.134}$$

$$\phi = \{\delta_b\}^T [K] \{\delta_b\} - \{\delta_b\}^T [G] \{\delta_b\} \tag{4.135}$$

Note: the negative sign in the above equation is a result of the assumption that the compression stress is positive producing a reduction in the potential energy.

The principle of minimum total potential energy requires that:

$$\left\{ \frac{\partial \phi}{\partial \{\delta_b\}} \right\} = \{0\} \tag{4.136}$$

Hence:

$$\left([K] - \lambda [G]\right) \{\delta_b\} = \{0\} \tag{4.137}$$

where:

λ is the load factor against buckling for the applied stresses

r is the size of the stiffness matrix [K] and the stability matrix [G]

$$r = 4 \times \mu \times n$$

μ is the number of series terms

n is the number of nodes of the section

4.7.2. The eigenvalue

The Eq.(4.137) is called a LINEAR EIGENVALUE PROBLEM. The r values of λ for which the determinant of $([K]-\lambda[G])$ is zero are called the EIGENVALUES. The r eigenvalues are the load factors for buckling in the r different series terms. Obviously the section will buckle at the lowest calculated value of λ. The eigenvalue λ is obtained from this equation by using Eigenvalue routine in Matlab.

4.7.3. The buckling modes

The r values of $\{\delta_b\}$ corresponding to the r values of λ are called the EIGENVECTORS. They are the amplitude of the buckling modes of the section which are obtained from below equation:

$$\left([K]-\lambda[G]\right)\{\delta_{bA}\}=\{0\} \tag{4.138}$$

Each eigenvector $\{\delta_{bA}\}$ corresponds to a partial eigenvalue λ in the above equation. The eigenvectors are computed by solving Eq.(4.138) in Matlab. In the calculation, the buckling mode is the eigenvector corresponds to the minimum eigenvalue λ and this is the amplitude buckling mode for whole section as shown in the Fig.4.8. This buckling mode vector has the same rows with the [K] and [G] matrices.
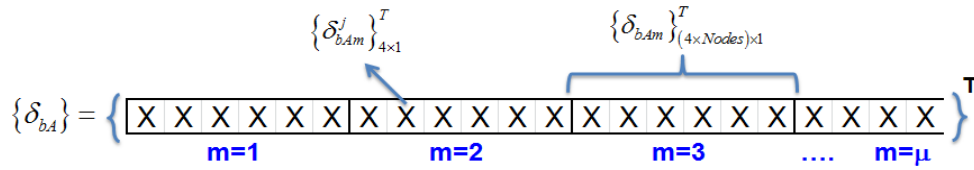
Figure 4.8: Amplitude of buckling modes vector

The buckling mode vector $\{\delta_{bA}\}$ is split up to the buckling mode vectors for each mode $\{\delta_{bAm}\}$ and the buckling mode vectors for each nodal line $\{\delta^j_{bAm}\}$

$$\left\{\delta^j_{bAm}\right\}=\left\{\delta^j_{bAXm} \quad \delta^j_{bAYm} \quad \delta^j_{bAZm} \quad \theta^j_{bAZm}\right\}^T$$

where:

   j is the nodal line

   $\{\delta_{bAm}\}$ is the amplitude of the buckling mode vector for series term m^{th} $\{\delta^j_{bAm}\}$ is the amplitude of the buckling mode vector of nodal line j, series term m^{th}

   The amplitudes of the buckling modes are multiplied with the displacement functions to get the buckling modes for all sections along the structural member.

$$\delta^j_{bXm}=\delta^j_{bAXm}X_{1m}(x_{sec}); \qquad \delta^j_{bYm}=\delta^j_{bAYm}X_{1m}(x_{sec})$$
$$\delta^j_{bZm}=\delta^j_{bAZm}X_{2m}(x_{sec}); \qquad \theta^j_{bZm}=\theta^j_{bAZm}X_{1m}(x_{sec}) \tag{4.139}$$

where:

δ^j_{bAXm}, δ^j_{bAYm}, δ^j_{bAZm}, θ^j_{bAZm} are the amplitudes of buckling mode of nodal line j, series term m^{th}

δ^j_{bXm}, δ^j_{bYm}, δ^j_{bZm}, θ^j_{bZm} are the buckling modes of node j, series term m^{th}

x_{sec} is the location of sections along the beam

The displacement of nodes along the beam is determined by doing the summation of the displacement in all series terms.

$$\delta^j_{bX} = \sum_{m=1}^{\mu} \delta^j_{bXm} \; ; \; \delta^j_{bY} = \sum_{m=1}^{\mu} \delta^j_{bYm}$$

$$\delta^j_{bX} = \sum_{m=1}^{\mu} \delta^j_{bZm} \; ; \; \theta^j_{bZ} = \sum_{m=1}^{\mu} \theta^j_{bZm}$$

(4.140)

where δ^j_{bX}, δ^j_{bY}, δ^j_{bZ}, θ^j_{bZ} are the buckling modes of node j

4.8. NUMERICAL EXAMPLE

Buckling analyses have been performed for a lipped channel section with rounded corners under localised loading using the THIN-WALL-2 V2.0 program. The geometry of the beam and the loading are shown in Fig.4.9. The beam is analysed with different boundary conditions for the web and the flanges of the end sections. In addition, lateral restraints are applied along the beam at Nodal Lines 11 and 35 to avoid twisting caused by eccentric loading. In the Simply-Free (SF) and Free-Free (FF) cases, the beam can move freely in the longitudinal direction, thus longitudinal restraints are applied at Nodal Lines 11 and 35 along the beam to prevent this movement. Furthermore, in the Free-Free (FF) case, the beam has no supports at both ends, thus vertical restraints are applied at Nodal Line 35 along the beam to prevent the movement of the beam in the vertical direction. The results from the elastic buckling analysis of the beam under localised loading include buckling modes and load factor. The buckling modes are obtained from Nodal Line 23 for all sections.

The beam has also been analysed using the ABAQUS software with an equivalent loading and boundary condition. It was meshed into 5mm x 5mm, except at the section's corners. The corners were modeled with 1mm x 5mm mesh to accurately represent the influence of corner radius. The buckling mode values are obtained from Nodal Line 23 for all sections.
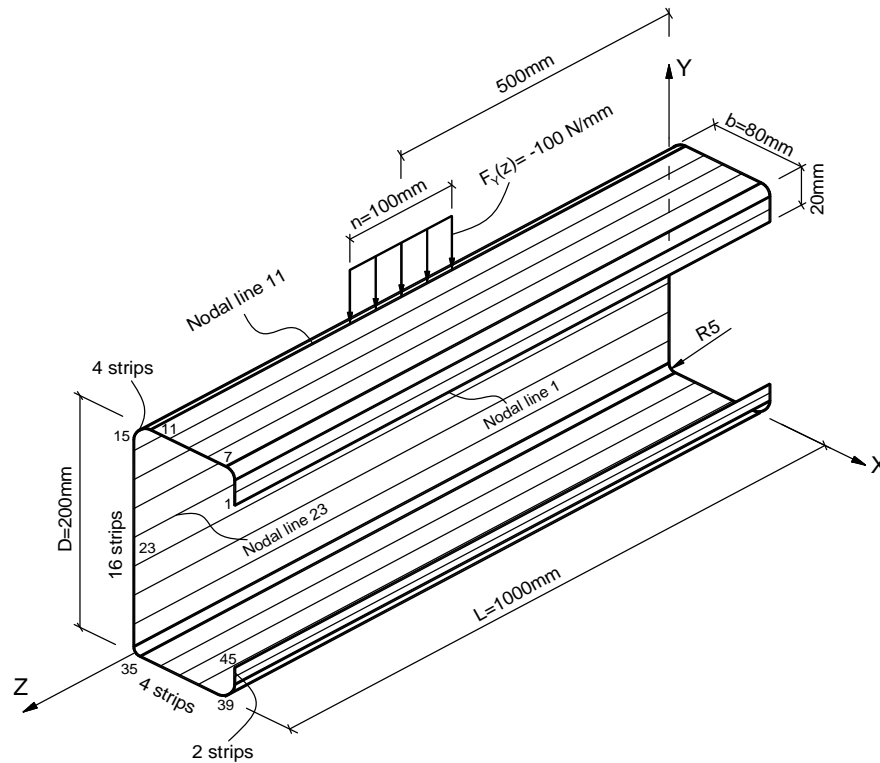
Figure 4.9: Lipped channel section under localised loading

Table 4.1: Buckling load factor (λ) comparison (L=1000mm, n=100mm)

Boundary conditions	FSM (THIN-WALL-2) (15 series terms)	FEM (Abaqus)	Difference (%)
SS	2.88402	2.87770	0.2196%
SC	3.23008	3.19310	1.1582%
SF	3.30027	3.30360	0.1008%
CC	3.45942	3.43930	0.5850%
CF	3.18921	3.18080	0.2643%
FF	2.88612	2.88610	0.0007%

The buckling analyses of the section have been performed for different boundary conditions by both the FSM using 15 series terms and the FEM. The detailed comparison of the buckling load factor λ for the different boundary conditions is shown in Table 4.1 with the difference from 0.0007% to 1.1582%. It is clear that the FSM provides accurate estimates of buckling load factor in comparison with the FEM.

The beam is subdivided into 21 equally spaced sections to calculate and plot the deformations along the beam. The comparison between the buckling modes from the FSM and the FEM are shown

in Figs.4.10 to 4.13 for the Clamped - Free (CF) case which uses the Bradford and Azhari [16] displacement functions with 15 series terms. The results for other boundary conditions are shown in Figs.D-1 to D-20 in Appendix D of the thesis.

(a) From THIN-WALL-2   (b) From Abaqus
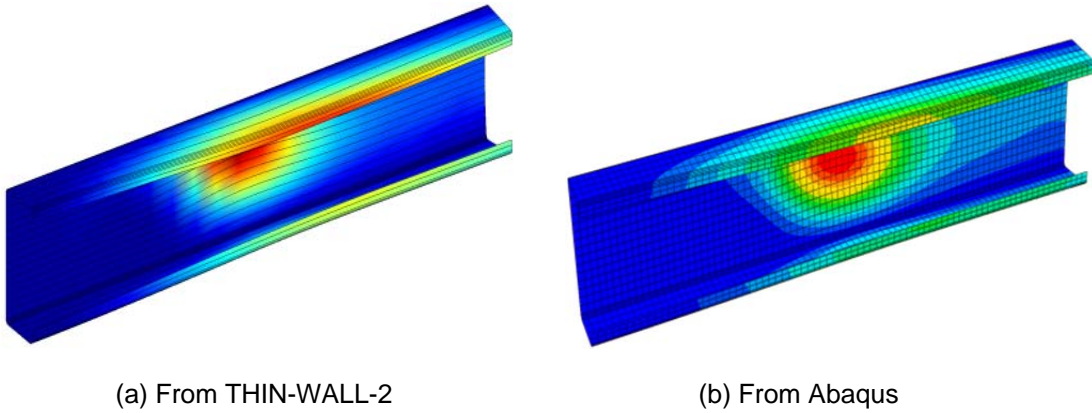
Figure 4.10: Buckling deformation comparison for the CF case
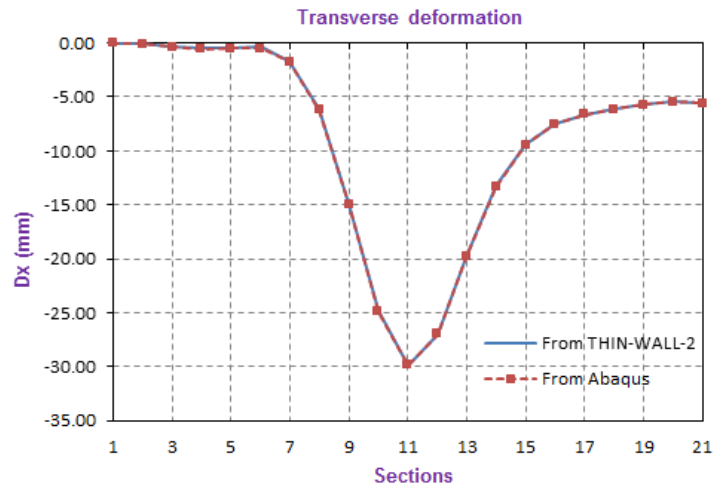
Figure 4.11: Transverse buckling deformation at Nodal Line 23 along the beam for the CF case
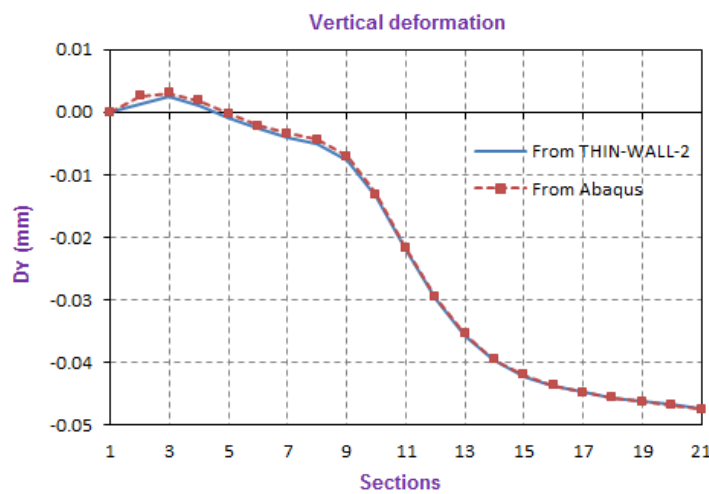
Figure 4.12: Vertical buckling deformation at Nodal Line 23 along the beam for the CF case
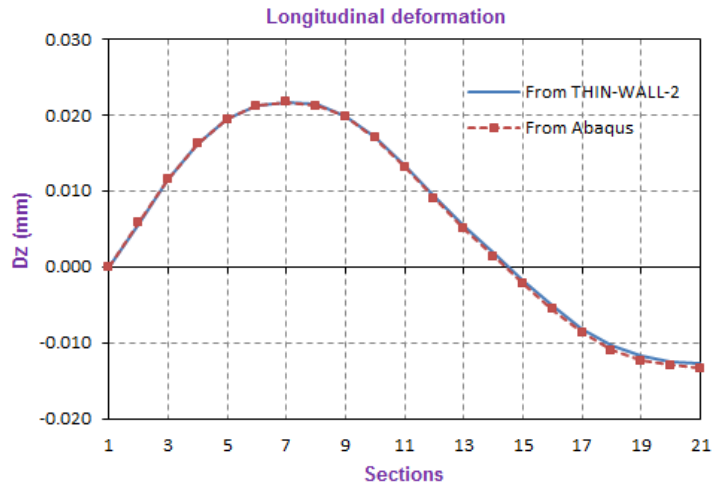
Figure 4.13: Longitudinal buckling deformation at Nodal Line 23 along the beam for the CF case

For the CF case, the selected maximum buckling deformation is -29.857 mm to obtain the buckling deformation in other sections and directions without scale factors.

4.9. CONVERGENCE STUDY

A study has been performed for the lipped channel section in Section 4.8 with the beam length is 1000mm and the load length is 100mm. Different boundary conditions and different number of series terms are performed to find the required number of series terms for a converged buckling analysis. The relationships between the load factor (λ) and the number of series terms are shown in Fig.4.14 for different boundary conditions. There is convergence of the buckling load factor (λ) when the number of series terms reaches 15 as shown in Table 4.2. It means that a smaller number of series terms is required for elastic buckling analysis in comparison with the number of series terms for pre-elastic buckling analysis as described in Chapter 3.

Table 4.2: Convergence of buckling load factors (λ), (L=1000mm and n=100mm)

Series terms (μ)	Buckling load factors (λ)					
	SS	SC	SF	CC	CF	FF
3	3.556	4.056	4.808	4.764	4.536	3.346
5	3.116	3.484	3.687	3.851	3.654	2.945
7	2.955	3.313	3.403	3.591	3.281	2.890
9	2.904	3.251	3.321	3.499	3.221	2.886
11	2.889	3.236	3.304	3.474	3.194	2.885
13	2.885	3.231	3.301	3.463	3.190	2.885
15	2.884	3.230	3.300	3.459	3.189	2.884
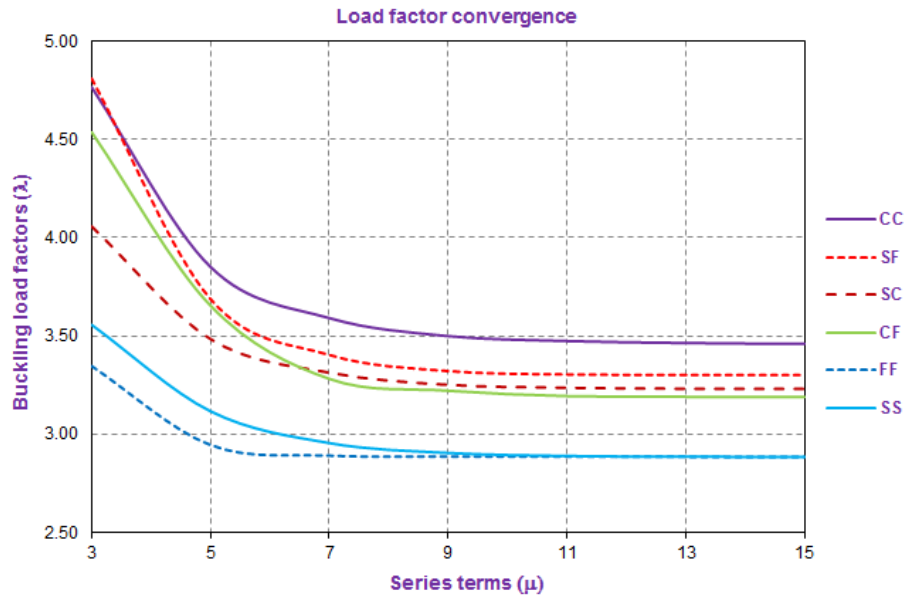
Figure 4.14: Convergence of load factor (λ)

(L=1000mm and n=100mm)

Similar convergence study has been performed for the same lipped channel section in Section 4.8 with the load length is 50mm and the beam length is 1000mm. The convergence of the buckling load factor is given in Table.4.3 and shown in Fig.4.15. It is clear that the solution is converged for the buckling load factors when the number of series terms reaches to 15 as previous example.

Table 4.3: Convergence of buckling load factors (λ), (L=1000mm and n=50mm)

Series terms (μ)	Buckling load factors (λ)					
	SS	SC	SF	CC	CF	FF
3	7.060	8.040	9.600	9.447	9.047	6.689
5	6.137	6.846	7.319	7.567	7.230	5.851
7	5.776	6.461	6.721	6.998	6.444	5.720
9	5.647	6.305	6.535	6.777	6.291	5.708
11	5.599	6.258	6.489	6.707	6.213	5.706
13	5.583	6.238	6.480	6.675	6.200	5.705
15	5.576	6.232	6.477	6.664	6.194	5.704
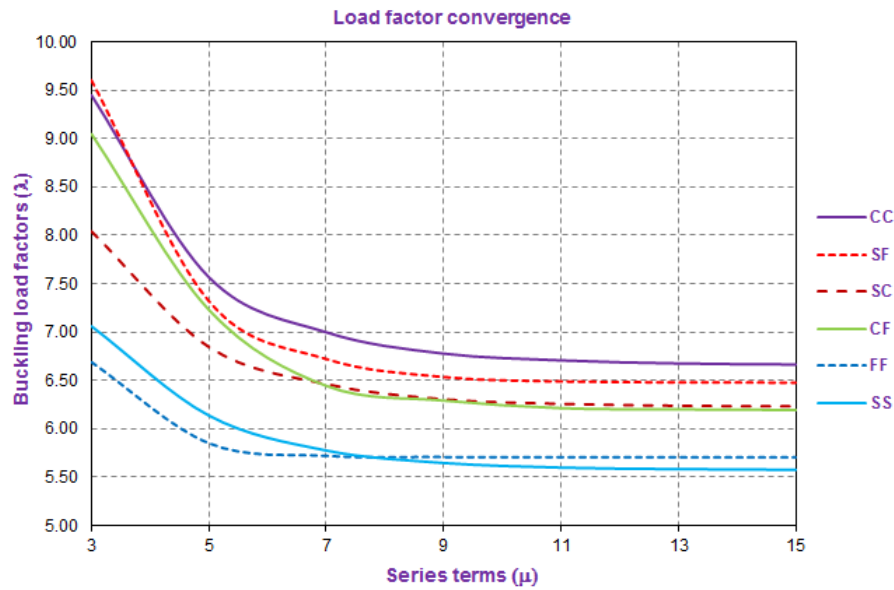
Figure 4.15: Convergence of load factor (λ) (L=1000mm and n=50mm)

4.10. CONCLUSION

The Finite Strip Method of elastic buckling analysis of thin-walled section under localised loading has been developed for general end boundary conditions. This method has proven to be accurate and efficient in comparison with the Finite Element Method.

Different displacement functions are required for flexural and membrane displacements for different support and loading conditions. The elastic buckling analysis requires a smaller number of series terms than the pre-buckling analysis to obtain the converged buckling load factor and buckling modes in comparison with the FEM.

CHAPTER 5

THIN-WALL-2 V2.0 PROGRAM

5.1. INTRODUCTION

The development of the Direct Strength Method (DSM) for design of cold-formed sections as specified in the North American Specification for the Design of Cold-Formed Steel Structural Members AISI S100-2012 [2] and the Australian/New Zealand Standard AS/NZS 4600:2005 [3] requires the ability to compute the elastic buckling loads of thin-walled sections including overall (Euler), distortional and local modes. Li and Schafer [17] developed the CUFSM computer program for buckling analysis of thin-walled members under compression and bending. The program is based on the Constrained Finite Strip Method (cFSM) developed by Ádány and Schafer [67]&[68]. Another computer program THIN-WALL was developed by Papangelis and Hancock [69] which is also used for analysis of thin-walled sections under compression and bending. This program is based on the Semi-Analytical Finite Strip Method (SAFSM) of analysis developed by Cheung [13] and then applied to the buckling of thin-walled sections under compression and bending by Plank and Wittrick [15]. Currently, both of these programs are not available for analysis of thin-walled sections under localised loading. An alternative approach based on Generalised Beam Theory (GBT) has been recently developed by D. Camotim and his colleagues in the program namely GBTWEB [55]. The latest version of this program allows for arbitrary cross-sections, and arbitrary loadings.

This Chapter introduces the new development of the THIN-WALL program namely THIN-WALL-2 Version 2.0 (THIN-WALL-2 V2.0) used for the analysis of thin-walled sections under generalised loading and general end boundary conditions. The Chapter gives a comparison among the three versions of the THIN-WALL program to compare the new developments.

5.2. FINITE STRIP METHOD - BRIEF OVERVIEW

The Finite Strip Method is an effective method for the static, stability, post-buckling and vibration analyses of thin-walled structures. In this method, in order to give compatibility between strips, the longitudinal harmonic series are chosen to satisfy the boundary conditions at the longitudinal ends of strips of structural members. In this case the FSM is known as the Semi-Analytical Finite Strip Method (SAFSM). In another case, the local spline functions are used instead of the harmonic series functions

in the longitudinal direction, the FSM then is developed to account for different boundary conditions. This is known as the Spline Finite Strip Method (SFSM).

The SAFSM analysis implemented in the THIN-WALL-2 program Version 1.0 described in Nguyen et al. [70] uses two different versions of the SAFSM buckling analysis. The first is bfinst7.cpp [71] for uniform loading which uses complex mathematical functions with no end constraints and so shear modes and the signature curve associated with shear are included as well as those associated with bending and compression. The second is bfinst10.cpp [12] for localised loading which assumes simply supported end boundary conditions and arbitrary loading. The theory including displacement functions used in the buckling analyses is described in detail in [72].

The FSM has been further developed for analysis of thin-walled sections under localised loading for general end boundary conditions as described in Chapters 3 and 4. This general theory is included in Version 2.0 of the THIN-WALL-2 program as described in this Chapter.

5.3. THE THIN-WALL-2 V2.0 PROGRAM OUTLINE

5.3.1. Domain of Application

The THIN-WALL-2 V2.0 program is written to define input data using a Graphical User Interface (GUI) to perform pre-buckling and buckling analyses of thin-walled sections under generalised loading. The loading may contain uniform stress and localised loading. The GUI is then used to display the results of the analyses. It is also possible to use this program to perform a cross-section analysis to generate the section properties. The cross-sections can be formed from different shapes includes open and closed sections or mixed sections.

5.3.2. Code Structure

The THIN-WALL-2 V2.0 program contains the GUI which calls three programs: bfinst7.cpp which is written using the C++ computer language and FSM module which is written using Matlab. The bfinst7.cpp program as described in [73] and [72] is used in a Uniform Stress module where the main functions are a cross-section analysis, a stress analysis and a buckling analysis of thin-walled sections under uniform stress. This is the same as in THIN-WALL-2 V1.0. The bfinst10.cpp is written using the C++ computer language and is used in a Localised Loading module for both pre-buckling and buckling analyses of thin-walled sections under localised loading with both end simply supported boundary condition as described in [12]. This is the same as in THIN-WALL-2 V1.0. The FSM module is written in Matlab and is used for analyses of thin-walled sections under localised loading with general end

---

boundary conditions as described in [74] and [79]. The main reason this module has been written in Matlab is to allow the challenging function integrations in Chapters 3 and 4 to be easily performed using in-built Matlab integrators.

The program sequence in THIN-WALL-2 V2.0 is shown in Fig.5.1. In the first step, the user defines the input data such as materials, element types, sections and the restraints. The second step includes two types of analysis of a structural member under loads. The first type is the analysis of a structural member under uniform stress. In this case, the user defines the half-wavelengths and assigns the uniform loads such as compression, bending and shear before running the section analysis, the stress analysis and the buckling analysis. The second type is the analysis of a structural member under localised loading. The user defines the series terms number, the boundary conditions and assign the localised loading before running the analyses. In the final step, the analytical results are displayed on the main window of THIN-WALL-2 V2.0 and exported into different data files.
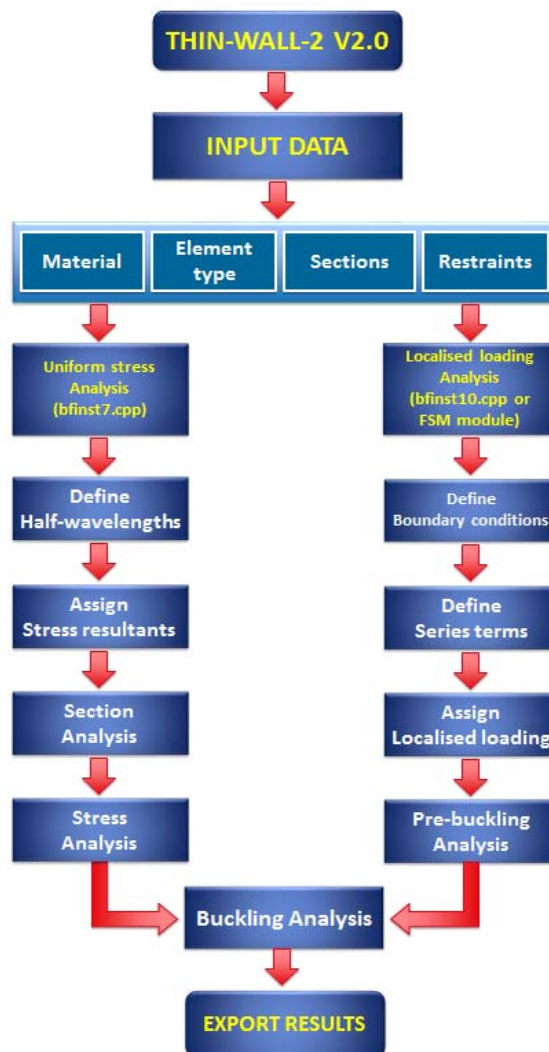
Figure 5.1: Sequence of THIN-WALL-2 V2.0

5.3.3. Comparison with the previous versions of the THIN-WALL program

The THIN-WALL-2 V2.0 program is developed by expanding the functions of the THIN-WALL and THIN-WALL-2 V1.0 programs. This expansion refers to the extension of THIN-WALL-2 V2.0 to pre-buckling and buckling analyses of thin-walled sections under generalised loading such as uniform stress or localised loading with general boundary condition compared to only uniform compression and bending in THIN-WALL and only simply supported boundary condition for localised loading analysis in THIN-WALL-2 V1.0. In addition, the new version improves the quality of some features related to the graphical interface.

Table 5.1 shows the comparison among three versions of the THIN-WALL program, making it possible to assess the new developments.

Table 5.1: Comparison of THIN-WALL versions

Features		THIN-WALL	THIN-WALL-2 V1.0	THIN-WALL-2 V2.0
Modeling	Material	Limited number of materials Isotropic material Corrugated webs	Unlimited number of materials Isotropic material	Unlimited number of materials Isotropic or orthotropic materials
	Element type	One element type	Many element types	Many element types
	Cross-section geometry	Default and general section types	Default and general section types	Default and general section types
	Boundary condition	One "standard" of end supports (S-S)	2 "standards" of end supports (Free to deform for uniform stress and simply supported boundary condition for localised loading)	6 "standards" of end supports (Free to deform for uniform stress and general end boundary conditions for localised loading)
	Restraint	Restraint by X,Y,Z axes and rotation by Z axis	Restraint by X,Y,Z axes and rotation by Z axis	Restraint by X,Y,Z axes and rotation by Z axis
Loading	Static loading	Uniform compression (N) and bending (M)	Uniform compression (N), bending (M), shear (V) or localised loading	Uniform compression (N), bending (M), shear (V) or localised loading

			(2 load cases IOF and ITF)	(4 load cases IOF, EOF, ITF and ETF)
Analysis	Cross-section analysis	Available	Available	Available
	Pre-Buckling analysis	----	Available	Available
	Buckling analysis	Available	Available	Available
Results	Deformation modes	One section	All sections	All sections
	Deformation shapes	2D view	2D and 3D views	2D and 3D views
	Stress	σ_x stress due to N or M	σ_x, σ_y and τ_{xy} stresses due to N, M, V and localised loading	σ_x, σ_y and τ_{xy} stresses due to N, M, V and localised loading
	Export data and report	Available	Not available	Available
Support	Introduction	Available	Not available	Available
	Tutorial	Available	Not available	Available
Other	Cross-section templates	17	9	9
	General section	Available	Available	Available
	Save/load data	Available	Available	Available
	Changing font style	Available	Not available	Available
	Changing unit	----	Not available	Available
	Output files type	*.txt (text file)	*.txt and *.xls files (text and excel files)	*.txt and *.xls files (text and excel files)
Public	The University of Sydney website	Available	Available	Not available

5.4. THE THIN-WALL-2 V2.0 PROGRAM, DETAILED DESCRIPTION

5.4.1. General

There are 11 menus which are created in THIN-WALL-2 V2.0 as shown in Fig.5.2. Each menu has different functions which help the user to manage the analyses effectively. The user can select these menus step by step following the analyses. In addition, there are some short cut buttons on the main window which have the same functions with selection from the menus, thus it is easier for the user to run the program.
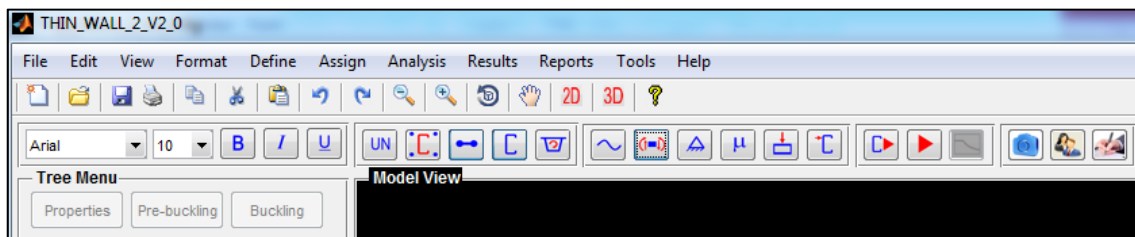
Figure 5.2: Program menu

5.4.2. File Menu

The main function of the File menu as shown in Fig.5.3 is to manage the data during the running process of THIN-WALL-2 V2.0. The user can create a new folder which includes all of the data files for each project. During the running process, data files are created in the main folder of THIN-WALL-2 V2.0 to provide support for the analytical steps. When the user closes the project, all data files are moved from the THIN-WALL-2 V2.0 folder to the new folder which the user has created. In addition, the user can open an old project and continue with a previous job. In this stage, all data files are moved from the old folder to the THIN-WALL-2 V2.0 folder and used during the analytical steps. With this feature, the user can manage and save the data files easily and use them for different purposes.
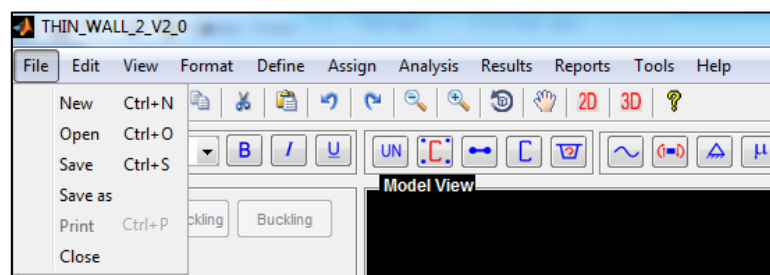
Figure 5.3: File menu

5.4.3. Edit Menu

The Edit menu as shown in Fig.5.4 is designed with the main function of supporting the user in managing objects during the analytical processes. The user can copy, cut and paste the input and the

output data from other programs such as Microsoft Word, Microsoft Excel or some image software into THIN-WALL-2 V2.0. Also, these data can be exported from THIN-WALL-2 V2.0 to other software.
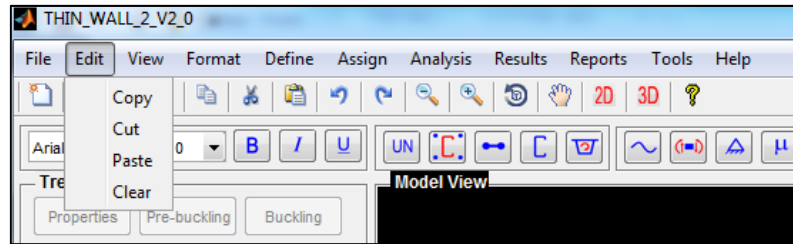
Figure 5.4: Edit menu

5.4.4. View Menu

The main function of the View menu as shown in Fig.5.5 is to help the user to control images in the main window. The user can choose 2D view, 3D view, they can also rotate, move, zoom in and zoom out objects to have the best views. In addition, there is a View-Bar designed on the right hand side of the main window which is used to control objects easily by selecting option buttons directly without selection from the menu.
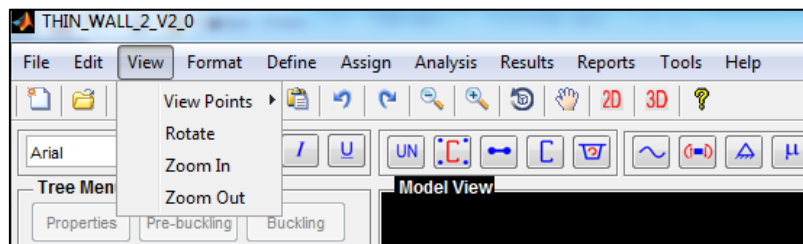
Figure 5.5: View menu

5.4.5. Format Menu

The Format menu, as shown in Fig.5.6, contains selections which the user can use to change the appearance of the program. For example, the user can define and change the units for the whole program by the Units option from the Format menu. The Unit_System window appears as shown in Fig.5.7 for the user to select the unit of length and the unit of force. After choosing the units and clicking on the OK button, the units are displayed in all relevant dialog boxes and the values which are defined in the previous steps are updated automatically with the new units.
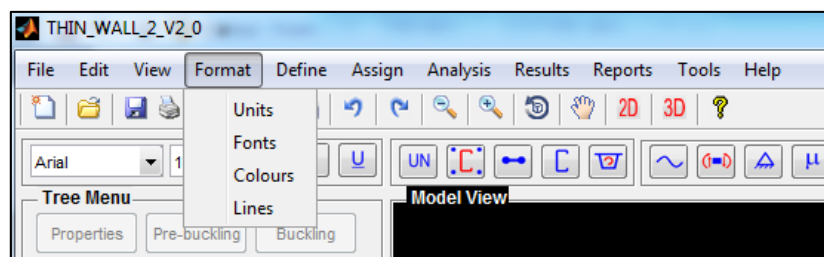
Figure 5.6: Format menu

In addition, there are other selections in the Format menu such as fonts, colours, lines which the user can change for objects in the program in order to have the best display solutions.
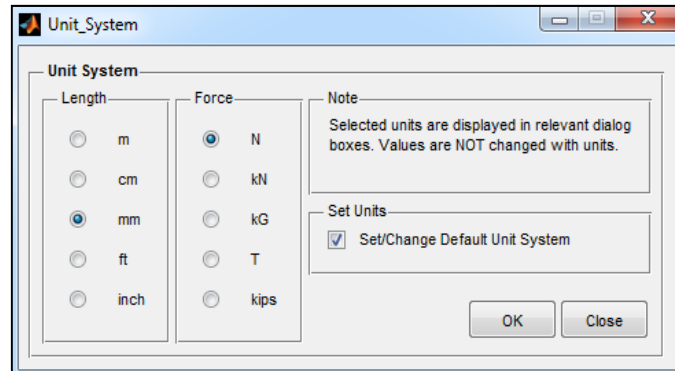
Figure 5.7: Define Units

5.4.6. Define Menu

5.4.6.1. General

The Define menu as shown in Fig.5.8 is used to define some input data for the program such as materials, element types, sections and section loops. When the user selects each of these options, some windows appear for the user to input and manage the input data.
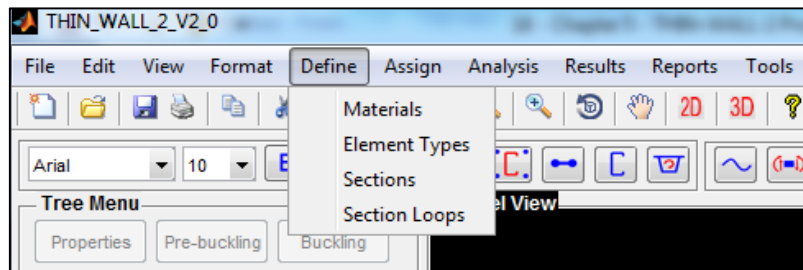
Figure 5.8: Define menu

5.4.6.2. Define materials

In the first step of the analytical process, the user has to define the materials for the structural member. The THIN-WALL-2 V2.0 program is designed for both isotropic and orthotropic materials with the same or different values of Young's modulus and Poisson's ratios in the longitudinal and transverse directions.

A steel material is created as the default material, so that if the user agrees with this, then they can click on the OK button to ignore the material definition step. In order to define a new material, the user clicks the Add button, so that a Materials_New window appears to input the material properties as shown in Fig.5.10. There are an unlimited number of materials; therefore, it is easier for the user to

analyse structures which are made from more than one material. The materials which have been defined are displayed in a table in the Materials window as shown in Fig.5.9.
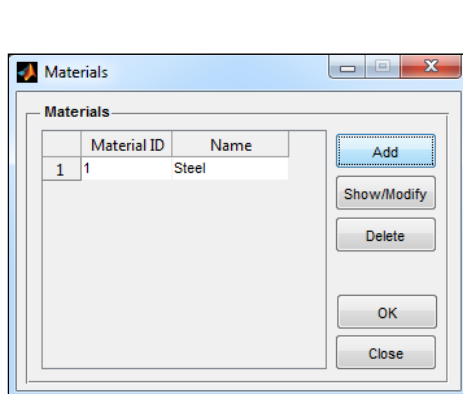
Figure 5.9: Define materials   Figure 5.10: Add new materials
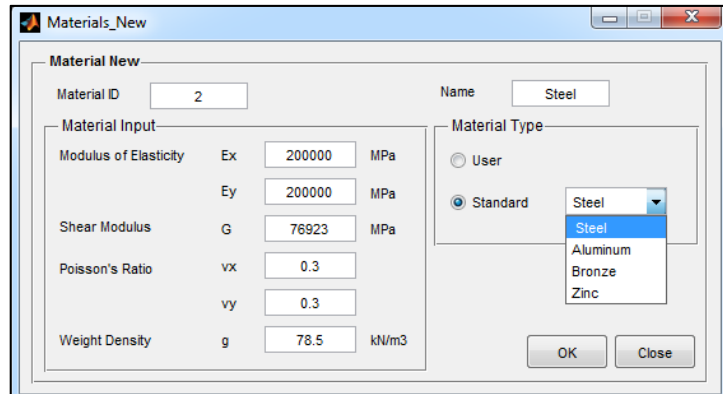
The user can select the material in the Materials table and click on the Modify button to change the material properties. The Materials_Modify window appears as shown in Fig.5.11 for the user to revise the properties for the selected material. Also, the user can delete any material which they defined by selecting material in the Materials table and clicking on the Delete button.
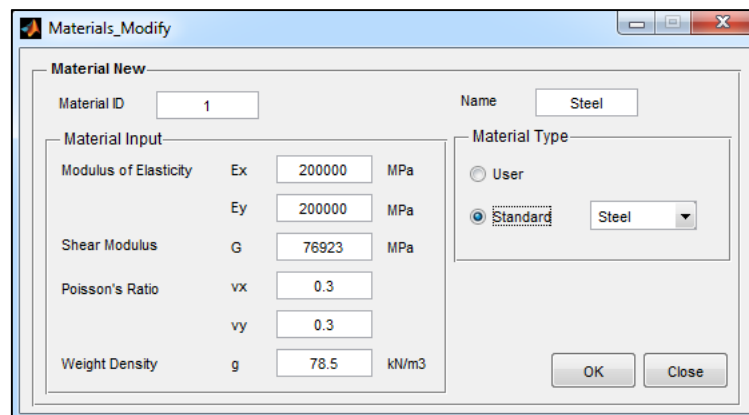
Figure 5.11: Modify materials

5.4.6.3. Define element types

After the material definition step, the user has to define the element types which include the properties of each strip such as the material, thickness for bending and thickness for shear which are used in the cross-section analysis. Similar to the material definition step, there is an Add button, a Modify button and a Delete button which are used to add new element types, modify element types or delete element types respectively. For example, when the user clicks on the Add button, the Element_Types_New window appears as shown in Fig.5.13 and the user can select material from the material list which is defined in the material definition step. After that, the user inputs the thickness for

bending and the thickness for shear of the new element type. The element types which have been defined are displayed in the Element Types window as shown in Fig.5.12.
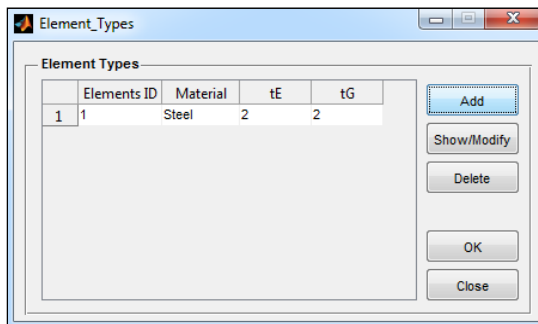
Figure 5.12: Define element types   Figure 5.13: Add a new element type
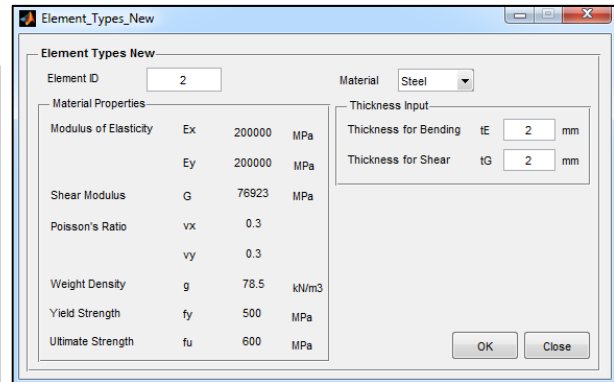
5.4.6.4. Define Sections

a. General

Before a computer analysis of a thin-walled section can be commenced, the geometry of the cross-section must be described to the computer. The method of computer data input is similar to the data for a plane structural framework being analysed on a computer. To achieve this similarity, a thin-walled cross-section should be divided into an assemblage of rectangular elements, with the ends of the elements intersecting at nodes.

The coordinates of the nodes of the cross-section based on an arbitrary axis system (X,Y) are input with the identification number for each node. The rectangular elements of the cross-section are input together with the identification number of the connected nodes. A number of different elements types can be defined, and the effective thickness and elastic moduli in flexure and shear, and Poisson's ratio for each type are also input. Any elements which form a closed loop must be included in the data for the section. The element number in the loop is preceded by a negative sign if the order of the node numbers which define the ends of the element is opposite to that for a clockwise traverse around the loop. By selecting the Sections option in the Define menu, a window appears as shown in Fig.5.14, the user can select the section type buttons then click on the Add button to define a new section. Currently, the program is available for three cross-section types which are C-sections, Z-section and General sections. In addition, the program allows define many sections and the user can set one section to become current by clicking on the Set Current button. Also, the user can select one section and click on the Show/Modify button to display all properties of the selected section.
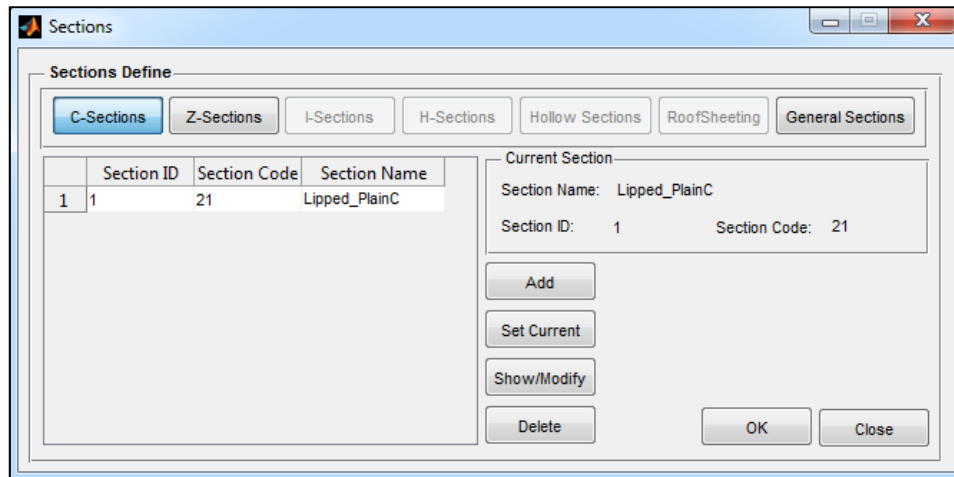
Figure 5.14: Define a new section

b. Channel sections

THIN-WALL-2 V2.0 is designed with three channel section types: an un-lipped channel section, a lipped channel section and a general channel section. Each type has four types of web stiffeners such as plain-C, rectangular stiffener, one triangular stiffener and two triangular stiffeners as shown in Fig.5.15. In this window, the user selects a channel section type and element type in order to assign default properties for the section. The dimensions of the section are overall dimensions but the program changes these dimensions automatically to centre to centre dimensions to calculate the section properties. Also, the user defines the strip subdivision for the section to determine the number of strips and nodes included in the section.

After finishing inputting the dimensions for the section, the user clicks on the Apply button to show the section data. The Section_Data window appears with two main data tables as in Fig.5.16. The first one is the Node_Data table with the nodal information such as nodal number, nodal co-ordinate. From this table, the user can add new nodes, insert nodes and delete nodes by clicking on the Add button, the Insert button and the Delete button respectively. The second one is the Strip_Data table which includes the strip number, start node and end node of each strip. The user can change the start node, the end node and reassign the element type for each strip. By clicking on the Apply button, then the section data is updated and shown in the Section Preview panel.
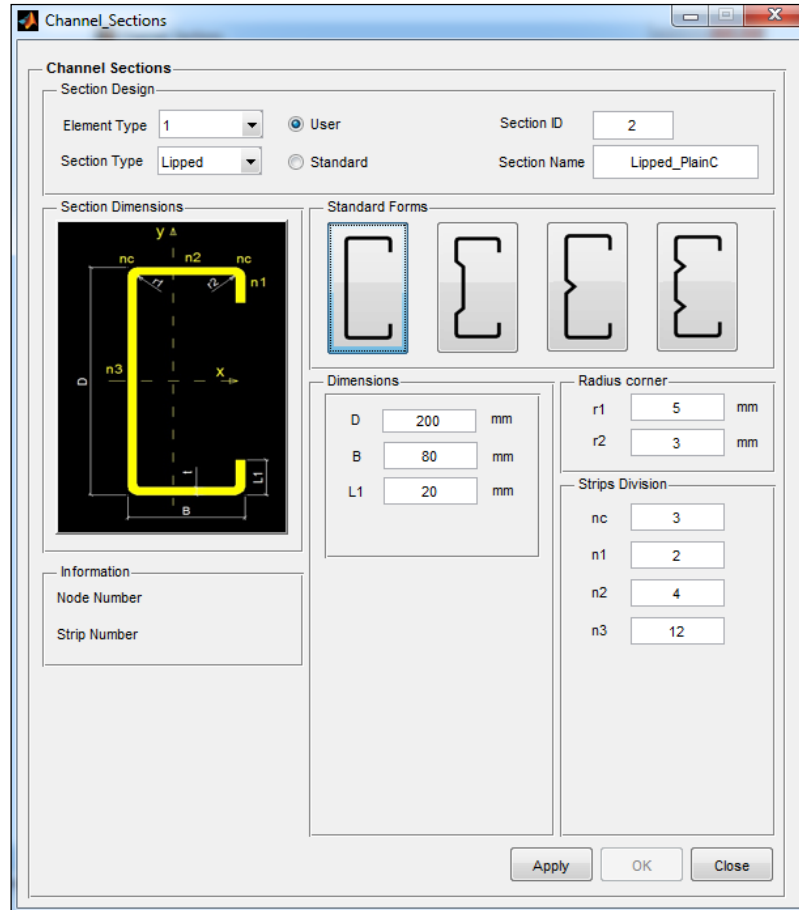
Figure 5.15: Define channel sections
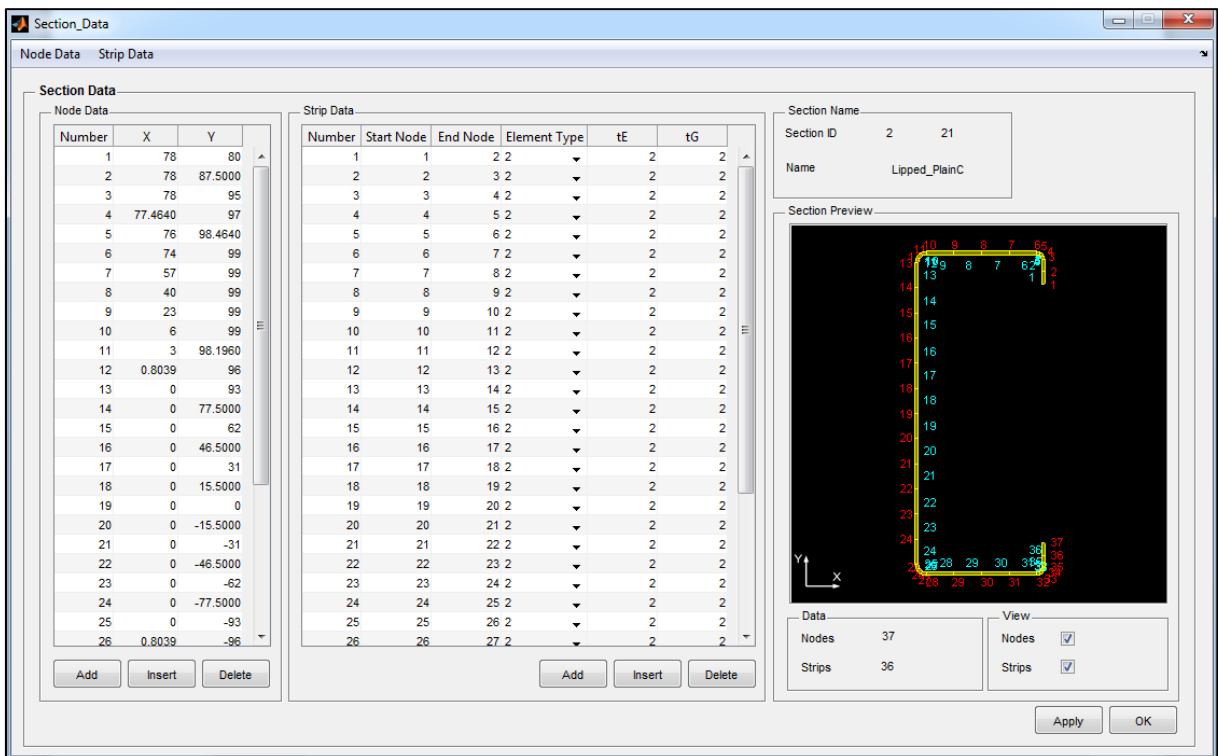
Figure 5.16: Section data

c. General sections

Recently, cold-formed steel has been applied with many section types, but some of them have not been created as template sections. In order to define these sections, the user selects the General Sections option from the Define/Sections menu, so that the General_Sections window appears as shown in Fig.5.17 which includes two tables. The first one is the Node_Data table where the user can input the nodal co-ordinates directly. The user can prepare the nodal co-ordinates in an Excel file, then copy and paste into this table. The second one is the Strip_Data table where the user can input the data for the strips. The user can click on the Default button to get the default definition for the Strip_Data table before changing the start node, the end node and the element type for the strip which the user may want to change. By clicking on the Apply button, then the section data is updated and shown in the Section Preview panel.
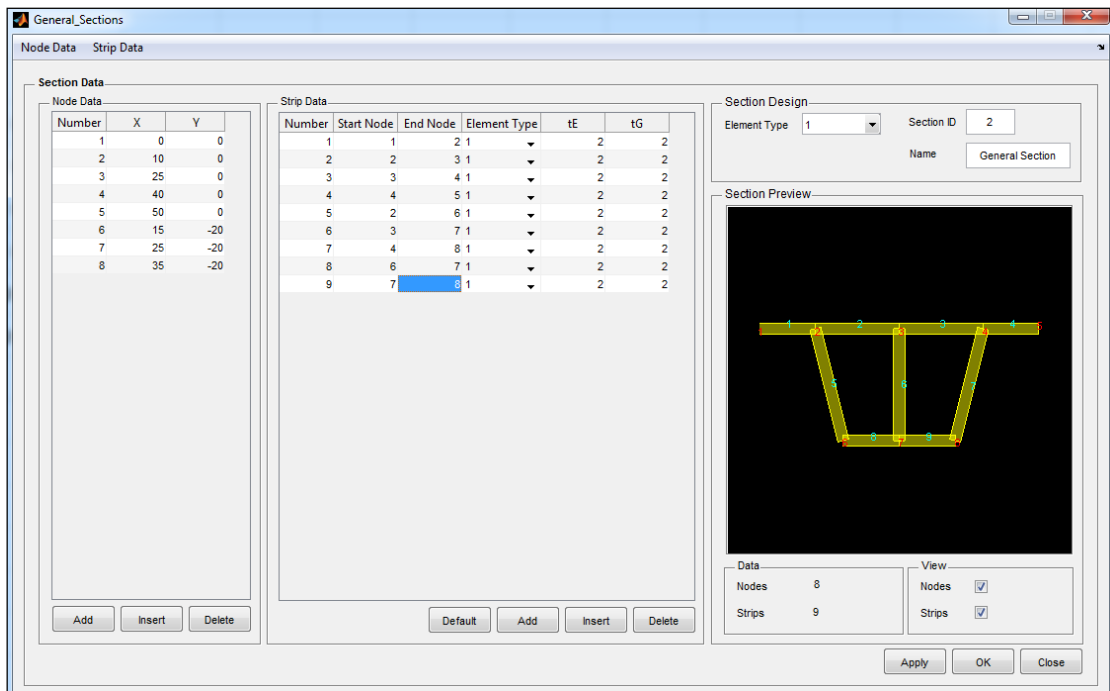
Figure 5.17: Define a general section

5.4.6.5. Define Section loops

For closed sections, the user needs to define the section loops. The section loops are clockwise. And the direction of strips is from the start node to the end node. If the direction of strips is the same with the loops, the sign of the strips is positive, otherwise the sign is negative.

When the user selects the Section Loops options from the Define menu, the Section_Loops window appear as shown in Fig.5.18. Then the user clicks on the Add button, the Section_Loops_New appear as shown in Fig.5.19 for the user to define a new section loop.
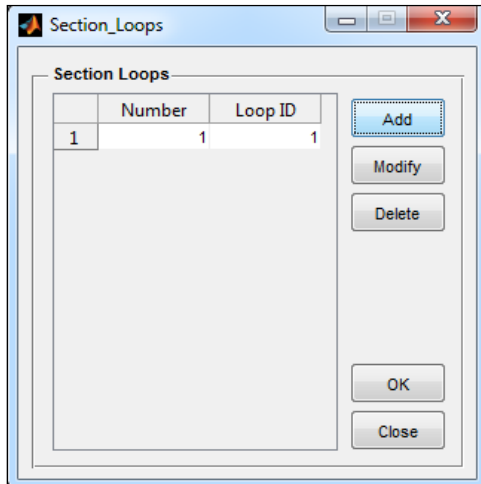
Figure 5.18: Define section loops   Figure 5.19: Add new section loops
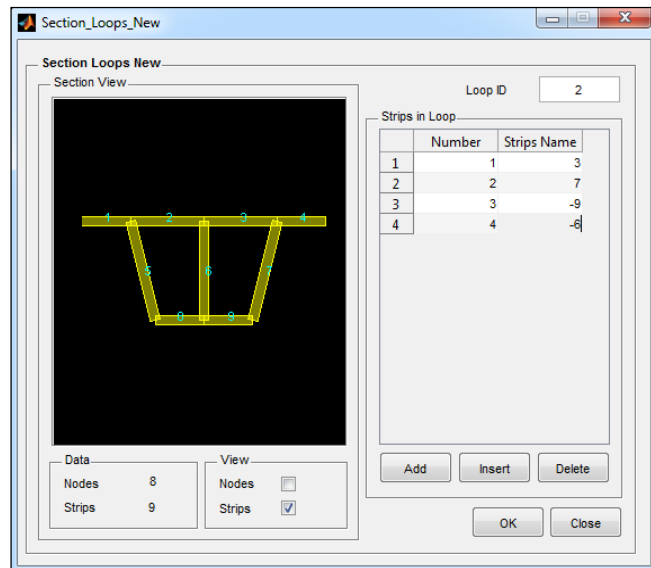
5.4.7. Assign Menu

5.4.7.1. General

The Assign menu as shown in Fig.5.20 is used to define some input data for the analysis steps such as half-wavelengths, stress resultants for analysis of sections under uniform stress and boundary conditions, series terms, localised loading for analysis of sections under localised loading.
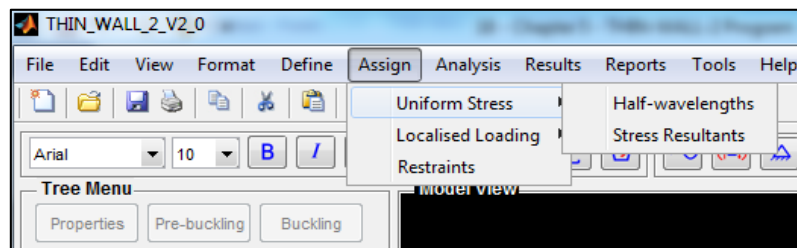
Figure 5.20: Assign menu

5.4.7.2. Assign stress resultants and half-wavelengths for the Uniform Stress module

a. Define half-wavelengths

THIN-WALL was written to analyse a structural member under uniform compression and bending alone over a range of half-wavelengths. Further development has been done for THIN-WALL-2 V2.0, so that it is possible to perform buckling analyses of a structural member under uniform compression, bending and shear or combinations of them over a range of half-wavelengths using the Uniform Stress module.

Before the definition of stress resultants, the user has to define the half-wavelengths by selecting the Half-wavelengths option from the Assign/Uniform Stress menu. The Half-wavelengths window appears as shown in Fig.5.21 with forty default half-wavelengths which are displayed on the

Half-wavelengths table. The minimum default half-wavelength is 30mm and the maximum default half-wavelength is 10000mm. In addition, the user can define more half-wavelengths, insert new half-wavelengths, modify half-wavelengths or delete half-wavelengths by clicking on the Add button, the Insert button, the Modify button or the Delete button respectively.
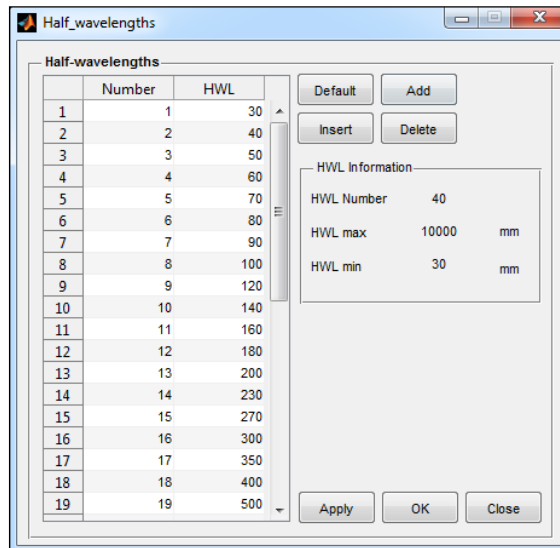
Figure 5.21: Define half-wavelengths

b. Assign stress resultants

After the definition of the half-wavelengths, the user selects the Stress Resultants option from the Assign/Uniform Stress menu. The Stress_Resultants window appears for the user to input the axial force, bending moments M_x, M_y, shear forces V_x, V_y, bimoment B, Saint-Venant (uniform) torque and warping (non-uniform) torque as shown in Fig.5.22.
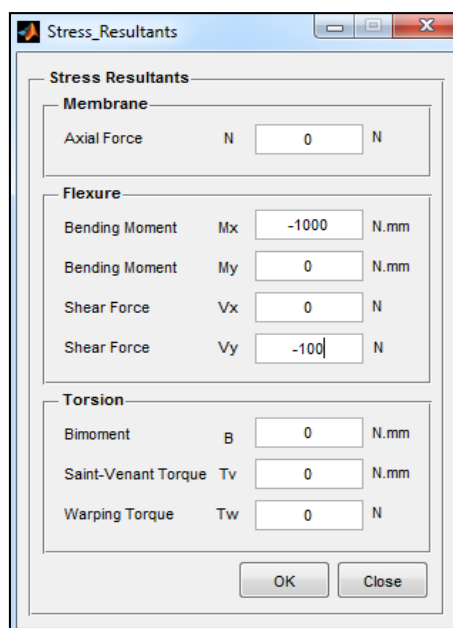
Figure 5.22: Assign stress resultants

5.4.7.3. Assign boundary condition, localised loading and series terms for the Localised Loading module

a. Assign boundary condition

Boundary condition refers to the support condition at the ends of the beam for use in the localised loading analyses using the Localised Loading module as described in Chapter 3. By selecting the Boundary conditions options from the Assign/Localised Loading menu, the Boundary_Conditions window appears as shown in Fig.5.23. From this window, the user can select six types of boundary conditions such as:

1. Both ends simply supported (SS)

2. One end simply supported and one end clamped (SC)

3. One end simply supported and one end free (SF)

4. Both ends clamped (CC)

5. One end clamped and one end free (CF)

6. Both ends free (FF)

For different boundary conditions, different displacement functions are required for both flexural and membrane displacements as described in [74]. The both ends simply supported is set up as a default boundary conditions for strips of the structural member.
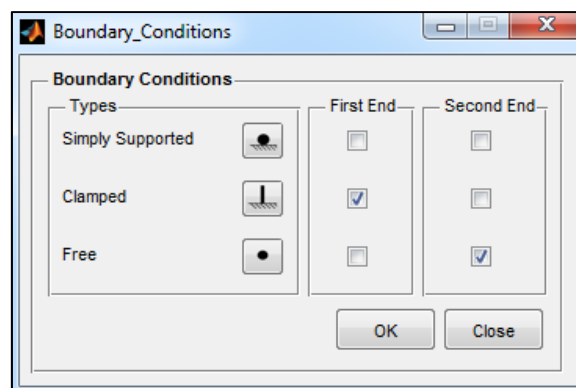
Figure 5.23: Define boundary conditions

b. Assign localised transverse loads

There are four localised loading cases as shown in Fig.5.24: Interior one-flange loading (IOF), Interior two-flange loading (ITF), End one-flange (EOF) loading and End two-flange (ETF) loading as described in Chapter 3.

The user selects the Localised Transverse Loads option from the Assign/Localised Loading menu, the Fig.5.25 appears to define the localised loading. Firstly, the user selects a loading case by

clicking on one of the four Load buttons, so that the loading case is displayed in the Load View panel. Secondly, the user inputs the length of the beam (L), the load length (n) and the load position. The user can select the relative assign or the absolute assign to define the position of loading on the beam. In addition, the value of loading must be input into the Load Value panel in the middle of this table. Finally, the user defines the applied loading points by selecting nodes in the Applied Loading Points table on the right side of this window.

a. IOF: Interior One-Flange Loading

b. ITF: Interior Two-Flange Loading

c. EOF: End One-Flange Loading

d. ETF: End Two-Flange Loading
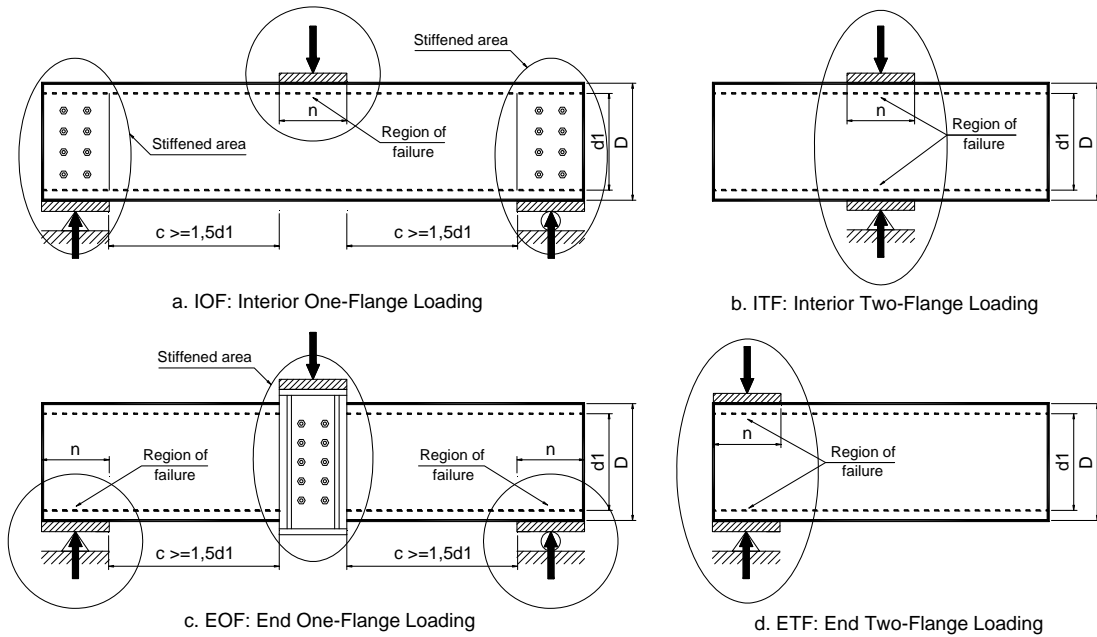
Figure 5.24: Localised loading cases
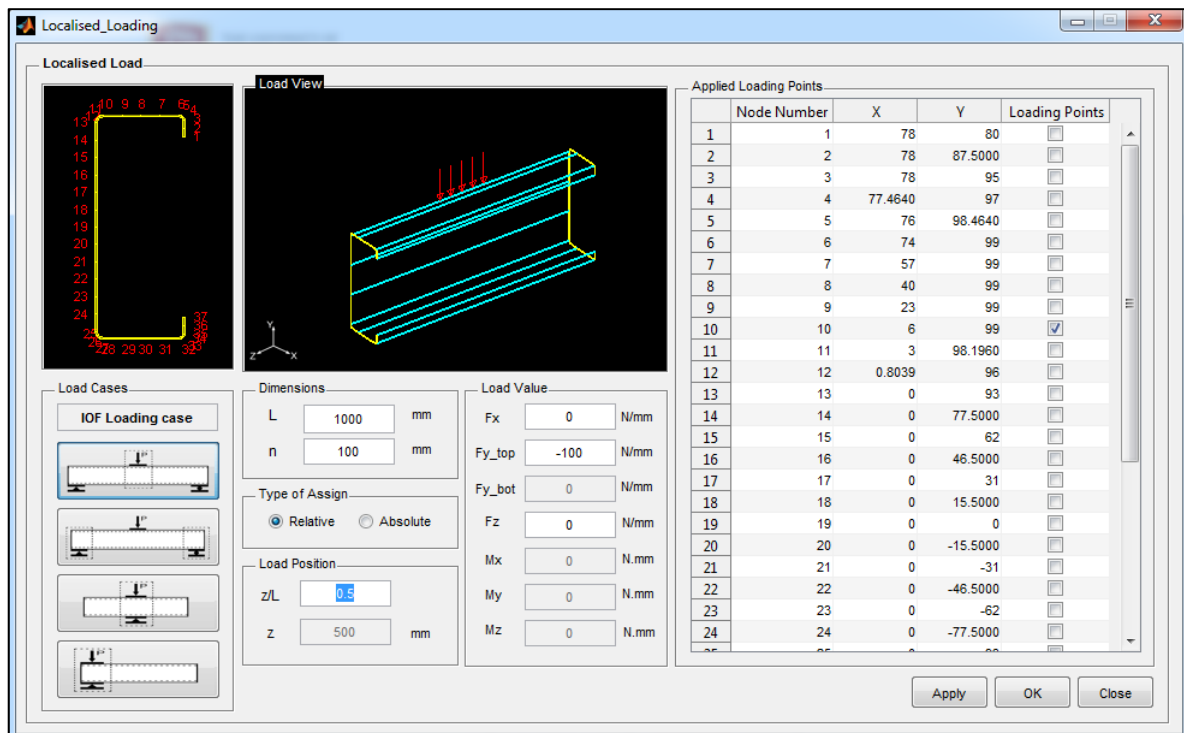
Figure 5.25: Assign localised loading

c. Assign series terms

In the buckling analysis of a structural member under localised loading, THIN-WALL-2 V2.0 calls the Localised Loading module to analyse the structure and export the results to data files. In this analysis, the Localised Loading module analyses the structure with multiple series terms in order to get the most accurate results. Therefore, the user has to define the number of series terms as shown in Fig.5.26 by selecting the Series Terms option from the Assign/Localised Loading menu. When using more series terms, the user gets more accurate results; however, the program runs longer because there are more degrees of freedom as described in [12]. In addition, the user can define different number of series terms for the pre-buckling and buckling analyses.
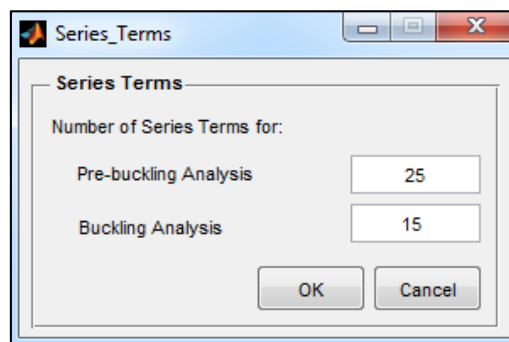
Figure 5.26: Assign series terms

5.4.7.4. Assign restraint

The Restraints window appears as shown in Fig.5.27 when the user selects the Restraints option from the Assign menu. There is a table which includes the nodal number and the nodal co-ordinates for the user to assign the restraint conditions. There are four degree of freedom for each node, thus the user can fix the nodal translation such as D_x, D_y, D_z in the X,Y,Z directions and the nodal rotation about the Z axis. By selecting the restraint condition for each node from the table and clicking on the Apply button, the restraint conditions for the whole section are updated and displayed on the Section View. For the analyses of standard sections under localised loading, the user can click on the Default button to apply the lateral restraints at localised loading points as described in 4.4.7.3.
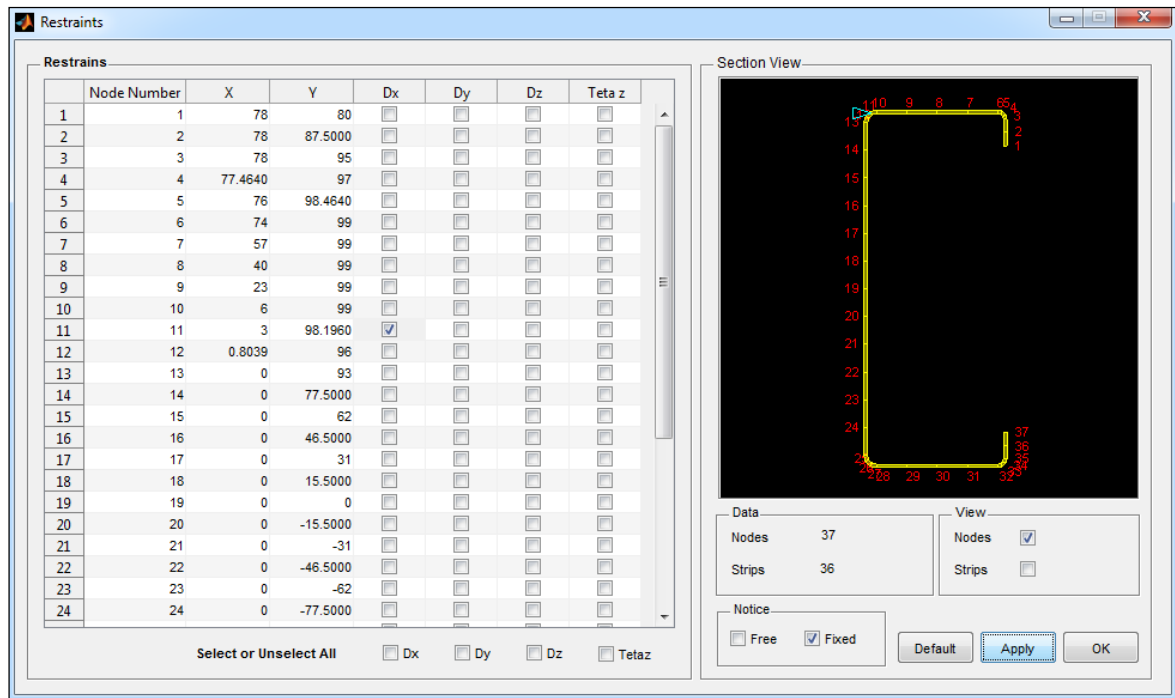
Figure 5.27: Assign restraints

5.4.8. Analysis Menu

5.4.8.1. General

The Analysis menu is shown in Fig.5.28 is used to manage the analysis steps such as section analysis, pre-buckling analysis and buckling analysis.
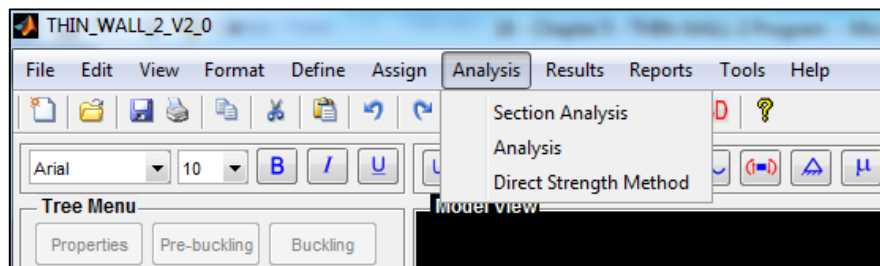
Figure 5.28: Analysis menu

5.4.8.2. Section analysis

The Uniform Stress module initially runs a cross-section analysis to achieve the section properties such as section area, moment of area, centroid, shear centre in rectangular axes and principal axes, mono-symmetry parameter, torsion and warping constants. In addition, the user can show these section properties on the properties panel, display images of the section properties on the main window and export images to other software as in 5.4.9.2.

5.4.8.3. Pre-buckling and buckling analyses

The Analysis window appears as shown in Fig.5.29 when the user selects the Analysis option from the Analysis menu or the Analysis button on the Analysis bar. From this window, the user can select the analysis type with suitable loading.
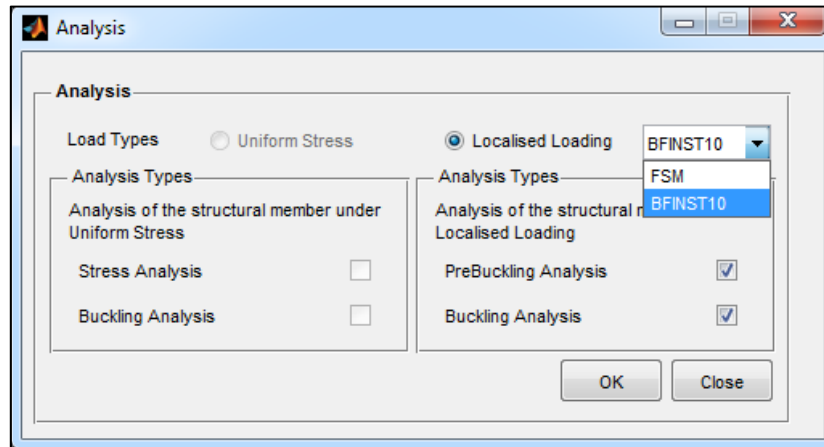
Figure 5.29: Analysis options

If the user selects the Uniform Stress option, the Uniform Stress module is called as shown in Fig.5.30 to run the analyses of the section under uniform stress. The user can select running stress analysis only or both stress and buckling analyses. The stresses and buckling modes are exported for 21 cross-sections and displayed on the Main Window as in 5.4.9.3.
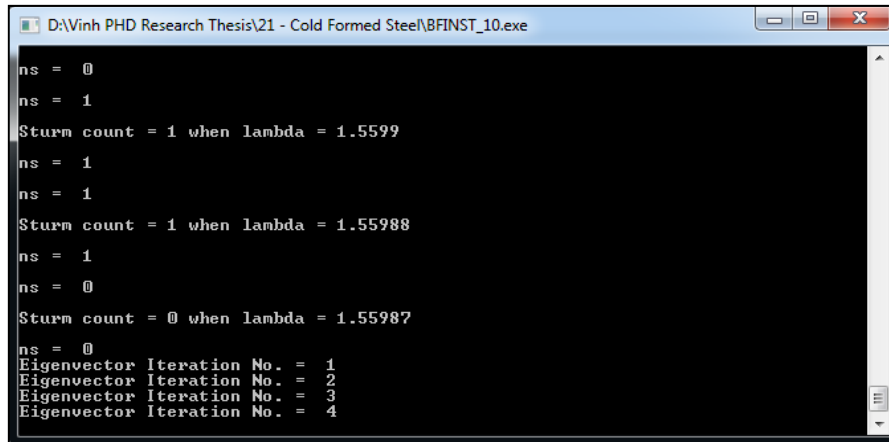
Figure 5.30: Running bfinst7.cpp for Uniform Stress analysis

If the user selects the Localised Loading option, the Main_Code box appears on the Analysis window. If the user selects BFINST10 option, the Localised Loading module is called to run the bfinst10.cpp engine as shown in Fig.5.31 for analyses of structural members under localised loading with both ends simply supported boundary condition. If the user selects the FSM option, the Localised Loading module is called to run the FSM module as shown in Fig.5.32 for analyses of structural members under localised loading with general boundary conditions. The user can select running pre-

buckling analysis only or both pre-buckling and buckling analyses. The stresses, deflections and buckling modes are exported for 21 cross-sections and displayed on the Main Window as in 5.4.9.4.

Figure 5.31: Running bfinst10.cpp for localised loading analysis
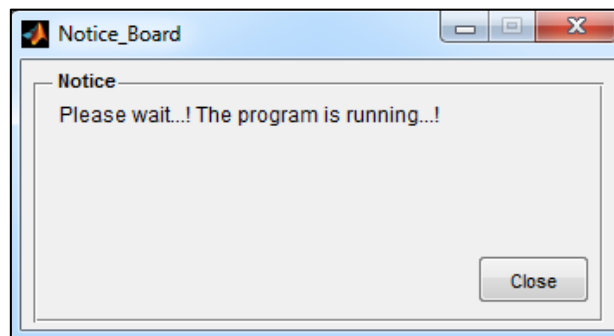
Figure 5.32: Running the FSM module for localised loading analysis

5.4.9. Results Menu

5.4.9.1. General

The Results menu as shown in Fig.5.33 is used to export the results from analytical steps such as section properties, stresses, deflections, buckling modes…
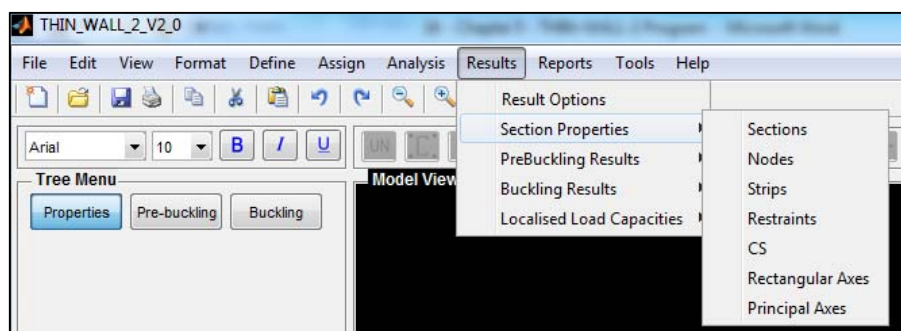
Figure 5.33: Results menu

All results of analytical processes are exported to data files and stored in the main folder of the THIN-WALL-2 V2.0. Three buttons appear on the tree menu such as the Properties button, the Pre-buckling button and the Buckling button to turn on and turn off the Properties panel, the Pre-buckling

panel and the Buckling panel respectively are shown in Fig.5.34(a),(b),(c). From these panels, the user can display the results on the main window of THIN-WALL-2 V2.0.
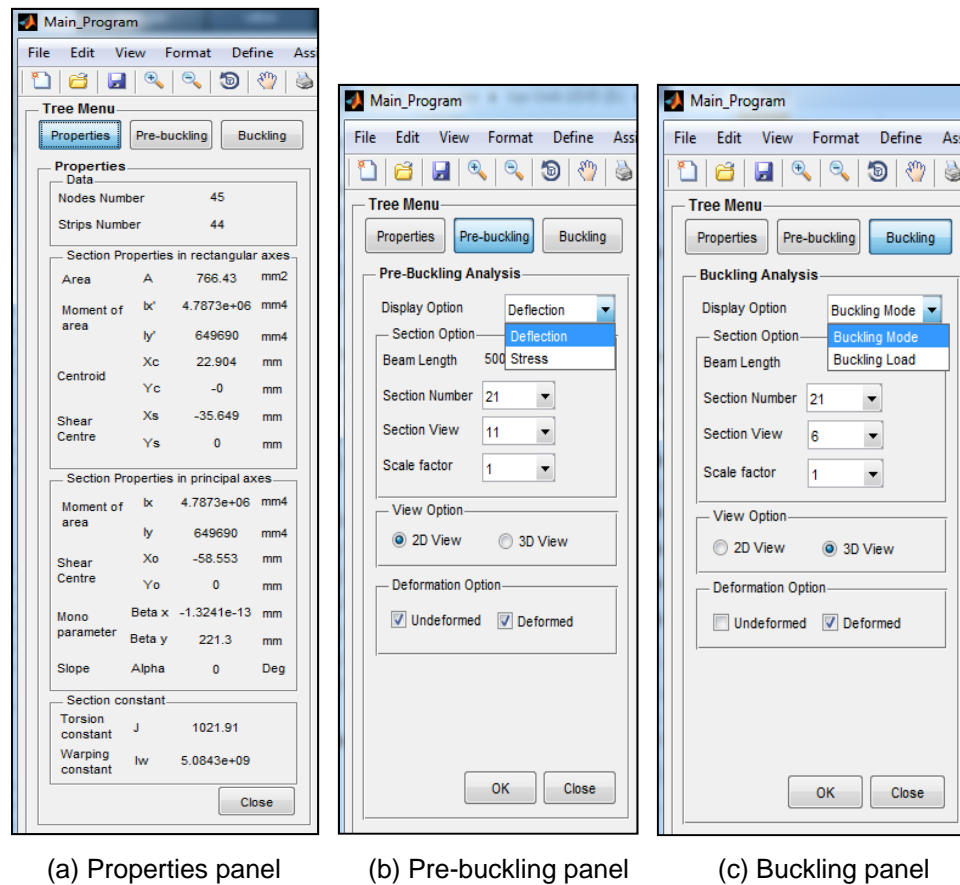
(a) Properties panel   (b) Pre-buckling panel   (c) Buckling panel

Figure 5.34: Panels on the tree menu

The user has to select the Result Options from the Results menu, so that the Result_Options window appears as shown in Fig.5.35. From this window, if the user selects the Uniform Stress option, then the GUI reads the data files which are exported from the Uniform Stress module to display on the main window. Alternatively, if the user selects the Localised Loading option, then the GUI reads the data files which are exported from the Localised Loading module.
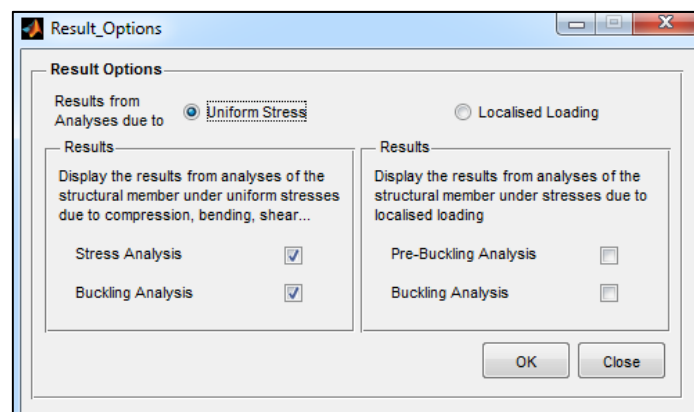
Figure 5.35: Result options

5.4.9.2. Section properties

The user can display the section properties after running the section analysis step. The Properties button appears on the tree menu as well as the Properties panel to display the section properties such as section area, moment of area, centroid, shear centre in rectangular and principal axes, torsion and warping constants and mono-symmetry parameters as shown in Fig.5.34(a).

A graphical-bar is designed on the right side of the main window with some special buttons which the user can click on to display section, node number, strip number, restraints, rectangular and principal axes on the main window as shown in Fig.5.36.
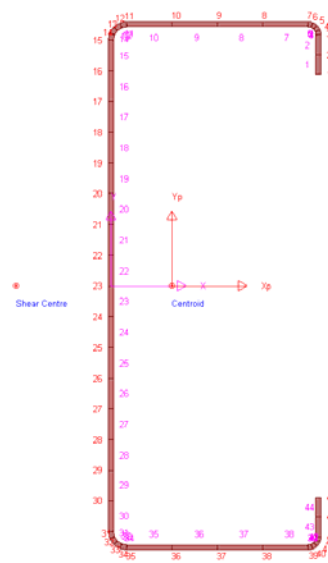
Figure 5.36: Section properties

5.4.9.3. Localised loading pre-buckling analysis results

After running the Pre-buckling analysis of a structural member under localised loading, the Pre-buckling button appears beside the Properties button on the tree menu. By clicking on this button, the Pre-buckling panel appears on this menu with two display options which are deflection and stress as shown in Fig.5.34(b). If the user chooses the Deflection option, two panels appear for the user to select 2D or 3D views and un-deformed or deformed views. The deflection modes and shapes of the structural member are displayed on the main window as shown in Fig.5.37. In the section option panel, the user can change the section displayed or scale the deflection of the sections.
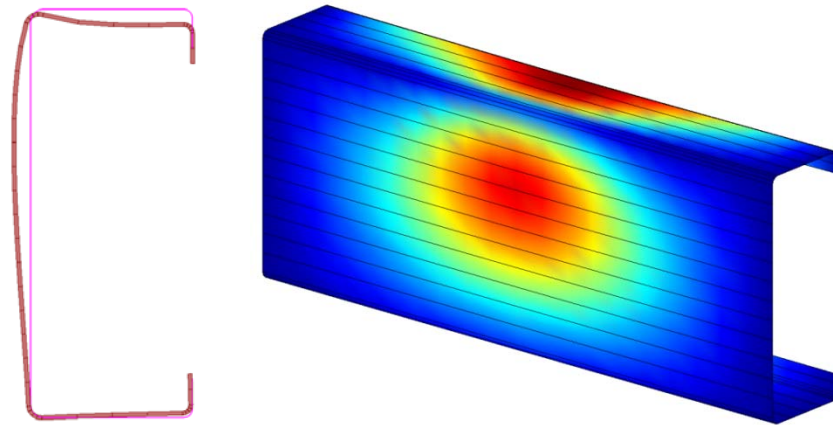
Figure 5.37: Pre-buckling deformation in 2D and 3D views

If the Stress option is selected, the stress panel appears for the user to select stress types such as longitudinal stress (S_x), transverse stress (S_y) or shear stress (T_{xy}). Also, the user can select display or un-display stress values and legends for each diagram on the main window as shown in Fig.5.38.
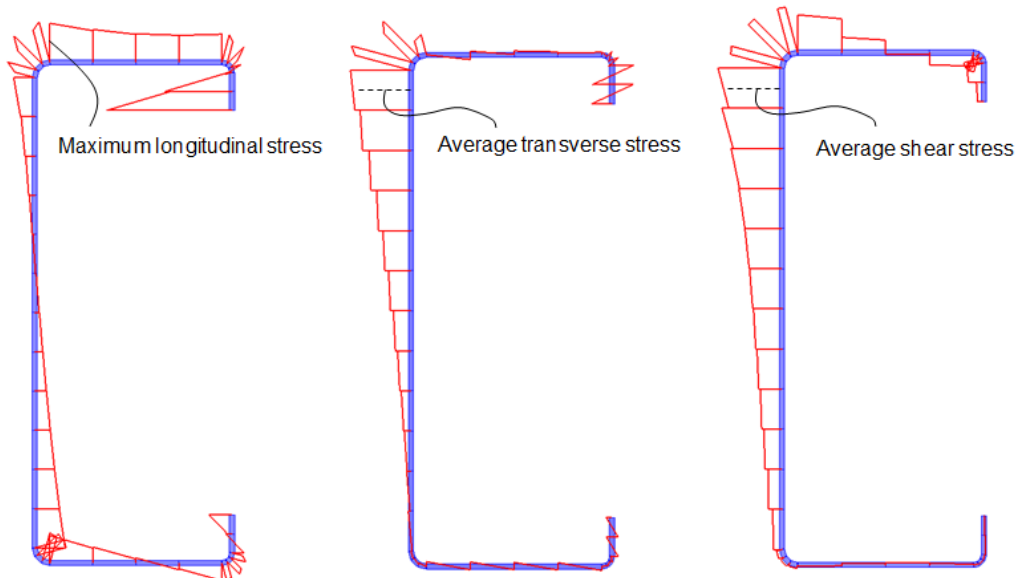
Longitudinal (0.5L), Transverse (0.5L) and Shear Stresses (0.45L)

Figure 5.38: Pre-buckling stresses

5.4.9.4. Localised loading buckling analysis results

After running the buckling analysis of a structural member under localised loading, the Buckling button appears beside the Pre-buckling button on the tree menu. When the user clicks on this button, the Buckling panel appears with two display options which are Buckling Mode and Buckling Load as shown in Fig.5.34(c).

If the Buckling Mode option is selected, the View panel and Deformation panel appear to select 2D or 3D views and un-deformed or deformed views. The buckling modes and shapes of the structural

member are displayed on the main window as shown in Fig.5.39. When the user selects the Buckling Load option, the Buckling_Loads window appears with the information about applied loads, buckling factor and buckling loads.
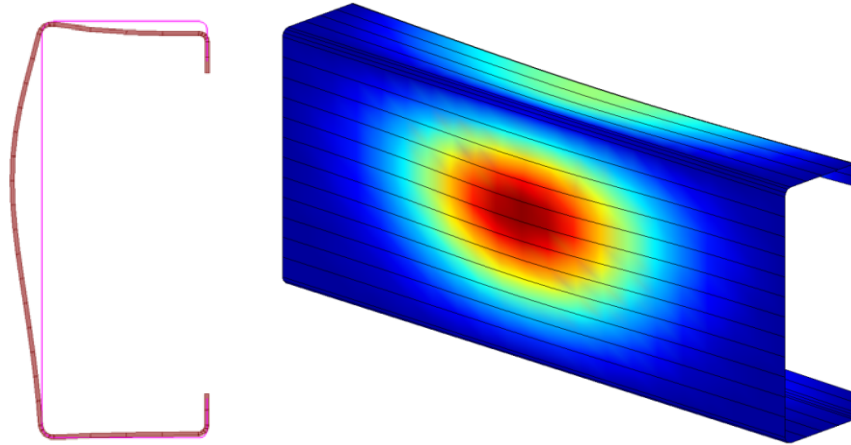
Figure 5.39: Buckling modes in 2D and 3D views

5.4.9.5. Uniform stress buckling analysis results

In the buckling analysis of a structural member under uniform compression, bending and shear, the Buckling panel appears with two display options which are buckling mode and signature curve. If the Buckling Mode option is selected, the View panel and Deformation panel appear to select 2D or 3D views and un-deformed or deformed views. If the Signature Curve option is selected, the Signature_Curve window appears with some other display options. The user can display the signature curve, buckling modes and buckled shapes together on this window. The signature curve illustrates the relationship between buckling load factors and half-wavelengths as shown in Fig.5.40.
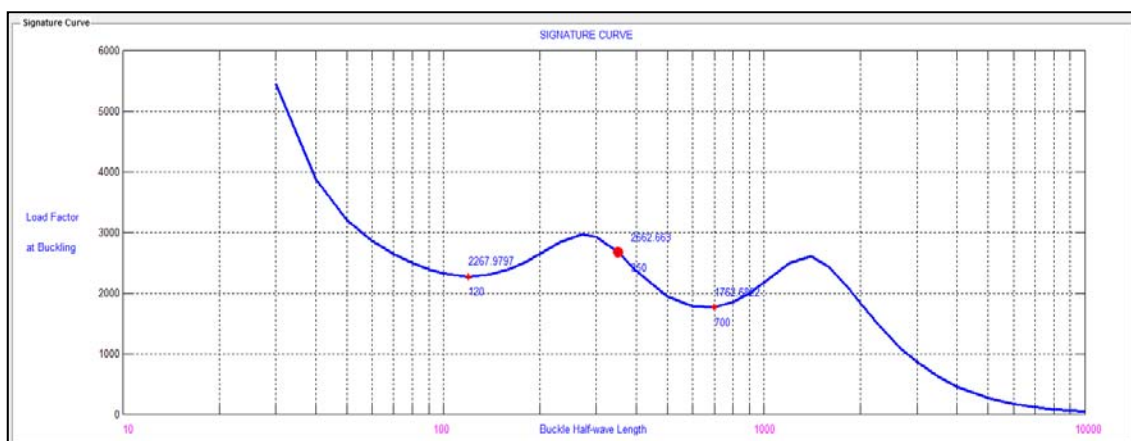
Figure 5.40: Signature curve

5.4.10. Report Menu

The Report menu as shown in Fig.5.41 is designed to write a report of the analyses. Firstly, the user input the personal information which should be included into the report. Secondly, by selecting the Create_Report option, a Report window appears as shown in Fig.5.42, from this the user can select some options to create a full report which contains the input data, the output data and the results of the analyses. Also, the user can export the data files into different files such as text files. In addition, the user can export images file by select the Pictures option from the Reports menu, a new window where the user can control the images with different colors, view-points before saving them in different formats.
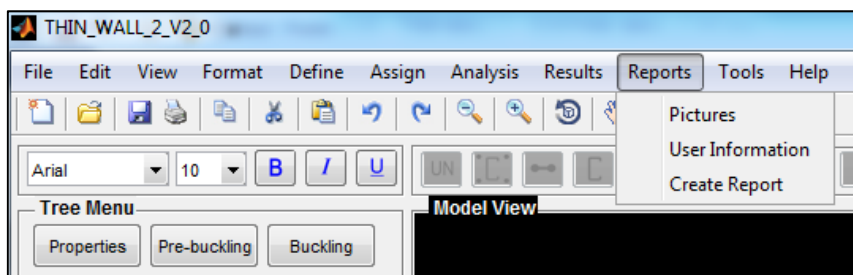
Figure 5.41: Reports menu
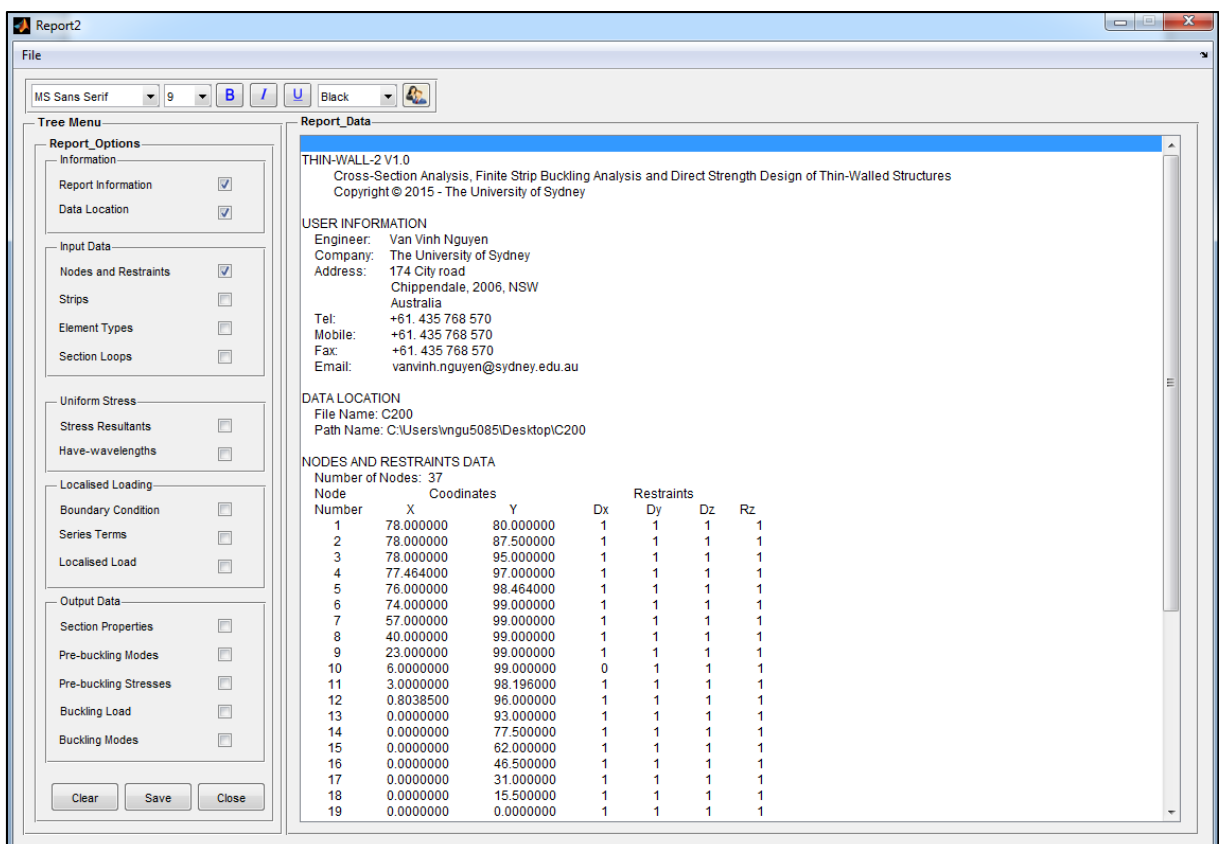
Figure 5.42: Report options

5.4.11. Tools Menu

The Tools menu as shown in Fig.5.43 is used to control the Main Window of the program with some selections such as lock and unlock the programs, turning on and off some tool bars in the Main Window.
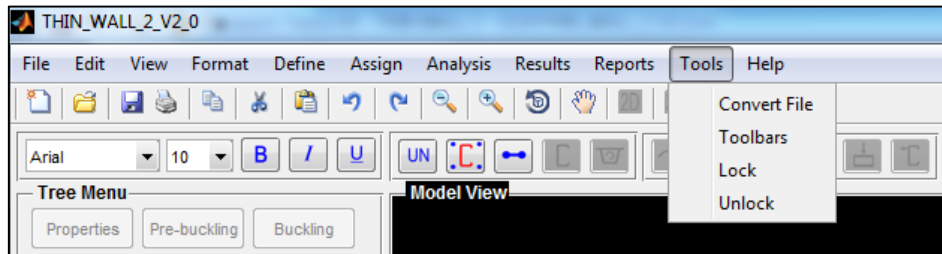
Figure 5.43: Tools menu

In order to support the user in using THIN-WALL-2 V2.0, there are tool-bars which are created on the main window. The first one is the Define bar where the main functions are defining materials, element types and sections. The second one is the Assign bar which is used to assign boundary condition, loadings and restraint. The Analysis bar contains the cross-section analysis button, the buckling analysis button and the un-lock and lock buttons. The user can click on these buttons to control the analyses. The Report bar is used to display the results of the analyses. Also, the user can export results into other format of data files in order to use for different purposes. The final one is the Result bars which is located on the right side of the main window. The user can click on buttons from this bar to display images on the main screen such as section, node number, strip number, buckling modes and shapes, signature curve, etc.

5.4.12. Help Menu

5.4.12.1. General

The Help menu as shown in Fig.5.44 is designed with some selections which help the user understand more about the THIN-WALL-2 V2.0 program, the SAFSM as well as the authors of the program as shown in Fig.5.45.
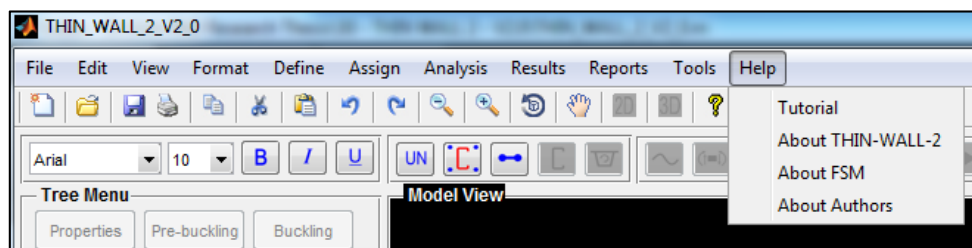
Figure 5.44: Help menu
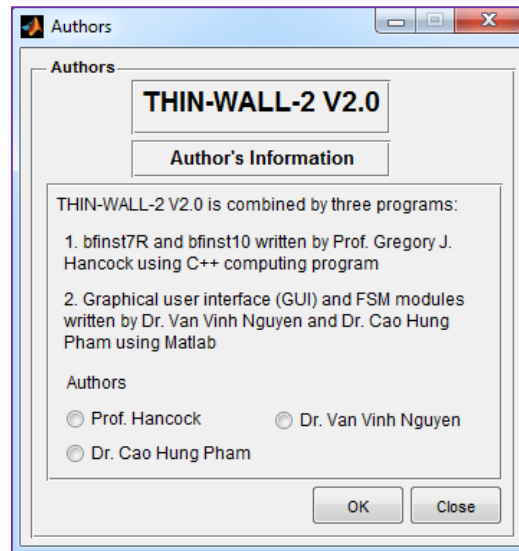
Figure 5.45: Author's information

5.4.12.2. Introduction about the SAFSM

THIN-WALL-2 V2.0 is written by relying on the theory of the SAFSM, thus it is necessary for the user to understand this theory. This function provides a brief introduction as well as advantages and disadvantages and the application of this method. In addition, some links are shown in this module which helps the user to find useful references.

5.4.12.3. Tutorial

There are some instructional files included in this module as well as a video which the user can download directly to study how to use THIN-WALL-2 V2.0. Also, if there is any problem, the user can contact the authors or the supporters by clicking to the Support button as shown in Fig.5.46 to gain the supports and the best solutions.
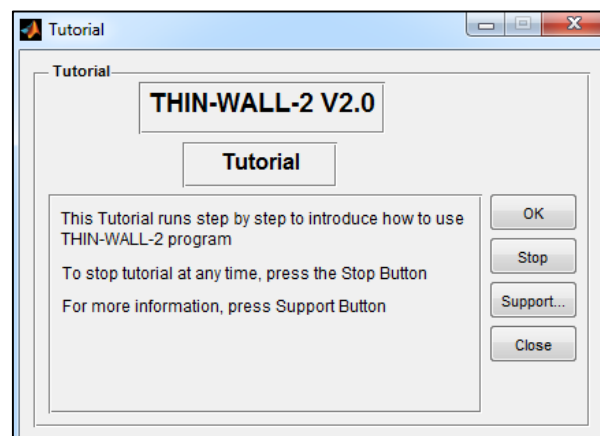
Figure 5.46: THIN-WALL-2 V2.0 tutorial

5.5. CONCLUSIONS

This Chapter provides a presentation of the THIN-WALL-2 V2.0 program which is based on the FSM. This second release extends the domain of application of the first one THIN-WALL [69]. It is possible to use this program to analyse structural members under uniform compression, bending and shear or localised loading and general end boundary conditions. The structural member may be made from both isotropic and orthotropic materials. In addition, with the general section module, THIN-WALL-2 V2.0 may be used to define and analyse all types of sections such as open sections, closed sections and mixed sections.

Finally, the GUI module which is included in THIN-WALL-2 V2.0 shows an improvement of this program in displaying the results from the analyses. The buckling modes and shapes are displayed in both 2D and 3D views, thus the user can understand the working of the structural member clearly.

CHAPTER 6

EXPERIMENTAL DATA, BUCKLING LOAD AND PLASTIC MECHANISM MODELS USED IN THE DIRECT STRENGTH METHOD APPLIED TO LOCALISED LOADING

6.1. INTRODUCTION

Experimental investigations have been performed in by many researchers to study the behaviour cold-formed steel members under localised loading. In addition, buckling analysis method and yielding analysis models have been proposed; however, these proposals still have limitations.

This Chapter summarises the experimental data which is used to develop the Direct Strength Method (DSM) for the design of cold-formed steel sections subjected to localised loading. This data is collected from previous literature for different localised load cases, cross-sections and flange fastened conditions. In addition, an introduction about the buckling analysis using THIN-WALL-2 V2.0 program to calculate the buckling load of structural members under localised loading is given. The Chapter also gives new plastic mechanism models used to estimate the yield load of the structural members. The buckling loads, the yield loads and the experimental data are used to establish the DSM equations for web crippling as described in Chapter 7.

6.2. EXPERIMENTAL DATA

6.2.1. Beshara and Schuster [36] (2000)

Beshara and Schuster [36] performed a statistical analysis on all available test data in order to develop more accurate coefficients for the Canadian standards as well as an experimental investigation into the web crippling capacities of fastened plain-C and plain-Z sections under the ITF and ETF load cases. The specimens were tested in pairs as shown in Fig.6.1 to avoid the twisting caused by eccentric loading. Table E-1 in Appendix E of the thesis shows the dimensions for 18 channel sections with different section depths, corner radii and bearing lengths of specimens under the ITF load case.
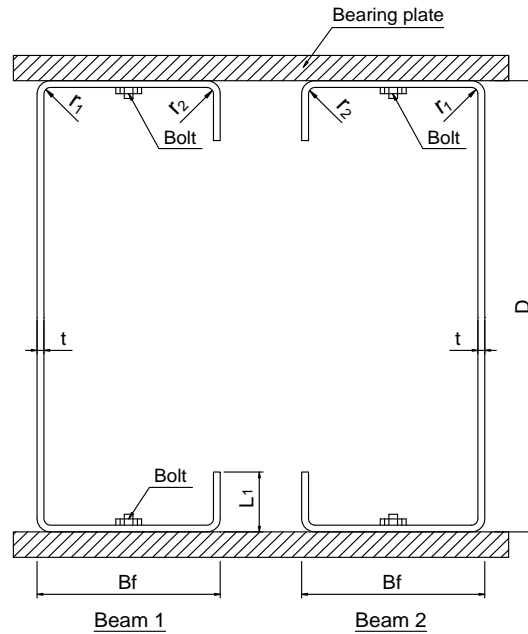
Figure 6.1: Fastened plain-C section under the ITF load case [36]

6.2.2. Young and Hancock [22] (2001)

Young and Hancock [22] performed a series of experimental tests on unlipped plain-C sections subjected to web crippling. The test specimens consisted of six different sectional sizes, having nominal thickness ranging from 4 to 6mm, a nominal depth of webs ranging from 75 to 300mm, and nominal flange widths ranging from 40 to 90mm. The specimens were tested as single element and flange unfastened condition as shown in Fig.6.2. Tables E-2 to E-5 in Appendix E of the thesis show the measured dimensions for 24 tested specimens under the IOF load case, 24 tested specimens under the EOF load case, 14 tested specimens under the ITF load case and 12 tested specimens under the ETF load case.
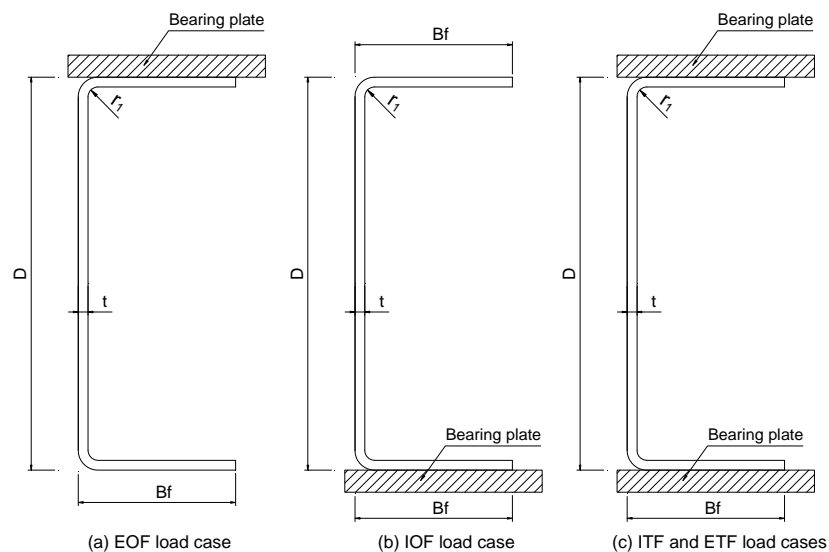
Figure 6.2: Unfastened plain-C sections under localised loads

6.2.3. Macdonald et al. [37] (2008)

Macdonald et al. [37] conducted tests on 36 fastened lipped plain-C sections under the EOF and the ETF load cases to investigate the effect of corner radius (r), web height (d_1) and bearing length (N) on web crippling. The specimens were tested as single element under loading as shown in Fig.6.3. The Finite Element Method (FEM) also was used to simulate the experimental investigation and validate the results. The detail sectional dimensions are given in Tables E-6 and E-7 in Appendix E of the thesis.
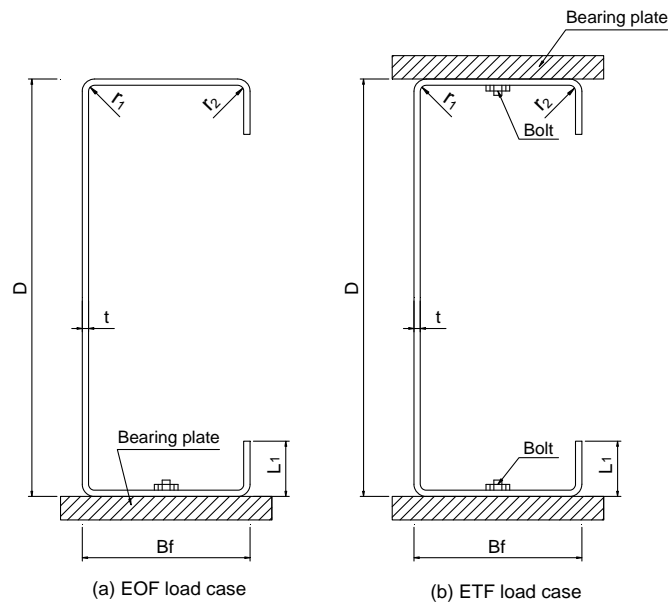
Figure 6.3: Fastened plain-C sections under the EOF and the ETF load cases

6.2.4. Uzzaman et al. [38] and [39] (2012)

Uzzaman performed a combination of experiments and non-linear finite element analyses to investigate the influence of holes on web crippling strength of cold-formed steel lipped plain-C sections under the EOF and the ETF load cases as described in [38] and [39]. In addition, both flange fastened and unfastened conditions were considered in the investigation as shown in Fig.6.4. Non-linear finite element models were conducted to compare against the experimental results. The data for 10 sections without holes under the ITF load case and 14 sections from Uzzaman et al. [38] and 23 sections from Uzzaman et al. [39] under the ETF load case is given in Tables E-8 to E-10 in Appendix E of the thesis.
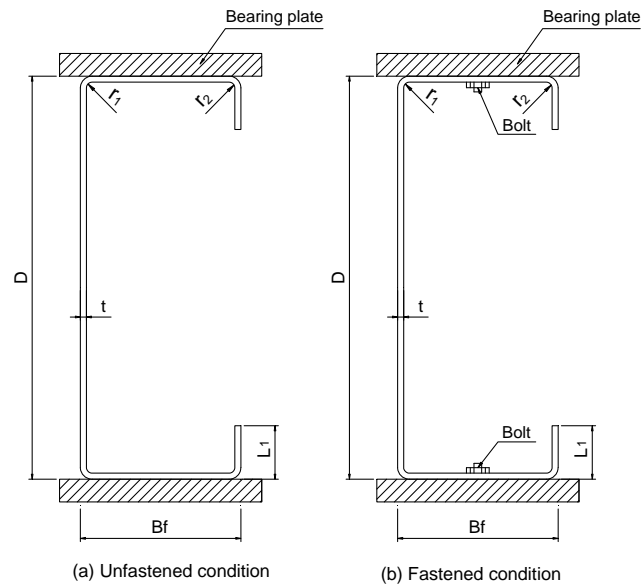
Figure 6.4: Plain-C sections under the ITF and ETF load cases

6.2.5. Morelli et al. [40] and Khatale et al. [41] (2014)

Experimental investigations involved the testing of two types of lipped channel sections: unstiffened web (plain-C sections) and stiffened web (DHS sections) were performed by Morelli et al. [40] for the IOF load case as shown in Fig.6.5 and Khatale et al. [41] for the ITF and ETF load cases. Two thicknesses 2.4mm and 3.0mm were tested with the depth of the sections remained constant at 300mm and the flange width ranging from 96 to 103mm. The detail dimensional data is given in Tables E-11 and E-12 for 32 specimens under the IOF load case, Tables E-13 and E-14 for 16 specimens under the ITF load case and Tables E-15 and E-16 for 16 specimens under the ETF load case in Appendix E of the thesis.
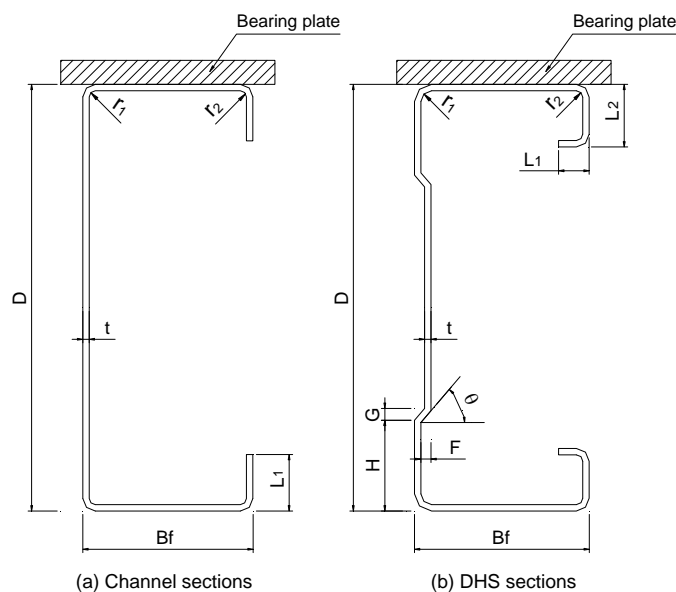
Figure 6.5: Plain-C and DHS sections under the IOF load case

6.2.6. Sundararajah et al. [19] (2015)

Sundararajah et al. [19] conducted 36 experiments to assess the web crippling behaviour and strength of unfastened lipped channel beams (LCBs) under the two-flange load cases (ITF and ETF) as shown in Fig.6.4(a). The experimental web crippling capacities were compared with the predictions from the current design rules from the Australian/New Zealand Standard AS/NZS 4600:2005 [3] and the North American Specification for the Design of Cold-Formed Steel Structural Members AISI S100-2012 [2]. The data of these experimental results are shown in Tables E-17 and E-18 in Appendix E of the thesis.

6.2.7. Efendy et al. [7] and Hadchiti et al. [8] (2015)

Experimental investigations were performed at the University of Sydney to study the behaviour of lipped plain-C and SupaCee sections under one-flange loading. Efendy et al. [7] performed experiments for 32 specimens under the IOF load case as shown in Fig.6.6, while Hadchiti et al. [8] conducted other 32 specimens under the EOF load case. The specimens were tested in pairs to avoid the twisting caused by eccentric loading. Also, both flange unfastened and fastened conditions were considered in this research. The sectional data and test results are shown in Tables E-19 and E-20 for the IOF load case and Tables E-21 and E-22 for the EOF load case in Appendix E of the thesis.

(a) Channel sections   (b) SupaCee sections
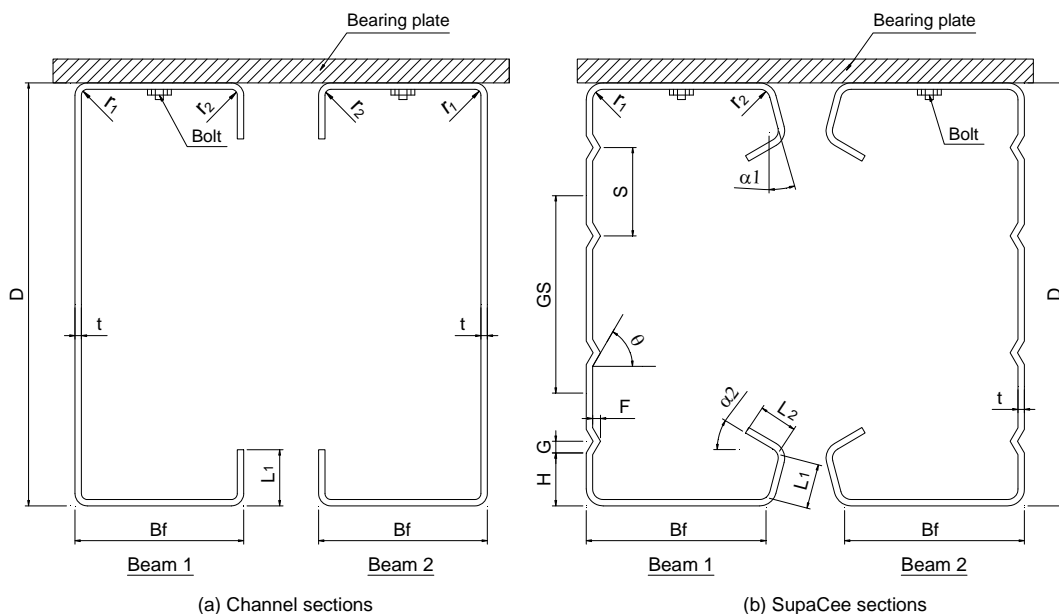
Figure 6.6: Plain-C and SupaCee sections under the IOF load case

6.2.8. Bartlett et al. [9] and Htet and Pham [10] (2016)

More recently, Bartlett et al. [9] and Htet and Pham [10] have performed experimental studies to investigate the capacities of cold-formed steel members under the ITF and ETF load cases respectively. In these studies, two types of cross-sections which are lipped plain-C sections and

SupaCee sections as shown in Fig.6.7 were tested to examine the effect of web stiffeners on sections. The specimens were tested in pairs to avoid the twisting caused by eccentric loading. Tables E-23 and E-24 for the ITF load case and Tables E-25 and E-26 for the ETF load case in Appendix E of the thesis show the sectional dimensions and test results from the experiments.

(a) Channel sections   (b) SupaCee sections
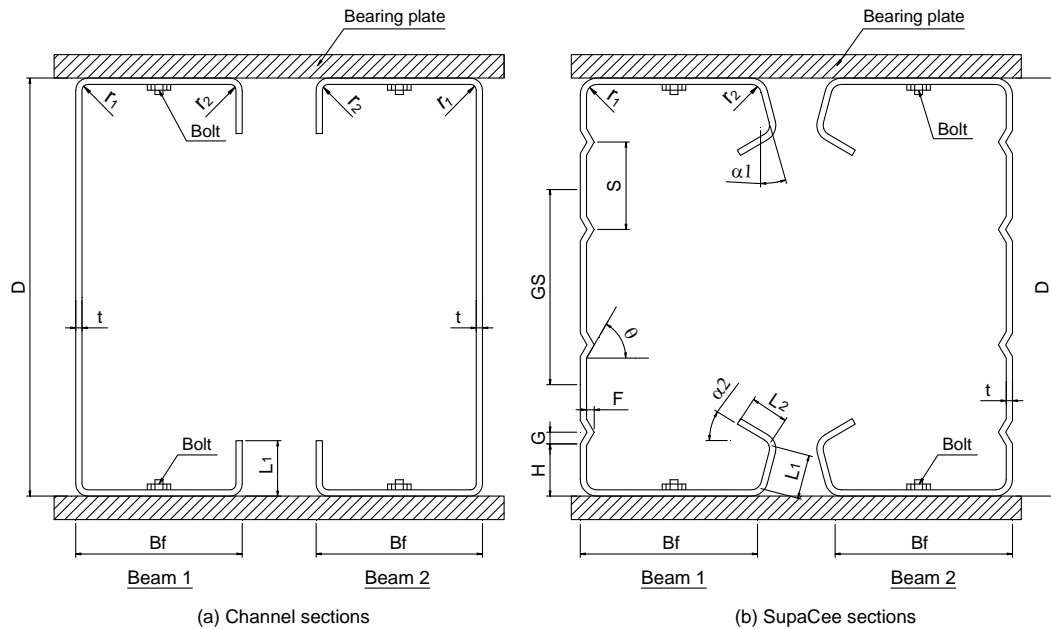
Figure 6.7: Plain-C and SupaCee sections under the ITF and ETF load cases

6.2.9. Lian et al. [42] (2016)

Lian et al. [42] performed a combination of tests and non-linear finite element analyses to investigate the impact of holes on web crippling under the EOF load case. The specimens were tested as single element as shown in Fig.6.3(a). The experimental data for 21 sections without hole is given in Table E-27 in Appendix E of the thesis.

6.3. BUCKLING LOAD

The buckling load is an important input of the DSM design equations for web crippling. Some investigations have been performed to determine the buckling load of thin-walled sections under localised loading; however, they still have limitations. In this thesis, the THIN-WALL-2 V2.0 program based on the FSM as described in Chapter 5 is selected to determine the buckling load of cold-formed sections subjected to localised loading. The program can perform the buckling analysis for all types of cross-sections, localised load cases and boundary conditions as described in Chapter 3. The buckling analysis results from THIN-WALL-2 V2.0 are benchmarked against the Finite Element Method (FEM) as described in Chapter 4. Thus, THIN-WALL-2 V2.0 can be seen as a good option for buckling

analysis of cold-formed steel sections under localised loading with general end boundary conditions.

Fig.6.8 shows the definition of localised load cases in the THIN-WALL-2 V2.0 program.
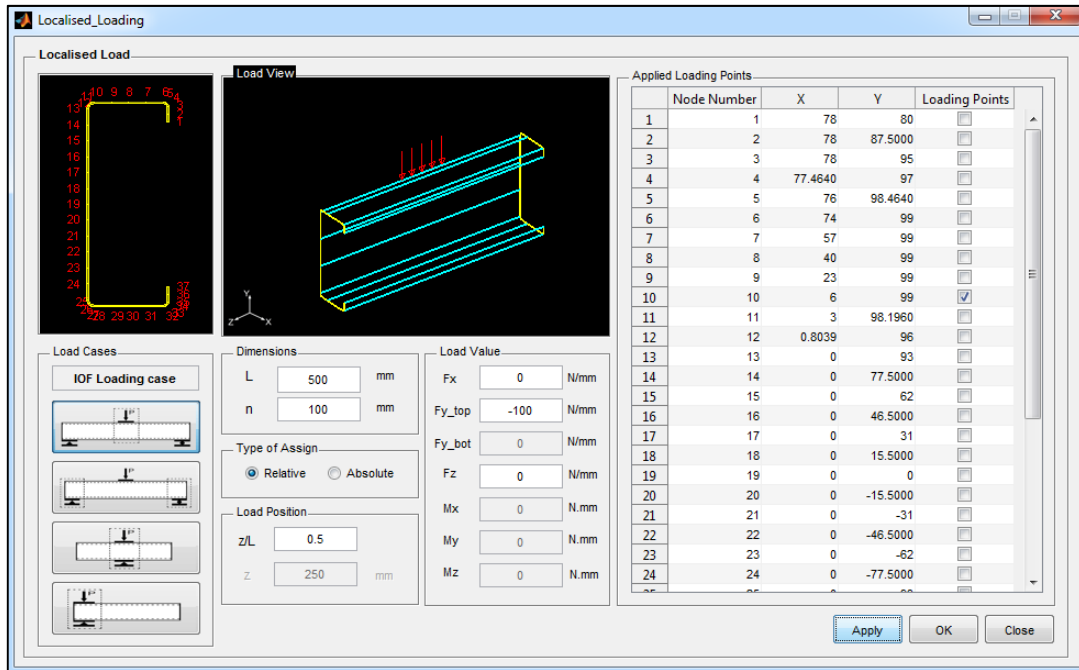
Figure 6.8: Assign localised loading

In the analysis of a beam under the IOF load case, the both ends Simply Supported (SS) boundary condition is assigned for the beam to match up with the practical boundary condition applied for the beam in experiments as shown in Fig.3.2(a). In addition, the localised load is applied on the top flange of the beam with interior locations. For the ITF load case as shown in Fig.3.2(b), the boundary condition is selected similar to the IOF load case; however, the localised loads are applied at both sides of the beam with interior locations.

In the experiment of the beam under the EOF load case as shown in Fig.3.2(c), the load is applied in the interior of the beam at a stiffened loading point in order to prevent failure around this area. With this loading condition, reactions appear at the ends of the beam which leads to web crippling. Thus, in the analysis, the beam length is taken as half of the original beam length from the experiment as shown in Fig.3.2(c) and the Clamped-Free (CF) is assigned to the beam. The localised load is applied at the end of the bottom flange.

For the ETF load case, the Simply-Free (SF) is assigned to the beam. Also, the longitudinal restraints are applied at the applied loading points to prevent the movement of the beam in the longitudinal direction. The beam length is equal to the original length of the beam as shown in Fig.3.2(d). The localised loads are applied at the end of the both flanges.

The buckling loads for the IOF and EOF load cases obtained from FSM using the THIN-WALL-2 V2.0 [76] program are compared against those from SFE using Abaqus [32] as shown in Figs.6.9 and 6.10. Similar comparisons for the ITF and ETF load cases are described in the Research Report 965 [77].
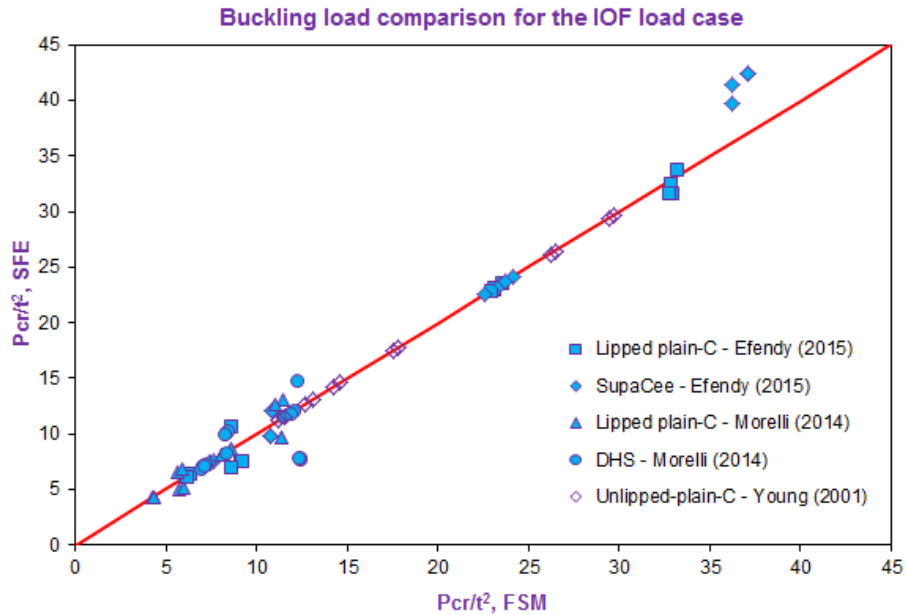
Figure 6.9: Buckling load comparison for the IOF load case
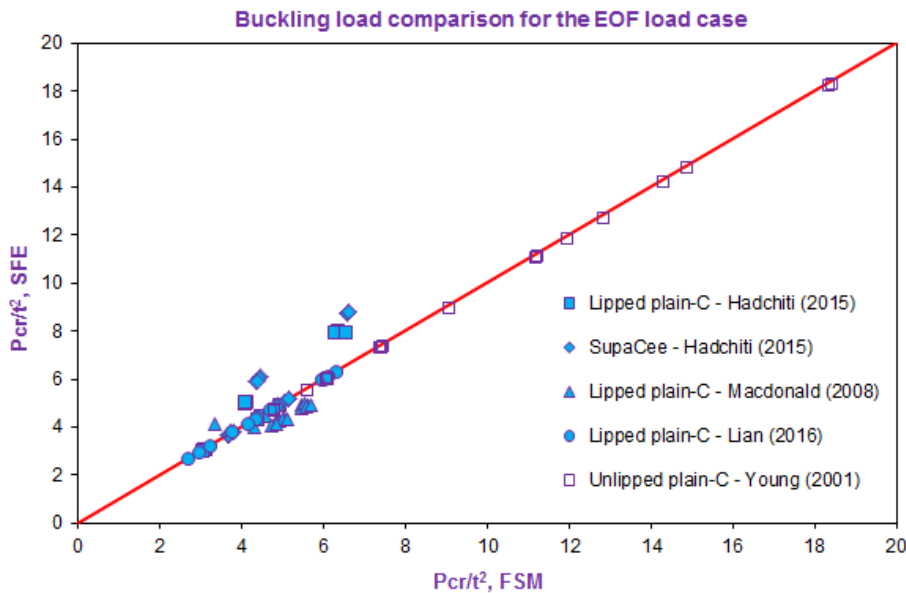
Figure 6.10: Buckling load comparison for the EOF load case

6.4. YIELD LOAD

The yield load is another key input to the DSM design equations for web crippling. Some models have been proposed to estimate the yield load of thin-walled sections under localised loading; however, these predictions still have some disadvantages. In this research, observations are performed from experiments to ascertain the failure modes of structural members under localised loading with different cross-sections, load cases and flange fastened conditions. From the data, new plastic mechanism models are built up based on the concept of the balance between the internal energy of the structural member and the external energy of the applied loads to estimate the yield load.

Regarding to the effect of inside radius to the yielding analysis, in general, all cold-formed sections have a corner radius and so the loads are eccentric from the web centreline. This can be compared with sections such as hot-rolled and welded I-sections where the web yielding is a direct result of bearing rather a plastic mechanism. This thesis concentrates on cold-formed steel sections with corner radii.

6.4.1. Plastic mechanism models for the IOF load case

The experiments were performed by Efendy et al. [7] at the University of Sydney for lipped plain-C sections and SupaCee sections under the IOF load case as shown in Fig.6.11(a). From the observation, it is found that for both flange unfastened and fastened conditions, the failure modes are similar which include two yield-lines. The first one is a straight line located on the top flange with the length equal to the bearing length, while the second one is a semi-circle from the top of the beam to the depth from 0.1D to 0.15D on the web (D is the overall depth of the beam) as shown in Fig.6.11(b).

(a) Experiment   (b) Failure modes
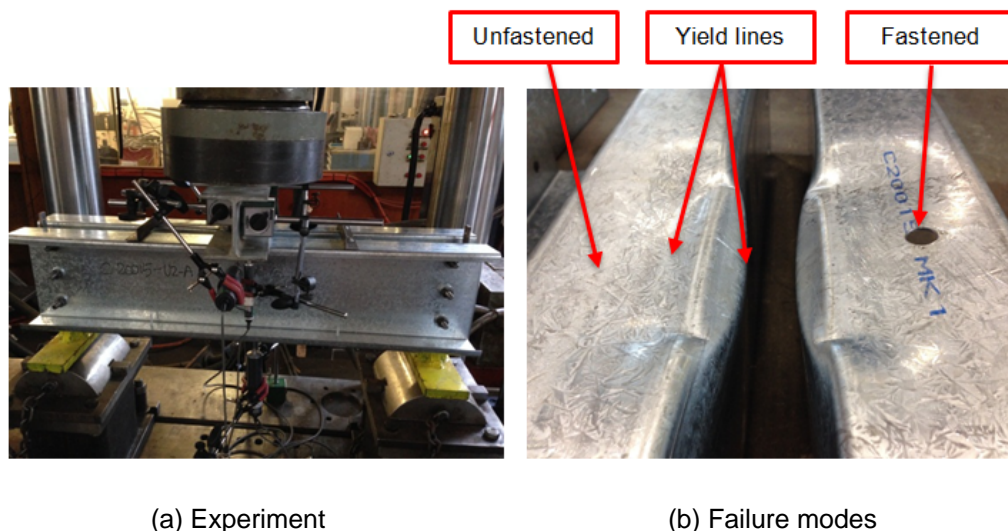
Figure 6.11: Experiment and failure modes for the IOF load case [7]

From the failure modes of the specimens under loading, a simplified plastic mechanism model is proposed as shown in Fig.6.12 to estimate the yield load for the IOF load case. In this model, there are two straight yield-lines matching up with two plastic hinges in the cross-section. The first one is located in the top flange with the length (N_{m1}) equal to the bearing length (N). The second one is located in the web which is the representative of the semi-circle yield-line on the specimen. The length of this line depends on the slope of two distribution lines from the bearing edges and its depth from the top of the beam. The model is simplified with horizontal hinges of length N_{m1} and N_{m2} to facilitate easy design.
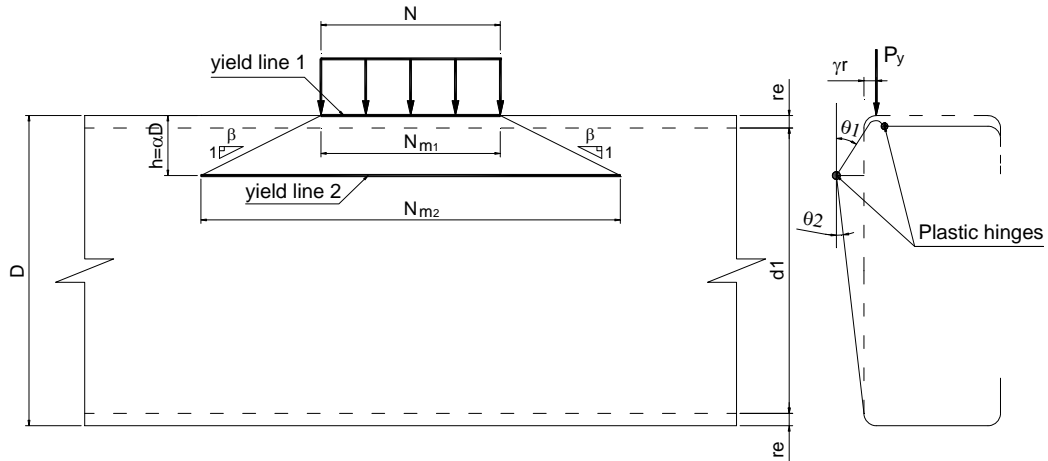
Figure 6.12: Plastic mechanism model for the IOF load case

The internal energy of the structural member must be equal to the external energy of the applied loads is given as:

$$P_y \gamma r \theta_1 = M_p \theta_1 N_{m1} + M_p \left(\theta_1 + \theta_2 \right) N_{m2} \tag{6.1}$$

Hence, the yield load is given as:

$$P_y = \frac{M_p}{\gamma r} \left[N_{m1} + \left(\frac{D}{D-h} \right) N_{m2} \right] \tag{6.2}$$

where:

θ_1, θ_2 are rotation angles of the top and the bottom web parts respectively

$$\theta_2 = \theta_1 \left(\frac{h}{D-h} \right)$$

t is the section thickness

D is the section depth

r_i, r and r_e are the interior, centre and outer radii respectively

$$r = r_i + \frac{t}{2}, \ r_e = r_i + t \tag{6.3}$$

γr is the load eccentricity from the web centre line

M_p is the plastic moment per unit length of plate

$$M_p = \frac{f_y t^2}{4} \tag{6.4}$$

f_y is the yield strength of steel

h is the depth of the second plastic hinge

$$h = \alpha D \tag{6.5}$$

α = 0.35 for unlipped plain-C sections

α = 0.125 for lipped plain-C and SupaCee sections

α = 0.07 for DHS sections

N is the bearing length

N_{m1} and N_{m2} are the yield-line lengths:

For unlipped plain-C sections:

$$N_{m1} = 0 \text{ and } N_{m2} = N + 2\beta h \tag{6.6}$$

For lipped plain-C, SupaCee and DHS sections

$$N_{m1} = N \text{ and } N_{m2} = N + 2\beta h \tag{6.7}$$

β is a yield-line distribution slope factor

$$\beta = \beta_o \beta_1 \tag{6.8}$$

β_1 is a slope factor,

β_1=1.0 for unlipped plain-C sections

β_1= 2.0 for lipped plain-C, SupaCee and DHS sections

β_o is a factor which depends on the bearing length ratio (N/D)

$$\frac{N}{D} = 0.15 \quad \beta_o = 1.6$$
$$\frac{N}{D} = 0.5 \quad \beta_o = 1.0 \tag{6.9}$$
$$\frac{N}{D} \geq 1.0 \quad \beta_o = 0$$

For other values of N/D, β is interpolated or extrapolated linearly

γ is a factor which depends on the radius ratio (r/t)

$$\gamma = \frac{1}{\gamma_o} \tag{6.10}$$

$$\frac{r_i}{t} = 2.5 \quad \gamma_o = 1.0$$
$$\frac{r_i}{t} = 1.5 \quad \gamma_o = 0.8 \tag{6.11}$$

For other values of r_i / t, γ_o is interpolated or extrapolated linearly

6.4.2. Plastic mechanism models for the EOF load case

The experiments were performed by Hadchiti et al. [8] at the University of Sydney for lipped plain-C and SupaCee sections under the EOF load case as shown in Fig.6.13(a). From observation of the tested beams, it is found that for both flange unfastened and fastened conditions, the failure modes are similar which include one inclined yield-line. The beginning point of this yield-line is located at 0.2D to 0.25D from the top of the beam, while the ending point is located at the junction between the web and the top flange as shown in Fig.6.13(b).

(a) Experiment   (b) Failure modes
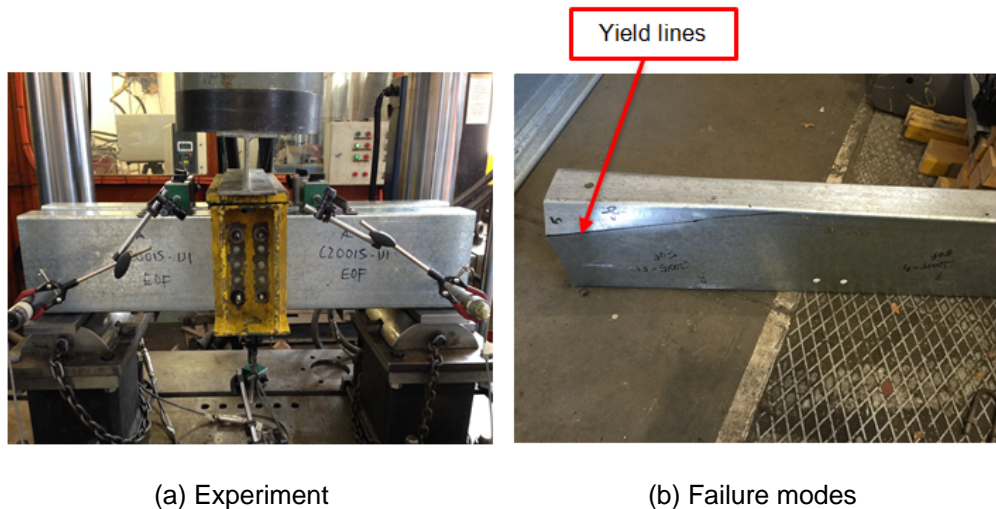
Figure 6.13: Experiment and failure modes for the EOF load case [8]

From the failure modes of the specimens under loading, a plastic mechanism model is proposed as shown in Fig.6.14 to estimate the yield load for the EOF load case. In this model, there is one yield-line matching up with one plastic hinge on the cross-section. In order to make a simple model for the calculation, the yield-line is assumed as a horizontal line. The length of this line depends on the slope of the distribution line from the bearing edge and its depth from the top of the beam.
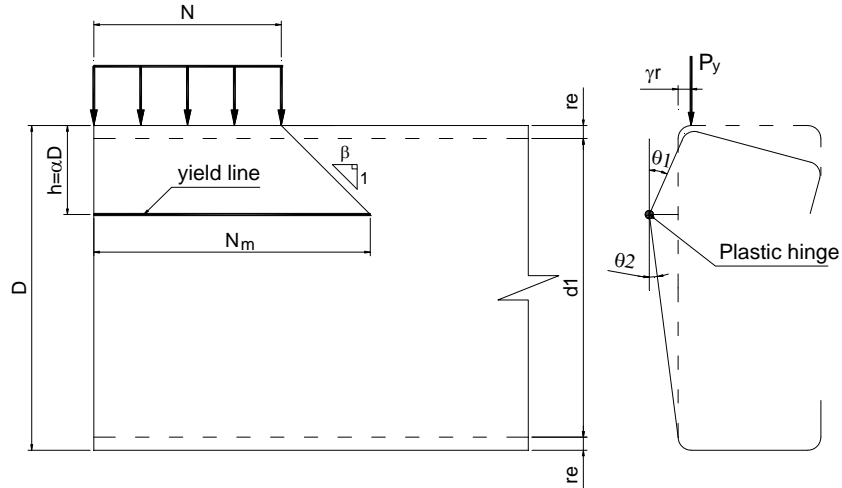
Figure 6.14: Plastic mechanism model for the EOF load case

The concept of the balance between the internal energy of the yield-line and the external energy of the applied load is given as:

$$P_y \gamma r \theta_1 = M_p \left(\theta_1 + \theta_2 \right) N_m \tag{6.12}$$

Hence, the yield load is given as:

$$P_y = \frac{M_p}{\gamma r} \left[\left(\frac{D}{D-h} \right) N_m \right] \tag{6.13}$$

where:

$$\theta_2 = \theta_1 \left(\frac{h}{D-h} \right)$$

$h = \alpha D$

$\alpha = 0.25$ for unlipped plain-C, lipped plain-C, SupaCee and DHS sections

N_m is the yield-line length

$$N_m = N + \beta h \tag{6.14}$$

$\beta = \beta_o \beta_1$

$\beta_1 = 1.0$ for unlipped plain-C, lipped plain-C, SupaCee and DHS sections

β_o is determined by Eq.(6.9)

γ is determined by Eqs.(6.10) & (6.11)

6.4.3. Plastic mechanism models for the ITF load case

The experiments were performed by Bartlett et al. [9] at the University of Sydney for lipped plain-C and SupaCee sections under the ITF load case as shown in Fig.6.15(a). It is found that the flange unfastened condition has different failure modes from the flange fastened condition. In this case, there

is only one yield-line located at the middle of the web as shown in Fig.6.15(b). From the failure modes of the specimens under the ITF load case with flange unfastened condition, a plastic mechanism model is proposed as shown in Fig.6.16 to estimate the yield load. In this model, there is one yield-line matching up with one plastic hinge at the middle of the web.

(a) Experiment   (b) Failure modes
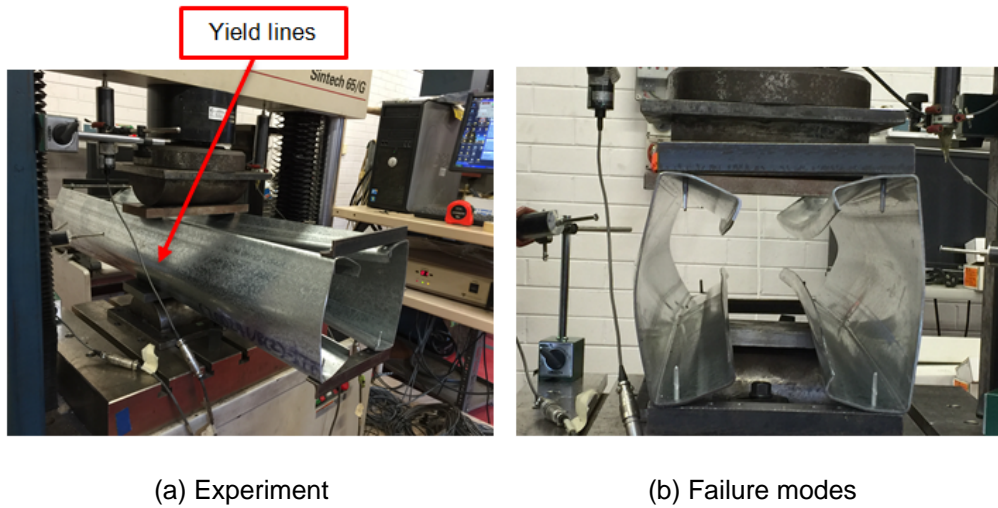
Figure 6.15: Experiment and failure modes for the ITF load case with flange unfastened condition [9]
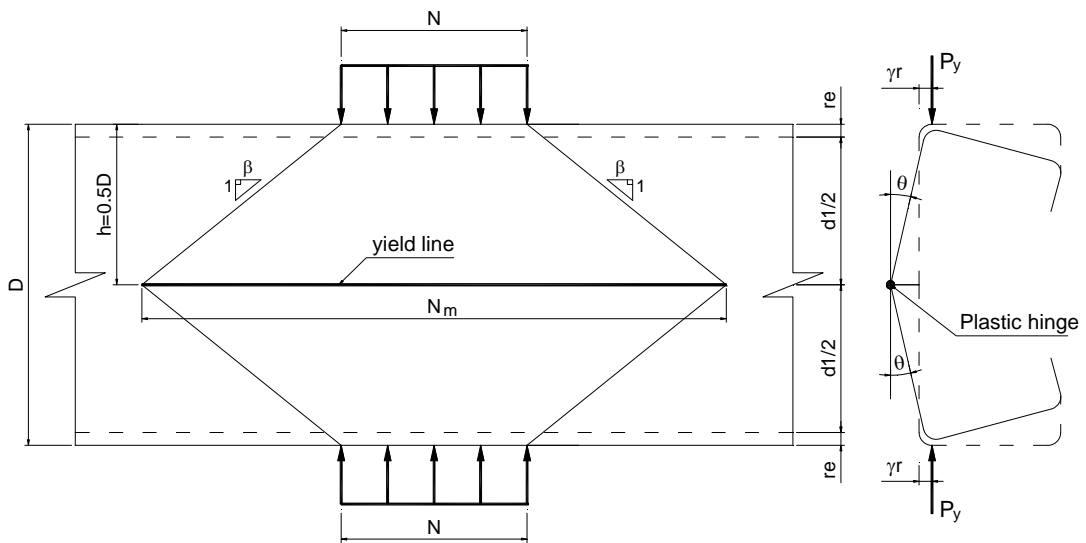
Figure 6.16: Plastic mechanism model for the ITF load case with flange unfastened condition

The yield load (P_y) for flange unfastened condition is given as:

$$2P_y \gamma r \theta = 2M_p \theta N_m \tag{6.15}$$

$$P_y = \frac{M_p N_m}{\gamma r} \tag{6.16}$$

where:

$h = \alpha D$

α = 0.5 for unlipped plain-C, lipped plain-C and SupaCee sections

α = 0.25 for DHS sections

N_m is the yield-line length

$$N_m = N + 2\beta h \qquad (6.17)$$

$\beta = \beta_o \beta_1$

β_1 = 1.5 for unlipped plain-C, lipped plain-C, SupaCee and DHS and sections

β_o is determined by Eq.(6.9)

γ is determined by Eqs.(6.10) & (6.11)

The flange fastened condition case is more complex than the flange unfastened condition with two yield-lines in the both flanges and three yield-lines in the web as shown in Fig.6.17. From the failure modes of the specimens under the ITF load case with flange fastened condition, a plastic mechanism model is proposed as shown in Fig.6.18 to estimate the yield load. In this model, there are two yield-lines in the both flanges with the length (N_{m1}) equal to the bearing length (N). There are two other yield-lines located in the web which are the representative of the semi-circle yield-lines in the specimen. The last one is located at the middle of the web.

(a) Experiment   (b) Failure modes
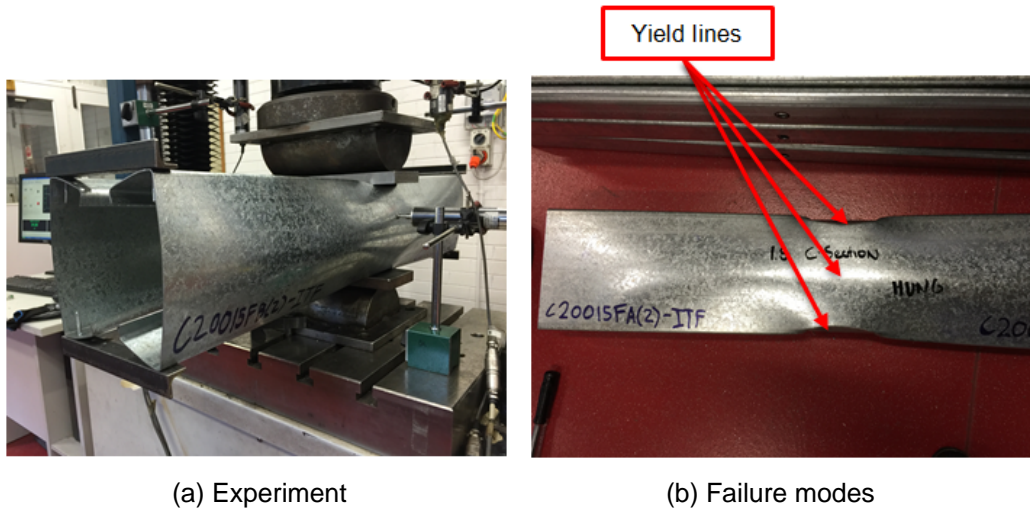
Figure 6.17: Experiment and failure modes for the ITF load case with flange fastened condition [9]
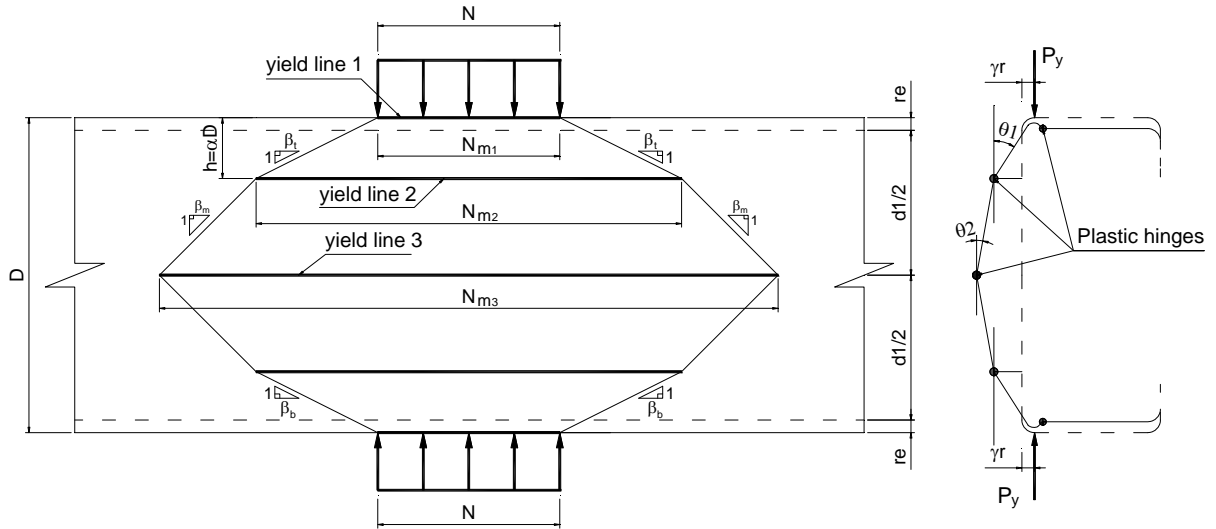
Figure 6.18: Plastic mechanism model for the ITF load case with flange fastened condition

The concept of the balance between the internal energy of the yield-line and the external energy of the applied load is given as:

$$2P_y \gamma r \theta = 2M_p \theta_1 N_{m1} + 2M_p \theta_1 N_{m2} + 2M_p \theta_2 N_{m3} \tag{6.18}$$

The yield load (P_y) for flange fastened condition is given as:

$$P_y = \frac{M_p}{\gamma r} \left[N_{m1} + N_{m2} + \left(\frac{2h}{D-2h} \right) N_{m3} \right] \tag{6.19}$$

where:

$$\theta_2 = \theta_1 \left(\frac{h}{D/2-h} \right)$$

$h = \alpha D$

$\alpha = 0.5$ for unlipped plain-C sections

$\alpha = 0.125$ for lipped plain-C, SupaCee and DHS sections

N_{m1}, N_{m2} and N_{m3} are the yield-line lengths

For unlipped plain-C sections

$$N_{m1} = 0, \ N_{m2} = N + 2\beta_t h, \ N_{m3} = 0 \tag{6.20}$$

For lipped plain-C, SupaCee and DHS sections

$$N_{m1} = N, \ N_{m2} = N + 2\beta_t h, \ N_{m3} = N_{m2} + 2\beta_m \left(\frac{D}{2} - h \right) \tag{6.21}$$

For the top and the bottom yield-lines in the web

$$\beta_t = \beta_b = \beta_o \beta_1 \tag{6.22}$$

$\beta_1 = 1.5$ for unlipped plain-C sections

β_1 = 2.0 for lipped plain-C, SupaCee and DHS sections

For the middle yield-line in the web

$$\beta_m = \beta_o \beta_2 \qquad (6.23)$$

β_2 is not available for unlipped plain-C sections

β_2 =1.0 for lipped plain-C, SupaCee and DHS sections

β_o is determined by Eq.(6.9)

γ is determined by Eqs.(6.10) & (6.11)

6.4.4. Plastic mechanism models for the ETF load case

The experiments were performed by Htet and Pham [10] at the University of Sydney for lipped plain-C and SupaCee sections under the ETF load case as shown in Fig.6.19(a). It can be seen that the flange unfastened and fastened conditions have similar failure modes which include one horizontal yield-line located at the middle of the web as shown in Fig.6.19(b). From the failure modes of the specimens under the ETF load case, a plastic mechanism model is proposed as shown in Fig.6.20 to estimate the yield load. In this model, there is one yield-line matching up with one plastic hinge at the middle of the web.

(a) Experiment   (b) Failure modes
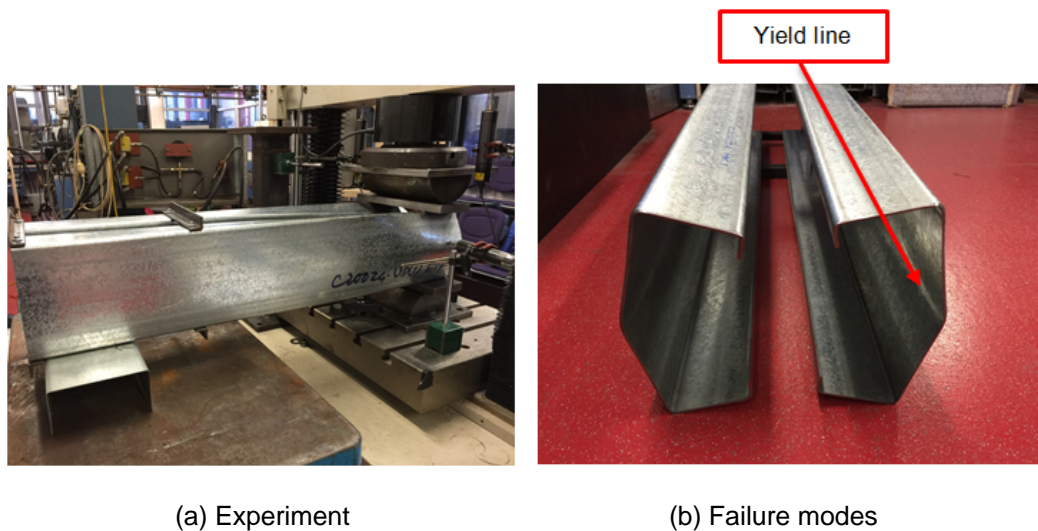
Figure 6.19: Plastic mechanism model for the ETF load case [10]
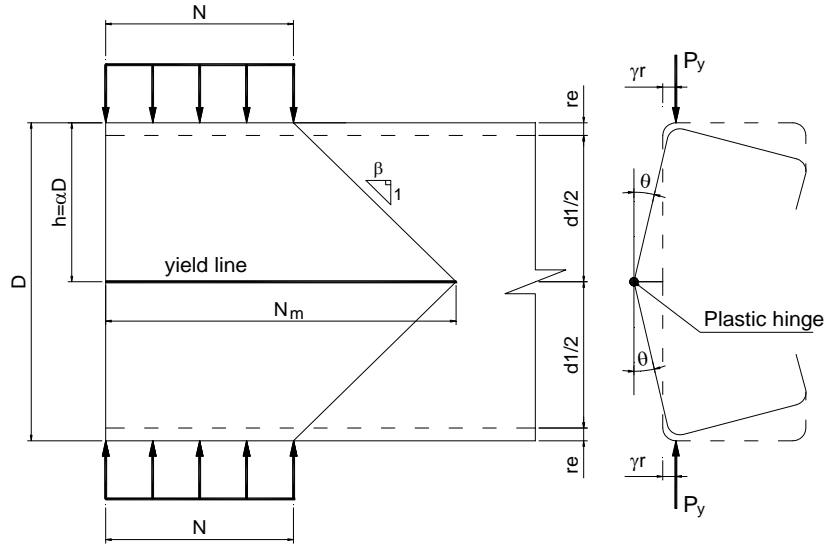
Figure 6.20: Plastic mechanism model for the ETF load case

The yield load (P_y) is given as:

$$2P_y \gamma r \theta = 2M_p \theta N_m \qquad (6.24)$$

$$P_y = \frac{M_p N_m}{\gamma r} \qquad (6.25)$$

where:

$h = \alpha D$

$\alpha = 0.5$ for unlipped plain-C, lipped plain-C and SupaCee sections

$\alpha = 0.25$ for DHS sections

N_m is the yield-line length

$$N_m = N + \beta h \qquad (6.26)$$

$\beta = \beta_o \beta_1$

$\beta_1 = 1.0$ for unlipped plain-C, lipped plain-C and SupaCee sections

$\beta_1 = 1.5$ for DHS sections

β_o is determined by Eq.(6.9)

γ is determined by Eqs.(6.10) & (6.11)

6.4.5. Summary of the plastic mechanism models

It is found that for different cross-sections, different plastic mechanism models are employed to estimate the yield load P_y. The factors for the different plastic mechanism models are given in Table 6.1 for different load cases, flange fastened conditions and cross-sections. It can be seen that for the

ITF load case, the factors for the flange unfastened condition are different from the factors for the flange fastened condition because of the different plastic mechanism models. For other cases, the factors are the same for both the flange unfastened and fastened conditions.

The values of the yield loads determined by the plastic mechanism models for the collected experimental data under different load cases are given in Tables E-1 to E-27 in Appendix E of the thesis.

Table 6.1: Factors for plastic mechanism models

Sections	Loading	Flange unfastening condition		Flange fastening condition		
		α	β_1	α	β_1	β_2
Unlipped plain-C	IOF	0.35	1.00	0.35	1.00	NA
	EOF	0.25	1.00	0.25	1.00	NA
	ITF	0.50	1.50	0.50	1.50	NA
	ETF	0.50	1.00	0.50	1.00	NA
Lipped plain-C and SupaCee	IOF	0.125	2.00	0.125	2.00	NA
	EOF	0.25	1.00	0.25	1.00	NA
	ITF	0.50	1.50	0.125	2.00	1.00
	ETF	0.50	1.00	0.50	1.00	NA
DHS	IOF	0.07	2.00	0.07	2.00	NA
	EOF	0.25	1.00	0.25	1.00	NA
	ITF	0.25	1.50	0.125	2.00	1.00
	ETF	0.25	1.50	0.25	1.50	NA

6.5. CONCLUSION

The buckling analysis using the THIN-WALL-2 V2.0 program based on the FSM described in Chapters 3, 4 and 5 has been selected to determine the buckling loads of the structural members under localised loading. Consistent and simplified plastic mechanism models have been developed for all four localised load cases to calculate the yield loads of the structural members. The parameters of the plastic mechanism models are adjusted due to the cross-sections types, loading conditions and flange fastening conditions. The experimental data is collected with the detail dimensions and yield stress values. This data is used to calculate the buckling loads and yield loads in order to build up the DSM design equations for structural members under localised loading as described in Chapter 7.

CHAPTER 7

A CONSISTENT AND SIMPLIFIED DIRECT STRENGTH METHOD FOR THE DESIGN OF COLD-FORMED STEEL SECTIONS UNDER LOCALISED LOADING

7.1. INTRODUCTION

The Direct Strength Method (DSM) has been seen as a reliable, consistent and well established design approach for cold-formed steel structural members under compression, bending and shear. For localised loading, many investigations have been performed to develop the DSM design equations; however these proposals are still not consistent.

This Chapter gives proposals of DSM equations for design of cold-formed steel sections under localised loading. These equations are built-up based on the buckling load (P_{cr}) obtained from the THIN-WALL-2 V2.0 program as described in Chapter 5 and the yield load (P_y) estimated from plastic mechanism models as described in the Chapter 6. This is a consistent, simplified and generalised model for all the localised load cases IOF, EOF, ITF and ETF. It includes both an inelastic reserve component as observed in testing and a yield load component. Also, the calibration is performed to validate the accuracy of the DSM predictions with the collected experimental data.

7.2. EXPERIMENTAL DATA, YIELD LOAD AND BUCKLING LOAD

The experimental data is collected from previous literature for structural members subjected to localised loading. The data includes four load cases such as the IOF, EOF, ITF, ETF and four types of cross sections such as unlipped plain-C, lipped plain-C, SupaCee and DHS sections. In addition, both flange unfastened and fastened conditions are considered in this collection. This data is used to determine the buckling load (P_{cr}) from the THIN-WALL-2 V2.0 program and the yield load (P_y) from plastic mechanism models as described in Chapter 6. The experimental data, the buckling loads and the yield loads are given in Tables F-1 to F-27 in Appendix F of the thesis.

7.3. DIRECT STRENGTH METHOD FOR WEB CRIPPLING

7.3.1. General DSM for web crippling

The Direct Strength Method (DSM) has been adopted for design of columns, beams and beam-columns as described in [2]. In order to develop the DSM design equation for localised loading, it is necessary to have three main inputs which are the buckling load (P_{cr}), the yield load (P_y) and the experimental failure load (P_{exp}). From these three components, a general set of DSM equations is

proposed to predict the nominal strength of structural members under localised loading as given in Eqs.(7.1) and (7.2).

$$\frac{P_n}{P_y} = \left[1 + \left(1 - \frac{\lambda}{\lambda_o} \right)(k_4 - 1) \right] \qquad \text{for} \qquad \lambda \leq \lambda_o \tag{7.1}$$

$$\frac{P_n}{P_y} = k_1 \left[1 - k_2 \left(\frac{P_{cr}}{P_y} \right)^{k3} \right] \left(\frac{P_{cr}}{P_y} \right)^{k3} \qquad \text{for} \qquad \lambda > \lambda_o \tag{7.2}$$

where:

λ is the sectional slenderness, $\lambda = \sqrt{P_y / P_{cr}}$

λ_o is the sectional slenderness when $P_n / P_y = 1$

k_1, k_2, k_3 are coefficients and exponents calibrated through a non-linear regression procedure, fitting the set of ratios $P_{\exp} / P_y$ to the right hand side of Eq.(7.2) which was proposed previously by Natário et al. [21]. For different load cases, different coefficients and exponents are employed to build up suitable DSM design equations.

For $\lambda \leq \lambda_o$ the nominal inelastic capacity of structural members is based on Eq.(7.3) which is itself based on the inelastic reserve equation for beams in the AISI S100:2012 Specification (Appendix 1, Sections 1.2.2.1.2.1.2 and 1.2.2.1.3.1.2). From this, Eq.(7.1) is proposed to predict the nominal inelastic capacity of structural members under localised loading.

$$P_n = P_y + \left(1 - \frac{1}{C_y^2} \right)(k_4 P_y - P_y) \tag{7.3}$$

where:

$C_y = \sqrt{\lambda_o / \lambda}$

k_4 is a mechanism strengthening effect coefficient. It has been chosen as k_4=1.8 in this study. The mechanism strengthening effect, which is observed experimentally, is probably caused by the moving hinge position in the flange under significant plastic deformation for stockier sections.

7.3.2. DSM design equations for the IOF load case

The experimental data for the IOF load case is collected from Efendy et al. [7] for lipped plain-C and SupaCee sections, Morelli et al. [40] for lipped plain-C and DHS sections and Young and Hancock [22]

for unlipped plain-C sections. The analyses are performed to obtain the buckling load and the yield load as described in Chapter 6. The relationship between P_{cr} and P_y is set up to propose new DSM design equations with the coefficients k_1=1, k_2=0.15, k_3=0.4 and k_4=1.8 as given in Eqs.(7.4) and (7.5) to predict the capacities of structural members under the IOF load case.

$$\frac{P_n}{P_y} = \left[1 + 0.8 \left(1 - \frac{\lambda}{0.776} \right) \right] \qquad \text{for} \qquad \lambda \leq 0.776 \tag{7.4}$$

$$\frac{P_n}{P_y} = \left[1 - 0.15 \left(\frac{P_{cr}}{P_y} \right)^{0.4} \right] \left(\frac{P_{cr}}{P_y} \right)^{0.4} \qquad \text{for} \qquad \lambda > 0.776 \tag{7.5}$$

where k_1 has been chosen as 1.0 to ensure the correct position for the cut off for the inelastic reserve equation. Eq.(7.5) has the same coefficients and exponents as the local buckling DSM equation in the AISI S100:2012 Specification (Appendix 1, Sections 1.2.2.1.2.1.1 and 1.2.1.2.1).

The DSM Eq.(7.5) for the IOF load case is plotted in Fig.7.1 with the test data. The cut-off $\left(P_n / P_y = 1 \right)$ is defined as the slenderness range for which the estimated web crippling load equals the yield load. From Eq.(7.4), the inelastic reserve capacity is plotted by a dash line in the same figure. Then, the DSM design curve is the combination of the continuous curve when $\lambda > 0.776$ and the dash line when $\lambda \leq 0.776$ as shown in Fig.7.1. It can be seen that the DSM curve fits the experimental data well.
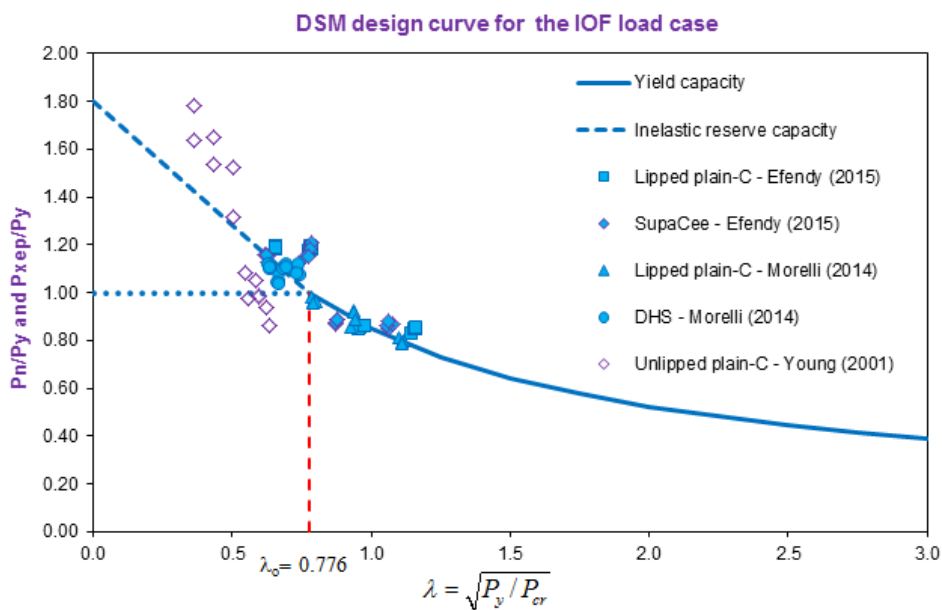
Figure 7.1: DSM design curve for the IOF load case

Comparisons between the experimental capacities (P_{exp}) and the nominal capacities (P_n) for each group of test data are given in the Tables F-1 to F-5 in Appendix F of the thesis. The summary of the mean values and the coefficient of variation of the ratios (P_{exp}/P_n) is given in Table 7.1. It is found that the average value of the ratios (P_{exp}/P_n) is 1.020, thus the predicted capacities are conservative in comparison with the experimental capacities and it is good for safe designs. The average value of the coefficient of variation is 8.30% which is less than 10%, thus it is acceptable variation. In addition, the relationship between the ratios (P_{exp}/P_n) is plotted as shown in Fig.7.2 to clarify that these values are close to the expected ratio (P_{exp}/P_n=1).
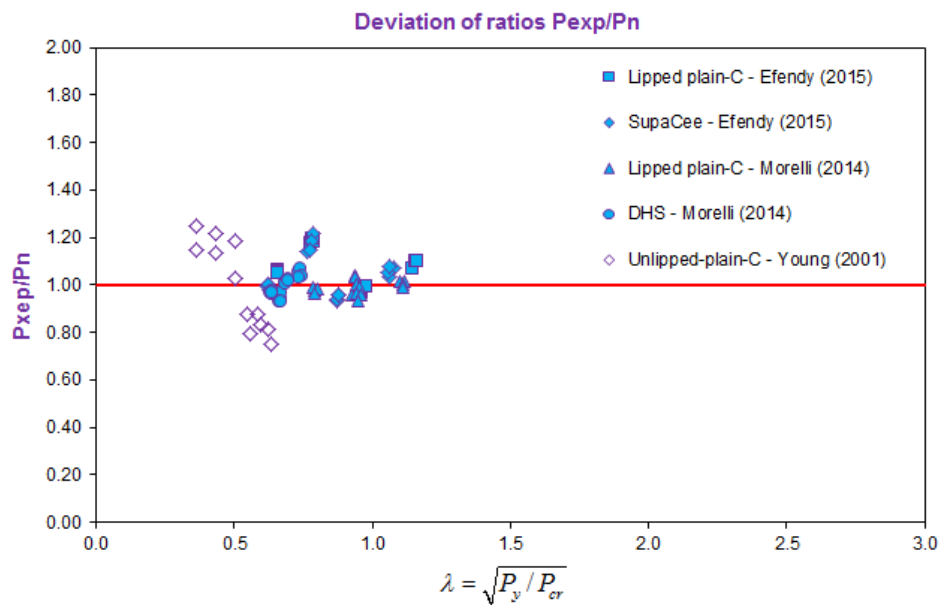
Figure 7.2: The ratios of P_{exp}/P_n for the IOF load case

Table 7.1: Summary of the ratios (P_{exp}/P_n) for the IOF load case

Load case	Authors	Year	Sections	P_{exp}/P_n		Average values	
				Mean	COV	Mean	COV
IOF load case	Efendy, Riyadi & Pham	2015	Lipped plain-C	1.082	7.24%	1.020	8.30%
			SupaCee	1.043	8.61%		
	Morelli, Batrounian, Pham & Papangelis	2014	Lipped plain-C	0.989	2.87%		
			DHS	0.996	4.44%		
	Young & Hancock	2001	Unlipped plain-C	0.993	18.36%		

7.3.3. DSM design equations for the EOF load case

Experiments for structural members under the EOF load case have been performed by many researchers such as Hadchiti et al. [8] for lipped plain-C and SupaCee sections, Macdonald et al. [37] and Lian et al. [42] for lipped plain-C sections and Young and Hancock [22] for unlipped plain-C

sections. This experimental data has been collected and the analyses have been performed to obtain the buckling loads and the yield loads. The DSM design equations have been proposed to predict the capacities of structural members under the EOF load case as given in Eqs.(7.6) and (7.7). These equations are the same as the DSM equations for the IOF load case.

$$\frac{P_n}{P_y} = \left[1 + 0.8\left(1 - \frac{\lambda}{0.776}\right)\right] \qquad \text{for} \qquad \lambda \le 0.776 \qquad (7.6)$$

$$\frac{P_n}{P_y} = \left[1 - 0.15\left(\frac{P_{cr}}{P_y}\right)^{0.4}\right]\left(\frac{P_{cr}}{P_y}\right)^{0.4} \qquad \text{for} \qquad \lambda > 0.776 \qquad (7.7)$$
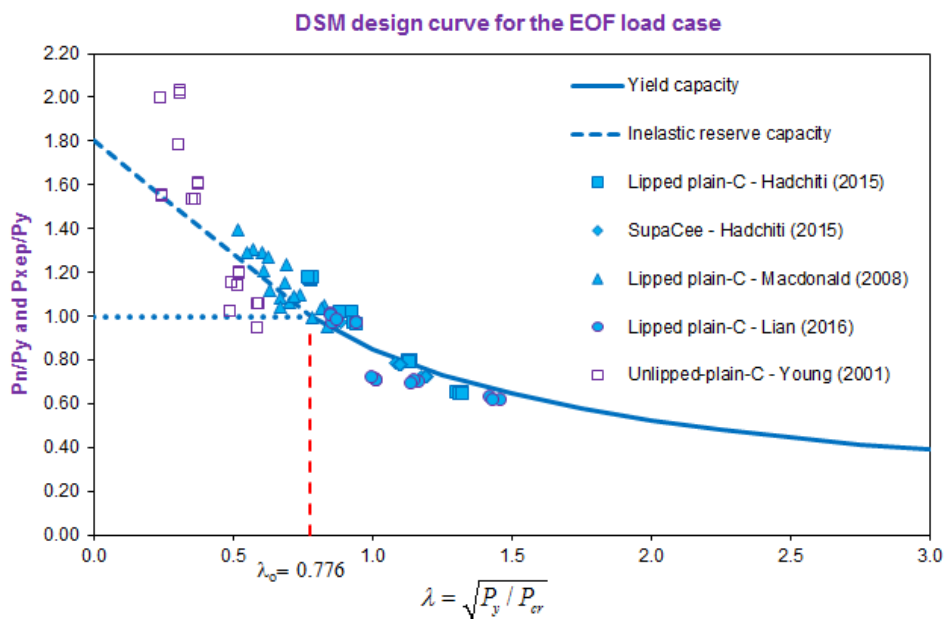
Figure 7.3: DSM design curve for the EOF load case

From Eqs.(7.6) and (7.7), the DSM design curve for the EOF load case has been plotted in Fig.7.3 with the experimental data. Some data points are located above and below but not far from the design curve. It means that the design curve captures the trend of the experimental data well.

Tables F-6 to F-10 in Appendix F of the thesis show the comparisons between the experimental capacities (P_{exp}) and the nominal capacities (P_n). Also, the ratios (P_{exp}/P_y) is plotted against the sectional slenderness (λ) to display the deviation of the experimental data as shown in Fig.7.4. The comparisons are summarised and given in Table 7.2 with the average values of the mean values and the coefficient of variation are 1.017 and 9.38% respectively. Similar to the IOF load case, these values prove that the predicted capacities (P_n) are conservative in comparison to the experimental capacities (P_{exp}) and are acceptable.
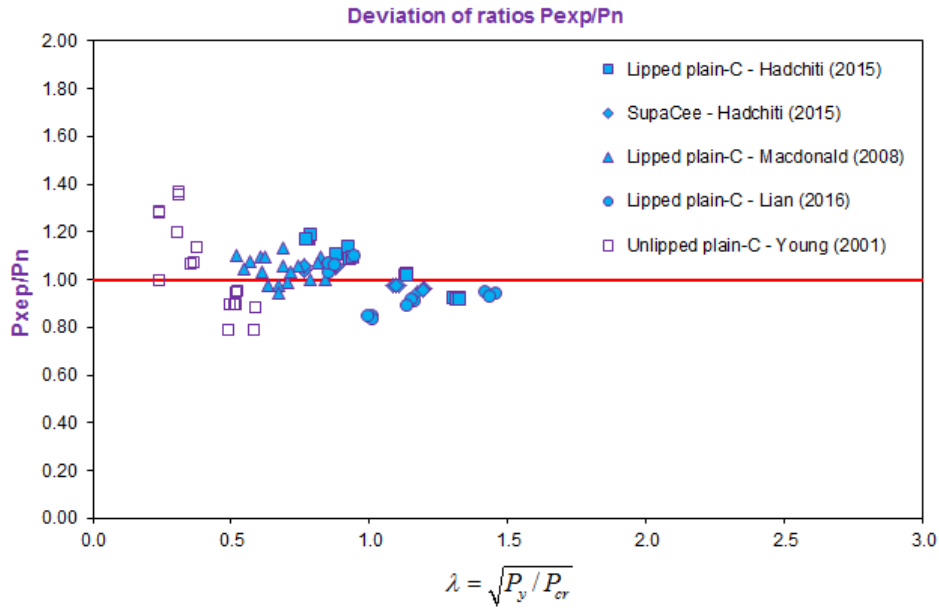
Figure 7.4: The ratios of P_{exp}/P_n for the EOF load case

Table 7.2: Summary of the ratios (P_{exp}/P_n) for the EOF load case

Load case	Authors	Year	Sections	P_{exp}/P_n		Average values	
				Mean	COV	Mean	COV
EOF load case	Hadchiti, Dalton & Pham	2015	Lipped plain-C	1.057	9.37%	1.017	9.38%
			SupaCee	1.008	4.44%		
	Macdonald et al.	2008	Lipped plain-C	1.042	5.15%		
	Lian et al.	2016	Lipped plain-C	0.951	9.84%		
	Young & Hancock	2001	Unlipped plain-C	1.025	18.07%		

7.3.4. DSM design equations for the ITF load case

From the previous literature, the experimental data for the ITF has been gathered from different sources. There are 32 specimens for lipped plain-C and SupaCee sections from Bartlett et al. [9], 16 tests for lipped plain-C and DHS sections from Khatale et al. [41], 18 specimens from Sundararajah et al. [19], 10 specimens from Uzzaman et al. [38], 18 specimens from Beshara and Schuster [36] for lipped plain-C sections and 14 specimens from Young and Hancock [22] for unlipped plain-C sections. The DSM design equations are established to predict the capacities of structural members subjected to the ITF load case as given in Eqs.(7.8) and (7.9) with the coefficients k_1=1, k_2=0.15, k_3=0.6 and k_4=1.8.

$$\frac{P_n}{P_y} = \left[1 + 0.8\left(1 - \frac{\lambda}{0.844}\right)\right] \qquad \text{for} \qquad \lambda \leq 0.844 \tag{7.8}$$

$$\frac{P_n}{P_y} = \left[1 - 0.15\left(\frac{P_{cr}}{P_y}\right)^{0.6}\right]\left(\frac{P_{cr}}{P_y}\right)^{0.6} \qquad \text{for} \qquad \lambda > 0.844 \tag{7.9}$$

where the value of k_1=1.0 has been chosen to ensure the correct position for the cut off for the inelastic reserve equation, while the value of k_3=0.6 is the same as used in the distortional buckling in compression equation in AISI S100:2012 (Appendix 1, Section 1.2.1.3.1). The choice of this equation is most likely related to the fact that the failure mode in Fig.6.13(b) for the ITF case involves more lip deformation than the IOF case in Fig.6.9(b).

From Eqs.(7.8) and (7.9), the DSM design curve for the ITF load case is plotted in Fig.7.5 with the experimental data. It can be seen that the data points are located close to the DSM curve. This prediction is proven by the comparisons between the experimental capacities (P_{exp}) and the nominal capacities (P_n) given in Tables F-11 to F-18 in Appendix F of the thesis and the summary of these comparisons given in Table 7.3. The average value of the ratios (P_{exp}/P_n) is 1.043 and the average value of the coefficient of variation is 7.69%. Also, the deviation of the ratios (P_{exp}/P_n) is close to the expected ratio (P_{exp}/P_n =1) as shown in Fig.7.6. It can be concluded that the proposed DSM design equations predict efficiently the capacities of structural members under the ITF load case.
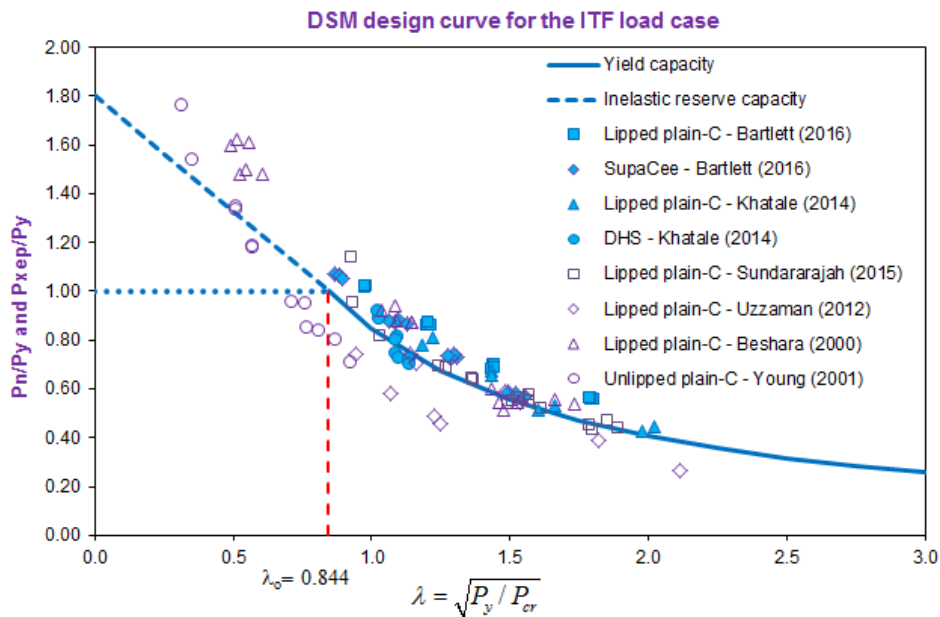
Figure 7.5: DSM design curve for the ITF load case
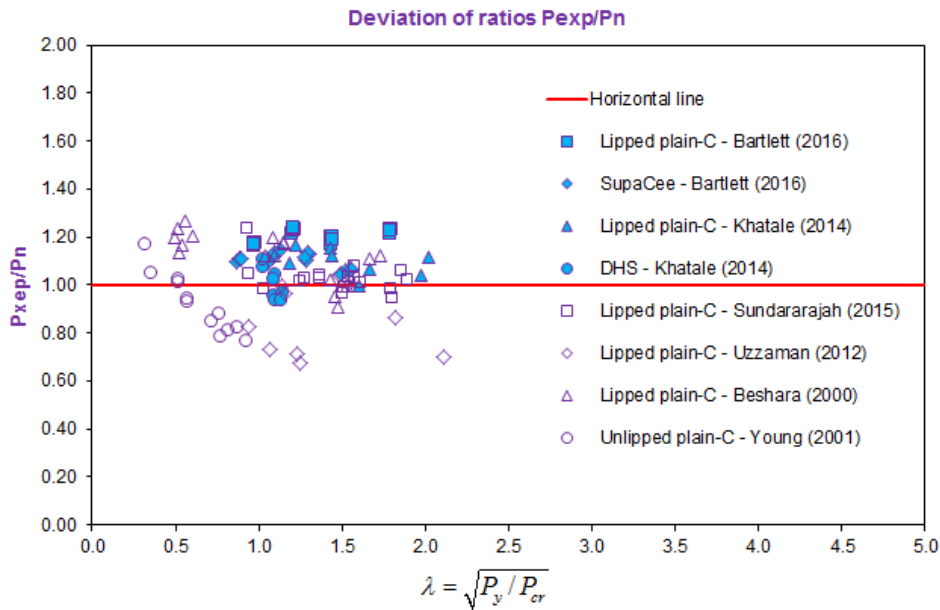
Figure 7.6: The ratios of P_{exp}/P_n for the ITF load case

Table 7.3: Summary of the ratios (P_{exp}/P_n) for the ITF load case

Load case	Authors	Year	Sections	P_{exp}/P_n		Average values	
				Mean	COV	Mean	COV
ITF load case	Bartlett, Nguyen & Pham	2016	Lipped plain-C	1.207	2.23%	1.043	7.69%
			SupaCee	1.103	2.68%		
	Khatale, Papangelis & Pham	2014	Lipped plain-C	1.093	5.20%		
			DHS	1.009	6.46%		
	Sundararajah et al.	2015	Lipped plain-C	1.036	6.17%		
	Uzzaman et al.	2012	Lipped plain-C	0.851	16.56%		
	Beshara & Schuster	2000	Lipped plain-C	1.125	8.95%		
	Young & Hancock	2001	Unlipped plain-C	0.923	13.30%		

7.3.5. DSM design equations for the ETF load case

The experimental data for the ETF load case includes 32 lipped plain-C and SupaCee sections from Htet and Pham [10], 16 lipped plain-C and DHS sections from Khatale et al. [41], 73 lipped plain-C sections from Macdonald et al. [37], Sundararajah et al. [19], Uzzaman et al. [38] & [39] and 12 unlipped plain-C sections from Young and Hancock [22]. Similar to other load cases, the experimental data is plotted as shown in Fig.7.7 in the relationship between the (P_{exp}/P_y) ratios and the sectional slenderness ($\lambda = \sqrt{P_y / P_{cr}}$). The DSM design equations to calculate the capacities of structural members under the ETF load case are proposed as given in Eqs.(7.10) and (7.11) with the coefficients k_1=1.0, k_2=0.25, k_3=1.0 and k_4=1.8.

$$\frac{P_n}{P_y} = \left[1 + 0.8 \left(1 - \frac{\lambda}{0.707} \right) \right] \qquad \text{for} \qquad \lambda \le 0.707 \qquad (7.10)$$

$$\frac{P_n}{P_y} = \left[1 - 0.25 \left(\frac{P_{cr}}{P_y} \right)^{1.0} \right] \left(\frac{P_{cr}}{P_y} \right)^{1.0} \qquad \text{for} \qquad \lambda > 0.707 \qquad (7.11)$$

where the value of k_1=1.0 has been chosen to ensure the correct position for the cut off for the inelastic reserve equation, while the value of k_3=1.0 implies the buckling phenomenon is closer to Euler than local or distortional. The choice of this equation is most likely related to the fact that the failure mode for the ETF case is Fig.6.17(b) is more like an eccentrically loaded strut than a localised failure.

From Eqs.(7.10) and (7.11), the DSM design curve for the ETF load case is plotted in Fig.7.7 with the experimental data. It is found that there is good agreement between the DSM design curve and the experimental data.
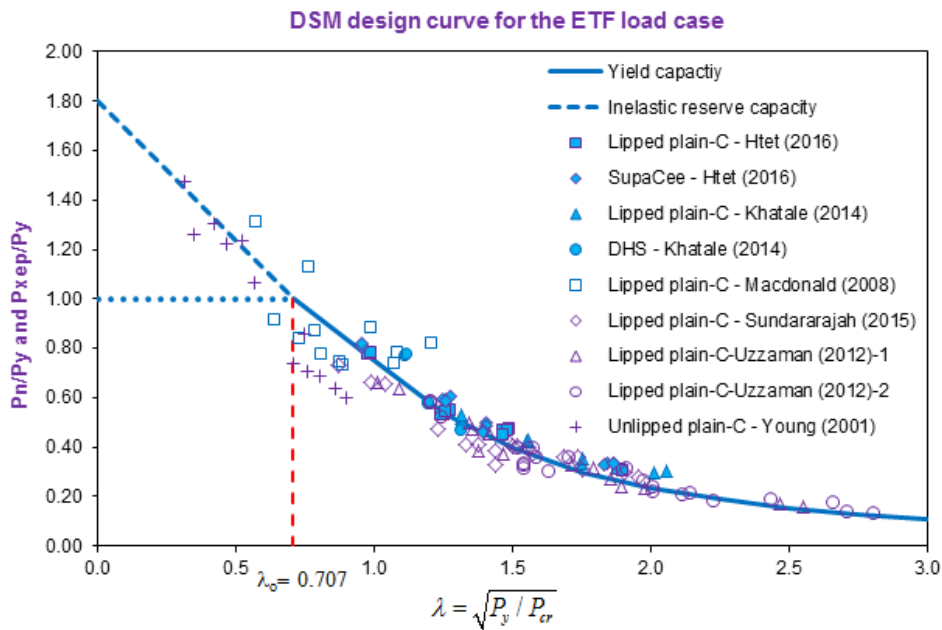
Figure 7.7: DSM design curve for the ETF load case

Table 7.4 shows the summary of the comparisons between the experimental capacities (P_{exp}) and the nominal capacities (P_n) which are given in Tables F-19 to F-27 in Appendix F of the thesis. From this summary, it is found that the average value of the ratios (P_{exp}/P_n) is 1.041, thus it is a conservative prediction of the nominal capacities. The average value of the coefficient of variation is 10.78% which is higher than the expected value 10% due to some scatter in the experimental data. These points are located far from the expected line (P_{exp}/P_n =1) as shown in Fig.7.8. However, the

prediction and the DSM design equation are acceptable and available to estimate the nominal capacities of structural member under the ETF load case.
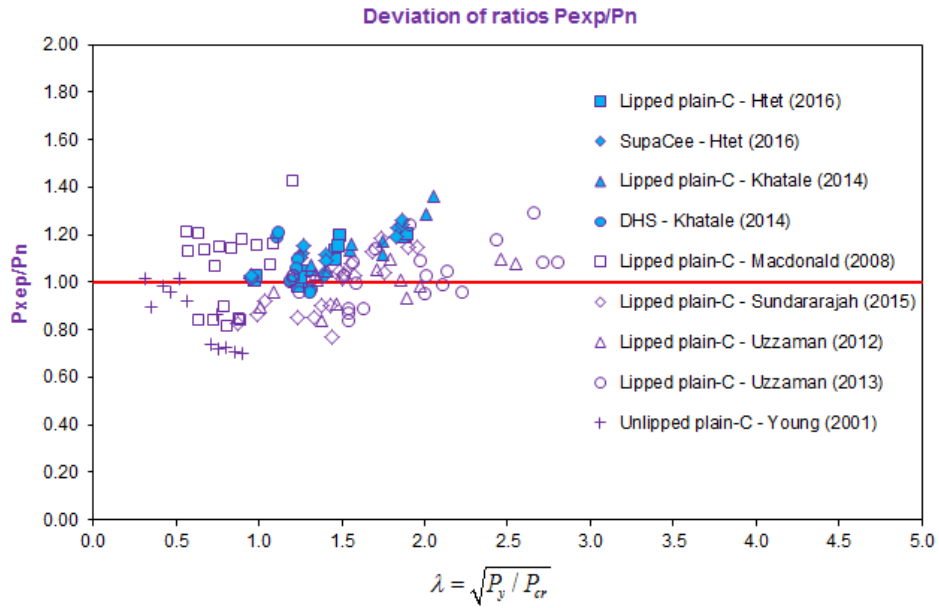
Figure 7.8: The ratios of P_{exp}/P_n for the ETF load case

Table 7.4: Summary of the ratios (P_{exp}/P_n) for the ETF load case

Load case	Authors	Year	Sections	P_{exp}/P_n		Average values	
				Mean	COV	Mean	COV
ETF load case	Htet & Pham	2016	Lipped plain-C	1.094	7.91%	1.041	10.78%
			SupaCee	1.110	7.65%		
	Khatale, Papangelis & Pham	2014	Lipped plain-C	1.169	9.06%		
			DHS	1.063	9.17%		
	Macdonald et al.	2008	Lipped plain-C	1.068	16.30%		
	Sundararajah et al.	2015	Lipped plain-C	0.985	12.91%		
	Uzzaman et al.	2012	Lipped plain-C	0.996	7.97%		
	Uzzaman et al.	2013	Lipped plain-C	1.031	10.98%		
	Young & Hancock	2001	Unlipped plain-C	0.854	15.08%		

7.3.6. Summary of the DSM models for web crippling

It is found that the same DSM equations with k_1=1.0, k_2=0.15, k_3=0.4 and k_4=1.8 are employed to predict the nominal capacities of structural members under the one-flange load cases (IOF and EOF). However, the two-flange load cases require different DSM equations with k_1=1.0, k_2=0.15, k_3=0.6 and k_4=1.8 for the ITF load case and k_1=1.0, k_2=0.25, k_3=1.0 and k_4=1.8 for the ETF load case. The summary of the DSM coefficients and the section slenderness (λ_o) for different load cases is given in Table 7.5.
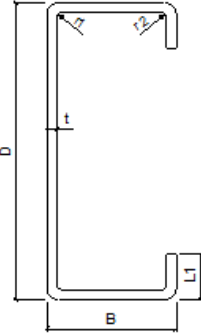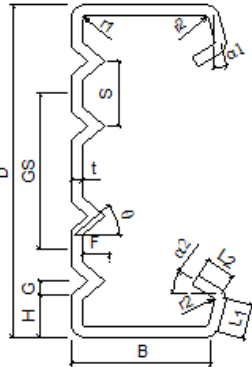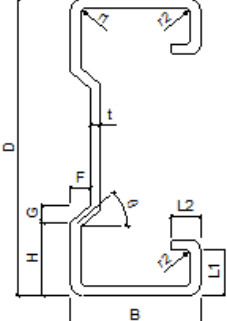
Table 7.5: DSM coefficients

Load cases	DSM coefficients				λ_o
	k_1	k_2	k_3	k_4	
IOF	1.00	0.15	0.40	1.80	0.776
EOF	1.00	0.15	0.40	1.80	0.776
ITF	1.00	0.15	0.60	1.80	0.844
ETF	1.00	0.25	1.00	1.80	0.707

In order to produce a DSM design method which is simple and align with the current DSM equation for compression, bending and shear, the coefficients (k_1, k_2, k_3) have been chosen to represent the type of behavior observed (such as local, distortional, Euler). It appears that the IOF and EOF cases fail in mainly a local mode and hence k_3 has been chosen as 0.4 similar to the DSM local buckling equation. The ITF case involves the lips and has a mode similar to distortional buckling, hence k_3 = 0.6. The ETF case looks more like a simple strut buckle and hence k_3=1.0 has been chosen similar to Euler.

The cross-sections which are used to develop the DSM design equations have dimensional limitations as shown in Table 7.6

Table 7.6: Limits for pre-qualified members subjected to web crippling

Section names	Section shapes	Geometric limitations
Unlipped and lipped plain-C sections		$19.30 < D/t < 206.90$ $10.47 < B/t < 73.28$ $6.56 < L_1/t < 28.18$ $0.89 < r_i/t < 12.07$
SupaCee sections		$80.47 < D/t < 138.00$ $24.36 < B/t < 45.37$ $4.52 < L_1/t < 12.32$ $4.71 < L_2/t < 9.36$ $1.98 < r_i/t < 3.33$ $1.08 < F/t < 2.80$ $33.50 < \alpha_1 < 49.50$ $39.00 < \alpha_1 < 57.50$
DHS sections		$97.08 < D/t < 122.86$ $32.08 < B/t < 41.94$ $12.98 < L_1/t < 17.14$ $3.57 < L_2/t < 5.95$ $1.60 < r_i/t < 2.04$ $1.28 < F/t < 1.87$

7.4. CALIBRATION OF DSM EQUATIONS FOR LOCALISED LOADING

7.4.1. Reliability analysis

The reliability of safety index β_o is a relative measure of the reliability or safety of a structure of structural element. When two designs are compared, the one with the larger β_o is more reliable. The reliability index accounts for the uncertainties and variabilities inherent in the design parameters, such as the material properties, geometry and applied load. To calculate the reliability index β_o, a first-order second moment (FOSM) method described by Ellingwood et al. [78] can be used. This method is outlined in Chapter F in the NAS (AISI 2007). The strength of the tested elements, assemblies, connections, or members shall satisfy Eq. (F1.1-1a) or Eq. (F1.1-1b) from the NAS (AISI 2007) as follows:

$$\sum \gamma_i Q_i \leq \phi R_n \tag{7.12}$$

where:

$\sum \gamma_i Q_i$ is the requires strength (factored loads) based on the most critical load combination determined in accordance with Section A5.1.2 for LRFD

γ_i and Q_i are the load factors and load effects, respectively

R_n is the average value of all test results

ϕ is resistance factor which is given by:

$$\phi = C_\phi \left(M_m F_m P_m \right) e^{-\beta_o \sqrt{V_M^2 + V_F^2 + C_P V_P^2 + V_Q^2}} \tag{7.13}$$

In which:

C_P is the correction factor

$$C_P = \frac{\left(1 + \dfrac{1}{n}\right)m}{(m-2)} \quad for \quad n \geq 4$$
$$C_P = 5.7 \quad for \quad n = 3$$

n is the number of tests

m=n-1 is degrees of freedom

C_ϕ is the calibration coefficient, C_ϕ =1.52 for LRFD as specified in Chapter F of the NAS (AISI 2007)

P_m is the mean value of professional factor, P. This factor gives the accuracy of the model by taking the ratio of the mean value of the tests R_n divided by the model

F_m is the mean value of fabrication factor, F. This is the ratio of the actual dimension to nominal dimension, normally thickness, because it is the most important dimension for thin-walled sections

M_m is the mean value of material factor, M.

V_F is the coefficient of variation of fabrication factor

V_M is the coefficient of variation of material factor

V_P is the coefficient of variation of test results

V_Q is the coefficient of variation of load effect, V_Q=0.21 for LRFD and LSD

β_o is the target reliability index, β_o=2.5 for cold-formed steel members

7.4.2. Results of reliability analysis

The results of the reliability analyses performed using Eq.7.13 are given in Table 7.7 which includes the results for the all localised load cases (IOF, EOF, ITF and ETF). The values of M_m, V_M, F_m and V_F are 1.10, 0.10. 1.00 and 0.05 which are exactly from Table F1 from the NAS (AISI 2007). The resulting safety indexes β_o are shown for ϕ=0.9. Alternatively, the resulting ϕ values are also shown for a safety index β_o=2.5.

Table 7.7: Reliability analysis results

Load cases	P_m	V_P	V_Q	C_ϕ	C_P	β_o (ϕ=0.9)	ϕ (β_o=2.5)
IOF	1.018	0.112	0.210	1.520	1.035	2.415	0.880
EOF	1.019	0.117	0.210	1.520	1.035	2.400	0.876
ITF	1.059	0.125	0.210	1.520	1.030	2.510	0.903
ETF	1.037	0.132	0.210	1.520	1.023	2.405	0.877

From the reliability analysis, it is indicated that the IOF load case has the best reliability results with the safety index β_o and resistance factor ϕ of 2.415 and 0.880 respectively in comparison with 2.400 and 0.876 for the EOF load case, 2.453 and 0.889 for the ITF load case and 2.510 and 0.903 for the ETF load case. For the IOF, EOF and ETF, the safety index β_o is lower than the target value 2.5, also the resistance factor ϕ is lower than the expected value 0.9 due to the wide range of the experimental data which was picked up from different sources. For the ITF, the safety index β_o is higher than the target value 2.5, also the resistance factor ϕ is higher than the expected value 0.9. Thus, resistance factor ϕ of 0.90 could be used with all DSM design equations for localised loading as appropriate.

7.5. COMPARISON BETWEEN THE PROPOSED DSM AND THE AS/NZS 4600

The nominal capacities of channel sections under different localised load cases can be calculated using the Australian/New Zealand Standard AS/NZS 4600:2005 [3] equation which is based on the North American Specification for the Design of Cold-Formed Steel Structural Members AISI S100-2012 [2] as follows:

$$R_b = C t_w^2 f_y \sin\theta \left(1 - C_r \sqrt{\frac{r_i}{t_w}}\right)\left(1 + C_l \sqrt{\frac{l_b}{t_w}}\right)\left(1 - C_w \sqrt{\frac{d_1}{t_w}}\right) \tag{7.14}$$

where

C is a coefficient

f_y is the yield strength of steel

t_w is the web thickness

θ is the angle between the plane of the web and the plane of the bearing surface. θ shall be within the following limits: $45^o \leq \theta \leq 90^o$

C_r is the coefficient of inside bent radius

r_i is the inside bent radius

C_l is the coefficient of bearing length

l_b is the actual bearing length. For the case of two equal and opposite concentrated loads distributed over unequal bearing length, the smaller value of l_b shall be taken

C_w is the coefficient of web slenderness

d_1 is the depth of the flat portion of the web measured along the plane of the web

The coefficients and capacity reduction factors are given in Tables 2.1 to 2.5 in the Australian/New Zealand Standard AS/NZS 4600:2005 [3].

The comparisons for the nominal capacities between the proposed DSM as described in Section 7.3 and the AS/NZS 4600 [3] equation are given in Figs.7.9 to 7.12. In general, the Eq.(7.14) gives higher nominal capacities of members under all different localised load cases in comparison with the proposed DSM. The AS/NZS 4600 standard is unconservative for the design for structural members under localised loading and consequently has lower ϕ factors 0.75 to 0.90 depending on the load case when compared with the proposed DSM model which has higher ϕ factors as explained before. In addition, this equation is only available for plain-C sections and it is not available for SupaCee and DHS sections. Also, there are too many coefficients used in this equation for different

load cases, fastened flange condition, stiffened flange condition as described in Section 2.2.2 in Chapter 2. Thus, the proposed DSM equations as described in this Chapter can be seen as more effective to determine the nominal capacities of members under web crippling.
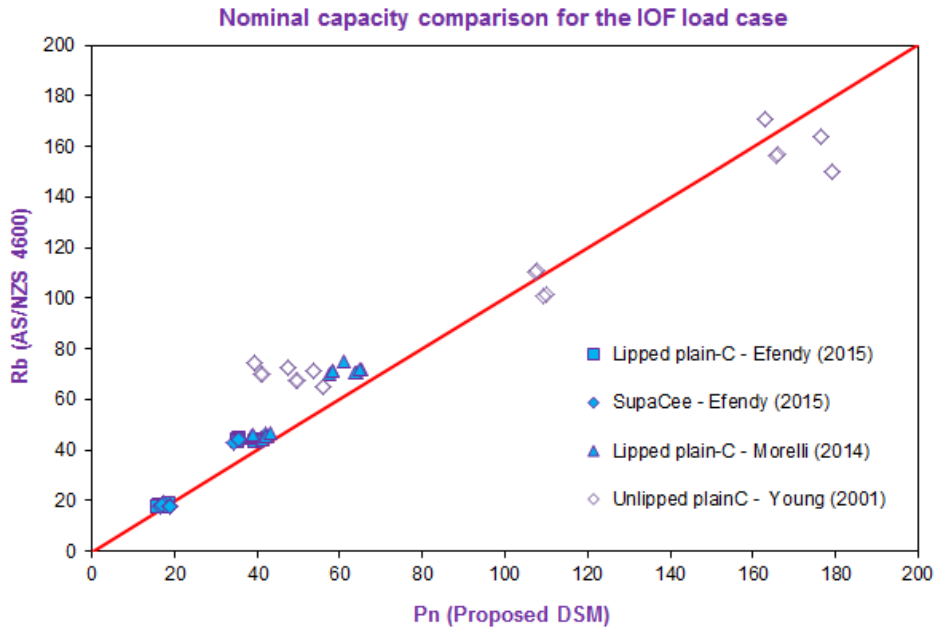
Figure 7.9: Nominal capacity comparison for the IOF load case
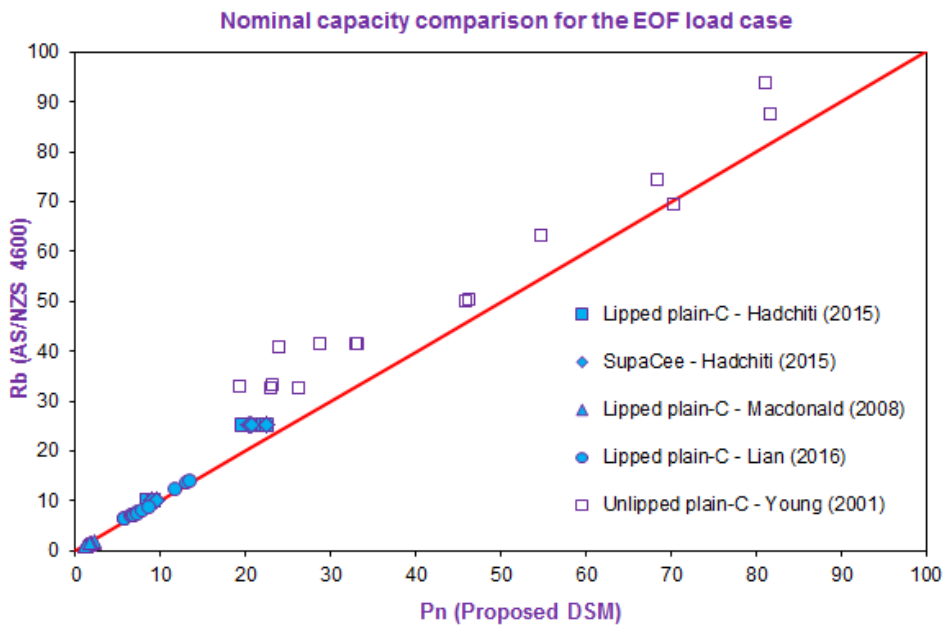
Figure 7.10: Nominal capacity comparison for the EOF load case
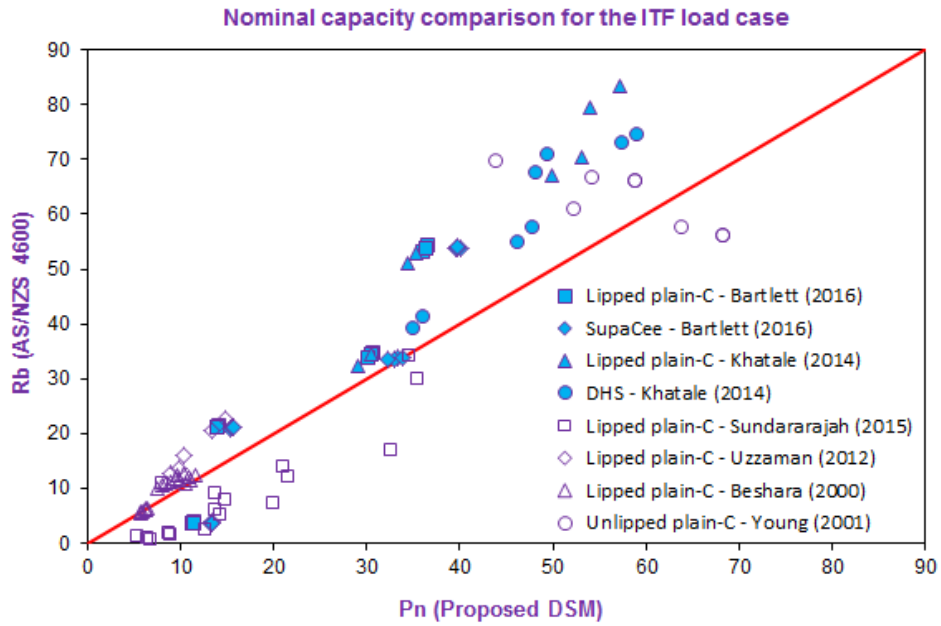
Figure 7.11: Nominal capacity comparison for the ITF load case
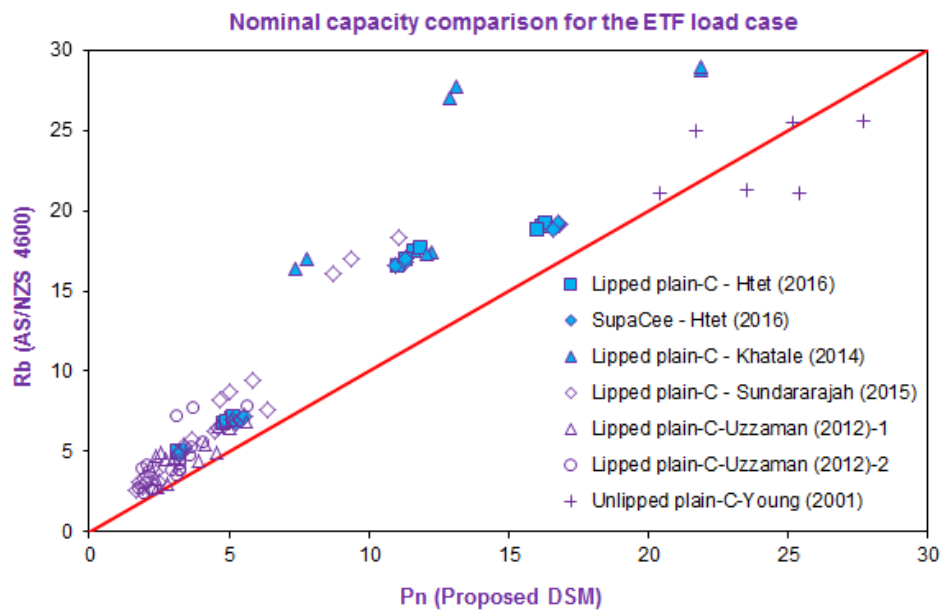
Figure 7.12: Nominal capacity comparison for the ETF load case

7.6. NUMERICAL EXAMPLES

7.6.1. General

Capacity determination has been performed for a lipped channel section with rounded corners under localised loading using the proposed DSM equation in this thesis. The geometry of the beam and the loading are shown in Fig.7.13. The beam has a thickness of 2mm and yield strength is 500MPa. Four localised loading cases such as IOF, EOF, ITF and ETF are considered in the calculations. The buckling loads are obtained from the THIN-WALL-2 V2.0 program as described in Section of 6.3, while the yield load are calculated by the plastic mechanism models as described in Section 6.4 of Chapter 6. From the input variables, the capacities of the beam are determined using the proposed DSM equations as described in this Chapter.
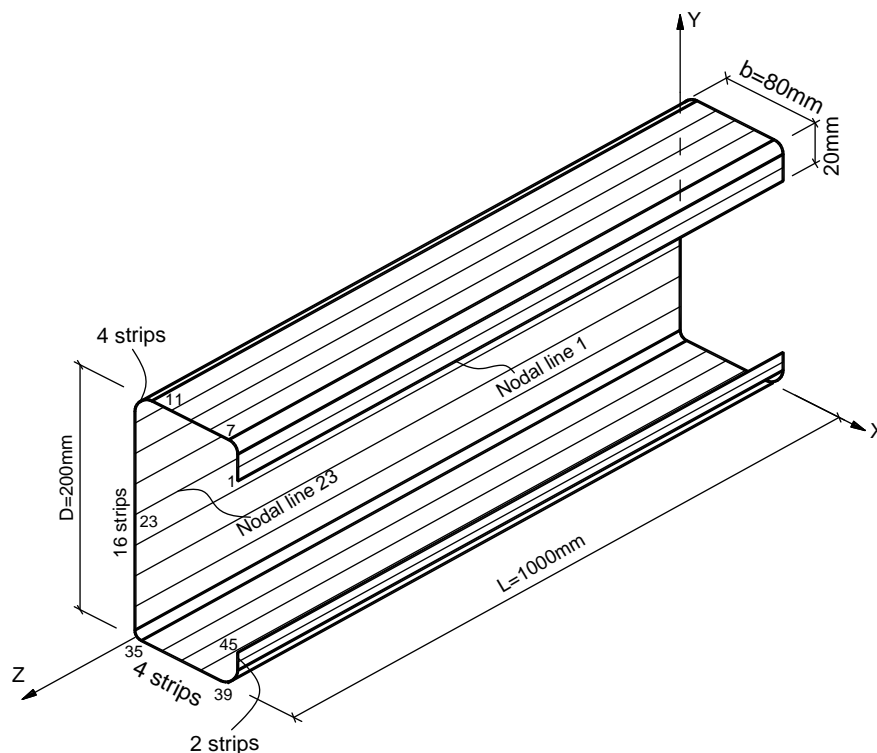
Figure 7.13: Lipped channel section dimensions

7.6.2. IOF load case

The buckling load is obtained from the THIN-WALL-2 V2.0 program: P_{cr} = 32.63 kN.

The plastic mechanism model is given in Fig.(7.14):
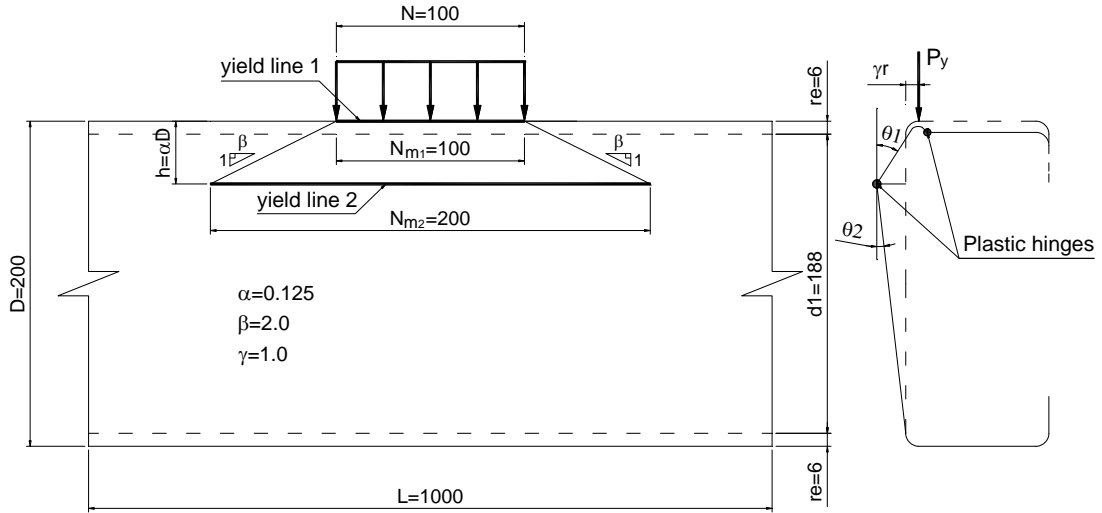
Figure 7.14: Plastic mechanism model for the section under the IOF load case

The yield load is determined by:

$$P_y = \frac{M_p}{\gamma r}\left[N_{m1} + \left(\frac{D}{D-h}\right)N_{m2}\right]$$

(7.15)

where:

M_p is the plastic moment per unit length of plate

$$M_p = \frac{f_y t^2}{4} = \frac{500 \times 2^2}{4} = 500 \text{ Nmm/mm}$$

(7.16)

h is the depth of the second plastic hinge

$$h = \alpha D = 0.125 \times 200 = 25 \text{ mm}$$

(7.17)

α = 0.125 for lipped plain-C section

β is a yield-line distribution slope factor

$$\beta = \beta_o \beta_1 = 2.0 \times 1.0 = 2.0$$

(7.18)

β_1 is a slope factor, β_1 = 2.0 for lipped plain-C

β_o is a factor which depends on the bearing length ratio (*N/D=0.5*), β_o = 1.0

N_{m1} and N_{m2} are the yield-line lengths:

$$N_{m1} = N = 100 \text{ mm}$$

(7.19)

$$N_{m2} = N + 2\beta h = 100 + 2 \times 2 \times 25 = 200 \text{ mm}$$

γ is a factor which depends on the radius ratio (*r_i/t*)

$$\gamma = \frac{1}{\gamma_o} = \frac{1}{1.0} = 1.0$$

(7.20)

γ_o = 1.0 for the radius ratio (*r_i/t=2.5*)

⇨ The yield load:

$$P_y = \frac{500}{1.0 \times 6} \times \left[100 + \left(\frac{200}{200-25} \right) \times 200 \right] = 27380 \text{ N} = 27.38 \text{ kN} \tag{7.21}$$

The slenderness:

$$\lambda = \sqrt{\frac{P_y}{P_{cr}}} = \sqrt{\frac{27.38}{32.63}} = 0.916 \tag{7.22}$$

Checking:

$$\lambda = 0.916 > 0.776$$

The nominal capacity is calculated by Eq.(7.5) as given:

$$P_n = P_y \left[1 - 0.15 \left(\frac{P_{cr}}{P_y} \right)^{0.4} \right] \left(\frac{P_{cr}}{P_y} \right)^{0.4} \tag{7.23}$$

$$\Rightarrow P_n = 27.38 \times \left[1 - 0.15 \times \left(\frac{32.63}{27.38} \right)^{0.4} \right] \times \left(\frac{32.63}{27.38} \right)^{0.4} = 24.64 \text{ kN}$$

The design capacity is given by:

$$\phi P_n = 0.9 \times 24.64 = 22.17 \text{ kN} \tag{7.24}$$

The design capacity from AS/NZS4600 [3]:

$$\phi R_b = 0.9 \times 28.60 = 25.74 \text{ kN} \tag{7.25}$$

7.6.3. EOF load case

The buckling load is obtained from the THIN-WALL-2 V2.0 program: P_{cr} = 16.73 kN.

The plastic mechanism model is given in Eq.(7.15):
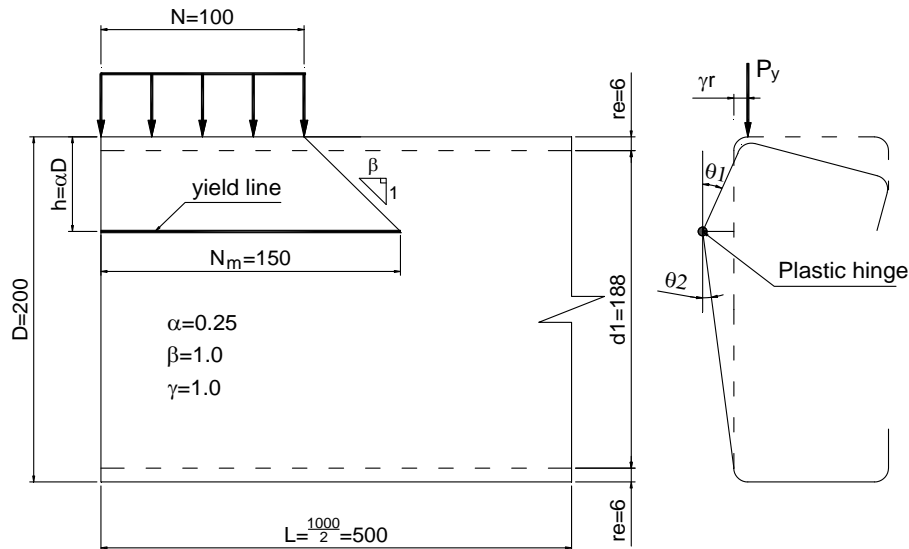
Figure 7.15: Plastic mechanism model for the section under the EOF load case

The yield load is determined by:

$$P_y = \frac{M_p}{\gamma r}\left[\left(\frac{D}{D-h}\right)N_m\right] \tag{7.26}$$

where:

M_p = 500 Nmm/mm as given in Eq.(7.16)

h is the depth of the second plastic hinge

$$h = \alpha D = 0.25 \times 200 = 50 \text{ mm} \tag{7.27}$$

α = 0.25 for lipped plain-C section

β is a yield-line distribution slope factor

$$\beta = \beta_o \beta_1 = 1.0 \times 1.0 = 1.0 \tag{7.28}$$

β_1 is a slope factor, β_1 = 1.0 for lipped plain-C

β_o is a factor which depends on the bearing length ratio ($N/D=0.5$), β_o = 1.0

N_m is the yield-line length:

$$N_m = N + \beta h = 100 + 1 \times 50 = 150 \text{ mm} \tag{7.29}$$

γ =1.0 as given in Eq (7.20)

⇨ The yield load:

$$P_y = \frac{500}{1.0 \times 6} \times \left[\left(\frac{200}{200-150}\right) \times 150\right] = 16670 \text{ N} = 16.67 \text{ kN} \tag{7.30}$$

The slenderness:

$$\lambda = \sqrt{\frac{P_y}{P_{cr}}} = \sqrt{\frac{16.67}{16.73}} = 0.998 \tag{7.31}$$

Checking:

$$\lambda = 0.998 > 0.776$$

The nominal capacity is calculated by Eq.(7.7) as given:

$$P_n = P_y\left[1 - 0.15\left(\frac{P_{cr}}{P_y}\right)^{0.4}\right]\left(\frac{P_{cr}}{P_y}\right)^{0.4} \tag{7.32}$$

$$\Rightarrow P_n = 16.67 \times \left[1 - 0.15 \times \left(\frac{16.73}{16.67}\right)^{0.4}\right] \times \left(\frac{16.73}{16.67}\right)^{0.4} = 14.18 \text{ kN}$$

The design capacity is given by:

$$\phi P_n = 0.9 \times 14.18 = 12.76 \text{ kN} \tag{7.33}$$

The design capacity from AS/NZS4600 [3]:

$$\phi R_b = 0.85 \times 17.47 = 13.97 \text{ kN}$$

(7.34)

7.6.4. ITF load case

a. Unfastened flanges condition

The buckling load is obtained from the THIN-WALL-2 V2.0 program: P_{cr} = 17.73 kN.

The plastic mechanism model is given in Eq.(7.16):
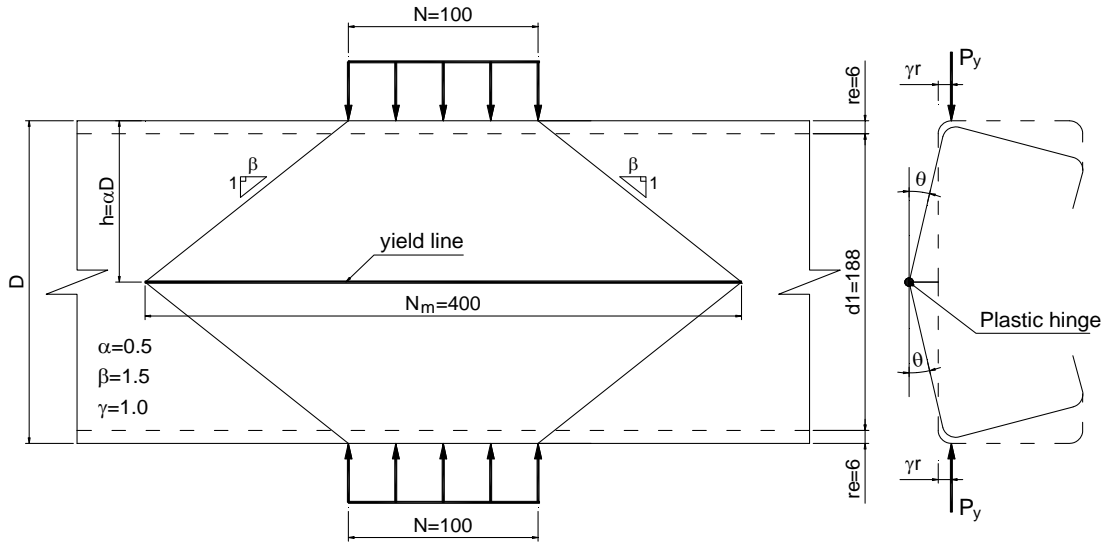
Figure 7.16: Plastic mechanism model for the section under the ITF load case - Unfastened

The yield load is determined by:

$$P_y = \frac{M_p N_m}{\gamma r}$$

(7.35)

where:

M_p = 500 Nmm/mm as given in Eq.(7.16)

h is the depth of the second plastic hinge

$$h = \alpha D = 0.5 \times 200 = 100 \text{ mm}$$

(7.36)

α = 0.5 for lipped plain-C section

β is a yield-line distribution slope factor

$$\beta = \beta_o \beta_1 = 1.0 \times 1.5 = 1.5$$

(7.37)

β_1 is a slope factor, β_1 = 1.5 for lipped plain-C

β_o is a factor which depends on the bearing length ratio (*N/D=0.5*), β_o = 1.0

N_{m1} and N_{m2} are the yield-line lengths:

$$N_m = N + 2\beta h = 100 + 2 \times 1.5 \times 100 = 400 \text{ mm}$$

(7.38)

γ=1.0 as given in Eq (7.20)

⇨ The yield load:

$$P_y = \frac{500 \times 400}{1.0 \times 6} = 33333 \text{ N} = 33.33 \text{ kN} \tag{7.39}$$

The slenderness:

$$\lambda = \sqrt{\frac{P_y}{P_{cr}}} = \sqrt{\frac{33.33}{17.73}} = 1.371 \tag{7.40}$$

Checking:

$\lambda = 0.998 > 0.844$

The nominal capacity is calculated by Eq.(7.9) as given:

$$P_n = P_y \left[1 - 0.15 \left(\frac{P_{cr}}{P_y} \right)^{0.6} \right] \left(\frac{P_{cr}}{P_y} \right)^{0.6} \tag{7.41}$$

$$\Rightarrow P_n = 33.33 \times \left[1 - 0.15 \times \left(\frac{17.73}{33.33} \right)^{0.6} \right] \times \left(\frac{17.73}{33.33} \right)^{0.6} = 20.48 \text{ kN}$$

The design capacity is given by:

$$\phi P_n = 0.9 \times 20.48 = 18.43 \text{ kN} \tag{7.42}$$

The design capacity from AS/NZS4600 [3]:

$$\phi R_b = 0.8 \times 17.42 = 13.93 \text{ kN} \tag{7.43}$$

b. Fastened flanges condition

The buckling load is obtained from the THIN-WALL-2 V2.0 program: P_{cr} = 25.36 kN.

The plastic mechanism model is given in Eq.(7.17):
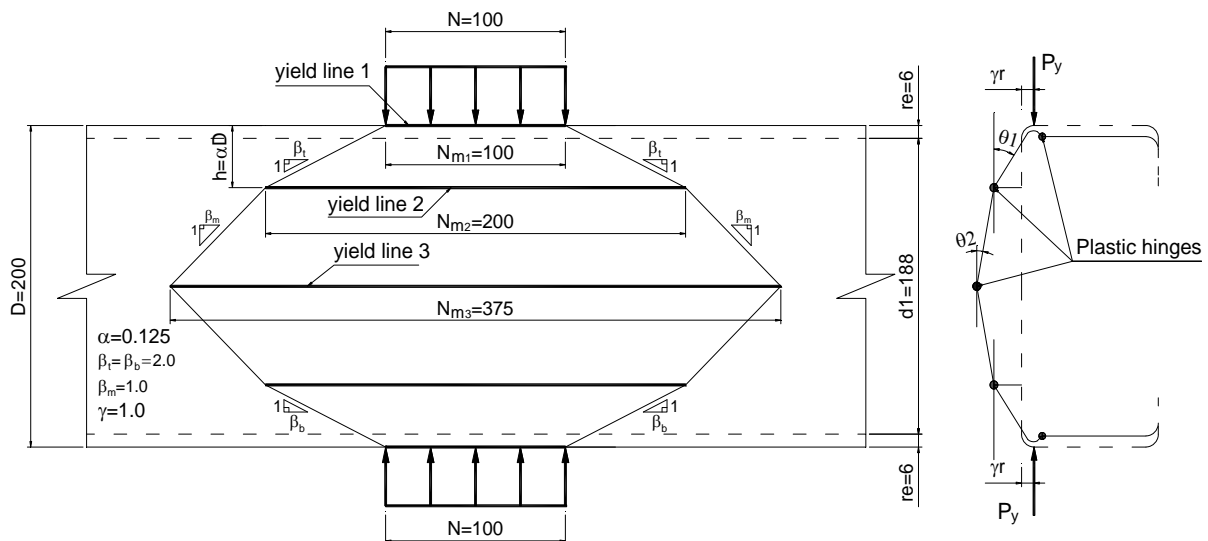
Figure 7.17: Plastic mechanism model for the section under the ITF load case - Fastened

The yield load is determined by:

$$P_y = \frac{M_p}{\gamma r}\left[N_{m1} + N_{m2} + \left(\frac{2h}{D-2h}\right)N_{m3}\right]$$
(7.44)

where:

M_p = 500 Nmm/mm as given in Eq.(7.16)

h is the depth of the second plastic hinge

$$h = \alpha D = 0.125 \times 200 = 25 \text{ mm}$$
(7.45)

α = 0.125 for lipped plain-C section

For the top and the bottom yield-lines in the web

$$\beta_t = \beta_b = \beta_o\beta_1 = 1.0 \times 2.0 = 2.0$$
(6.46)

β_1 = 2.0 for lipped plain-C section

β_o is a factor which depends on the bearing length ratio ($N/D=0.5$), $\beta_o = 1.0$

For the middle yield-line in the web

$$\beta_m = \beta_o\beta_2 = 1.0 \times 1.0 = 1.0$$
(6.47)

β_2 =1.0 for lipped plain-C section

N_{m1}, N_{m2} and N_{m3} are the yield-line lengths:

$$N_{m1} = N = 100 \text{ mm}$$

$$N_{m2} = N + 2\beta_t h = 100 + 2 \times 2.0 \times 25 = 200 \text{ mm}$$
(6.48)

$$N_{m3} = N_{m2} + 2\beta_m h = 200 + 2 \times 1.0 \times \left(\frac{200}{2} - 25\right) = 275 \text{ mm}$$

γ =1.0 as given in Eq (7.20)

⇨ The yield load:

$$P_y = \frac{500}{1.0 \times 6.0}\left[100 + 200 + \left(\frac{2 \times 25}{200 - 2 \times 25}\right) \times 275\right] = 32.64 \text{ mm}$$
(7.49)

The slenderness:

$$\lambda = \sqrt{\frac{P_y}{P_{cr}}} = \sqrt{\frac{32.64}{25.36}} = 1.134$$
(7.50)

Checking:

$$\lambda = 1.134 > 0.844$$

The nominal capacity is calculated by Eq.(7.9) as given:

$$P_n = P_y \left[1 - 0.15 \left(\frac{P_{cr}}{P_y} \right)^{0.6} \right] \left(\frac{P_{cr}}{P_y} \right)^{0.6}$$

(7.51)

$$\Rightarrow P_n = 32.64 \times \left[1 - 0.15 \times \left(\frac{25.36}{32.64} \right)^{0.6} \right] \times \left(\frac{25.36}{32.64} \right)^{0.6} = 24.44 \text{ kN}$$

The design capacity is given by:

$$\phi P_n = 0.9 \times 24.44 = 21.99 \text{ kN}$$

(7.52)

The design capacity from AS/NZS4600 [3]:

$$\phi R_b = 0.85 \times 36.96 = 31.42 \text{ kN}$$

(7.53)

7.6.5. ETF load case

The buckling load is obtained from the THIN-WALL-2 V2.0 program: P_{cr} = 8.04 kN.

The plastic mechanism model is given in Eq.(7.18):
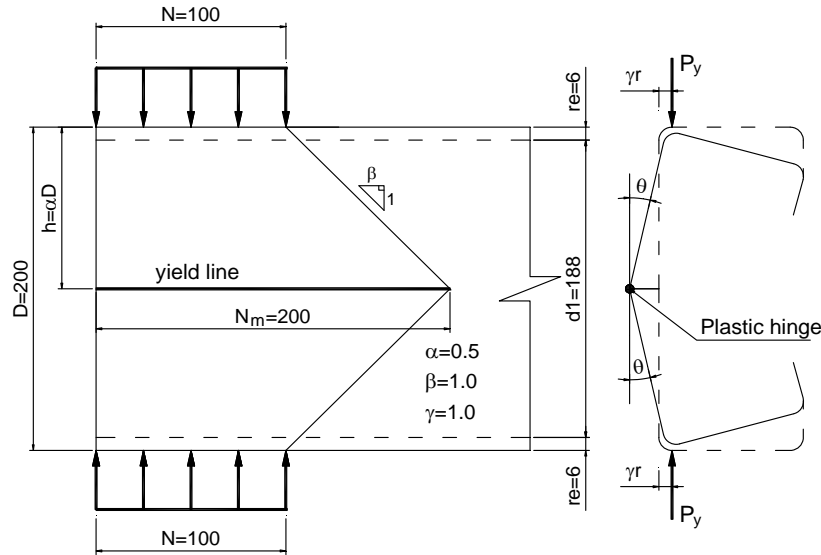
Figure 7.18: Plastic mechanism model for the section under the ETF load case

The yield load is determined by:

$$P_y = \frac{M_p N_m}{\gamma r}$$

(7.54)

where:

M_p = 500 Nmm/mm as given in Eq.(7.16)

h is the depth of the second plastic hinge

$$h = \alpha D = 0.5 \times 200 = 100 \text{ mm}$$

(7.55)

α = 0.5 for lipped plain-C section

β is a yield-line distribution slope factor

$$\beta = \beta_o \beta_1 = 1.0 \times 1.0 = 1.0 \qquad (7.56)$$

β_1 is a slope factor, $\beta_1 = 1.0$ for lipped plain-C

β_o is a factor which depends on the bearing length ratio (*N/D=0.5*), $\beta_o = 1.0$

N_m is the yield-line length:

$$N_m = N + \beta h = 100 + 1.0 \times 100 = 200 \text{ mm} \qquad (7.57)$$

$\gamma = 1.0$ as given in Eq (7.20)

⇨ The yield load:

$$P_y = \frac{500 \times 200}{1.0 \times 6} = 16670 \text{ N} = 16.67 \text{ kN} \qquad (7.58)$$

The slenderness:

$$\lambda = \sqrt{\frac{P_y}{P_{cr}}} = \sqrt{\frac{16.67}{8.07}} = 1.440 \qquad (7.59)$$

Checking:

$$\lambda = 1.440 > 0.707$$

The nominal capacity is calculated by Eq.(7.11) as given:

$$P_n = P_y \left[1 - 0.25 \left(\frac{P_{cr}}{P_y} \right)^{1.0} \right] \left(\frac{P_{cr}}{P_y} \right)^{1.0} \qquad (7.60)$$

$$\Rightarrow P_n = 16.67 \times \left[1 - 0.25 \times \left(\frac{8.04}{16.67} \right)^{1.0} \right] \times \left(\frac{8.04}{16.67} \right)^{0.6} = 7.07 \text{ kN}$$

The design capacity is given by:

$$\phi P_n = 0.9 \times 7.07 = 6.36 \text{ kN} \qquad (7.61)$$

The design capacity from AS/NZS4600 [3]:

$$\phi R_b = 0.9 \times 10.68 = 9.61 \text{ kN} \qquad (7.62)$$

7.7. CONCLUSION

The DSM has been developed using generalised design equations to predict both the yield load and inelastic capacities of structural members subjected to different localised load cases. The same DSM equations are used to calculate the nominal capacities of structural members under the one-flange loading cases (IOF and EOF), while the two-flange load cases (ITF and ETF) require different DSM equations. These equations are benchmarked against the experimental data collected from different investigations. A resistance factor ϕ of 0.90 is recommended to use for the DSM equations for all

localised load cases (IOF, EOF, ITF and ETF) in the design of cold-formed steel sections under localised loading.

The two main inputs which are used to build up the DSM equations are the buckling load and the yield load. The buckling load is obtained from THIN-WALL-2 V2.0 program based on the FSM, while the yield load is determined from plastic mechanism models.

CHAPTER 8

CONCLUSIONS AND RECOMMENDATIONS

FOR FUTURE STUDIES

8.1. INTRODUCTION

This Chapter summarizes the outcomes of this thesis in both pre-buckling and buckling analyses of thin-walled sections under localised loading as well as the development of the THIN-WALL-2 V2.0 program. In addition, an overview about the plastic mechanism models for yielding analysis of cold-formed steel sections subjected to web crippling is given. The Chapter summarises the development of the DSM for the design of cold-formed steel sections under localised loading. Finally, recommendations for future studies in this research area are suggested.

8.2. ANALYSIS OF THIN-WALLED SECTIONS UNDER LOCALISED LOADING

8.2.1. Pre-buckling analysis

Pre-buckling analysis of cold-formed steel members under localised loading is an important step which provides membrane stresses used in the buckling analysis step. In this thesis, the Finite Strip Method (FSM) has been developed for pre-buckling analysis of thin-walled sections under localised loading with general end boundary conditions. This method has been benchmarked against the Finite Element Method (FEM) as described in Chapter 3. There are six possible different combinations of boundary conditions which can be applied to structural members, as follows:

1. Both ends simply supported (SS),

2. One end simply supported and the other end clamped (SC),

3. One end simply supported and the other end free (SF),

4. Both ends clamped (CC),

5. One end clamped and the other end free (CF),

6. Both ends free (FF).

For different boundary conditions at supports and locations of applied loads, different displacement functions are required for both flexural and membrane displacements. In this research, the displacement functions introduced by Cheung [13] have been selected for the SS, SC, SF and CC boundary conditions, while the displacement functions from Bradford and Azhari [16] have been

employed for the CF boundary condition. In addition, a new set of displacement functions have been proposed for the FF boundary conditions as described in Chapter 3.

As stresses are not uniform along the member due to localised loading, the pre-buckling analysis also requires multiple series terms with orthogonal functions. The larger the number of series terms used, the more accurate results obtained from the pre-buckling analysis. A convergence study has been performed with the beam length is 1000mm and the load length is 100mm to understand the relationship between the convergence of the stresses and the number of series terms. It is indicated that the stresses converged when the number of series terms reaches 25. It means that about 25 series terms are required to get the converged stresses as well as deflections in the pre-buckling analysis for a localised load one tenth the length of the member. The more localised is the loading, the larger the number of series terms required to get the accurate results in the pre-buckling analysis.

8.2.2. Buckling analysis

In this thesis, the FSM has been developed for the buckling analysis of thin-walled sections under localised loading with general end boundary conditions. This method has proven to be accurate and efficient in comparison with the FEM as described in Chapter 4. For different boundary conditions, different functions are required to express the stresses of a strip in the structural member. The stress functions are employed the same as the displacement functions as described in the pre-buckling analysis.

Similar to the pre-buckling analysis, multiple series terms are required in the buckling analysis to get more accurate results. A convergence study has been performed to understand the relationship between the convergence of buckling load factors and the number of series terms. It is found that there is convergence of the buckling load factor (λ) when the number of series terms reaches 15. It means that a smaller number of series terms are required for buckling analysis in comparison with those in the pre-buckling analysis.

8.2.3. THIN-WALL-2 V2.0 program

The FSM theory has been developed for both pre-buckling and buckling analyses of thin-walled sections under localised loading for general end boundary conditions. This theory has been included in the THIN-WALL-2 V2.0 as described in Chapter 5. The program contains a Graphical User Interface (GUI) which calls three programs: bfinst7.cpp, bfinst10.cpp written by using C++ computer language and a FSM module written by Matlab. The bfinst7.cpp program as described in [73] and [72] is used in

a Uniform Stress module where the main functions are a cross-section analysis, a stress analysis and a buckling analysis of thin-walled sections under uniform stresses. The bfinst10.cpp program is used in a Localised Loading module for both pre-buckling and buckling analyses of structural members under localised loading with both ends simply supported boundary condition as described in [12]. The FSM module is developed for analysis of structural members under localised loading with general end boundary conditions as described in Chapters 3 and 4.

In general, the THIN-WALL-2 V2.0 program can be used to define input data using the GUI to perform pre-buckling and buckling analyses of thin-walled sections under generalised loading. The loading may contain uniform stresses due to compression, bending, shear or combinations of these loading and localised loading. The structural members may be made from both isotropic and orthotropic materials. It is also possible to use this program to perform a cross-section analysis to generate the section properties. The cross-sections can be formed from different shapes includes open and closed sections or mixed sections. In addition, the buckling modes and shapes are displayed in both 2D and 3D views, thus the user can understand the working of the structural member clearly.

Simulations have been modeled by the FEM using Abaqus [32] for analysis of structural members under localised loading. It is found that there is agreement between the results from the THIN-WALL-2 V2.0 program and those from Abaqus. Thus, the THIN-WALL-2 V2.0 program has been seen as a good alternative software which can be used in analysis of thin-walled sections under generalised loading.

8.3. YIELDING ANALYSIS

Yield load (P_y) is an important input to develop the DSM for web crippling. In this thesis, new and simple plastic mechanism models have been developed for all four localised load cases to calculate the yield loads of the structural members under loalised loading. The parameters of the models are adjusted due to the cross-sections types, loading conditions and flange fastened conditions. Currently, the plastic mechanism models are proposed for unlipped plain-C, lipped plain-C, SupaCee and DHS channels as described in Chapter 6.

8.4. DIRECT STRENGTH METHOD FOR WEB CRIPPLING

In this thesis, the DSM has been developed for the design of cold-formed steel sections subjected to localised loading. In order to develop this method for web crippling, the experimental data has been

collected from previous literature for different cross-section types, localised load cases and flange fastened conditions. In addition, the buckling load (P_{cr}) is obtained from the THIN-WALL-2 V2.0 program, while the yield load (P_y) is determined by the plastic mechanism models. From these inputs, a consistent and simplified DSM equations for design of cold-formed sections under localised loading are proposed. The DSM has been developed using generalised design equations to predict both the yield load and inelastic capacities of structural members subjected to different localised load cases. The same DSM equations are used to calculate the nominal capacities of structural members under the one-flange loading cases (IOF and EOF), while the two-flange load cases (ITF and ETF) require different DSM equations.

The DSM equations for each load case have been plotted with the experimental data as described in Chapter 7. It is indicated that the DSM equations are benchmarked against the experimental data collected from different investigations. In addition, a resistance factor ϕ of 0.90 is recommended to use for the DSM equations for all localised load cases (IOF, EOF, ITF and ETF) in the design of cold-formed steel sections under localised loading.

8.5. RECOMMENDATIONS FOR FUTURE STUDIES

The FSM method has been developed for analysis of thin-walled sections under localised loading for general end boundary conditions and has been included in the THIN-WALL-2 V2.0 program. However, it still has some limitations which need to be improved in the future work:

1. The displacement functions for the SC, SF boundary conditions are combinations of sin, cos, sinh and cosh functions as described in Chapter 3. These functions make the integrations in both the pre-buckling and buckling analyses become more complicated. Consequently, the THIN-WALL-2 V2.0 program runs slowly in solving the integrations in the analytical processes. Thus, it is necessary to discover simpler displacement functions for the SC and SF boundary conditions for faster execution is required.

2. The displacement functions for the SC and the CF cases still have problems with the shear stress results. The SC case has symmetric shear stress at both ends of structural members and these values are not matching with the shear stress from the FEM (Abaqus). Especially for the CF case, shear stresses equal to zero at the clamped end occur which does not appear in the results from Abaqus. These problems do not affect the final results from the buckling analysis as explained in Chapter 3; however, it is still important to discover more

suitable displacement functions for the SC and CF cases to get accurate results for the pre-buckling analysis.

3. In this research, the boundary condition refers to the support conditions at the ends of all strips of structural members included strips on the web, flanges and lips. However, for members in practical structures or in experiments, it is difficult to apply the boundary conditions for the lips and flanges alone. It means that the boundary condition for strips on the web may be simply supported, clamped or free, while the boundary condition for strips on the lips and flanges are always free. Hence, the boundary conditions for structural members can be mixed boundary conditions. Consequently, different displacement functions are required and applied for strips in different parts of the structural member. Thus, it is necessary to develop the FSM theory for analysis of cold-formed steel members subjected to web crippling with mixed boundary conditions.

4. The FSM has been developed for analysis of thin-walled sections under compression, bending, shear force and localised loading. However, the method has not developed for analysis of thin-walled sections subjected to combinations these above loads. Thus, this is an important research direction in the future which makes the FSM method become more general.

The DSM has been proposed for design of cold-formed steel members subjected to web crippling. It seems to be a consistent and simplified proposal in comparison with other previous DSM predictions. However, the proposals still have some restrictions as follows:

1. Currently, the plastic mechanism models, which provide the yield load (P_y) for the DSM, have been developed in this thesis for un-lipped plain-C, lipped plain-C, SupaCee and DHS, channels. The experimental data is still limited for other cross-section types such as hat sections, Z-sections and box sections as shown in Fig.8.1, channel sections with hollow flanges as shown in Fig.8.2, roof sheeting and decking. Thus, it is essential to gather more experimental data for different cross-sections to further develop the plastic mechanism models.
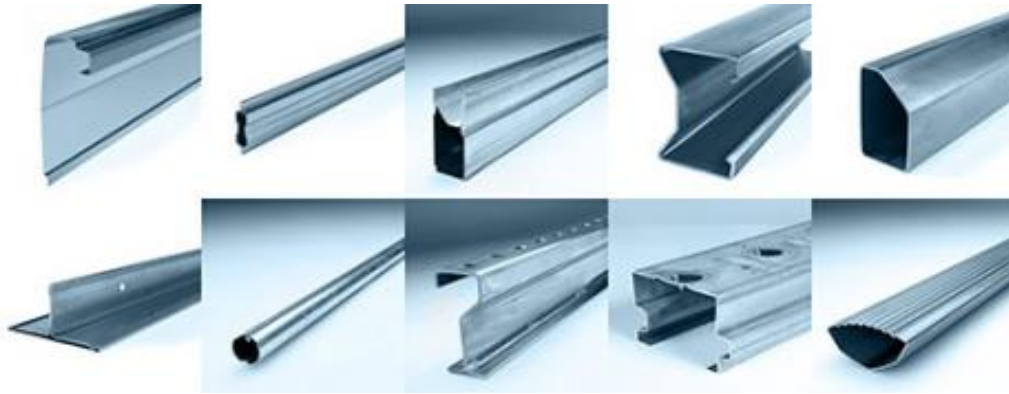
Figure 8.1: Different cold-formed steel sections

Figure 8.2: Channel section with hollow flanges

2. In this thesis, the DSM is proposed for cold-formed steel members without holes; however, structural members with web openings are used widely for different purposes as shown in Fig.8.3. The creation of holes decreases the strength of members under loading. Also, the behaviour of members with holes is different from members without holes. Thus, it is important to develop the DSM to predict the capacities of structural members with holes subjected to localised loading.

Figure 8.3: Cold-formed steel members with holes

CHAPTER 9

REFERENCES

1.   Rogers, C.A., D. Yang, and G.J. Hancock, *Stability and ductility of thin high strength G550 steel members and connections.* Thin-Walled Structures, 2003. 41(2-3): p. 149-166.

2.   North American Specification for the Design of Cold-Formed Steel Structural Members AISI S100-2012, *American Iron and Steel Institute (AISI).* 2012.

3.   Australian/New Zealand Standard AS/NZS 4600:2005, *Cold-Formed Steel Structures. Standards Australia/Standards New Zealand.* 2005.

4.   British Standards BS5950, *Structural use of steelwork in buildings*, in *Part 5: Code of practice for the design of cold-formed sections.* 1998, British Standards Institution: London.

5.   Eurocode-3, *Design of steel structures*, in *Part 1.3: General rules - Supplementary rules for cold-formed members and sheeting.* 1996, European Committee for Standardization: Brussels, Belgium.

6.   Chinese Standard GB 50018-2002, *Technical Code of Cold-formed Thin-wall Steel Structures (English Version).* 2002, MOC, AQSIQ: China.

7.   Efendy, W., D. Riyadi, and C.H. Pham, *Bearing capacity of cold-formed steel channels subjected to interior one flange loading*, in *School of Civil Engineering.* 2015, Bachelor of Engineering Thesis, The University of Sydney: Australia.

8.   Hadchiti, M., J.C. Dalton, and C.H. Pham, *Bearing capacity of cold-formed steel channels subjected to exterior one flange loading*, in *School of Civil Engineering.* 2015, Bachelor of Engineering Thesis, The University of Sydney: Australia.

9.   Bartlett, A.D., K.H. Nguyen, and C.H. Pham, *Web Crippling of Cold-Formed Steel with Web Swage Stiffeners subject to Interior-Two-Flange Loading*, in *School of Civil Engineering.* 2016, Bachelor of Engineering Thesis, The University of Sydney: Australia.

10.   Htet, A.K. and C.H. Pham, *Bearing capacity of cold-formed steel channels subjected to End two flanges loading*, in *School of Civil Engieering.* 2016, Master of Engineering Thesis, The University of Sydney: Australia.

11.   Schafer, B.W. and T. Pekoz, *Direct Strength Prediction of cold-formed steel members using numerical elastic buckling solutions*, in *Fourteenth International Specialty Conference on Cold-Formed Steel Structures.* 1998: St. Louis, Missouri, USA.

12. Hancock, G.J. and C.H. Pham, *Buckling analysis of thin-walled sections under localised loading using the semi-analytical finite strip method.* Thin-Walled Structures, 2015. 86: p. 35-46.

13. Cheung, Y.K., *Finite Strip Method in structural analysis. New York, NY: Pergamon Press, Inc.* 1976.

14. Przmieniecki, J.S.D., *Finite Element Structural Analysis of Local Instability.* Journal of the American Institute of Aeronautics and Astronautics, 1973. 11(1).

15. Plank, R.J. and W.H. Wittrick, *Buckling under combined loading of thin,flar-walled structures by a complex Finite Strip Method.* International Journal for numerical methods in engineering, 1974. 8: p. 323-339.

16. Bradford, M.A. and M. Azhari, *Buckling of plates with different end conditions using the finite strip method.* Computers & Structures, 1995. 56(1): p. 75-83.

17. Li, Z. and B.W. Schafer, *Buckling analysis of cold-formed steel members with general boundary conditions using CUFSM:conventional and constrained finite strip methods*, in *Twentieth International Specialty Conference on Cold-Formed Steel Structures*. 2010: Saint Louis, Missouri, USA. p. 15.

18. Keerthan, P., M. Mahendran, and E. Steau, *Experimental study of web crippling behaviour of hollow flange channel beams under two flange load cases.* Thin-Walled Structures, 2014. 85: p. 207-219.

19. Sundararajah, L., M. Mahendran, and P. Keerthan, *Experimental studies of lipped channel beams subjected to web crippling under ETF and ITF load cases*, in *Eighth International Conference on Advances in Steel Structures*. 2015: Lisbon, Portugal.

20. Dara, M. and C. Yu, *Direct Strength Method for Web Crippling of Cold-formed Steel C- and Zsections Subjected to One-flange Loading.* Journal of Steel Structures & Constructions, 2015. 1(1): p. 4.

21. Natário, P., N. Silvestre, and D. Camotim, *Direct strength prediction of web crippling failure of beams under ETF loading.* Thin-Walled Structures, 2016(98): p. 360-374.

22. Young, B. and G.J. Hancock, *Design of Cold-Formed channels subjected to Web crippling.* Journal of Structural Engineering (ASCE), 2001. 127(10): p. 1137-1144.

23. Cook, R.D., *Concepts and Applications of Finite Element Analysis; a Treatment of the Finite Element Method as Used for the Analysis of Displacement, Strain and Stress.* 1974, the University of Michigan, USA: Wiley, 1974. 402.

24. Rajasekaran, S. and D.W. Murray, *Incremental Finite Element Matrices.* Journal of the Structural Division, 1973. 99(12): p. 2423-2438.

25. Hancock, G.J. and N.S. Trahair, *Finite Element analysis of the lateral buckling of continuously restrained beam-columns.* Institution of Engineers, 1978. CE2(2): p. p. 120-127.

26. Hancock, G.J. and O. Roos, *Flexural-Torsional Buckling of Storage Rack Columns*, in *8th ISCCFSS*. 1986: St. Louis, Missouri, USA.

27. Clarke, M.J. and G.J. Hancock, *A finite element non-linear analysis of stressed arch frames, JSE, ASCE.* International Journal for numerical methods in engineering, 1991. 117(10): p. Pages 2819-2837.

28. Schafer, B.W., *Cold-formed steel behavior and design: analytical and numerical modeling of elements and members with longitudinal stiffeners.* 1997, PhD thesis, Cornell University: USA.

29. Schafer, B.W. and T. Peköz, *Computational modeling of cold-formed steel: characterizing geometric imperfections and residual stresses.* Journal of Constructional Steel Research, 1998. 47(3): p. 193-210.

30. Natário, P., N. Silvestre, and D. Camotim, *Web crippling failure using quasi-static FE models.* Thin-Walled Structures, 2014. 84: p. 34-49.

31. Natário, P., N. Silvestre, and D. Camotim, *Computational modelling of flange crushing in cold-formed steel sections.* Thin-Walled Structures, 2014. 84: p. 393-405.

32. ABAQUS/Standard Version 6.13, *ABAQUS/CAE User's Manual. Dassault Systèmes: Simulia Corp., Providence: RI, USA.* 2008.

33. North American Specification for the Design of Cold-Formed Steel Structural Members AISI S100-2012, *Commentary to the AISI Specifications.* 2012.

34. S909-08, A., *Standard Test Method for determining the Web Crippling Strength of Cold-Formed steel beams.* 2008.

35. Cain, D.E. and R.A. LaBoube, *The effect of flange restraint on web crippling strength of cold-formed steel Z- and I-sections*, in *Wei-Wen Yu Center for Cold-Formed Steel Structures.* 1995: Baltimore, Maryland , USA. p. 106.

36. Beshara, B. and R.M. Schuster, *Web crippling of cold formed steel C and Z sections*, in *15th International Specialty Conference on Cold-Formed Steel Structures*. 2000: Baltimore, Maryland, USA. p. 21.

37. Macdonald, M., M.A. Heiyantuduwa Don, and J. Rhodes, *Web crippling behaviour of thin-walled lipped channel beams subjected to EOF and ETF loading*, in *19th International Specialty Conference on Cold-Formed Steel Structures*. 2008: St. Louis, Missouri, USA.

38. Uzzaman, A., et al., *Cold-formed steel sections with web openings subjected to web crippling under two-flange loading conditions-part I:Tests and finite element analysis.* Thin-Walled Structures, 2012. 56: p. 38-48.

39. Uzzaman, A., et al., *Web crippling behaviour of cold-formed steel channel sections with offset web holes subjected to interior-two-flange loading.* Thin-Walled Structures, 2012. 50: p. 76-86.

40. Morelli, M., et al., *Bearing capacity of cold-formed steel channels with web stiffeners subjected to interior one-flange loading*, in *School of Civil Engineering*. 2014, Bachelor of Engineering Thesis, The University of Sydney. p. 89.

41. Khatale, G.D., J.P. Papangelis, and C.H. Pham, *Bearing capacity of channels with web stiffeners subjected to two-flange loading*, in *School of Civil Engineering*. 2014, Master of Engineering Thesis, The University of Sydney. p. 69.

42. Lian, Y., et al., *Effect of web holes on web crippling strength of cold-formed steel channel sections under end-one-flange loading condition – PartI:Tests and finite element analysis.* Thin-Walled Structures, 2016. 107: p. 443-452.

43. Saint-Venant, M., *Discussion in Theorie De L'elasticité Des Corp Solids*. 1883.

44. Bryan, G.H. *On the Stability of Plane Plate under Thrust in Its Own Plane with Applications on the Buckling of the Sides of a Ship*. in *London Math*. 1891. London.

45. Yu, W.W., *Colf Formed Steel Design*. 1991, New York.

46. Timoshenko, S.P. and J.M. Gere, *Theory of Elastic Stability*. 1961: McGraw-Hill Book Co. Inc, New York, N.Y.

47. Girkmann, K., *Stability of the webs of plate girders taking account of concentrated loads*. 1936, International Association of Bridge and Structural Engineering, Final Report. p. 607-11.

48. Khan, M.Z. and A.C. Walker, *Buckling of Plates subjected to Localised Edge Loading.* The Structural Engineer, 1972. 50(June): p. 225-232.

49. Zetlin, L., *Elastic Instability of flat plates subjected to partial edge loadings.* Journal of Structural Division, ASCE Proceedings, 1955. 81.

50. Rockey, K.C. and D.K. Bagchi, *Buckling of plate girder webs under partial edge loadings.* Journal of Mechanic Science, 1970: p. 61-76.

51. Khan, M.Z., K.C. Johns, and B. Hayman, *Buckling of Plates with Partially Loaded Edges.* Journal of the Structural Division, ASCE Proceeding, 1977. 103.

52. Chin, C.K., F.G.A. Al-Bermani, and S. Kitipornchai, *Finite element method for buckling analysis of plate structures.* Journal of Structural Engineering (ASCE), 1993.

53. Johansson, B. and O. Lagerqvist, *Resistance of plate edges to concentrated forces.* Journal of Constructional Steel Research, 1995. 32(1): p. 69-105.

54. Natário, P., N. Silvestre, and D. Camotim, *Localized web buckling analysis of beams subjected to concentrated loads using GBT.* Thin-Walled Structures, 2012. 61: p. 27-41.

55. Natário, P., N. Silvestre, and D. Camotim, *GBTWEB, GBT-based code for web buckling analysis of members under localised loads.* 2015.

56. Hetrakul, N. and W. Yu, *Webs for cold-formed steel flexural members; structural behaviour of beam webs subjected to web crippling and a combination of web crippling and bending.* 1978: University of Missouri, Missouri, USA.

57. Chu, X., et al., *Buckling behaviour of cold-formed channel sections under uniformly distributed loads.* Thin-Walled Structures, 2005. 43(4): p. 531-542.

58. Bui, H.C., *Buckling analysis of thin-walled sections under general loading conditions.* Thin-Walled Structures, 2009. 47(6–7): p. 730-739.

59. Hancock, G.J. and C.H. Pham, *Shear buckling of channel sections with simply supported ends using the Semi-Analytical Finite Strip Method.* Thin-Walled Structures, 2013. 71: p. 72-80.

60. Australian/New Zealand Standard AS/NZS 4100:1998, *Steel Structures. Standards Australia/Standards New Zealand.* 1998.

61. Natário, P., N. Silvestre, and D. Camotim, *On the Strength Prediction of Web Crippling Failure in Cold-Formed Steel Beams*, in *Advances in Steel and Aluminum Structures (ICSAS).* 2011: Singapore.

62. Natário, P., N. Silvestre, and D. Camotim, *DSM for Web Crippling under two-flange conditions*, in *CCFSS2016.* 2016: Baltimore, Maryland, USA. p. 20.

63.   Natário, P., N. Silvestre, and D. Camotim, *Web crippling of beams under ITF loading: A novel DSM-based design approach.* Journal of Constructional Steel Research, 2017. 128: p. 812-824.

64.   Macdonald, M., et al., *Web crippling behaviour of thin-walled lipped channel beams.* Thin-Walled Structures, 2011. 49(5): p. 682-690.

65.   Sundararajah, L., M. Mahendran, and P. Keerthan, *Web crippling capacity of Cold-formed channel sections with and without longitudinal web stiffeners subjected to two-flange load cases*, in *7th International Conference on Coupled Instabilities in Metal Structures*. 2016: Baltimore, Mareland, USA.

66.   Natário, P., N. Silvestre, and D. Camotim, *Localised failure of Thin-Walled Steel Members subjected to Concentrated loads - Analysis, behaviour and design*. 2015, Universidade de Lisboa, Portugal: Instituto Superio Tecnico.

67.   Ádány, S. and B.W. Schafer, *Generalized constrained finite strip method for thin-walled members with arbitrary cross-section: Primary modes.* Thin-Walled Structures, 2014a. 84: p. 150-169.

68.   Ádány, S. and B.W. Schafer, *Generalized constrained finite strip method for thin-walled members with arbitrary cross-section: Secondary modes, orthogonality, examples.* Thin-Walled Structures, 2014b. 84: p. 123-133.

69.   Papangelis, J.P. and G.J. Hancock, *Computer analysis of thin-walled structural members.* Computers & Structures, 1994. 56(1): p. 157-176.

70.   Nguyen, V.V., G.J. Hancock, and C.H. Pham, *Development of the THIN-WALL-2 program for buckling analysis of thin-walled sections under generalised loading*, in *Eighth International Conference on Advances in Steel Structures*. 2015: Lisbon, Portugal. p. 20.

71.   Hancock, G.J. and C.H. Pham, *Direct Strength Method of Design for Shear of Cold-Formed Channel Sections based on a Shear Signature Curve*, in *Proceedings, 21st International Specialty Conference on Cold-Formed Steel Structures*. 2012: St Louis, Missouri, USA. p. 207-221.

72.   Hancock, G.J. and C.H. Pham, *Relationship between the Semi-analytical finite strip methods for buckling of thin-walled sections under uniform and localised loading*, in *Eighth International Conference on Advances in Steel Structures*. 2015: Lisbon, Portugal. p. 20.

73. Pham, S.H., C.H. Pham, and G.J. Hancock, *Direct strength method of design for shear including sections with longitudinal web stiffeners.* Thin-Walled Structures, 2014. 81: p. 19-28.

74. Nguyen, V.V., G.J. Hancock, and C.H. Pham, *Analyses of thin-walled sections under localised loading for general end boundary conditions - Part 1: Pre-buckling*, in *CCFSS2016*. 2016a: Baltimore, Maryland, USA. p. 20.

75. Nguyen, V.V., G.J. Hancock, and C.H. Pham, *Pre-buckling analysis of thin-walled sections under localised loading for general end boundary conditions*, in *Research report R958*. 2016, The University of Sydney: Sydney, Australia. p. 40.

76. Nguyen, V.V., G.J. Hancock, and C.H. Pham, *Application of the THIN-WALL-2 V2.0 program for analysis of thin-walled sections under localised loading*, in *International conference CIGOS2017 - New challenges in Civil Engineering*. 2017: Ho Chi Minh city, Viet Nam.

77. Nguyen, V.V., G.J. Hancock, and C.H. Pham, *Experimental data, buckling loads and plastic mechanism models used in the Direct Strength Method (DSM) applied to localised loading*, in *Research Report R965*. 2017, The University of Sydney: Sydney, Australia.

78. Ellingwood, B., et al., *Development of a probability based load criterion for American National Standard A58: Building requirements for minimum design loads in buildings and other structures*, in *15th International Specialty Conference on Cold-Formed Steel Structures*. 1980: St, Louis, MO, USA.

APPENDIX A: FLEXURAL AND MEMBRANE STIFFNESS MATRICES

1. Flexural stiffness matrix

The evaluation matrix of the flexural displacement functions at nodal line.

$$
[C_F] = \begin{bmatrix} 1 & 0 & 0 & 0 \\ 0 & \dfrac{1}{b} & 0 & 0 \\ 1 & 1 & 1 & 1 \\ 0 & \dfrac{1}{b} & \dfrac{2}{b} & \dfrac{3}{b} \end{bmatrix}
\qquad
[C_F]^{-1} = \begin{bmatrix} 1 & 0 & 0 & 0 \\ 0 & b & 0 & 0 \\ -3 & -2b & 3 & -b \\ 2 & b & -2 & b \end{bmatrix}
\tag{A-1}
$$

The property matrix of flexural displacement of a strip

$$
[D_F] = \begin{bmatrix} D_x & D_1 & 0 \\ D_1 & D_y & 0 \\ 0 & 0 & D_{xy} \end{bmatrix}
\tag{A-2}
$$

$$
D_x = \frac{E_x t^3}{12(1 - \nu_y \nu_x)}
\qquad
D_y = \frac{E_y t^3}{12(1 - \nu_y \nu_x)}
$$

$$
D_1 = \nu_x D_y = \nu_y D_x
\qquad
D_{xy} = \frac{G t^3}{12}
\tag{A-3}
$$

E_x, E_y are the moduli of elasticity of the longitudinal and transverse directions of a strip respectively

ν_x, ν_y are the poisson's ratios

G is the shear modulus of a strip

The strain matrix of flexural displacement

$$
[B_{Fm}] = \begin{bmatrix} -X_{1m}'' & -\bar{y} X_{1m}'' & -\bar{y}^2 X_{1m}'' & -\bar{y}^3 X_{1m}'' \\ 0 & 0 & -\dfrac{2}{b^2} X_{1m} & -\dfrac{6\bar{y}}{b^2} X_{1m} \\ 0 & \dfrac{2}{b} X_{1m}' & \dfrac{4\bar{y}}{b} X_{1m}' & \dfrac{6\bar{y}^2}{b} X_{1m}' \end{bmatrix}
\tag{A-4}
$$

Matrix *A*:

$$A = [D_F][B_{Fn}] \tag{A-5}$$

$$A = \begin{bmatrix} D_x & D_1 & 0 \\ D_1 & D_y & 0 \\ 0 & 0 & D_{xy} \end{bmatrix} \begin{bmatrix} -X_{1n}^{"} & -\overline{y}X_{1n}^{"} & -\overline{y}^2 X_{1n}^{"} & -\overline{y}^3 X_{1n}^{"} \\ 0 & 0 & -\dfrac{2}{b^2}X_{1n} & -\dfrac{6\overline{y}}{b^2}X_{1n} \\ 0 & \dfrac{2}{b}X_{1n}^{'} & \dfrac{4\overline{y}}{b}X_{1n}^{'} & \dfrac{6\overline{y}^2}{b}X_{1n}^{'} \end{bmatrix} = \begin{bmatrix} A_{11} & A_{12} & A_{13} & A_{14} \\ A_{21} & A_{22} & A_{23} & A_{24} \\ A_{31} & A_{32} & A_{33} & A_{34} \end{bmatrix}$$

In which:

$$A_{11} = -D_x X_{1n}^{"}$$

$$A_{23} = -\overline{y}^2 D_1 X_{1n}^{"} - \frac{2}{b^2}D_y X_{1n}$$

$$A_{12} = -\overline{y}D_x X_{1n}^{"}$$

$$A_{24} = -\overline{y}^3 D_1 X_{1n}^{"} - \frac{6\overline{y}}{b^2}D_y X_{1n}$$

$$A_{13} = -\overline{y}^2 D_x X_{1n}^{"} - \frac{2}{b^2}D_1 X_{1n}$$

$$A_{31} = 0$$

$$A_{14} = -\overline{y}^3 D_x X_{1n}^{"} - \frac{6\overline{y}}{b^2}D_1 X_{1n}$$

$$A_{32} = \frac{2}{b}D_{xy} X_{1n}^{'}$$

$$A_{21} = -D_1 X_{1n}^{"}$$

$$A_{33} = \frac{4\overline{y}}{b}D_{xy} X_{1n}^{'}$$

$$A_{22} = -\overline{y}D_1 X_{1n}^{"}$$

$$A_{34} = \frac{6\overline{y}^2}{b}D_{xy} X_{1n}^{'}$$

Matrix *B*:

$$B = [B_{Fm}]^T [D_F][B_{Fn}] \tag{A-6}$$

$$B = \begin{bmatrix} -X_{1m}^{"} & 0 & 0 \\ -\overline{y}X_{1m}^{"} & 0 & \dfrac{2}{b}X_{1m}^{'} \\ -\overline{y}^2 X_{1m}^{"} & -\dfrac{2}{b^2}X_{1m} & \dfrac{4\overline{y}}{b}X_{1m}^{'} \\ -\overline{y}^3 X_{1m}^{"} & -\dfrac{6\overline{y}}{b^2}X_{1m} & \dfrac{6\overline{y}^2}{b}X_{1m}^{'} \end{bmatrix} \begin{bmatrix} A_{11} & A_{12} & A_{13} & A_{14} \\ A_{21} & A_{22} & A_{23} & A_{24} \\ A_{31} & A_{32} & A_{33} & A_{34} \end{bmatrix} = \begin{bmatrix} B_{11} & B_{12} & B_{13} & B_{14} \\ B_{21} & B_{22} & B_{23} & B_{24} \\ B_{31} & B_{32} & B_{33} & B_{34} \\ B_{41} & B_{42} & B_{43} & B_{44} \end{bmatrix}$$

In which:

$$B_{11} = D_x X_{1m}^{"} X_{1n}^{"} \qquad\qquad B_{12} = \overline{y} D_x X_{1m}^{"} X_{1n}^{"}$$

$$B_{13} = \overline{y}^2 D_x X_{1m}^{"} X_{1n}^{"} + \frac{2}{b^2} D_1 X_{1m}^{"} X_{1n} \qquad\qquad B_{14} = \overline{y}^3 D_x X_{1m}^{"} X_{1n}^{"} + \frac{6\overline{y}}{b^2} D_1 X_{1m}^{"} X_{1n}$$

$$B_{21} = \overline{y} D_x X_{1m}^{"} X_{1n}^{"}$$

$$B_{22} = \overline{y}^2 D_x X_{1m}^{"} X_{1n}^{"} + \frac{4}{b^2} D_{xy} X_{1m}^{'} X_{1n}^{'}$$

$$B_{23} = \overline{y}^3 D_x X_{1m}^{"} X_{1n}^{"} + \frac{2\overline{y}}{b^2} D_1 X_{1m}^{"} X_{1n} + \frac{8\overline{y}}{b^2} D_{xy} X_{1m}^{'} X_{1n}^{'}$$

$$B_{24} = \overline{y}^4 D_x X_{1m}^{"} X_{1n}^{"} + \frac{6\overline{y}^2}{b^2} D_1 X_{1m}^{"} X_{1n} + \frac{12\overline{y}^2}{b^2} D_{xy} X_{1m}^{'} X_{1n}^{'}$$

$$B_{31} = \overline{y}^2 D_x X_{1m}^{"} X_{1n}^{"} + \frac{2}{b^2} D_1 X_{1m} X_{1n}^{"}$$

$$B_{32} = \overline{y}^3 D_x X_{1m}^{"} X_{1n}^{"} + \frac{2\overline{y}}{b^2} D_1 X_{1m} X_{1n}^{"} + \frac{8\overline{y}}{b^2} D_{xy} X_{1m}^{'} X_{1n}^{'}$$

$$B_{33} = \overline{y}^4 D_x X_{1m}^{"} X_{1n}^{"} + \frac{2\overline{y}^2}{b^2} D_1 X_{1m}^{"} X_{1n} + \frac{2\overline{y}^2}{b^2} D_1 X_{1m} X_{1n}^{"} + \frac{4}{b^4} D_y X_{1m} X_{1n} + \frac{16\overline{y}^2}{b^2} D_{xy} X_{1m}^{'} X_{1n}^{'}$$

$$B_{34} = \overline{y}^5 D_x X_{1m}^{"} X_{1n}^{"} + \frac{6\overline{y}^3}{b^2} D_1 X_{1m}^{"} X_{1n} + \frac{2\overline{y}^3}{b^2} D_1 X_{1m} X_{1n}^{"} + \frac{12\overline{y}}{b^4} D_y X_{1m} X_{1n} + \frac{24\overline{y}^3}{b^2} D_{xy} X_{1m}^{'} X_{1n}^{'}$$

$$B_{41} = \overline{y}^3 D_x X_{1m}^{"} X_{1n}^{"} + \frac{6\overline{y}}{b^2} D_1 X_{1m} X_{1n}^{"}$$

$$B_{42} = \overline{y}^4 D_x X_{1m}^{"} X_{1n}^{"} + \frac{6\overline{y}^2}{b^2} D_1 X_{1m} X_{1n}^{"} + \frac{12\overline{y}^2}{b^2} D_{xy} X_{1m}^{'} X_{1n}^{'}$$

$$B_{43} = \overline{y}^5 D_x X_{1m}^{"} X_{1n}^{"} + \frac{2\overline{y}^3}{b^2} D_1 X_{1m}^{"} X_{1n} + \frac{6\overline{y}^3}{b^2} D_1 X_{1m} X_{1n}^{"} + \frac{12\overline{y}}{b^4} D_y X_{1m} X_{1n} + \frac{24\overline{y}^3}{b^2} D_{xy} X_{1m}^{'} X_{1n}^{'}$$

$$B_{44} = \overline{y}^6 D_x X_{1m}^{"} X_{1n}^{"} + \frac{6\overline{y}^4}{b^2} D_1 X_{1m}^{"} X_{1n} + \frac{6\overline{y}^4}{b^2} D_1 X_{1m} X_{1n}^{"} + \frac{36\overline{y}^2}{b^4} D_y X_{1m} X_{1n} + \frac{36\overline{y}^4}{b^2} D_{xy} X_{1m}^{'} X_{1n}^{'}$$

Matrix C:

$$C = \int_0^{\bar{y}=1} \left[B_{Fm}\right]^T \left[D_F\right]\left[B_{Fn}\right]d\bar{y} = \begin{bmatrix} C_{11} & C_{12} & C_{13} & C_{14} \\ C_{21} & C_{22} & C_{23} & C_{24} \\ C_{31} & C_{32} & C_{33} & C_{34} \\ C_{41} & C_{42} & C_{43} & C_{44} \end{bmatrix} \tag{A-7}$$

In which:

$$C_{11} = D_x X_{1m}^{"} X_{1n}^{"} \qquad\qquad C_{12} = \frac{1}{2} D_x X_{1m}^{"} X_{1n}^{"}$$

$$C_{13} = \frac{1}{3} D_x X_{1m}^{"} X_{1n}^{"} + \frac{2}{b^2} D_1 X_{1m}^{"} X_{1n} \qquad C_{14} = \frac{1}{4} D_x X_{1m}^{"} X_{1n}^{"} + \frac{6}{2b^2} D_1 X_{1m}^{"} X_{1n}$$

$$C_{21} = \frac{1}{2} D_x X_{1m}^{"} X_{1n}^{"} \qquad\qquad C_{22} = \frac{1}{3} D_x X_{1m}^{"} X_{1n}^{"} + \frac{4}{b^2} D_{xy} X_{1m}^{'} X_{1n}^{'}$$

$$C_{23} = \frac{1}{4} D_x X_{1m}^{"} X_{1n}^{"} + \frac{2}{2b^2} D_1 X_{1m}^{"} X_{1n} + \frac{8}{2b^2} D_{xy} X_{1m}^{'} X_{1n}^{'}$$

$$C_{24} = \frac{1}{5} D_x X_{1m}^{"} X_{1n}^{"} + \frac{6}{3b^2} D_1 X_{1m}^{"} X_{1n} + \frac{12}{3b^2} D_{xy} X_{1m}^{'} X_{1n}^{'}$$

$$C_{31} = \frac{1}{3} D_x X_{1m}^{"} X_{1n}^{"} + \frac{2}{b^2} D_1 X_{1m} X_{1n}^{"}$$

$$C_{32} = \frac{1}{4} D_x X_{1m}^{"} X_{1n}^{"} + \frac{2}{2b^2} D_1 X_{1m} X_{1n}^{"} + \frac{8}{2b^2} D_{xy} X_{1m}^{'} X_{1n}^{'}$$

$$C_{33} = \frac{1}{5} D_x X_{1m}^{"} X_{1n}^{"} + \frac{2}{3b^2} D_1 X_{1m}^{"} X_{1n} + \frac{2}{3b^2} D_1 X_{1m} X_{1n}^{"} + \frac{4}{b^4} D_y X_{1m} X_{1n} + \frac{16}{3b^2} D_{xy} X_{1m}^{'} X_{1n}^{'}$$

$$C_{34} = \frac{1}{6} D_x X_{1m}^{"} X_{1n}^{"} + \frac{6}{4b^2} D_1 X_{1m}^{"} X_{1n} + \frac{2}{4b^2} D_1 X_{1m} X_{1n}^{"} + \frac{12}{2b^4} D_y X_{1m} X_{1n} + \frac{24}{4b^2} D_{xy} X_{1m}^{'} X_{1n}^{'}$$

$$C_{41} = \frac{1}{4} D_x X_{1m}^{"} X_{1n}^{"} + \frac{6}{2b^2} D_1 X_{1m} X_{1n}^{"}$$

$$C_{42} = \frac{1}{5} D_x X_{1m}^{"} X_{1n}^{"} + \frac{6}{3b^2} D_1 X_{1m} X_{1n}^{"} + \frac{12}{3b^2} D_{xy} X_{1m}^{'} X_{1n}^{'}$$

$$C_{43} = \frac{1}{6} D_x X_{1m}^{"} X_{1n}^{"} + \frac{2}{4b^2} D_1 X_{1m}^{"} X_{1n} + \frac{6}{4b^2} D_1 X_{1m} X_{1n}^{"} + \frac{12}{2b^4} D_y X_{1m} X_{1n} + \frac{24}{4b^2} D_{xy} X_{1m}^{'} X_{1n}^{'}$$

$$C_{44} = \frac{1}{7} D_x X_{1m}^{"} X_{1n}^{"} + \frac{6}{5b^2} D_1 X_{1m}^{"} X_{1n} + \frac{6}{5b^2} D_1 X_{1m} X_{1n}^{"} + \frac{36}{3b^4} D_y X_{1m} X_{1n} + \frac{36}{5b^2} D_{xy} X_{1m}^{'} X_{1n}^{'}$$

Matrix D:

$$D = \int\limits_{0}^{\xi=\pi} \int\limits_{0}^{\overline{y}=1} \left[B_{Fm}\right]^{T} \left[D_{F}\right] \left[B_{Fn}\right] d\overline{y} d\xi = \begin{bmatrix} D_{11} & D_{12} & D_{13} & D_{14} \\ D_{21} & D_{22} & D_{23} & D_{24} \\ D_{31} & D_{32} & D_{33} & D_{34} \\ D_{41} & D_{42} & D_{43} & D_{44} \end{bmatrix} \tag{A-8}$$

In which:

$$D_{11} = D_{x} I_{4F\xi}$$

$$D_{13} = \frac{1}{3} D_{x} I_{4F\xi} + \frac{2}{b^{2}} D_{1} I_{2F\xi}$$

$$D_{12} = \frac{1}{2} D_{x} I_{4F\xi}$$

$$D_{14} = \frac{1}{4} D_{x} I_{4F\xi} + \frac{3}{b^{2}} D_{1} I_{2F\xi}$$

$$D_{21} = \frac{1}{2} D_{x} I_{4F\xi}$$

$$D_{23} = \frac{1}{4} D_{x} I_{4F\xi} + \frac{1}{b^{2}} D_{1} I_{2F\xi} + \frac{4}{b^{2}} D_{xy} I_{5F\xi}$$

$$D_{22} = \frac{1}{3} D_{x} I_{4F\xi} + \frac{4}{b^{2}} D_{xy} I_{5F\xi}$$

$$D_{24} = \frac{1}{5} D_{x} I_{4F\xi} + \frac{2}{b^{2}} D_{1} I_{2F\xi} + \frac{4}{b^{2}} D_{xy} I_{5F\xi}$$

$$D_{31} = \frac{1}{3} D_{x} I_{4F\xi} + \frac{2}{b^{2}} D_{1} I_{3F\xi}$$

$$D_{32} = \frac{1}{4} D_{x} I_{4F\xi} + \frac{1}{b^{2}} D_{1} I_{3F\xi} + \frac{4}{b^{2}} D_{xy} I_{5F\xi}$$

$$D_{33} = \frac{1}{5} D_{x} I_{4F\xi} + \frac{2}{3b^{2}} D_{1} I_{3F\xi} + \frac{2}{3b^{2}} D_{1} I_{2F\xi} + \frac{4}{b^{4}} D_{y} I_{1F\xi} + \frac{16}{3b^{2}} D_{xy} I_{5F\xi}$$

$$D_{34} = \frac{1}{6} D_{x} I_{4F\xi} + \frac{3}{2b^{2}} D_{1} I_{2F\xi} + \frac{1}{2b^{2}} D_{1} I_{3F\xi} + \frac{6}{b^{4}} D_{y} I_{1F\xi} + \frac{6}{b^{2}} D_{xy} I_{5F\xi}$$

$$D_{41} = \frac{1}{4} D_{x} I_{4F\xi} + \frac{3}{b^{2}} D_{1} I_{3F\xi}$$

$$D_{42} = \frac{1}{5} D_{x} I_{4F\xi} + \frac{2}{b^{2}} D_{1} I_{3F\xi} + \frac{4}{b^{2}} D_{xy} I_{5F\xi}$$

$$D_{43} = \frac{1}{6} D_{x} I_{4F\xi} + \frac{1}{2b^{2}} D_{1} I_{2F\xi} + \frac{3}{2b^{2}} D_{1} I_{3F\xi} + \frac{6}{b^{4}} D_{y} I_{1F\xi} + \frac{6}{b^{2}} D_{xy} I_{5F\xi}$$

$$D_{44} = \frac{1}{7} D_{x} I_{4F\xi} + \frac{6}{5b^{2}} D_{1} I_{2F\xi} + \frac{6}{5b^{2}} D_{1} I_{3F\xi} + \frac{12}{b^{4}} D_{y} I_{1F\xi} + \frac{36}{5b^{2}} D_{xy} I_{5F\xi}$$

In which:

$$I_{1F\xi} = \int\limits_{o}^{\xi=\pi} X_{1m}(\xi) X_{1n}(\xi) d\xi$$

$$I_{4F\xi} = \int\limits_{o}^{\xi=\pi} X_{1m}^{"}(\xi) X_{1n}^{"}(\xi) d\xi$$

$$I_{2F\xi} = \int\limits_{o}^{\xi=\pi} X_{1m}^{"}(\xi) X_{1n}(\xi) d\xi \qquad\qquad I_{5F\xi} = \int\limits_{o}^{\xi=\pi} X_{1m}^{'}(\xi) X_{1n}^{'}(\xi) d\xi$$

$$I_{3F\xi} = \int\limits_{o}^{\xi=\pi} X_{1m}(\xi) X_{1n}^{"}(\xi) d\xi$$

$$X_{1m}^{'} = \frac{d\left(X_{1m}(\xi)\right)}{dx} = \left(\frac{\pi}{L}\right)\frac{d\left(X_{1m}(\xi)\right)}{d\left(\dfrac{\pi x}{L}\right)} = \left(\frac{\pi}{L}\right)\frac{d\left(X_{1m}(\xi)\right)}{d\xi}$$

$$X_{1m}^{"} = \left(\frac{\pi}{L}\right)^{2}\frac{d^{2}\left(X_{1m}(\xi)\right)}{d\xi^{2}}$$

2. Membrane stiffness matrix

The evaluation matrix of the membrane displacement functions at nodal line.

$$[C_M] = \begin{bmatrix} 1 & 0 & 0 & 0 \\ 0 & 0 & 1 & 0 \\ 1 & 1 & 0 & 0 \\ 0 & 0 & 1 & 1 \end{bmatrix} \qquad\qquad [C_M]^{-1} = \begin{bmatrix} 1 & 0 & 0 & 0 \\ -1 & 0 & 1 & 0 \\ 0 & 1 & 0 & 0 \\ 0 & -1 & 0 & 1 \end{bmatrix} \qquad\text{(A-9)}$$

The property matrix of membrane displacement

$$[D_M] = \begin{bmatrix} E_2 & E_{12} & 0 \\ E_{12} & E_1 & 0 \\ 0 & 0 & G \end{bmatrix} \qquad\qquad\qquad\text{(A-10)}$$

$$E_2 = \frac{E_x}{(1-\nu_y\nu_x)}; \qquad E_1 = \frac{E_y}{(1-\nu_y\nu_x)}; \qquad\qquad\text{(A-11)}$$

$$E_{12} = \frac{\nu_x E_y}{(1-\nu_y\nu_x)} = \frac{\nu_y E_x}{(1-\nu_y\nu_x)}$$

The strain matrix of membrane displacement

$$[B_{Mm}] = \begin{bmatrix} 0 & 0 & X_{2m}^{'} & \overline{y}X_{2m}^{'} \\ 0 & \dfrac{1}{b}X_{1m} & 0 & 0 \\ X_{1m}^{'} & \overline{y}X_{1m}^{'} & 0 & \dfrac{1}{b}X_{2m} \end{bmatrix} \qquad\qquad\text{(A-12)}$$

Matrix *M*:

$$M = [D_M][B_{Mn}]$$
(A-13)

$$M = \begin{bmatrix} E_2 & E_{12} & 0 \\ E_{12} & E_1 & 0 \\ 0 & 0 & G \end{bmatrix} \begin{bmatrix} 0 & 0 & X_{2n}^{'} & \overline{y}X_{2n}^{'} \\ 0 & \dfrac{1}{b}X_{1n} & 0 & 0 \\ X_{1n}^{'} & \overline{y}X_{1n}^{'} & 0 & \dfrac{1}{b}X_{2n} \end{bmatrix} = \begin{bmatrix} M_{11} & M_{12} & M_{13} & M_{14} \\ M_{21} & M_{22} & M_{23} & M_{24} \\ M_{31} & M_{32} & M_{33} & M_{34} \end{bmatrix}$$

In which:

$$M_{11} = 0 \qquad\qquad M_{23} = E_{12}X_{2n}^{'}$$

$$M_{12} = \frac{E_{12}}{b}X_{1n} \qquad\qquad M_{24} = E_{12}\overline{y}X_{2n}^{'}$$

$$M_{13} = E_2X_{2n}^{'} \qquad\qquad M_{31} = GX_{1n}^{'}$$

$$M_{14} = E_2\overline{y}X_{2n}^{'} \qquad\qquad M_{32} = G\overline{y}X_{1n}^{'}$$

$$M_{21} = 0 \qquad\qquad M_{33} = 0$$

$$M_{22} = \frac{E_1}{b}X_{1n} \qquad\qquad M_{34} = \frac{G}{b}X_{2n}$$

Matrix *N*:

$$N = [B_{Mm}]^T[D_M][B_{Mn}]$$
(A-14)

$$N = \begin{bmatrix} 0 & 0 & X_{1m}^{'} \\ 0 & \dfrac{1}{b}X_{1m} & \overline{y}X_{1m}^{'} \\ X_{2m}^{'} & 0 & 0 \\ \overline{y}X_{2m}^{'} & 0 & \dfrac{1}{b}X_{2m} \end{bmatrix} \begin{bmatrix} M_{11} & M_{12} & M_{13} & M_{14} \\ M_{21} & M_{22} & M_{23} & M_{24} \\ M_{31} & M_{32} & M_{33} & M_{34} \end{bmatrix} = \begin{bmatrix} N_{11} & N_{12} & N_{13} & N_{14} \\ N_{21} & N_{22} & N_{23} & N_{24} \\ N_{31} & N_{32} & N_{33} & N_{34} \\ N_{41} & N_{42} & N_{43} & N_{44} \end{bmatrix}$$

In which:

$$N_{11} = GX_{1m}^{'}X_{1n}^{'} \qquad\qquad N_{31} = 0$$

$$N_{12} = G\overline{y}X_{1m}^{'}X_{1n}^{'} \qquad\qquad N_{32} = \frac{E_{12}}{b}X_{2m}^{'}X_{1n}$$

$$N_{13} = 0 \qquad\qquad N_{33} = E_2X_{2m}^{'}X_{2n}^{'}$$

$$N_{14} = \frac{G}{b} X_{1m}^{'} X_{2n} \qquad N_{34} = E_2 \bar{y} X_{2m}^{'} X_{2n}^{'}$$

$$N_{21} = G \bar{y} X_{1m}^{'} X_{1n}^{'} \qquad N_{41} = \frac{G}{b} X_{2m} X_{1n}^{'}$$

$$N_{22} = \frac{E_1}{b^2} X_{1m} X_{1n} + G \bar{y}^2 X_{1m}^{'} X_{1n}^{'} \qquad N_{42} = \frac{E_{12}}{b} \bar{y} X_{2m}^{'} X_{1n} + \frac{G}{b} \bar{y} X_{2m} X_{1n}^{'}$$

$$N_{23} = \frac{E_{12}}{b} X_{1m} X_{2n}^{'} \qquad N_{43} = E_2 \bar{y} X_{2m}^{'} X_{2n}^{'}$$

$$N_{24} = \frac{E_{12}}{b} \bar{y} X_{1m} X_{2n}^{'} + \frac{G}{b} \bar{y} X_{1m}^{'} X_{2n} \qquad N_{44} = E_2 \bar{y}^2 X_{2m}^{'} X_{2n}^{'} + \frac{G}{b^2} X_{2m} X_{2n}$$

Matrix P:

$$P = \int_0^{\bar{y}=1} \left[B_{Mm} \right]^T \left[D_M \right] \left[B_{Mn} \right] d\bar{y} = \begin{bmatrix} P_{11} & P_{12} & P_{13} & P_{14} \\ P_{21} & P_{22} & P_{23} & P_{24} \\ P_{31} & P_{32} & P_{33} & P_{34} \\ P_{41} & P_{42} & P_{43} & P_{44} \end{bmatrix} \qquad \text{(A-15)}$$

In which:

$$P_{11} = G X_{1m}^{'} X_{1n}^{'} \qquad P_{31} = 0$$

$$P_{12} = \frac{G}{2} X_{1m}^{'} X_{1n}^{'} \qquad P_{32} = \frac{E_{12}}{b} X_{2m}^{'} X_{1n}$$

$$P_{13} = 0 \qquad P_{33} = E_2 X_{2m}^{'} X_{2n}^{'}$$

$$P_{14} = \frac{G}{b} X_{1m}^{'} X_{2n} \qquad P_{34} = \frac{E_2}{2} X_{2m}^{'} X_{2n}^{'}$$

$$P_{21} = \frac{G}{2} X_{1m}^{'} X_{1n}^{'} \qquad P_{41} = \frac{G}{b} X_{2m} X_{1n}^{'}$$

$$P_{22} = \frac{E_1}{b^2} X_{1m} X_{1n} + \frac{G}{3} X_{1m}^{'} X_{1n}^{'} \qquad P_{42} = \frac{E_{12}}{2b} X_{2m}^{'} X_{1n} + \frac{G}{2b} X_{2m} X_{1n}^{'}$$

$$P_{23} = \frac{E_{12}}{b} X_{1m} X_{2n}^{'} \qquad P_{43} = \frac{E_2}{2} X_{2m}^{'} X_{2n}^{'}$$

$$P_{24} = \frac{E_{12}}{2b} X_{1m} X_{2n}^{'} + \frac{G}{2b} X_{1m}^{'} X_{2n} \qquad P_{44} = \frac{E_2}{3} X_{2m}^{'} X_{2n}^{'} + \frac{G}{b^2} X_{2m} X_{2n}$$

Matrix Q:

$$Q = \int\limits_0^{\xi=\pi} \int\limits_0^{\bar{y}=1} \left[B_{Mm} \right]^T \left[D_M \right] \left[B_{Mn} \right] d\bar{y} d\xi = \begin{bmatrix} Q_{11} & Q_{12} & Q_{13} & Q_{14} \\ Q_{21} & Q_{22} & D_{23} & Q_{24} \\ Q_{31} & Q_{32} & D_{33} & Q_{34} \\ Q_{41} & Q_{42} & D_{43} & Q_{44} \end{bmatrix} \qquad \text{(A-16)}$$

where:

$$Q_{11} = GI_{5M\xi} \qquad\qquad Q_{31} = 0$$

$$Q_{12} = \frac{G}{2} I_{5M\xi} \qquad\qquad Q_{32} = \frac{E_{12}}{b} I_{2M\xi}$$

$$Q_{13} = 0 \qquad\qquad Q_{33} = E_2 I_{4M\xi}$$

$$Q_{14} = \frac{G}{b} I_{6M\xi} \qquad\qquad Q_{34} = \frac{E_2}{2} I_{4M\xi}$$

$$Q_{21} = \frac{G}{2} I_{5M\xi} \qquad\qquad Q_{41} = \frac{G}{b} I_{7M\xi}$$

$$Q_{22} = \frac{E_1}{b^2} I_{1M\xi} + \frac{G}{3} I_{5M\xi} \qquad\qquad Q_{42} = \frac{E_{12}}{2b} I_{2M\xi} + \frac{G}{2b} I_{7M\xi}$$

$$Q_{23} = \frac{E_{12}}{b} I_{3M\xi} \qquad\qquad Q_{43} = \frac{E_2}{2} I_{4M\xi}$$

$$Q_{24} = \frac{E_{12}}{2b} I_{3M\xi} + \frac{G}{2b} I_{6M\xi} \qquad\qquad Q_{44} = \frac{E_2}{3} I_{4M\xi} + \frac{G}{b^2} I_{8M\xi}$$

In which:

$$I_{1M\xi} = \int\limits_o^{\xi=\pi} X_{1m}(\xi) X_{1n}(\xi) d\xi \qquad\qquad I_{5M\xi} = \int\limits_o^{\xi=\pi} X_{1m}^{'}(\xi) X_{1n}^{'}(\xi) d\xi$$

$$I_{2M\xi} = \int\limits_o^{\xi=\pi} X_{2m}^{'}(\xi) X_{1n}(\xi) d\xi \qquad\qquad I_{6M\xi} = \int\limits_o^{\xi=\pi} X_{1m}^{'}(\xi) X_{2n}(\xi) d\xi$$

$$I_{3M\xi} = \int\limits_o^{\xi=\pi} X_{1m}(\xi) X_{2n}^{'}(\xi) d\xi \qquad\qquad I_{7M\xi} = \int\limits_o^{\xi=\pi} X_{2m}(\xi) X_{1n}^{'}(\xi) d\xi$$

$$I_{4M\xi} = \int\limits_o^{\xi=\pi} X_{2m}^{'}(\xi) X_{2n}^{'}(\xi) d\xi \qquad\qquad I_{8M\xi} = \int\limits_o^{\xi=\pi} X_{2m}(\xi) X_{2n}(\xi) d\xi$$

3. Transformation matrix

The transformation matrix $[C]^{-T}$

$$[C]^{-T} = \begin{bmatrix} & & & & 0 & 0 & 1 & -1 \\ & & & & 1 & -1 & 0 & 0 \\ 1 & 0 & -3 & 2 & & & & \\ 0 & b & -2b & b & & & & \\ & & & & 0 & 0 & 0 & 1 \\ & & & & 0 & 1 & 0 & 0 \\ 0 & 0 & 3 & -2 & & & & \\ 0 & 0 & -b & b & & & & \end{bmatrix} \tag{A-17}$$

The rotation matrix $[R]$

$$[R] = \begin{bmatrix} 0 & \cos\beta & -\sin\beta & 0 & & & & \\ 0 & \sin\beta & \cos\beta & 0 & & & & \\ 1 & 0 & 0 & 0 & & & & \\ 0 & 0 & 0 & 1 & & & & \\ & & & & 0 & \cos\beta & -\sin\beta & 0 \\ & & & & 0 & \sin\beta & \cos\beta & 0 \\ & & & & 1 & 0 & 0 & 0 \\ & & & & 0 & 0 & 0 & 1 \end{bmatrix} \tag{A-18}$$

The transformation matrix $[A]$

$$[A] = \begin{bmatrix} -\sin\beta & 3\sin\beta & -2\sin\beta & \cos\beta & -\cos\beta & & \\ \cos\beta & -3\cos\beta & 2\cos\beta & \sin\beta & -\sin\beta & & \\ & & & & & 1 & -1 \\ & b & -2b & b & & & \\ & -3\sin\beta & 2\sin\beta & & \cos\beta & & \\ & 3\cos\beta & -2\cos\beta & & \sin\beta & & \\ & & & & & 1 & \\ & -b & b & & & & \end{bmatrix} \tag{A-19}$$

APPENDIX B: PRE-BUCKLING COMPARISON BETWEEN THE FSM AND THE FEM FOR DIFFERENT BOUNDARY CONDITIONS

1. Both ends Simply supported (SS)

Stress comparison:
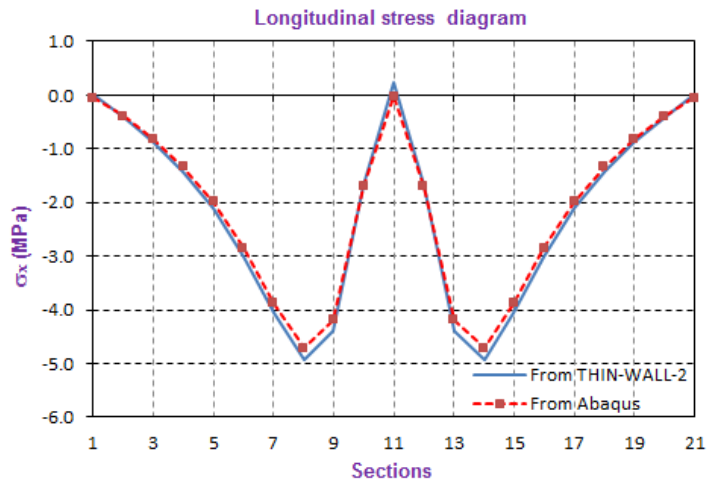
Figure B-1: Longitudinal stress at Nodal Line 23 along the beam for the SS case
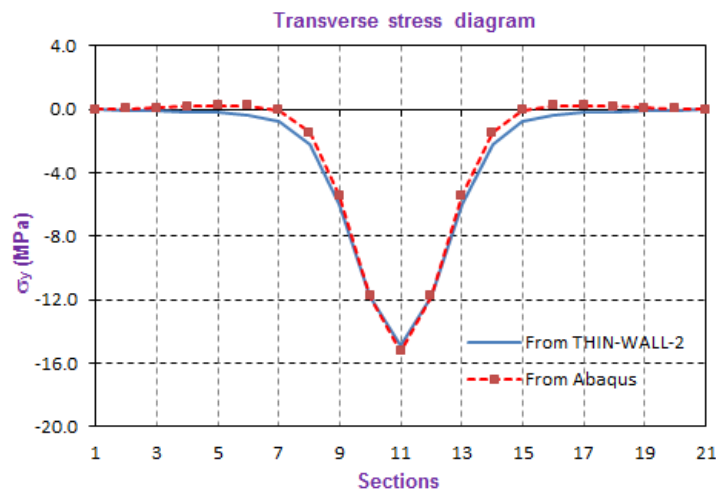
Figure B-2: Transverse stress at Nodal Line 23 along the beam for the SS case
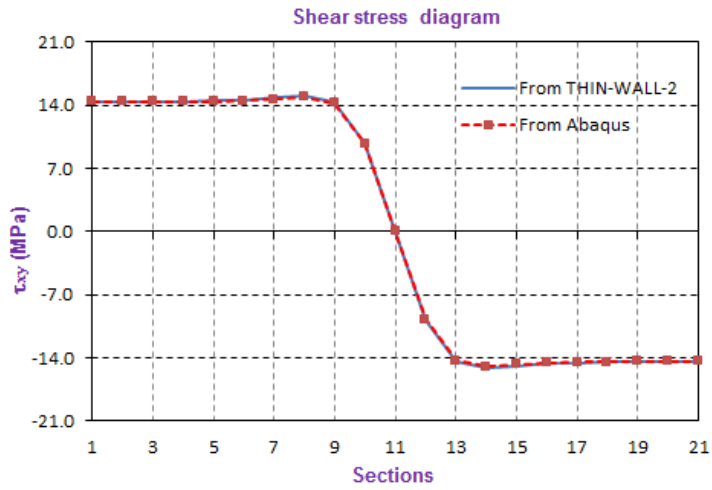
Figure B-3: Shear stress at Nodal Line 23 along the beam for the SS case

Pre-buckling deformation comparison:

(a) From THIN-WALL-2   (b) From Abaqus
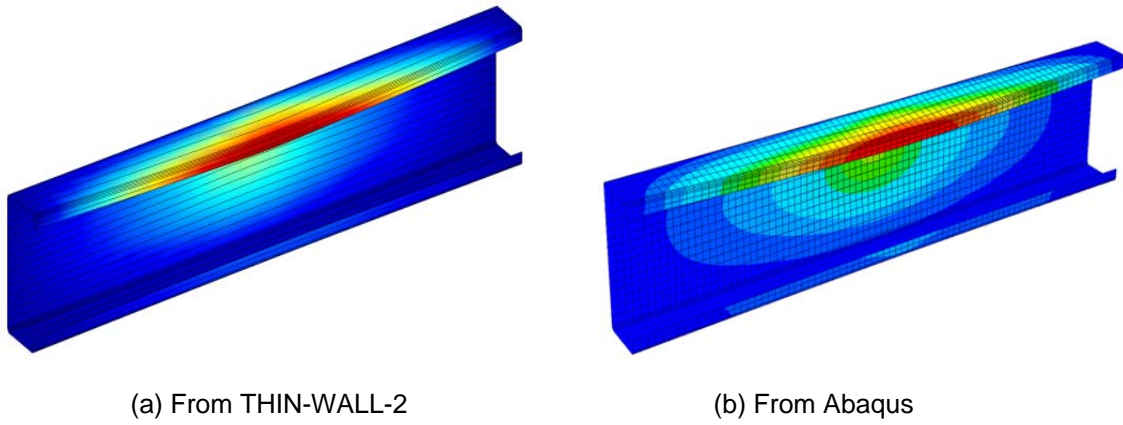
Figure B-4: Pre-buckling deformation comparison for the SS case

Deformation comparison:
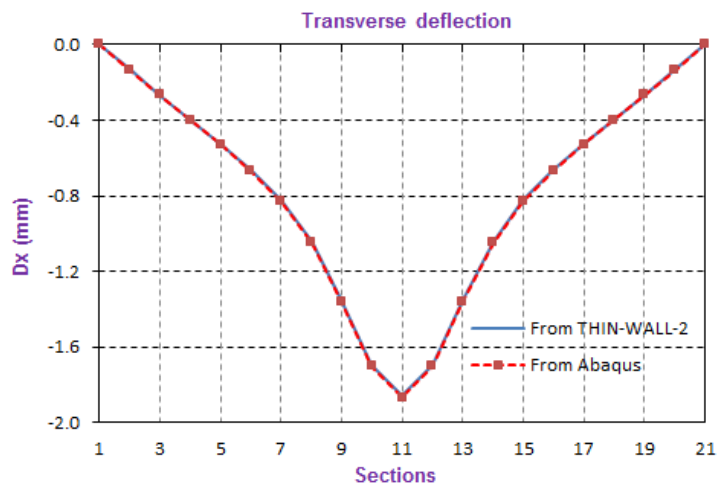
Figure B-5: Transverse pre-buckling deformation at Nodal Line 23 along the beam for the SS case
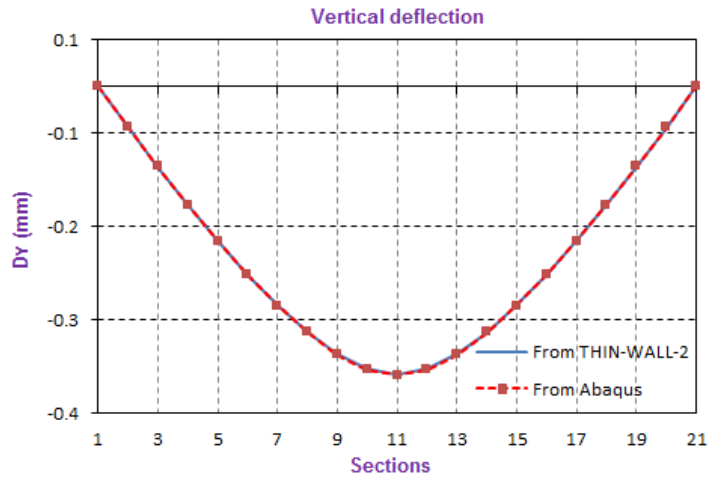
Figure B-6: Vertical pre-buckling deformation at Nodal Line 23 along the beam for the SS case
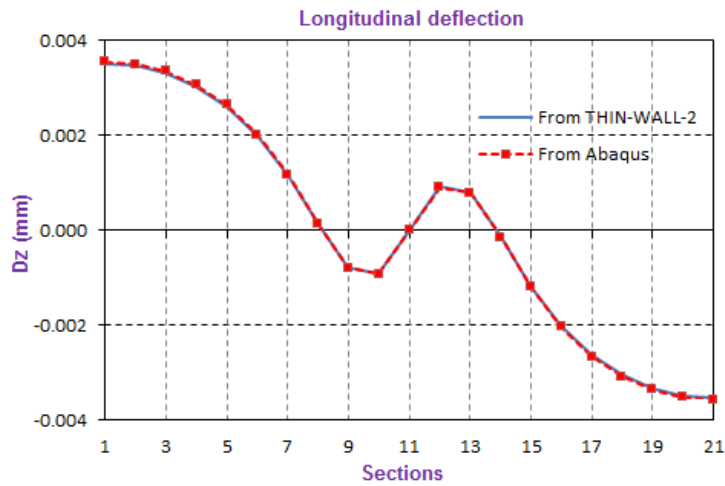
Figure B-7: Longitudinal pre-buckling deformation at Nodal Line 23 along the beam for the SS case

2. One end Simply supported and one end Clamped (SC)

Stress comparison:
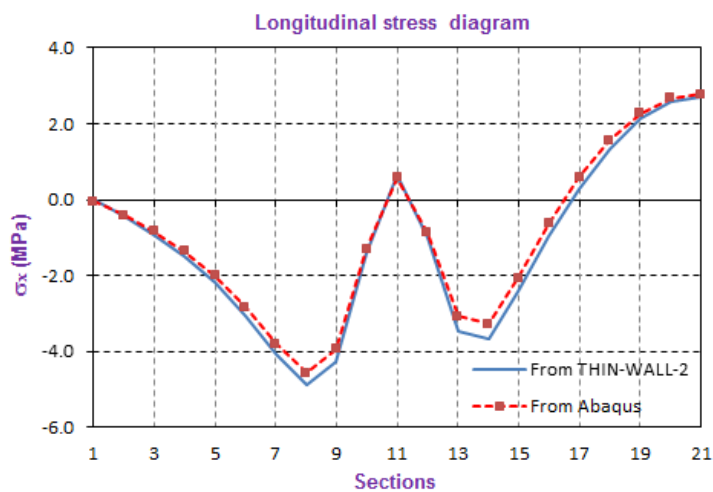
Figure B-8: Longitudinal stress at Nodal Line 23 along the beam for the SC case
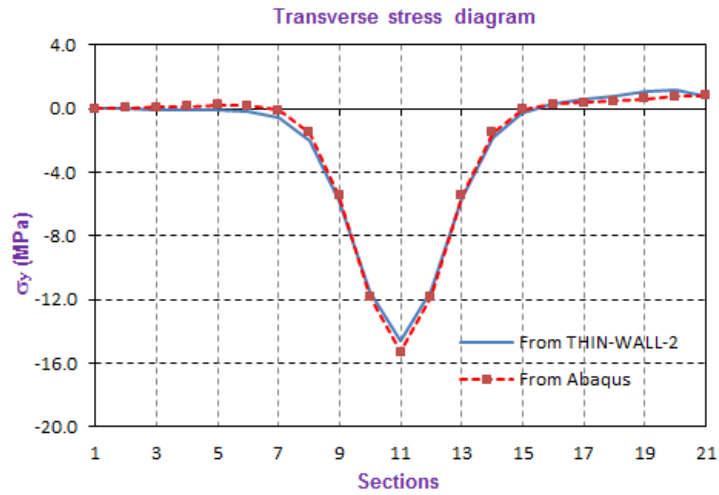
Figure B-9: Transverse stress at Nodal Line 23 along the beam for the SC case
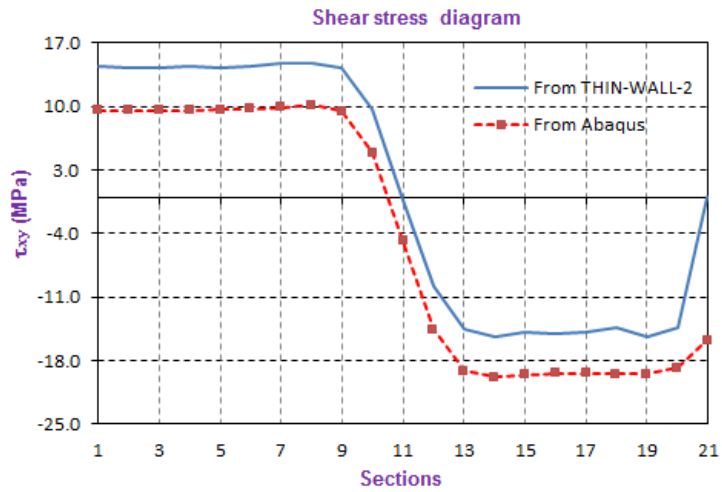
Figure B-10: Shear stress at Nodal Line 23 along the beam for the SC case

Pre-buckling deformation comparison:

(a) From THIN-WALL-2   (b) From Abaqus
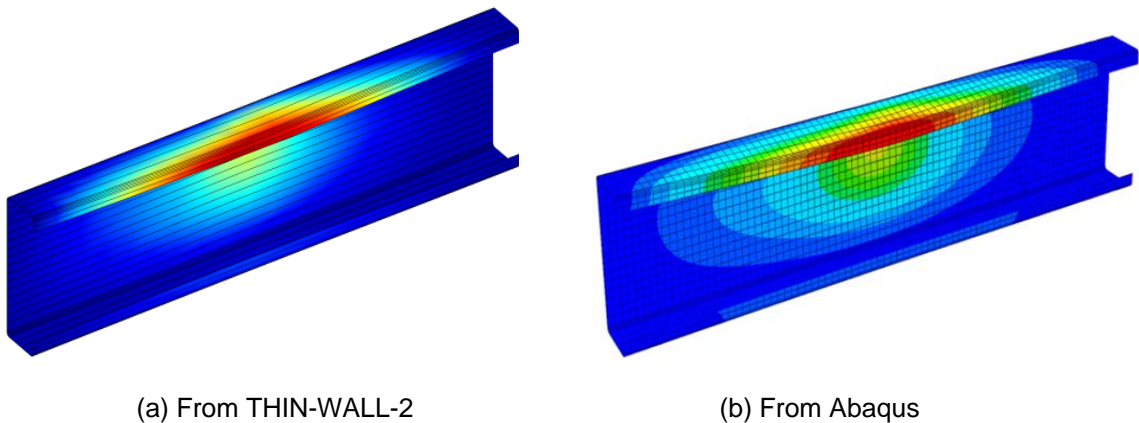
Figure B-11: Pre-buckling deformation comparison for the SC case
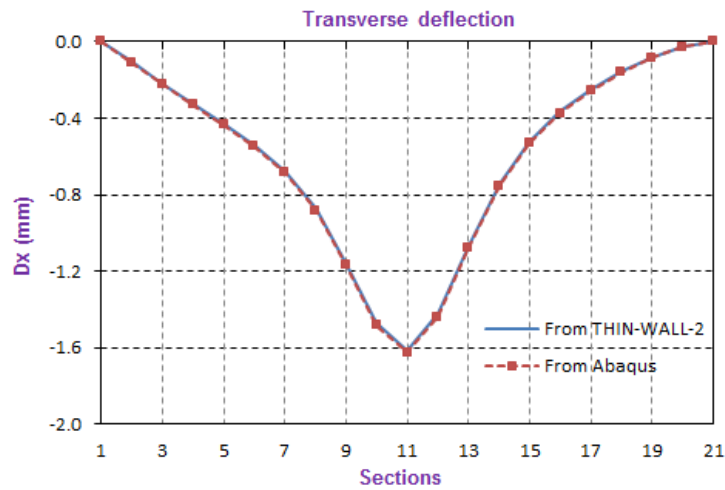
Figure B-12: Transverse pre-buckling deformation at Nodal Line 23 along the beam for the SC case
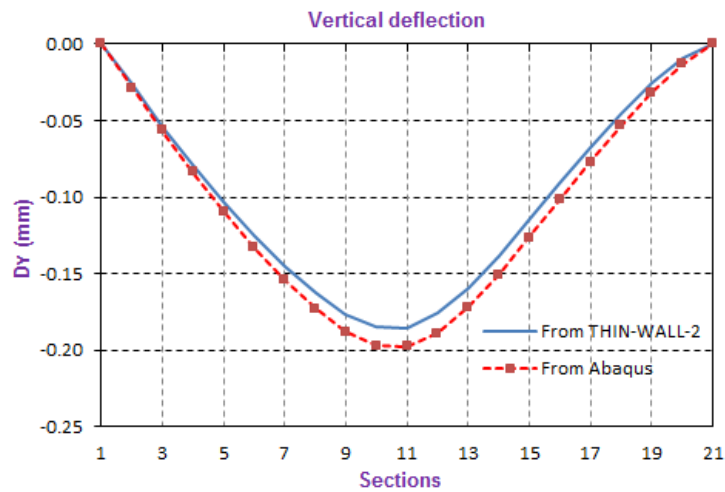
Figure B-13: Vertical pre-buckling deformation at Nodal Line 23 along the beam for the SC case
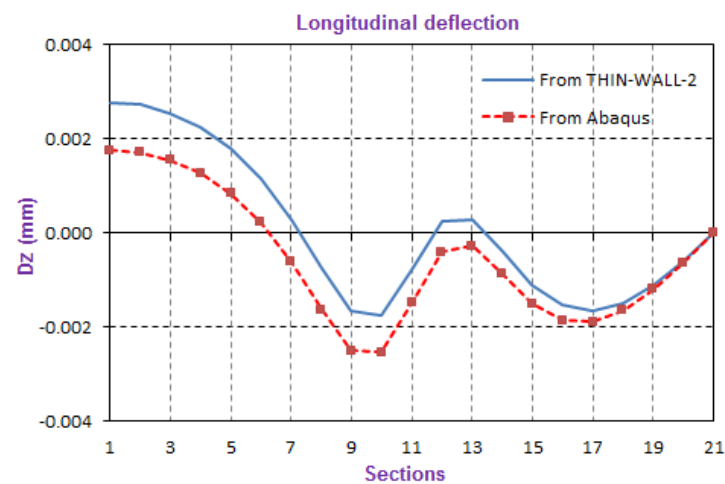
Figure B-14: Longitudinal pre-buckling deformation at Nodal Line 23 along the beam for the SC case

3. One end Simply supported and one end Free (SF)

Stress comparison:
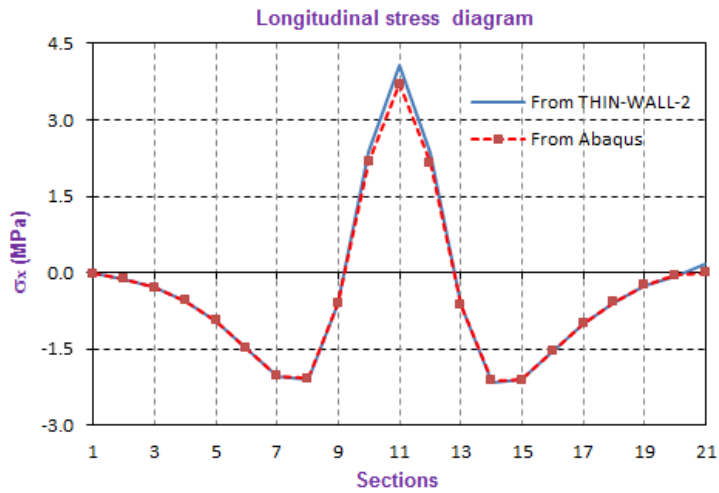
Figure B-15: Longitudinal stress at Nodal Line 23 along the beam for the SF case
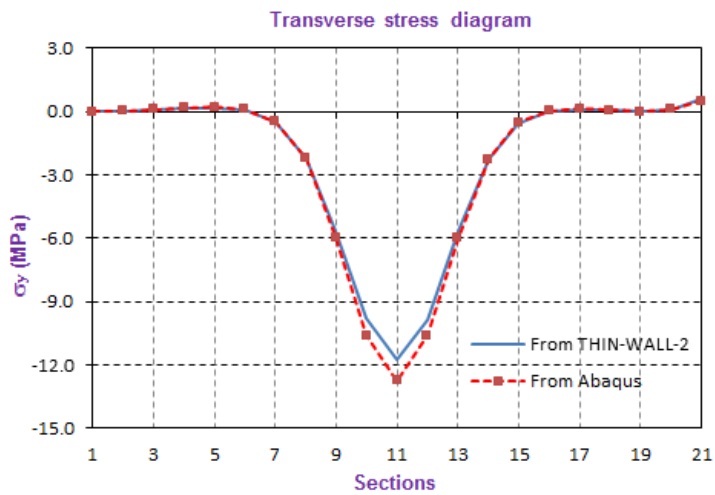
Figure B-16: Transverse stress at Nodal Line 23 along the beam for the SF case
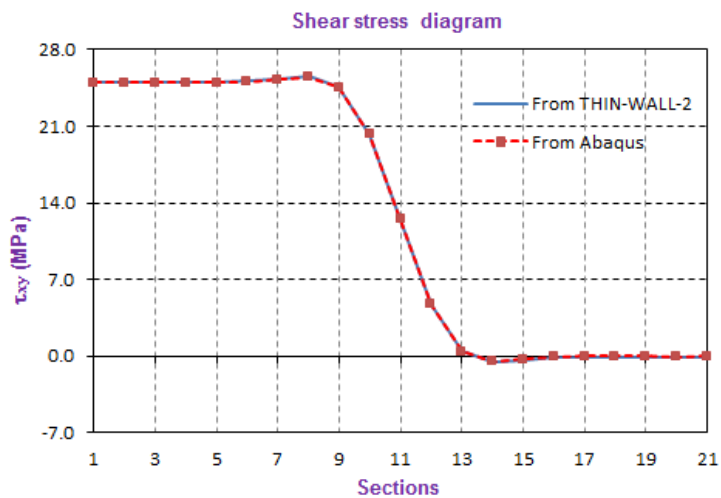
Figure B-17: Shear stress at Nodal Line 23 along the beam for the SF case

Pre-buckling deformation comparison:

(a) From THIN-WALL-2   (b) From Abaqus
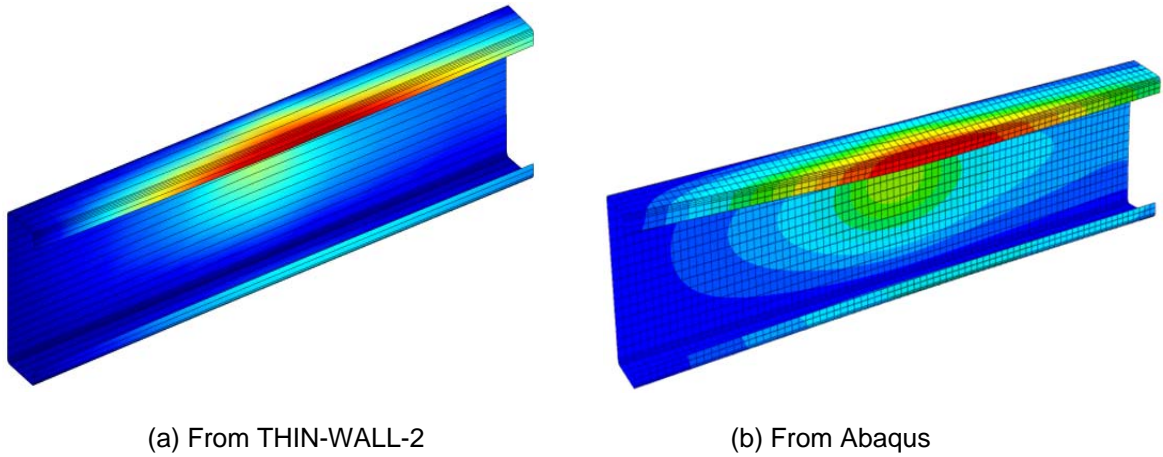
Figure B-18: Pre-buckling deformation comparison for the SF case
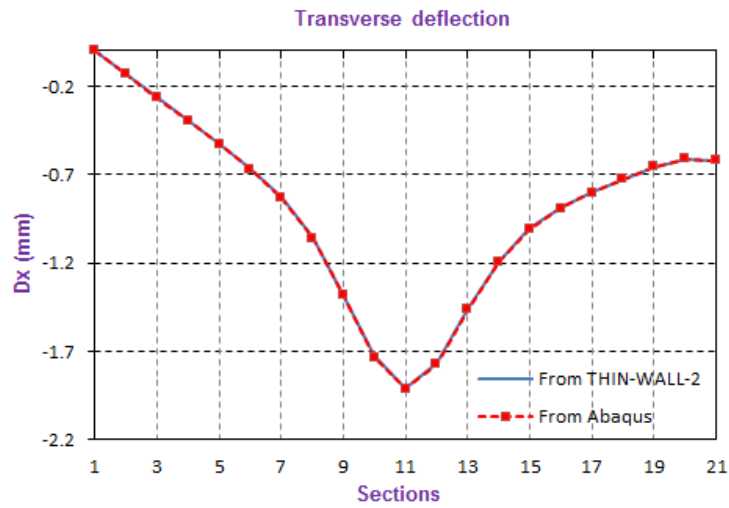
Figure B-19: Transverse pre-buckling deformation at Nodal Line 23 along the beam for the SF case
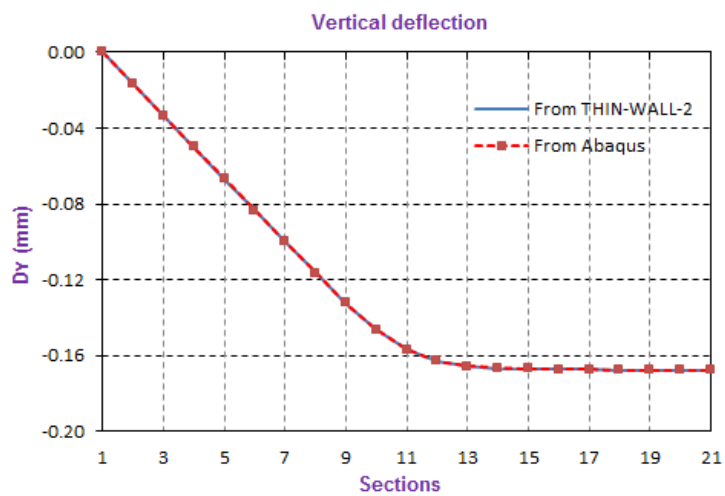
Figure B-20: Vertical pre-buckling deformation at Nodal Line 23 along the beam for the SF case
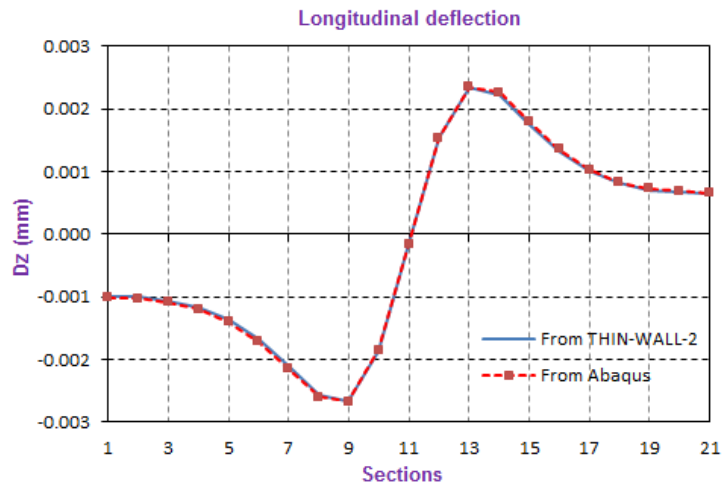
Figure B-21: Longitudinal pre-buckling deformation at Nodal Line 23 along the beam for the SF case

4. Both ends Clamped (CC)

Stress comparison:
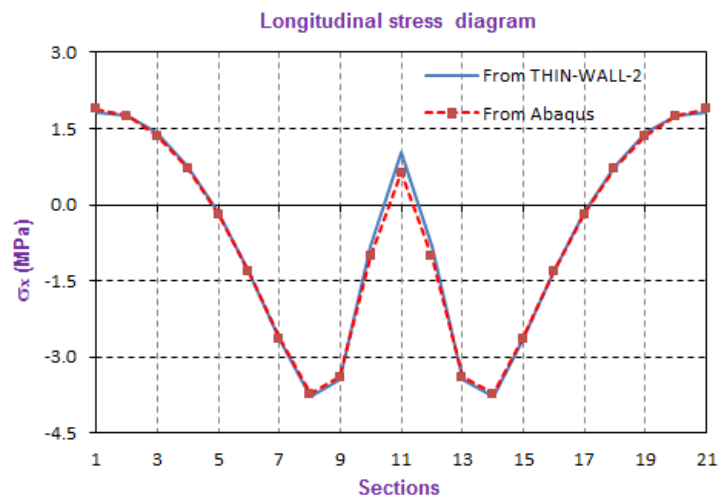
Figure B-22: Longitudinal stress at Nodal Line 23 along the beam for the CC case
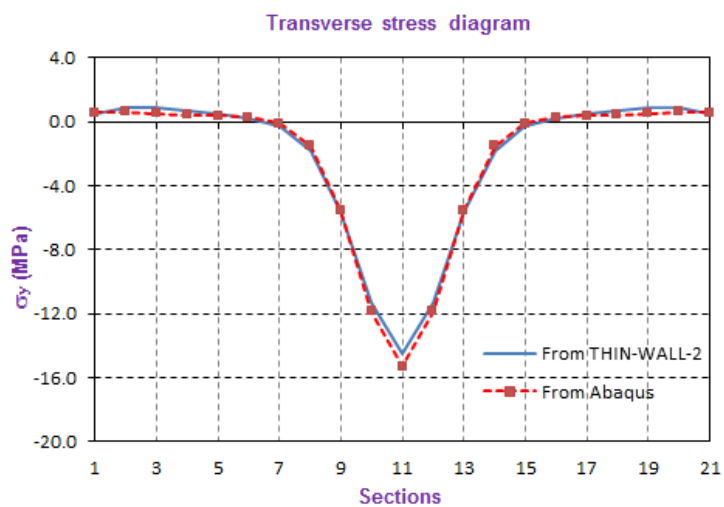
Figure B-23: Transverse stress at Nodal Line 23 along the beam for the CC case
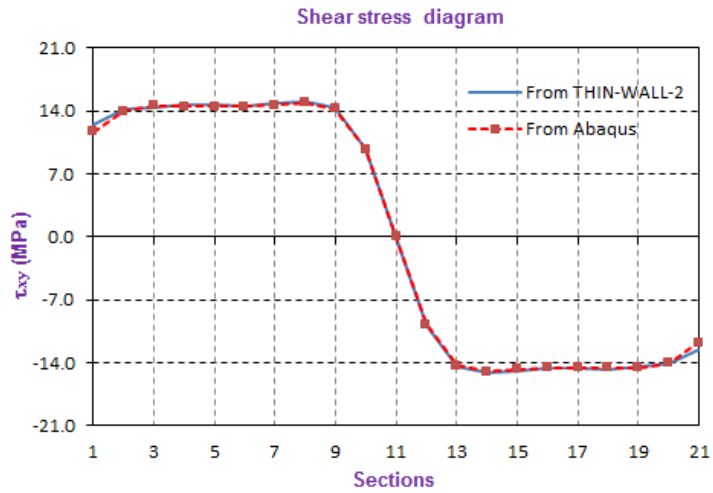
Figure B-24: Shear stress at Nodal Line 23 along the beam for the CC case

Pre-buckling deformation comparison:

(a) From THIN-WALL-2   (b) From Abaqus
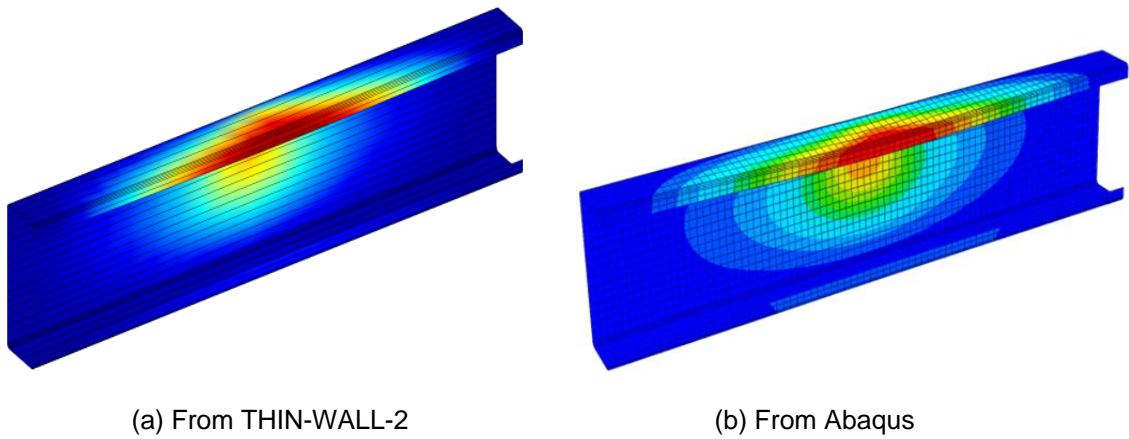
Figure B-25: Pre-buckling deformation comparison for the CC case
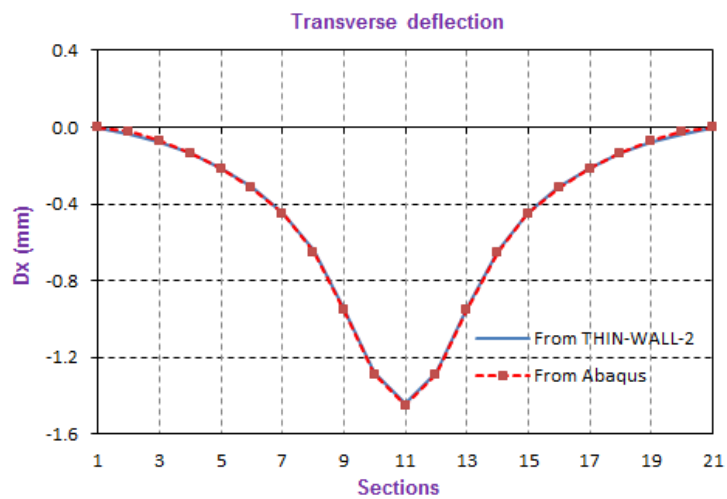
Figure B-26: Transverse pre-buckling deformation at Nodal Line 23 along the beam for the CC case
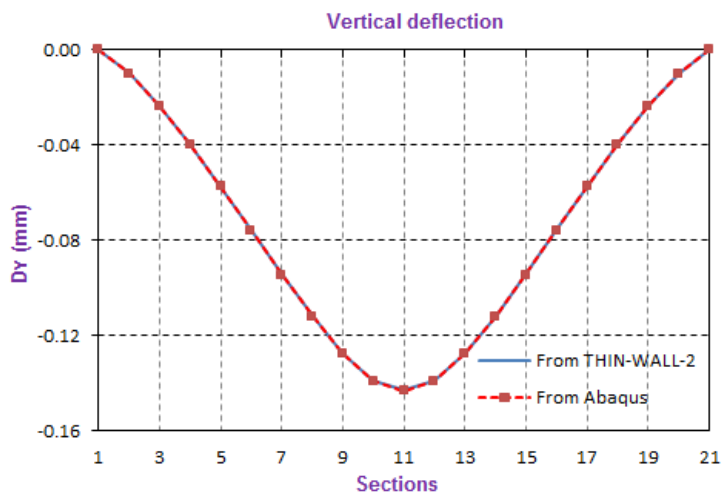
Figure B-27: Vertical pre-buckling deformation at Nodal Line 23 along the beam for the CC case
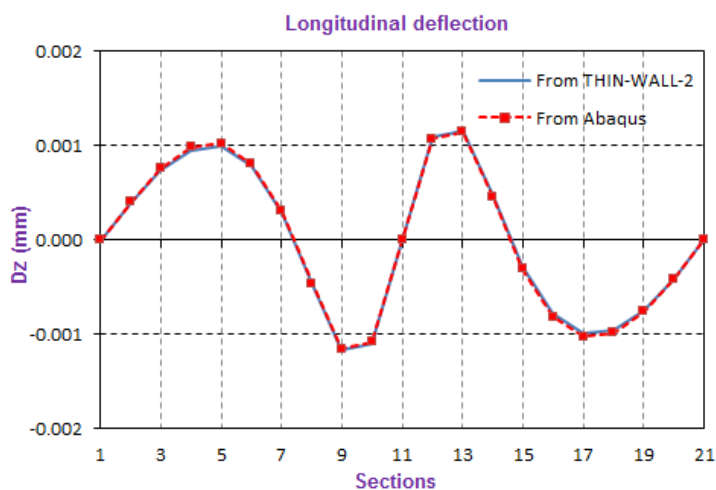
Figure B-28: Longitudinal pre-buckling deformation at Nodal Line 23 along the beam for the CC case

5. Both ends Free (FF)

Stress comparison:
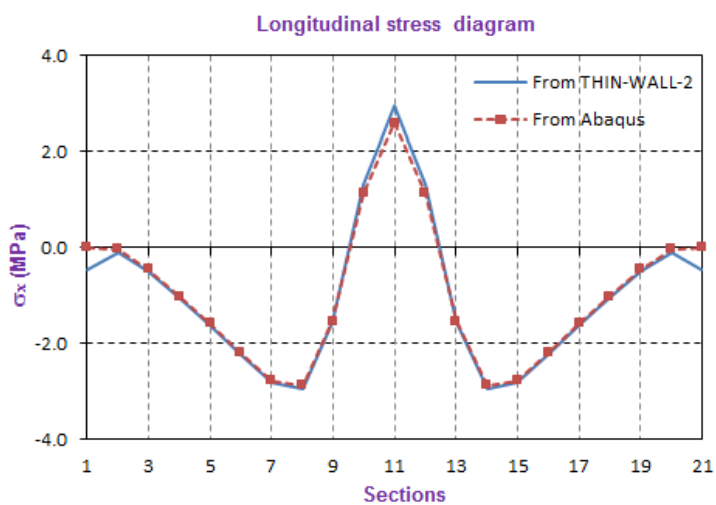
Figure B-29: Longitudinal stress at Nodal Line 23 along the beam for the FF case
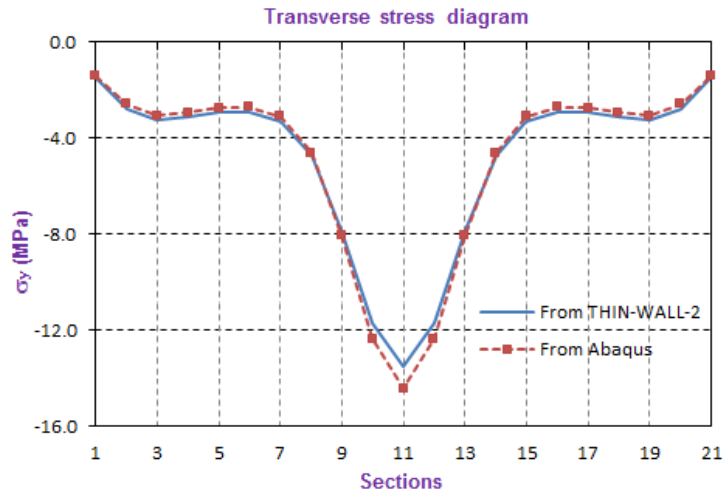
Figure B-30: Transverse stress at Nodal Line 23 along the beam for the FF case
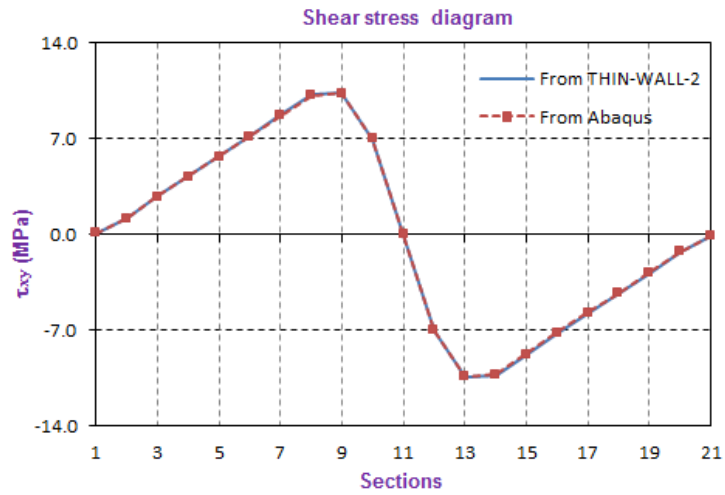
Figure B-31: Shear stress at Nodal Line 23 along the beam for the FF case

Pre-buckling deformation comparison:

(a) From THIN-WALL-2   (b) From Abaqus
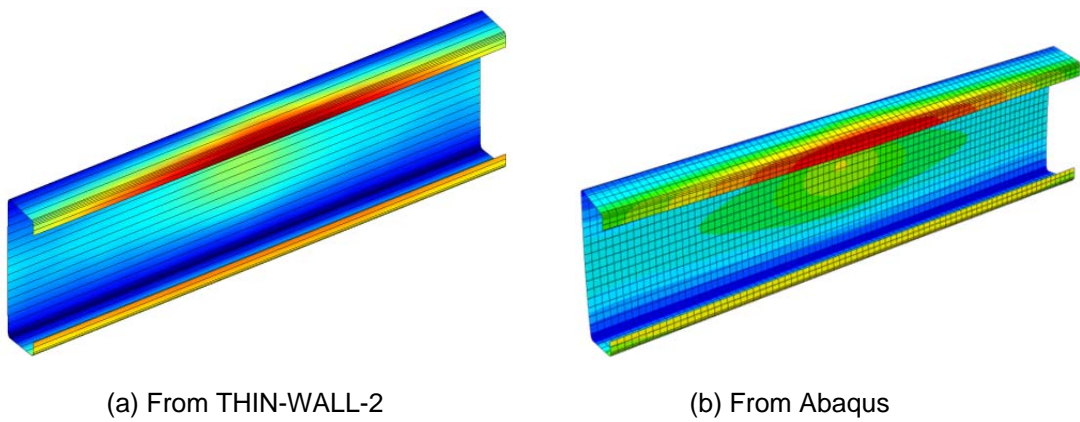
Figure B-32: Pre-buckling deformation comparison for the FF case
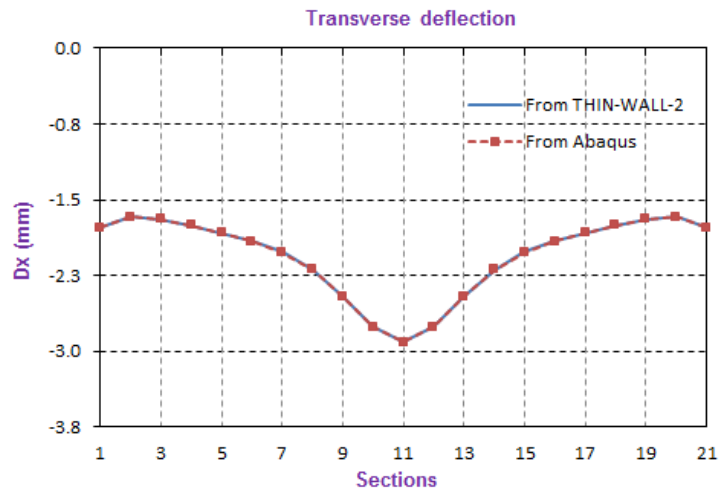
Figure B-33: Transverse pre-buckling deformation at Nodal Line 23 along the beam for the FF case
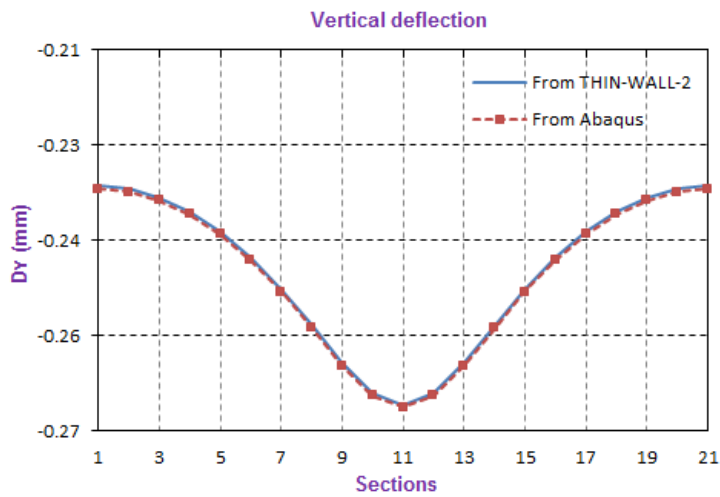
Figure B-34: Vertical pre-buckling deformation at Nodal Line 23 along the beam for the FF case
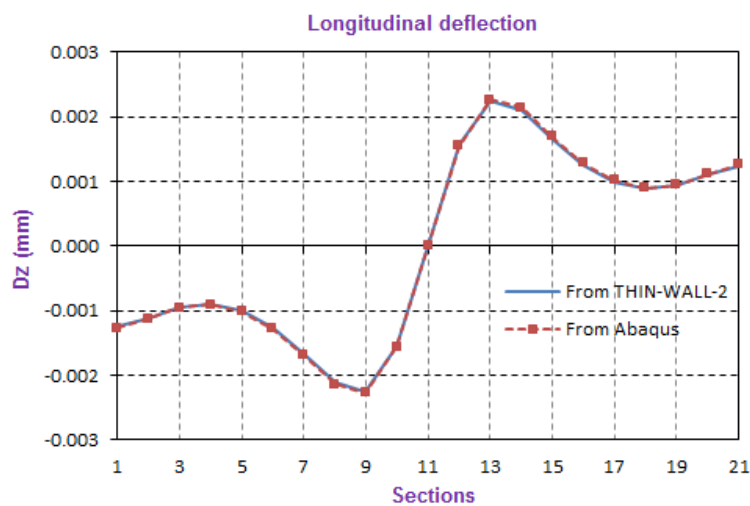
Figure B-35: Longitudinal pre-buckling deformation at Nodal Line 23 along the beam for the FF case

APPENDIX C: FLEXURAL AND MEMBRANE STABILITY MATRICES

1. Flexural stability matrix

The evaluation matrix of the flexural displacement functions at nodal line.

$$
[C_F] = \begin{bmatrix} 1 & 0 & 0 & 0 \\ 0 & \dfrac{1}{b} & 0 & 0 \\ 1 & 1 & 1 & 1 \\ 0 & \dfrac{1}{b} & \dfrac{2}{b} & \dfrac{3}{b} \end{bmatrix}
\qquad
[C_F]^{-1} = \begin{bmatrix} 1 & 0 & 0 & 0 \\ 0 & b & 0 & 0 \\ -3 & -2b & 3 & -b \\ 2 & b & -2 & b \end{bmatrix}
\tag{C-1}
$$

The property matrix of flexural displacement of a strip

$$
[D_F] = \begin{bmatrix} D_x & D_1 & 0 \\ D_1 & D_y & 0 \\ 0 & 0 & D_{xy} \end{bmatrix}
\tag{C-2}
$$

$$
D_x = \frac{E_x t^3}{12(1-\nu_y \nu_x)}
\qquad\qquad
D_y = \frac{E_y t^3}{12(1-\nu_y \nu_x)}
\tag{C-3}
$$

$$
D_1 = \nu_x D_y = \nu_y D_x
\qquad\qquad
D_{xy} = \frac{G t^3}{12}
$$

E_x, E_y are the moduli of elasticity of the longitudinal and transverse directions of a strip respectively

ν_x, ν_y are the poisson's ratios

G is the shear modulus of a strip

The strain matrix of flexural displacement

$$
[B_{Fk}] = \begin{bmatrix} -X_{1k}^{"} & -\overline{y} X_{1k}^{"} & -\overline{y}^2 X_{1k}^{"} & -\overline{y}^3 X_{1k}^{"} \\ 0 & 0 & -\dfrac{2}{b^2} X_{1k} & -\dfrac{6\overline{y}}{b^2} X_{1k} \\ 0 & \dfrac{2}{b} X_{1k}^{'} & \dfrac{4\overline{y}}{b} X_{1k}^{'} & \dfrac{6\overline{y}^2}{b} X_{1k}^{'} \end{bmatrix}
\tag{C-4}
$$

The flexural stability matrix of a strip:

$$
[g_{Fmn}] = [C_F]^{-T} [g_{\alpha Fmn}][C_F]^{-1}
\tag{C-5}
$$

$$\left[g_{\alpha Fmn} \right] = \begin{pmatrix} \left[g_{\alpha FL1mn} \right] + \left[g_{\alpha FL2mn} \right] + \left[g_{\alpha FT1mn} \right] + \left[g_{\alpha FT2mn} \right] + \\ + \left[g_{\alpha FS11mn} \right] + \left[g_{\alpha FS12mn} \right] + \left[g_{\alpha FS21mn} \right] + \left[g_{\alpha FS22mn} \right] \end{pmatrix} \tag{C-6}$$

Components of the flexural stability matrix

$$\left[g_{\alpha FL1mn} \right] = \left[\left(\frac{V}{\pi} \right) \sum_{k=1}^{\mu} \left(B_{FL1} C_{Lw1mnk} \right) \right] \tag{C-7}$$

$$\left[g_{\alpha FL2mn} \right] = \left[\left(\frac{V}{\pi} \right) \sum_{k=1}^{\mu} \left(B_{FL2} C_{Lw2mnk} \right) \right] \tag{C-8}$$

$$\left[g_{\alpha FT1mn} \right] = \left[\left(\frac{V}{\pi b^2} \right) \sum_{k=1}^{\mu} \left(B_{FT1} C_{T1mnk} \right) \right] \tag{C-9}$$

$$\left[g_{\alpha FT2mn} \right] = \left[\left(\frac{V}{\pi b^2} \right) \sum_{k=1}^{\mu} \left(B_{FT2} C_{T2mnk} \right) \right] \tag{C-10}$$

$$\left[g_{\alpha FS11mn} \right] = \left[\left(\frac{V}{\pi b} \right) \sum_{k=1}^{\mu} \left(B_{FS11} C_{S11mnk} \right) \right] \tag{C-11}$$

$$\left[g_{\alpha FS12mn} \right] = \left[\left(\frac{V}{\pi b} \right) \sum_{k=1}^{\mu} \left(B_{FS12} C_{S12mnk} \right) \right] \tag{C-12}$$

$$\left[g_{\alpha FS21mn} \right] = \left[\left(\frac{V}{\pi b} \right) \sum_{k=1}^{\mu} \left(B_{FS21} C_{S21mnk} \right) \right] \tag{C-13}$$

$$\left[g_{\alpha FS22mn} \right] = \left[\left(\frac{V}{\pi b} \right) \sum_{k=1}^{\mu} \left(B_{FS22} C_{S22mnk} \right) \right] \tag{C-14}$$

V is the strip volume, *V=bLt*

Matrices for calculation of the flexural stability matrix

$$B_{FL1} = \begin{bmatrix} \left(\sigma_{L1k} \right) & \left(\dfrac{\sigma_{L1k}}{2} \right) & \left(\dfrac{\sigma_{L1k}}{3} \right) & \left(\dfrac{\sigma_{L1k}}{4} \right) \\ \left(\dfrac{\sigma_{L1k}}{2} \right) & \left(\dfrac{\sigma_{L1k}}{3} \right) & \left(\dfrac{\sigma_{L1k}}{4} \right) & \left(\dfrac{\sigma_{L1k}}{5} \right) \\ \left(\dfrac{\sigma_{L1k}}{3} \right) & \left(\dfrac{\sigma_{L1k}}{4} \right) & \left(\dfrac{\sigma_{L1k}}{5} \right) & \left(\dfrac{\sigma_{L1k}}{6} \right) \\ \left(\dfrac{\sigma_{L1k}}{4} \right) & \left(\dfrac{\sigma_{L1k}}{5} \right) & \left(\dfrac{\sigma_{L1k}}{6} \right) & \left(\dfrac{\sigma_{L1k}}{7} \right) \end{bmatrix} \tag{C-15}$$

$$B_{FL2} = \begin{bmatrix} \left(\sigma_{L2k} + \dfrac{\sigma_{L3k}}{2}\right) & \left(\dfrac{\sigma_{L2k}}{2} + \dfrac{\sigma_{L3k}}{3}\right) & \left(\dfrac{\sigma_{L2k}}{3} + \dfrac{\sigma_{L3k}}{4}\right) & \left(\dfrac{\sigma_{L2k}}{4} + \dfrac{\sigma_{L3k}}{5}\right) \\ \left(\dfrac{\sigma_{L2k}}{2} + \dfrac{\sigma_{L3k}}{3}\right) & \left(\dfrac{\sigma_{L2k}}{3} + \dfrac{\sigma_{L3k}}{4}\right) & \left(\dfrac{\sigma_{L2k}}{4} + \dfrac{\sigma_{L3k}}{5}\right) & \left(\dfrac{\sigma_{L2k}}{5} + \dfrac{\sigma_{L3k}}{6}\right) \\ \left(\dfrac{\sigma_{L2k}}{3} + \dfrac{\sigma_{L3k}}{4}\right) & \left(\dfrac{\sigma_{L2k}}{4} + \dfrac{\sigma_{L3k}}{5}\right) & \left(\dfrac{\sigma_{L2k}}{5} + \dfrac{\sigma_{L3k}}{6}\right) & \left(\dfrac{\sigma_{L2k}}{6} + \dfrac{\sigma_{L3k}}{7}\right) \\ \left(\dfrac{\sigma_{L2k}}{4} + \dfrac{\sigma_{L3k}}{5}\right) & \left(\dfrac{\sigma_{L2k}}{5} + \dfrac{\sigma_{L3k}}{6}\right) & \left(\dfrac{\sigma_{L2k}}{6} + \dfrac{\sigma_{L3k}}{7}\right) & \left(\dfrac{\sigma_{L2k}}{7} + \dfrac{\sigma_{L3k}}{8}\right) \end{bmatrix} \tag{C-16}$$

$$B_{FT1} = \begin{bmatrix} 0 & 0 & 0 & 0 \\ 0 & \sigma_{T1k} & \sigma_{T1k} & \sigma_{T1k} \\ 0 & \sigma_{T1k} & \dfrac{4\sigma_{T1k}}{3} & \dfrac{6\sigma_{T1k}}{4} \\ 0 & \sigma_{T1k} & \dfrac{6\sigma_{T1k}}{4} & \dfrac{9\sigma_{T1k}}{5} \end{bmatrix} \qquad B_{FT2} = \begin{bmatrix} 0 & 0 & 0 & 0 \\ 0 & \sigma_{T2k} & \sigma_{T2k} & \sigma_{T2k} \\ 0 & \sigma_{T2k} & \dfrac{4\sigma_{T2k}}{3} & \dfrac{6\sigma_{T2k}}{4} \\ 0 & \sigma_{T2k} & \dfrac{6\sigma_{T2k}}{4} & \dfrac{9\sigma_{T2k}}{5} \end{bmatrix} \tag{C-17}$$

$$B_{FS11} = \begin{bmatrix} 0 & \tau_{1k} & \tau_{1k} & \tau_{1k} \\ 0 & \dfrac{\tau_{1k}}{2} & \dfrac{2\tau_{1k}}{3} & \dfrac{3\tau_{1k}}{4} \\ 0 & \dfrac{\tau_{1k}}{3} & \dfrac{2\tau_{1k}}{4} & \dfrac{3\tau_{1k}}{5} \\ 0 & \dfrac{\tau_{1k}}{4} & \dfrac{2\tau_{1k}}{5} & \dfrac{3\tau_{1k}}{6} \end{bmatrix} \qquad B_{FS12} = \begin{bmatrix} 0 & \tau_{2k} & \tau_{2k} & \tau_{2k} \\ 0 & \dfrac{\tau_{2k}}{2} & \dfrac{2\tau_{2k}}{3} & \dfrac{3\tau_{2k}}{4} \\ 0 & \dfrac{\tau_{2k}}{3} & \dfrac{2\tau_{2k}}{4} & \dfrac{3\tau_{2k}}{5} \\ 0 & \dfrac{\tau_{2k}}{4} & \dfrac{2\tau_{2k}}{5} & \dfrac{3\tau_{2k}}{6} \end{bmatrix} \tag{C-18}$$

$$B_{FS21} = \begin{bmatrix} 0 & 0 & 0 & 0 \\ \tau_{1k} & \dfrac{\tau_{1k}}{2} & \dfrac{\tau_{1k}}{3} & \dfrac{\tau_{1k}}{4} \\ \tau_{1k} & \dfrac{2\tau_{1k}}{3} & \dfrac{2\tau_{1k}}{4} & \dfrac{2\tau_{1k}}{5} \\ \tau_{1k} & \dfrac{3\tau_{1k}}{4} & \dfrac{3\tau_{1k}}{5} & \dfrac{3\tau_{1k}}{6} \end{bmatrix} \qquad B_{FS22} = \begin{bmatrix} 0 & 0 & 0 & 0 \\ \tau_{2k} & \dfrac{\tau_{2k}}{2} & \dfrac{\tau_{2k}}{3} & \dfrac{\tau_{2k}}{4} \\ \tau_{2k} & \dfrac{2\tau_{2k}}{3} & \dfrac{2\tau_{2k}}{4} & \dfrac{2\tau_{2k}}{5} \\ \tau_{2k} & \dfrac{3\tau_{2k}}{4} & \dfrac{3\tau_{2k}}{5} & \dfrac{3\tau_{2k}}{6} \end{bmatrix} \tag{C-19}$$

Integrals for calculation of the flexural stability matrix

$$C_{L1wmnk} = \int_0^{\xi=\pi} X_{1m}^{'}(\xi)\,\sigma_{1k}(\xi)\,X_{1n}^{'}(\xi)\,d\xi \tag{C-20}$$

$$C_{L2wmnk} = \int_0^{\xi=\pi} X_{1m}^{'}(\xi)\,\sigma_{2k}(\xi)\,X_{1n}^{'}(\xi)\,d\xi \tag{C-21}$$

$$C_{T1mnk} = \int_0^{\xi=\pi} X_{1m}(\xi)\,\sigma_{1k}(\xi)\,X_{1n}(\xi)\,d\xi \tag{C-22}$$

$$C_{T2mnk} = \int\limits_{0}^{\xi=\pi} X_{1m}(\xi)\,\sigma_{2k}(\xi)\,X_{1n}(\xi)\,d\xi \tag{C-23}$$

$$C_{S11mnk} = \int\limits_{0}^{\xi=\pi} X_{1m}^{'}(\xi)\,\tau_{1k}(\xi)\,X_{1n}(\xi)\,d\xi \tag{C-24}$$

$$C_{S12mnk} = \int\limits_{0}^{\xi=\pi} X_{1m}^{'}(\xi)\,\tau_{2k}(\xi)\,X_{1n}(\xi)\,d\xi \tag{C-25}$$

$$C_{S21mnk} = \int\limits_{0}^{\xi=\pi} X_{1m}(\xi)\,\tau_{1k}(\xi)\,X_{1n}^{'}(\xi)\,d\xi \tag{C-26}$$

$$C_{S22mnk} = \int\limits_{0}^{\xi=\pi} X_{1m}(\xi)\,\tau_{2k}(\xi)\,X_{1n}^{'}(\xi)\,d\xi \tag{C-27}$$

$\xi = \left(\dfrac{\pi x}{L}\right)$, when x changes from 0 to L, then ξ changes from 0 to π

$\overline{y} = \dfrac{y}{b}$, when y changes from 0 to b, then $\overline{y}$ changes from 0 to 1

$$X_{1m}^{'} = \frac{d\left(X_{1m}(\xi)\right)}{dx} = \left(\frac{\pi}{L}\right)\frac{d\left(X_{1m}(\xi)\right)}{d\left(\dfrac{\pi x}{L}\right)} = \left(\frac{\pi}{L}\right)\frac{d\left(X_{1m}(\xi)\right)}{d\xi}$$

$$X_{1m}^{''} = \left(\frac{\pi}{L}\right)^2 \frac{d^2\left(X_{1m}(\xi)\right)}{d\xi^2}$$

Stress functions

$$\sigma_{1k}(x) = X_{1k}(x) \text{ and } \sigma_{2k}(x) = X_{2k}^{'}(x) \tag{C-28}$$

$$\tau_{1k}(x) = X_{1m}^{'}(x) \text{ and } \tau_{2k}(x) = X_{2m}(x) \tag{C-29}$$

$$\sigma_{L1k} = \alpha_{2Mm}\frac{E_{12}}{b}; \sigma_{L2k} = \alpha_{3Mm}E_2 \text{ and } \sigma_{L3k} = \alpha_{4Mm}E_2 \tag{C-30}$$

$$\sigma_{T1k} = \alpha_{2Mm}\frac{E_1}{b} \text{ and } \sigma_{T2k} = \left[\alpha_{3Mm}E_{12} + \frac{1}{2}\alpha_{4Mm}E_{12}\right] \tag{C-31}$$

$$\tau_{1k} = \left[\alpha_{1Mm}G + \frac{1}{2}\alpha_{2Mm}G\right] \text{ and } \tau_{2k} = \alpha_{4Mm}\frac{G}{b} \tag{C-32}$$

2. Membrane stability matrix

The evaluation matrix of the membrane displacement functions at nodal line.

$$[C_M] = \begin{bmatrix} 1 & 0 & 0 & 0 \\ 0 & 0 & 1 & 0 \\ 1 & 1 & 0 & 0 \\ 0 & 0 & 1 & 1 \end{bmatrix} \qquad [C_M]^{-1} = \begin{bmatrix} 1 & 0 & 0 & 0 \\ -1 & 0 & 1 & 0 \\ 0 & 1 & 0 & 0 \\ 0 & -1 & 0 & 1 \end{bmatrix}$$ (C-33)

The property matrix of membrane displacement

$$[D_M] = \begin{bmatrix} E_2 & E_{12} & 0 \\ E_{12} & E_1 & 0 \\ 0 & 0 & G \end{bmatrix}$$ (C-34)

$$E_2 = \frac{E_x}{(1-\nu_y\nu_x)}; \qquad E_1 = \frac{E_y}{(1-\nu_y\nu_x)};$$ (C-35)

$$E_{12} = \frac{\nu_x E_y}{(1-\nu_y\nu_x)} = \frac{\nu_y E_x}{(1-\nu_y\nu_x)}$$

The strain matrix of membrane displacement

$$[B_{Mm}] = \begin{bmatrix} 0 & 0 & X'_{2m} & \bar{y}X'_{2m} \\ 0 & \dfrac{1}{b}X_{1m} & 0 & 0 \\ X'_{1m} & \bar{y}X'_{1m} & 0 & \dfrac{1}{b}X_{2m} \end{bmatrix}$$ (C-26)

The membrane stability matrix of a strip:

$$[g_{Mmn}] = [C_M]^{-T}[g_{\alpha Mmn}][C_M]^{-1}$$ (C-37)

$$[g_{\alpha Mmn}] = \left([g_{\alpha Mv1mn}] + [g_{\alpha Mv2mn}] + [g_{\alpha Mu1mn}] + [g_{\alpha Mu2mn}]\right)$$ (C-38)

Components of the membrane stability matrix

$$[g_{\alpha Mv1mn}] = \left[\left(\frac{V}{\pi}\right)\sum_{k=1}^{\mu}\left(B_{Mv1}C_{Lv1mnk}\right)\right]$$ (C-39)

$$[g_{\alpha Mv2mn}] = \left[\left(\frac{V}{\pi}\right)\sum_{k=1}^{\mu}\left(B_{Mv2}C_{Lv2mnk}\right)\right]$$ (C-40)

$$[g_{\alpha Mu1mn}] = \left[\left(\frac{V}{\pi}\right)\sum_{k=1}^{\mu}\left(B_{Mu1}C_{Lu1mnk}\right)\right]$$ (C-41)

$$[g_{\alpha Mu2mn}] = \left[\left(\frac{V}{\pi}\right)\sum_{k=1}^{\mu}\left(B_{Mu2}C_{Lu2mnk}\right)\right]$$ (C-42)

Matrices for calculation of the membrane stability matrix

$$B_{Mv1} = \begin{bmatrix} \left(\sigma_{L1k}\right) & \left(\dfrac{\sigma_{L1k}}{2}\right) & 0 & 0 \\[2mm] \left(\dfrac{\sigma_{L1k}}{2}\right) & \left(\dfrac{\sigma_{L1k}}{3}\right) & 0 & 0 \\[2mm] 0 & 0 & 0 & 0 \\[1mm] 0 & 0 & 0 & 0 \end{bmatrix}$$

(C-43)

$$B_{Mv2} = \begin{bmatrix} \left(\sigma_{L2k} + \dfrac{\sigma_{L3k}}{2}\right) & \left(\dfrac{\sigma_{L2k}}{2} + \dfrac{\sigma_{L3k}}{3}\right) & 0 & 0 \\[2mm] \left(\dfrac{\sigma_{L2k}}{2} + \dfrac{\sigma_{L3k}}{3}\right) & \left(\dfrac{\sigma_{L2k}}{3} + \dfrac{\sigma_{L3k}}{4}\right) & 0 & 0 \\[2mm] 0 & 0 & 0 & 0 \\[1mm] 0 & 0 & 0 & 0 \end{bmatrix}$$

(C-44)

$$B_{Mu1} = \begin{bmatrix} 0 & 0 & 0 & 0 \\[1mm] 0 & 0 & 0 & 0 \\[1mm] 0 & 0 & \left(\sigma_{L1k}\right) & \left(\dfrac{\sigma_{L1k}}{2}\right) \\[2mm] 0 & 0 & \left(\dfrac{\sigma_{L1k}}{2}\right) & \left(\dfrac{\sigma_{L1k}}{3}\right) \end{bmatrix}$$

(C-45)

$$B_{Mu2} = \begin{bmatrix} 0 & 0 & 0 & 0 \\[1mm] 0 & 0 & 0 & 0 \\[1mm] 0 & 0 & \left(\sigma_{L2k} + \dfrac{\sigma_{L3k}}{2}\right) & \left(\dfrac{\sigma_{L2k}}{2} + \dfrac{\sigma_{L3k}}{3}\right) \\[2mm] 0 & 0 & \left(\dfrac{\sigma_{L2k}}{2} + \dfrac{\sigma_{L3k}}{3}\right) & \left(\dfrac{\sigma_{L2k}}{3} + \dfrac{\sigma_{L3k}}{4}\right) \end{bmatrix}$$

(C-46)

Integrals for calculation of the membrane stability matrix

$$C_{Lv1mnk} = \int_{0}^{\xi=\pi} X_{1m}^{'}\left(\xi\right)\sigma_{1k}\left(\xi\right)X_{1n}^{'}\left(\xi\right)d\xi = C_{L1wmnk}$$

(C-47)

$$C_{Lv2mnk} = \int_{0}^{\xi=\pi} X_{1m}^{'}\left(\xi\right)\sigma_{2k}\left(\xi\right)X_{1n}^{'}\left(\xi\right)d\xi = C_{L2wmnk}$$

(C-48)

$$C_{Lu1mnk} = \int_{0}^{\xi=\pi} X_{2m}^{'}\left(\xi\right)\sigma_{1k}\left(\xi\right)X_{2n}^{'}\left(\xi\right)d\xi$$

(C-49)

$$C_{Lu2mnk} = \int_{0}^{\xi=\pi} X_{2m}^{'}\left(\xi\right)\sigma_{2k}\left(\xi\right)X_{2n}^{'}\left(\xi\right)d\xi$$

(C-50)

APPENDIX D: BUCKLING COMPARISON BETWEEN THE FINITE STRIP METHOD AND THE FINITE ELEMENT METHOD FOR DIFFERENT BOUNDARY CONDITIONS

1. Both ends Simply supported (SS)

Buckling deformation comparison:

(a) From THIN-WALL-2   (b) From Abaqus
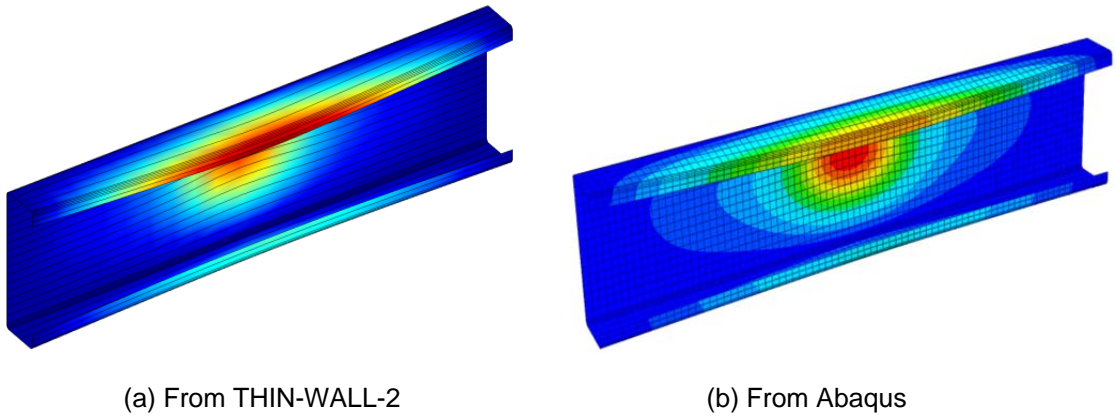
Figure D-1: Buckling deformation comparison for the SS case
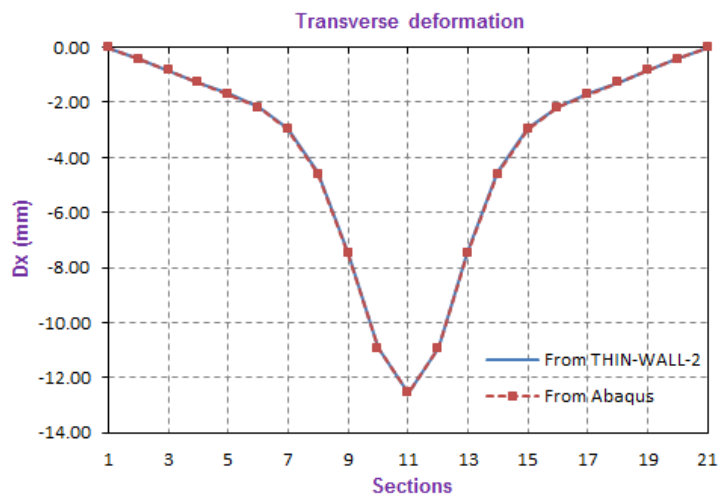
Figure D-2: Transverse buckling deformation at Nodal Line 23 along the beam for the SS case
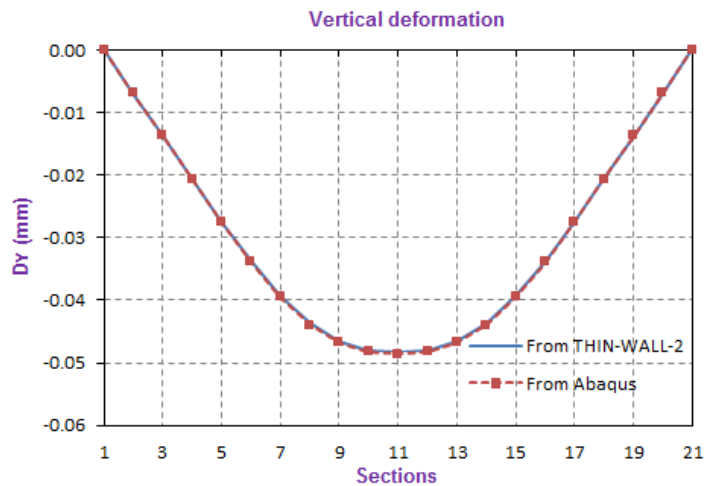
Figure D-3: Vertical buckling deformation at Nodal Line 23 along the beam for the SS case
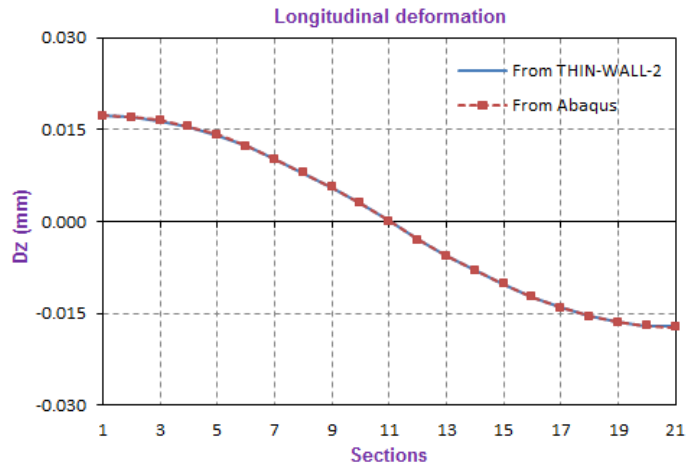
Figure D-4: Longitudinal buckling deformation at Nodal Line 23 along the beam for the SS case

For the SS case, the selected maximum buckling deformation is -12.545 mm to obtain the buckling deformation in other sections and directions without scale factors.

2. One end Simply supported and one end Clamped (SC)

Buckling deformation comparison:

(a) From THIN-WALL-2   (b) From Abaqus
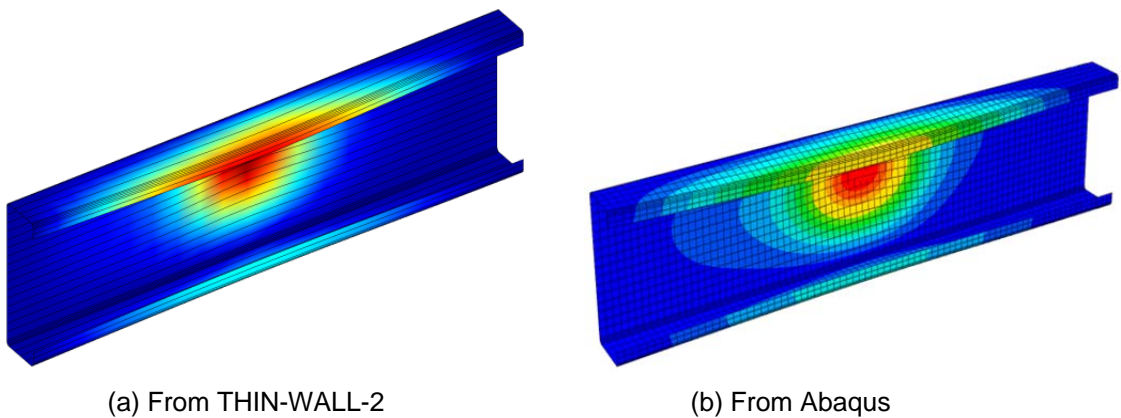
Figure D-5: Buckling deformation comparison for the SC case
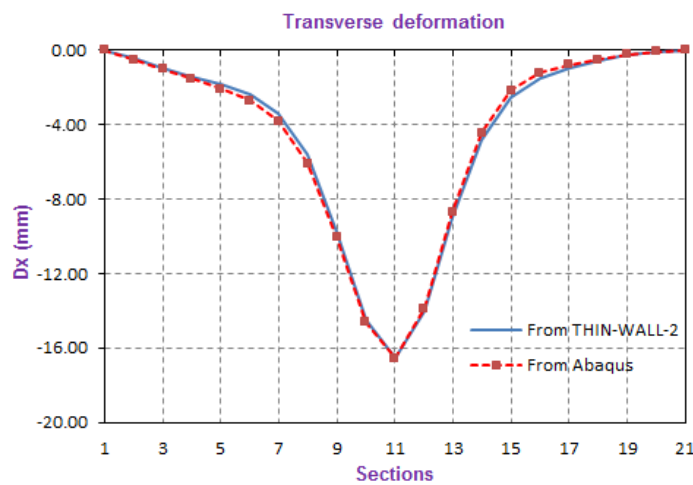
Figure D-6: Transverse buckling deformation at Nodal Line 23 along the beam for the SC case
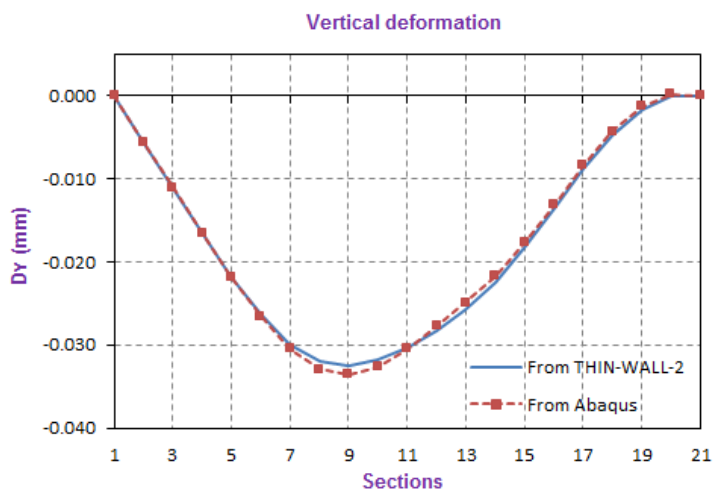
Figure D-7: Vertical buckling deformation at Nodal Line 23 along the beam for the SC case
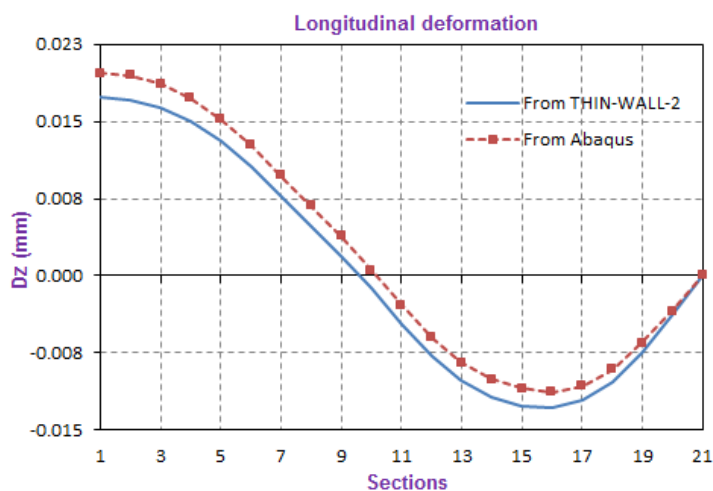
Figure D-8: Longitudinal buckling deformation at Nodal Line 23 along the beam for the SC case

For the SC case, the selected maximum buckling deformation is -16.527 mm to obtain the buckling deformation in other sections and directions without scale factors.

3. One end Simply supported and one end Free (SF)

Buckling deformation comparison:

(a) From THIN-WALL-2   (b) From Abaqus
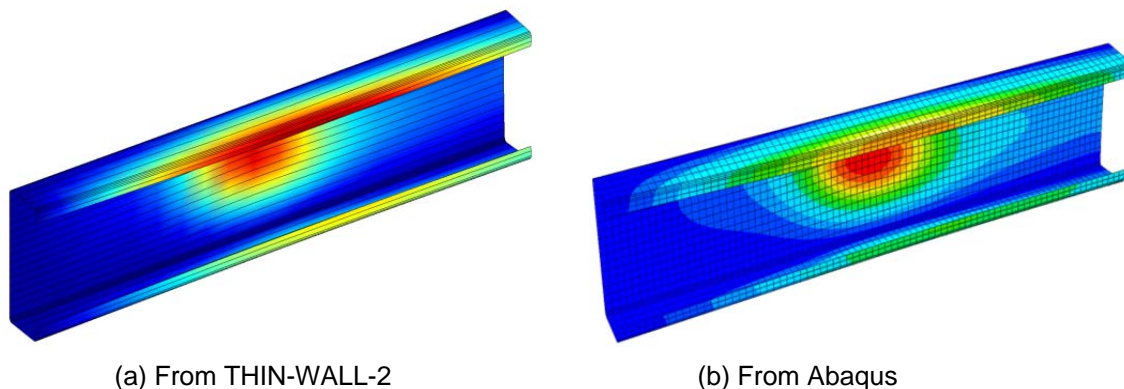
Figure D-9: Buckling deformation comparison for the SF case
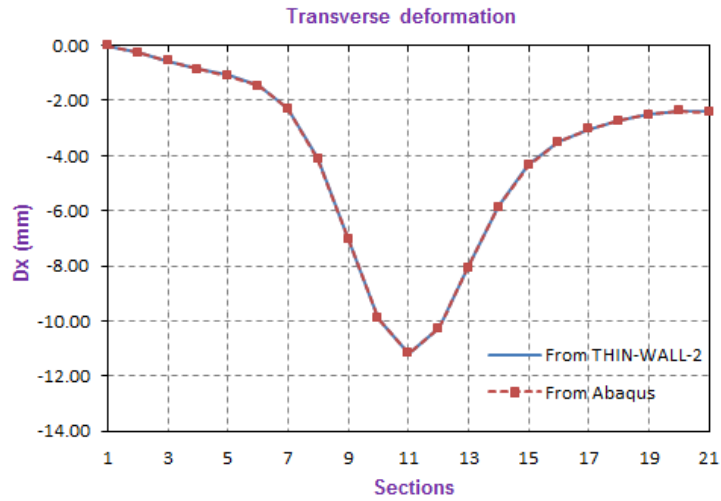
Figure D-10: Transverse buckling deformation at Nodal Line 23 along the beam for the SF case
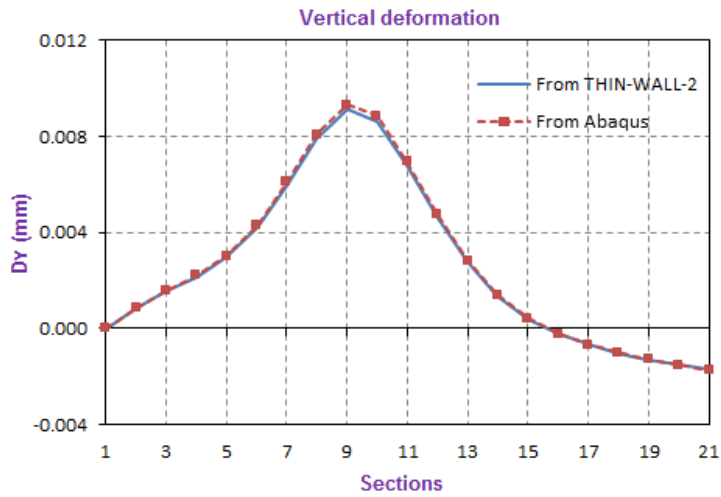
Figure D-11: Vertical buckling deformation at Nodal Line 23 along the beam for the SF case
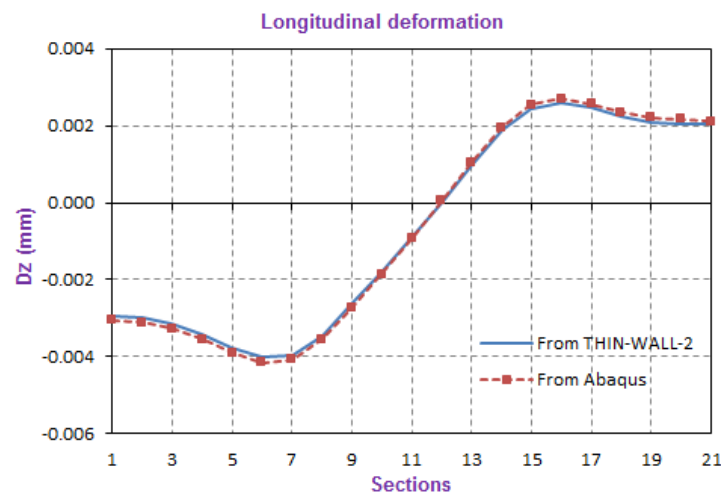
Figure D-12: Longitudinal buckling deformation at Nodal Line 23 along the beam for the SF case

For the SF case, the selected maximum buckling deformation is -11.173 mm to obtain the buckling deformation in other sections and directions without scale factors.

4. Both ends Clamped (CC)

Buckling deformation comparison:

(a) From THIN-WALL-2   (b) From Abaqus
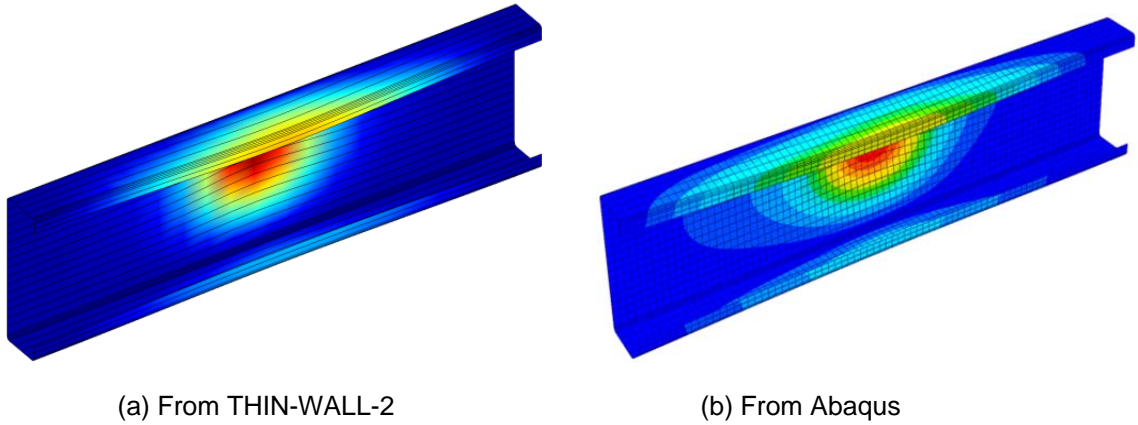
Figure D-13: Buckling deformation comparison for the CC case
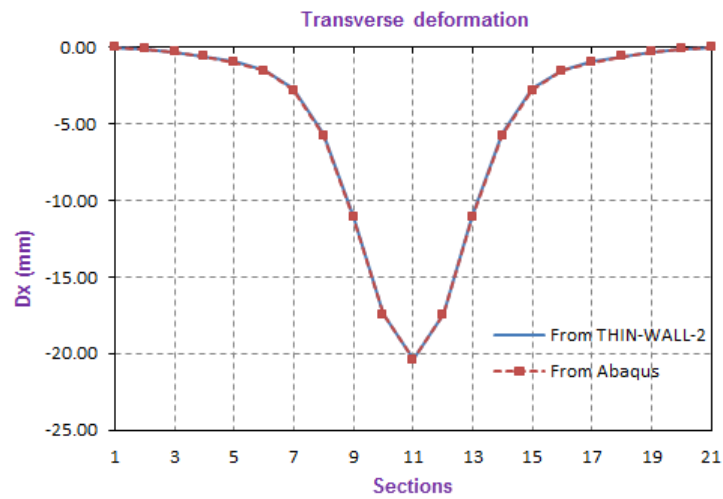
Figure D-14: Transverse buckling deformation at Nodal Line 23 along the beam for the CC case
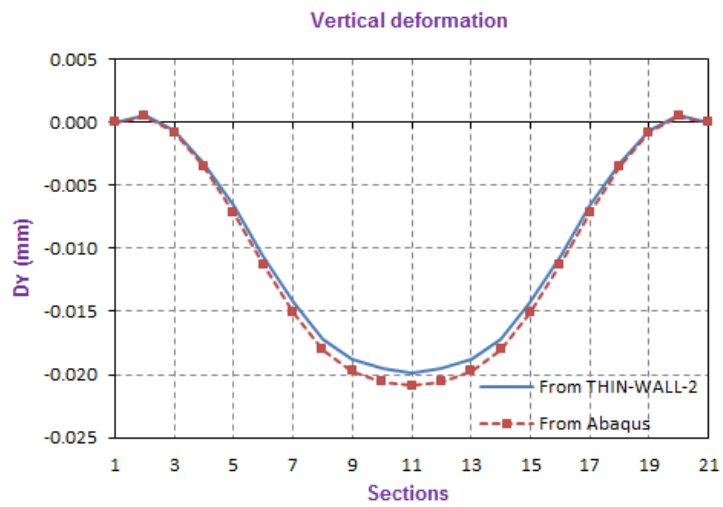
Figure D-15: Vertical buckling deformation at Nodal Line 23 along the beam for the CC case
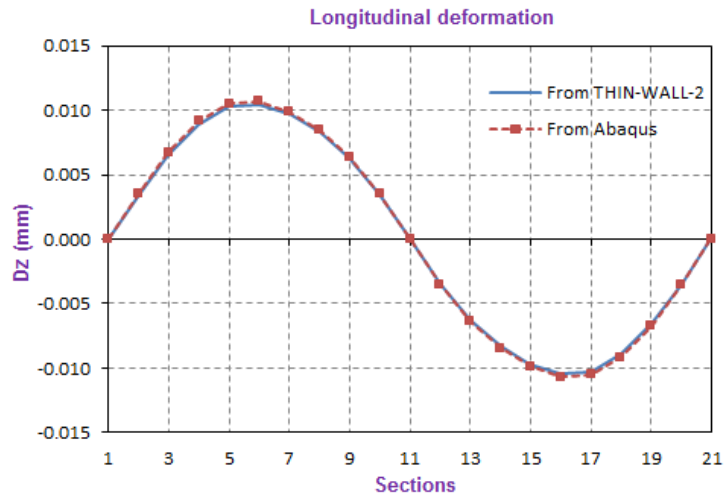
Figure D-16: Longitudinal buckling deformation at Nodal Line 23 along the beam for the CC case

For the CC case, the selected maximum buckling deformation is -20.395 mm to obtain the buckling deformation in other sections and directions without scale factors.

5. Both ends Free (FF)

Buckling deformation comparison:

(a) From THIN-WALL-2   (b) From Abaqus
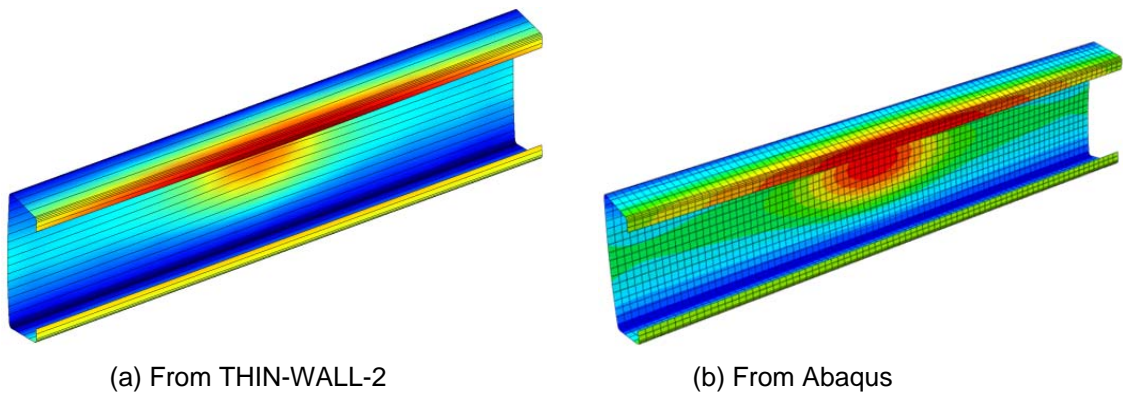
Figure D-17: Buckling deformation comparison for the FF case
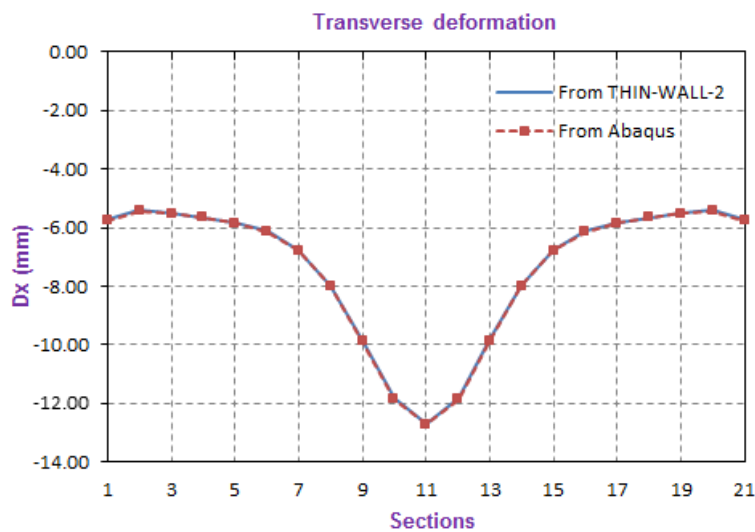
Figure D-18: Transverse buckling deformation at Nodal Line 23 along the beam for the FF case
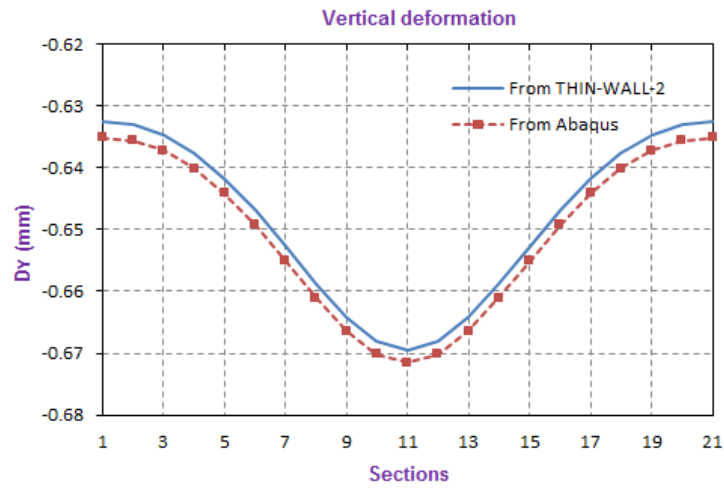
Figure D-19: Vertical buckling deformation at Nodal Line 23 along the beam for the FF case
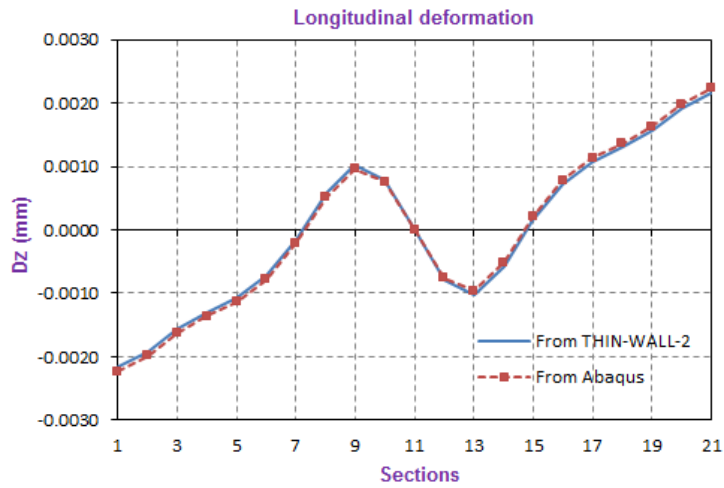
Figure D-20: Longitudinal buckling deformation at Nodal Line 23 along the beam for the FF case

For the CF case, the selected maximum buckling deformation is -12.713 mm to obtain the buckling deformation in other sections and directions without scale factors.

APPENDIX E: EXPERIMENTAL DATA, BUCKLING LOADS AND YIELD LOADS FOR WEB CRIPPLING.

1. Beshara and Schuster [36] (2000)

Table E-1: Lipped plain-C sections under the ITF load case

Specimens	Wed D (mm)	Flanges B_f (mm)	Lips L (mm)	Thickness t_w (mm)	r_1 (mm)	r_2 (mm)	Length L_o (mm)	Yield strength f_y (MPa)	Yield load P_y (kN)	Buckling load P_{cr} (kN)	Experiment load P_{exp} (kN)
C120-7-30F	121.00	62.80	27.60	1.45	7.00	7.00	610	332.00	6.64	21.28	10.70
C120-7-60F	121.00	62.70	27.50	1.45	7.00	7.00	610	332.00	7.96	21.82	11.80
C120-10-30F	121.00	68.10	30.40	1.45	10.00	10.00	610	332.00	6.14	23.44	9.96
C120-10-60F	121.00	68.00	30.10	1.45	10.00	10.00	610	332.00	7.36	24.75	11.00
C120-14-30F	118.00	82.10	28.20	1.45	14.00	14.00	610	332.00	5.66	23.33	9.06
C120-14-60F	118.00	82.30	28.40	1.45	14.00	14.00	610	332.00	6.81	25.02	10.10
C200-7-30F	200.00	67.32	32.40	1.16	7.00	7.00	1220	328.00	7.66	6.51	7.20
C200-7-60F	200.00	66.72	32.20	1.16	7.00	7.00	1220	328.00	8.65	6.57	7.56
C200-10-30F	199.00	78.62	31.30	1.16	10.00	10.00	1220	328.00	7.12	6.64	6.57
C200-10-60F	200.00	78.92	31.00	1.16	10.00	10.00	1220	328.00	8.08	6.79	7.08
C200-14-60F	201.00	91.32	27.90	1.16	14.00	14.00	1220	328.00	7.71	5.88	6.72
C200-14-100F	201.00	90.52	27.80	1.16	14.00	14.00	1220	328.00	8.69	6.21	7.08
C300-7-30F	300.00	62.20	16.30	1.45	7.00	7.00	1500	448.00	19.86	7.17	11.00
C300-7-60F	300.00	63.70	15.90	1.45	7.00	7.00	1500	448.00	21.65	7.21	11.60
C300-10-30F	299.00	68.30	17.40	1.45	10.00	10.00	1500	448.00	18.29	8.59	9.99
C300-10-60F	300.00	71.60	19.40	1.45	10.00	10.00	1500	448.00	19.99	8.56	10.90
C300-14-60F	300.00	82.60	18.50	1.45	14.00	14.00	1500	448.00	18.84	9.19	11.30
C300-14-100F	300.00	81.80	19.60	1.45	14.00	14.00	1500	448.00	20.57	9.43	10.60

2. Young and Hancock [22] (2001)

Table E-2: Unlipped plain-C sections under the IOF load case

Specimens	Depth D (mm)	Flanges Bf (mm)	Lips L (mm)	Thickness tw (mm)	Radius ri (mm)	Length Lo (mm)	Yield strength fy (MPa)	Yield load Py (kN)	Buckling load Pcr (kN)	Experiment load Pexp (kN)
IOF75N40A	74.60	40.40	0.00	3.85	3.90	444.30	450.00	27.53	210.56	49.00
IOF75N40B	74.60	40.30	0.00	3.85	3.90	446.80	450.00	27.53	210.60	49.00
IOF75N20A	74.60	40.40	0.00	3.86	3.90	424.80	450.00	28.87	216.74	47.20
IOF75N20B	74.50	40.40	0.00	3.86	3.90	424.10	450.00	28.83	216.74	47.20
IOF100N50A	99.20	50.40	0.00	3.83	4.10	529.20	440.00	35.06	187.56	57.90
IOF100N50B	99.20	50.50	0.00	3.83	4.10	530.90	440.00	35.06	187.56	57.90
IOF100N25A	99.20	50.40	0.00	3.84	4.10	505.00	440.00	36.66	194.58	56.30
IOF100N25B	99.30	50.40	0.00	3.84	4.10	506.00	440.00	36.70	194.58	56.30
IOF125N65A	125.00	65.70	0.00	3.86	3.90	618.50	405.00	41.78	165.75	63.60
IOF125N65B	125.00	65.60	0.00	3.86	3.90	619.30	405.00	41.78	165.75	63.60
IOF125N32A	125.00	65.50	0.00	3.86	3.90	587.00	405.00	43.63	171.36	57.40
IOF125N32B	125.00	65.70	0.00	3.86	3.90	586.80	405.00	43.63	171.36	57.40
IOF200N75A	198.90	75.90	0.00	4.74	4.20	855.20	415.00	90.04	264.15	94.50
IOF200N75B	198.70	75.90	0.00	4.73	4.20	854.20	415.00	89.68	264.15	94.50
IOF200N37A	198.70	75.90	0.00	4.72	4.20	816.80	415.00	92.21	260.04	91.20
IOF200N37B	198.80	75.90	0.00	4.74	4.20	817.50	415.00	92.80	260.04	91.20
IOF250N90A	249.80	89.90	0.00	5.99	7.90	1023.00	445.00	132.05	440.64	142.80
IOF250N90B	249.60	89.80	0.00	5.99	7.90	1020.00	445.00	131.94	440.64	142.80
IOF250N45A	249.20	90.00	0.00	5.98	7.90	974.30	445.00	135.28	436.46	132.30
IOF250N45B	249.30	90.00	0.00	5.99	7.90	976.40	445.00	135.65	436.46	132.30
IOF300N90A	298.70	91.30	0.00	6.00	8.40	1169.00	435.00	152.61	392.85	143.40
IOF300N90B	298.80	90.90	0.00	6.00	8.40	1169.80	435.00	152.66	392.85	143.40
IOF300N45A	298.60	91.30	0.00	6.00	8.40	1125.00	435.00	156.26	388.58	134.60
IOF300N45B	298.50	91.30	0.00	6.00	8.40	1124.30	435.00	156.21	388.58	134.60

Table E-3: Unlipped plain-C sections under the EOF load case

Specimens	Depth D (mm)	Flanges B$_f$ (mm)	Lips L (mm)	Thickness t$_w$ (mm)	Radius r$_i$ (mm)	web d$_1$ (mm)	Length L$_o$ (mm)	Yield strength f$_f$ (MPa)	Yield load P$_y$ (kN)	Buckling load P$_{cr}$ (kN)	Experiment load P$_{exp}$ (kN)
EOF75N40A	74.50	40.20	0.00	3.84	3.90	59.02	397.00	450	15.35	270.21	23.90
EOF75N40B	74.40	40.30	0.00	3.84	3.90	58.92	396.00	450	15.34	271.43	23.90
EOF75N20A	74.30	40.30	0.00	3.84	3.90	58.82	355.20	450	12.27	219.18	24.60
EOF75N20B	74.40	40.40	0.00	3.84	3.90	58.92	354.00	450	12.28	219.18	24.60
EOF100N50A	99.30	50.40	0.00	3.85	4.10	83.4	490.00	440	19.21	211.63	34.40
EOF100N50B	99.30	50.40	0.00	3.85	4.10	83.4	490.70	440	19.21	211.58	34.40
EOF100N25A	99.30	50.50	0.00	3.85	4.10	83.4	440.00	440	15.54	166.10	31.40
EOF100N25B	99.20	50.40	0.00	3.83	4.10	83.34	439.70	440	15.41	163.74	31.40
EOF125N65A	125.00	65.50	0.00	3.85	3.90	109.5	594.00	405	22.97	177.02	35.30
EOF125N65B	124.90	65.50	0.00	3.84	3.90	109.42	593.40	405	22.88	188.92	35.30
EOF125N32A	125.60	65.70	0.00	3.84	3.90	110.12	528.80	405	18.42	133.19	29.70
EOF125N32B	125.40	65.60	0.00	3.84	3.90	109.92	529.20	405	18.40	133.43	29.70
EOF200N75A	198.70	75.80	0.00	4.71	4.20	180.88	839.80	415	42.91	164.41	49.30
EOF200N75B	198.80	75.80	0.00	4.71	4.20	180.98	839.50	415	42.92	164.28	49.30
EOF200N37A	198.80	76.00	0.00	4.72	4.20	180.96	764.60	415	36.13	134.73	43.70
EOF200N37B	198.80	75.80	0.00	4.74	4.20	180.92	764.50	415	36.34	136.35	43.70
EOF250N90A	249.30	90.10	0.00	5.99	7.90	221.52	1018.10	445	62.37	263.62	64.30
EOF250N90B	249.30	90.00	0.00	5.99	7.90	221.52	1014.30	445	62.37	263.64	64.30
EOF250N45A	249.70	89.90	0.00	5.99	7.90	221.92	925.90	445	52.85	218.36	61.30
EOF250N45B	249.50	89.80	0.00	5.99	7.90	221.72	921.80	445	52.81	218.61	61.30
EOF300N90A	298.60	90.90	0.00	6.00	8.40	269.8	1169.00	435	67.88	201.02	64.80
EOF300N90B	298.50	91.10	0.00	6.00	8.40	269.7	1169.80	435	67.87	201.22	64.80
EOF300N45A	298.60	91.00	0.00	6.00	8.40	269.8	1125.00	435	58.70	171.45	62.50
EOF300N45B	298.40	91.10	0.00	6.00	8.40	269.6	1124.30	435	58.67	171.65	62.50

Table E-4: Unlipped plain-C sections under the ITF load case

Specimens	Depth D (mm)	Flanges B$_f$ (mm)	Lips L (mm)	Thickness t$_w$ (mm)	Radius r$_i$ (mm)	Length L$_o$ (mm)	Yield strength f$_y$ (MPa)	Yield load P$_y$ (kN)	Buckling load P$_{cr}$ (kN)	Experiment load P$_{exp}$ (kN)
ITF75-N40	74.50	40.50	0.00	3.84	3.90	263.80	450.00	29.07	302.28	51.30
ITF75-N20	74.60	40.50	0.00	3.84	3.90	243.00	450.00	35.60	290.56	54.90
ITF100-N50	99.30	50.40	0.00	3.83	4.10	200.20	440.00	37.93	247.75	24.80
ITF100-N25	99.20	50.40	0.00	3.83	4.10	175.00	440.00	45.60	253.28	22.60
ITF125-N65A	125.00	65.60	0.00	3.84	3.90	440.00	405.00	44.70	171.60	60.40
ITF125-N65B	124.90	65.50	0.00	3.84	3.90	440.10	405.00	44.65	171.73	59.60
ITF125-N32A	125.10	65.60	0.00	3.85	3.90	407.70	405.00	54.17	166.82	64.40
ITF125-N32B	124.90	65.30	0.00	3.85	3.90	407.50	405.00	54.07	166.82	63.80
ITF200-N75	198.70	75.90	0.00	4.72	4.20	675.20	415.00	104.80	183.23	100.10
ITF200-N37	198.80	76.00	0.00	4.73	4.20	638.00	415.00	118.41	180.71	99.80
ITF250-N90	249.60	90.00	0.00	6.01	7.90	838.40	445.00	155.04	306.18	148.50
ITF250-N45	249.50	89.90	0.00	5.99	7.90	796.50	445.00	174.25	298.17	148.40
ITF300-N90	298.80	90.90	0.00	6.00	8.40	990.00	435.00	185.08	246.15	149.10
ITF300-N45	298.60	91.00	0.00	5.97	8.40	944.10	435.00	203.87	239.99	144.60

Table E-5: Unlipped plain-C sections under the ETF load case

Specimens	Depth D (mm)	Flanges B_f (mm)	Lips L (mm)	Thickness t_w (mm)	Radius r_i (mm)	Length L_o (mm)	Yield strength f_y (MPa)	Yield load P_y (kN)	Buckling load P_{cr} (kN)	Experiment load P_{exp} (kN)
ETF75N40	74.30	40.50	0.00	3.85	3.90	152.00	450.00	15.01	153.88	22.10
ETF75N20	74.40	40.40	0.00	3.84	3.90	133.60	450.00	14.52	120.14	18.30
ETF100N50	99.10	50.40	0.00	3.83	4.10	200.20	440.00	18.99	107.32	24.80
ETF100N25	99.40	50.30	0.00	3.83	4.10	175.00	440.00	18.44	85.61	22.60
ETF125N65	125.60	65.40	0.00	3.83	3.90	252.50	405.00	22.87	84.56	28.20
ETF125N32	125.30	65.30	0.00	3.84	3.90	219.80	405.00	21.97	67.78	23.40
ETF200N75	198.90	75.90	0.00	4.72	4.20	375.30	415.00	47.01	84.25	40.20
ETF200N37	198.70	75.90	0.00	4.72	4.20	336.90	415.00	45.34	70.79	31.20
ETF250N90	249.20	89.80	0.00	5.99	7.90	465.10	445.00	68.37	136.60	50.60
ETF250N45	249.40	89.90	0.00	5.98	7.90	421.00	445.00	66.43	116.16	46.90
ETF300N90	298.50	90.90	0.00	5.98	8.40	539.60	435.00	77.69	105.33	49.40
ETF300N45	298.30	91.20	0.00	6.01	8.40	495.20	435.00	75.92	94.17	45.40

3. Macdonald et al. [37] (2008)

Table E-6: Lipped plain-C sections under the EOF load case

Specimen	Depth D (mm)	Flanges B_f (mm)	Lips l (mm)	Thickness t_w (mm)	Radius r_i (mm)	Wed L_o (mm)	Yield strength f_y (MPa)	Yield load P_y (kN)	Buckling load P_{cr} (kN)	Experiment load P_{exp} (kN)
EOF-25F-1	104.76	57.16	19.04	0.78	4.00	600.00	220.00	0.98	2.62	1.18
EOF-25F2	102.26	54.51	19.10	0.78	2.60	600.00	220.00	1.08	2.27	1.24
EOF-25F-3	101.26	52.61	19.46	0.78	1.20	600.00	220.00	1.39	2.04	1.46
EOF-100F-4	104.76	57.16	19.04	0.78	4.00	600.00	220.00	1.64	3.32	1.74
EOF-100F-5	102.26	54.51	19.10	0.78	2.60	600.00	220.00	1.82	3.31	2.00
EOF-100F-6	101.26	52.61	19.46	0.78	1.20	600.00	220.00	2.36	3.37	2.25
EOF-50F-7	102.26	54.51	19.10	0.78	2.60	600.00	220.00	1.32	2.96	1.43
EOF-50F-8	101.26	52.61	19.46	0.78	1.20	600.00	220.00	1.71	2.79	1.70
EOF-50F-9	104.76	57.16	19.04	0.78	4.00	600.00	220.00	1.20	3.00	1.34
EOF-50F-10	77.26	40.61	14.66	0.78	1.20	600.00	220.00	1.46	3.07	1.80
EOF-50F-11	76.76	41.76	14.00	0.78	2.60	600.00	220.00	1.12	3.04	1.44
EOF-50F-12	78.76	44.16	13.84	0.78	4.00	600.00	220.00	1.01	3.11	1.32
EOF-25F-13	77.26	40.61	14.66	0.78	1.20	600.00	220.00	1.14	2.92	1.44
EOF-25F-14	76.76	41.76	14.00	0.78	2.60	600.00	220.00	0.87	2.89	1.12
EOF-25F-15	78.76	44.16	13.84	0.78	4.00	600.00	220.00	0.79	2.95	1.10
EOF-100F-16	77.26	40.61	14.66	0.78	1.20	600.00	220.00	2.27	3.41	2.35
EOF-100F-17	76.76	41.76	14.00	0.78	2.60	600.00	220.00	1.74	3.38	1.90
EOF-100F-18	78.76	44.16	13.84	0.78	4.00	600.00	220.00	1.55	3.46	1.62

Table E-7: Lipped plain-C sections under the ETF load case

Specimen	Depth D (mm)	Flanges B$_f$ (mm)	Lips l (mm)	Thickness t$_w$ (mm)	Radius r$_i$ (mm)	Length L$_o$ (mm)	Yield strength f$_y$ (MPa)	Yield load P$_y$ (kN)	Buckling load P$_{cr}$ (kN)	Experiment load P$_{exp}$ (kN)
ETF-25F-1	77.76	41.26	14.60	0.78	1.60	400.00	220	1.16	1.53	0.87
ETF-25F-2	79.76	43.06	14.68	0.78	2.40	400.00	220	1.04	1.62	0.81
ETF-25F-3	76.76	44.16	13.04	0.78	5.00	400.00	220	0.83	2.06	0.76
ETF-25F-4	102.96	53.86	19.64	0.78	1.60	400.00	220	1.52	1.05	1.25
ETF-25F-5	102.56	54.46	19.24	0.78	2.40	400.00	220	1.32	1.16	0.98
ETF-25F-6	101.36	56.46	17.96	0.78	5.00	400.00	220	1.08	1.39	0.80
ETF-50F-7	77.76	41.26	14.60	0.78	1.60	400.00	220	1.21	2.11	1.38
ETF-50F-8	79.76	43.06	14.68	0.78	2.40	400.00	220	1.09	2.08	0.92
ETF-50F-9	76.76	44.16	13.04	0.78	5.00	400.00	220	0.87	2.68	1.14
ETF-50F-10	102.96	53.86	19.64	0.78	1.60	400.00	220	1.57	1.35	1.24
ETF-50F-11	102.56	54.46	19.24	0.78	2.40	400.00	220	1.37	1.42	1.22
ETF-50F-12	101.36	56.46	17.96	0.78	5.00	400.00	220	1.12	1.84	0.98
ETF-100F-13	77.76	41.26	14.60	0.78	1.60	400.00	220	1.53	3.50	1.84
ETF-100F-14	79.76	43.06	14.68	0.78	2.40	400.00	220	1.34	3.35	1.76
ETF-100F-15	76.76	44.16	13.04	0.78	5.00	400.00	220	1.11	3.58	1.58
ETF-100F-16	102.96	53.86	19.64	0.78	1.60	400.00	220	1.68	2.12	1.72
ETF-100F-17	102.56	54.46	19.24	0.78	2.40	400.00	220	1.47	2.14	1.56
ETF-100F-18	101.36	56.46	17.96	0.78	5.00	400.00	220	1.20	2.25	1.28

4. Uzzaman et al. [38],[39] (2012)

Table E-8: Lipped plain-C sections under the ITF load case (2012)

Specimen	Wed D (mm)	Flanges B$_f$ (mm)	Lips L (mm)	Thickness t$_w$ (mm)	web d$_1$ (mm)	Radius		Wed L$_o$ (mm)	Yield strength f$_y$ (MPa)	Yield load P$_y$ (kN)	Buckling load P$_{cr}$ (kN)	Experiment load P$_{exp}$ (kN)
						r$_1$ (mm)	r$_2$ (mm)					
C142N90A0U	142.20	58.60	15.90	1.23	130.14	4.80	4.80	337.50	455.00	10.36	9.05	6.03
C142N120A0U	141.80	58.90	15.60	1.24	129.72	4.80	4.80	350.00	455.00	8.49	9.52	6.32
C172N120A0U	172.80	64.10	15.60	1.27	160.26	5.00	5.00	400.00	534.00	14.40	9.53	7.05
C202N150A0U	202.10	63.10	17.50	1.45	189.20	5.00	5.00	450.00	513.00	18.34	11.75	8.40
C262N150A0U	263.40	63.40	14.40	1.56	249.28	5.50	5.50	550.00	525.00	30.53	6.83	8.19
C142N90A0F	142.20	58.60	15.90	1.23	130.14	4.80	4.80	337.50	455.00	12.08	9.31	8.97
C142N120A0F	141.80	58.90	15.60	1.24	129.72	4.80	4.80	350.00	455.00	13.39	9.92	9.44
C172N120A0F	172.80	64.10	15.60	1.27	160.26	5.00	5.00	400.00	534.00	18.26	8.32	10.72
C202N150A0F	202.10	63.10	17.50	1.45	189.20	5.00	5.00	450.00	513.00	24.85	10.51	13.51
C262N150A0F	263.40	63.40	14.40	1.56	249.28	5.50	5.50	550.00	525.00	32.71	9.87	12.78

Table E-9: Lipped plain-C sections under the ETF load case (2012)

Specimen	Depth D (mm)	Flanges B$_f$ (mm)	Lips L (mm)	Thickness t$_w$ (mm)	Radius r$_1$ (mm)	r$_2$ (mm)	Length L$_o$ (mm)	Yield strength f$_y$ (MPa)	Yield load P$_y$ (kN)	Buckling load P$_{cr}$ (kN)	Experiment load P$_{exp}$ (kN)
C142N90A0U	142.20	58.60	15.90	1.23	4.80	4.80	337.50	455.00	5.90	2.74	2.21
C142N120A0U	141.80	58.90	15.60	1.24	4.80	4.80	350.00	455.00	6.12	3.23	2.35
C172N120A0U	172.80	64.10	15.60	1.27	5.00	5.00	400.00	534.00	8.74	2.54	2.37
C202N120A0U	202.10	63.10	17.50	1.45	5.00	5.00	425.00	513.00	11.48	2.94	2.70
C202N150A0U	202.10	63.10	17.50	1.45	5.00	5.00	450.00	513.00	11.72	3.27	2.84
C262N120A0U	263.40	63.40	14.40	1.56	5.50	5.50	525.00	525.00	16.04	2.46	2.55
C262N150A0U	263.40	63.40	14.40	1.56	5.50	5.50	550.00	525.00	16.31	2.69	2.82
C142N90A0F	142.20	58.60	15.90	1.23	4.80	4.80	337.50	455.00	5.90	4.96	3.75
C142N120A0F	141.80	58.90	15.60	1.24	4.80	4.80	350.00	455.00	6.12	6.00	4.06
C172N120A0F	172.80	64.10	15.60	1.27	5.00	5.00	400.00	534.00	8.74	4.77	4.16
C202N120A0F	202.10	63.10	17.50	1.45	5.00	5.00	425.00	513.00	11.48	5.72	5.24
C202N150A0F	202.10	63.10	17.50	1.45	5.00	5.00	450.00	513.00	11.72	6.53	5.82
C262N120A0F	263.40	63.40	14.40	1.56	5.50	5.50	525.00	525.00	16.04	5.00	5.06
C262N150A0F	263.40	63.40	14.40	1.56	5.50	5.50	550.00	525.00	16.31	5.57	5.37

Table E-10: Lipped plain-C sections under the ETF load case (2012)

Specimen	Depth D (mm)	Flanges B$_f$ (mm)	Lips L (mm)	Thickness t$_w$ (mm)	Radius r$_1$ (mm)	r$_2$ (mm)	L$_o$ (mm)	Yield strength f$_y$ (MPa)	Yield load P$_y$ (kN)	Buckling load P$_{cr}$ (kN)	Experiment load P$_{exp}$ (kN)
C142N30A0U	142.15	58.57	15.85	1.23	4.75	4.75	275.40	455.00	5.56	2.09	1.68
C142N60A0U1	141.75	58.94	15.56	1.24	4.75	4.75	300.56	455.00	5.78	2.45	1.95
C142N60A0U2	141.75	58.94	15.56	1.24	4.75	4.75	300.56	455.00	5.78	2.45	1.83
C142N60A0U3	141.75	58.94	15.56	1.24	4.75	4.75	300.56	455.00	5.78	2.45	1.91
C172N32.5A0U	172.76	64.05	15.61	1.27	5.00	5.00	327.41	534.00	8.12	1.82	1.70
C172N65A0FU	172.58	64.28	15.25	1.28	5.00	5.00	356.39	534.00	8.42	2.10	1.88
C202N32.5A0U	202.06	63.11	17.51	1.45	5.00	5.00	375.84	513.00	10.77	2.18	1.98
C202N65A0U	202.44	64.20	16.50	1.45	5.00	5.00	400.91	513.00	11.05	2.42	2.39
C262N32.5A0U	263.43	63.35	14.42	1.56	5.50	5.50	450.93	525.00	15.28	1.94	2.04
C262N65A0U	262.39	64.05	15.33	1.55	5.50	5.50	497.18	525.00	15.38	2.09	2.19
C302N44A0U	305.47	86.78	20.77	1.94	5.00	5.00	549.73	483.00	22.41	3.17	3.96
C302N90A0U	303.55	87.06	21.29	1.97	5.50	5.50	596.45	483.00	22.54	3.81	4.30
C142N30A0F	143.48	59.82	15.80	1.24	4.75	4.75	275.52	455.00	5.67	3.69	2.96
C142N60A0F1	142.96	61.01	14.88	1.21	4.75	4.75	302.46	455.00	5.65	3.90	3.32
C142N60A0F2	142.96	61.01	14.88	1.21	4.75	4.75	302.46	455.00	5.65	3.90	3.31
C142N60A0F3	142.96	61.01	14.88	1.21	4.75	4.75	302.46	455.00	5.65	3.90	3.27
C172N32.5A0F	173.22	63.48	15.36	1.26	5.00	5.00	325.01	534.00	8.06	3.21	2.88
C172N65A0F	173.27	64.29	14.64	1.26	5.00	5.00	351.45	534.00	8.29	3.61	3.31
C202N32.5A0F	202.43	63.97	16.19	1.38	5.00	5.00	376.43	513.00	10.13	3.49	3.63
C202N65A0F	202.37	63.91	16.44	1.45	5.00	5.00	401.84	513.00	11.05	4.48	4.37
C262N32.5A0F	263.55	63.38	14.84	1.55	5.50	5.50	452.21	525.00	15.16	3.76	3.63
C262N65A0F	262.66	65.33	15.17	1.52	5.50	5.50	499.22	525.00	15.01	3.86	3.94
C302N44A0F	304.52	86.59	19.77	1.96	5.50	5.50	544.52	483.00	21.96	6.02	6.95

5. Morelli et al. [40] (2014)

Table E-11: Lipped plain-C sections under the IOF load case

Specimen	Depth D (mm)	Flanges B_f (mm)	Lips L (mm)	Thickness t_w (mm)	Radius r_1 (mm)	Radius r_2 (mm)	Wed L_o (mm)	Yield strength f_y (MPa)	Yield load P_y (kN)	Buckling load P_cr (kN)	Experiment load P_exp (kN)
C30030U-T1A	299.70	96.50	32.10	3.03	5.00	5.00	1100.00	511.73	65.00	73.98	60.00
C30030U-T1B	299.10	96.10	31.50	3.05	5.00	5.00	1100.00	511.73	65.49	74.85	60.00
C30030U-T2A	301.00	96.00	31.00	3.13	5.00	5.00	1100.00	511.42	68.13	79.18	58.50
C30030U-T2B	301.00	96.50	30.50	3.06	5.00	5.00	1100.00	511.42	66.05	74.08	58.50
C30030F-T1A	301.00	96.00	35.00	3.09	5.00	5.00	1100.00	503.22	65.87	105.52	63.50
C30030F-T1B	297.00	97.00	34.00	3.07	5.00	5.00	1100.00	503.22	64.65	104.56	63.50
C30030F-T2A	297.00	98.00	30.00	3.05	5.00	5.00	1100.00	509.77	64.91	101.43	62.50
C30030F-T2B	297.00	97.00	34.00	3.07	5.00	5.00	1100.00	509.77	65.49	104.56	62.50
C30024U-T1A	297.00	96.30	28.50	2.44	5.00	5.00	1100.00	513.31	48.22	39.72	39.00
C30024U-T1B	301.00	96.50	28.20	2.44	5.00	5.00	1100.00	513.31	48.70	38.97	39.00
C30024U-T2A	296.00	96.00	27.00	2.45	5.00	5.00	1100.00	514.41	48.48	39.45	38.50
C30024U-T2B	299.00	95.50	28.00	2.46	5.00	5.00	1100.00	514.41	49.10	39.92	38.50
C30024F-T1A	296.00	96.00	26.00	2.43	5.00	5.00	1100.00	507.82	47.33	51.92	41.00
C30024F-T1B	296.00	96.00	30.00	2.46	5.00	5.00	1100.00	507.82	48.12	54.36	41.00
C30024F-T2A	296.00	97.00	26.00	2.44	5.00	5.00	1100.00	515.07	48.27	52.45	40.50
C30024F-T2B	297.00	97.00	30.00	2.47	5.00	5.00	1100.00	515.07	49.20	54.72	40.50

Table E-12: DHS sections under the IOF load case

Specimen	Depth D (mm)	Flanges B_f (mm)	Thickness t_w (mm)	Lips l_1 (mm)	Lips l_2 (mm)	Web H (mm)	Web F (mm)	Web G (mm)	Yield strength f_y (MPa)	Yield load P_y (kN)	Buckling load P_cr (kN)	Experiment load P_exp (kN)
DHS30030U-T1A	303.50	100.10	3.10	40.50	13.00	70.00	4.00	10.10	511.73	50.27	113.21	53.00
DHS30030U-T1B	302.50	100.00	3.05	41.50	12.00	72.00	4.00	9.50	511.73	49.08	110.32	53.00
DHS30030U-T2A	302.50	105.00	3.11	41.50	12.00	70.00	4.00	9.50	511.42	50.38	115.64	52.50
DHS30030U-T2B	302.90	100.10	3.12	40.50	12.10	69.00	4.00	10.00	511.42	50.64	114.20	52.50
DHS30030F-T1A	303.00	105.00	3.00	40.00	11.00	71.00	4.00	9.00	503.22	47.23	118.07	53.00
DHS30030F-T1B	302.00	105.00	3.01	41.00	11.00	69.00	4.00	11.00	503.22	47.36	119.12	53.00
DHS30030F-T2A	302.50	104.00	3.01	41.00	13.00	70.00	4.00	10.00	509.77	48.02	119.74	53.00
DHS30030F-T2B	302.50	104.00	3.00	41.00	13.00	69.00	4.00	10.00	509.77	47.80	118.21	53.00
DHS30024U-T1A	301.00	104.00	2.48	39.50	11.00	70.00	4.60	9.00	513.31	37.04	69.58	41.00
DHS30024U-T1B	301.50	100.50	2.46	40.00	11.50	68.00	4.60	10.00	513.31	36.67	67.81	41.00
DHS30024U-T2A	301.00	101.00	2.46	38.00	11.00	69.00	4.50	11.00	514.41	36.71	66.32	39.50
DHS30024U-T2B	301.00	100.00	2.45	42.00	13.00	68.00	4.50	12.00	514.41	36.51	68.39	39.50
DHS30024F-T1A	300.00	103.00	2.52	40.00	9.00	70.00	4.60	9.00	507.82	37.38	80.02	41.50
DHS30024F-T1B	300.00	102.00	2.53	40.00	11.00	69.00	4.60	9.00	507.82	37.58	80.87	41.50
DHS30024F-T2A	301.00	103.00	2.52	39.00	15.00	68.00	4.60	10.00	515.07	37.98	79.56	42.50
DHS30024F-T2B	301.00	100.00	2.54	39.00	11.00	65.00	4.60	10.00	515.07	38.39	80.16	42.50

Corner radius: $r_1 = 5$ mm, $r_2 = 3$ mm; Beam length L=1100 mm

6. Khatale et al. [41] (2014)

Table E-13: Lipped plain-C sections under the ITF load case

Specimen	Wed D (mm)	Flanges B_f (mm)	Lips L (mm)	Thickness t_w (mm)	Radius r_1 (mm)	Radius r_2 (mm)	Wed L_o (mm)	Yield strength f_y (MPa)	Yield load P_y (kN)	Buckling load P_cr (kN)	Experiment load P_exp (kN)
C30030-UA	299.70	97.40	31.15	3.05	5.00	5.00	1500.00	511.73	102.33	39.78	52.83
C30030-UB	300.10	97.30	31.10	3.00	5.00	5.00	1500.00	511.42	100.15	36.16	53.21
C30030-FA	300.00	96.70	31.30	3.05	5.00	5.00	1500.00	503.22	79.99	56.99	62.58
C30030-FB	299.70	96.70	30.70	2.96	5.00	5.00	1500.00	509.77	77.71	52.15	62.77
C30024-UA	299.20	95.95	28.70	2.40	5.00	5.00	1500.00	513.31	73.91	18.88	31.73
C30024-UB	300.00	96.00	28.40	2.35	5.00	5.00	1500.00	514.41	72.23	17.69	32.35
C30024-FA	299.40	95.75	28.15	2.42	5.00	5.00	1500.00	507.82	58.80	28.69	39.72
C30024-FB	299.90	95.80	28.05	2.44	5.00	5.00	1500.00	515.07	60.39	29.34	39.69

Table E-14: DHS sections under the ITF load case

Specimens	Wed D (mm)	Flanges B_f (mm)	Thickness t_w (mm)	Lips l_1 (mm)	Lips l_2 (mm)	Web H (mm)	Web F (mm)	Web G (mm)	Yield strength f_y (MPa)	Yield load P_y (kN)	Buckling load P_cr (kN)	Experiment load P_exp (kN)
DHS30030-UA	302.20	99.75	3.06	40.00	13.20	72.50	4.00	7.70	511.73	59.51	56.52	53.08
DHS30030-UB	300.60	102.30	3.01	40.20	13.20	72.80	4.00	8.00	511.42	57.82	55.59	53.47
DHS30030-FA	303.30	102.15	2.90	41.40	14.00	67.90	4.00	7.80	503.22	75.32	63.80	56.51
DHS30030-FB	299.90	102.85	2.85	42.20	11.90	67.40	4.00	8.20	509.77	73.83	61.58	54.00
DHS30024-UA	300.10	101.35	2.50	39.30	12.55	65.50	4.60	7.30	513.31	44.98	37.66	36.69
DHS30024-UB	300.00	101.05	2.54	39.30	12.45	71.90	4.60	8.20	514.41	46.04	39.14	37.01
DHS30024-FA	300.60	101.30	2.50	38.80	12.25	70.10	4.60	7.70	507.82	61.65	47.75	44.75
DHS30024-FB	300.30	101.20	2.54	39.00	12.20	69.00	4.60	7.90	515.07	63.84	49.56	44.89

Corner radius: r_1 = 5 mm, r_2 = 3 mm; Beam length L=1500 mm

Table E-15: Lipped plain-C sections under the ETF load case

Specimen	Depth D (mm)	Flanges B_f (mm)	Lips L (mm)	Thickness t_w (mm)	Radius r_1 (mm)	Radius r_2 (mm)	L_o (mm)	Yield strength f_y (MPa)	Yield load P_y (kN)	Buckling load P_cr (kN)	Experiment load P_exp (kN)
C30030-UA	300.00	96.70	31.65	2.97	5.00	5.00	750.00	513.31	42.77	14.01	14.34
C30030-UB	302.10	97.25	31.05	3.00	5.00	5.00	750.00	514.41	43.75	14.27	15.39
C30030-FA	301.80	97.00	30.10	3.05	5.00	5.00	750.00	507.82	44.13	25.56	22.96
C30030-FB	300.00	96.40	30.75	3.04	5.00	5.00	750.00	515.07	44.31	25.56	23.50
C30024-UA	299.70	95.60	28.15	2.49	5.00	5.00	750.00	511.73	33.50	8.27	9.96
C30024-UB	302.70	96.05	28.40	2.46	5.00	5.00	750.00	511.42	33.25	7.86	10.09
C30024-FA	302.40	96.10	27.70	2.47	5.00	5.00	750.00	503.22	32.87	13.66	13.88
C30024-FB	300.10	96.10	27.95	2.45	5.00	5.00	750.00	509.77	32.69	13.47	13.99

Table E-16: DHS sections under the ETF load case

Specimen	Wed D (mm)	Flanges B_f (mm)	Thickness t_w (mm)	Lips		Web			Yield strength f_y (MPa)	Yield load P_y (kN)	Buckling load P_cr (kN)	Experiment load P_exp (kN)
				l_1 (mm)	l_2 (mm)	H (mm)	F (mm)	G (mm)				
DHS30030-UA	301.90	102.70	3.02	42.90	12.00	77.80	4.00	6.50	513.31	36.75	25.92	21.44
DHS30030-UB	299.80	102.80	3.04	42.60	12.00	68.10	4.00	10.80	514.31	36.94	26.04	21.59
DHS30030-FA	300.00	102.20	3.03	42.65	11.80	69.60	4.00	7.00	515.31	36.86	30.10	28.58
DHS30030-FB	301.40	102.20	3.02	42.75	11.35	70.90	4.00	5.80	516.31	36.92	29.73	28.79
DHS30024-UA	300.20	101.00	2.52	39.50	12.45	67.10	4.60	6.90	513.31	28.58	16.60	13.82
DHS30024-UB	300.40	101.55	2.53	39.70	12.35	67.20	4.60	7.40	514.31	28.80	16.79	13.71
DHS30024-FA	300.10	101.10	2.51	39.10	13.70	69.20	4.60	7.50	515.31	28.53	18.87	17.28
DHS30024-FB	300.80	101.40	2.54	39.20	12.50	69.20	4.60	7.60	516.31	29.10	19.41	17.14

Corner radius: r_1 = 5 mm, r_2 = 3 mm; Beam length L=750 mm

7. Sundararajah et al. [19] (2015)

Table E-17: Lipped plain-C sections under the ITF load case

Specimen	Wed D (mm)	Flanges B_f (mm)	Lips L (mm)	Thickness t_w (mm)	Radius		Length L_o (mm)	Yield strength f_y (MPa)	Yield load P_y (kN)	Buckling load P_cr (kN)	Experiment load P_exp (kN)
					r_1 (mm)	r_2 (mm)					
C10010U-25	99.90	50.60	14.00	1.03	3.50	3.50	510.00	581.00	10.82	5.87	7.05
C10015U-25	101.10	51.20	14.00	1.52	4.00	4.00	510.00	582.00	17.57	16.78	14.43
C15012U-25	150.30	62.10	18.00	1.21	4.00	4.00	760.00	583.00	20.41	5.74	9.13
C15015U-25	150.10	62.50	18.00	1.52	4.50	4.50	760.00	584.00	26.53	10.86	15.36
C20019U-25	203.60	76.40	19.00	1.91	5.00	5.00	1015.00	585.00	48.41	14.18	22.99
C20024U-25	203.70	76.60	19.00	2.41	5.00	5.00	1015.00	586.00	66.27	27.16	36.71
C10010U-50	100.40	50.30	14.00	1.03	3.50	3.50	510.00	587.00	9.20	5.99	6.41
C10015U-50	101.10	50.00	14.00	1.52	4.00	4.00	510.00	588.00	14.87	17.20	14.30
C15012U-50	151.10	62.00	18.00	1.21	4.00	4.00	760.00	589.00	18.61	5.78	8.16
C15015U-50	150.80	61.40	18.00	1.52	4.50	4.50	760.00	590.00	24.16	10.90	13.17
C20019U-50	203.60	76.60	19.00	1.91	5.00	5.00	1015.00	591.00	45.27	14.30	20.70
C20024U-50	203.60	76.70	19.00	2.41	5.00	5.00	1019.00	592.00	61.93	27.41	34.41
C10010U-100	100.10	50.70	14.00	1.03	3.50	3.50	510.00	593.00	5.62	6.63	6.45
C10015U-100	100.80	50.90	14.00	1.52	4.00	4.00	510.00	594.00	9.15	19.20	14.34
C15012U-100	150.40	62.30	18.00	1.21	4.00	4.00	760.00	595.00	14.38	6.13	8.14
C15015U-100	150.00	62.70	18.00	1.52	4.50	4.50	760.00	596.00	18.63	11.63	12.92
C20019U-100	203.10	77.30	19.00	1.91	5.00	5.00	1015.00	597.00	38.24	14.84	20.19
C20024U-100	203.60	76.70	19.00	2.41	5.00	5.00	1013.00	598.00	52.50	28.33	33.68

Table E-18: Lipped plain-C sections under the ETF load case

Specimen	Depth D (mm)	Flanges B_f (mm)	Lips L (mm)	Thickness t_w (mm)	Radius r_1 (mm)	Radius r_2 (mm)	L_o (mm)	Yield strength f_y (MPa)	Yield load P_y (kN)	Buckling load P_cr (kN)	Experiment load P_exp (kN)
C10010U-25	100.40	50.50	14.00	1.03	3.50	3.50	306.00	581	4.38	1.91	1.76
C10015U-25	100.00	50.00	14.00	1.52	4.00	4.00	307.00	540	6.48	6.01	4.24
C15012U-25	150.00	62.00	18.00	1.21	4.00	4.00	456.00	556	7.33	1.92	2.06
C15015U-25	150.20	62.50	18.00	1.52	4.50	4.50	456.00	531	9.11	3.76	3.63
C20019U-25	203.70	77.00	19.00	1.91	5.00	5.00	609.00	506	15.29	5.07	5.51
C20024U-25	203.60	76.50	19.00	2.41	5.00	5.00	609.00	526	21.69	9.81	9.10
C10010U-50	100.30	50.50	14.00	1.03	3.50	3.50	306.00	581	4.54	2.20	1.74
C10015U-50	100.90	51.30	14.00	1.52	4.00	4.00	307.00	540	6.78	6.94	4.47
C15012U-50	150.70	61.80	18.00	1.21	4.00	4.00	456.00	556	7.55	2.09	2.23
C15015U-50	150.00	62.50	18.00	1.52	4.50	4.50	456.00	531	9.32	4.14	3.74
C20019U-50	203.40	76.50	19.00	1.91	5.00	5.00	609.00	506	15.55	5.47	5.63
C20024U-50	203.50	76.40	19.00	2.41	5.00	5.00	606.00	526	22.09	10.67	7.20
C10010U-100	99.80	50.20	14.00	1.03	3.50	3.50	306.00	581	4.53	2.99	2.13
C10015U-100	100.40	50.90	14.00	1.52	4.00	4.00	306.00	540	7.23	9.54	5.27
C15012U-100	150.90	61.90	18.00	1.21	4.00	4.00	456.00	556	7.92	2.58	2.46
C15015U-100	150.00	60.00	18.00	1.52	4.50	4.50	456.00	531	9.78	5.16	4.03
C20019U-100	203.40	76.50	19.00	1.91	5.00	5.00	606.00	506	16.11	6.51	6.01
C20024U-100	203.50	76.40	19.00	2.41	5.00	5.00	609.00	526	22.89	12.90	9.45

8. Efendy et al. [7] (2015)

Table E-19: Lipped plain-C sections under the IOF load case

Specimen	Depth D (mm)	Flanges B_f (mm)	Lips L (mm)	Thickness t_w (mm)	Radius r_i (mm)	Wed L_o (mm)	Yield strength f_y (MPa)	Yield load P_y (kN)	Buckling load P_cr (kN)	Experiment load P_exp (kN)
C20015-U1A	203.30	76.35	15.86	1.58	5.00	900.00	513.40	20.82	15.90	17.31
C20015-U1B	203.41	75.53	16.40	1.55	5.00	900.00	513.40	20.31	15.24	17.31
C20015-U2A	203.34	75.71	15.66	1.56	5.00	900.00	513.40	20.48	15.27	17.46
C20015-U2B	203.10	76.47	15.52	1.56	5.00	900.00	513.40	20.46	15.28	17.46
C20015-F1A	203.36	75.79	16.17	1.58	5.00	900.00	513.40	20.82	22.77	17.76
C20015-F1B	203.15	77.20	15.59	1.59	5.00	900.00	513.40	20.98	23.05	17.76
C20015-F2A	203.43	77.60	15.31	1.55	5.00	900.00	513.40	20.31	21.39	17.49
C20015-F2B	203.23	77.05	15.55	1.55	5.00	900.00	513.40	20.30	21.46	17.49
C20024-U1A	202.83	77.02	21.57	2.47	5.00	900.00	483.49	35.49	58.80	41.88
C20024-U1B	204.43	75.43	21.75	2.46	5.00	900.00	483.49	35.47	57.65	41.88
C20024-U2A	202.50	75.82	21.85	2.45	5.00	900.00	483.49	35.06	57.76	41.91
C20024-U2B	204.62	74.83	22.23	2.45	5.00	900.00	483.49	35.30	57.26	41.91
C20024-F1A	202.15	77.13	21.64	2.45	5.00	900.00	483.49	35.02	82.07	41.94
C20024-F1B	203.60	75.32	22.02	2.46	5.00	900.00	483.49	35.38	82.89	41.94
C20024-F2A	202.15	77.24	22.17	2.45	5.00	900.00	483.49	35.02	82.23	41.78
C20024-F2B	203.74	75.91	22.20	2.45	5.00	900.00	483.49	35.20	81.81	41.78

Table E-20: SupaCee sections under the IOF load case

Specimen	Wed D (mm)	Flanges B_f (mm)	Thickness t_w (mm)	Lips l_1 (mm)	Lips l_2 (mm)	Lip angles α_1 (degrees)	Lip angles α_2 (degrees)	Web stiffeners H (mm)	Yield strength f_y (MPa)	Yield load P_y (kN)	Buckling load P_{cr} (kN)	Experiment load P_{exp} (kN)
SC20015-U1A	205.13	58.60	1.58	14.50	10.65	31.00	40.00	21.85	513.40	20.94	18.56	17.73
SC20015-U1B	205.16	57.86	1.55	14.25	11.23	32.00	36.00	23.92	513.40	20.43	17.51	17.73
SC20015-U2A	203.40	57.61	1.60	13.62	11.36	30.00	34.00	21.47	513.40	21.17	18.99	18.28
SC20015-U2B	205.29	59.83	1.57	14.50	11.34	37.00	43.00	22.62	513.40	20.78	18.38	18.28
SC20015-F1A	204.21	58.75	1.56	14.08	10.19	36.00	43.00	21.67	513.40	20.54	27.02	17.86
SC20015-F1B	203.08	61.70	1.56	14.30	11.37	33.00	38.00	22.49	513.40	20.46	27.06	17.86
SC20015-F2A	204.97	60.88	1.56	14.55	11.03	36.00	41.00	22.69	513.40	20.59	26.81	18.25
SC20015-F2B	204.18	59.91	1.56	13.06	9.98	37.00	49.00	20.98	513.40	20.53	26.81	18.25
SC20024-U1A	204.80	63.68	2.42	13.70	12.97	37.00	41.60	22.93	483.49	34.73	56.35	42.00
SC20024-U1B	204.81	62.53	2.46	14.22	12.88	40.00	42.00	23.11	483.49	35.51	58.51	42.00
SC20024-U2A	203.44	63.34	2.46	15.34	11.58	27.00	36.00	21.64	483.49	35.36	60.34	40.69
SC20024-U2B	203.20	64.26	2.46	14.41	12.03	33.00	37.00	22.35	483.49	35.33	59.28	40.69
SC20024-F1A	203.22	61.72	2.47	15.00	12.08	32.00	36.00	22.08	483.49	35.53	92.68	41.11
SC20024-F1B	202.78	61.39	2.52	13.70	12.95	34.00	42.00	20.61	483.49	36.46	92.68	41.11
SC20024-F2A	204.58	62.14	2.46	13.89	12.01	42.00	54.00	22.21	483.49	35.49	90.47	40.78
SC20024-F2B	204.50	60.17	2.45	14.38	13.30	33.00	36.00	24.14	483.49	35.28	90.47	40.78

Corner radius: $r_1 = r_2 = 5$ mm; Web stiffeners: G = 2.90mm, F = 4.20 mm; Beam length L=900 mm

9. Hadchiti et al. [8] (2015)

Table E-21: Lipped plain-C sections under the EOF load case

Specimen	Wed D (mm)	Flanges B (mm)	Lips L (mm)	Thickness t_w (mm)	Radius r_i (mm)	Length L_o (mm)	Yield strength f_y (MPa)	Yield load P_y (kN)	Buckling load P_{cr} (kN)	Experiment load P_{exp} (kN)
C20015-U1A	206.00	77.25	15.75	1.50	5.00	900.00	512.00	11.90	6.81	7.77
C20015-U1B	203.50	77.50	16.00	1.50	5.00	900.00	512.00	11.81	6.99	7.77
C20015-U2A	204.50	77.25	15.75	1.50	5.00	900.00	512.00	11.85	6.88	7.69
C20015-U2B	205.50	77.50	15.50	1.50	5.00	900.00	512.00	11.89	6.80	7.69
C20015-F1A	203.50	77.25	15.70	1.50	5.00	900.00	512.00	11.81	9.16	9.48
C20015-F1B	203.50	77.75	15.95	1.50	5.00	900.00	512.00	11.81	9.16	9.48
C20015-F2A	202.50	77.00	16.25	1.50	5.00	900.00	512.00	11.78	9.25	9.39
C20015-F2B	203.50	76.45	16.25	1.50	5.00	900.00	512.00	11.81	9.20	9.39
C20024-U1A	202.50	78.00	21.50	2.40	5.00	900.00	512.00	21.97	28.41	22.49
C20024-U1B	203.50	77.50	16.50	2.40	5.00	900.00	512.00	22.04	25.86	22.49
C20024-U2A	204.00	77.35	16.25	2.40	5.00	900.00	512.00	22.07	25.66	21.49
C20024-U2B	205.50	77.15	15.75	2.40	5.00	900.00	512.00	22.17	25.17	21.49
C20024-F1A	204.50	77.75	16.00	2.40	5.00	900.00	512.00	22.10	36.31	25.82
C20024-F1B	203.50	77.00	16.50	2.40	5.00	900.00	512.00	22.04	36.67	25.82
C20024-F2A	205.50	77.50	16.50	2.40	5.00	900.00	512.00	22.17	36.13	26.23
C20024-F2B	205.50	77.50	16.50	2.40	5.00	900.00	512.00	22.17	37.70	26.23

Table E-22: SupaCee sections under the EOF load case

Specimen	Wed D (mm)	Flanges B$_f$ (mm)	Thickness t$_w$ (mm)	Lips		Lip angles		Web stiffeners H (mm)	Yield strength f$_y$ (MPa)	Yield load P$_y$ (kN)	Buckling load P$_{cr}$ (kN)	Experiment load P$_{exp}$ (kN)
				l$_1$ (mm)	l$_2$ (mm)	α$_1$ (degrees)	α$_2$ (degrees)					
SC20015-U1A	203.50	63.00	1.50	14.95	12.79	37.00	41.50	20.10	512.00	11.81	8.22	8.55
SC20015-U1B	204.00	63.00	1.50	16.40	13.74	37.00	42.50	20.85	512.00	11.83	8.59	8.55
SC20015-U2A	203.50	63.50	1.50	14.02	13.69	33.50	40.00	20.35	512.00	11.81	8.31	8.58
SC20015-U2B	205.00	63.00	1.50	15.22	13.49	35.50	41.00	22.35	512.00	11.87	8.33	8.58
SC20015-F1A	204.50	61.25	1.50	16.20	14.04	37.00	41.50	21.35	512.00	11.85	10.07	9.28
SC20015-F1B	206.00	62.25	1.50	15.97	13.69	34.50	41.00	20.60	512.00	11.90	9.95	9.29
SC20015-F2A	207.00	62.50	1.50	14.35	12.64	36.00	43.50	21.35	512.00	11.94	9.80	9.29
SC20015-F2B	206.00	60.75	1.50	14.52	12.74	34.50	40.00	19.10	512.00	11.90	9.88	9.29
SC20024-U1A	206.00	64.90	2.40	16.10	14.63	35.00	39.50	22.35	512.00	22.21	28.98	21.59
SC20024-U1B	205.00	62.90	2.40	15.94	13.60	37.50	42.50	20.85	512.00	22.14	28.23	21.59
SC20024-U2A	201.80	67.40	2.40	16.47	12.96	34.50	42.00	20.38	512.00	21.92	29.78	21.61
SC20024-U2B	203.00	65.40	2.40	16.91	14.02	36.50	43.00	20.10	512.00	22.00	29.78	21.61
SC20024-F1A	205.00	63.65	2.40	14.10	13.82	34.00	39.50	20.98	512.00	22.14	37.87	23.29
SC20024-F1B	206.00	63.40	2.40	16.02	14.10	36.00	41.00	22.85	512.00	22.21	37.85	23.29
SC20024-F2A	204.00	64.90	2.40	15.32	12.85	35.00	40.00	21.35	512.00	22.07	38.06	23.75
SC20024-F2B	204.00	64.90	2.40	14.88	13.90	35.00	39.00	20.60	512.00	22.07	38.06	23.75

Corner radius: r$_1$ = r$_2$ = 5 mm; Web stiffeners: G = 2.90mm, F = 4.20 mm; Beam length L=900 mm

10. Bartlett et al. [9] (2016)

Table E-23: Lipped plain-C sections under the ITF load case

Specimen	Wed D (mm)	Flanges B$_f$ (mm)	Lips L (mm)	Thickness t$_w$ (mm)	Radius		Wed L$_o$ (mm)	Yield strength f$_y$ (MPa)	Yield load P$_y$ (kN)	Buckling load P$_{cr}$ (kN)	Experiment load P$_{exp}$ (kN)
					r$_1$ (mm)	r$_2$ (mm)					
C20015-U1A	204.10	74.42	16.64	1.54	5.00	5.00	1000.00	513.40	24.95	7.80	14.01
C20015-U1B	204.28	75.45	16.60	1.53	5.00	5.00	1000.00	513.40	24.77	7.68	14.01
C20015-U2A	203.41	75.12	16.58	1.53	5.00	5.00	1000.00	513.40	24.62	7.71	14.02
C20015-U2B	203.35	75.02	17.01	1.53	5.00	5.00	1000.00	513.40	24.61	7.77	14.02
C20015-F1A	202.39	74.18	16.75	1.53	5.00	5.00	1000.00	513.40	23.76	11.59	16.75
C20015-F1B	202.87	74.35	15.92	1.53	5.00	5.00	1000.00	513.40	23.80	11.53	16.75
C20015-F2A	203.11	74.45	16.65	1.54	5.00	5.00	1000.00	513.40	24.03	11.75	16.56
C20015-F2B	203.04	74.26	15.89	1.53	5.00	5.00	1000.00	513.40	23.82	11.53	16.56
C20024-U1A	202.78	77.22	20.59	2.45	5.00	5.00	1000.00	483.49	43.16	30.36	37.42
C20024-U1B	203.44	77.41	20.38	2.44	5.00	5.00	1000.00	483.49	43.11	29.93	37.42
C20024-U2A	204.72	75.91	20.75	2.44	5.00	5.00	1000.00	483.49	43.49	29.69	37.63
C20024-U2B	203.14	77.21	20.58	2.43	5.00	5.00	1000.00	483.49	42.79	29.69	37.63
C20024-F1A	203.37	77.60	20.32	2.43	5.00	5.00	1000.00	483.49	41.52	44.00	42.75
C20024-F1B	203.47	77.53	20.30	2.44	5.00	5.00	1000.00	483.49	41.77	44.52	42.75
C20024-F2A	204.34	74.97	20.82	2.42	5.00	5.00	1000.00	483.49	41.44	43.60	42.62
C20024-F2B	203.01	77.33	20.26	2.43	5.00	5.00	1000.00	483.49	41.46	44.10	42.62

Table E-24: SupaCee sections under the ITF load case

Specimen	Wed D (mm)	Flanges B_f (mm)	Thickness t_w (mm)	Lips l_1 (mm)	Lips l_2 (mm)	Lip angles α_1 (degrees)	Lip angles α_2 (degrees)	Web stiffeners G (mm)	Web stiffeners F (mm)	Web stiffeners H (mm)	Yield strength f_y (MPa)	Yield load P_y (kN)	Buckling load P_cr (kN)	Experiment load P_exp (kN)
SC20015-U1A	204.09	68.24	1.54	18.39	13.66	46.50	46.50	5.56	3.24	24.98	513.40	24.94	10.35	14.26
SC20015-U1B	202.64	67.80	1.53	17.66	13.86	42.50	52.50	5.69	3.30	24.85	513.40	24.49	10.60	14.26
SC20015-U2A	204.20	66.45	1.53	17.28	13.75	39.50	46.50	5.97	3.15	27.10	513.40	24.75	10.26	14.15
SC20015-U2B	201.34	67.44	1.52	18.72	13.86	40.50	48.50	5.98	3.36	24.21	513.40	24.07	10.77	14.15
SC20015-F1A	203.77	67.55	1.52	18.00	13.65	45.00	50.50	6.06	3.13	26.65	513.40	23.68	13.89	17.25
SC20015-F1B	203.02	66.15	1.53	17.16	13.82	40.00	41.50	6.24	3.15	25.06	513.40	23.81	14.36	17.25
SC20015-F2A	203.26	69.42	1.53	16.91	13.65	45.00	52.00	5.78	3.23	24.07	513.40	23.84	14.21	17.63
SC20015-F2B	203.39	66.36	1.53	17.66	13.58	41.50	49.50	6.70	3.30	24.75	513.40	23.85	14.64	17.63
SC20024-U1A	202.79	69.64	2.43	16.97	15.57	43.50	57.00	5.54	4.18	25.56	483.49	42.69	36.23	37.36
SC20024-U1B	202.48	69.75	2.42	18.03	15.34	47.00	56.00	5.97	3.78	25.07	483.49	42.36	35.42	37.36
SC20024-U2A	204.39	67.43	2.42	17.90	14.99	47.00	54.00	5.44	3.46	24.53	483.49	42.91	33.84	37.18
SC20024-U2B	201.31	69.07	2.43	18.58	15.64	37.00	42.00	6.54	4.25	26.53	483.49	42.25	37.49	37.18
SC20024-F1A	202.61	70.11	2.43	18.76	15.70	43.50	57.50	5.53	4.11	25.50	483.49	41.40	52.73	44.03
SC20024-F1B	201.04	69.39	2.43	18.65	15.41	41.50	49.50	5.82	4.46	25.87	483.49	41.16	54.65	44.03
SC20024-F2A	202.56	69.86	2.43	18.76	14.76	36.00	48.00	6.26	4.00	25.11	483.49	41.39	53.06	44.06
SC20024-F2B	204.68	69.44	2.44	18.42	15.02	41.50	54.00	6.19	3.87	25.40	483.49	41.95	52.56	44.06

Corner radius: $r_1 = r_2 = 5$ mm; Beam length L=1000 mm

11. Htet and Pham [10] (2016)

Table E-25: Lipped plain-C sections under the ETF load case

Specimen	Depth D (mm)	Flanges B_f (mm)	Lips L (mm)	Thickness t_w (mm)	Radius r_1 (mm)	Radius r_2 (mm)	L_o (mm)	Yield strength f_y (MPa)	Yield load P_y (kN)	Buckling load P_cr (kN)	Experiment load P_exp (kN)
C20015-U1A	203.00	74.82	17.12	1.51	5.00	5.00	1000.00	513.40	11.99	3.39	3.79
C20015-U1B	203.00	75.51	16.38	1.52	5.00	5.00	1000.00	513.40	12.09	3.42	3.79
C20015-U2A	203.00	75.53	16.49	1.52	5.00	5.00	1000.00	513.40	12.09	3.43	3.80
C20015-U2B	204.00	75.02	15.98	1.52	5.00	5.00	1000.00	513.40	12.14	3.38	3.80
C20015-F1A	203.00	75.39	16.57	1.53	5.00	5.00	1000.00	513.40	12.19	5.73	5.73
C20015-F1B	203.00	75.42	17.03	1.50	5.00	5.00	1000.00	513.40	11.88	5.41	5.73
C20015-F2A	203.00	75.33	16.51	1.51	5.00	5.00	1000.00	513.40	11.99	5.51	5.64
C20015-F2B	204.00	74.93	16.77	1.54	5.00	5.00	1000.00	513.40	12.35	5.81	5.64
C20024-U1A	204.00	75.49	20.25	2.45	5.00	5.00	1000.00	483.49	21.56	13.82	11.61
C20024-U1B	203.00	76.63	20.48	2.46	5.00	5.00	1000.00	483.49	21.58	14.13	11.61
C20024-U2A	204.00	75.95	20.60	2.40	5.00	5.00	1000.00	483.49	20.97	13.07	11.58
C20024-U2B	203.00	76.72	20.44	2.42	5.00	5.00	1000.00	483.49	21.11	13.48	11.58
C20024-F1A	202.00	76.14	19.99	2.41	5.00	5.00	1000.00	483.49	20.90	21.96	16.37
C20024-F1B	203.00	75.19	20.22	2.40	5.00	5.00	1000.00	483.49	20.87	21.63	16.37
C20024-F2A	202.00	77.02	19.94	2.42	5.00	5.00	1000.00	483.49	21.01	22.16	16.42
C20024-F2B	203.00	76.33	19.91	2.40	5.00	5.00	1000.00	483.49	20.87	21.53	16.42

Table E-26: SupaCee sections under the ETF load case

Specimen	Depth D (mm)	Flanges B_f (mm)	Thickness t_w (mm)	Lips l_1 (mm)	l_2 (mm)	Lip angles α_1 (degrees)	α_2 (degrees)	Web stiffeners G (mm)	F (mm)	H (mm)	Yield strength f_y (MPa)	Yield load P_y (kN)	Buckling load P_cr (kN)	Experiment load P_exp (kN)
SC20015-U1A	203.00	61.14	1.50	13.31	12.02	45.00	47.00	5.15	3.10	17.38	513.40	11.88	3.51	4.01
SC20015-U1B	203.00	63.10	1.53	10.84	12.01	46.50	54.00	6.11	2.62	19.50	513.40	12.19	3.64	4.01
SC20015-U2A	204.00	62.55	1.51	12.96	9.57	45.50	50.50	6.32	2.72	19.03	513.40	12.04	3.46	4.00
SC20015-U2B	203.00	64.09	1.50	12.09	9.89	45.50	54.00	6.46	2.36	17.15	513.40	11.88	3.42	4.00
SC20015-F1A	202.00	62.93	1.50	12.54	10.95	45.50	53.50	6.10	2.80	18.58	513.40	11.83	6.00	5.86
SC20015-F1B	203.00	63.01	1.52	12.09	11.00	46.00	45.50	5.99	2.68	18.47	513.40	12.09	6.15	5.86
SC20015-F2A	204.00	62.48	1.52	11.31	11.46	44.00	45.50	5.30	3.06	18.26	513.40	12.14	6.26	5.67
SC20015-F2B	203.00	62.10	1.54	11.07	10.85	46.50	54.50	5.52	2.58	19.12	513.40	12.30	6.35	5.67
SC20024-U1A	204.00	65.28	2.42	10.93	13.41	41.00	42.00	5.00	2.82	18.01	483.49	21.21	13.40	12.63
SC20024-U1B	204.00	67.09	2.40	11.03	12.70	49.50	44.00	5.05	3.41	17.99	483.49	20.97	12.95	12.63
SC20024-U2A	203.00	67.17	2.41	12.26	13.23	41.50	48.50	5.01	3.20	19.35	483.49	20.99	13.51	12.48
SC20024-U2B	204.00	65.25	2.42	11.69	13.21	44.00	47.50	5.37	2.98	18.29	483.49	21.21	13.46	12.48
SC20024-F1A	204.00	64.16	2.42	12.10	12.86	43.50	47.00	5.10	2.98	20.56	483.49	21.21	23.17	17.10
SC20024-F1B	203.00	66.17	2.41	12.39	12.01	44.50	45.00	6.13	3.14	19.68	483.49	20.99	23.03	17.10
SC20024-F2A	203.00	65.50	2.42	12.56	12.81	44.00	44.50	5.31	2.61	19.67	483.49	21.11	23.07	17.06
SC20024-F2B	203.00	64.10	2.40	12.42	11.41	45.50	46.50	5.97	3.14	19.38	483.49	20.87	22.83	17.06

Corner radius: $r_1 = r_2 = 5$ mm; Beam length L=1000 mm

12. Lian et al. [42] (2016)

Table E-27: Lipped plain-C sections under the EOF load case

Specimen	Wed D (mm)	Flanges B (mm)	Lips L (mm)	Thickness t_w (mm)	Radius r_i (mm)	Length L_o (mm)	Yield strength f_y (MPa)	Yield load P_y (kN)	Buckling load P_cr (kN)	Experiment load P_exp (kN)
C142N100A0U1	142.70	59.79	13.23	1.23	4.80	360.00	457.00	6.72	6.60	4.78
C142N100A0U2	142.17	59.98	13.18	1.23	4.80	360.00	457.00	6.71	6.63	4.81
C142N100A0U3	142.40	60.04	13.00	1.23	4.80	360.00	457.00	6.72	6.58	4.76
C142N120A0U	142.09	60.07	13.34	1.25	4.80	380.00	457.00	7.48	7.57	5.41
C142N100A0F1	142.13	60.06	13.17	1.27	4.80	360.00	457.00	6.99	9.66	7.07
C142N100A0F2	142.20	60.09	13.09	1.27	4.80	360.00	457.00	6.99	9.65	6.80
C142N100A0F3	142.18	60.01	13.10	1.27	4.80	360.00	457.00	6.99	9.65	7.04
C142N120A0F	142.15	60.09	13.06	1.24	4.80	380.00	457.00	7.41	9.72	7.33
C142N150A0F	142.27	59.99	13.14	1.23	4.80	410.00	457.00	8.17	9.23	7.97
C202N100A0F	202.01	65.57	14.51	1.35	5.00	450.00	464.00	9.30	6.89	6.53
C202N120A0F	202.02	65.39	14.71	1.35	5.00	469.50	464.00	10.01	7.58	7.11
C202N150A0F	202.01	65.45	14.75	1.35	5.00	499.50	464.00	11.06	8.58	7.73
C302N100A0F	302.91	88.61	18.66	1.76	5.00	599.85	479.00	17.77	8.39	11.07
C302N120A0F	303.36	89.06	18.79	1.80	5.00	621.00	479.00	19.38	9.64	12.31
C302N150A0F	303.36	88.65	18.63	1.75	5.00	649.00	479.00	20.20	9.88	12.58

APPENDIX F: DIRECT STRENGTH METHOD DATA

1. IOF load case

Table F-1: Lipped plain-C sections (Efendy et al. [7])

Specimen	Yield Load P_y (kN)	Buckling P_{cr} (kN)	Ratio P_{cr}/P_y	$\lambda = \sqrt{P_y/P_{cr}}$	Ratio k_1	k_2	k_3	k_4	Nominal P_n (kN)	Experiment P_{exp} (kN)	Ratio P_{exp}/P_n
C20015-U1A	20.82	15.90	0.76	1.14	1	0.15	0.4	1.8	16.17	17.31	1.070
C20015-U1B	20.31	15.24	0.75	1.15	1	0.15	0.4	1.8	15.69	17.31	1.104
C20015-U2A	20.48	15.27	0.75	1.16	1	0.15	0.4	1.8	15.78	17.46	1.106
C20015-U2B	20.46	15.28	0.75	1.16	1	0.15	0.4	1.8	15.78	17.46	1.107
C20015-F1A	20.82	22.77	1.09	0.96	1	0.15	0.4	1.8	18.23	17.76	0.974
C20015-F1B	20.98	23.05	1.10	0.95	1	0.15	0.4	1.8	18.39	17.76	0.966
C20015-F2A	20.31	21.39	1.05	0.97	1	0.15	0.4	1.8	17.56	17.49	0.996
C20015-F2B	20.30	21.46	1.06	0.97	1	0.15	0.4	1.8	17.57	17.49	0.995
C20024-U1A	35.49	58.80	1.66	0.78	1	0.15	0.4	1.8	35.46	41.88	1.181
C20024-U1B	35.47	57.65	1.63	0.78	1	0.15	0.4	1.8	35.23	41.88	1.189
C20024-U2A	35.06	57.76	1.65	0.78	1	0.15	0.4	1.8	34.97	41.91	1.199
C20024-U2B	35.30	57.26	1.62	0.79	1	0.15	0.4	1.8	35.04	41.91	1.196
C20024-F1A	35.02	82.07	2.34	0.65	1	0.15	0.4	1.8	39.45	41.94	1.063
C20024-F1B	35.38	82.89	2.34	0.65	1	0.15	0.4	1.8	39.85	41.94	1.053
C20024-F2A	35.02	82.23	2.35	0.65	1	0.15	0.4	1.8	39.47	41.78	1.059
C20024-F2B	35.20	81.81	2.32	0.66	1	0.15	0.4	1.8	39.55	41.78	1.056
Mean											1.082
COV											7.24%

Table F-2: SupaCee sections (Efendy et al. [7])

Specimen	Yield Load P_y (kN)	Buckling P_{cr} (kN)	Ratio P_{cr}/P_y	$\lambda = \sqrt{P_y/P_{cr}}$	Ratio k_1	k_2	k_3	k_4	Nominal P_n (kN)	Experiment P_{exp} (kN)	Ratio P_{exp}/P_n
SC20015-U1A	20.94	18.56	0.89	1.06	1	0.15	0.4	1.8	17.10	17.73	1.037
SC20015-U1B	20.43	17.51	0.86	1.08	1	0.15	0.4	1.8	16.50	17.73	1.075
SC20015-U2A	21.17	18.99	0.90	1.06	1	0.15	0.4	1.8	17.36	18.28	1.053
SC20015-U2B	20.78	18.38	0.88	1.06	1	0.15	0.4	1.8	16.96	18.28	1.078
SC20015-F1A	20.54	27.02	1.32	0.87	1	0.15	0.4	1.8	19.08	17.86	0.936
SC20015-F1B	20.46	27.06	1.32	0.87	1	0.15	0.4	1.8	19.04	17.86	0.938
SC20015-F2A	20.59	26.81	1.30	0.88	1	0.15	0.4	1.8	19.07	18.25	0.957
SC20015-F2B	20.53	26.81	1.31	0.88	1	0.15	0.4	1.8	19.03	18.25	0.959
SC20024-U1A	34.73	56.35	1.62	0.79	1	0.15	0.4	1.8	34.48	42.00	1.218
SC20024-U1B	35.51	58.51	1.65	0.78	1	0.15	0.4	1.8	35.42	42.00	1.186
SC20024-U2A	35.36	60.34	1.71	0.77	1	0.15	0.4	1.8	35.74	40.69	1.139
SC20024-U2B	35.33	59.28	1.68	0.77	1	0.15	0.4	1.8	35.47	40.69	1.147
SC20024-F1A	35.53	92.68	2.61	0.62	1	0.15	0.4	1.8	41.27	41.11	0.996
SC20024-F1B	36.46	92.68	2.54	0.63	1	0.15	0.4	1.8	42.04	41.11	0.978
SC20024-F2A	35.49	90.47	2.55	0.63	1	0.15	0.4	1.8	40.96	40.78	0.996
SC20024-F2B	35.28	90.47	2.56	0.62	1	0.15	0.4	1.8	40.79	40.78	1.000
Mean											1.043
COV											8.61%

Table F-3: Lipped plain-C sections (Morelli et al. [40])

Specimen	Yield Load P_y (kN)	Buckling P_{cr} (kN)	Ratio P_{cr}/P_y	$\lambda = \sqrt{P_y / P_{cr}}$	Ratio				Nominal P_n (kN)	Experiment P_{exp} (kN)	Ratio P_{exp}/P_n
					k_1	k_2	k_3	k_4			
C30030U-T1A	65.00	73.98	1.14	0.94	1	0.15	0.4	1.8	57.64	60.00	1.041
C30030U-T1B	65.49	74.85	1.14	0.94	1	0.15	0.4	1.8	58.15	60.00	1.032
C30030U-T2A	68.13	79.18	1.16	0.93	1	0.15	0.4	1.8	60.83	58.50	0.962
C30030U-T2B	66.05	74.08	1.12	0.94	1	0.15	0.4	1.8	58.29	58.50	1.004
C30030F-T1A	65.87	105.52	1.60	0.79	1	0.15	0.4	1.8	65.13	63.50	0.975
C30030F-T1B	64.65	104.56	1.62	0.79	1	0.15	0.4	1.8	64.11	63.50	0.990
C30030F-T2A	64.91	101.43	1.56	0.80	1	0.15	0.4	1.8	63.68	62.50	0.981
C30030F-T2B	65.49	104.56	1.60	0.79	1	0.15	0.4	1.8	64.69	62.50	0.966
C30024U-T1A	48.22	39.72	0.82	1.10	1	0.15	0.4	1.8	38.43	39.00	1.015
C30024U-T1B	48.70	38.97	0.80	1.12	1	0.15	0.4	1.8	38.43	39.00	1.015
C30024U-T2A	48.48	39.45	0.81	1.11	1	0.15	0.4	1.8	38.47	38.50	1.001
C30024U-T2B	49.10	39.92	0.81	1.11	1	0.15	0.4	1.8	38.96	38.50	0.988
C30024F-T1A	47.33	51.92	1.10	0.95	1	0.15	0.4	1.8	41.47	41.00	0.989
C30024F-T1B	48.12	54.36	1.13	0.94	1	0.15	0.4	1.8	42.57	41.00	0.963
C30024F-T2A	48.27	52.45	1.09	0.96	1	0.15	0.4	1.8	42.16	40.50	0.961
C30024F-T2B	49.20	54.72	1.11	0.95	1	0.15	0.4	1.8	43.30	40.50	0.935
Mean											0.989
COV											2.87%

Table F-4: DHS sections (Morelli et al. [40])

Specimen	Yield Load P_y (kN)	Buckling P_{cr} (kN)	Ratio P_{cr}/P_y	$\lambda = \sqrt{P_y / P_{cr}}$	Ratios				Nominal P_n (kN)	Experiment P_{exp} (kN)	Ratio P_{exp}/P_n
					k_1	k_2	k_3	k_4			
DHS30030U-T1A	50.27	113.21	2.25	0.67	1	0.15	0.4	1.8	55.95	53.00	0.947
DHS30030U-T1B	49.08	110.32	2.25	0.67	1	0.15	0.4	1.8	54.59	53.00	0.971
DHS30030U-T2A	50.38	115.64	2.30	0.66	1	0.15	0.4	1.8	56.39	52.50	0.931
DHS30030U-T2B	50.64	114.20	2.26	0.67	1	0.15	0.4	1.8	56.38	52.50	0.931
DHS30030F-T1A	47.23	118.07	2.50	0.63	1	0.15	0.4	1.8	54.21	53.00	0.978
DHS30030F-T1B	47.36	119.12	2.52	0.63	1	0.15	0.4	1.8	54.45	53.00	0.973
DHS30030F-T2A	48.02	119.74	2.49	0.63	1	0.15	0.4	1.8	55.08	53.00	0.962
DHS30030F-T2B	47.80	118.21	2.47	0.64	1	0.15	0.4	1.8	54.70	53.00	0.969
DHS30024U-T1A	37.04	69.58	1.88	0.73	1	0.15	0.4	1.8	38.80	41.00	1.057
DHS30024U-T1B	36.67	67.81	1.85	0.74	1	0.15	0.4	1.8	38.20	41.00	1.073
DHS30024U-T2A	36.71	66.32	1.81	0.74	1	0.15	0.4	1.8	37.92	39.50	1.042
DHS30024U-T2B	36.51	68.39	1.87	0.73	1	0.15	0.4	1.8	38.21	39.50	1.034
DHS30024F-T1A	37.38	80.02	2.14	0.68	1	0.15	0.4	1.8	40.94	41.50	1.014
DHS30024F-T1B	37.58	80.87	2.15	0.68	1	0.15	0.4	1.8	41.23	41.50	1.007
DHS30024F-T2A	37.98	79.56	2.09	0.69	1	0.15	0.4	1.8	41.31	42.50	1.029
DHS30024F-T2B	38.39	80.16	2.09	0.69	1	0.15	0.4	1.8	41.71	42.50	1.019
Mean											0.996
COV											4.44%

Table F-5: Unlipped plain-C sections (Young and Hancock [22])

Specimen	Yield Load P_y (kN)	Buckling P_{cr} (kN)	Ratio P_{cr}/P_y	$\lambda = \sqrt{P_y/P_{cr}}$	Ratio k_1	k_2	k_3	k_4	Nominal P_n (kN)	Experiment P_{exp} (kN)	Ratio P_{exp}/P_n
IOF75N40A	27.53	210.56	7.65	0.36	1	0.15	0.4	1.8	39.29	49.00	1.247
IOF75N40B	27.53	210.60	7.65	0.36	1	0.15	0.4	1.8	39.29	49.00	1.247
IOF75N20A	28.87	216.74	7.51	0.36	1	0.15	0.4	1.8	41.11	47.20	1.148
IOF75N20B	28.83	216.74	7.52	0.36	1	0.15	0.4	1.8	41.06	47.20	1.150
IOF100N50A	35.06	187.56	5.35	0.43	1	0.15	0.4	1.8	47.48	57.90	1.220
IOF100N50B	35.06	187.56	5.35	0.43	1	0.15	0.4	1.8	47.48	57.90	1.220
IOF100N25A	36.66	194.58	5.31	0.43	1	0.15	0.4	1.8	49.58	56.30	1.135
IOF100N25B	36.70	194.58	5.30	0.43	1	0.15	0.4	1.8	49.63	56.30	1.134
IOF125N65A	41.78	165.75	3.97	0.50	1	0.15	0.4	1.8	53.58	63.60	1.187
IOF125N65B	41.78	165.75	3.97	0.50	1	0.15	0.4	1.8	53.58	63.60	1.187
IOF125N32A	43.63	171.36	3.93	0.50	1	0.15	0.4	1.8	55.83	57.40	1.028
IOF125N32B	43.63	171.36	3.93	0.50	1	0.15	0.4	1.8	55.83	57.40	1.028
IOF200N75A	90.04	264.15	2.93	0.58	1	0.15	0.4	1.8	107.86	94.50	0.876
IOF200N75B	89.68	264.15	2.95	0.58	1	0.15	0.4	1.8	107.54	94.50	0.879
IOF200N37A	92.21	260.04	2.82	0.60	1	0.15	0.4	1.8	109.36	91.20	0.834
IOF200N37B	92.80	260.04	2.80	0.60	1	0.15	0.4	1.8	109.87	91.20	0.830
IOF250N90A	132.05	440.64	3.34	0.55	1	0.15	0.4	1.8	163.15	142.80	0.875
IOF250N90B	131.94	440.64	3.34	0.55	1	0.15	0.4	1.8	163.05	142.80	0.876
IOF250N45A	135.28	436.46	3.23	0.56	1	0.15	0.4	1.8	165.84	132.30	0.798
IOF250N45B	135.65	436.46	3.22	0.56	1	0.15	0.4	1.8	166.19	132.30	0.796
IOF300N90A	152.61	392.85	2.57	0.62	1	0.15	0.4	1.8	176.61	143.40	0.812
IOF300N90B	152.66	392.85	2.57	0.62	1	0.15	0.4	1.8	176.66	143.40	0.812
IOF300N45A	156.26	388.58	2.49	0.63	1	0.15	0.4	1.8	179.09	134.60	0.752
IOF300N45B	156.21	388.58	2.49	0.63	1	0.15	0.4	1.8	179.05	134.60	0.752
Mean											0.993
COV											18.36%

2. EOF load case

Table F-6: Lipped plain-C sections (Hadchiti et al. [8])

Specimen	Yield Load P_y (kN)	Buckling P_{cr} (kN)	Ratio P_{cr}/P_y	$\lambda = \sqrt{P_y / P_{cr}}$	Ratio				Nominal P_n (kN)	Experiment P_{exp} (kN)	Ratio P_{exp}/P_n
					k_1	k_2	k_3	k_4			
C20015-U1A	11.90	6.81	0.57	1.32	1	0.15	0.4	1.8	8.38	7.77	0.927
C20015-U1B	11.81	6.99	0.59	1.30	1	0.15	0.4	1.8	8.41	7.77	0.924
C20015-U2A	11.85	6.88	0.58	1.31	1	0.15	0.4	1.8	8.39	7.69	0.917
C20015-U2B	11.89	6.80	0.57	1.32	1	0.15	0.4	1.8	8.36	7.69	0.919
C20015-F1A	11.81	9.16	0.78	1.14	1	0.15	0.4	1.8	9.22	9.48	1.028
C20015-F1B	11.81	9.16	0.78	1.14	1	0.15	0.4	1.8	9.22	9.48	1.028
C20015-F2A	11.78	9.25	0.79	1.13	1	0.15	0.4	1.8	9.24	9.39	1.017
C20015-F2B	11.81	9.20	0.78	1.13	1	0.15	0.4	1.8	9.24	9.39	1.017
C20024-U1A	21.97	28.41	1.29	0.88	1	0.15	0.4	1.8	20.30	22.49	1.108
C20024-U1B	22.04	25.86	1.17	0.92	1	0.15	0.4	1.8	19.74	22.49	1.139
C20024-U2A	22.07	25.66	1.16	0.93	1	0.15	0.4	1.8	19.71	21.49	1.091
C20024-U2B	22.17	25.17	1.14	0.94	1	0.15	0.4	1.8	19.64	21.49	1.094
C20024-F1A	22.10	36.31	1.64	0.78	1	0.15	0.4	1.8	22.03	25.82	1.172
C20024-F1B	22.04	36.67	1.66	0.78	1	0.15	0.4	1.8	22.05	25.82	1.171
C20024-F2A	22.17	36.13	1.63	0.78	1	0.15	0.4	1.8	22.04	26.23	1.190
C20024-F2B	22.17	37.70	1.70	0.77	1	0.15	0.4	1.8	22.38	26.23	1.172
Mean											1.057
COV											9.37%

Table F-7: SupaCee sections (Hadchiti et al. [8])

Specimen	Yield Load P_y (kN)	Buckling P_{cr} (kN)	Ratio P_{cr}/P_y	$\lambda = \sqrt{P_y / P_{cr}}$	Ratio				Nominal P_n (kN)	Experiment P_{exp} (kN)	Ratio P_{exp}/P_n
					k_1	k_2	k_3	k_4			
SC20015-U1A	11.81	8.22	0.70	1.20	1	0.15	0.4	1.8	8.89	8.55	0.962
SC20015-U1B	11.83	8.59	0.73	1.17	1	0.15	0.4	1.8	9.03	8.55	0.946
SC20015-U2A	11.81	8.31	0.70	1.19	1	0.15	0.4	1.8	8.93	8.58	0.961
SC20015-U2B	11.87	8.33	0.70	1.19	1	0.15	0.4	1.8	8.96	8.58	0.958
SC20015-F1A	11.85	10.07	0.85	1.08	1	0.15	0.4	1.8	9.54	9.28	0.973
SC20015-F1B	11.90	9.95	0.84	1.09	1	0.15	0.4	1.8	9.53	9.29	0.974
SC20015-F2A	11.94	9.80	0.82	1.10	1	0.15	0.4	1.8	9.50	9.29	0.978
SC20015-F2B	11.90	9.88	0.83	1.10	1	0.15	0.4	1.8	9.51	9.29	0.977
SC20024-U1A	22.21	28.98	1.31	0.88	1	0.15	0.4	1.8	20.58	21.59	1.049
SC20024-U1B	22.14	28.23	1.28	0.89	1	0.15	0.4	1.8	20.37	21.59	1.060
SC20024-U2A	21.92	29.78	1.36	0.86	1	0.15	0.4	1.8	20.58	21.61	1.050
SC20024-U2B	22.00	29.78	1.35	0.86	1	0.15	0.4	1.8	20.63	21.61	1.047
SC20024-F1A	22.14	37.87	1.71	0.76	1	0.15	0.4	1.8	22.40	23.29	1.040
SC20024-F1B	22.21	37.85	1.70	0.77	1	0.15	0.4	1.8	22.43	23.29	1.038
SC20024-F2A	22.07	38.06	1.72	0.76	1	0.15	0.4	1.8	22.40	23.75	1.060
SC20024-F2B	22.07	38.06	1.72	0.76	1	0.15	0.4	1.8	22.40	23.75	1.060
Mean											1.008
COV											4.44%

Table F-8: Lipped plain-C sections (Macdonald et al. [37])

Specimen	Yield Load P_y (kN)	Buckling P_{cr} (kN)	Ratio P_{cr}/P_y	$\lambda = \sqrt{P_y / P_{cr}}$	Ratio				Nominal P_n (kN)	Experiment P_{exp} (kN)	Ratio P_{exp}/P_n
					k_1	k_2	k_3	k_4			
EOF-25F-1	0.98	2.62	2.68	0.61	1	0.15	0.4	1.8	1.14	1.18	1.033
EOF-25F2	1.08	2.27	2.11	0.69	1	0.15	0.4	1.8	1.17	1.24	1.057
EOF-25F-3	1.39	2.04	1.47	0.83	1	0.15	0.4	1.8	1.34	1.46	1.092
EOF-100F-4	1.64	3.32	2.02	0.70	1	0.15	0.4	1.8	1.76	1.74	0.987
EOF-100F-5	1.82	3.31	1.82	0.74	1	0.15	0.4	1.8	1.89	2.00	1.060
EOF-100F-6	2.36	3.37	1.43	0.84	1	0.15	0.4	1.8	2.25	2.25	1.000
EOF-50F-7	1.32	2.96	2.24	0.67	1	0.15	0.4	1.8	1.47	1.43	0.973
EOF-50F-8	1.71	2.79	1.63	0.78	1	0.15	0.4	1.8	1.70	1.70	0.998
EOF-50F-9	1.20	3.00	2.50	0.63	1	0.15	0.4	1.8	1.37	1.34	0.975
EOF-50F-10	1.46	3.07	2.10	0.69	1	0.15	0.4	1.8	1.59	1.80	1.132
EOF-50F-11	1.12	3.04	2.72	0.61	1	0.15	0.4	1.8	1.31	1.44	1.097
EOF-50F-12	1.01	3.11	3.08	0.57	1	0.15	0.4	1.8	1.22	1.32	1.078
EOF-25F-13	1.14	2.92	2.57	0.62	1	0.15	0.4	1.8	1.31	1.44	1.096
EOF-25F-14	0.87	2.89	3.32	0.55	1	0.15	0.4	1.8	1.07	1.12	1.044
EOF-25F-15	0.79	2.95	3.75	0.52	1	0.15	0.4	1.8	1.00	1.10	1.101
EOF-100F-16	2.27	3.41	1.51	0.81	1	0.15	0.4	1.8	2.20	2.35	1.069
EOF-100F-17	1.74	3.38	1.94	0.72	1	0.15	0.4	1.8	1.85	1.90	1.029
EOF-100F-18	1.55	3.46	2.23	0.67	1	0.15	0.4	1.8	1.72	1.62	0.942
Mean											1.042
COV											5.15%

Table F-9: Lipped plain-C sections (Lian et al. [42])

Specimen	Yield Load P_y (kN)	Buckling P_{cr} (kN)	Ratio P_{cr}/P_y	$\lambda = \sqrt{P_y / P_{cr}}$	Ratio				Nominal P_n (kN)	Experiment P_{exp} (kN)	Ratio P_{exp}/P_n
					k_1	k_2	k_3	k_4			
C142N100A0U1	6.72	6.60	0.98	1.01	1	0.15	0.4	1.8	5.68	4.78	0.842
C142N100A0U2	6.71	6.63	0.99	1.01	1	0.15	0.4	1.8	5.68	4.81	0.847
C142N100A0U3	6.72	6.58	0.98	1.01	1	0.15	0.4	1.8	5.67	4.76	0.839
C142N120A0U	7.48	7.57	1.01	0.99	1	0.15	0.4	1.8	6.39	5.41	0.847
C142N100A0F1	6.99	9.66	1.38	0.85	1	0.15	0.4	1.8	6.60	7.07	1.072
C142N100A0F2	6.99	9.65	1.38	0.85	1	0.15	0.4	1.8	6.60	6.80	1.031
C142N100A0F3	6.99	9.65	1.38	0.85	1	0.15	0.4	1.8	6.60	7.04	1.067
C142N120A0F	7.41	9.72	1.31	0.87	1	0.15	0.4	1.8	6.88	7.33	1.066
C142N150A0F	8.17	9.23	1.13	0.94	1	0.15	0.4	1.8	7.23	7.97	1.102
C202N100A0F	9.30	6.89	0.74	1.16	1	0.15	0.4	1.8	7.15	6.53	0.913
C202N120A0F	10.01	7.58	0.76	1.15	1	0.15	0.4	1.8	7.75	7.11	0.917
C202N150A0F	11.06	8.58	0.78	1.14	1	0.15	0.4	1.8	8.64	7.73	0.895
C302N100A0F	17.77	8.39	0.47	1.46	1	0.15	0.4	1.8	11.70	11.07	0.946
C302N120A0F	19.38	9.64	0.50	1.42	1	0.15	0.4	1.8	13.00	12.31	0.947
C302N150A0F	20.20	9.88	0.49	1.43	1	0.15	0.4	1.8	13.47	12.58	0.934
Mean											0.951
COV											9.84%

Table F-10: Unlipped plain-C sections (Young and Hancock [22])

Specimen	Ratio r_i/t_w	Yield Load P_y (kN)	Plastic P_p (kN)	Buckling P_{cr} (kN)	Ratio P_{cr}/P_y	$\lambda = \sqrt{P_y/P_{cr}}$	Ratios				Nominal P_n (kN)	Experiment P_{exp} (kN)	Ratio P_{exp}/P_n
							k_1	k_2	k_3	k_4			
EOF75N40A	1.02	15.35	17.91	270.21	17.60	0.24	1	0.15	0.4	1.8	23.86	23.90	1.002
EOF75N40B	1.02	15.34	17.89	271.43	17.70	0.24	1	0.15	0.4	1.8	23.85	23.90	1.002
EOF75N20A	1.02	12.27	14.32	219.18	17.86	0.24	1	0.15	0.4	1.8	19.10	24.60	1.288
EOF75N20B	1.02	12.28	14.33	219.18	17.84	0.24	1	0.15	0.4	1.8	19.11	24.60	1.287
EOF100N50A	1.06	19.21	23.80	211.63	11.02	0.30	1	0.15	0.4	1.8	28.61	34.40	1.202
EOF100N50B	1.06	19.21	23.80	211.58	11.01	0.30	1	0.15	0.4	1.8	28.61	34.40	1.202
EOF100N25A	1.06	15.54	19.24	166.10	10.69	0.31	1	0.15	0.4	1.8	23.07	31.40	1.361
EOF100N25B	1.07	15.41	19.09	163.74	10.62	0.31	1	0.15	0.4	1.8	22.87	31.40	1.373
EOF125N65A	1.01	22.97	28.93	177.02	7.71	0.36	1	0.15	0.4	1.8	32.82	35.30	1.076
EOF125N65B	1.02	22.88	28.81	188.92	8.26	0.35	1	0.15	0.4	1.8	32.97	35.30	1.071
EOF125N32A	1.02	18.42	23.20	133.19	7.23	0.37	1	0.15	0.4	1.8	26.09	29.70	1.138
EOF125N32B	1.02	18.40	23.17	133.43	7.25	0.37	1	0.15	0.4	1.8	26.07	29.70	1.139
EOF200N75A	0.89	42.91	53.76	164.41	3.83	0.51	1	0.15	0.4	1.8	54.63	49.30	0.902
EOF200N75B	0.89	42.92	53.78	164.28	3.83	0.51	1	0.15	0.4	1.8	54.64	49.30	0.902
EOF200N37A	0.89	36.13	45.27	134.73	3.73	0.52	1	0.15	0.4	1.8	45.74	43.70	0.955
EOF200N37B	0.89	36.34	45.54	136.35	3.75	0.52	1	0.15	0.4	1.8	46.07	43.70	0.949
EOF250N90A	1.32	62.37	74.29	263.62	4.23	0.49	1	0.15	0.4	1.8	80.99	64.30	0.794
EOF250N90B	1.32	62.37	74.29	263.64	4.23	0.49	1	0.15	0.4	1.8	80.99	64.30	0.794
EOF250N45A	1.32	52.85	62.94	218.36	4.13	0.49	1	0.15	0.4	1.8	68.32	61.30	0.897
EOF250N45B	1.32	52.81	62.90	218.61	4.14	0.49	1	0.15	0.4	1.8	68.30	61.30	0.898
EOF300N90A	1.40	67.88	83.49	201.02	2.96	0.58	1	0.15	0.4	1.8	81.51	64.80	0.795
EOF300N90B	1.40	67.87	83.47	201.22	2.96	0.58	1	0.15	0.4	1.8	81.52	64.80	0.795
EOF300N45A	1.40	58.70	72.19	171.45	2.92	0.59	1	0.15	0.4	1.8	70.24	62.50	0.890
EOF300N45B	1.40	58.67	72.15	171.65	2.93	0.58	1	0.15	0.4	1.8	70.23	62.50	0.890
Mean													1.025
COV													18.07%

3. ITF load case

Table F-11: Lipped plain-C sections (Bartlett et al. [9])

Specimens	Yield Load P_y (kN)	Buckling P_{cr} (kN)	Ratio P_{cr}/P_y	$\lambda = \sqrt{P_y/P_{cr}}$	Ratios				Nominal P_n (kN)	Experiment P_{exp} (kN)	Ratio P_{exp}/P_n
					k_1	k_2	k_3	k_4			
C20015-U1A	24.95	7.80	0.31	1.79	1	0.15	0.6	1.8	11.49	14.01	1.219
C20015-U1B	24.77	7.68	0.31	1.80	1	0.15	0.6	1.8	11.36	14.01	1.234
C20015-U2A	24.62	7.71	0.31	1.79	1	0.15	0.6	1.8	11.35	14.02	1.235
C20015-U2B	24.61	7.77	0.32	1.78	1	0.15	0.6	1.8	11.39	14.02	1.231
C20015-F1A	23.76	11.59	0.49	1.43	1	0.15	0.6	1.8	13.94	16.75	1.202
C20015-F1B	23.80	11.53	0.48	1.44	1	0.15	0.6	1.8	13.91	16.75	1.204
C20015-F2A	24.03	11.75	0.49	1.43	1	0.15	0.6	1.8	14.12	16.56	1.173
C20015-F2B	23.82	11.53	0.48	1.44	1	0.15	0.6	1.8	13.91	16.56	1.190
C20024-U1A	43.16	30.36	0.70	1.19	1	0.15	0.6	1.8	30.70	37.42	1.219
C20024-U1B	43.11	29.93	0.69	1.20	1	0.15	0.6	1.8	30.46	37.42	1.229
C20024-U2A	43.49	29.69	0.68	1.21	1	0.15	0.6	1.8	30.46	37.63	1.235
C20024-U2B	42.79	29.69	0.69	1.20	1	0.15	0.6	1.8	30.23	37.63	1.245
C20024-F1A	41.52	44.00	1.06	0.97	1	0.15	0.6	1.8	36.31	42.75	1.177
C20024-F1B	41.77	44.52	1.07	0.97	1	0.15	0.6	1.8	36.63	42.75	1.167
C20024-F2A	41.44	43.60	1.05	0.97	1	0.15	0.6	1.8	36.11	42.62	1.180
C20024-F2B	41.46	44.10	1.06	0.97	1	0.15	0.6	1.8	36.33	42.62	1.173
Mean											1.207
COV											2.23%

Table F-12: SupaCee sections (Bartlett et al. [9])

Specimens	Yield Load P_y (kN)	Buckling P_{cr} (kN)	Ratio P_{cr}/P_y	$\lambda = \sqrt{P_y/P_{cr}}$	Ratios				Nominal P_n (kN)	Experiment P_{exp} (kN)	Ratio P_{exp}/P_n
					k_1	k_2	k_3	k_4			
SC20015-U1A	24.94	10.35	0.42	1.55	1	0.15	0.6	1.8	13.42	14.26	1.063
SC20015-U1B	24.49	10.60	0.43	1.52	1	0.15	0.6	1.8	13.48	14.26	1.058
SC20015-U2A	24.75	10.26	0.41	1.55	1	0.15	0.6	1.8	13.30	14.15	1.064
SC20015-U2B	24.07	10.77	0.45	1.50	1	0.15	0.6	1.8	13.48	14.15	1.050
SC20015-F1A	23.68	13.89	0.59	1.31	1	0.15	0.6	1.8	15.32	17.25	1.126
SC20015-F1B	23.81	14.36	0.60	1.29	1	0.15	0.6	1.8	15.63	17.25	1.103
SC20015-F2A	23.84	14.21	0.60	1.30	1	0.15	0.6	1.8	15.55	17.63	1.134
SC20015-F2B	23.85	14.64	0.61	1.28	1	0.15	0.6	1.8	15.80	17.63	1.116
SC20024-U1A	42.69	36.23	0.85	1.09	1	0.15	0.6	1.8	33.43	37.36	1.118
SC20024-U1B	42.36	35.42	0.84	1.09	1	0.15	0.6	1.8	32.92	37.36	1.135
SC20024-U2A	42.91	33.84	0.79	1.13	1	0.15	0.6	1.8	32.37	37.18	1.149
SC20024-U2B	42.25	37.49	0.89	1.06	1	0.15	0.6	1.8	33.84	37.18	1.099
SC20024-F1A	41.40	52.73	1.27	0.89	1	0.15	0.6	1.8	39.57	44.03	1.113
SC20024-F1B	41.16	54.65	1.33	0.87	1	0.15	0.6	1.8	40.12	44.03	1.098
SC20024-F2A	41.39	53.06	1.28	0.88	1	0.15	0.6	1.8	39.68	44.06	1.110
SC20024-F2B	41.95	52.56	1.25	0.89	1	0.15	0.6	1.8	39.78	44.06	1.107
Mean											1.089
COV											3.11%

Table F-13: Lipped plain-C sections (Khatale et al. [41])

Specimens	Yield Load P_y (kN)	Buckling P_{cr} (kN)	$\lambda = \sqrt{P_y/P_{cr}}$	Ratios				Nominal P_n (kN)	Experiment P_{exp} (kN)	Ratio P_{exp}/P_n
				k_1	k_2	k_3	k_4			
C30030-UA	102.33	39.78	1.60	1	0.15	0.6	1.8	53.11	52.83	0.995
C30030-UB	100.15	36.16	1.66	1	0.15	0.6	1.8	49.92	53.21	1.066
C30030-FA	79.99	56.99	1.18	1	0.15	0.6	1.8	57.28	62.58	1.093
C30030-FB	77.71	52.15	1.22	1	0.15	0.6	1.8	53.95	62.77	1.164
C30024-UA	73.91	18.88	1.98	1	0.15	0.6	1.8	30.44	31.73	1.043
C30024-UB	72.23	17.69	2.02	1	0.15	0.6	1.8	29.05	32.35	1.114
C30024-FA	58.80	28.69	1.43	1	0.15	0.6	1.8	34.50	39.72	1.151
C30024-FB	60.39	29.34	1.43	1	0.15	0.6	1.8	35.35	39.69	1.123
Mean										1.093
COV										5.20%

Table F-14: DHS sections (Khatale et al. [41])

Specimens	Yield Load P_y (kN)	Buckling P_{cr} (kN)	Ratio P_{cr}/P_y	$\lambda = \sqrt{P_y / P_{cr}}$	Ratios				Nominal P_n (kN)	Experiment P_{exp} (kN)	Ratio P_{exp}/P_n
					k_1	k_2	k_3	k_4			
DHS30030-UA	59.51	56.52	0.95	1.03	1	0.15	0.6	1.8	49.31	53.08	1.077
DHS30030-UB	57.82	55.59	0.96	1.02	1	0.15	0.6	1.8	48.20	53.47	1.109
DHS30030-FA	75.32	63.80	0.85	1.09	1	0.15	0.6	1.8	58.92	56.51	0.959
DHS30030-FB	73.83	61.58	0.83	1.09	1	0.15	0.6	1.8	57.31	54.00	0.942
DHS30024-UA	44.98	37.66	0.84	1.09	1	0.15	0.6	1.8	34.98	36.69	1.049
DHS30024-UB	46.04	39.14	0.85	1.08	1	0.15	0.6	1.8	36.08	37.01	1.026
DHS30024-FA	61.65	47.75	0.77	1.14	1	0.15	0.6	1.8	46.08	44.75	0.971
DHS30024-FB	63.84	49.56	0.78	1.13	1	0.15	0.6	1.8	47.78	44.89	0.940
Mean											1.009
COV											6.46%

Table F-15: Lipped plain-C sections (Sundararajah et al. [19])

Specimens	Yield Load P_y (kN)	Buckling P_{cr} (kN)	Ratio P_{cr}/P_y	$\lambda = \sqrt{P_y / P_{cr}}$	Ratios				Nominal P_n (kN)	Experiment P_{exp} (kN)	Ratio P_{exp}/P_n
					k_1	k_2	k_3	k_4			
C10010U-25	10.82	5.87	0.54	1.36	1	0.15	0.6	1.8	6.72	7.05	1.049
C10015U-25	17.57	16.78	0.96	1.02	1	0.15	0.6	1.8	14.60	14.43	0.989
C15012U-25	20.41	5.74	0.28	1.89	1	0.15	0.6	1.8	8.87	9.13	1.030
C15015U-25	26.53	10.86	0.41	1.56	1	0.15	0.6	1.8	14.16	15.36	1.085
C20019U-25	48.41	14.18	0.29	1.85	1	0.15	0.6	1.8	21.51	22.99	1.069
C20024U-25	66.27	27.16	0.41	1.56	1	0.15	0.6	1.8	35.40	36.71	1.037
C10010U-50	9.20	5.99	0.65	1.24	1	0.15	0.6	1.8	6.29	6.41	1.020
C10015U-50	14.87	17.20	1.16	0.93	1	0.15	0.6	1.8	13.57	14.30	1.054
C15012U-50	18.61	5.78	0.31	1.79	1	0.15	0.6	1.8	8.54	8.16	0.955
C15015U-50	24.16	10.90	0.45	1.49	1	0.15	0.6	1.8	13.59	13.17	0.969
C20019U-50	45.27	14.30	0.32	1.78	1	0.15	0.6	1.8	20.97	20.70	0.987
C20024U-50	61.93	27.41	0.44	1.50	1	0.15	0.6	1.8	34.48	34.41	0.998
C10010U-100	5.62	6.63	1.18	0.92	1	0.15	0.6	1.8	5.18	6.45	1.245
C15012U-100	14.38	6.13	0.43	1.53	1	0.15	0.6	1.8	7.85	8.14	1.038
C15015U-100	18.63	11.63	0.62	1.27	1	0.15	0.6	1.8	12.46	12.92	1.037
C20019U-100	38.24	14.84	0.39	1.61	1	0.15	0.6	1.8	19.83	20.19	1.018
C20024U-100	52.50	28.33	0.54	1.36	1	0.15	0.6	1.8	32.50	33.68	1.036
Mean											1.036
COV											6.17%

Table F-16: Lipped plain-C sections (Uzzaman et al. [38])

Specimens	Yield Load P_y (kN)	Buckling P_{cr} (kN)	Ratio P_{cr}/P_y	$\lambda = \sqrt{P_y/P_{cr}}$	k_1	k_2	k_3	k_4	Nominal P_n (kN)	Experiment P_{exp} (kN)	Ratio P_{exp}/P_n
C142N90A0U	10.36	9.05	0.87	1.07	1	0.15	0.6	1.8	8.23	6.03	0.733
C142N120A0U	8.49	9.52	1.12	0.94	1	0.15	0.6	1.8	7.63	6.32	0.828
C172N120A0U	14.40	9.53	0.66	1.23	1	0.15	0.6	1.8	9.93	7.05	0.710
C202N150A0U	18.34	11.75	0.64	1.25	1	0.15	0.6	1.8	12.43	8.40	0.676
C262N150A0U	30.53	6.83	0.22	2.11	1	0.15	0.6	1.8	11.67	8.19	0.702
C142N90A0F	12.08	9.31	0.77	1.14	1	0.15	0.6	1.8	9.01	8.97	0.996
C142N120A0F	13.39	9.92	0.74	1.16	1	0.15	0.6	1.8	9.78	9.44	0.965
C172N120A0F	18.26	8.32	0.46	1.48	1	0.15	0.6	1.8	10.33	10.72	1.038
C202N150A0F	24.85	10.51	0.42	1.54	1	0.15	0.6	1.8	13.50	13.51	1.001
C262N150A0F	32.71	9.87	0.30	1.82	1	0.15	0.6	1.8	14.77	12.78	0.865
Mean											0.851
COV											16.56%

Table F-17: Lipped plain-C sections (Beshara and Schuster [36])

Specimens	Yield Load P_y (kN)	Buckling P_{cr} (kN)	$\lambda = \sqrt{P_y/P_{cr}}$	k_1	k_2	k_3	k_4	Nominal P_n (kN)	Experiment P_{exp} (kN)	Ratio P_{exp}/P_n
C120-7-30F	6.64	21.28	0.56	1	0.15	0.6	1.8	8.44	10.70	1.268
C120-7-60F	7.96	21.82	0.60	1	0.15	0.6	1.8	9.78	11.80	1.207
C120-10-30F	6.14	23.44	0.51	1	0.15	0.6	1.8	8.07	9.96	1.234
C120-10-60F	7.36	24.75	0.55	1	0.15	0.6	1.8	9.44	11.00	1.165
C120-14-30F	5.66	23.33	0.49	1	0.15	0.6	1.8	7.55	9.06	1.200
C120-14-60F	6.81	25.02	0.52	1	0.15	0.6	1.8	8.89	10.10	1.136
C200-7-30F	7.66	6.51	1.08	1	0.15	0.6	1.8	6.00	7.20	1.199
C200-7-60F	8.65	6.57	1.15	1	0.15	0.6	1.8	6.40	7.56	1.181
C200-10-30F	7.12	6.64	1.04	1	0.15	0.6	1.8	5.85	6.57	1.124
C200-10-60F	8.08	6.79	1.09	1	0.15	0.6	1.8	6.29	7.08	1.125
C200-14-60F	7.71	5.88	1.14	1	0.15	0.6	1.8	5.72	6.72	1.175
C200-14-100F	8.69	6.21	1.18	1	0.15	0.6	1.8	6.23	7.08	1.136
C300-7-30F	19.86	7.17	1.66	1	0.15	0.6	1.8	9.90	11.00	1.111
C300-7-60F	21.65	7.21	1.73	1	0.15	0.6	1.8	10.32	11.60	1.124
C300-10-30F	18.29	8.59	1.46	1	0.15	0.6	1.8	10.51	9.99	0.950
C300-10-60F	19.99	8.56	1.53	1	0.15	0.6	1.8	10.93	10.90	0.997
C300-14-60F	18.84	9.19	1.43	1	0.15	0.6	1.8	11.05	11.30	1.022
C300-14-100F	20.57	9.43	1.48	1	0.15	0.6	1.8	11.67	10.60	0.908
Mean										1.126
COV										8.69%

Table F-18: Unlipped plain-C sections (Young and Hancock [22])

| Specimens | Yield Load P_y (kN) | Buckling P_{cr} (kN) | Ratio P_{cr}/P_y | $\lambda = \sqrt{P_y / P_{cr}}$ | Ratios | | | | Nominal P_n (kN) | Experiment P_{exp} (kN) | Ratio P_{exp}/P_n |
					k_1	k_2	k_3	k_4			
ITF75-N40	29.07	302.28	10.40	0.31	1	0.15	0.6	1.8	43.79	51.30	1.171
ITF75-N20	35.60	290.56	8.16	0.35	1	0.15	0.6	1.8	52.27	54.90	1.050
ITF100-N50	37.93	247.75	6.53	0.39	1	0.15	0.6	1.8	54.22	24.80	0.457
ITF100-N25	45.60	253.28	5.55	0.42	1	0.15	0.6	1.8	63.75	22.60	0.354
ITF125-N65A	44.70	171.60	3.84	0.51	1	0.15	0.6	1.8	58.84	60.40	1.026
ITF125-N65B	44.65	171.73	3.85	0.51	1	0.15	0.6	1.8	58.80	59.60	1.014
ITF125-N32A	54.17	166.82	3.08	0.57	1	0.15	0.6	1.8	68.26	64.40	0.943
ITF125-N32B	54.07	166.82	3.09	0.57	1	0.15	0.6	1.8	68.16	63.80	0.936
ITF200-N75	104.80	183.23	1.75	0.76	1	0.15	0.6	1.8	113.54	100.10	0.882
ITF200-N37	118.41	180.71	1.53	0.81	1	0.15	0.6	1.8	122.32	99.80	0.816
ITF250-N90	155.04	306.18	1.97	0.71	1	0.15	0.6	1.8	174.54	148.50	0.851
ITF250-N45	174.25	298.17	1.71	0.76	1	0.15	0.6	1.8	187.44	148.40	0.792
ITF300-N90	185.08	246.15	1.33	0.87	1	0.15	0.6	1.8	180.53	149.10	0.826
ITF300-N45	203.87	239.99	1.18	0.92	1	0.15	0.6	1.8	187.64	144.60	0.771
Mean											0.849
COV											25.91%

4. ETF load case

Table F-19: Lipped plain-C sections (Htet and Pham [10])

| Specimens | Yield Load P_y (kN) | Buckling P_{cr} (kN) | $\lambda = \sqrt{P_y / P_{cr}}$ | Ratios | | | | Nominal P_n (kN) | Experiment P_{exp} (kN) | Ratio P_{exp}/P_n |
				k_1	k_2	k_3	k_4			
C20015-U1A	11.99	3.39	1.88	1	0.25	1	1.8	3.15	3.79	1.204
C20015-U1B	12.09	3.42	1.88	1	0.25	1	1.8	3.18	3.79	1.191
C20015-U2A	12.09	3.43	1.88	1	0.25	1	1.8	3.19	3.80	1.191
C20015-U2B	12.14	3.38	1.90	1	0.25	1	1.8	3.15	3.80	1.207
C20015-F1A	12.19	5.73	1.46	1	0.25	1	1.8	5.05	5.73	1.134
C20015-F1B	11.88	5.41	1.48	1	0.25	1	1.8	4.79	5.73	1.195
C20015-F2A	11.99	5.51	1.47	1	0.25	1	1.8	4.88	5.64	1.155
C20015-F2B	12.35	5.81	1.46	1	0.25	1	1.8	5.13	5.64	1.099
C20024-U1A	21.56	13.82	1.25	1	0.25	1	1.8	11.60	11.61	1.000
C20024-U1B	21.58	14.13	1.24	1	0.25	1	1.8	11.82	11.61	0.982
C20024-U2A	20.97	13.07	1.27	1	0.25	1	1.8	11.03	11.58	1.050
C20024-U2B	21.11	13.48	1.25	1	0.25	1	1.8	11.33	11.58	1.022
C20024-F1A	20.90	21.96	0.98	1	0.25	1	1.8	16.19	16.37	1.011
C20024-F1B	20.87	21.63	0.98	1	0.25	1	1.8	16.03	16.37	1.022
C20024-F2A	21.01	22.16	0.97	1	0.25	1	1.8	16.32	16.42	1.006
C20024-F2B	20.87	21.53	0.98	1	0.25	1	1.8	15.98	16.42	1.028
Mean										1.094
COV										7.91%

Table F-20: SupaCee sections (Htet and Pham [10])

Specimens	Yield Load P_y (kN)	Buckling P_{cr} (kN)	Ratio P_{cr}/P_y	$\lambda = \sqrt{P_y/P_{cr}}$	Ratios				Nominal P_n (kN)	Experiment P_{exp} (kN)	Ratio P_{exp}/P_n
					k_1	k_2	k_3	k_4			
SC20015-U1A	11.88	3.51	0.30	1.84	1	0.25	1	1.8	3.25	4.01	1.233
SC20015-U1B	12.19	3.64	0.30	1.83	1	0.25	1	1.8	3.37	4.01	1.189
SC20015-U2A	12.04	3.46	0.29	1.86	1	0.25	1	1.8	3.22	4.00	1.244
SC20015-U2B	11.88	3.42	0.29	1.86	1	0.25	1	1.8	3.17	4.00	1.261
SC20015-F1A	11.83	6.00	0.51	1.40	1	0.25	1	1.8	5.24	5.86	1.118
SC20015-F1B	12.09	6.15	0.51	1.40	1	0.25	1	1.8	5.36	5.86	1.092
SC20015-F2A	12.14	6.26	0.52	1.39	1	0.25	1	1.8	5.45	5.67	1.040
SC20015-F2B	12.30	6.35	0.52	1.39	1	0.25	1	1.8	5.53	5.67	1.026
SC20024-U1A	21.21	13.40	0.63	1.26	1	0.25	1	1.8	11.28	12.63	1.119
SC20024-U1B	20.97	12.95	0.62	1.27	1	0.25	1	1.8	10.95	12.63	1.153
SC20024-U2A	20.99	13.51	0.64	1.25	1	0.25	1	1.8	11.33	12.48	1.101
SC20024-U2B	21.21	13.46	0.63	1.26	1	0.25	1	1.8	11.33	12.48	1.101
SC20024-F1A	21.21	23.17	1.09	0.96	1	0.25	1	1.8	16.84	17.10	1.016
SC20024-F1B	20.99	23.03	1.10	0.95	1	0.25	1	1.8	16.71	17.10	1.023
SC20024-F2A	21.11	23.07	1.09	0.96	1	0.25	1	1.8	16.77	17.06	1.017
SC20024-F2B	20.87	22.83	1.09	0.96	1	0.25	1	1.8	16.59	17.06	1.028
Mean											1.110
COV											7.65%

Table F-21: Lipped plain-C sections (Khatale et al. [41])

Specimens	Yield Load P_y (kN)	Buckling P_{cr} (kN)	Ratio P_{cr}/P_y	$\lambda = \sqrt{P_y/P_{cr}}$	Ratios				Nominal P_n (kN)	Experiment P_{exp} (kN)	Ratio P_{exp}/P_n
					k_1	k_2	k_3	k_4			
C30030-UA	42.77	14.01	0.33	1.75	1	0.25	1	1.8	12.87	14.34	1.115
C30030-UB	43.75	14.27	0.33	1.75	1	0.25	1	1.8	13.11	15.39	1.174
C30030-FA	44.13	25.56	0.58	1.31	1	0.25	1	1.8	21.86	22.96	1.050
C30030-FB	44.31	25.56	0.58	1.32	1	0.25	1	1.8	21.87	23.50	1.074
C30024-UA	33.50	8.27	0.25	2.01	1	0.25	1	1.8	7.76	9.96	1.284
C30024-UB	33.25	7.86	0.24	2.06	1	0.25	1	1.8	7.40	10.09	1.364
C30024-FA	32.87	13.66	0.42	1.55	1	0.25	1	1.8	12.24	13.88	1.134
C30024-FB	32.69	13.47	0.41	1.56	1	0.25	1	1.8	12.08	13.99	1.158
Mean											1.169
COV											9.06%

Table F-22: DHS sections (Khatale et al. [41])

Specimens	Yield Load P_y (kN)	Buckling P_{cr} (kN)	Ratio P_{cr}/P_y	$\lambda = \sqrt{P_y/P_{cr}}$	Ratios				Nominal P_n (kN)	Experiment P_{exp} (kN)	Ratio P_{exp}/P_n
					k_1	k_2	k_3	k_4			
DHS30030-UA	36.75	25.92	0.71	1.19	1	0.25	1	1.8	21.35	21.44	1.004
DHS30030-UB	36.94	26.04	0.71	1.19	1	0.25	1	1.8	21.45	21.59	1.006
DHS30030-FA	36.86	30.10	0.82	1.11	1	0.25	1	1.8	23.95	28.58	1.193
DHS30030-FB	36.92	29.73	0.81	1.11	1	0.25	1	1.8	23.74	28.79	1.213
DHS30024-UA	28.58	16.60	0.58	1.31	1	0.25	1	1.8	14.19	13.82	0.974
DHS30024-UB	28.80	16.79	0.58	1.31	1	0.25	1	1.8	14.34	13.71	0.956
DHS30024-FA	28.53	18.87	0.66	1.23	1	0.25	1	1.8	15.75	17.28	1.097
DHS30024-FB	29.10	19.41	0.67	1.22	1	0.25	1	1.8	16.18	17.14	1.060
Mean											1.063
COV											9.17%

Table F-23: Lipped plain-C sections (Macdonald et al. [37])

Specimens	Yield Load P_y (kN)	Buckling P_{cr} (kN)	Ratio P_{cr}/P_y	$\lambda = \sqrt{P_y/P_{cr}}$	Ratios				Nominal P_n (kN)	Experiment P_{exp} (kN)	Ratio P_{exp}/P_n
					k_1	k_2	k_3	k_4			
ETF-25F-1	1.16	1.53	1.32	0.87	1	0.25	1	1.8	1.02	0.87	0.849
ETF-25F-2	1.04	1.62	1.56	0.80	1	0.25	1	1.8	0.99	0.81	0.820
ETF-25F-3	0.83	2.06	2.49	0.63	1	0.25	1	1.8	0.90	0.76	0.847
ETF-25F-4	1.52	1.05	0.69	1.20	1	0.25	1	1.8	0.87	1.25	1.434
ETF-25F-5	1.32	1.16	0.88	1.07	1	0.25	1	1.8	0.91	0.98	1.080
ETF-25F-6	1.08	1.39	1.29	0.88	1	0.25	1	1.8	0.94	0.80	0.848
ETF-50F-7	1.21	2.11	1.73	0.76	1	0.25	1	1.8	1.19	1.38	1.157
ETF-50F-8	1.09	2.08	1.92	0.72	1	0.25	1	1.8	1.08	0.92	0.848
ETF-50F-9	0.87	2.68	3.09	0.57	1	0.25	1	1.8	1.00	1.14	1.136
ETF-50F-10	1.57	1.35	0.86	1.08	1	0.25	1	1.8	1.06	1.24	1.167
ETF-50F-11	1.37	1.42	1.04	0.98	1	0.25	1	1.8	1.05	1.22	1.161
ETF-50F-12	1.12	1.84	1.64	0.78	1	0.25	1	1.8	1.08	0.98	0.904
ETF-100F-13	1.53	3.50	2.29	0.66	1	0.25	1	1.8	1.61	1.84	1.143
ETF-100F-14	1.34	3.35	2.51	0.63	1	0.25	1	1.8	1.45	1.76	1.212
ETF-100F-15	1.11	3.58	3.24	0.56	1	0.25	1	1.8	1.30	1.58	1.219
ETF-100F-16	1.68	2.12	1.26	0.89	1	0.25	1	1.8	1.45	1.72	1.185
ETF-100F-17	1.47	2.14	1.46	0.83	1	0.25	1	1.8	1.36	1.56	1.147
ETF-100F-18	1.20	2.25	1.88	0.73	1	0.25	1	1.8	1.19	1.28	1.071
Mean											1.068
COV											16.30%

Table F-24: Lipped plain-C sections (Sundararajah et al. [19])

Specimens	Yield Load P_y (kN)	Buckling P_{cr} (kN)	Ratio P_{cr}/P_y	$\lambda = \sqrt{P_y / P_{cr}}$	Ratios				Nominal P_n (kN)	Experiment P_{exp} (kN)	Ratio P_{exp}/P_n
					k_1	k_2	k_3	k_4			
C10010U-25	4.38	1.91	0.44	1.52	1	0.25	1	1.8	1.70	1.76	1.035
C10015U-25	6.48	6.01	0.93	1.04	1	0.25	1	1.8	4.61	4.24	0.919
C15012U-25	7.33	1.92	0.26	1.95	1	0.25	1	1.8	1.79	2.06	1.148
C15015U-25	9.11	3.76	0.41	1.56	1	0.25	1	1.8	3.37	3.63	1.076
C20019U-25	15.29	5.07	0.33	1.74	1	0.25	1	1.8	4.65	5.51	1.185
C20024U-25	21.69	9.81	0.45	1.49	1	0.25	1	1.8	8.70	9.10	1.046
C10010U-50	4.54	2.20	0.48	1.44	1	0.25	1	1.8	1.93	1.74	0.900
C10015U-50	6.78	6.94	1.02	0.99	1	0.25	1	1.8	5.17	4.47	0.865
C15012U-50	7.55	2.09	0.28	1.90	1	0.25	1	1.8	1.94	2.23	1.148
C15015U-50	9.32	4.14	0.44	1.50	1	0.25	1	1.8	3.68	3.74	1.015
C20019U-50	15.55	5.47	0.35	1.69	1	0.25	1	1.8	4.99	5.63	1.128
C20024U-50	22.09	10.67	0.48	1.44	1	0.25	1	1.8	9.38	7.20	0.767
C10010U-100	4.53	2.99	0.66	1.23	1	0.25	1	1.8	2.49	2.13	0.854
C10015U-100	7.23	9.54	1.32	0.87	1	0.25	1	1.8	6.39	5.27	0.824
C15012U-100	7.92	2.58	0.33	1.75	1	0.25	1	1.8	2.37	2.46	1.040
C15015U-100	9.78	5.16	0.53	1.38	1	0.25	1	1.8	4.48	4.03	0.900
C20019U-100	16.11	6.51	0.40	1.57	1	0.25	1	1.8	5.85	6.01	1.027
C20024U-100	22.89	12.90	0.56	1.33	1	0.25	1	1.8	11.08	9.45	0.853
Mean											0.985
COV											12.91%

Table F-25: Lipped plain-C sections (Uzzaman et al. [38])

Specimens	Yield Load P_y (kN)	Buckling P_{cr} (kN)	Ratio P_{cr}/P_y	$\lambda = \sqrt{P_y / P_{cr}}$	Ratios				Nominal P_n (kN)	Experiment P_{exp} (kN)	Ratio P_{exp}/P_n
					k_1	k_2	k_3	k_4			
C142N90A0U	5.90	2.74	0.47	1.47	1	0.25	1	1.8	2.43	2.21	0.911
C142N120A0U	6.12	3.23	0.53	1.38	1	0.25	1	1.8	2.80	2.35	0.838
C172N120A0U	8.74	2.54	0.29	1.86	1	0.25	1	1.8	2.35	2.37	1.007
C202N120A0U	11.48	2.94	0.26	1.98	1	0.25	1	1.8	2.75	2.70	0.981
C202N150A0U	11.72	3.27	0.28	1.89	1	0.25	1	1.8	3.04	2.84	0.933
C262N120A0U	16.04	2.46	0.15	2.55	1	0.25	1	1.8	2.37	2.55	1.076
C262N150A0U	16.31	2.69	0.16	2.46	1	0.25	1	1.8	2.58	2.82	1.095
C142N90A0F	5.90	4.96	0.84	1.09	1	0.25	1	1.8	3.92	3.75	0.957
C142N120A0F	6.12	6.00	0.98	1.01	1	0.25	1	1.8	4.53	4.06	0.897
C172N120A0F	8.74	4.77	0.55	1.35	1	0.25	1	1.8	4.12	4.16	1.010
C202N120A0F	11.48	5.72	0.50	1.42	1	0.25	1	1.8	5.01	5.24	1.047
C202N150A0F	11.72	6.53	0.56	1.34	1	0.25	1	1.8	5.62	5.82	1.036
C262N120A0F	16.04	5.00	0.31	1.79	1	0.25	1	1.8	4.61	5.06	1.097
C262N150A0F	16.31	5.57	0.34	1.71	1	0.25	1	1.8	5.10	5.37	1.054
Mean											0.996
COV											7.97%

Table F-26: Lipped plain-C sections (Uzzaman et al. [39])

Specimens	Yield Load P_y (kN)	Buckling P_{cr} (kN)	Ratio P_{cr}/P_y	$\lambda = \sqrt{P_y/P_{cr}}$	Ratios				Nominal P_n (kN)	Experiment P_{exp} (kN)	Ratio P_{exp}/P_n
					k_1	k_2	k_3	k_4			
C142N30A0U	5.56	2.09	0.38	1.63	1	0.25	1	1.8	1.89	1.68	0.887
C142N60A0U1	5.78	2.45	0.42	1.54	1	0.25	1	1.8	2.19	1.95	0.892
C142N60A0U2	5.78	2.45	0.42	1.54	1	0.25	1	1.8	2.19	1.83	0.837
C142N60A0U3	5.78	2.45	0.42	1.54	1	0.25	1	1.8	2.19	1.91	0.873
C172N32.5A0U	8.12	1.82	0.22	2.11	1	0.25	1	1.8	1.72	1.70	0.988
C172N65A0FU	8.42	2.10	0.25	2.00	1	0.25	1	1.8	1.97	1.88	0.956
C202N32.5A0U	10.77	2.18	0.20	2.22	1	0.25	1	1.8	2.07	1.98	0.957
C202N65A0U	11.05	2.42	0.22	2.14	1	0.25	1	1.8	2.28	2.39	1.047
C262N32.5A0U	15.28	1.94	0.13	2.81	1	0.25	1	1.8	1.88	2.04	1.086
C262N65A0U	15.38	2.09	0.14	2.71	1	0.25	1	1.8	2.02	2.19	1.083
C302N44A0U	22.41	3.17	0.14	2.66	1	0.25	1	1.8	3.06	3.96	1.295
C302N90A0U	22.54	3.81	0.17	2.43	1	0.25	1	1.8	3.65	4.30	1.178
C142N30A0F	5.67	3.69	0.65	1.24	1	0.25	1	1.8	3.09	2.96	0.957
C142N60A0F1	5.65	3.90	0.69	1.20	1	0.25	1	1.8	3.23	3.32	1.029
C142N60A0F2	5.65	3.90	0.69	1.20	1	0.25	1	1.8	3.23	3.31	1.026
C142N60A0F3	5.65	3.90	0.69	1.20	1	0.25	1	1.8	3.23	3.27	1.013
C172N32.5A0F	8.06	3.21	0.40	1.58	1	0.25	1	1.8	2.89	2.88	0.995
C172N65A0F	8.29	3.61	0.44	1.51	1	0.25	1	1.8	3.22	3.31	1.028
C202N32.5A0F	10.13	3.49	0.34	1.70	1	0.25	1	1.8	3.19	3.63	1.139
C202N65A0F	11.05	4.48	0.41	1.57	1	0.25	1	1.8	4.03	4.37	1.085
C262N32.5A0F	15.16	3.76	0.25	2.01	1	0.25	1	1.8	3.53	3.63	1.029
C262N65A0F	15.01	3.86	0.26	1.97	1	0.25	1	1.8	3.61	3.94	1.090
C302N44A0F	21.96	6.02	0.27	1.91	1	0.25	1	1.8	5.61	6.95	1.240
Mean											1.031
COV											10.98%

Table F-27: Unlipped plain-C sections (Young and Hancock [22])

Specimens	Yield Load P_y (kN)	Buckling P_{cr} (kN)	Ratio P_{cr}/P_y	Ratios				Nominal P_n (kN)	Experiment P_{exp} (kN)	Ratio P_{exp}/P_n
				k_1	k_2	k_3	k_4			
ETF75N40	15.01	153.88	10.25	1	0.25	1	1.8	21.72	22.10	1.018
ETF75N20	14.52	120.14	8.27	1	0.25	1	1.8	20.43	18.30	0.896
ETF100N50	18.99	107.32	5.65	1	0.25	1	1.8	25.15	24.80	0.986
ETF100N25	18.44	85.61	4.64	1	0.25	1	1.8	23.51	22.60	0.961
ETF125N65	22.87	84.56	3.70	1	0.25	1	1.8	27.71	28.20	1.018
ETF125N32	21.97	67.78	3.09	1	0.25	1	1.8	25.39	23.40	0.922
ETF200N75	47.01	84.25	1.79	1	0.25	1	1.8	46.50	40.20	0.865
ETF200N37	45.34	70.79	1.56	1	0.25	1	1.8	43.16	31.20	0.723
ETF250N90	68.37	136.60	2.00	1	0.25	1	1.8	68.37	50.60	0.740
ETF250N45	66.43	116.16	1.75	1	0.25	1	1.8	65.38	46.90	0.717
ETF300N90	77.69	105.33	1.36	1	0.25	1	1.8	69.63	49.40	0.709
ETF300N45	75.92	94.17	1.24	1	0.25	1	1.8	64.97	45.40	0.699
Mean										0.854
COV										15.08%